

# Machine Learning and Blockchain Technology for Smart Healthcare and Human Health 2021

Lead Guest Editor: Yang Gao

Guest Editors: Yuan Yuan, Xinchun Wang, and Weiwei Cai





---

# **Machine Learning and Blockchain Technology for Smart Healthcare and Human Health 2021**

**Machine Learning and Blockchain  
Technology for Smart Healthcare and  
Human Health 2021**

Lead Guest Editor: Yang Gao

Guest Editors: Yuan Yuan, Xinchun Wang, and  
Weiwei Cai



Copyright © 2023 Hindawi Limited. All rights reserved.

This is a special issue published in “Journal of Healthcare Engineering.” All articles are open access articles distributed under the Creative Commons Attribution License, which permits unrestricted use, distribution, and reproduction in any medium, provided the original work is properly cited.

## Associate Editors

Xiao-Jun Chen , China  
Feng-Huei Lin , Taiwan  
Maria Lindén, Sweden

## Academic Editors

Cherif Adnen, Tunisia  
Saverio Affatato , Italy  
Óscar Belmonte Fernández, Spain  
Sweta Bhattacharya , India  
Prabadevi Boopathy , India  
Weiwei Cai, USA  
Gin-Shin Chen , Taiwan  
Hongwei Chen, USA  
Daniel H.K. Chow, Hong Kong  
Gianluca Ciardelli , Italy  
Olawande Daramola, South Africa  
Elena De Momi, Italy  
Costantino Del Gaudio , Italy  
Ayush Dogra , India  
Luobing Dong, China  
Daniel Espino , United Kingdom  
Sadiq Fareed , China  
Mostafa Fatemi, USA  
Jesus Favela , Mexico  
Jesus Fontecha , Spain  
Agostino Forestiero , Italy  
Jean-Luc Gennisson, France  
Badicu Georgian , Romania  
Mehdi Gheisari , China  
Luca Giancardo , USA  
Antonio Gloria , Italy  
Kheng Lim Goh , Singapore  
Carlos Gómez , Spain  
Philippe Gorce, France  
Vincenzo Guarino , Italy  
Muhammet Gul, Turkey  
Valentina Hartwig , Italy  
David Hewson , United Kingdom  
Yan Chai Hum, Malaysia  
Ernesto Iadanza , Italy  
Cosimo Ieracitano, Italy

Giovanni Improta , Italy  
Norio Iriguchi , Japan  
Mihajlo Jakovljevic , Japan  
Rutvij Jhaveri, India  
Yizhang Jiang , China  
Zhongwei Jiang , Japan  
Rajesh Kaluri , India  
Venkatachalam Kandasamy , Czech Republic  
Pushpendu Kar , India  
Rashed Karim , United Kingdom  
Pasi A. Karjalainen , Finland  
John S. Katsanis, Greece  
Smith Khare , United Kingdom  
Terry K.K. Koo , USA  
Srinivas Koppu, India  
Jui-Yang Lai , Taiwan  
Kuruva Lakshmanna , India  
Xiang Li, USA  
Lun-De Liao, Singapore  
Qiu-Hua Lin , China  
Aiping Liu , China  
Zufu Lu , Australia  
Basem M. ElHalawany , Egypt  
Praveen Kumar Reddy Maddikunta , India  
Ilias Maglogiannis, Greece  
Saverio Maietta , Italy  
M.Sabarimalai Manikandan, India  
Mehran Moazen , United Kingdom  
Senthilkumar Mohan, India  
Sanjay Mohapatra, India  
Rafael Morales , Spain  
Mehrbakhsh Nilashi , Malaysia  
Sharnil Pandya, India  
Jialin Peng , China  
Vincenzo Positano , Italy  
Saeed Mian Qaisar , Saudi Arabia  
Alessandro Ramalli , Italy  
Alessandro Reali , Italy  
Vito Ricotta, Italy  
Jose Joaquin Rieta , Spain  
Emanuele Rizzuto , Italy

Dinesh Rokaya, Thailand  
Sébastien Roth, France  
Simo Saarakkala , Finland  
Mangal Sain , Republic of Korea  
Nadeem Sarwar, Pakistan  
Emiliano Schena , Italy  
Prof. Asadullah Shaikh, Saudi Arabia  
Jiann-Shing Shieh , Taiwan  
Tiago H. Silva , Portugal  
Sharan Srinivas , USA  
Kathiravan Srinivasan , India  
Neelakandan Subramani, India  
Le Sun, China  
Fabrizio Taffoni , Italy  
Jinshan Tang, USA  
Ioannis G. Tollis, Greece  
Ikram Ud Din, Pakistan  
Sathishkumar V E , Republic of Korea  
Cesare F. Valenti , Italy  
Qiang Wang, China  
Uche Wejinya, USA  
Yuxiang Wu , China  
Ying Yang , United Kingdom  
Elisabetta Zanetti , Italy  
Haihong Zhang, Singapore  
Ping Zhou , USA

# Contents

**Retracted: Models of Artificial Intelligence-Assisted Diagnosis of Lung Cancer Pathology Based on Deep Learning Algorithms**

Journal of Healthcare Engineering

Retraction (1 page), Article ID 9874292, Volume 2023 (2023)

**Retracted: Design of Optimal Scheduling Model for Emergency Medical Supplies by Blockchain Technology**

Journal of Healthcare Engineering

Retraction (1 page), Article ID 9846831, Volume 2023 (2023)

**Retracted: Qualitative Diagnosis of Liver Tumors Based on Ultrasound-Guided Automatic Biopsy**

Journal of Healthcare Engineering

Retraction (1 page), Article ID 9848645, Volume 2023 (2023)

**Retracted: Construction of Sports and Health Data Resources and Transformation of Teachers' Orientation Based on Web Database**

Journal of Healthcare Engineering

Retraction (1 page), Article ID 9852340, Volume 2023 (2023)

**Retracted: Technical Evaluation of Commercial Sperm DFI Quality Control Products in SCSA Testing**

Journal of Healthcare Engineering

Retraction (1 page), Article ID 9812053, Volume 2023 (2023)

**Retracted: Deep Learning-Based Cervical Spine Posterior Percutaneous Endoscopic Disc Nucleus Resection for the Treatment of Cervical Spondylotic Radiculopathy**

Journal of Healthcare Engineering

Retraction (1 page), Article ID 9810452, Volume 2023 (2023)

**Retracted: Analysis and Improvement of Nursing Quality Based on Standardized Information Integration**

Journal of Healthcare Engineering

Retraction (1 page), Article ID 9791476, Volume 2023 (2023)

**Retracted: Investigation on Quality of Life and Economic Burden of Children with Cerebral Palsy in Changzhou**

Journal of Healthcare Engineering

Retraction (1 page), Article ID 9789538, Volume 2023 (2023)

**Retracted: Construction of Community Medical Communication Service and Rehabilitation Model for Elderly Patients under the Internet of Things**

Journal of Healthcare Engineering

Retraction (1 page), Article ID 9784075, Volume 2023 (2023)

**Retracted: Correlation Analysis of Magnetic Resonance Imaging Characteristics and Prognosis of Invasive Pituitary Adenomas in Neurosurgery Hospitals**

Journal of Healthcare Engineering

Retraction (1 page), Article ID 9815014, Volume 2023 (2023)

**Retracted: Discussion on Health Service System of Mobile Medical Institutions Based on Internet of Things and Cloud Computing**

Journal of Healthcare Engineering

Retraction (1 page), Article ID 9892481, Volume 2023 (2023)

**Retracted: The Potential Mechanism of Exercise Combined with Natural Extracts to Prevent and Treat Postmenopausal Osteoporosis**

Journal of Healthcare Engineering

Retraction (1 page), Article ID 9875621, Volume 2023 (2023)

**Retracted: The Role of Three-Dimensional Reconstruction of Medical Images and Virtual Reality in Nursing Experimental Teaching**

Journal of Healthcare Engineering

Retraction (1 page), Article ID 9838194, Volume 2023 (2023)

**Retracted: Effect of Protein Nutrition Level on Protein Metabolism during Volleyball Exercise Based on Edge Computing in the Medical System**

Journal of Healthcare Engineering

Retraction (1 page), Article ID 9830421, Volume 2023 (2023)

**Retracted: An Early Warning of Atrial Fibrillation Based on Short-Time ECG Signals**

Journal of Healthcare Engineering


Retraction (1 page), Article ID 9860546, Volume 2023 (2023)

**Retracted: Immunomodulatory Effect of *Lycium barbarum* Polysaccharides against Liver Fibrosis Based on the Intelligent Medical Internet of Things**

Journal of Healthcare Engineering



Retraction (1 page), Article ID 9852810, Volume 2023 (2023)

**[Retracted] Correlation Analysis of Magnetic Resonance Imaging Characteristics and Prognosis of Invasive Pituitary Adenomas in Neurosurgery Hospitals**

Jinan Bai, Xin Li, Ailiang Ge, and Jianhua Gu 


Research Article (11 pages), Article ID 8280540, Volume 2022 (2022)

**[Retracted] Construction of Community Medical Communication Service and Rehabilitation Model for Elderly Patients under the Internet of Things**

Xiaoxia Zhang , Fang Wang , Dan Wang, Yanhua Xiang, and Zhongwei Zhang

Research Article (12 pages), Article ID 9689769, Volume 2022 (2022)



**[Retracted] Models of Artificial Intelligence-Assisted Diagnosis of Lung Cancer Pathology Based on Deep Learning Algorithms**

Su Chen 

Research Article (12 pages), Article ID 3972298, Volume 2022 (2022)

# Contents

**[Retracted] The Role of Three-Dimensional Reconstruction of Medical Images and Virtual Reality in Nursing Experimental Teaching**

Min Zhu, Chunhui Li, Shuangping Zhao, Liang Chen , and Xueping Zhao 


Research Article (13 pages), Article ID 3853193, Volume 2022 (2022)

**[Retracted] Technical Evaluation of Commercial Sperm DFI Quality Control Products in SCSA Testing**

Tao Pang and Xinzong Zhang 


Research Article (14 pages), Article ID 9552123, Volume 2022 (2022)

**[Retracted] Design of Optimal Scheduling Model for Emergency Medical Supplies by Blockchain Technology**

Yan Zhao 


Research Article (10 pages), Article ID 4608761, Volume 2022 (2022)

**[Retracted] Analysis and Improvement of Nursing Quality Based on Standardized Information Integration**

Huixia He, Huiling Li, Kong Qiao, Bin Hao, and Dong Yu 


Research Article (10 pages), Article ID 9172416, Volume 2022 (2022)

**[Retracted] Construction of Sports and Health Data Resources and Transformation of Teachers' Orientation Based on Web Database**

Jiawen Yang and Min Chen 




Research Article (10 pages), Article ID 4372406, Volume 2022 (2022)

**[Retracted] Immunomodulatory Effect of *Lycium barbarum* Polysaccharides against Liver Fibrosis Based on the Intelligent Medical Internet of Things**

Yanzhen Han , Yan Zhou, Tiejing Shan, Wei Li, and Haiping Liu

Research Article (13 pages), Article ID 6280265, Volume 2022 (2022)

**[Retracted] An Early Warning of Atrial Fibrillation Based on Short-Time ECG Signals**

Tianxia Zhao , Xin'an Wang , and Changpei Qiu 


Research Article (7 pages), Article ID 2205460, Volume 2022 (2022)

**[Retracted] Effect of Protein Nutrition Level on Protein Metabolism during Volleyball Exercise Based on Edge Computing in the Medical System**

Jicheng Yang, Ning Du , Wei Jiang, and Chenzhe Liu


Research Article (9 pages), Article ID 1614748, Volume 2022 (2022)

**Performance Prediction of Listed Companies in Smart Healthcare Industry: Based on Machine Learning Algorithms**

Baobao Dong , Xiangming Wang, and Qi Cao

Research Article (7 pages), Article ID 8091383, Volume 2022 (2022)

**[Retracted] Discussion on Health Service System of Mobile Medical Institutions Based on Internet of Things and Cloud Computing**

Jinzhou Tang 


Research Article (12 pages), Article ID 5235349, Volume 2022 (2022)

**[Retracted] Investigation on Quality of Life and Economic Burden of Children with Cerebral Palsy in Changzhou**

Chaorong Bian , Feng Peng , Haibin Guo , and Kejin Chen 


Research Article (9 pages), Article ID 1519689, Volume 2022 (2022)

**[Retracted] The Potential Mechanism of Exercise Combined with Natural Extracts to Prevent and Treat Postmenopausal Osteoporosis**

Tongxi Zhou, Zhuo Gai, Xing Gao, and Li Li 


Review Article (9 pages), Article ID 2852661, Volume 2021 (2021)

**[Retracted] Deep Learning-Based Cervical Spine Posterior Percutaneous Endoscopic Disc Nucleus Resection for the Treatment of Cervical Spondylotic Radiculopathy**

Yang Zhang, Hengjie Zhu, Zheng Zhou, Yinming Sun, Xiang Shen, Jixiang Wu, and Chengcun Li 

Research Article (12 pages), Article ID 7245566, Volume 2021 (2021)

**[Retracted] Qualitative Diagnosis of Liver Tumors Based on Ultrasound-Guided Automatic Biopsy**

Bin Peng 

Research Article (12 pages), Article ID 8585887, Volume 2021 (2021)

## Retraction

# Retracted: Models of Artificial Intelligence-Assisted Diagnosis of Lung Cancer Pathology Based on Deep Learning Algorithms

### Journal of Healthcare Engineering

Received 10 October 2023; Accepted 10 October 2023; Published 11 October 2023

Copyright © 2023 Journal of Healthcare Engineering. This is an open access article distributed under the Creative Commons Attribution License, which permits unrestricted use, distribution, and reproduction in any medium, provided the original work is properly cited.

This article has been retracted by Hindawi following an investigation undertaken by the publisher [1]. This investigation has uncovered evidence of one or more of the following indicators of systematic manipulation of the publication process:

- (1) Discrepancies in scope
- (2) Discrepancies in the description of the research reported
- (3) Discrepancies between the availability of data and the research described
- (4) Inappropriate citations
- (5) Incoherent, meaningless and/or irrelevant content included in the article
- (6) Peer-review manipulation

The presence of these indicators undermines our confidence in the integrity of the article's content and we cannot, therefore, vouch for its reliability. Please note that this notice is intended solely to alert readers that the content of this article is unreliable. We have not investigated whether authors were aware of or involved in the systematic manipulation of the publication process.

In addition, our investigation has also shown that one or more of the following human-subject reporting requirements has not been met in this article: ethical approval by an Institutional Review Board (IRB) committee or equivalent, patient/participant consent to participate, and/or agreement to publish patient/participant details (where relevant).

Wiley and Hindawi regrets that the usual quality checks did not identify these issues before publication and have since put additional measures in place to safeguard research integrity.

We wish to credit our own Research Integrity and Research Publishing teams and anonymous and named external researchers and research integrity experts for contributing to this investigation.

The corresponding author, as the representative of all authors, has been given the opportunity to register their agreement or disagreement to this retraction. We have kept a record of any response received.

### References

- [1] S. Chen, "Models of Artificial Intelligence-Assisted Diagnosis of Lung Cancer Pathology Based on Deep Learning Algorithms," *Journal of Healthcare Engineering*, vol. 2022, Article ID 3972298, 12 pages, 2022.

## Retraction

# Retracted: Design of Optimal Scheduling Model for Emergency Medical Supplies by Blockchain Technology

### Journal of Healthcare Engineering

Received 10 October 2023; Accepted 10 October 2023; Published 11 October 2023

Copyright © 2023 Journal of Healthcare Engineering. This is an open access article distributed under the Creative Commons Attribution License, which permits unrestricted use, distribution, and reproduction in any medium, provided the original work is properly cited.

This article has been retracted by Hindawi following an investigation undertaken by the publisher [1]. This investigation has uncovered evidence of one or more of the following indicators of systematic manipulation of the publication process:

- (1) Discrepancies in scope
- (2) Discrepancies in the description of the research reported
- (3) Discrepancies between the availability of data and the research described
- (4) Inappropriate citations
- (5) Incoherent, meaningless and/or irrelevant content included in the article
- (6) Peer-review manipulation

The presence of these indicators undermines our confidence in the integrity of the article's content and we cannot, therefore, vouch for its reliability. Please note that this notice is intended solely to alert readers that the content of this article is unreliable. We have not investigated whether authors were aware of or involved in the systematic manipulation of the publication process.

Wiley and Hindawi regrets that the usual quality checks did not identify these issues before publication and have since put additional measures in place to safeguard research integrity.

We wish to credit our own Research Integrity and Research Publishing teams and anonymous and named external researchers and research integrity experts for contributing to this investigation.

The corresponding author, as the representative of all authors, has been given the opportunity to register their agreement or disagreement to this retraction. We have kept a record of any response received.

### References

- [1] Y. Zhao, "Design of Optimal Scheduling Model for Emergency Medical Supplies by Blockchain Technology," *Journal of Healthcare Engineering*, vol. 2022, Article ID 4608761, 10 pages, 2022.

## Retraction

# Retracted: Qualitative Diagnosis of Liver Tumors Based on Ultrasound-Guided Automatic Biopsy

### Journal of Healthcare Engineering

Received 29 August 2023; Accepted 29 August 2023; Published 30 August 2023

Copyright © 2023 Journal of Healthcare Engineering. This is an open access article distributed under the Creative Commons Attribution License, which permits unrestricted use, distribution, and reproduction in any medium, provided the original work is properly cited.

This article has been retracted by Hindawi following an investigation undertaken by the publisher [1]. This investigation has uncovered evidence of one or more of the following indicators of systematic manipulation of the publication process:

- (1) Discrepancies in scope
- (2) Discrepancies in the description of the research reported
- (3) Discrepancies between the availability of data and the research described
- (4) Inappropriate citations
- (5) Incoherent, meaningless and/or irrelevant content included in the article
- (6) Peer-review manipulation

The presence of these indicators undermines our confidence in the integrity of the article's content and we cannot, therefore, vouch for its reliability. Please note that this notice is intended solely to alert readers that the content of this article is unreliable. We have not investigated whether authors were aware of or involved in the systematic manipulation of the publication process.

Wiley and Hindawi regrets that the usual quality checks did not identify these issues before publication and have since put additional measures in place to safeguard research integrity.

We wish to credit our own Research Integrity and Research Publishing teams and anonymous and named external researchers and research integrity experts for contributing to this investigation.

The corresponding author, as the representative of all authors, has been given the opportunity to register their agreement or disagreement to this retraction. We have kept a record of any response received.

### References

- [1] B. Peng, "Qualitative Diagnosis of Liver Tumors Based on Ultrasound-Guided Automatic Biopsy," *Journal of Healthcare Engineering*, vol. 2021, Article ID 8585887, 12 pages, 2021.

## Retraction

# Retracted: Construction of Sports and Health Data Resources and Transformation of Teachers' Orientation Based on Web Database

### Journal of Healthcare Engineering

Received 11 July 2023; Accepted 11 July 2023; Published 12 July 2023

Copyright © 2023 Journal of Healthcare Engineering. This is an open access article distributed under the Creative Commons Attribution License, which permits unrestricted use, distribution, and reproduction in any medium, provided the original work is properly cited.

This article has been retracted by Hindawi following an investigation undertaken by the publisher [1]. This investigation has uncovered evidence of one or more of the following indicators of systematic manipulation of the publication process:

- (1) Discrepancies in scope
- (2) Discrepancies in the description of the research reported
- (3) Discrepancies between the availability of data and the research described
- (4) Inappropriate citations
- (5) Incoherent, meaningless and/or irrelevant content included in the article
- (6) Peer-review manipulation

The presence of these indicators undermines our confidence in the integrity of the article's content and we cannot, therefore, vouch for its reliability. Please note that this notice is intended solely to alert readers that the content of this article is unreliable. We have not investigated whether authors were aware of or involved in the systematic manipulation of the publication process.

Wiley and Hindawi regrets that the usual quality checks did not identify these issues before publication and have since put additional measures in place to safeguard research integrity.

We wish to credit our own Research Integrity and Research Publishing teams and anonymous and named external researchers and research integrity experts for contributing to this investigation.

The corresponding author, as the representative of all authors, has been given the opportunity to register their agreement or disagreement to this retraction. We have kept a record of any response received.

### References

- [1] J. Yang and M. Chen, "Construction of Sports and Health Data Resources and Transformation of Teachers' Orientation Based on Web Database," *Journal of Healthcare Engineering*, vol. 2022, Article ID 4372406, 10 pages, 2022.

## Retraction

# Retracted: Technical Evaluation of Commercial Sperm DFI Quality Control Products in SCSA Testing

### Journal of Healthcare Engineering

Received 11 July 2023; Accepted 11 July 2023; Published 12 July 2023

Copyright © 2023 Journal of Healthcare Engineering. This is an open access article distributed under the Creative Commons Attribution License, which permits unrestricted use, distribution, and reproduction in any medium, provided the original work is properly cited.

This article has been retracted by Hindawi following an investigation undertaken by the publisher [1]. This investigation has uncovered evidence of one or more of the following indicators of systematic manipulation of the publication process:

- (1) Discrepancies in scope
- (2) Discrepancies in the description of the research reported
- (3) Discrepancies between the availability of data and the research described
- (4) Inappropriate citations
- (5) Incoherent, meaningless and/or irrelevant content included in the article
- (6) Peer-review manipulation

The presence of these indicators undermines our confidence in the integrity of the article's content and we cannot, therefore, vouch for its reliability. Please note that this notice is intended solely to alert readers that the content of this article is unreliable. We have not investigated whether authors were aware of or involved in the systematic manipulation of the publication process.

Wiley and Hindawi regrets that the usual quality checks did not identify these issues before publication and have since put additional measures in place to safeguard research integrity.

We wish to credit our own Research Integrity and Research Publishing teams and anonymous and named external researchers and research integrity experts for contributing to this investigation.

The corresponding author, as the representative of all authors, has been given the opportunity to register their agreement or disagreement to this retraction. We have kept a record of any response received.

### References

- [1] T. Pang and X. Zhang, "Technical Evaluation of Commercial Sperm DFI Quality Control Products in SCSA Testing," *Journal of Healthcare Engineering*, vol. 2022, Article ID 9552123, 14 pages, 2022.

## Retraction

# Retracted: Deep Learning-Based Cervical Spine Posterior Percutaneous Endoscopic Disc Nucleus Resection for the Treatment of Cervical Spondylotic Radiculopathy

### Journal of Healthcare Engineering

Received 11 July 2023; Accepted 11 July 2023; Published 12 July 2023

Copyright © 2023 Journal of Healthcare Engineering. This is an open access article distributed under the Creative Commons Attribution License, which permits unrestricted use, distribution, and reproduction in any medium, provided the original work is properly cited.

This article has been retracted by Hindawi following an investigation undertaken by the publisher [1]. This investigation has uncovered evidence of one or more of the following indicators of systematic manipulation of the publication process:

- (1) Discrepancies in scope
- (2) Discrepancies in the description of the research reported
- (3) Discrepancies between the availability of data and the research described
- (4) Inappropriate citations
- (5) Incoherent, meaningless and/or irrelevant content included in the article
- (6) Peer-review manipulation

The presence of these indicators undermines our confidence in the integrity of the article's content and we cannot, therefore, vouch for its reliability. Please note that this notice is intended solely to alert readers that the content of this article is unreliable. We have not investigated whether authors were aware of or involved in the systematic manipulation of the publication process.

In addition, our investigation has also shown that one or more of the following human-subject reporting requirements has not been met in this article: ethical approval by an Institutional Review Board (IRB) committee or equivalent, patient/participant consent to participate, and/or agreement to publish patient/participant details (where relevant).

Wiley and Hindawi regrets that the usual quality checks did not identify these issues before publication and have since put additional measures in place to safeguard research integrity.

We wish to credit our own Research Integrity and Research Publishing teams and anonymous and named external researchers and research integrity experts for contributing to this investigation.

The corresponding author, as the representative of all authors, has been given the opportunity to register their agreement or disagreement to this retraction. We have kept a record of any response received.

### References

- [1] Y. Zhang, H. Zhu, Z. Zhou et al., "Deep Learning-Based Cervical Spine Posterior Percutaneous Endoscopic Disc Nucleus Resection for the Treatment of Cervical Spondylotic Radiculopathy," *Journal of Healthcare Engineering*, vol. 2021, Article ID 7245566, 12 pages, 2021.

## Retraction

# Retracted: Analysis and Improvement of Nursing Quality Based on Standardized Information Integration

### Journal of Healthcare Engineering

Received 11 July 2023; Accepted 11 July 2023; Published 12 July 2023

Copyright © 2023 Journal of Healthcare Engineering. This is an open access article distributed under the Creative Commons Attribution License, which permits unrestricted use, distribution, and reproduction in any medium, provided the original work is properly cited.

This article has been retracted by Hindawi following an investigation undertaken by the publisher [1]. This investigation has uncovered evidence of one or more of the following indicators of systematic manipulation of the publication process:

- (1) Discrepancies in scope
- (2) Discrepancies in the description of the research reported
- (3) Discrepancies between the availability of data and the research described
- (4) Inappropriate citations
- (5) Incoherent, meaningless and/or irrelevant content included in the article
- (6) Peer-review manipulation

The presence of these indicators undermines our confidence in the integrity of the article's content and we cannot, therefore, vouch for its reliability. Please note that this notice is intended solely to alert readers that the content of this article is unreliable. We have not investigated whether authors were aware of or involved in the systematic manipulation of the publication process.

Wiley and Hindawi regrets that the usual quality checks did not identify these issues before publication and have since put additional measures in place to safeguard research integrity.

We wish to credit our own Research Integrity and Research Publishing teams and anonymous and named external researchers and research integrity experts for contributing to this investigation.

The corresponding author, as the representative of all authors, has been given the opportunity to register their agreement or disagreement to this retraction. We have kept a record of any response received.

### References

- [1] H. He, H. Li, K. Qiao, B. Hao, and D. Yu, "Analysis and Improvement of Nursing Quality Based on Standardized Information Integration," *Journal of Healthcare Engineering*, vol. 2022, Article ID 9172416, 10 pages, 2022.

## Retraction

# Retracted: Investigation on Quality of Life and Economic Burden of Children with Cerebral Palsy in Changzhou

### Journal of Healthcare Engineering

Received 11 July 2023; Accepted 11 July 2023; Published 12 July 2023

Copyright © 2023 Journal of Healthcare Engineering. This is an open access article distributed under the Creative Commons Attribution License, which permits unrestricted use, distribution, and reproduction in any medium, provided the original work is properly cited.

This article has been retracted by Hindawi following an investigation undertaken by the publisher [1]. This investigation has uncovered evidence of one or more of the following indicators of systematic manipulation of the publication process:

- (1) Discrepancies in scope
- (2) Discrepancies in the description of the research reported
- (3) Discrepancies between the availability of data and the research described
- (4) Inappropriate citations
- (5) Incoherent, meaningless and/or irrelevant content included in the article
- (6) Peer-review manipulation

The presence of these indicators undermines our confidence in the integrity of the article's content and we cannot, therefore, vouch for its reliability. Please note that this notice is intended solely to alert readers that the content of this article is unreliable. We have not investigated whether authors were aware of or involved in the systematic manipulation of the publication process.

Wiley and Hindawi regrets that the usual quality checks did not identify these issues before publication and have since put additional measures in place to safeguard research integrity.

We wish to credit our own Research Integrity and Research Publishing teams and anonymous and named external researchers and research integrity experts for contributing to this investigation.

The corresponding author, as the representative of all authors, has been given the opportunity to register their agreement or disagreement to this retraction. We have kept a record of any response received.

### References

- [1] C. Bian, F. Peng, H. Guo, and K. Chen, "Investigation on Quality of Life and Economic Burden of Children with Cerebral Palsy in Changzhou," *Journal of Healthcare Engineering*, vol. 2022, Article ID 1519689, 9 pages, 2022.

## Retraction

# Retracted: Construction of Community Medical Communication Service and Rehabilitation Model for Elderly Patients under the Internet of Things

### Journal of Healthcare Engineering

Received 11 July 2023; Accepted 11 July 2023; Published 12 July 2023

Copyright © 2023 Journal of Healthcare Engineering. This is an open access article distributed under the Creative Commons Attribution License, which permits unrestricted use, distribution, and reproduction in any medium, provided the original work is properly cited.

This article has been retracted by Hindawi following an investigation undertaken by the publisher [1]. This investigation has uncovered evidence of one or more of the following indicators of systematic manipulation of the publication process:

- (1) Discrepancies in scope
- (2) Discrepancies in the description of the research reported
- (3) Discrepancies between the availability of data and the research described
- (4) Inappropriate citations
- (5) Incoherent, meaningless and/or irrelevant content included in the article
- (6) Peer-review manipulation

The presence of these indicators undermines our confidence in the integrity of the article's content and we cannot, therefore, vouch for its reliability. Please note that this notice is intended solely to alert readers that the content of this article is unreliable. We have not investigated whether authors were aware of or involved in the systematic manipulation of the publication process.

Wiley and Hindawi regrets that the usual quality checks did not identify these issues before publication and have since put additional measures in place to safeguard research integrity.

We wish to credit our own Research Integrity and Research Publishing teams and anonymous and named external researchers and research integrity experts for contributing to this investigation.

The corresponding author, as the representative of all authors, has been given the opportunity to register their agreement or disagreement to this retraction. We have kept a record of any response received.

### References

- [1] X. Zhang, F. Wang, D. Wang, Y. Xiang, and Z. Zhang, "Construction of Community Medical Communication Service and Rehabilitation Model for Elderly Patients under the Internet of Things," *Journal of Healthcare Engineering*, vol. 2022, Article ID 9689769, 12 pages, 2022.

## Retraction

# Retracted: Correlation Analysis of Magnetic Resonance Imaging Characteristics and Prognosis of Invasive Pituitary Adenomas in Neurosurgery Hospitals

### Journal of Healthcare Engineering

Received 27 June 2023; Accepted 27 June 2023; Published 28 June 2023

Copyright © 2023 Journal of Healthcare Engineering. This is an open access article distributed under the Creative Commons Attribution License, which permits unrestricted use, distribution, and reproduction in any medium, provided the original work is properly cited.

This article has been retracted by Hindawi following an investigation undertaken by the publisher [1]. This investigation has uncovered evidence of one or more of the following indicators of systematic manipulation of the publication process:

- (1) Discrepancies in scope
- (2) Discrepancies in the description of the research reported
- (3) Discrepancies between the availability of data and the research described
- (4) Inappropriate citations
- (5) Incoherent, meaningless and/or irrelevant content included in the article
- (6) Peer-review manipulation

The presence of these indicators undermines our confidence in the integrity of the article's content and we cannot, therefore, vouch for its reliability. Please note that this notice is intended solely to alert readers that the content of this article is unreliable. We have not investigated whether authors were aware of or involved in the systematic manipulation of the publication process.

In addition, our investigation has also shown that one or more of the following human-subject reporting requirements has not been met in this article: ethical approval by an Institutional Review Board (IRB) committee or equivalent, patient/participant consent to participate, and/or agreement to publish patient/participant details (where relevant).

Wiley and Hindawi regrets that the usual quality checks did not identify these issues before publication and have since put additional measures in place to safeguard research integrity.

We wish to credit our own Research Integrity and Research Publishing teams and anonymous and named external researchers and research integrity experts for contributing to this investigation.

The corresponding author, as the representative of all authors, has been given the opportunity to register their agreement or disagreement to this retraction. We have kept a record of any response received.

### References

- [1] J. Bai, X. Li, A. Ge, and J. Gu, "Correlation Analysis of Magnetic Resonance Imaging Characteristics and Prognosis of Invasive Pituitary Adenomas in Neurosurgery Hospitals," *Journal of Healthcare Engineering*, vol. 2022, Article ID 8280540, 11 pages, 2022.

## Retraction

# Retracted: Discussion on Health Service System of Mobile Medical Institutions Based on Internet of Things and Cloud Computing

### Journal of Healthcare Engineering

Received 16 November 2022; Accepted 16 November 2022; Published 24 January 2023

Copyright © 2023 Journal of Healthcare Engineering. This is an open access article distributed under the Creative Commons Attribution License, which permits unrestricted use, distribution, and reproduction in any medium, provided the original work is properly cited.

*Journal of Healthcare Engineering* has retracted the article titled “Discussion on Health Service System of Mobile Medical Institutions Based on Internet of Things and Cloud Computing” [1] due to concerns that the peer review process has been compromised.

Following an investigation conducted by the Hindawi Research Integrity team [2], significant concerns were identified with the peer reviewers assigned to this article; the investigation has concluded that the peer review process was compromised. We therefore can no longer trust the peer review process, and the article is being retracted with the agreement of the Chief Editor.

### References

- [1] J. Tang, “Discussion on Health Service System of Mobile Medical Institutions Based on Internet of Things and Cloud Computing,” *Journal of Healthcare Engineering*, vol. 2022, Article ID 5235349, 12 pages, 2022.
- [2] L. Ferguson, “Advancing Research Integrity Collaboratively and with Vigour,” 2022, <https://www.hindawi.com/post/advancing-research-integrity-collaboratively-and-vigour/>.

## Retraction

# Retracted: The Potential Mechanism of Exercise Combined with Natural Extracts to Prevent and Treat Postmenopausal Osteoporosis

### Journal of Healthcare Engineering

Received 16 November 2022; Accepted 16 November 2022; Published 23 January 2023

Copyright © 2023 Journal of Healthcare Engineering. This is an open access article distributed under the Creative Commons Attribution License, which permits unrestricted use, distribution, and reproduction in any medium, provided the original work is properly cited.

*Journal of Healthcare Engineering* has retracted the article titled “The Potential Mechanism of Exercise Combined with Natural Extracts to Prevent and Treat Postmenopausal Osteoporosis” [1] due to concerns that the peer review process has been compromised.

Following an investigation conducted by the Hindawi Research Integrity team [2], significant concerns were identified with the peer reviewers assigned to this article; the investigation has concluded that the peer review process was compromised. We therefore can no longer trust the peer review process, and the article is being retracted with the agreement of the Chief Editor.

The authors do not agree to the retraction.

### References

- [1] T. Zhou, Z. Gai, X. Gao, and L. Li, “The Potential Mechanism of Exercise Combined with Natural Extracts to Prevent and Treat Postmenopausal Osteoporosis,” *Journal of Healthcare Engineering*, vol. 2021, Article ID 2852661, 9 pages, 2021.
- [2] L. Ferguson, “Advancing Research Integrity Collaboratively and with Vigour,” 2022, <https://www.hindawi.com/post/advancing-research-integrity-collaboratively-and-vigour/>.

## *Retraction*

# **Retracted: The Role of Three-Dimensional Reconstruction of Medical Images and Virtual Reality in Nursing Experimental Teaching**

### **Journal of Healthcare Engineering**

Received 16 November 2022; Accepted 16 November 2022; Published 23 January 2023

Copyright © 2023 Journal of Healthcare Engineering. This is an open access article distributed under the Creative Commons Attribution License, which permits unrestricted use, distribution, and reproduction in any medium, provided the original work is properly cited.

*Journal of Healthcare Engineering* has retracted the article titled “The Role of Three-Dimensional Reconstruction of Medical Images and Virtual Reality in Nursing Experimental Teaching” [1] due to concerns that the peer review process has been compromised.

Following an investigation conducted by the Hindawi Research Integrity team [2], significant concerns were identified with the peer reviewers assigned to this article; the investigation has concluded that the peer review process was compromised. We therefore can no longer trust the peer review process, and the article is being retracted with the agreement of the Chief Editor.

### **References**

- [1] M. Zhu, C. Li, S. Zhao, L. Chen, and X. Zhao, “The Role of Three-Dimensional Reconstruction of Medical Images and Virtual Reality in Nursing Experimental Teaching,” *Journal of Healthcare Engineering*, vol. 2022, Article ID 3853193, 13 pages, 2022.
- [2] L. Ferguson, “Advancing Research Integrity Collaboratively and with Vigour,” 2022, <https://www.hindawi.com/post/advancing-research-integrity-collaboratively-and-vigour/>.

## *Retraction*

# **Retracted: Effect of Protein Nutrition Level on Protein Metabolism during Volleyball Exercise Based on Edge Computing in the Medical System**

### **Journal of Healthcare Engineering**

Received 16 November 2022; Accepted 16 November 2022; Published 20 January 2023

Copyright © 2023 Journal of Healthcare Engineering. This is an open access article distributed under the Creative Commons Attribution License, which permits unrestricted use, distribution, and reproduction in any medium, provided the original work is properly cited.

*Journal of Healthcare Engineering* has retracted the article titled “Effect of Protein Nutrition Level on Protein Metabolism during Volleyball Exercise Based on Edge Computing in the Medical System” [1] due to concerns that the peer review process has been compromised.

Following an investigation conducted by the Hindawi Research Integrity team [2], significant concerns were identified with the peer reviewers assigned to this article; the investigation has concluded that the peer review process was compromised. We therefore can no longer trust the peer review process, and the article is being retracted with the agreement of the Chief Editor.

The authors do not agree to the retraction.

### **References**

- [1] J. Yang, N. Du, W. Jiang, and C. Liu, “Effect of Protein Nutrition Level on Protein Metabolism during Volleyball Exercise Based on Edge Computing in the Medical System,” *Journal of Healthcare Engineering*, vol. 2022, Article ID 1614748, 9 pages, 2022.
- [2] L. Ferguson, “Advancing Research Integrity Collaboratively and with Vigour,” 2022, <https://www.hindawi.com/post/advancing-research-integrity-collaboratively-and-vigour/>.

## *Retraction*

# **Retracted: An Early Warning of Atrial Fibrillation Based on Short-Time ECG Signals**

### **Journal of Healthcare Engineering**

Received 16 November 2022; Accepted 16 November 2022; Published 19 January 2023

Copyright © 2023 Journal of Healthcare Engineering. This is an open access article distributed under the Creative Commons Attribution License, which permits unrestricted use, distribution, and reproduction in any medium, provided the original work is properly cited.

*Journal of Healthcare Engineering* has retracted the article titled “An Early Warning of Atrial Fibrillation Based on Short-Time ECG Signals” [1] due to concerns that the peer review process has been compromised.

Following an investigation conducted by the Hindawi Research Integrity team [2], significant concerns were identified with the peer reviewers assigned to this article; the investigation has concluded that the peer review process was compromised. We therefore can no longer trust the peer review process, and the article is being retracted with the agreement of the Chief Editor.

The authors do not agree to the retraction.

### **References**

- [1] T. Zhao, X. Wang, and C. Qiu, “An Early Warning of Atrial Fibrillation Based on Short-Time ECG Signals,” *Journal of Healthcare Engineering*, vol. 2022, Article ID 2205460, 7 pages, 2022.
- [2] L. Ferguson, “Advancing Research Integrity Collaboratively and with Vigour,” 2022, <https://www.hindawi.com/post/advancing-research-integrity-collaboratively-and-vigour/>.

## Retraction

# Retracted: Immunomodulatory Effect of *Lycium barbarum* Polysaccharides against Liver Fibrosis Based on the Intelligent Medical Internet of Things

### Journal of Healthcare Engineering

Received 9 December 2022; Accepted 9 December 2022; Published 3 January 2023

Copyright © 2023 Journal of Healthcare Engineering. This is an open access article distributed under the Creative Commons Attribution License, which permits unrestricted use, distribution, and reproduction in any medium, provided the original work is properly cited.

*Journal of Healthcare Engineering* has retracted the article titled “Immunomodulatory Effect of *Lycium barbarum* Polysaccharides against Liver Fibrosis Based on the Intelligent Medical Internet of Things” [1] due to concerns that the peer review process has been compromised.

Following an investigation conducted by the Hindawi Research Integrity team [2], significant concerns were identified with the peer reviewers assigned to this article; the investigation has concluded that the peer review process was compromised. We therefore can no longer trust the peer review process, and the article is being retracted with the agreement of the Chief Editor.

The authors agree to the retraction; author Wei Li could not be reached by the publisher using the e-mail address provided with the article submission.

### References

- [1] Y. Han, Y. Zhou, T. Shan, W. Li, and H. Liu, “Immunomodulatory Effect of *Lycium barbarum* Polysaccharides against Liver Fibrosis Based on the Intelligent Medical Internet of Things,” *Journal of Healthcare Engineering*, vol. 2022, Article ID 6280265, 13 pages, 2022.
- [2] L. Ferguson, “Advancing Research Integrity Collaboratively and with Vigour,” 2022, <https://www.hindawi.com/post/advancing-research-integrity-collaboratively-and-vigour/>.

## Retraction

# Retracted: Correlation Analysis of Magnetic Resonance Imaging Characteristics and Prognosis of Invasive Pituitary Adenomas in Neurosurgery Hospitals

### Journal of Healthcare Engineering

Received 27 June 2023; Accepted 27 June 2023; Published 28 June 2023

Copyright © 2023 Journal of Healthcare Engineering. This is an open access article distributed under the Creative Commons Attribution License, which permits unrestricted use, distribution, and reproduction in any medium, provided the original work is properly cited.

This article has been retracted by Hindawi following an investigation undertaken by the publisher [1]. This investigation has uncovered evidence of one or more of the following indicators of systematic manipulation of the publication process:

- (1) Discrepancies in scope
- (2) Discrepancies in the description of the research reported
- (3) Discrepancies between the availability of data and the research described
- (4) Inappropriate citations
- (5) Incoherent, meaningless and/or irrelevant content included in the article
- (6) Peer-review manipulation

The presence of these indicators undermines our confidence in the integrity of the article's content and we cannot, therefore, vouch for its reliability. Please note that this notice is intended solely to alert readers that the content of this article is unreliable. We have not investigated whether authors were aware of or involved in the systematic manipulation of the publication process.

In addition, our investigation has also shown that one or more of the following human-subject reporting requirements has not been met in this article: ethical approval by an Institutional Review Board (IRB) committee or equivalent, patient/participant consent to participate, and/or agreement to publish patient/participant details (where relevant).

Wiley and Hindawi regrets that the usual quality checks did not identify these issues before publication and have since put additional measures in place to safeguard research integrity.

We wish to credit our own Research Integrity and Research Publishing teams and anonymous and named external researchers and research integrity experts for contributing to this investigation.

The corresponding author, as the representative of all authors, has been given the opportunity to register their agreement or disagreement to this retraction. We have kept a record of any response received.

### References

- [1] J. Bai, X. Li, A. Ge, and J. Gu, "Correlation Analysis of Magnetic Resonance Imaging Characteristics and Prognosis of Invasive Pituitary Adenomas in Neurosurgery Hospitals," *Journal of Healthcare Engineering*, vol. 2022, Article ID 8280540, 11 pages, 2022.

## Research Article

# Correlation Analysis of Magnetic Resonance Imaging Characteristics and Prognosis of Invasive Pituitary Adenomas in Neurosurgery Hospitals

Jinan Bai, Xin Li, Ailiang Ge, and Jianhua Gu 

Department of Neurosurgery, Yangzhou Hongquan Hospital, Yangzhou 225200, Jiangsu, China

Correspondence should be addressed to Jianhua Gu; 201800153@yangtzeu.edu.cn

Received 18 January 2022; Revised 27 March 2022; Accepted 6 April 2022; Published 21 April 2022

Academic Editor: Yang Gao

Copyright © 2022 Jinan Bai et al. This is an open access article distributed under the Creative Commons Attribution License, which permits unrestricted use, distribution, and reproduction in any medium, provided the original work is properly cited.

The incidence of pituitary adenoma is second only to glioma and meningioma, and its incidence ranks third among intracranial tumors. Most pituitary adenomas are benign and noninvasive tumors, but invasive pituitary adenomas pose a great threat to human health. In order to explore the risk factors that affect the clinical aggressive behavior of patients with pituitary adenoma, analyze the correlation between different classification methods and clinical aggressive behavior, and lay the foundation for early judgment and individualized treatment of clinical aggressive behavior of patients with pituitary adenoma. We conducted statistical research on patients who were treated for pituitary adenomas in the city's Yangzhou Hongquan Hospital. The results of the study showed that six patients in this study showed aggressiveness in the clinical symptomatic outcome, six patients showed aggressiveness in the serological outcome, and seven patients showed aggressiveness in imaging. In the multimodal classification, the clinical aggressiveness of pituitary adenomas in the invasion + atypical group was significantly higher than that in other groups, and the difference was statistically significant ( $P < 0.05$ ). The correlation analysis of magnetic resonance imaging features and prognosis of invasive pituitary adenomas were verified to be feasible for the treatment of patients.

## 1. Introduction

Pituitary tumors are monoclonal cell tumors originating from the adenohypophysis. According to statistical studies, their incidence accounts for about 17% of all intracranial tumors. It is second only to intracranial gliomas and meningiomas and is the third most common intracranial tumor. According to the endocrine society's autopsy report of 3,048 individuals, it grows chronically in many directions, and studies have reported that the autopsy rate of pituitary adenomas can be as high as 30%. For pituitary adenomas, the first choice is bromocriptine drug treatment. If the drug is not well controlled or the tumor is progressively enlarged, surgical treatment can be considered. Most other patients with pituitary adenomas are treated with surgery, and a few patients require postoperative adjuvant radiotherapy, chemotherapy. The prognosis and quality of life of most patients are relatively high, and individual studies have reported that

the survival period of patients with pituitary adenoma can be as long as 15 years or even longer. However, there are still a small number of patients with tumor invasion into surrounding structures, such as erosion of the sellar dura, parasellar bone, upward breakthrough of the saddle septum, part of the internal carotid artery, and so on. The tumor invasion leads to the total surgical resection rate. There is no strict boundary between invasive and noninvasive pituitary adenomas. The difference lies in the size of the invasiveness. In clinical work, patients with invasive pituitary adenoma face multiple operations and high hospitalization costs, which brings huge economic pressure to society and families and at the same time greatly reduces the patient's quality of life and life span and increases the patient's life. The case fatality rate has brought huge challenges to clinicians' diagnosis and treatment.

Invasive pituitary adenomas in the imaging classification and atypical adenomas in the pathology classification are

often considered to have a poor prognosis. These two classifications guide the treatment of clinicians to a certain extent. And we have found in a lot of clinical work that the postoperative pathology of invasive pituitary adenomas can be suggested to be typical, and the pathological classification of noninvasive pituitary adenomas is also atypical. Therefore, whether it is based on imaging Neither classification nor histopathological classification can indicate the growth characteristics of pituitary adenomas and the prognosis of patients, nor can it link the clinical features of pituitary adenomas with clinical aggressive behavior, so these two classifications have certain limitations. Therefore, the early judgment of the clinical aggressive behavior of pituitary adenomas has always been a difficult problem faced by neurosurgeons.

Regarding the clinical aggressive behavior of pituitary adenomas, domestic and foreign experts also have many studies. Boling retrospectively analyzed patients who underwent endoscopic pituitary adenoma surgery at six international centers from 2002 to 2014. Standard demographic and comorbidity data were collected, as well as information about tumor extent and treatment. Logistic regression was used to check the following 30-day results for risk factors: systemic complications, intracranial complications, postoperative cerebrospinal fluid (CSF) leakage, length of hospital stay, readmission, and reoperation. Results data were collected from 982 patients with an average age of 52 years. The median body mass index (BMI) of all patients was 30.9 kg/m<sup>2</sup>, and 56% of them were women. The median length of hospital stay was 5 days, and 23.8% of patients had postoperative adverse events [1]. Chang speculates that the tumor is related to the activating mutation of  $\beta$ -catenin and speculates that pituitary stem cells (SCs) may play a role in the tumorigenesis of human ACP. SCs have also been found in pituitary adenomas. The purpose is to characterize the expression patterns of ABCG2, CD44, DLL4, NANOG, NOTCH2, POU5F1/OCT4, SOX2, and SOX9 SC markers in human ACP and pituitary adenomas. *Methods and Results.* We studied 33 patients (9 ACP and 24 adenomas) using real-time quantitative PCR (real-time fluorescence quantitative PCR) and immunohistochemistry. SOX9 is upregulated in ACP, shows positive immunostaining in epithelium and stroma, and is highest in relapsed patients. Immunohistochemistry confirmed that CD44 is overexpressed in ACP [2]. Johnson P modified the treatment plan for 6 patients with pituitary adenomas to include positions each shot and 0.5 mm and 1 mm movement in each basic direction. Twelve new plans were created for each patient, and changes in target coverage and maximum doses to surrounding critical structures were recorded. Of particular interest is the tolerability of optic nerve device doses exceeding 8 Gy or brainstem doses exceeding 10–12 Gy. The target volume range is 0.8–4.7 cc, and the prescription dose range is 12–20 Gy. *Results.* Target coverage only has a significant effect on the smallest lesions. In this case, moving up or down by 1 mm will result in a 10% loss of coverage. Moving up by 0.5 mm will cause a loss of coverage of 4% [3]. For the first time, Svro and Salehi reported the efficacy of temozolomide in

the treatment of prolactinoma. The clinical symptoms and signs of the patients were significantly improved, and the serum MGMT expression was low. It was confirmed that temozolomide was effective for such tumors. Follow-up studies by Kovacs et al. also further confirmed this view. However, Kovacs et al. subsequently used temozolomide to treat a case of corticotropin adenoma and did not achieve the same effect. Immunohistochemical staining showed that the tumor cell nucleus MGMT of this patient was highly expressed [4]. These studies have provided us with some references, but due to various reasons, such as the number of samples and the type of tumor included, most of these experiments are difficult to reproduce, and the data can only provide some references.

This article classifies pituitary adenomas (invasive adenomas and noninvasive adenomas) according to the tumor's appearance on magnetic resonance imaging (MRI) and compares the imaging differences of different classifications. The influence of invasive adenoma and noninvasive adenoma on pituitary adenoma treatment patients, and the correlation between MRI characteristics and prognosis of invasive pituitary adenoma were analyzed. the characteristics of different types of adenomas are obtained, which provides clinical treatment. The system designed in this paper classifies the patient's condition based on the multimodal classification method. Compared with the traditional pituitary adenoma, it can more effectively judge the clinical violations of pituitary adenoma and solve and provide solutions that cannot be formulated for patients by traditional surgery.

## 2. MRI Features and Prognostic Correlation Analysis Method

**2.1. Pituitary Adenoma.** From the perspective of cell morphology, pituitary tumors can be divided into typical adenomas, atypical adenomas, and pituitary carcinomas. Atypical adenomas show higher aggressiveness, enhanced mitotic activity, excessive p53 protein immune response, and MIB-1 proliferation index greater than 3%. The patient may have multiple relapses. Malignant prolactinoma is a rare tumor with cerebrospinal fluid, meninges, or distant metastasis. They usually have a MIB-1 proliferation index greater than 12%, a large number of mitosis characterized by nuclear pleomorphism, and active immune response to the p53 protein [5]. Compared with other pituitary tumors, prolactinoma is the only option for first-line treatment with medication alone. In general, treatment with dopamine receptor agonists, such as cabergoline and bromocriptine, has a high success rate in prolactin levels, reducing tumor size, and restoring sexual function [6]. Although most pituitary adenomas are benign, drug-resistant treatment remains a problem. If the level of prolactin is abnormal and the tumor volume does not decrease by 50%, the treatment is considered a failure. Although most pituitary adenomas initially choose surgery or drug therapy alone as the first-line treatment, the treatment of these types of tumors is challenging due to local invasion and recurrence of these tumors. Due to the lack of identification of consistent and effective

chemotherapeutics, systemic chemotherapy has been reserved as a “last resort” to treat such pituitary adenomas.

In the initial pathological studies, people classified pituitary adenomas into chromophobic adenomas, eosinophilic adenomas, and basophilic adenomas based on the difference in cytoplasmic hematoxylin-eosin staining. Later, mixed adenomas were introduced. Classification of adenomas [7]. However, in the gradual clinical application, it has been found that these pathological types cannot be linked to the clinical manifestations and endocrine characteristics of the tumor. A pathological type of adenoma often has more than one endocrine symptom. It can also belong to different pathological types. Therefore, it is of little help to clinical diagnosis and treatment. In 2004, the WHO classified pituitary adenomas at the molecular level by revealing the decisive transcription factors for the development of pituitary adenomas from cancer stem cells to various types of tumors. Its various detection methods and subtype structure also determine that this classification is not suitable for clinical use [8]. This pathological classification divides pituitary adenomas into typical adenomas, atypical adenomas, and pituitary carcinomas.

**2.2. Image Classification.** Jefferson first gave a rough description of invasive pituitary adenomas in 1940; Hardy first proposed the grading standard for invasive pituitary adenomas of grades 0–IV in 1969 and defined grades III and IV as invasive pituitary adenomas, as shown in Figure 1.

Grade I is normal or local expansion, tumor <10 mm; grade II is an expansion of sella  $\geq 10$  mm of sphenoid bone; grade III is local perforation of the sella floor; grade IV is diffuse destruction of the sella floor with distant spread.

Wilson subsequently made improvements on this basis, divided it into ABCDE stages according to the degree of involvement of the adenomas on the supracarpal and paracarpal adenomas, and defined stages C, D, and E as aggressive pituitary adenomas, as shown in Figure 2.

Neither the traditional imaging classification nor the pathological classification can indicate the clinical aggressive behavior of pituitary adenomas, nor can it guide clinicians to accurately judge the prognosis of patients with adenomas [9]. Regarding the prognosis of patients with pituitary adenomas, neurosurgeons often pay too much attention to the residual degree of tumors in imaging, ignoring clinical symptoms and signs and changes in serum pituitary hormone levels. The changes in imaging tumor volume are the expressions of the clinical aggressive behavior of pituitary adenomas. Comprehensive analysis of the clinical aggressive behavior of different pituitary adenomas is very important for the prognosis of patients. In the multimodal classification of imaging and pathology proposed in this study, the incidence of clinical symptoms and imaging aggressive behavior (37.5%) of patients in the “invasion + atypical” group was significantly higher than that of “invasion + typical.” The difference between “noninvasive + typical” and “noninvasive + atypical” groups was statistically significant ( $P < 0.05$ ), which confirmed the application value of our proposed multimodal classification method for pituitary

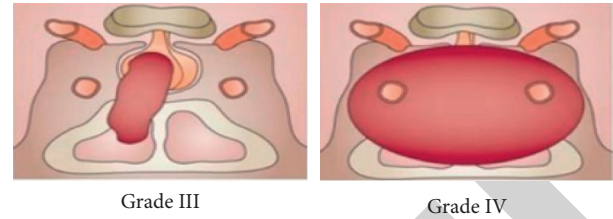


FIGURE 1: Grading of aggressive pituitary adenoma.

adenomas. Multimodal classification can predict early clinical aggressive behavior expression in patients with pituitary adenoma [10].

Some studies have found that the aggressiveness of pituitary adenomas is related to the type of adenoma, but the study did not explain the relationship between the ability to exhibit aggressiveness and its pathological types and hormone levels, and no further follow-up and observation have been carried out, so no conclusions have been made. Which clinical features of pituitary adenomas are more likely to recur [11, 12]? Previous studies have shown that invasive pituitary adenoma means expanding to the surrounding area, invading the dura mater, bone tissue, cavernous sinus, and other surrounding tissue structures around the sella area. Therefore, it is an indicator of postoperative tumor recurrence and poor prognosis. We believe that the invasive pituitary adenoma defined in the traditional imaging classification is judged based only on the staged manifestations of the tumor's invasion of surrounding tissues after a certain period of time while ignoring the proliferation characteristics of the tumor itself. What are the two? What is the cause and what is the effect or the interaction are still unable to draw conclusions [13].

The aggressive behavior of pituitary adenomas is manifested in three aspects: clinical symptoms, serology, and imaging, while the traditional classification method is different in the judgment of the aggressive behavior of adenomas, and none of them can make clear the aggressive expression of adenomas. The explanation shows that the traditional methods of judging the aggressiveness of pituitary adenomas have certain limitations [14].

At present, there are no satisfactory molecular diagnostic markers that can predict the high-risk recurrence of pituitary adenomas, and multimodal classification based on imaging and pathology can help us better judge the prognosis of patients with different pituitary adenomas. The final imaging effect is very good, which can provide help for the characteristics and prognosis of pituitary adenomas. So far, similar articles have reported on the classification method combining imaging and pathology. They classify patients with adenomas into grade 1a (noninvasive + nonproliferative group), grade 1b (noninvasive + proliferative group), and grade 2a (invasive + proliferation group), grade 2b (invasive + nonproliferative group), and grade 3 (pituitary cancer group) reported that the prognosis of pituitary adenomas above grade 2a in this classification is worse [15, 16]. This also supports our conclusion from the side, and considering that pituitary cancer is extremely rare and has a small composition, this study focuses on a comprehensive analysis of the clinical behavior of pituitary

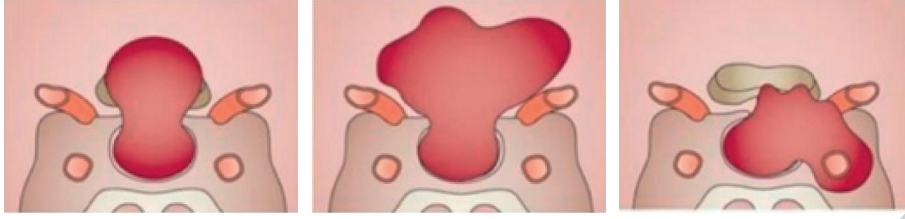


FIGURE 2: Invasive pituitary adenoma as defined by Wilson.

adenomas; we have eliminated the composition of pituitary adenoma and made it simpler. We classify pituitary adenomas according to the degree of tumor expansion and invasion on MRI. Pituitary adenomas are divided into “invasive + atypical” group and other groups that include “invasive + typical,” “noninvasive + typical,” and “noninvasive + atypical” groups [17, 18]. Studies have proved that neither imaging classification nor pathological classification can accurately indicate the correlation between the growth characteristics of pituitary adenomas and the prognosis of patients, the “invasive + atypical” multimodal classification method is useful for the early prediction of clinical aggressive behavior. It is very important to believe that this method of multimodal classification analysis is more clinically applicable. It is useful for predicting the risk classification of patients with different pituitary adenomas expressing clinical aggressive behavior and identifying patients with early pituitary adenomas who are at risk of recurrence or progression. Future clinical trials for clinicians to formulate the best treatment plan, adjust treatment strategies, and early intervention treatment will provide more information [19].

**2.3. Medical Images.** Hospital image enhancement is the main development purpose of technology realization and function realization. In the current medical environment and actual rehabilitation treatment, how to more comprehensively understand and transform the expectations and needs of users, and how to improve the form, structure, and function of products to meet the needs of users is an urgent problem to be solved in augmented reality technology and its clinical application [20]. The magnetic resonance imaging used in this article conforms to the following formula:

$$\kappa = x \frac{\omega^n y + b}{f(x)1/\min \sum_2^1 \alpha_j \omega^{n-1} x_i + b}, \quad (1)$$

$$\omega = \max \sum_{i=1}^n \alpha_i - \frac{1}{2} \sum_{i,j=1}^n \alpha_i \alpha_j \beta_i \beta_j. \quad (2)$$

According to the characteristics of the medical system, we have improved the relevant calculation functions as follows:

$$f(i) = x_0 + x_1 y_1 + x_2 y_2 + x_3 y_3, \quad (3)$$

$$W = \frac{N_1 r_1^2}{2} + \frac{N_2 r_2^2}{2} + N_2 d_2^2 + \left( \frac{N_3 r_3^2}{2} + N_3 d_3^2 \right) * 0.1 + \frac{2}{3} N. \quad (4)$$

The corresponding equation is

$$-div\left(\frac{\nabla u}{|\nabla u|}\right) - \lambda(u_0 - u) = 0. \quad (5)$$

It can be transformed into an optimization problem of a function. Let the error function be

$$E(x, y) = div\left(\frac{\nabla u}{|\nabla u|}\right) - \lambda(u - u_0). \quad (6)$$

Assuming that the final output is an ideal model, we can get

$$u(x, y) = N(u_0(x, y), w), \quad (7)$$

$$t(s) = \exp\left(-\int_0^s \kappa(t) dt\right). \quad (8)$$

The quadratic performance indicators are as follows:

$$K = \sum_{k=1}^{\infty} [x^i(k)Jx(k) + r^i(k)cJ], \quad (9)$$

where the weighting matrix  $Q$  is

$$Q = \frac{1}{2a^2 r^{-1}} \left( \frac{2b^2}{a^2 r^{-1}} p - t \right)^{-1} [a^2 r^{-1} t^2 + 2(1 - b^2)t]. \quad (10)$$

The image is subject to external and internal interference during the acquisition and preprocessing, resulting in some noise. Noise will degrade the image quality and affect the subsequent image processing results. Therefore, this paper uses adaptive median filtering and Wiener filtering to remove these noises. The traditional median filter formula is as follows:

$$g(x, y) = med\{f(x - k, y - l), (k, l) \in S\}, \quad (11)$$

where  $f(x, y)$  represents the input image,  $S$  represents the neighborhood filter window  $(x, y)$  of the pixel, and  $g(x, y)$  represents the output response. Calculate the local mean and variance of each pixel as follows:

$$\mu = \frac{1}{MN} \sum_{(n_1, n_2) \in \mu} g(n_1, n_2), \quad (12)$$

$$\sigma^2 = \frac{1}{MN} \sum_{(n_1, n_2) \in \kappa} [g(n_1, n_2) - \kappa]^2. \quad (13)$$

According to the characteristics of the image, the histogram specification is adopted to improve the contrast of the image and highlight the target information. Finally, the adaptive median filter and Wiener filter are used for denoising processing, which provides a good premise for the subsequent images.

**2.4. Prognosis of Pituitary Adenoma.** A pituitary adenoma is a very complex disease, and its pathogenesis is not yet clear. However, in recent years, more views believe that pituitary adenoma is a monoclonal tumor, which is believed to be related to growth factors, receptors, and transcription factors, and factors such as abnormal cell signaling pathways are closely related, and some people believe that it is related to the alpha subunit of the G protein gene or the mutation of the AIP gene [21]. Pituitary adenomas are also the most common neuroendocrine tumors. They are often misdiagnosed because of differences in tumor size, shape, and degree of involvement of surrounding structures, as well as differences in endocrine hormone levels in different pituitary adenomas. Due to the numerous clinical symptoms of pituitary adenomas and the inaccurate treatment effect, there is still a risk of recurrence even when the tumor is completely resected. At present, there is no unified diagnosis and treatment standard.

We believe that the treatment of pituitary adenomas should implement a multidisciplinary joint diagnosis and treatment system to form a standardized diagnosis and treatment model, and this model includes standardized management of preoperative preparation, surgical treatment, and perioperative and postoperative follow-up. Preoperative preparation include assessment of cardiopulmonary function, treatment of underlying diseases, perfect visual field and endocrine examination, and assessment of adrenal gland, thyroid, and gonadal function, combined with imaging department to clarify the deformed structure of sella and the tumor and peripheral optic nerve, internal carotid artery, pituitary stalk, and other brains. The adjacent relationship of the tissues strictly grasps the surgical indications and contraindications of each surgical approach and determines the best surgical plan; during the operation, using the navigation and positioning function to remove the tumor within the maximum safety range, the pituitary function is protected, and a good job is done in the repair of the sellar area and cerebrospinal fluid leakage [22].

Nursing work at the end of the operation: using hormone replacement therapy and symptomatic treatment with

fluid replacement within 24 hours after surgery, observing changes in patients' vision and neurological function, monitoring electrolytes and 24-hour urine output, actively dealing with complications such as cerebrospinal fluid leakage, and diabetes insipidus, and reviewing endocrine hormone, and assess changes in adrenal, thyroid, and gonadal function. The functional changes of pituitary MRI were reviewed within 3 days after operation. Pituitary hormones should be reviewed within 6–12 weeks after surgery to evaluate the function of the pituitary gland and each target gland. The pituitary MRI was re-examined 3 months after the operation, combined with multidisciplinary consultation again, and hormone replacement therapy, radiotherapy, and chemotherapy were decided according to the residual tumor, histopathology, pituitary hormones, and clinical symptoms. Except for specific types of tumors such as PRL, the treatment of pituitary adenomas is mainly through surgical treatment. Although the apparent cure of surgery is recognized, it can alleviate some of the patients' symptoms and signs and avoid permanent damage to the organ system caused by hormone overdose. However, surgery is not the only treatment for pituitary adenomas. There are still some patients who need to undergo a comprehensive treatment process such as drugs and radiotherapy, and there is a risk of recurrence after surgery. However, it is very important for clinicians to recognize this aggressive growth of pituitary adenomas early and to adopt postoperative intensive treatment strategies. There are few reports on the clinical aggressive behavior of pituitary adenomas at home and abroad. Due to the complexity and diversity of pituitary adenomas, various problems will still be encountered during each treatment process. Therefore, we need to form a standardized diagnosis and treatment model and strengthen further follow-up to ensure the efficacy and safety of each treatment plan.

### 3. MRI Features and Prognosis Correlation Analysis Experiment

**3.1. Case Collection.** Collect 58 patients with pituitary adenoma who were admitted to the Department of Neurosurgery of the Yangzhou Hongquan Hospital in our city from January 2015 to December 2020. The sample data include 58 cases. Postoperative medical examination, postoperative hormone levels, and so on were grouped according to the diagnostic criteria of IPA. There were 32 males and 26 females. The age range was 29–82 years (the average age was 48.9 years). The results of the disease examination revealed hormone types: 7 cases of growth hormone type adenoma, 8 cases of prolactin type adenoma, 2 cases of corticotropin type adenoma, 1 case of thyroid-stimulating hormone type adenoma, 33 cases of mixed functional adenoma, and 7 cases of nonfunctional adenomas.

**3.2. Diagnostic Criteria.** This study used 2004 WHO diagnostic screening criteria: Knosp classification is based on the coronary artery scan enhanced by MRI of the pituitary

gland, and used the middle and outer rectangular lines of the carotid sinus (C4) and the superior clone (C2) as reference lines to determine the relationship between the pituitary gland and sinus cavity infiltration. The classification is as follows: grade 0: the cavity is not penetrated, and the volume is restricted to the intraline arteries between the saddle and the inner wall of the carotid artery; grade I: the tumor is located in the centerline of the internal carotid artery, and the central venous network is inserted and disappeared; grade 2: the volume is located inside the lateral wall of the internal carotid artery, and the internal, superior, and inferior venous network disappears; and grade 3: the tumor passed through the lateral wall of the internal carotid artery, passed through the cervical vagina and venous stroma, entered the cervicovaginal cavity, and disappeared. The external cavity of the sinus cavity also disappeared, and the sidewall was enlarged to the extent that the carotid artery in the sinus cavity was partially wrapped, or the tumor and venous network disappeared completely. We call it invasive pituitary, which shows grades III and IV as shown in Figure 3.

**3.3. Results Judgment.** The results should be analyzed and confirmed by two experienced pathologists. The pathological section was placed under an optical microscope, and the positive cells were counted according to the percentage of positive cells in all cells in the field of view and the color intensity. The specific situation is shown in Table 1.

**3.4. Statistical Methods.** In this paper, SPSS 20.0 software was used for statistical analysis and processing. The results of immunohistochemistry used the Wilcoxon rank-sum test, and the results of immunohistochemistry used the *t*-test. The difference was statistically significant with a bilateral  $P < 0.05$ . In the correlation test of clinical case characteristics, the correlation between the imaging grades adopts the Spearman rank correlation analysis method, and the difference is statistically significant with a bilateral  $P < 0.05$ .

## 4. MRI Features and Prognosis Correlation Analysis Experimental Analysis

**4.1. Patient Information.** We categorized the collected patient data according to age, gender, and disease course to facilitate data statistics. Among the 58 pituitary adenoma patients in this study, 33 were male patients (56.9%), and 25 were female patients (43.1%). The average age is  $49.3 \pm 10.9$  years, and the age is between 25 and 74 years, as shown in Table 2.

We investigated the course of these patients, as shown in Table 3.

It can be seen that the median value of patients with pituitary adenoma in this article is 6.5 months. On the whole, the number of male patients is slightly larger than that of female patients. The age of patients is mainly between 40 and 69 years old, accounting for 75% of the total number of patients.

The clinical symptoms of patients with pituitary adenoma are different. We have made statistics on the different clinical conditions, as shown in Table 4.

In this study, there were 24 patients (41.4%) with headache, 15 patients (25.9%) with dizziness, 23 patients (39.7%) with visual field defect, 23 patients (39.7%) with decreased vision, 6 patients (10.3%) with decreased libido, 2 patients (3.4%) with irregular menstruation, 3 patients (5.2%) with amenorrhea and lactation, 6 patients (10.3%) with acromegaly, and 3 patients (5.2%) with asymptomatic patients. Different patients can show mixed symptoms, of which 21 cases have only 1 symptom, 24 cases have 2 symptoms, 7 cases have 3 symptoms, 2 cases have 4 symptoms, 1 case has 5 symptoms, and 3 patients have no clinical symptoms due to accidental physical examination.

**4.2. Image of Patients with Pituitary Adenoma.** All patients completed the pituitary MRI scan + enhanced examination before and 3 days after the operation and 3 months after the operation. According to the different extent of tumor expansion and invasion on MRI, the pituitary adenomas are classified by imaging. Among them, the adenomas growing on the saddle are classified according to the Hardy grade III or IV or the Hardy-Wilson staging CE. In the stage, adenomas growing near the sella use Knosp grade III or IV as the criterion for invasive pituitary adenomas. In this study, 52 invasive pituitary adenomas (Figure 4(a) - 4(c)) and 6 noninvasive pituitary adenomas (Figure 4(d)) were selected.

Eliminate patients without complete data; cross-categorize patients with different imaging and pathology; use chi-square test, *t*-test, and Fisher's exact probability method for analysis; use mean and standard deviation for continuous variables; and use the medium for categorical data. Digits and percentiles are used for statistical description. Image detection of pituitary adenomas in different patients is shown in Figure 5.

**4.3. Changes before and after Treatment.** In this study, MRI high spatial resolution 3D structural data automatic volume measurement algorithm was used to calculate the tumor volume, and the tumor volume changes before surgery, 3 days after surgery, and 3 months after surgery were obtained by magnetic resonance imaging. The sagittal and coronal positions of the pituitary MRI before surgery are shown in Figure 6.

It can be seen from the figure that before the operation, the patient's pituitary adenoma is more obvious, and the tumor is located in the middle of the brain, which is more harmful to the human body. We analyze the images of the pituitary adenoma in different periods after treatment, as shown in Figure 7.

The aggressive standard of clinical symptoms is that the postoperative clinical symptoms and signs are not relieved or reappear and aggravate after remission; the aggressive standard of serology is that the level of serum pituitary endocrine hormones does not decrease or decreases after the operation; imaging aggressiveness. The standard is that the

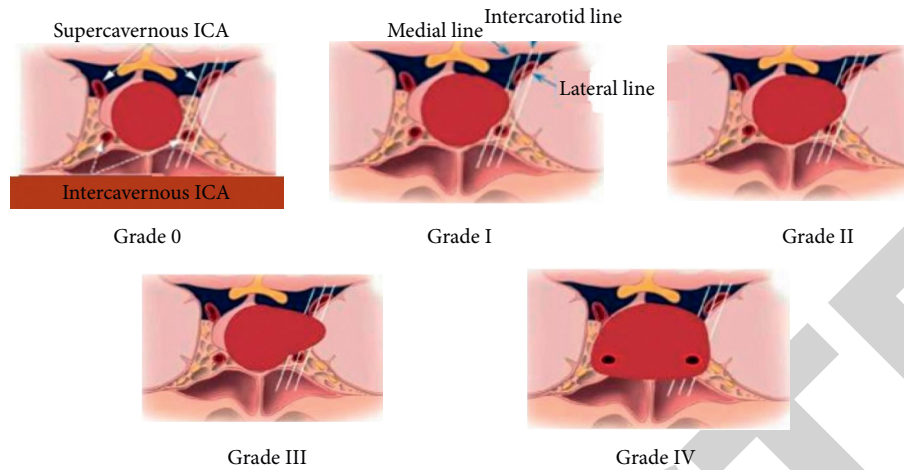


FIGURE 3: Classification of invasive pituitary adenomas.

TABLE 1: Result judgment evaluation.

Scoring	Dyeing intensity	Positive cell ratio
0	No coloring	$\leq 5\%$
1	Light yellow	6%–25%
2	Yellow	26%–50%
3	Brownish yellow	51%–75%
4	Brown	$>75\%$

TABLE 2: Specific conditions of patients.

	Male	Female	Total
20–29	2	0	2
30–39	6	3	9
40–49	13	8	21
50–59	9	6	15
60–69	6	2	8
70–79	2	1	3

TABLE 3: Course of disease.

	Male	Female	Total
$\leq 3$	6	2	8
3 days < course $\leq 6$ months	13	8	21
6 months < course $\leq 12$ months	7	3	10
12 months < course $\leq 18$ months	1	0	1
18 months < course $\leq 24$ months	5	2	7

TABLE 4: Clinical situation of patients.

	Headache	Vision loss	Visual impairment	Dizzy	Amenorrhea and lactation	Acromegaly	Decreased libido	Asymptomatic
Number of people	24	23	23	15	6	6	3	3

increase in tumor volume at 3 months after surgery is greater than 6% of the tumor volume at 3 days after surgery. It can be seen from the figure that after treatment, the patient's tumor has improved significantly. In order to understand the impact of prognostic measures on the patient, we have made statistics on the patient's postoperative prognostic rehabilitation effect, as shown in Figure 8.

It can be seen from the figure that after the operation, the recovery efficiency of different surgical methods is different. The MRI method used in this article can clearly understand the location of the tumor, so the pituitary adenoma can be easily removed during the operation. Therefore, the prognosis of patients is better, and the incidence of complications is lower than that of other surgical groups.

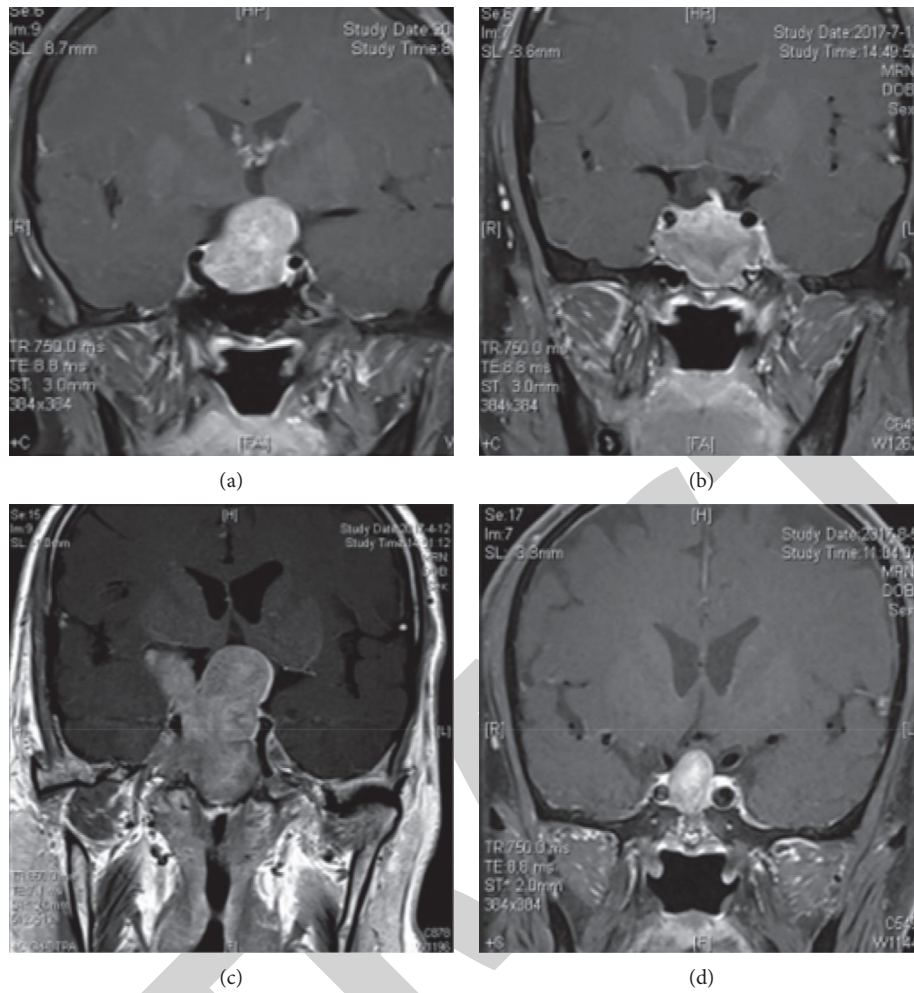


FIGURE 4: Image classification of pituitary adenoma: (a) invasive pituitary adenoma, (b) invasive pituitary adenoma, (c) invasive pituitary adenoma, and (d) noninvasive pituitary adenoma.

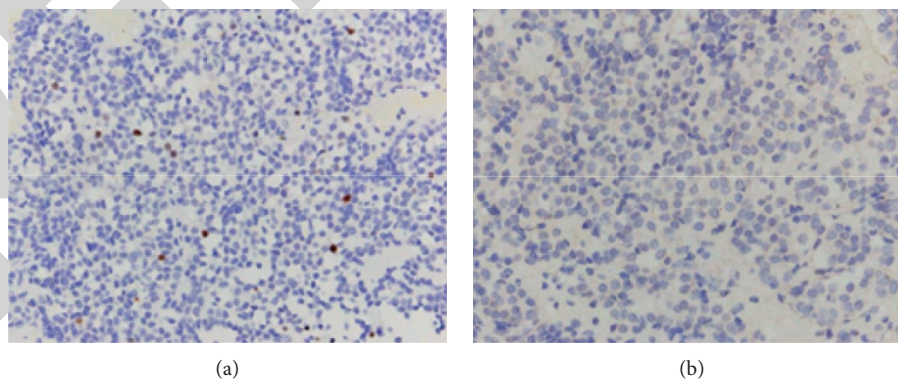


FIGURE 5: Continued.

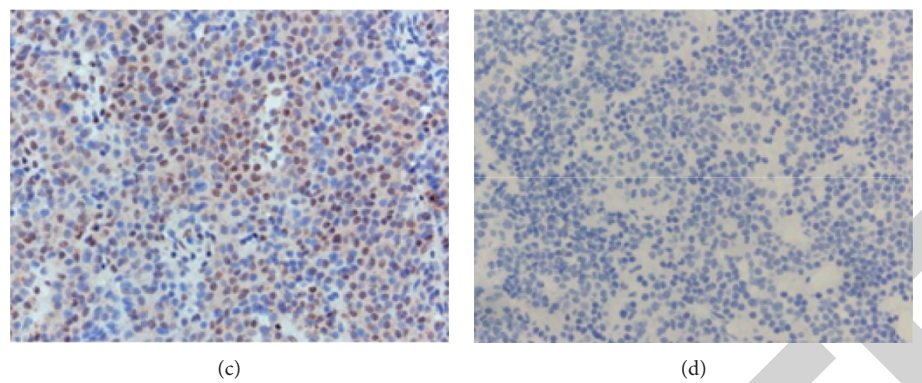


FIGURE 5: Imaging of different pituitary adenomas: (a) Ki-67 positive expression (immunohistochemical staining,  $\times 400$ ), (b) Ki-67 negative expression (immunohistochemical staining,  $\times 400$ ), (c) p53 positive expression (immunohistochemical staining,  $\times 400$ ), and (d) p53 negative expression (immunohistochemical staining,  $\times 400$ ).

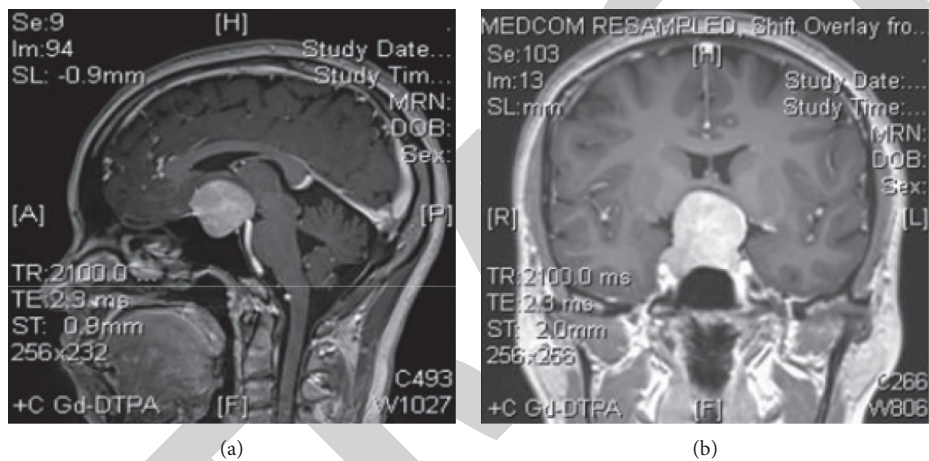


FIGURE 6: Preoperative MRI of the pituitary gland in the sagittal and coronal positions: (a) preoperative pituitary MRI sagittal position and (b) preoperative MRI coronal position of the pituitary gland.

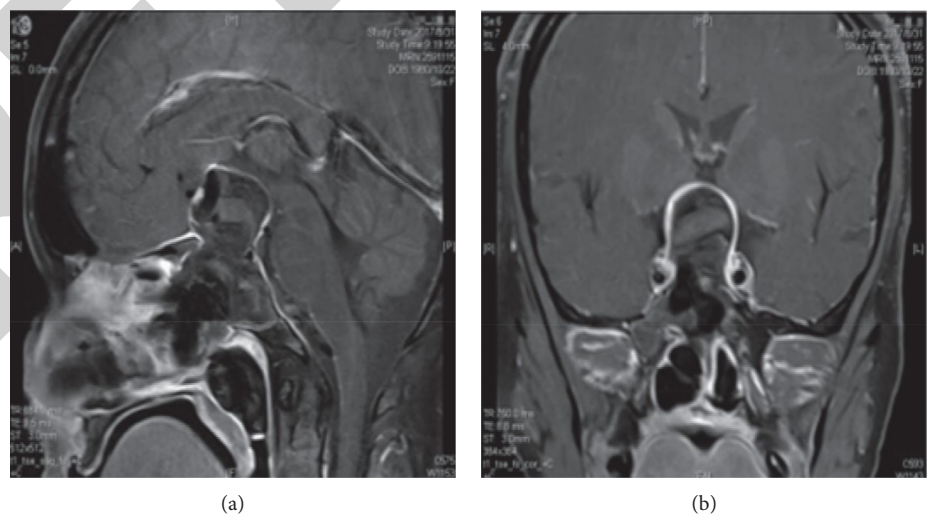


FIGURE 7: Continued.

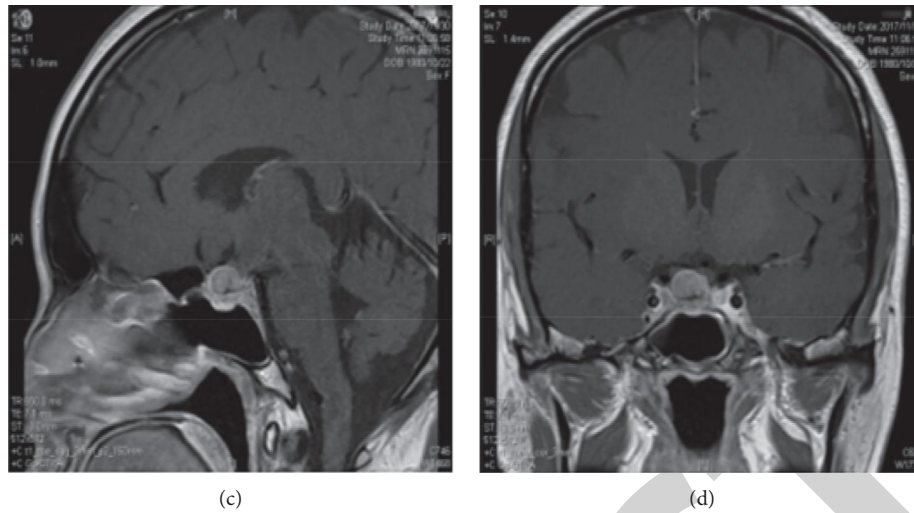


FIGURE 7: Pituitary adenomas in different periods after treatment: (a) 3 days after surgery, pituitary MRI sagittal; (b) 3 days after surgery, pituitary MRI sagittal; (c) 3 months postoperative pituitary MRI sagittal position; and (d) pituitary MRI sagittal position 3 months after the operation.

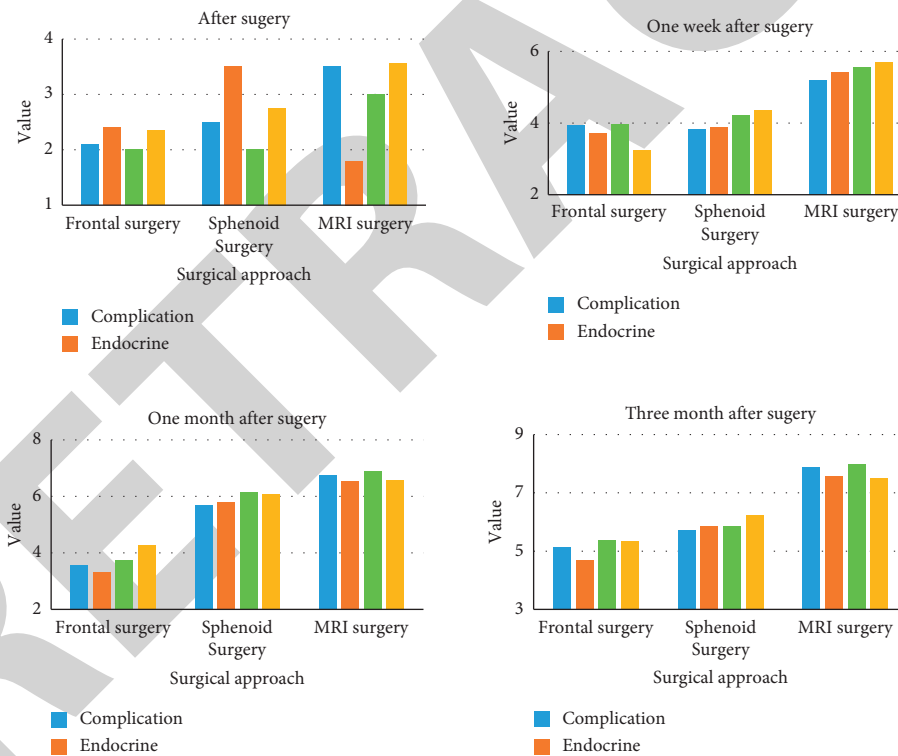


FIGURE 8: The prognosis of different operations.

## 5. Conclusion

The correct classification of pituitary adenomas through MRI effects is an important research area. Only by correctly classifying and grading pituitary adenomas can we implement individualized and precise treatment plans for early diagnosis and early treatment of patients with adenomas, so as to effectively improve the prognosis of patients. The traditional single pituitary adenoma classification method cannot effectively judge the clinical aggressive behavior of

pituitary adenomas, while the multimodal classification method combined with imaging and pathology can prompt the clinical aggressive behavior of pituitary adenomas, which can be formulated for clinicians. The best treatment plan as well as the implementation of early intervention treatment in the future clinical trials and individualized treatment provides more information. Of course, there are some shortcomings in this article. The income sample is only 58 cases in the city; the number is small; and multicenter, large-sample research cannot be carried out to improve the credibility of

## Retraction

# Retracted: Construction of Community Medical Communication Service and Rehabilitation Model for Elderly Patients under the Internet of Things

### Journal of Healthcare Engineering

Received 11 July 2023; Accepted 11 July 2023; Published 12 July 2023

Copyright © 2023 Journal of Healthcare Engineering. This is an open access article distributed under the Creative Commons Attribution License, which permits unrestricted use, distribution, and reproduction in any medium, provided the original work is properly cited.

This article has been retracted by Hindawi following an investigation undertaken by the publisher [1]. This investigation has uncovered evidence of one or more of the following indicators of systematic manipulation of the publication process:

- (1) Discrepancies in scope
- (2) Discrepancies in the description of the research reported
- (3) Discrepancies between the availability of data and the research described
- (4) Inappropriate citations
- (5) Incoherent, meaningless and/or irrelevant content included in the article
- (6) Peer-review manipulation

The presence of these indicators undermines our confidence in the integrity of the article's content and we cannot, therefore, vouch for its reliability. Please note that this notice is intended solely to alert readers that the content of this article is unreliable. We have not investigated whether authors were aware of or involved in the systematic manipulation of the publication process.

Wiley and Hindawi regrets that the usual quality checks did not identify these issues before publication and have since put additional measures in place to safeguard research integrity.

We wish to credit our own Research Integrity and Research Publishing teams and anonymous and named external researchers and research integrity experts for contributing to this investigation.

The corresponding author, as the representative of all authors, has been given the opportunity to register their agreement or disagreement to this retraction. We have kept a record of any response received.

### References

- [1] X. Zhang, F. Wang, D. Wang, Y. Xiang, and Z. Zhang, "Construction of Community Medical Communication Service and Rehabilitation Model for Elderly Patients under the Internet of Things," *Journal of Healthcare Engineering*, vol. 2022, Article ID 9689769, 12 pages, 2022.

## Research Article

# Construction of Community Medical Communication Service and Rehabilitation Model for Elderly Patients under the Internet of Things

Xiaoxia Zhang<sup>1</sup>, Fang Wang<sup>1</sup>, Dan Wang<sup>1</sup>, Yanhua Xiang<sup>1</sup> and Zhongwei Zhang<sup>2</sup>

<sup>1</sup>Changsha Social Work College, Changsha, Hunan, China

<sup>2</sup>Dongfang Electric Corporation, Chengdu, Sichuan, China

Correspondence should be addressed to Fang Wang; wangfang\_731@163.com

Received 16 October 2021; Revised 16 December 2021; Accepted 8 January 2022; Published 29 March 2022

Academic Editor: Yang Gao

Copyright © 2022 Xiaoxia Zhang et al. This is an open access article distributed under the Creative Commons Attribution License, which permits unrestricted use, distribution, and reproduction in any medium, provided the original work is properly cited.

The objective of this study was to discuss the health management of elderly patients in the community and the management of community rehabilitation under the support of the new Internet of Things (IoT). The IoT technology was adopted to monitor the wearable devices through mobile medical physiological data. The heart rate, blood pressure, respiratory rate, and other physiological indicators of the elderly were collected in real time. The support vector machine (SVM) algorithm was selected as the core algorithm for the elderly physiological index disease risk assessment, the fuzzy comprehensive evaluation method was adopted as the core method of the elderly disease risk quantitative assessment model to process the physiological indicators, and finally, a reasonable physiological index processing model and quantitative indicators of disease risk were obtained. The data on vascular disease were selected from the MIMIC database. In addition, the advantages and disadvantages of the SVM algorithm and the Backpropagation Neural Network (BPNN) algorithm were compared and analysed. The final verification results showed that the fusion accuracy of the SVM processing MIMIC database and the University of California Irvine (UCI) dataset was 0.8327 and 0.8045, respectively, while the fusion accuracy of the BPNN algorithm in processing the same data was 0.7792 and 0.7288, respectively. It was obvious that the fusion accuracy of the SVM algorithm was higher than that of the BPNN algorithm, and the accuracy difference of the SVM algorithm was lower than that of the BPNN algorithm in different groups of data. In the verification of the elderly disease risk quantitative assessment model, the results were consistent with the selected data, which verified the effectiveness of the design model in this study. Therefore, it can be used as a quantitative assessment model of general elderly physiological indicators of disease risk and can be applied to the community medical communication management system. It proved that the model of medical communication and rehabilitation services for elderly patients in the community constructed in this study can definitely help the development of community service for the elderly.

## 1. Introduction

With the development of society, the aging society has become an important social problem that most countries inevitably need to face [1]. According to relevant investigations and studies, as of the end of 2019, the number of elderly people aged 60 and over in China totalled 253.88 million as of the end of 2019, accounting for 18.1% of the total population of the country, of which, there are 176.03 million people aged 65 and over, accounting for 12.6% of the total population of the whole country. Compared with 17.9%

of the elderly population aged 60 and above in 2018 and 17.3% in 2017, the current aging trend is becoming increasingly severe [2–4]. With the gradual severity of the aging problem, there are currently 37,021 legally registered and licensed elderly care institutions in China as of the end of 2019, with a total of 4.674 million beds. It means that the vast majority of elderly people find it difficult to enjoy the services of social public elderly care, and they are more dependent on families and individuals. According to the latest survey, the family pension model for the elderly in 2020 is still not the current main pension model, accounting

for 90% of the national pension, while the institutional pension and the community pension account for only 7% and 3%, respectively. This data are especially highlighted in the vast rural areas [5]. The incidence of chronic diseases and malignant tumours increases with age. After illness, the probability of complications increases significantly, making the disease management and prognosis of the elderly extremely complicated and slow in progress [6–8]. Therefore, it is difficult to meet the actual needs of the elderly simply by family support, and community support has become the best solution at present. It not only satisfies the “acquaintance” environment pursued by the elderly but also allows the community to provide relatively professional management of the elderly, and it can give full play to the advantages of grassroots management in China [9–12].

Community elderly care mainly introduces elderly care services into the community so that the elderly can provide for the elderly at home. It not only respects the willingness of the elderly to provide for elderly care at home but also combines the professionalism and convenience of social elderly care. It is a new and characteristic elderly care method for the aging society in China. Community care and elderly care services are gradually established through government supervision, social participation, and market management. The community service for the elderly, with family care as the core, community services as the support, and professionalism as the guide, is to provide the elderly care services in all aspects of daily life, health management, spiritual civilization, and cultural entertainment. The development of various convenient services is inseparable from the role of communication terminal equipment for the elderly and the intelligent platform for the elderly in the community [13–16].

Internet of Things (IoT) refers to the collection of information through various sensors, real-time collection of any required information, and transmission through the Internet to achieve a wide range of connections among objects and people and objects and to achieve intelligent identification and connection of objects [17]. In layman’s terms, IoT is based on the Internet through smart devices to realize the collection and artificial intelligence processing of surrounding objects and various types of information. In China, IoT has long been widely used in smart cities, traffic diversion, environmental remediation, government work, social stability, logistics and transportation, smart homes, industrial production, campus life, food safety, public services, life and health, and personal care [18]. The development of IoT is not only a demand of society but also a demand for people who aspire to make life more convenient in the future [19–21].

With the continuous deepening of IoT technology in the health field, the continuous reform and innovation of wearable devices function so that they can fully meet the current technical needs of the health and rehabilitation management of the elderly. Applying this technology to the health management of elderly patients in the community can solve the inconvenience, psychological resistance, and long-term continuous physiological monitoring of elderly patients and can locate and notify community personnel and

medical staff in a timely manner under abnormal physiological conditions. Some elderly people can communicate and supervise the rehabilitation information. It makes up for the lack of community care for the health management of the elderly and improves the monitoring of the physiological conditions of the elderly by the community and medical staff. In the case of not affecting the normal life of the elderly as much as possible, managing the physical health of each elderly person has played a key auxiliary role in community elderly care [22–24].

In summary, the aging of the population is currently a major problem facing the country and society. How to meet the needs of the elderly and society needs to be solved urgently. Therefore, this work discusses the health management of elderly patients in the community and the support of the new Internet of Things. The application of community rehabilitation management is different from previous studies. This work uses the popular Internet of Things technology in recent years, combines community medical services for elderly patients, and adopts intelligent electronic equipment to realize automated monitoring of various physiological indicators of elderly patients, with a view to providing new strategies for the rehabilitation management of elderly patients in the community.

## 2. Technologies and Methods

**2.1. Wearable Devices.** With the advent of Google Glass in 2012, the “first year of smart wearable devices” also kicked off. Nowadays, with the commercial application of high-precision sensors, wearable devices have long been used in the daily lives of most people. The common sports bracelets, smartwatches, smart rings, smart glasses, and smart gloves generally have requirements for biometric identification, such as long-term continuous monitoring of electrocardiogram, body temperature, blood pressure, heart rate, and blood oxygen. At present, the domestic wearable devices market is mainly concentrated in major Internet manufacturers such as Huawei, Xiaomi, Apple, and OV. According to the China Wearable Devices Market Quarterly Tracking Report, the Fourth Quarter of 2020, released by Internet Data Center (IDC) data agency, the wearable devices market shipments in the fourth quarter of 2020 were 30.26 million units in China, with a year-on-year increase of 7.7%. Among them, basic wearable devices were 25.18 million units, with a year-on-year increase of 10.3%, and smart wearable devices were 5.08 million units, with a year-on-year decrease of 3.6%. In foreign markets, Apple still tops the list with 55.6 million units, with a market share of 36.2%, followed by Xiaomi with 13.5 million units, with a market share of 8.8%, and then followed by Samsung with 13 million units and Huawei 10.2 million units. The continuous hot industry growth has never stopped the development of technology.

**2.2. Construction on Community Medical Communication Service and Rehabilitation Model.** With the continuous upgrading of wireless sensing technology in wearable devices

in recent years, the accuracy and stability of physiological data monitoring of the human body have gradually increased [25]. For elderly patients, the daily records of physiological indicators such as blood pressure, blood sugar, heart rate, weight, and sleep quality are very important. These data not only reflect the current physical health of the elderly but also can predict future physical health. In traditional elderly care services, it is often necessary for the elderly to go to the community for testing or community personnel to collect data daily, which is time-consuming and laborious and cannot achieve the effect of real-time monitoring. Introducing wearable devices into community pensions and applying IoT technology to the health monitoring of the elderly can solve the above problems. The community elderly medical information supervision system is shown in Figure 1.

**2.3. IoT Technology.** IoT refers to the collection of information through various sensors and real-time collection of any required information and transmission via the Internet to achieve a wide range of connections among objects, people, and objects and to achieve intelligent identification and connection of objects. IoT can be roughly divided into a three-tier architecture, including information collection, data transmission, and smart port. Information collection mainly comes from the real-time collection of peripheral information by various sensors, periodically obtaining the required information and continuously updating and classifying the collected data. Data transmission is the real-time transmission of collected data through various wired or wireless networks to ensure information security and data accuracy during the transmission process. It is the most core technology in the entire IoT technology link. The smart port is a port for IoT to interact with enterprises and individuals. It can transmit the collected data to the user interface and perform personalized processing so that it can meet the needs of users and finally implement the personalized smart applications of the IoT.

Sensor technology refers to a chip or device that can stably sense and convert the monitored information into a signal that can be transmitted according to a certain logic. Nowadays, the requirements for sensors are not satisfied with the general data transmission, and a certain amount of intelligent processing is needed. It needs to have a certain degree of self-adaptation to the changes of external information and be able to perform data preprocessing and diagnosis.

Embedded technology refers to a system or software that is controlled by an internal computer to perform personalized customization functions. The embedded system is completely customized for the specific role of the user. It is mostly composed of a microcontrol module, a nonvolatile read-only memory module, a volatile random access memory module, a sensor module, an analog-to-digital conversion module, a control module, a display module, and a lightweight embedded operating system. Among them, the monolithic microcontroller is the core of most embedded systems.

**2.4. Electronization of Elderly Ability Assessment.** The Elderly Ability Quantitative Table is a subjective quantitative evaluation system for the elderly to assess their own abilities. After the electronization, it not only saves the dependence on paper quality but also facilitates the update and retention of evaluations in the future, facilitates the elderly to fill in anytime and anywhere, and reduces the workload of the elderly and community workers.

For the selection of the scale, the Abilities Assessment of the Elderly issued by the MCA is undertaken as the basis of the scale. The assessment refers to the ability assessment system for the elderly in Europe, America, and surrounding areas of China, Taiwan, and Hong Kong and establishes the ability of the elderly to evaluate the content and corresponding grades with Chinese characteristics.

The Elderly Ability Assessment scale is divided into 4 first-level indicators in this study, and the first-level indicators are graded into 25 second-level indicators. The specific items are shown in Table 1.

Each grade is divided into three levels: 0 points require great assistance from others or complete assistance from others; 5 points require partial assistance from others or rarely require assistance from others; and 10 points can be completed independently. Each level indicator has a corresponding score coefficient, and the basic coefficient is 0.5. For some basic ability indicators such as walking on flat ground, holding and placing, and level of consciousness, the coefficient needs to be increased to 1. The final score and other vector data are filed together with the community medical workstation, and the specific value is judged by the medical staff.

**2.5. Monitoring Technology of Physiological Indicators.** At present, there are relatively mature and commercial high-precision sensors all over the world, which can continuously monitor electrocardiograph (ECG), body temperature, blood pressure, heart rate, blood oxygen, and other parameters for a long time. In addition, the high-precision sensors have been applied to wearable devices for commercialization and integrate the global position system (GPS) positioning and Wireless Fidelity (Wi-Fi) module.

Photoplethysmography (PPG) is commonly used at present. This technology irradiates the skin. Because blood is highly impermeable, it will reflect red light and absorb green light. The reflected light is collected by the sensor through projection or reflection, converted into electrical signals, and converted into PPG through corresponding processing. The principle is shown in Figure 2.

In Figure 2,  $X$  is the incident light intensity,  $X_{\max}$  is the maximum output light, and  $X_{\min}$  refers to the minimum output light. According to the Lambert-Beer law between blood composition and absorbance, equation (1) can be obtained:

$$\Delta Y^\lambda = \lg \frac{X_O^\lambda}{X_{\min}^\lambda \lg(X_O^\lambda / X_{\max}^\lambda)} \quad (1)$$

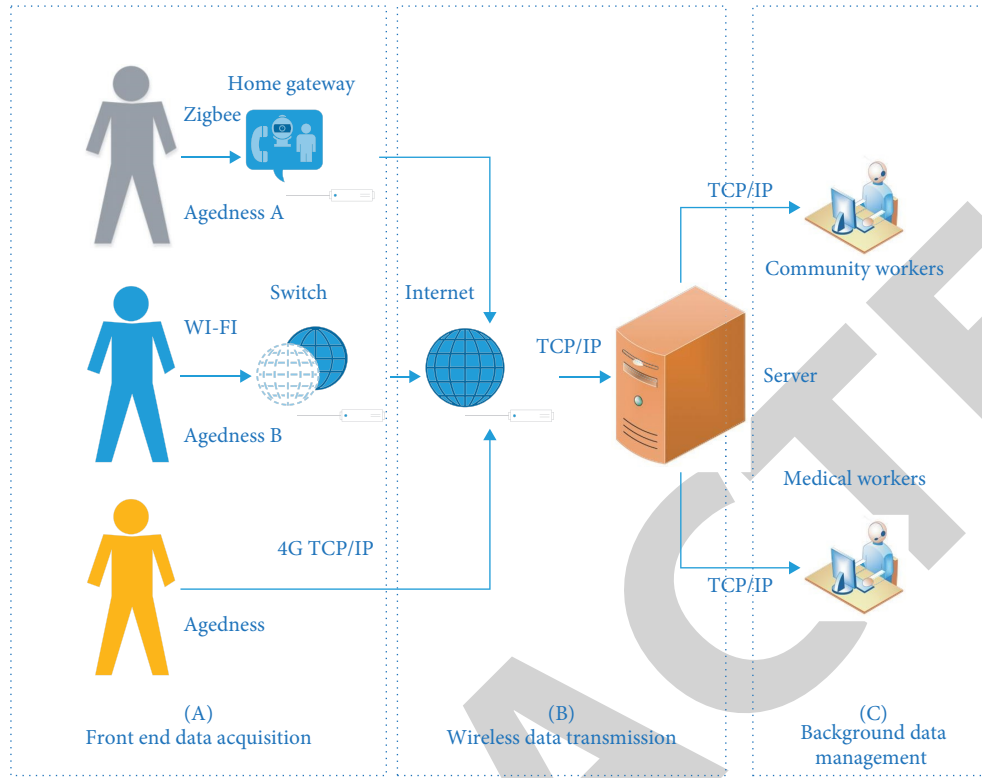


FIGURE 1: The structure of the medical information monitoring system for the elderly in the community. (a) Front-end data collection, (b) wireless data transmission, and (c) background data management.

TABLE 1: Items for elderly ability assessment.

First-level indicators	Second-level indicators
Behavioral ability	Eating, going to the toilet, walking on level ground, walking on slopes, walking on stairs, picking and placing, moving, hanging and taking, self-care, and exercise
Mental state	Emotional cognition, emotional expression, depressive symptoms, aggression, irritability, and self-awareness
Receive feedback	Listening, speaking, reading, writing, spatial positioning, and level of consciousness
Social participation	Interpersonal communication, activity participation, character identification, and workability

In the above equation,  $\Delta Y^\lambda$  refers to the absorbance of pulsating arterial blood at the wavelength  $\lambda$ ;  $X_O^\lambda$ ,  $X_{\max}^\lambda$ , and  $X_{\min}^\lambda$  represent the intensity of the incident light, the maximum output light, and the minimum output light, respectively. Equation (1) can be simplified to equation (2).

$$\Delta Y^\lambda = \sum_x^n \varepsilon_x \cdot c_x \cdot l. \quad (2)$$

In equation (2),  $\varepsilon_x$ ,  $c_x$ , and  $l$  represent the molar extinction coefficient and concentration of the  $x$ -th component in the blood and the equivalent optical path length of the pulsating blood in the maximum filling state, respectively.

The wearable device collects human body-related data through sensors and performs PPG processing, which can directly obtain physiological data such as heart rate, blood pressure, and pulse that are required for daily monitoring.

**2.6. GPS Positioning.** In this experiment, the geographic location of the elderly wearing is displayed on the map in real time by connecting to the open API interface of

AutoNavi Map. The three-axis acceleration sensor is adopted to collect the changes in the wearer's spatial position and sudden spatial changes such as falling and violent exercises. In addition, specific elderly people are dealt with accordingly.

The specific working principle of the three-axis acceleration sensor is shown in Figure 3. It can be judged whether the wearer is in a spatial abnormal state by monitoring the position values in the  $X$ ,  $Y$ , and  $Z$  directions of the coordinate axis.

**2.7. Radio Technology.** Wearable monitoring devices can currently use Bluetooth, ZigBee, Wi-Fi, and mobile communication mainstream transmission methods. Among them, Bluetooth is suitable for short-distance high-speed transmission, but its power consumption and cost are relatively high. ZigBee is suitable for short-distance, low-latency, low-power, and high-security transmission protocols. It is currently mainly used in various

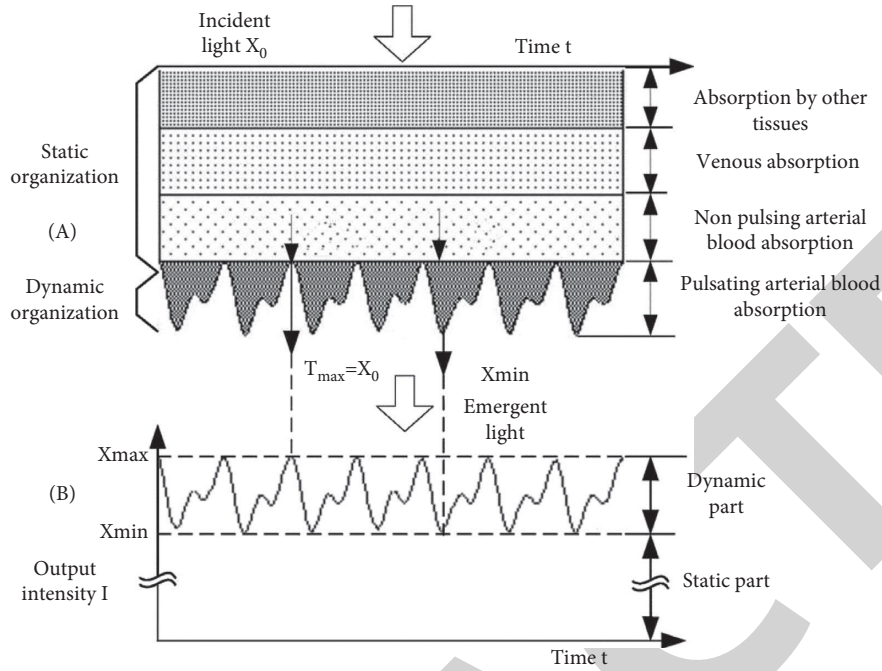


FIGURE 2: Schematic diagram of photoplethysmography: (A) the light transmission of the human body and (B) the sensor data collection.

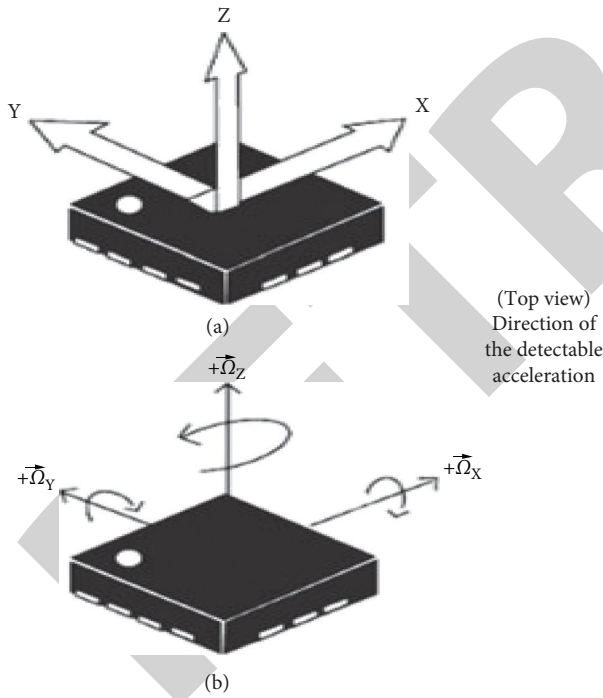


FIGURE 3: Working principle of three-axis acceleration sensor: (a) the three-axis detection of the three-axis sensor and (b) the acceleration detection of the three-axis sensor.

short-distance mechanical control, medical, home intelligent control, and other fields. Wi-Fi is suitable for the construction and wireless connection of mobile networking in a small area. The mobile communications (3G, 4G, 5G, etc.) are suitable for large-scale high-speed and high-quality communications.

**2.8. Analysis of Physiological Indicators for Elderly Patients.** Based on the initial analysis of the physiological indicators of the elderly in the community, the community health information files are established and classified, and all the physiological indicators of the elderly can be studied. The specific mode is shown in Figure 4.

The data of physiological indicators for the elderly in the community can be undertaken as a benchmark to learn and train the support vector machine (SVM). SVM is a common method to solve data classification and analysis. It uses the optimal hyperplane in data classification and processes two-dimensional linear inseparable samples through the high-dimensional mapping of the kernel function to obtain the global optimal solution.

The fuzzy comprehensive evaluation method (FCEM) is used as the evaluation method for the physiological indicators of the elderly group for abnormal tendency. Determining the index weight and selecting the membership function are the most critical technical issues.

For the index weight, principal component analysis (PCA) is selected as the method of determination. PCA combines  $x$  physiological indicators with certain connections to form  $n$  independent parameters to replace the original indicators. Its mathematical model is shown in equation (3).

$$\begin{cases} M_1 = a_{11}Z_1 + a_{21}Z_2 + \dots + a_{x1}Z_x, \\ M_2 = a_{12}Z_1 + a_{22}Z_2 + \dots + a_{x2}Z_x, \\ \dots \\ M_n = a_{1n}Z_1 + a_{2n}Z_2 + \dots + a_{xn}Z_x. \end{cases} \quad (3)$$

In equation (3),  $M$  is the principal component, with a total of  $n$  groups, where  $a_{11} \dots a_{xn}$  represent the eigenvector

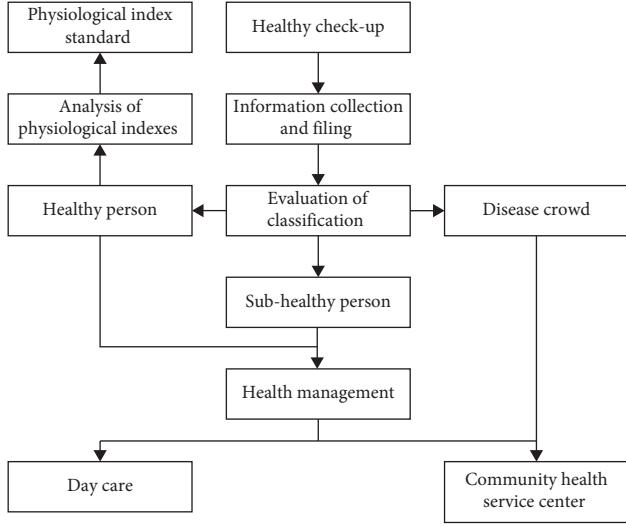


FIGURE 4: The first health survey of the elderly population in the community.

corresponding to the eigenvalue of the original data  $Z(Z_1, Z_2, \dots, Z_x)$  covariance matrix and  $Z_1 \dots Z_x$  represent the normalized vector of the data. The principal component contribution rate can be calculated with the following equation:

$$f_n = \frac{\sum_{q=1}^n \lambda_q}{\sum_{q=1}^x \lambda_q} \quad (n = 1, \dots, x). \quad (4)$$

It is assumed that the contribution rate  $f_1 + f_2$  corresponding to the first and second principal components  $M1$  and  $M2 > 85\%$  and the pair of  $M1$  and  $M2$  can describe the original information. Regarding its weight, it can be calculated with the following equation:

$$g_1 = \frac{a_{11}f_1 + a_{12}f_2}{f_1 + f_2}. \quad (5)$$

Similarly, the  $g_n$  weight equation is shown as follows:

$$g_n = \frac{a_{n1}f_1 + a_{n2}f_2}{f_1 + f_2}. \quad (6)$$

In this study, the  $K$ th parabolic function is selected as the membership function of the risk level, which can be calculated with the following equations:

$$T(x) = \begin{cases} 1, & x < a, \\ \left(\frac{b-x}{b-a}\right)^k, & a \leq x \leq b, \\ 1, & b \leq x, \end{cases} \quad (7)$$

$$T(x) = \begin{cases} 0, & x < a, \\ \left(\frac{x-a}{b-a}\right)^k, & a \leq x \leq b, \\ 1, & b < x, \end{cases} \quad (8)$$

$$T(x) = \begin{cases} \left(\frac{x-a}{b-a}\right)^k, & a \leq x \leq b, \\ \left(\frac{d-x}{d-c}\right)^k, & c \leq x \leq d \\ 0, & x < a, d < x. \end{cases} \quad (9)$$

Equation (7) is small-sized, equation (8) is medium-sized, and equation (9) is large-sized;  $a, b, c$ , and  $d$  are the four types of indicators for the analysis and evaluation of the specific physiological indicators of elderly patients. The model is shown in Figure 5.

In the process, the collected data has to be preprocessed firstly. The min-max normalization in the linear method is adopted in the normalization process in this study, which is specifically shown in equation (10):

$$x^* = \frac{x-a}{b-a}. \quad (10)$$

In the equation above,  $a$  is the minimum value in the sample data, and  $b$  is the maximum value in the sample data.

Attribute reduction is to eliminate repetitive and useless attributes through algorithms so that the reduced subset can get the same attribute results as the original conditions. The steps are shown in Figure 6.

$$f(x) = k \left( 1 - \frac{\text{card}(x)}{n} \right) + (1-k) \frac{\gamma_c(D)}{\gamma_c(D)}. \quad (11)$$

In equation (11),  $\text{card}(x)$  is the number of particle attributes,  $n$  is the total number of attributes,  $\gamma_c(D)$  is the particle dependency,  $\gamma_c(D)$  is the dependency of the total set of attributes under the original conditions, and  $k$  refers to a self-defined parameter. If more sensitive information is calculated, it should appropriately reduce  $k$ ; and if fewer attributes are required, it can increase the value of  $k$  appropriately.

**2.9. Attribute Reduction and Parameter Optimization Based on Improved PSO-SVM.** Particle swarm optimization (PSO) is a population-based stochastic optimization technology that optimizes the accuracy of the parameters in the SVM algorithm by selecting the PSO algorithm so as to improve the accuracy of the vector machine for grading and evaluating the abnormal physiological parameters of the elderly. The specific process is shown in Figure 7.

**2.10. Verification Experiment of Fusion Algorithm.** The data of 90 patients from the MIMIC database, Numeric/055n database, and 180 patients with vascular disease from the UCI database were randomly selected as the verification data for algorithm verification. The Backpropagation Neural Networks (BPNN) algorithm is adopted to verify the SVM algorithm used in this study. The database data are fused, and the fusion accuracy is judged to determine the pros and cons of the SVM algorithm and the BPNN algorithm.

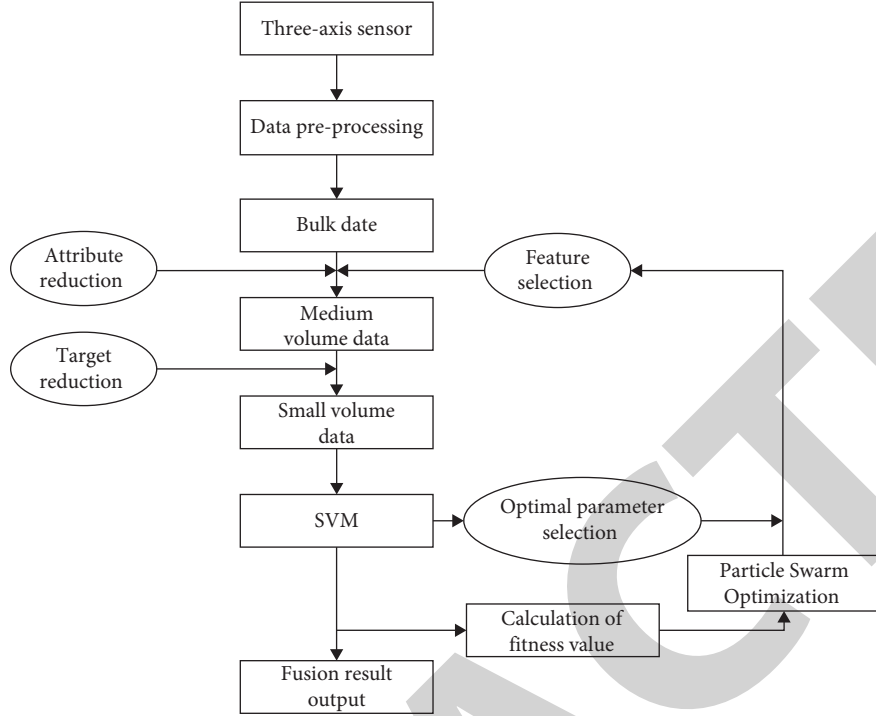


FIGURE 5: Results of risk analysis and evaluation of physiological indicators for the elderly.

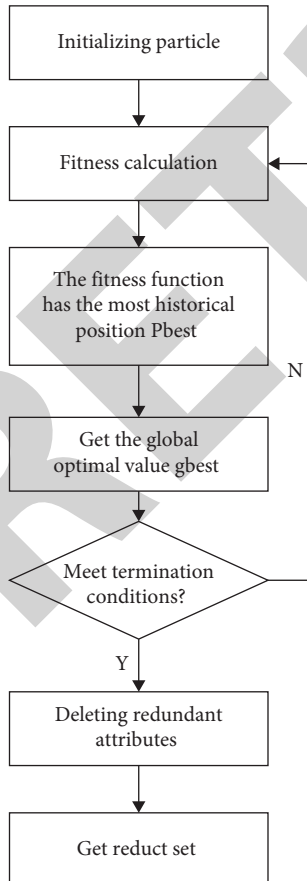


FIGURE 6: Steps for attribute reduction algorithm. The particle fitness value can be calculated with equation (11).

**2.11. Fuzzy Comprehensive Assessment of Disease Risk.** Due to the high coupling and nonlinear relationship of physiological indicators, disease risk assessment mainly relies on the subjective judgment of professional knowledge and experience of medical staff. The fuzzy comprehensive assessment is adopted as a quantitative assessment method of disease risk in the elderly, and the fuzzy membership function and fuzzy product rule are selected to simulate the medical staff system and professional knowledge in this study.

The fuzzy relationship matrix is represented by  $F (F_1, F_2, \dots, F_n)$ , and its specific relationship is shown in equation (12):

$$F = \begin{Bmatrix} F_1 \\ F_2 \\ \dots \\ F_n \end{Bmatrix} = \begin{bmatrix} f_{11} & f_{12} & \dots & f_{1n} \\ f_{21} & f_{22} & \dots & f_{2n} \\ \dots & \dots & \dots & \dots \\ f_{x1} & f_{x2} & \dots & f_{xn} \end{bmatrix}. \quad (12)$$

Here,  $n$  is the number of influencing factors, and  $x$  refers to the evaluation level.  $B$  is defined to be the set of evaluation value vectors in the evaluation set, and  $B$  represents the probability of a certain risk level and the degree of occurrence at this level. The equation is as follows:

$$B = A \circ F = (a_1, a_2, \dots, a_x) \circ \begin{bmatrix} f_{11} & f_{12} & \dots & f_{1n} \\ f_{21} & f_{22} & \dots & f_{2n} \\ \dots & \dots & \dots & \dots \\ f_{x1} & f_{x2} & \dots & f_{xn} \end{bmatrix}. \quad (13)$$

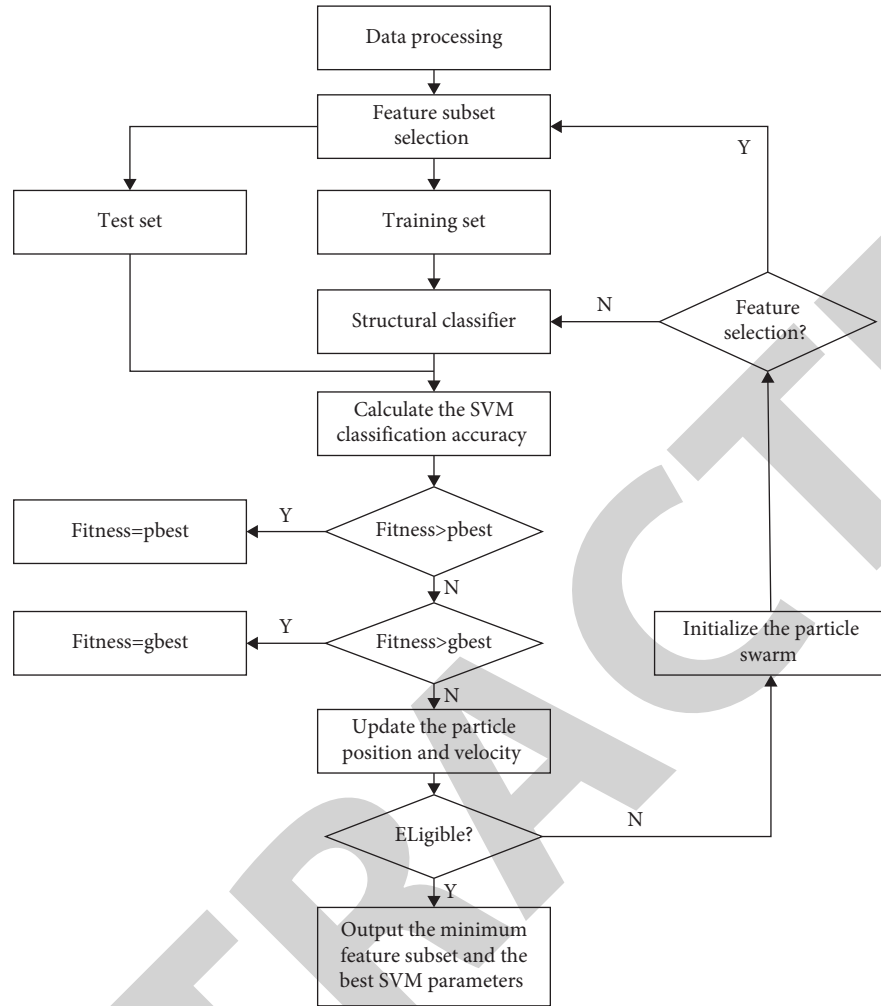


FIGURE 7: Flowchart for attribute reduction and parameter optimization based on PSO-SVM.

In equation (13),  $A$  refers to the weight vector  $A = (a_1, a_2, \dots, a_x)$  ( $0 \leq a_i \leq 1, i = 1, \dots, x$ ), and  $\circ$  is the operator.  $M(\cdot, \oplus)$  is selected for operation in this study. The specific algorithm is shown in equation (14):

$$U_c = \min \left( 1, \sum_{t=1}^x a_t f_{tc} \right). \quad (14)$$

In equation (14),  $U_c$  represents the membership degree of the graded fuzzy subset  $r_i$  in the fuzzy comment set  $R$  for evaluating disease risk,  $c = 1, 2, \dots, n$ ,  $\cdot$  is a real number operation, and  $\oplus$  refers to the sum operation up to 1.

The final risk level is to avoid losing too much information and getting wrong information. The weighted average principle is adopted to calculate the number of cases as follows:

$$j^* = \frac{\sum_{i=1}^x \mu(r_i) \cdot u_i}{\sum_{i=1}^x u_i}. \quad (15)$$

In equation (15),  $\mu(r_i)$  is the evaluation grade value variable, with the principle of maximum membership  $U = \max\{u_1, u_2, \dots, u_i\}$ . In the end, the risk value of a certain factor influencing the elderly's illness is calculated as shown in equation (16):

$$f = \frac{0.5}{L - M} \times (\text{cur\_val} - M) + 0.5. \quad (16)$$

In the equation above,  $L$  represents the maximum value of factor risk, corresponding to fuzzy risk level 1;  $M$  refers to the median value of factor risk, corresponding to fuzzy risk level 0.5; and  $\text{cur\_val}$  represents the current measured value of the factor.

**2.12. Examples of Quantitative Disease Risk Assessment.** A case of data from the MIMIC database, Numeric/055n, is selected as a model for elderly disease risk assessment in the community based on fuzzy comprehensive assessment. The specific data used is shown in Table 2.

This model is brought into the above-mentioned physiological indicators risk assessment model for the elderly. Firstly, its membership function is determined, and then a fuzzy matrix is constructed based on the fuzzy value of each influencing factor. The fuzzy comprehensive score is calculated from the fuzzy relationship and the weight matrix. According to the principle of nearest neighbour value, the risk level of elderly disease is judged.

TABLE 2: Risk assessment models for elderly diseases.

Average blood pressure (mmhg)	Risk grade	Pulmonary arterial pressure (mmhg)	Heart rate (time/min)	SpO <sub>2</sub> (%)	Body temperature (°C)	Breathing rate (time/min)
114	2	26	108	98	36.7	20

**2.13. Family Health Self-Management.** Family health self-management is an important connection part between elderly patients and medical staff and between family and community medical workstations. The above-mentioned system is adopted to assess the health risks of elderly patients. Medical staff receive the information on risk factors, conduct real-time and continuous online monitoring of health conditions, and then provide targeted health advice and guidance for elderly patients. For elderly patients with higher health risks, medical staff can take targeted health interventions to help them deal with health matters.

In addition, real-time communication and video chat are also important means to protect the physical and mental health of elderly patients. Based on real-time communication, it can grasp the physical and mental conditions of elderly patients, provide health interventions and guidance (including correction of bad living habits and eating patterns), and provide mental health guidance and spiritual comfort. It can give full play to the advantages of traditional Chinese medicine (TCM) in “preventing disease,” suggest targeted treatments such as medicated diet to elderly patients, provide targeted rehabilitation training and guidance to elderly patients in need of rehabilitation, and give corresponding supervisions.

For elderly patients living alone at home, a one-button call for help function is provided, equipped with the GPS system, to facilitate timely call for help to community medical institutions when needed.

**2.14. Construction of Community Medical Workstation.** Community medical workstations take IoT as the core and play a role as a link among elderly patients, communities, and hospitals. The workstation monitors the physiological indicators of the elderly in the community on a daily basis and establishes long-term electronic information files for the elderly. In addition, the health risk assessment feedback from the intelligent system is verified and further analysed, and targeted health interventions are made for elderly patients to provide professional physical, psychological, and social support. If required by elderly patients, they can consider providing further on-site services or contacting an ambulance.

**2.15. Training of Medical Personnel.** As the community undertakes the health management of elderly patients, the shortage of grassroots medical personnel has become an important factor restricting the development of community care for the elderly. In response to the rapid increase in the incidence of chronic diseases in elderly patients, community medical staff are more inclined to health prevention, health management, and rehabilitation. In order to solve the current shortage of community medical personnel, lack of

professionalism, and irrational distribution of personnel, a training mechanism that integrates medical care and maintenance should be adopted. For community medical stations, relevant government departments propose targeted training norms and the transformation of in-service personnel. It can cultivate relevant technical professionals in colleges and technical schools to engage in community health management services for elderly patients and provide follow-up learning and promotion channels.

### 3. Results and Discussion

**3.1. Comparison Results of Fusion Algorithms.** The selected two sets of physiological data are fused on SVM and BPNN, respectively, and the fusion accuracy is shown in Figure 8.

As given in Figure 8, the SVM algorithm is generally higher than the BPNN algorithm from the overall fusion accuracy point of view; the difference of SVM algorithm in different data fusion results is 0.0282, while the difference of BPNN algorithm is 0.0504 in terms of fusion results. This proves that the SVM algorithm is better than the BPNN algorithm in overall fusion accuracy. When different results are processed, the SVM algorithm fusion results show less difference, indicating that the SVM algorithm has reduced dependence on typical samples; in this study, selection data are common due to the study of elderly patients in the community. For special patients, targeted observation is adopted, which is not within the scope of home monitoring. Therefore, the SVM algorithm is more suitable for the construction of the algorithm used in this study.

Tafreshi. et al. [26] used fuzzy algorithms to reduce the false alarm rate of blood pressure and ECG monitors, which can measure the blood pressure-ECG delay. Mainardi et al. [27] proposed a bipartite interpolation recursive identification model for the measurement of beat-to-beat parameters, which helps describe and detect the heart rate, arterial blood pressure, and neuromodulation of the patients. Tashiro et al. [28] proposed the use of neural network algorithms for the independent recognition of high-frequency ECG signals. This method can reduce the transfer of samples between high-frequency ECG and neural network algorithms, effectively optimizing the data recognition accuracy and classification efficiency.

**3.2. Results of Quantitative Disease Risk Assessment.** The risk level is set as  $F = \{f_1, f_2, f_3\}$ , which are high-risk, low-risk, and health, respectively. Their level fuzzy value is  $F = \{0.9, 0.5, 0.1\}$ . According to the physiological indicators risk quantitative assessment model for the elderly,  $f_1 \sim f_3$  are introduced in the fuzzy membership function,  $k$  is set to 1.1, and its function is as follows:

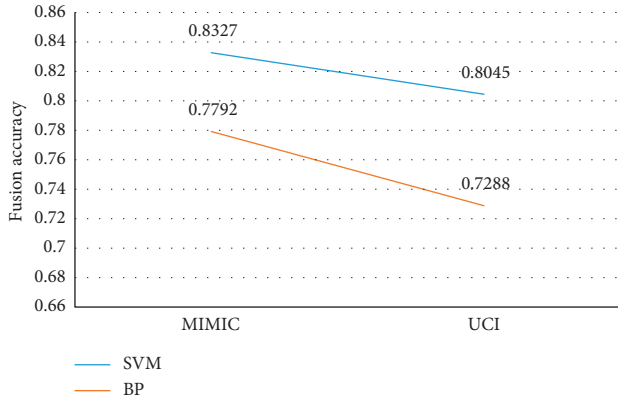


FIGURE 8: Comparison results of fusion algorithms.

$$T_1(x) = \begin{cases} 1, & x > 0.9, \\ \left(\frac{x-0.5}{0.4}\right)^{1.1}, & 0.5 \leq x \leq 0.9, \\ 0, & x \leq 0.5, \end{cases} \quad (17)$$

$$T_2(x) = \begin{cases} 0, & x < 0.1, \\ \left(\frac{x-0.1}{0.35}\right)^{1.1}, & 0.1 \leq x \leq 0.45, \\ 1, & 0.45 \leq x \leq 0.55, \\ \left(\frac{0.9-x}{0.35}\right)^{1.1}, & 0.55 \leq x \leq 0.9, \\ 0, & x \geq 0.9, \end{cases} \quad (18)$$

$$T_3(x) = \begin{cases} 0, & x > 0.5, \\ \left(\frac{0.5-X}{0.35}\right)^{1.1}, & 0.1 \leq x \leq 0.5, \\ 1, & x < 0.1. \end{cases} \quad (19)$$

Equations (17)~(19) are fuzzy membership functions  $f_1 \sim f_3$ . All influencing factors are processed according to the fuzzy calculation model, and the fuzzy value of the risk degree of each factor is obtained, which are 0.59, 0.25, 0.42, 0.76, 0.91, and 0.27, respectively. According to the above results, the membership function is introduced to construct a fuzzy relationship matrix, and then according to the weight vector, the quantitative risk assessment results of the elderly physiological indicators are judged. The fuzzy relation matrix is shown in equation (18):

$$F = \begin{bmatrix} 0.211 & 0.795 & 0 \\ 0 & 0.38 & 0.54 \\ 0 & 0.929 & 0.123 \\ 0.649 & 0.276 & 0 \\ 1 & 0 & 0 \\ 0 & 0.44 & 0.486 \end{bmatrix}. \quad (20)$$

The six parameters of the selected data in the MIMIC database, Numeric/055n database, are used for the PCA, and the weights of these six influencing factors are calculated. Part of the data in the database is shown in Table 3.

The physiological indicators data are normalized, and then their characteristic values and contribution rates are calculated. The results are shown in Table 4.

The first two rows of data are undertaken as the main parameters to build the principal component model:

$$\begin{cases} T_1(x) = 0.2634x_1 + 0.2393x_2 + 0.2445x_3 - 0.1334x_4 + 0.085x_5 + 0.2571x_6, \\ T_2(x) = 0.1668x_1 + 0.3816x_2 - 0.2337x_3 + 0.6967x_4 - 0.3876x_5 + 0.1882x_6. \end{cases} \quad (21)$$

In equation (21),  $x_1 \sim x_6$  are the six related parameters in Table 3 except risk grade. The weight value of each parameter can be calculated according to equation (21) to obtain the weight vector  $Q$ :

$$Q = (0.2421, 0.2723, 0.1332, 0.0611, 0.0276, 0.2409). \quad (22)$$

According to the weight vector, the fuzzy evaluation value  $A$  is calculated according to equation (13):

$$A = Q \circ F = (0.119, 0.549, 0.283). \quad (23)$$

In the equation above,  $F$  is the fuzzy relationship matrix of equation (18), and the membership level  $j^*$  is calculated by the weighted average principle according to equation (15):

$$j^* = \frac{\sum_{i=1}^x \mu(r_i) \cdot u_i}{\sum_{i=1}^x u_i} = \frac{0.119 \times 0.9 + 0.549 \times 0.5 + 0.283 \times 0.1}{0.119 + 0.549 + 0.283} = 0.431. \quad (24)$$

If the calculated membership grade of 0.431 is near 0.5 in the comment concentration, it means that the disease risk factor of the physiological indicators is 0.5 (low risk), which is consistent with the sample grade label 2 (low risk) of the data in the MIMIC database, Numeric/055n database. It shows that the fuzzy comprehensive evaluation model based on the PCA method provided in this study is effective and can be used for the quantitative evaluation of the disease risk of normal elderly physiological indicators.

Tonekabonipour et al. [29] compared and verified the fuzzy neural algorithm and the network neural algorithm in the accuracy of ECG processing, and the results showed that the fuzzy neural algorithm is superior to ECG. Lai et al. [30] believed that the SVM combined with particle swarm optimization (PSO) algorithm has greatly improved the accuracy of classification and recognition and general application compared with other classification methods.

TABLE 3: Some elderly physiological indicators in the database.

Average blood pressure (mmhg)	Risk grade	Pulmonary arterial pressure (mmhg)	Heart rate (time/min)	SpO2 (%)	Body temperature (°C)	Breathing rate (time/min)
114	2	26	108	98	36.7	20
112	2	24	102	98	36.8	19
121	2	24	104	99	36.8	18
118	2	27	103	98	36.8	20
116	2	28	105	98	36.7	20
118	2	26	112	98	37.1	22
120	2	29	121	95	37.1	25
102	2	33	132	97	36.9	25

TABLE 4: Characteristic values and contribution rate of sample data.

Eigenvalue	3.6107	1.1032	0.9037	0.2304	0.1425	0.0603
Contribution rate	70.056	16.746	6.8935	3.7425	2.2469	0.8825

#### 4. Conclusion

Based on the IoT, a model of medical communication and rehabilitation service is constructed for elderly patients in the community in this study. On the basis of mobile communication medical testing wearable devices, artificial intelligence is used to monitor elderly physiological indicators, quantitatively evaluate disease risks, and complete long-term and continuous monitoring of the physical condition of the elderly in the jurisdiction by the community. In addition, it helps community medical stations to carry out rehabilitation service and daily health management for elderly patients. Based on the existing basis, the physiological data of the human body are combined with the SVM by analysing physiological parameters, GPS, and other data to design a reasonable physiological indicator processing model and disease risk quantitative indicators. The quantitative relationship between six physiological indicators and disease risk is analysed, and the dimensionality of feature attributes is reduced to improve the quantum swarm algorithm to obtain the best combination of parameters and finally verify the effectiveness of the model through testing. The results suggested that the SVM algorithm showed better fusion accuracy and lower accuracy difference. Therefore, the community-based medical communication and rehabilitation service model for elderly patients constructed in this study was definitely helpful to the development of community services for the elderly. However, when the model is built, a single physiological factor is considered only in this study, and it fails to consider some special diseases such as upper and lower limb disabilities. In the construction of the disease risk quantitative assessment model, the accuracy can still be further classified. It is believed that, with the continuous growth of the community elderly care industry, more talents will be devoted to the industry, and more and more detailed evaluation models can be put forward for community elderly care communications and medical care. In general, the results of this study provide theoretical support for the development of the rehabilitation service model and daily health management of community

medical stations for elderly patients and meet the rehabilitation service needs of the majority of elderly groups.

#### Data Availability

All data included in this study are available upon request by contact with the corresponding author.

#### Conflicts of Interest

There are no potential conflicts of interest in the article.

#### Authors' Contributions

The authors declare that there are no conflicts of interest.

#### References

- [1] G. Duns, "Ageing," *Australian journal of general practice*, vol. 48, no. 7, p. 421, 2019.
- [2] F. F. Evandro, C. L. Xie, and J. A. Schenkel, "A research agenda for ageing in China in the 21st century (2nd edition): focusing on basic and translational research, long-term care, policy and social networks," *Ageing Research Reviews*, vol. 64, Article ID 101174, 2020.
- [3] P.-C. Ko and W.-J. J. Yeung, "An ecological framework for active aging in China," *Journal of Aging and Health*, vol. 30, no. 10, pp. 1642–1676, 2018.
- [4] J. Li, X. Chen, X. Han, and G. Zhang, "Spatiotemporal matching between medical resources and population ageing in China from 2008 to 2017," *BMC Public Health*, vol. 20, no. 1, p. 845, 2020.
- [5] B. Qu, X. Li, J. Liu, and J. Mao, "Analysis of the current situation regarding the aging rural population in china and proposed countermeasures," *Population Health Management*, vol. 15, no. 3, pp. 181–185, 2012.
- [6] G. G. Huang, Y. Duan, and F. Guo, "Prevalence and related influencing factors of depression symptoms among empty-nest older adults in China," *Archives of Gerontology and Geriatrics*, vol. 91, Article ID 104183, 2020.
- [7] W. He, L. Jiang, X. Ge et al., "Quality of life of empty-nest elderly in China: a systematic review and meta-analysis," *Psychology, Health & Medicine*, vol. 25, no. 2, pp. 131–147, 2020.
- [8] H. Su, J. Cao, Y. Zhou, L. Wang, and L. Xing, "The mediating effect of coping style on personality and mental health among elderly Chinese empty-nester: a cross-sectional study," *Archives of Gerontology and Geriatrics*, vol. 75, pp. 197–201, 2018.

## Retraction

# Retracted: Models of Artificial Intelligence-Assisted Diagnosis of Lung Cancer Pathology Based on Deep Learning Algorithms

### Journal of Healthcare Engineering

Received 10 October 2023; Accepted 10 October 2023; Published 11 October 2023

Copyright © 2023 Journal of Healthcare Engineering. This is an open access article distributed under the Creative Commons Attribution License, which permits unrestricted use, distribution, and reproduction in any medium, provided the original work is properly cited.

This article has been retracted by Hindawi following an investigation undertaken by the publisher [1]. This investigation has uncovered evidence of one or more of the following indicators of systematic manipulation of the publication process:

- (1) Discrepancies in scope
- (2) Discrepancies in the description of the research reported
- (3) Discrepancies between the availability of data and the research described
- (4) Inappropriate citations
- (5) Incoherent, meaningless and/or irrelevant content included in the article
- (6) Peer-review manipulation

The presence of these indicators undermines our confidence in the integrity of the article's content and we cannot, therefore, vouch for its reliability. Please note that this notice is intended solely to alert readers that the content of this article is unreliable. We have not investigated whether authors were aware of or involved in the systematic manipulation of the publication process.

In addition, our investigation has also shown that one or more of the following human-subject reporting requirements has not been met in this article: ethical approval by an Institutional Review Board (IRB) committee or equivalent, patient/participant consent to participate, and/or agreement to publish patient/participant details (where relevant).

Wiley and Hindawi regrets that the usual quality checks did not identify these issues before publication and have since put additional measures in place to safeguard research integrity.

We wish to credit our own Research Integrity and Research Publishing teams and anonymous and named external researchers and research integrity experts for contributing to this investigation.

The corresponding author, as the representative of all authors, has been given the opportunity to register their agreement or disagreement to this retraction. We have kept a record of any response received.

### References

- [1] S. Chen, "Models of Artificial Intelligence-Assisted Diagnosis of Lung Cancer Pathology Based on Deep Learning Algorithms," *Journal of Healthcare Engineering*, vol. 2022, Article ID 3972298, 12 pages, 2022.

## Research Article

# Models of Artificial Intelligence-Assisted Diagnosis of Lung Cancer Pathology Based on Deep Learning Algorithms

Su Chen 

*The First Affiliated Hospital, Sun Yat-Sen University, Guangzhou 510030, Guangdong, China*

Correspondence should be addressed to Su Chen; [chens57@mail.sysu.edu.cn](mailto:chens57@mail.sysu.edu.cn)

Received 15 December 2021; Revised 19 January 2022; Accepted 18 February 2022; Published 26 March 2022

Academic Editor: Yang Gao

Copyright © 2022 Su Chen. This is an open access article distributed under the Creative Commons Attribution License, which permits unrestricted use, distribution, and reproduction in any medium, provided the original work is properly cited.

In this article, in order to explore the application of a diagnosis system for lung cancer, we use an auxiliary diagnostic system to predict and diagnose the good and evil attributes of chest CT pulmonary nodules. This research improves the new diagnosis method based on the convolutional neural network (CNN) and the recurrent neural network (RNN) and combines the dual effects of the two algorithms to process the classification of benign and malignant nodules. By collecting H-E-stained pathological slices of 652 patients' lung lesions from two hospitals between January 2018 and January 2019, the output results of the improved 3D U-net system and the consistent results of two-person reading were compared. This article analyzes the sensitivity, specificity, positive flammability rate, and negative flammability rate of different lung nodule detection methods. In addition, the artificial intelligence system's and the radiologist's judgment results of benign and malignant pulmonary nodules are used to draw ROC curves for further analysis. The improved model has an accuracy rate of 92.3% for predicting malignant lung nodules and an accuracy rate of 82.8% for benign lung nodules. The new diagnostic method using the convolutional neural network and the recurrent neural network can be very effective for improving the accuracy of predicting lung cancer diagnosis. It can play a very effective role in the disease prediction of lung cancer patients, thereby improving the treatment effect.

## 1. Introduction

In the last decade, the mortality and morbidity of malignant tumors have been increasing, which has led to a very serious situation in cancer prevention and cancer treatment. From the perspective of cancer incidence, lung cancer has the highest incidence among the top ten cancers, and deaths due to lung cancer ranks first among the top ten cancer deaths. After investigation, it is found that the symptoms of lung cancer are not so obvious in the early stage. The patient does not feel any abnormality in the body at the early stage. Only when the body is abnormal, it is diagnosed as lung cancer. The stage of the patient diagnosed with lung cancer is normally intermediate to advanced stage. For patients in the advanced stage, the current medical level of clinical surgery has no effect, so generally, patients in the late stage will give up treatment, and their survival rate is relative. However, for early lung cancer patients, it can be treated by clinical surgery, and there is a very high survival rate.

Research on the diagnosis system for lung cancer based on text and images can provide reference value for clinicians. It can effectively reduce the workload of clinicians to screen early lung cancer patients manually and prevent missed screening due to fatigue and other factors. It can provide effective tools for the early detection and diagnosis and increase the chance of curing lung cancer patients.

Pulmonary sarcoidosis is a multisystem and multiorgan granulomatous disease of unknown etiology, which often invades the lungs, bilateral hilar lymph nodes, eyes, skin, and other organs, and the chest invasion rate is as high as 80%–90%. In recent years, the application of deep learning algorithms in medicine has developed rapidly, and research in this area has also emerged in an endless stream. Zheng S applied MIP images to improve the efficiency of automatic lung nodule detection using the CNN [1]. Meanwhile, Koning H J investigated this issue and obtained relevant data from the registry. Data analysis showed that in high-risk trials, lung cancer mortality was significantly lower in

patients screened with volumetric CT than in untested patients [2]. In the research of deep transfer learning, Zhao tested the deep learning model. For the external test set, the transferred model has good generalization ability [3]. Jae-Hong developed a new CNN-based system combining a pretrained deep CNN structure and a self-training network [4]. Wang proposed a new method for breast cancer screening and diagnosis based on the CNN model. This method produced a CNN-based breast cancer CT image detection model and a breast cancer screening model [5]. Artificial intelligence is also used for auxiliary diagnosis of cervical cancer. Zhu used the TBS report artificial intelligence cervical fluid thin layer cytology auxiliary diagnosis system jointly developed by Southern Medical University and Guangzhou Fuqiang Pathology Technology Co. Ltd. to diagnose all clinical specimens [6]. Although artificial intelligence can achieve good results in medical applications, there are still difficulties in application. Reliable deep learning models require additional effort and cost. To this end, Guo Ke proposed a new medical-aided diagnosis model as a service. This will help medical institutions obtain reliable medical aid diagnostic models quickly and efficiently [7]. Although deep learning is increasingly used in medical diagnosis, it is not without its drawbacks. Compared with traditional algorithms, when the amount of data processed is too large, deep learning algorithms are slower than traditional algorithms, and a series of problems are prone to occur in practical applications. Therefore, we urgently need a more stable and processing power algorithm model [8].

The innovations of this article are as follows: (1) This article uses a multitask deep neural network technology based on three-dimensional convolution, and its advantage is that it can assign weights to similar structures. (2) This article uses an improved 3D U-net system and compares it with the original system. The improved sensitivity and specificity changes were investigated, and it was determined that the improved 3D U-net system is more suitable for lung nodule identification. (3) This article also uses an ROC curve to distinguish invasive adenocarcinoma from noninvasive lung cancer and discusses the further application of the artificial intelligence system in lung cancer diagnosis.

## 2. Artificial Intelligence-Assisted Diagnosis of Lung Cancer Pathology

**2.1. Medical-Related Technologies.** In the medical field, lung cancer-related examinations mainly include CT images to detect lung nodules, CT image descriptions for analysis, and test reports to further test some information such as tumor markers. This section mainly introduces the lung nodules, the principle of CT imaging, the source of the examination description, and the related information of the examination report [9].

**2.1.1. Lung Nodules.** Pulmonary nodule is a disease of the lung tissue, it occurs in the early stage of lung cancer, it is a granulomatous disease, and the cause is unknown [10]. The CT image of the lung nodules is shown in Figure 1.

**2.1.2. CT Image.** The expansion of CT is computed tomography. Generally speaking, CT in clinical practice uses X-rays as the radiation source to emit X-rays, and the final tomographic image is X-ray CT. What we need to know is that all processes that can create images and use computers to build tomograms can be called CT [11–13].

The absorption of X-rays by objects plays a major role in CT imaging. A specific detector is used to receive the X-rays that pass through this layer; the received X-rays are converted into visible light through a converter and then converted into digital signals by an analog/digital converter, which are then input to a computer for processing [14]. The principle of CT is shown in Figure 2.

**2.1.3. Inspection Report.** The test report mainly includes sputum cytology, pleural fluid examination, blood routine examination, and tumor marker screening. Cytology examination of sputum and pleural fluid mainly determines whether there are tumor cells in the sputum and pleural fluid. Routine blood tests include determining the count of white blood cells, red blood cells, and platelets, as well as cell acidity and alkalinity [15]. The inspection items are shown in Table 1.

## 2.2. Image-Processing Technology

**2.2.1. Image Enhancement: Binarization.** The relationship between white and black is divided into several levels according to the logarithmic relationship, which is called the “gray level”. The range is generally from 0 to 255, where white is 255 and black is 0, so black and white images are also called grayscale images, which are widely used in the fields of medicine and image recognition. Image binarization is a necessary step in pre-image processing. It is mainly to set the gray value of the pixels on the image to 0 or 255, which can eliminate a lot of noise interference, and the entire image will show only black and white visual effects [16–18].

- (1) Binary thresholding: The gray value is set greater than the threshold to maxval, and the threshold is set to 0 in other cases.

$$D(a, b) \begin{cases} \text{max val,} & S(a, b) > \text{threshold,} \\ 0, & \text{other wise.} \end{cases} \quad (1)$$

- (2) Anti-binary thresholding: The gray value is set greater than the threshold to 0, and the threshold is set to maxval in other cases.

$$D(a, b) \begin{cases} \text{max val,} & S(a, b) \leq \text{threshold,} \\ 0, & \text{other wise.} \end{cases} \quad (2)$$

- (3) Threshold of truncation: The threshold to the gray value is set greater than the threshold, and the threshold setting remains unchanged in other cases.

$$D(a, b) \begin{cases} \text{threshold,} & S(a, b) \leq \text{threshold,} \\ S(a, b), & \text{other wise.} \end{cases} \quad (3)$$

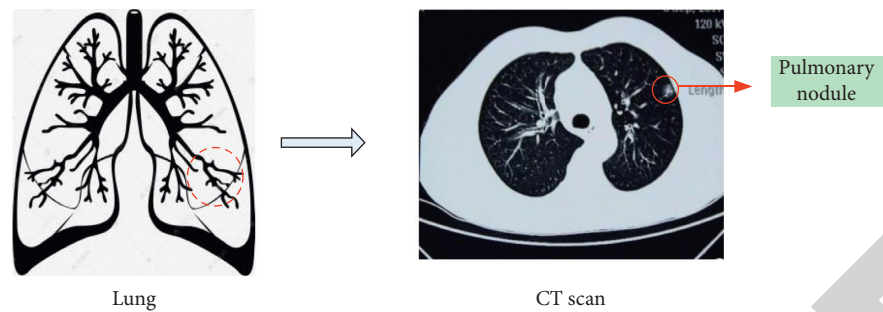


FIGURE 1: CT image of lung nodules.

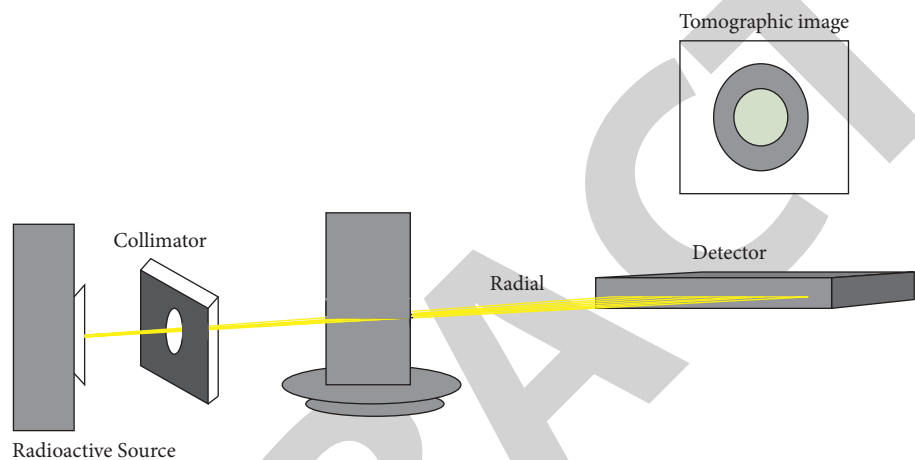


FIGURE 2: CT principle.

TABLE 1: Inspection items.

	Reference range	Inspection name	State	Result value
Blood routine examination Sputum examination	0–0.10	Basophils	Normal	0.02
	0.05–0.5	Eosinophils	Normal	0.06
	0–1	Basophil ratio	Normal	0.30%
	110–160	Hemoglobin	Normal	135 g/L
	100–300	Platelets	Normal	158 g/L
	3.5–5.5	Red blood cells	Normal	3.94
	37–50	Erythrocyte distribution width	Normal	45.31%
	4–10	White blood cells	Normal	7.21 g/L
Tumor markers	86–100	Mean red blood cell volume	Normal	89.4 fL
	No tumor cells	Sputum cells	Normal	No tumor cells
	<5 g/ml	CEA	Normal	2.36 g/ml
	<30 U/ml	CA125	Normal	12.5 U/ml
	<8.20 U/ml	CA72-4	Normal	2.24 U/ml
	<16.3 ng/ml	NSE	Normal	14.15 ng/ml
Hydrothorax examination	<1.5 ng/ml	SCC	Normal	1.17 ng/ml
	<2.0 ng/ml	CYFRA21-1	High	6.38 ng/ml
	0.38–2.1	Triglyceride	Normal	0.68 mmol/L
	0.8–1.95	High-density lipoprotein	Normal	1.23 mmol/L
	3.8–6.1	Glucose	High	10.08 mmol/L
	2–4	Low-density lipoprotein	Normal	1.76 mmol/L
	109–271	Lactate dehydrogenase	Normal	174.1 U/L
	0–6.8	Direct bilirubin	Normal	3.18 umol/L
	3.6–5.9	Total cholesterol	Low	3.36 mmol/L
	20–45	Globulin	Normal	33.5 g/L

- (4) Threshold is 0: The gray value greater than the threshold is unchanged, and the gray value of the threshold is set to 0 in other cases.

$$D(a, b) \begin{cases} S(a, b), & S(a, b) > \text{threshold}, \\ 0, & \text{other wise.} \end{cases} \quad (4)$$

- (5) Dethresholding to 0: The gray value not greater than the threshold is unchanged, and the threshold gray value is set to 0 in other cases.

$$D(a, b) \begin{cases} S(a, b), & S(a, b) \leq \text{threshold}, \\ 0, & \text{other wise.} \end{cases} \quad (5)$$

**2.2.2. Image Filtering.** In simple terms, image filtering is a method of image noise reduction, which is mainly divided into linear noise reduction methods and nonlinear noise reduction methods. Linear noise reduction methods mainly include box, mean, and Gaussian methods [19]. The nonlinear noise reduction method is mainly median filtering. In the mean method in the linear noise reduction method, the mean filter using the neighborhood mean method is very suitable for removing grain noise in the image obtained by scanning. The domain averaging method can effectively suppress the noise, and at the same time, it also causes the blurring phenomenon due to averaging; the blurring degree

is proportional to the radius of the neighborhood. The median noise reduction in the nonlinear noise reduction method is a commonly performed using a nonlinear smoothing filter. Its main function is to change the pixel with a large difference in the gray value of the surrounding pixels to a value close to the surrounding pixel value so as to eliminate the isolated noise points, so the median filter is very effective in filtering out the salt and pepper noise of the image.

Image filtering can be calculated by the formula

$$O(i, j) = \sum_{m,n} I(i+m, j+n) \cdot K(m, n). \quad (6)$$

$(I, j)$  is the position of the pixel in the picture;  $(m, n)$  is the position/coordinates in the convolution kernel, and the coordinates of its center point are  $(0, 0)$ .

$K(m, n)$  is the weight parameter on  $(m, n)$  in the convolution kernel.

$I(i+m, j+n)$  is the picture pixel value corresponding to  $K(m, n)$ ;  $o(i, j)$  is the filtering/convolution result of  $(i, j)$  pixels in the picture.

**(1) Box filtering.** Box filtering is the simplest processing, where all pixels have the same weighting factor.

The core is

$$h = \alpha \begin{bmatrix} 1 & \dots & 1 \\ \vdots & \ddots & \vdots \\ 1 & \dots & 1 \end{bmatrix} \alpha = \begin{cases} \frac{1}{\text{hsize.width} * \text{hsize.height}}, & \text{normalize} = \text{true}, \\ 1, & \text{otherwise.} \end{cases} \quad (7)$$

However, when `normalize` is true, it becomes a mean filter.

**(2) Mean filtering.** The mean filtering method is a method that takes the average of the target pixel to achieve the purpose of filtering. For the pixels to be processed, the mean filtering method selects a template. The template is composed of several adjacent pixels.

Its core is

$$\text{kore} = \frac{1}{\text{kore}_{\text{width}} \cdot \text{kore}_{\text{height}}} \begin{bmatrix} 1 & \dots & 1 \\ \vdots & \ddots & \vdots \\ 1 & \dots & 1 \end{bmatrix}. \quad (8)$$

**(3) Gaussian filtering.** Gaussian filtering is a linear filtering and an important method for smoothing the image. The image processed by Gaussian filtering looks more natural than the image processed by the ordinary template [20, 21].

There are two main functional forms of Gaussian filtering. The first is a one-dimensional Gaussian filtering function:

$$G(x) = \frac{1}{\sqrt{2\pi}\sigma} e^{-x^2/2\sigma^2}. \quad (9)$$

The second is the two-dimensional Gaussian filter function:

$$G(x, y) = \frac{1}{2\pi\sigma^2} e^{-x^2+y^2/2\sigma^2}. \quad (10)$$

**2.2.3. Edge Sharpening.** Edge sharpening is an image processing filter that enhances the edge contrast of an image or video. Visually, images with clear boundaries are preferred by users. Edge sharpening mainly includes expansion, corrosion, opening operation, and closing operation. The edge contrast of an image or video is enhanced by edge sharpening, and its sharpness or clarity can be significantly improved [22].

**2.3. Related Technologies of Deep Learning.** In real life, deep learning methods are widely used to extract and analyze image semantic features, laying a solid foundation for the research of image classification technology.

**2.3.1. The Emergence of Deep Learning.** In 2006, the concept of deep learning was first proposed. It is a complex algorithm. After years of development, there are many deep learning frameworks [23]. A restricted Boltzmann machine (RBM) is a generative stochastic artificial neural network that learns probability distribution over its input set. The first-generation neural network perception model is shown in Figure 3.

Further research on the RBM model is one of the core contents of deep learning and has very important significance [24]. The RBM power model is shown in Figure 4.

RBM is an undirected graph probability model, which is based on power. We combine the power function of the input layer vector  $x$  and the hidden layer vector  $h$  to define the joint probability distribution as

$$O(x, h) = \frac{g^{-\text{power}(x, h)}}{f}. \quad (11)$$

$$\begin{aligned} \frac{\partial \log O(x)}{\partial \theta} &= -\frac{\partial \text{free Power}(x)}{\partial \theta} + \frac{1}{f} \sum_{\hat{x}} g^{-\text{free Power}(\hat{x})} \frac{\partial \text{free Power}(\hat{x})}{\partial \theta} = \\ &= -\frac{\partial \text{free Power}(x)}{\partial \theta} + \sum_{\hat{x}} O(\hat{x}) \frac{\partial \text{free Power}(\hat{x})}{\partial \theta}. \end{aligned} \quad (15)$$

In order to deal with the difficult RBM calculation problem of the partition function, the approximate value of the log-likelihood gradient  $\partial \log O(x) / \partial \theta$  is usually used for training. The sample  $x \sim O(x)$  subject is used for data

$$P_{\hat{O}} \left[ \frac{\partial \log O(x)}{\partial \theta} \right] = -P_{\hat{O}} \left[ \frac{\partial \text{free Power}(x)}{\partial \theta} \right] + P_{\hat{O}} \left[ \frac{\partial \text{free Power}(\hat{x})}{\partial \theta} \right]. \quad (16)$$

Among them,  $O$  is the model probability distribution,  $P_{\hat{O}}$  and  $P_O$  are the expected values under the corresponding probability distribution, and  $\hat{O}$  is the empirical probability distribution of the training data set. The first term of (16) is relatively simple, and it is generally replaced by training sample expectations; the second term contains samples obtained from model  $O$ .

**2.3.2. Deep Learning Model: Convolutional Neural Network Model.** Convolutional neural networks (CNN) are feed-forward neural networks, which are a feature extraction and classification method for images [25]. Figure 5 shows a simple convolutional neural network model.

The normalization constant is  $F = \sum_{x, h} g^{-\text{power}(x, h)}$ . The marginal probability distribution of the observable input data  $x$  is

$$\begin{aligned} O(x) &= \sum_h O(x, h) \\ &= \sum_h \frac{g^{-\text{power}(x, h)}}{f}. \end{aligned} \quad (12)$$

Introducing free power changes (12) into

$$O(x) = \frac{g^{-\text{free Power}(x)}}{f}. \quad (13)$$

$f = \sum_x g^{-\text{free Power}(x)}$  is used in formula (13), that is,

$$\text{free Power}(x) = -\log \sum_h g^{-\text{power}(x, h)}. \quad (14)$$

$\theta$  is introduced to represent the parameters of the model; taking the logarithm of (13) and deriving it result in

distribution and the free power gradient on the sample  $\hat{x} \sim O(\hat{x})$  subject is used for model distribution to define the model parameter update rule as

It can be seen from Figure 5 that, unlike the multilayer feedforward sensor, the convolutional neural network limits the network structure by using the local connection of the receiving area.

(1) Before training, the ownership value of the convolutional neural network is initialized with different small random numbers for supervised training. There are two stages to training a folded neural network:

(a) In the prepropagation stage, samples are taken from the sample set and input  $X$  to the network, where  $E$  is the weight of the network and  $Y$  is the mapping function. The information is passed on

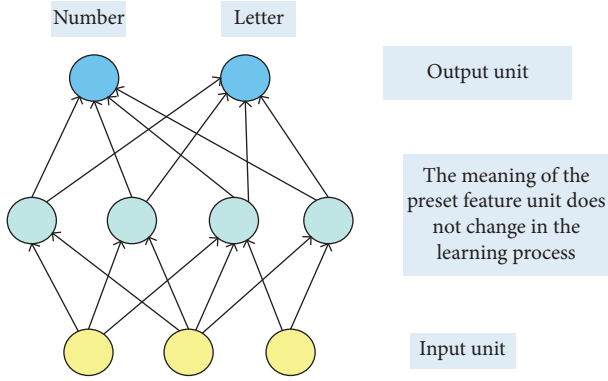


FIGURE 3: The first-generation neural network perception model.

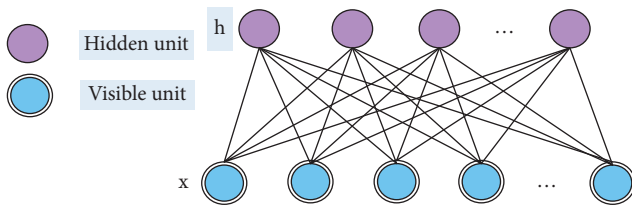


FIGURE 4: RBM power model.

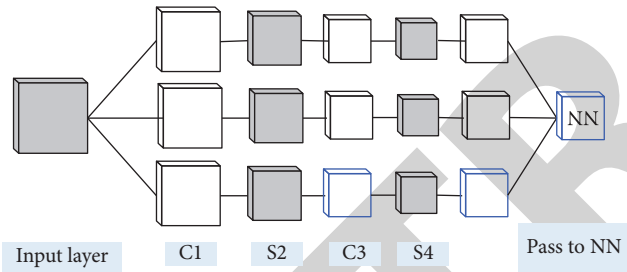


FIGURE 5: Convolutional neural network.

and the corresponding actual output is calculated:

$$B_p = Y_n (\cdots (Y_2 (Y_1 (X E_1) E_2) \cdots) E_n). \quad (17)$$

(b) In the retrospective phase,

$$E_p = \frac{1}{2} \sum_j (Y_{pj} - O_{pj})^2. \quad (18)$$

(2) Activation function. The sigmoid function and tanh function are the first nonlinear activation functions used in neural networks.

The sigmoid function not only increases monotonically but its inverse function also increases monotonously. Therefore, the sigmoid function is very suitable to be used as a threshold function of a neural network, and its function value is between 0 and 1.

The analytical formula of the function is

$$\text{sigmoid}(x) = \frac{1}{1 + e^{-x}}. \quad (19)$$

The output value of the tanh function can be scaled nonlinearly in the range of  $(-1, 1)$ , which is convenient for normalizing the model characteristics.

The analytical formula of the function is

$$T(x) = \frac{e^x - e^{-x}}{e^x + e^{-x}}. \quad (20)$$

**2.3.3. Long- and Short-Memory Neural Network.** The structure diagram of long short-term memory (LSTM) is shown in Figure 6, and each line represents a vector. The yellow rectangle represents the activation function in this neural network layer. The pink circles represent point-by-point operations between vectors, such as vector multiplication and vector addition. Compared with other models, the LSTM model can handle the semantics of long-distance context better in text. Therefore, the LSTM model has become the current mainstream word segmentation task model.

**2.3.4. Deep Learning Algorithm of 3D U-Net Model.** The deep learning algorithm used in this experiment is a 3D U-net model. In this model, each green cuboid is a module. Each module has a fixed network structure (Figure 7), including 3D convolution, normalization, an activation function, and a pooling layer.

### 3. Artificial Intelligence-Assisted Diagnosis of Lung Cancer Pathology Experiment and Analysis

**3.1. Basic Characteristics of Research Objects.** This study retrospectively collected H-E-stained pathological sections of lung lesions in 652 patients from three tertiary hospitals, mainly Jiangxi Provincial People's Hospital, from January 2018 to January 2019. There were 301 males (accounting for 46.2%) and 351 females (accounting for 53.8%), ranging from 24 to 92 years old, with an average age of  $(61.8 \pm 10.5)$  years. Among them, 278 (41.2%) had malignant lesions, 396 (58.8%) had benign lesions, and 674 had lung nodules, where 488 had solid nodules, 186 had subsolid nodules, 124 had partial solid nodules, and 62 had ground glass nodules; 8 had tiny nodules with a diameter of less than 5 mm in the lung nodules, 74 had small nodules with a diameter of  $5 \text{ mm} \leq 10 \text{ mm}$ , and 592 had nodules with a diameter  $>10 \text{ mm}$ . Among them, there were 387 nodules between 10 and 20 mm and 205 nodules between 20 and 30 mm. There were 218 nodules in the upper lobe of the left lung, 99 nodules in the lower left lobe, 156 nodules in the upper right lung, 69 nodules in the middle right lung, and 132 nodules in the lower right lung (details are shown in Table 2).

**3.2. Detection of Lung Nodules.** Of the 652 patients included, there were a total of 674 pulmonary nodules. There were 633 cases of 1 target lung nodule and 20 cases of 2 target lung nodules. Among them, the improved 3D U-net network-assisted diagnosis system detected a total of 674 target

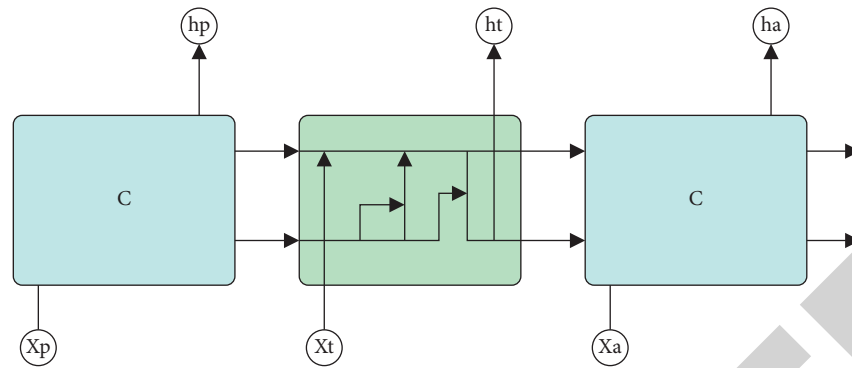


FIGURE 6: LSTM network structure diagram.

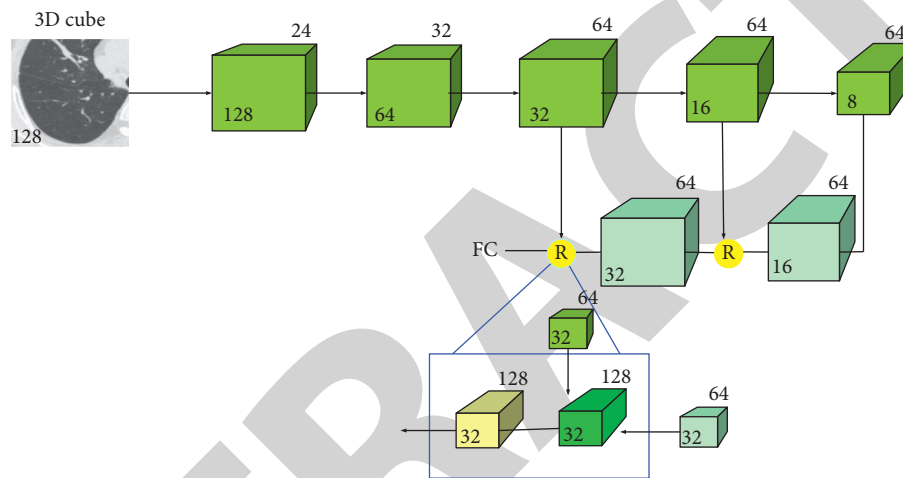


FIGURE 7: Improved 3D U-net model diagram.

TABLE 2: Basic characteristics of lung nodules.

Features	Classification	Number of nodules	Proportion (%)
Density classification	Reality	488	72.4
	Partial realness	124	18.4
	Ground glass	62	9.2
Position	Upper lobe of left lung	218	32.3
	Lower lobe of left lung	99	14.7
	Upper lobe of right lung	156	23.1
	Middle lobe of right lung	69	10.2
	Lower lobe of right lung	132	19.6
Diameter	$d < 5$ mm	8	1.2
	$5\text{ mm} \leq d \leq 10$ mm	74	11.0
	$10\text{ mm} \leq d \leq 30$ mm	592	87.8
Pathological type	Benign	396	58.8
	Malignant	278	41.2
Gender	Male	301	46.2
	Female	351	53.8
Age	Age 24–92 years old; average age $(61.8 \pm 10.5)$ years		

nodules, with a detection rate of 100.0% (674/674). Radiologists reported a total of 673 target sections, with a detection rate of 99.9% (673/674), as shown in Table 3.

Figure 8 shows the difference between the AI model, pathologists, and pathology gold standard. The gold standard refers to the dispute between two pathologists with

TABLE 3: Pathological types of lung nodules.

Pathological types of pulmonary nodules	Number of nodules	Proportion (%)
Benign nodule	396	58.8
Tuberculoma	313	46.4
Hamartoma	62	9.2
Sclerosing alveolar cell tumor	21	3.1
Malignant nodule	278	41.2
Adenocarcinoma	259	38.4
Squamous cell carcinoma	19	2.8
Total	674	100.0

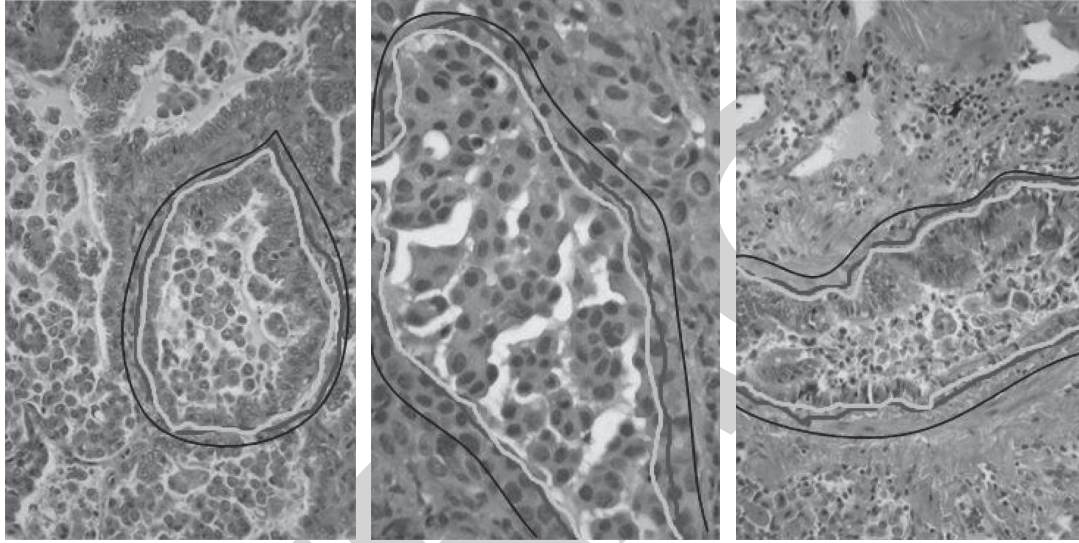


FIGURE 8: Pathological gold standard, AI model, and pathological regions segmented by pathologists (black line: AI model, gray line: gold standard, and white line: pathologist).

more than 5 years of experience in the diagnosis of lung diseases. The chief physician discusses the final result of the decision.

### 3.3. Diagnosis of Benign and Malignant Pulmonary Nodules

**3.3.1. Prediction of Benign and Malignant.** In principle, the 674 cases in this study were divided into two groups at a ratio of 3 : 1: a training group and a research group, with 506 cases in the training group and 168 cases in the testing group. The training group data are used to train the benign and malignant classification models of lung lesions, and the test group data are used to test the model. After the model is tested and refined, the performance indicators of the final classification model are recorded.

In this study, the prediction results of the 168 lung nodules in the test group based on the model established by the deep learning algorithm are shown in Table 4.

It can be seen that there are a total of 104 malignant lung nodules, and the model successfully predicted that 96 of them are malignant, accounting for 92.3% of the total. Among them, 8 were misdiagnosed, accounting for 7.7%. Among all 64 benign nodules, the model successfully predicted 53 benign nodules, accounting for 82.8%. 11 cases were misdiagnosed, accounting for 17.2%.

TABLE 4: The prediction results of 168 benign and malignant lung nodules by the deep learning algorithm model.

Pathology	Forecast		Total
	Malignant	Benign	
Malignant	96 (TP)	8 (FN)	104 (P)
Benign	11 (FP)	53 (TN)	64 (N)
Total	107	61	168

Note: TP : true positive. FN : false negative. TN : true negative.

### 3.3.2. Comparison between AI's and Doctor's Reading.

The 3D U-net can be moved in all three directions (image height, width, and channels). At each position, element-wise multiplication and addition provide a numerical value. Because the filter slides through a 3D space, the output values are also arranged in 3D space. The improved 3D U-net, the original 3D U-net, and the doctor's sensitivity, specificity, negative likelihood ratio, and positive likelihood ratio for benign and malignant judgments are shown in Table 5. The three sets of data are compared in pairs, and the two artificial intelligence systems have their own advantages and disadvantages in judging the benign and malignant pulmonary nodules. The improved 3D U-net system has high sensitivity, high specificity, and a positive likelihood ratio of the 3D U-net system, and the overall performance of

TABLE 5: Comparison of benign and malignant judgments between the improved 3D U-net, the original 3D U-net, and the physician.

Object	Sensitivity	Specificity	Positive fuel-like ratio	Negative fuel-like ratio
Improved 3D U-net	95.51%97.22–95.46%	34.46%27.86–46.85%	1.211.05–1.39	0.200.10–0.35
3D U-net	91.83%82.70–92.37%	58.69%47.33–66.95%	2.131.47–2.48	0.220.10–0.35
Physician	85.1%76.43–88.67%	70.15%60.22–75.68%	2.812.16–3.64	0.230.10–0.35

the latter is slightly stronger. The positive likelihood ratios of the three were 1.21, 2.13, and 2.81, among which that of radiologists was the highest, but none of the three had a high diagnostic value for benign and malignant pulmonary nodules.

The flammability ratio is the ratio of the mass of air to fuel in the mixture. It is generally expressed in grams of air consumed per gram of fuel when burned. The two artificial intelligence systems are used to judge the benign and malignant pulmonary nodules, and the radiologist draws the ROC curve (Figure 9). The AUC area of the 3D U-net system was 0.583 [ $P = 0.02$  ( $<0.05$ )]. The AUC area of the improved 3D U-net system was 0.729 [ $P = 0.02$  ( $<0.05$ )]. The improved 3D U-net system has certain accuracy in the diagnosis of benign and malignant pulmonary nodules, and its performance is close to that of radiologists. The AUC area of the radiologist group was 0.794 [ $P = 0.01$  ( $<0.05$ )]. The accuracy of manual image reading for the diagnosis of benign and malignant pulmonary nodules was higher than that of the two artificial intelligence systems, but the overall accuracy was average.

**3.3.3. Using ROC Curve to Distinguish Invasive Adenocarcinoma from Noninvasive Lung Cancer.** The ROC curve is used for analysis, and the nodule diameter, CT value, and malignant probability are used as the cutting points for the differential diagnosis of invasive adenocarcinoma and noninvasive tissue (preinvasive lesion/microinvasive adenocarcinoma). They are 11.38 mm,  $-377.2$  HU, and 95%; the corresponding areas under the ROC curve are 0.931, 0.887, and 0.876, and the sensitivities are 87.9%, 79.5%, and 81.6%, respectively. The specificities were 87.5%, 91.4%, and 75.7%, and the accuracy was 88.2%, 85.3%, and 80.8%, respectively (Figure 10). CT value is a measurement unit for measuring the density of a local tissue or organ in the human body, usually called Heinz unit; for air, it is  $-1000$ , and for dense bone, it is  $+1000$ . The cleavage site is a commonly used linking sequence for fusion proteins in genetic engineering expression systems, and the target protein in the fusion protein can be separated from the peptide segments of the nontarget protein by drug treatment.

#### 4. Discussion

In this study, the improved 3D U-net network-assisted diagnosis system detected 674 target nodules, with a detection rate of 100.0% (674/674). Radiologists detected 673 target sections, with a detection rate of 99.9% (673/674). What the radiologist missed was a solid pulmonary nodule located in the basal segment of the right lower lobe, with a diameter of 29 mm and an unclear boundary with the

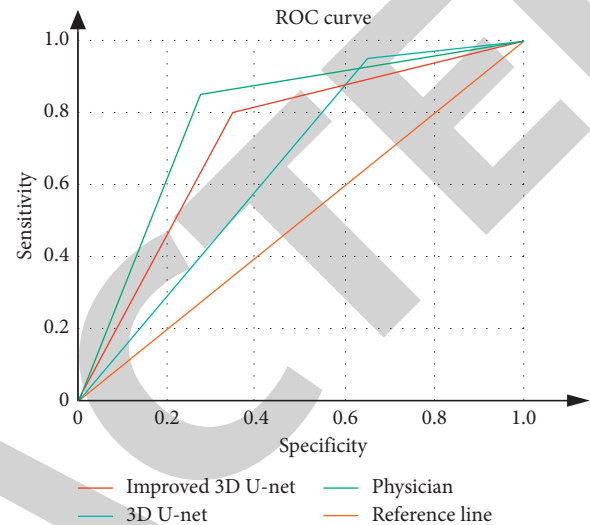


FIGURE 9: ROC curve of artificial intelligence reading and physician reading.

surrounding tissues. If the artificial intelligence system wants to accurately screen out lung nodules and judge their nature, it needs to go through lung parenchymal segmentation, lung nodule detection, lung nodule segmentation, and lung nodule diagnosis—a total of 4 steps. The first 3 steps are responsible for screening and segmenting lung nodules, and the fourth step is to distinguish between benign and malignant lung nodules. Any failure in any of the first 3 steps will result in missed or false detection of lung nodules. When artificial intelligence extracts nodules, compared with isolated solid nodules, the extraction of adhesion pleural nodules and adhesion vascular nodules is more difficult. Pulmonary nodules adhere to the pleura, blood vessels, and other tissues, and their CT values are similar to those of surrounding tissues, which brings great interference to the extraction of the nodules.

In this study, the improved 3D U-net system's, the original 3D U-net system's, and the physician's sensitivity in judging benign and malignant lung nodules was 95.51%, 91.83%, and 85.1%, respectively. The specificities were 34.46%, 58.69%, and 70.15%, respectively. The positive likelihood ratios were 1.21, 2.13, and 2.81, respectively. The negative likelihood ratios were 0.20, 0.22, and 0.23, respectively. The positive likelihood ratios of the three are less than 10, which is of low value. Comparing the two artificial intelligence systems, the improved 3D U-net system has higher diagnostic sensitivity and poorer specificity than the 3D U-net system. Both artificial intelligence systems are based on the use scenarios of the 3D-CNN system to screen for lung nodules. It is designed to detect lung nodules; the

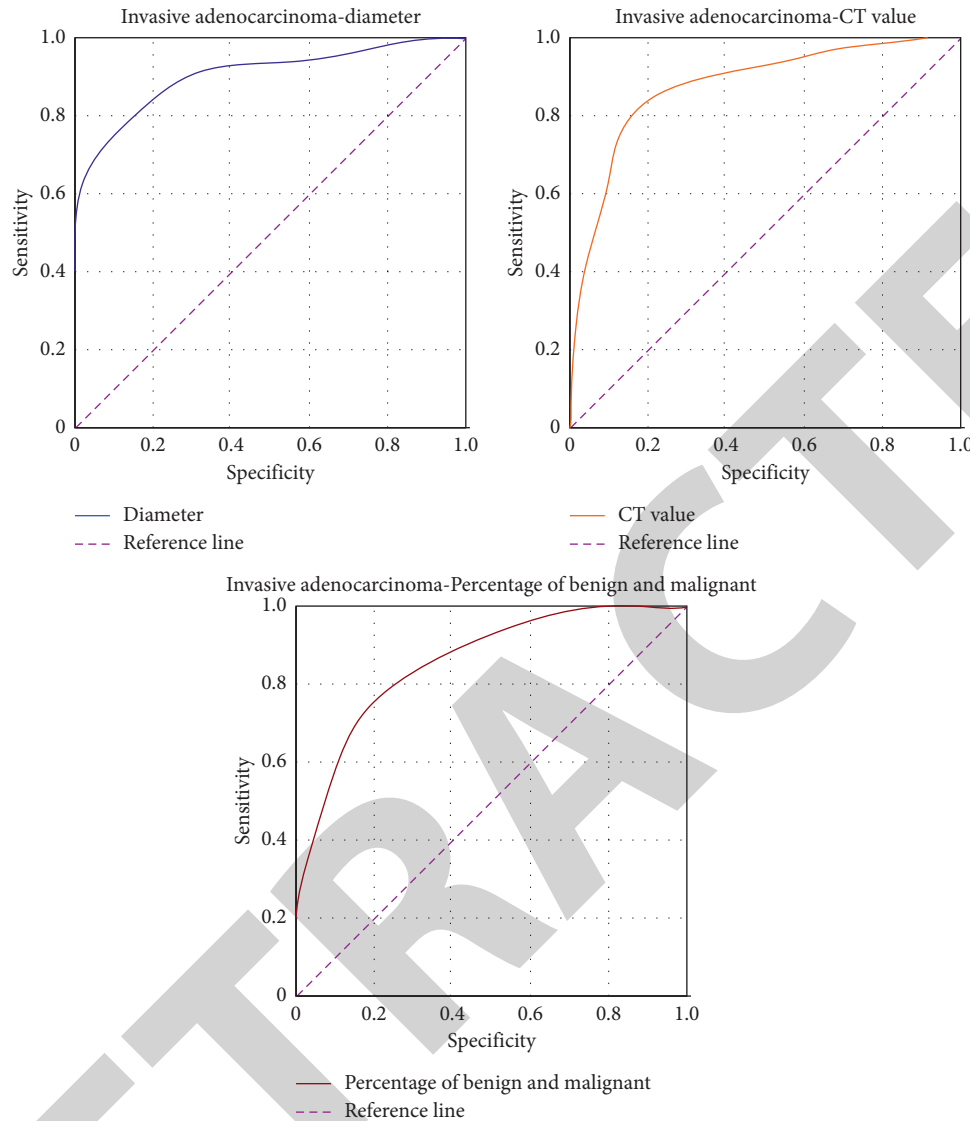


FIGURE 10: ROC curve of diameter, CT value, and malignant probability.

algorithm is optimized for sensitivity, resulting in low specificity, and the ability to cut lung nodules is stronger. The improved algorithm has changed with respect to the optimization direction, so its performance is different. Comparing the two artificial intelligence systems to radiologists, the sensitivity of judging the nature of pulmonary nodules is higher than that of radiologists. In terms of specificity, radiologists lead.

The AUC areas for judging benign and malignant pulmonary nodules are 0.583 AUC area of the original 3D U-net system and 0.729 AUC area of the improved 3D U-net system. The AUC area of the radiologist group was 0.794. The original 3D U-net system has low accuracy in judging benign and malignant pulmonary nodules. The improved 3D U-net system and radiologists have certain accuracy in judging benign and malignant pulmonary nodules. The use of the CNN helps improve the accuracy

of CT volume measurement and nodule differentiation in patients with lung nodules in computer-aided detection. At this stage, artificial intelligence shows good performance in judging benign and malignant pulmonary nodules and has a very promising application prospect.

The intelligent diagnosis system based on the improved 3D U-net network can automatically detect lung nodules through automatic segmentation of lesions, automatic measurement of quantitative and qualitative parameters, judgment of nodule types, automatic analysis of benign and malignant nodules, etc. This experiment detected 674 cases of pathological lung nodules. The results showed that mixed ground glass nodules and pure ground glass nodules were more common in adenocarcinoma and only solid nodules were seen in squamous cell carcinoma. The accuracy of distinguishing and diagnosing invasive adenocarcinoma and

noninvasive adenocarcinoma in groups was based on the standard diameter of the nodule, CT value, and “malignant probability,” which were 88.2%, 85.3%, and 80.8%, respectively.

There are many shortcomings in this study: because it is impossible to obtain the pathological results of all nodules, the gold standard for judging the true and false of nodules in this study was confirmed by three senior chest CT diagnostic physicians after reading the pictures. The comparative analysis with the artificial intelligence system is carried out by two intermediate-level doctors, and there may be more human errors. The detection method of pulmonary nodules is closely related to their density, location, and shape. The analysis of the detection efficiency of this study only considers the density of nodules, and the influence of factors such as the location of nodules is not included in the scope of the study; further experimental studies are needed in the future. It is believed that as the deep learning research driven by big data continues to deepen, new signs are constantly being explored, and new algorithms are constantly being developed; the auxiliary diagnosis value of artificial intelligence auxiliary diagnosis systems will definitely achieve satisfactory results.

## 5. Conclusion

This paper improves the convolutional neural network model on the original basis and applies it to the diagnosis of benign and malignant lung nodules to assist in the diagnosis of lung cancer. In experiments on a large number of samples, it is verified that the improved model used in this study reduces the complexity of the algorithm while increasing the overall lung nodule detection rate and reducing the misdiagnosis rate. It proves that the artificial intelligence-assisted diagnosis system can help clinicians screen and diagnose patients, improve work efficiency, and reduce workload. In this study, a 3D U-net model obtained by fusion of the convolutional neural network (CNN) and the long short-term memory (LSTM) recurrent neural network (RNN) was used. Compared with the single-modal learning method that scholars of comparative research only use CT images, this method can enable the network model to learn more subtle features. The accuracy of this model for predicting malignant pulmonary nodules can reach 92.3%, and the accuracy of predicting benign pulmonary nodules can reach 82.8%, which prove that the system is feasible and effective. Based on the prediction model designed in this paper, it can play a very important role in the diagnosis of lung cancer, and it can also indirectly improve the treatment of lung cancer in the future.

## Data Availability

No data were used to support this study.

## Conflicts of Interest

The author declares that there are no conflicts of interest with any financial organizations regarding the material reported in this article.

## References

- [1] S. Zheng, J. Guo, X. Cui, R. N. J. Veldhuis, M. Oudkerk, and P. M. A. van Ooijen, “Automatic pulmonary nodule detection in CT scans using convolutional neural networks based on maximum intensity projection,” *IEEE Transactions on Medical Imaging*, vol. 39, no. 3, pp. 797–805, 2020.
- [2] H. J. de Koning, C. M. van der Aalst, P. A. de Jong et al., “Reduced lung-cancer mortality with volume CT screening in a randomized trial,” *New England Journal of Medicine*, vol. 382, no. 6, pp. 503–513, 2020.
- [3] D. Zhao, N. Y. Che, Z. G. Song et al., “Pathological diagnosis of lung cancer based on deep transfer learning,” *Zhonghua bing li xue za zhi Chinese journal of pathology*, vol. 49, no. 11, pp. 1120–1125, 2020.
- [4] L. Jae-Hong, K. Do-Hyung, J. Seong-Nyum, and C. Seong-Ho, “Diagnosis and prediction of periodontally compromised teeth using a deep learning-based convolutional neural network algorithm,” *Journal of Periodontal & Implant Science*, vol. 48, no. 2, pp. 114–123, 2018.
- [5] Y. Wang, F. Yang, J. Zhang, H. Wang, X. Yue, and S. Liu, “Application of artificial intelligence based on deep learning in breast cancer screening and imaging diagnosis,” *Neural Computing & Applications*, vol. 33, no. 15, pp. 9637–9647, 2021.
- [6] X. H. Zhu, X. M. Li, W. L. Zhang et al., “Application of artificial intelligence-assisted diagnosis for cervical liquid-based thin-layer cytology,” *Zhonghua bing li xue za zhi Chinese journal of pathology*, vol. 50, no. 4, pp. 333–338, 2021.
- [7] K. Guo, S. Ren, M. Z. A. Bhuiyan et al., “MDMAAS: medical-assisted diagnosis model as a service with artificial intelligence and trust,” *IEEE Transactions on Industrial Informatics*, vol. 16, no. 3, pp. 2102–2114, 2020.
- [8] R. L. Siegel, K. D. Miller, and A. Jemal, “Cancer statistics, 2019,” *CA: A Cancer Journal for Clinicians*, vol. 69, no. 1, pp. 7–34, 2019.
- [9] M. Alruwaili, A. Shehab, and S. Abd El-Ghany, “COVID-19 diagnosis using an enhanced inception-ResNetV2 deep learning model in CXR images,” *Journal of Healthcare Engineering*, vol. 2021, no. 4, pp. 1–16, 2021.
- [10] L. Cong, W. Feng, Z. Yao, X. Zhou, and W. Xiao, “Deep learning model as a new trend in computer-aided diagnosis of tumor pathology for lung cancer,” *Journal of Cancer*, vol. 11, no. 12, pp. 3615–3622, 2020.
- [11] S. A. Agnes and J. Anitha, “Appraisal of deep-learning techniques on computer-aided lung cancer diagnosis with computed tomography screening,” *Journal of Medical Physics*, vol. 45, no. 2, pp. 98–106, 2020.
- [12] M. Elhoseny, G. Ramirez-Gonzalez, O. M. Abu-Elnasr, S. A. Shawkat, N. Arunkumar, and A. Farouk, “Secure medical data transmission model for IoT-based healthcare systems,” *Ieee Access*, vol. 6, Article ID 20596, 2018.
- [13] M. Abdolmaleky, M. Naseri, J. Batle, A. Farouk, and L.-H. Gong, “Red-Green-Blue multi-channel quantum representation of digital images,” *Optik*, vol. 128, pp. 121–132, 2017.
- [14] P. P. Massion, S. Antic, S. Ather et al., “Assessing the accuracy of a deep learning method to risk stratify indeterminate pulmonary nodules,” *American Journal of Respiratory and Critical Care Medicine*, vol. 202, no. 2, pp. 241–249, 2020.
- [15] N. Murty and M. Babu, “A critical study of classification algorithms for LungCancer disease detection and diagnosis,” *International Journal of Computational Intelligence Research*, vol. 13, no. 3, pp. 1041–1048, 2017.

## *Retraction*

# **Retracted: The Role of Three-Dimensional Reconstruction of Medical Images and Virtual Reality in Nursing Experimental Teaching**

### **Journal of Healthcare Engineering**

Received 16 November 2022; Accepted 16 November 2022; Published 23 January 2023

Copyright © 2023 Journal of Healthcare Engineering. This is an open access article distributed under the Creative Commons Attribution License, which permits unrestricted use, distribution, and reproduction in any medium, provided the original work is properly cited.

*Journal of Healthcare Engineering* has retracted the article titled “The Role of Three-Dimensional Reconstruction of Medical Images and Virtual Reality in Nursing Experimental Teaching” [1] due to concerns that the peer review process has been compromised.

Following an investigation conducted by the Hindawi Research Integrity team [2], significant concerns were identified with the peer reviewers assigned to this article; the investigation has concluded that the peer review process was compromised. We therefore can no longer trust the peer review process, and the article is being retracted with the agreement of the Chief Editor.

### **References**

- [1] M. Zhu, C. Li, S. Zhao, L. Chen, and X. Zhao, “The Role of Three-Dimensional Reconstruction of Medical Images and Virtual Reality in Nursing Experimental Teaching,” *Journal of Healthcare Engineering*, vol. 2022, Article ID 3853193, 13 pages, 2022.
- [2] L. Ferguson, “Advancing Research Integrity Collaboratively and with Vigour,” 2022, <https://www.hindawi.com/post/advancing-research-integrity-collaboratively-and-vigour/>.

## Research Article

# The Role of Three-Dimensional Reconstruction of Medical Images and Virtual Reality in Nursing Experimental Teaching

Min Zhu,<sup>1</sup> Chunhui Li,<sup>2</sup> Shuangping Zhao,<sup>3</sup> Liang Chen <sup>4</sup> and Xueping Zhao <sup>2</sup>

<sup>1</sup>Anhui Vocational College of City Management, Hefei 230011, Anhui, China

<sup>2</sup>School of Nursing, Medical College of Soochow University, Suzhou 215006, Jiangsu, China

<sup>3</sup>The First Affiliated Hospital of Soochow University, Suzhou 215006, Jiangsu, China

<sup>4</sup>School of Mechanical and Electric Engineering, Soochow University, Suzhou 215021, Jiangsu, China

Correspondence should be addressed to Xueping Zhao; zxp@suda.edu.cn

Received 16 November 2021; Accepted 12 January 2022; Published 8 March 2022

Academic Editor: Yang Gao

Copyright © 2022 Min Zhu et al. This is an open access article distributed under the Creative Commons Attribution License, which permits unrestricted use, distribution, and reproduction in any medium, provided the original work is properly cited.

With the continuous advancement of medicine and computer science, medical image processing technology is also constantly advancing, and at the same time, it puts forward the needs of its own development. The purpose of this article is to combine the three-dimensional reconstruction of medical images and virtual reality (VR) technology in nursing experiment teaching to help students understand more easily and to simplify the teachers' teaching process and make the VR application technology. It is the most popular and effective in medical teaching. This article proposes the C-V model and the geometric active contour model to help us more clearly understand the pathology in this environment, where the specific symptoms appear, and bring a more easy-to-understand model for teaching and improving teaching quality. This article also designs nursing experiment teaching. The experimental results of this paper show that, after using VR courseware for teaching, the optimal test rate of the experimental class is 15% higher than that of the control class, and the transition rate is 8%. The actual test excellent rate and success rate of the experimental class are much higher than those of the control class. Therefore, it can be concluded that the application of VR technology in nursing teaching helps teachers improve their practical ability. The excellent teaching feedback rate is 95%, which is higher than 80.5% in the control group, indicating that the patient teaching simulation is approved by the observation group. The program can effectively improve the feedback rate of excellent teaching and provide students with better teaching services.

## 1. Introduction

**1.1. Background.** The Internet, also known as the international network, refers to the huge network connected between the network and the network. These networks are connected by a set of common protocols to form a logically single huge international network. With the development of computer graphics technology, imaging technology, human-computer interaction technology, electronic vision, and other disciplines, VR technology was born on the basis of the increasing intersection of disciplines. It has the characteristics of immersion, realism, and interactivity and significantly improves human interaction, the ability of information interaction between people. With the help of two-dimensional medical image sequences, imaging

technicians can observe the location of lesions. If the characteristic information of the image is too little, the relevant biological information is difficult to determine the indication. It usually needs to be based on the doctor's work experience. Obviously, two-dimensional medical images are difficult to fully reflect three-dimensional objects, and it is difficult to determine the spatial distribution relationship of human tissues and organs. Therefore, the two-dimensional images are imaged by medical image analysis technology. After segmentation, recognition, and imaging, the image can form a three-dimensional model, which will be more convenient for doctors to find relevant indications and improve the certainty and reliability of diagnosis. The three-dimensional visualization of medical images through VR technology, and the combination of three-dimensional

visualization technology and VR, not only can obtain volume data, but also, more importantly, can create a virtual environment, which can help us in nursing teaching to help students reduce some errors in practical operations. It can also increase the effect of teaching and help us to be more stable and effective in medical teaching.

*1.2. Significance.* VR plays a very important role in medicine. Based on the three-dimensional reconstruction of medical images, VR technology can be effectively used in situations such as auxiliary disease judgment, virtual surgery, and medical simulation demonstrations. The use of VR technology to assist disease judgment can help determine and quantify the disease, and provide correct and intuitive diagnosis and treatment plans based on the doctor's experience, avoiding misdiagnosis that may be caused by traditional medical diagnosis. Surgical plan involves choosing the best surgical approach, avoiding potential problems during the operation, and increasing the success rate of the operation; the virtual surgical system can be used for teaching and simulation exercises at the same time, and students can operate the virtual human model intuitively and concretely. It has high superiority and repeatability and can reduce the tension of the hands and feet during the first operation. In summary, the medical image processing system with the help of VR can play an important auxiliary role in medical teaching, virtual surgery, and various medical research teaching. The application of VR technology in the experimental training of nursing specialty is conducive to improving students' clinical adaptability, comprehensive skills, and practical ability. Through the integration of training content, the lung examination skills are integrated or integrated into the health assessment, the treatment of chronic obstructive pulmonary disease and other medical diseases, and the basic nursing skills such as oxygen inhalation and oxygen inhalation. On the one hand, it can strengthen the functions and skills of students' basic nursing technology application; on the other hand, it can cultivate students' ability to analyze, summarize, and judge problems and comprehensive clinical skills.

*1.3. Related Work.* After reading a lot of related literature, the authors found that there are many research studies on the combination of 3D reconstruction of medical images and virtual reality, but their research is not very comprehensive. Just like in Chen SH et al.'s study, their team proposed the dislocation and destruction of three-dimensional images of nerve fibers, blood vessels, and lesions in 35 patients. The anatomical relationship between ligaments and tumors and important fiber bundles, arteries, and veins was clearly identified, and virtual operation simulations and surgical plans for 35 patients were successfully completed. The 3D images obtained from VR are close to real surgery. The research in this article provides us with the best individualized surgical methods that help to design the best, which in turn can improve the outcome of the surgery. However, there are still many problems in the article, and the technology is not mature enough [1]. In the Department of

Neurosurgery's research, the team discussed the basic knowledge, reconstruction technology, practicability, and limitations of three-dimensional (3D) fusion imaging methods. Reconstructing standard 3D images by relatively simple processing of a kind of image data is widely used and has excellent spatial information and construction simplicity. However, due to the relatively low resolution of anatomical information, this information is not sufficient for preoperative simulation [2]. In Ruiz-Moya A et al.'s literature, the team believe that if CT angiography (CTA) can be (3D) virtual reconstruction, it will be better used for breast planning and reconstruction of deep inferior epigastric artery perforator (DIEP). Although the operation is likely to produce diffuse venous congestion, scientists have not found its mechanism [3]. In Mou et al.'s research, the team collected relevant information by investigating patients, through literature review, consulting professionals, organizing case discussion, consulting relevant literature, and establishing the damage assessment model according to relevant data. The results showed that there were significant differences in the microvessel structure of SPN with different stages and properties. With the help of intelligent medical VR image system, it can be seen that the correlation between DDPCR and vascular parameters (especially the lumen vascular ratio) is good compared with other detection methods, and the accuracy is improved by about 10%. Their accuracy has improved, but the system structure in the article in their experiment is not optimized enough and is a bit complicated [4]. According to Zhou Rui et al.'s research, the biomechanical properties of the blood vessel wall during virtual reality (VR)-assisted percutaneous transluminal angioplasty (PTA) and its effect on lower extremity arteriosclerosis obliterans (LEAO) are well matched. The results show that a normal and narrow blood vessel and blood model have been successfully constructed; compared with normal blood vessels, if the pressure of the blood vessel at stenosis is greatly reduced, the blood vessel wall will bear greater stress, and the blood return area can be formed in the poststenosis stage. However, there is still such a problem in their research that the experimental technology is not mature enough [5]. In the research of Rozin, the author put forward the reasons that prevented Schedrovitsky and members of the Moscow methodology circle from understanding the essence of thinking, abandoning the interpretation of the world view as an activity, and turning to the development of the theory of mental activity. VR is combined with the role of psychology in the real scene. However, the research is a bit too theoretical, and no technology is used to explain the study [6]. In Kerrebroeck et al.'s research, the team proposed that mobile VR provides marketers with innovative ways to reach consumers. This research examines the impact of VR in the context of transforming brand experience demands. This research is of great practical value, but their system structure is not complete yet, and further research is needed [7]. In the research of Yubao et al., they put forward the successful application of virtual simulation technology in experimental and practical teaching processes and also mentioned new research directions, which can point out the direction for experimental teaching workers.

The new research results provide additional technical support and guarantee for the training of qualified college students. However, there are many problems in the current experimental teaching and practical teaching processes. The structure of medical images is complex, and it is difficult for students to understand their structure and working principle [8]. Most of the above documents are about medical imaging, three-dimensional reconstruction, and virtual reality. Although they do not combine the three, they still have certain reference value and need to be explored in this article.

**1.4. Innovation.** This article studies the establishment of observable three-dimensional models to improve breakthroughs in medical education, so that they can better benefit society. Nursing practice teaching is the most important link to improve the quality of teaching. Because traditional nursing practice teaching cannot use technology to be contextualized and be in real time, and also lacks variable factors, the experimental model is easily damaged and the simulated environment is not realistic enough. There are relatively few experiments, and the initial operation training is not suitable for direct use on the human body. It is imperative to reform practical teaching. Virtual experimental teaching can not only meet the three-dimensional requirements of visual knowledge learning but also change the ratio of traditional experimental instruments to the low number of students. In addition to the high cost of laboratory construction, maintenance, and transformation, VR technology is basically mature, and it is completely feasible to establish a virtual laboratory. It is currently widely used in developed countries and has become the development direction of international nursing practice teaching and has gradually been recognized by domestic medical education. This research combines basic training and clinical practice to try to establish a new training framework for experimental teaching of nursing, in order to improve the quality of practical teaching. Combining the three-dimensional reconstruction of medical images and VR technology in nursing teaching can help students understand the teaching more easily, and it can also help them truly master these technologies more vividly. It can also reduce the errors that will be caused during the actual operation.

## 2. Introduction of Technical Methods

**2.1. Three-Dimensional Reconstruction of Medical Images.** Medical three-dimensional reconstruction refers to the establishment of a mathematical model suitable for computer representation and processing of three-dimensional objects. It is the basis for processing, operating, and analyzing its properties in a computer environment. It is also a key technology for establishing virtual reality that expresses the objective world in a computer. Medical image processing and analysis is a technology developed on the basis of graphics and computer medicine. It can help medical staff conduct research, diagnosis, and treatment. The cross-sectional image is converted into a format that can be processed

by the computer. The image of the region of interest is preprocessed by two-dimensional filtering and image processing and interpretation techniques to obtain human body data; the image is preprocessed to complete the fragmentation of different tissues and organs. Sorting and registration and fusion of the same slice images produced by different devices in different time periods are done to further realize the region of interest; finally, 3D reconstruction is performed to restore the 3D model of the object. For example, vision VTK and ITK are the two most popular algorithm platforms. VTK is an open-source vision algorithm platform based on OpenGL for application data. It adopts object-oriented design concepts for design and implementation research and development, which incorporates some commonly used algorithms and visual applications. The relevant details are placed in the background. With powerful functions, strong compatibility, and support for platform development, ITK is a platform that supports both open-source platform and cross-platform and mainly provides medical image segmentation and registration algorithms, which can be used for general research and development. All medical image segmentation and registration algorithms are in ITK, and the research and development of medical images has almost begun, such as the VolView system developed based on VTK and ITK. Although they are the most common medical image processing and analysis platforms, they have their own limitations due to various initial stages. For example, when VTK was born, it was defined in the field of general visualization in the field of medical imaging. The goal is to reduce the cost that is very important for the user without optimizing a specific algorithm. It is also difficult to design a good platform, such as VolView, which is very limited depending on its development. This can increase the intuitiveness of medicine, help doctors make better judgments, and reduce doctor's misjudgments of patient's pain and the inability to explain this, leading to missing the best time for treatment, and at the same time, this also has an impact on education. The huge role can help us in this experimental study to reduce the risk of nurses just starting to operate. Medical three-dimensional reconstruction is involved in various image fields, which helps us greatly in image extraction and analysis. The medical imaging process is shown in Figure 1.

**2.2. VR Technology.** VR technology is a new intelligent interactive teaching method developed in recent years. It can truly simulate the characteristics of multiple perception, interaction, and autonomy in the natural environment and realize the combination of text, text, and text in VR technologies such as anatomy, radiology, and endoscopy. In this study, VR technology was applied to the holistic first aid experiment of comprehensive nursing skills to evaluate the application of VR technology in nursing experiment teaching. VR technology is a new type of intelligent interactive education method developed in recent years, which has the advantages of repeatability and versatility. The nursing experiment teaching training framework is shown in Figure 2. The figure shows how students conduct

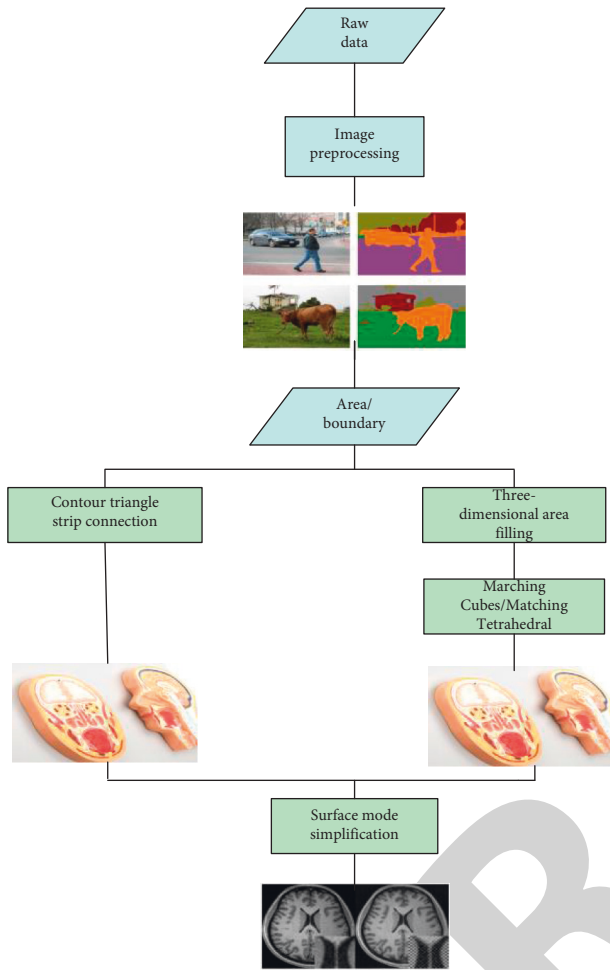


FIGURE 1: Medical 3D reconstruction process.

experiments and how to improve their knowledge reserves, including how to inject patients and how to resuscitate a patient's heart. During this time, to improve oneself, it has specific learning methods and steps [9]. The visualization of scientific computing is a technology for the intuitive display of data, which aims to use the principles and methods of computer graphics or general graphics to convert large-scale data generated by scientific and engineering calculations into graphics and images [10]. It is the focus of computer graphics research, involving multidisciplinary fields such as computer graphics, image processing, computer vision, computer-aided design, and graphical user interface. Various applied studies have shown that the introduction of VR technology into medical teaching can effectively express educational content, effectively create a real educational environment, improve the effectiveness of teachers' knowledge and skills, and make it easier for teachers to express teaching ideas and content. It can also make learners more intuitively and easily understand the ideas and content of teaching, as a teaching method, to provide instinctive and intuitive thinking materials in a direct way of transmitting information. VR can be summarized as follows: VR medical teaching is the use of VR software development tools to reproduce the abstract and practical content of medical

teaching in the VR system. The VR desktop technology is applied in medical teaching. The VR teaching system provides real-time feedback information through information exchange between the teacher and the learning content in the VR teaching system. The operation of the teacher object in the virtual environment promotes student learning and teaching content understanding and knowledge.

**2.3. Geometric Active Contour Model.** Image segmentation and boundary extraction are very important for image understanding, image analysis, pattern recognition, computer vision, etc., while the active contour model is one of the important tools for image segmentation and boundary extraction [11]. It mainly includes the parameter active contour model and geometric active contour model. A curve with an irregular motion state can be represented by two parameters. The geometric active contour model is developed based on the curve evolution theory, which makes the curve move to the edge of the object under the action of the two geometric parameters of normal vector and curvature. When the curve approaches or coincides with the edge of the object, the image segmentation is realized. Assuming that the unit vector of the curve is the unit tangent direction vector of the  $r$  curve, the movement of the  $g$  curve can be described by the movement of each point on the curve in the direction of  $r$  and  $k$ , and then the evolution process of the contour curve  $c(s, t)$  can be described as in formula (1) [12]. The C-V model is an active contour model based on the simplified Mumford–Shah model. It uses the level set idea to have evolve the curve by minimizing the energy function:

$$\frac{VC}{Vt} = \alpha r + \beta g, \quad (1)$$

where  $t$  is the time,  $V$  represents the rate of change of the curve along the tangent direction, and  $\beta$  represents the rate of change of the curve in the normal direction. At the actual rate of change, only the change in the normal vector needs to be considered. Changing the tangent direction will not affect the relatively large motion state of the curve. The above formula can be simplified to

$$\frac{vc}{vt} = v(n) \cdot g, \quad (2)$$

where  $v(n)$  is the rate of change of the curve, which is affected by the rate. A simple contour curve is shown in Figure 3.

On a two-dimensional plane, one can use the function  $y=f(x)$  to express the curve, that is, when the two of them are equal, let the function

$$\phi(x) = y - f(x). \quad (3)$$

We call  $\phi(x) = 0$  the implicit function of the curve. A closed curve can divide a two-dimensional plane into two parts. The part of  $\phi(x) > 0$  is inside the curve, and the part of  $\phi(x) < 0$  is outside the curve, while  $\phi(x) = 0$  represents the contour curve itself, as shown in Figure 4.

As time  $t$  changes, this set of levels continues to evolve repeatedly, as shown in Figure 4. There are three processes from left to right. The blue level in the figure is the sum of the

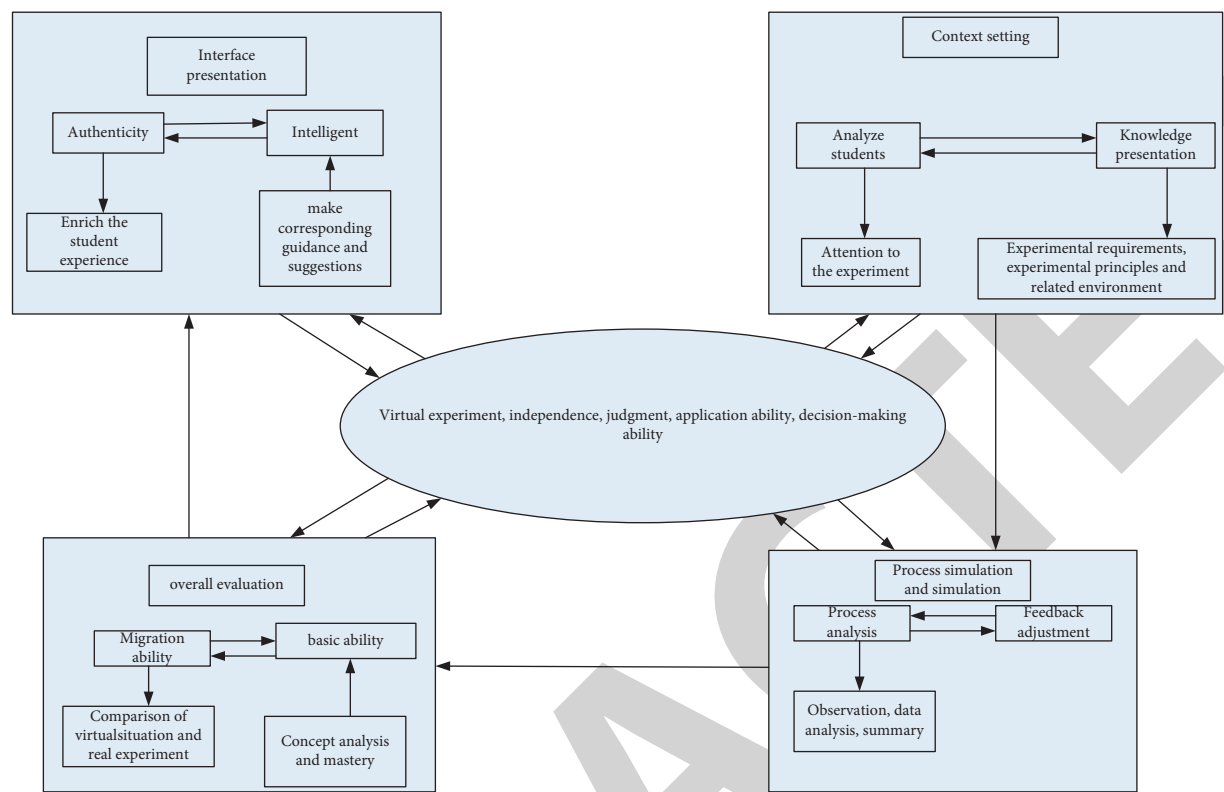


FIGURE 2: Nursing experimental teaching training framework.

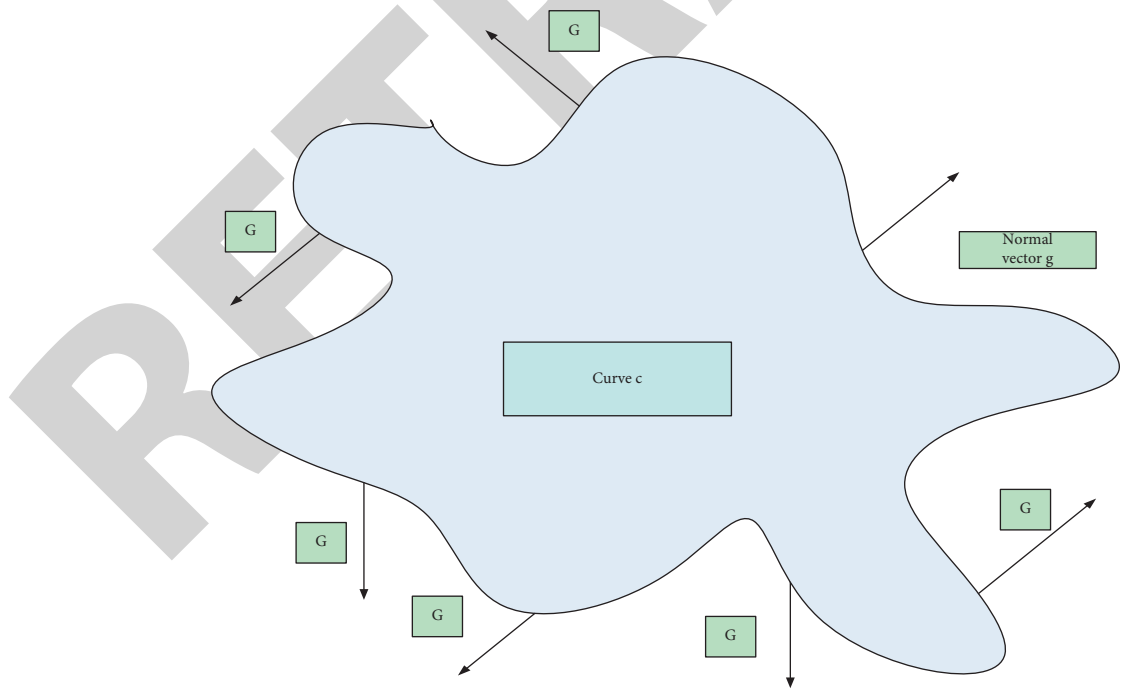


FIGURE 3: Schematic diagram of curve movement.

zero level. With the continuous movement of the lowered zero level, the interface between it and the three-dimensional surface is a contour line, that is, a gray pattern from top to bottom. As the curve evolves, it is continuously divided into

two parts to simulate the continuous change process of the curve or surface to realize the change of the curve topology [13]. The level adjustment method cleverly changes the evolution process of the curve relative to the high-

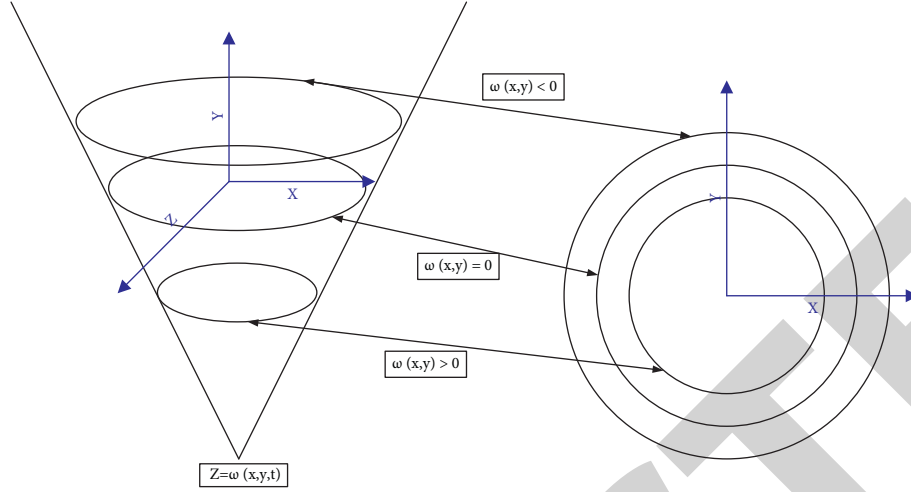


FIGURE 4: Schematic diagram of the level set method.

dimensional space. In the repeated update process, the curve  $C(s, t)$  is represented by the level function set:

$$\omega(c(s, t), t) = 0, \quad (4)$$

where  $s$  is the curve parameter and  $t$  is the time.

Since the change of the tangent direction has no effect on the shape of the curve, the above formula can be simplified as

$$\omega(c(t), t) = 0. \quad (5)$$

Derivatives on both sides of the above equation at the same time can be obtained:

$$\begin{aligned} \frac{\delta\phi(c(t), t)}{\delta t} &= \frac{\delta\phi(x(t), y(t), t)}{\delta t} \\ &= \nabla\phi \frac{\delta c}{\delta t} + \frac{\delta\phi}{\delta t} \\ &= 0. \end{aligned} \quad (6)$$

In the above formula, CC is the gradient of CC. From the definition of the level set, we can know that the normal direction of CC and the curve is the same, so they have a unit vector [14]:

$$g = \frac{\nabla\delta}{|\nabla\delta|}. \quad (7)$$

Combining equations (6) and (7), we can get the differential equation:

$$\frac{\delta\phi}{\delta t} + v(n)|\nabla\phi| = 0, \quad (8)$$

where  $v(n)$  depends on  $n$ , and the curvature  $n$  can be calculated by the following formula:

$$\begin{aligned} n &= \text{div}\left(\frac{\nabla\delta}{|\nabla\delta|}\right) \\ &= \frac{\delta_{xy}\delta_y^2 - 2\delta_x\delta_y\delta_{xy} + \delta_{xy}\delta_x^2}{(\delta_x^2 + \delta_y^2)^{3/2}}. \end{aligned} \quad (9)$$

The flow chart of the horizontal image segmentation method is shown in Figure 5.

It is easy to calculate without considering various parameters of contour operation. We only need to use Euler's method to calculate the specified area, which can simplify the entire calculation process. In mathematics and computer science, Euler's method, named after its inventor Leonhard Euler, is a first-order numerical method for solving ordinary differential equations with given initial values. It is the most basic type of explicit method for solving numerical ordinary differential equations. Compared with the parameterized processing of the contour function, the illusion of the curve is closer to the limit. By simulating the evolution of the curve, including each inflection point and sharp point, it can be handled well, so that we can correlate them through the medical image. The dimensionality reduction processing is given in [15]. The C-V model is a model that is widely used in image processing. It builds a model based on the level set equation and constructs an energy function.

**2.4. C-V Model.** Chan and Vese proposed a new active contour model in 2001, based on the simplified Mumford-Shah model, using the level set idea, to have evolve the curve by minimizing the energy function. The previous methods are based on image edge segmentation. They mainly rely on the edge information of the image. At the same time, this method relies too much on the gradient information of the image. When the edge information of the image is poor or the gradient information is not obvious, the segmentation effect of the method is not so ideal. The curve will often pass through the edge and cause the segmentation to fail. Therefore, the method of splitting each region appears. The C-V model is simplified by the M-S model. The M-S model uses smooth trajectory-based operations to describe areas with fixed gray values and uses the association of short smooth curves to describe areas with strong gray neuroticism and uses one to describe similar areas and boundaries:

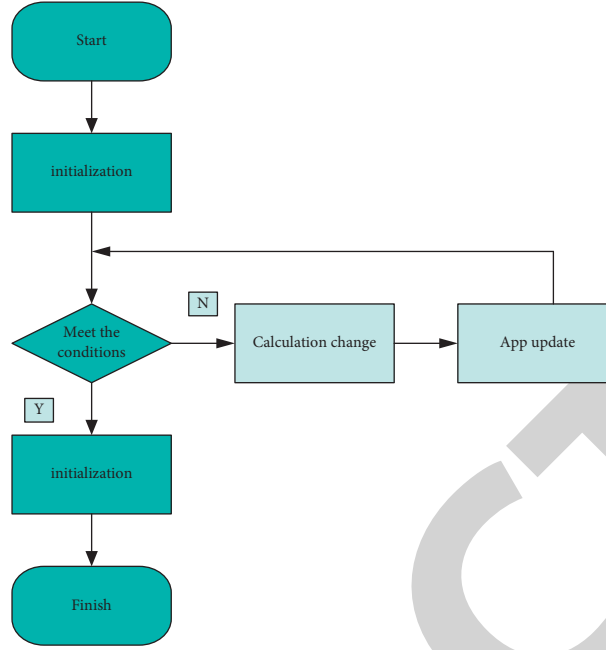


FIGURE 5: Flow chart of the level set segmentation method.

$$F(u, c) = \lambda \iint_{\Omega} |u_0(x, y) - u(x, y)|^2 dx dy + \nu \iint_{\Omega/c} |\nabla u|^2 dx dy + \mu |c|, \quad (10)$$

where  $u$  is the approximate image of  $u_0$ ,  $F$  is the slice smooth function,  $c$  is the set of curves, the absolute value of  $c$  is the length of the curve, and  $\mu, \nu, \lambda$  are the parameters.

The C-V model is to change this function to a constant function  $u$ , the intermediate target medical image is  $\Omega$ , the

target area is divided into two parts  $\Omega_1$  and  $\Omega_2$ , and their common gray value is similar, assuming the gray value of each part. The mean values are  $L_1$  and  $L_2$ , so that we can get

$$u(x, y) = \begin{cases} L_1, & \text{if } (x, y) \in \Omega_1, \\ L_2, & \text{if } (x, y) \in \Omega_2. \end{cases} \quad (11)$$

At this time, when we add the area calculation, we can get the following formula:

$$\begin{aligned} F_{lv}(u, c) &= \lambda \iint_{\Omega} |u_0(x, y) - u(x, y)|^2 dx dy + \mu \cdot \text{length}(c) + \nu \cdot \text{ar}(\text{inside}(c)) \\ &= \lambda \iint_{\Omega_1} |u_0(x, y) - L_1|^2 dx dy + \lambda \iint_{\Omega_2} |u_0(x, y) - L_2|^2 dx dy + \mu \cdot \text{length}(c) + \nu \cdot \text{ar}(\Omega_1). \end{aligned} \quad (12)$$

The  $\mu, \lambda_1, \lambda_2$  between them are parameters, and length and ar describe the length and area of the curve. The level set method is a numerical technique for interface tracking and

shape modeling. Assuming that the level set is passed, we can get the following energy function:

$$F_{cv}(l_1, l_2, \vartheta) = \lambda_1 \int_{\vartheta > 0} |u_0(x, y) - l_1|^2 dx dy + \lambda_2 \int_{\vartheta < 0} |u_0(x, y) - l_2|^2 dx dy + \mu \cdot \text{length}\{\vartheta(x, y) = 0\} + \nu \cdot \text{ar}(\vartheta(x, y) \geq 0). \quad (13)$$

In order to define the function  $h$  and dir function,

$$H(x) = \begin{cases} 1, & \text{if } x \geq 0, \\ 0, & \text{if } x < 0. \end{cases} \quad (14)$$

Then, the coefficients of the energy function are

$$\begin{aligned} |c|_{\text{length}\{\vartheta = 0\}} &= \int_{\Omega} |\nabla h(\vartheta(x, y))| dx dy \\ &= \int_{\Omega} \delta(\vartheta(x, y)) |\nabla(\vartheta(x, y))| dx dy, \\ \text{ar}(\text{inside}(c)) &= \text{ar}(\vartheta \geq 0) \\ &= \int_{\Omega} h(\vartheta(x, y)) dx dy, \\ \int_{\vartheta \geq 0} |u_0(x, y) - l_1|^2 dx dy &= \int_{\Omega} |u_0(x, y) - l_1|^2 h(\vartheta(x, y)) dx dy, \\ \int_{\vartheta < 0} |u_0(x, y) - l_2|^2 dx dy &= \int_{\Omega} |u_0(x, y) - l_2|^2 [1 - h(\vartheta(x, y))] dx dy. \end{aligned} \quad (15)$$

$L_1$  and  $L_2$  can be calculated by the following formulas:

$$\begin{aligned} L_1 &= \frac{\int_{\Omega} u_0 h(\vartheta) dx dy}{\int_{\Omega} h(\vartheta) dx dy}, \\ L_2 &= \frac{\int_{\Omega} u_0 [1 - h(\vartheta)] dx dy}{\int_{\Omega} [1 - h(\vartheta)] dx dy}. \end{aligned} \quad (16)$$

After we add the time variable, we can get the initial curve profile when  $t = 0$ , whose formula is

$$\frac{\delta \vartheta}{\delta t} = \delta_{\sigma}(\vartheta) \left\{ -\lambda_1 (u_0 - l_1)^2 + \lambda_2 (u_0 - c_2)^2 + \mu \text{div} \left( \frac{\nabla \vartheta}{|\nabla \vartheta|} \right) - \nu \right\}. \quad (17)$$

Finally, we obtain the segmentation result of the C-V model by calculating the convergence.

The RC algorithm is an earlier encryption algorithm with mature technology. In the symmetric encryption algorithm, the data sender processes the plaintext and the encryption key together with a special encryption algorithm to make it a complex encrypted ciphertext and send it out. According to the related algorithm (RC algorithm), the three-dimensional visualization of the segmented and identified two-dimensional thyroid slices is shown in Figure 6. After the normal thyroid image is three-dimensionally reconstructed, the result of the three-dimensional visualization of the diseased thyroid image is shown in Figure 6. In order to facilitate observation, the lesion is marked with a red line. Through this, we can have a certain understanding of the principle and location of this lesion, so that students can understand where the problem occurred when they actually encountered it [16].

### 3. Experiment and Analysis

**3.1. Subjects.** We select 263 nursing undergraduates from a medical school as the research objects. 131 students in

Nursing Class 1 served as the control group, including 7 boys (5%) and 124 girls (95%), aged 18–22 ( $19.60 \pm 1.45$ ) years and with admission scores of 412–498 ( $451.2 \pm 29.8$ ) points. 132 students in Nursing Class 2 were the experimental group, including 11 boys (8%) and 121 girls (92%), aged 17–23 ( $20.00 \pm 1.70$ ) years and with admission scores of 418–492 ( $460.2 \pm 27.4$ ) points. There was no statistically significant difference between the two groups in gender ( $\chi^2 = 0.74$ ,  $P = 0.390$ ), age ( $t = -0.71$ ,  $P = 0.486$ ), and school scores ( $t = -0.70$ ,  $P = 0.491$ ) ( $P > 0.05$ ). The scores of each student are collected for comparison, and then the results are analyzed to draw conclusions. Their population composition is shown in Figure 7 [17].

The function of aseptic technique is one of the topics of nurse skills training in the laboratory, and it is also an important skill training [18]. In the laboratory practice platform, after passing the online real-name authentication, the trainees will enter the page to select training topics after registering and logging in. Students perform aseptic operations through the virtual Internet. There is feedback at every step of the process from environmental preparation, article preparation, to operation. The scoring system synchronized with the training will point out the error points and the points that have been eliminated in detail. When students make mistakes, the screen will provide correction information on time, which solves the shortcomings of teachers in the area that does not guide. For example, in the aseptic technique mode, if the student dipped a cotton swab by mistake, a warning symbol would appear on the screen. For the first time, it asks the student to think about what is wrong, until the task is correct before proceeding to the next step. For the purpose of open experimental teaching, in addition to the traditional appointment laboratory, which uses laboratory space, cargo, and simulation for flight practice, it also mainly uses the computer network system to allow students to enter the virtual simulation of the laboratory and then select the relevant flying objects on the page.

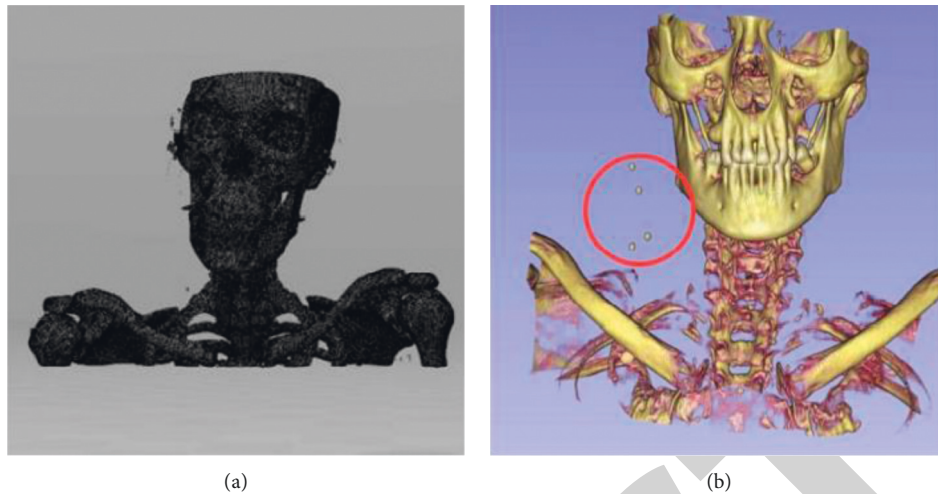


FIGURE 6: Three-dimensional rendering of the thyroid body. (a) A three-dimensional image of a normal thyroid body. (b) A three-dimensional image of a diseased thyroid body.

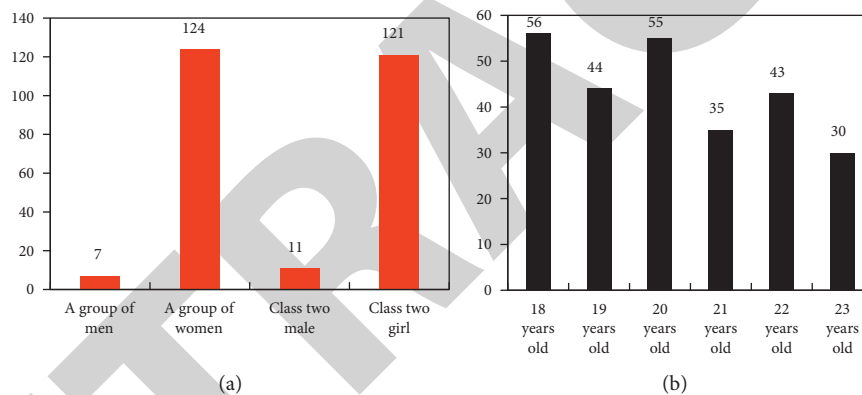


FIGURE 7: Composition of experimental subjects. (a) Number composition. (b) Age composition.

If they have computers or mobile phones in every corner of the university, they can go to the practice of online skill business and finally feedback the results. The functional structure diagram of the virtual simulation experiment system is shown in Figure 8.

Using VR technology for teaching, the boring single skill training of first aid is compiled into a computer-operable teaching task that students can complete by playing different roles [19]. At the same time, before virtual teaching, students need to increase the time of self-study before class to familiarize themselves with the virtual case, in order to complete the role task assignment and plan the operation time [20,21]. After class, one can also make an appointment in the laboratory to conduct rescue exercises of virtual cases again to consolidate first aid knowledge and skills [22]. The use of simulated humans in VR technology can repeatedly present rare or critical illnesses, allowing students to be exposed to more clinical cases within a limited time. The specific experimental screen is shown in Figure 9 [23]. Through the use of some experiments on the software to operate, equipment is selected, and as long as there is an

error in the operating steps, the experiment will stop; if one is correct, they can proceed to the next step [24].

**3.2. Experimental Results.** In order to study the performance of each student, this article collects the performance of each student and compares them. After the relevant research of each student, the students in the experimental group provided “patient” data, including medical records, through the virtual experimental platform. The monitor directly focused on the vital points of the “patient” and the oxygen saturation in the blood and analyzed “the main factors of the patient’s basic measures for ‘health problems’ and hospitalization to provide rapid treatment for ‘patients,’ such as oxygen inhalation and establishment of venous access. During the application process, if an error occurs or the prescribed time is exceeded, the procedure will automatically stop or speed up the introduction of correction information.” On the basis of the previous training, students modify the “patient” program according to the information and simulate the implementation. After the training, the students write the

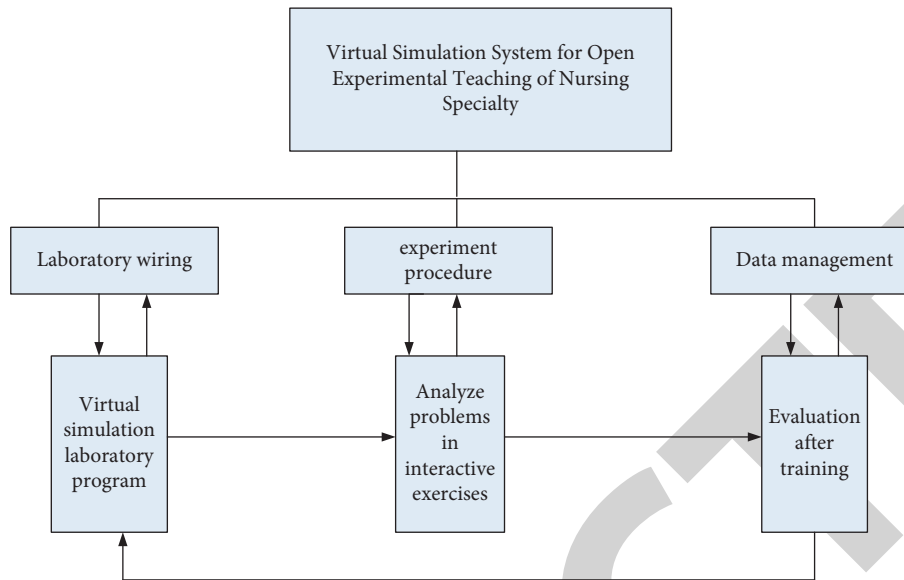


FIGURE 8: Functional structure diagram of the virtual simulation experiment system.



FIGURE 9: Nursing teaching in virtual reality.

experimental experience and communicate with the teacher, while the students in the control group had a specific understanding of the cases and the required nursing skills through the way of previewing and consulting materials after class. The experiment was divided into six groups for case analysis, which discussed nursing assessment, diagnosis, planning, implementation, and evaluation according to nursing procedures [25]. Finally, each group of students exchanged their experiences, and the teacher gave on-site guidance and teaching summaries to the problems found in the teaching process [26]. When establishing 3D reconstruction models of medical images and virtual reality in nursing experimental teaching, the transmission efficiency and accuracy are problems that need to be solved. The score distribution of the students participating in the experiment is shown in Tables 1 and 2. From the tables, we can clearly see that combined with VR, the teaching method of image 3D reconstruction has brought different learning effects to children due to the previous methods [27].

**3.3. Result Analysis.** The students also reflected that their classes showed the real content they need to teach in the

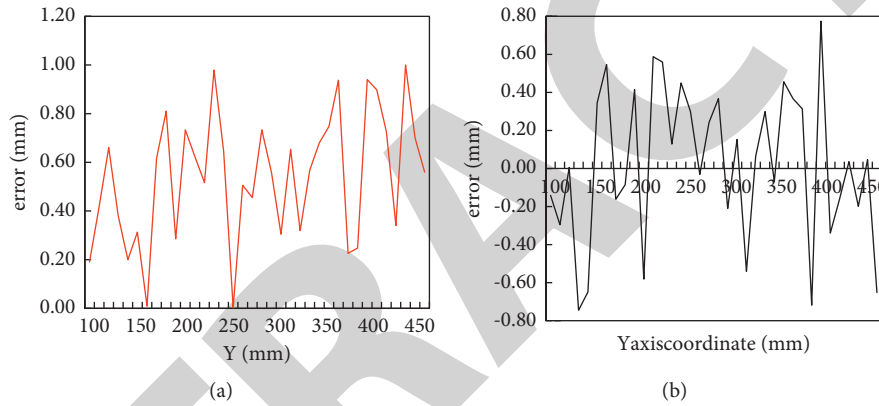
classroom. It is very intuitive. It can not only deepen the memory of knowledge but also cultivate rich 3D reconstruction capabilities. It is generally difficult to make 3D models [28]. The staff summarized several conclusions about the application of VR technology in medical education: (1) It improves the intuition and interest of medical knowledge, and interest is a factor of student enthusiasm and initiative. Reality presents medical knowledge to students in an intuitive and vivid way and helps learners apply the knowledge they have learned to real life through technical means. Expressed in a traditional way, therefore, in terms of teaching content, the intuitiveness of virtual medical reality is an incomparable advantage of traditional teaching methods. (2) It is practical and fully reflects the teacher's theme status. An important feature of VR medicine is that it can reflect the subject status of teachers in the learning process. Virtual practice training is an important part of VR medical courses, and function is the most important part of virtual practice. Therefore, the practical and functional virtual medical reality fully embodies the dominant position of medical students in the learning process. Modern pedagogy believes that the subjective status of teachers and the leading role of teachers are one of the teaching principles.

TABLE 1: Comparison of students' academic performance.

Group	CPR	ECG monitoring	Sputum suction technique	Oxygen technology
Experimental group ( $n = 132$ )	$87.01 \pm 6.24$	$95.88 \pm 2.42$	$86.62 \pm 8.17$	$95.62 \pm 2.19$
Control group ( $n = 131$ )	$80.32 \pm 5.86$	$86.27 \pm 3.17$	$80.21 \pm 6.39$	$85.92 \pm 2.26$
T value	-12.56	-14.62	-11.38	-15.52
P value	<0.001	<0.001	<0.001	<0.001

TABLE 2: Practical performance of students.

Group	Ventilator use	Tracheal tube care	Skill assessment results
Experimental group ( $n = 132$ )	$86.86 \pm 7.02$	$90.01 \pm 2.79$	$90.33 \pm 5.58$
Control group ( $n = 131$ )	$79.17 \pm 6.39$	$84.62 \pm 3.18$	$82.75 \pm 4.82$
Tvalue	-12.08	-11.33	-13.47
P value	<0.001	<0.001	<0.001

FIGURE 10: Reconstruction error of (a)  $x$ -axis and (b)  $z$ -axis.

Activities can also internalize medical knowledge into cognitive results and ultimately realize the construction of “meaning.”

## 4. Discussion

**4.1. Errors in 3D Reconstruction of Medical Images.** As shown in Figure 10, we can clearly see that we still have certain errors in the 3D reconstruction of medical images. In the graph of the  $z$ -axis reconstruction error, we will find that the  $x$ -axis reconstruction error receives an increase in the  $y$ -axis, and it is also more affected than that in the  $z$ -axis.

**4.2. The Number of Virtual Experiments Increases the Reflection of Teaching Quality.** As shown in Figure 11, in addition to intuitive imaging, medical VR courses also have a significant advantage, that is, three-dimensional interaction, which simulates the actual operation of medical VR courses, allows medical students to practice repeatedly and concentrate on practice. At the same time, the VR medical course also judges whether the virtual object is working normally according to the medical

students in the virtual site and provides real-time feedback information [29].

**4.3. Distribution of Student Performance.** As shown in Figure 12, in the context of VR medical imaging teaching, student performance has improved rapidly, and the rate of excellence and specialization has increased unabated. The conversion rate is 8% higher. The excellence rate and success rate of the practical exam in the experimental class are much higher than those in the control class. Therefore, it can be concluded that the application of VR technology in nursing teaching is conducive to improving the practical ability of teaching teachers. Technology is a new intelligent interactive education method developed in recent years. It has the advantages of repeatability, zero risk, multiperson function, etc. The knowledge and understanding of students' real medical environment is conducive to timely contacting with clinical practice [30]. Currently, VR technology is mainly used to train specific medical skills. The education and transfusion of bronchoscopy, surgery, and vascular intervention in clinical medicine have been integrated into nursing teaching, and

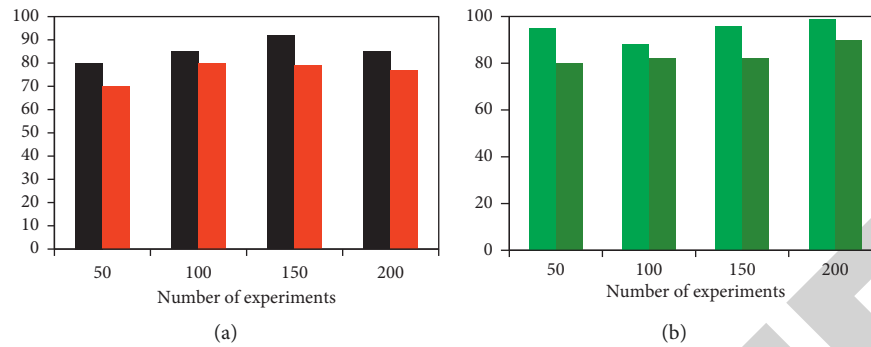


FIGURE 11: Effect of increasing the number of experiments on student performance. (a) Practical scores of the experimental group and the control group. (b) Success rate of the experimental group and the control group in the practical operation.

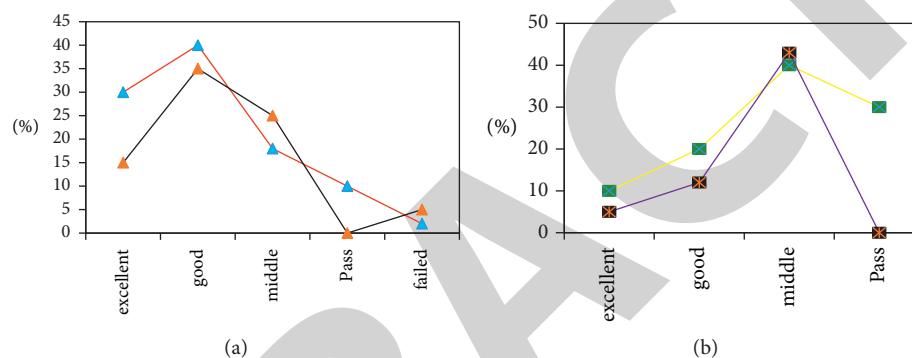


FIGURE 12: Distribution of student performance. (a) Under VR medical image teaching. (b) Achievements under traditional teaching.

certain teaching effects have been achieved. The audit team's independent learning ability, information technology application, and team spirit are slightly inferior to the audit team.

## 5. Conclusions

Medical image imaging is an important branch in the field of computer imaging in medicine and computer science. It integrates many technologies such as computer graphics, digital image processing, and biomedical engineering, integrates 3D graphics technology into medical engineering, and realizes the discovery of medicine. It has been a research hotspot for more than 20 years. It cultivates students' practical work ability, cultivates students' thinking and expression ability, consolidates students' learning mentality, and identifies students' learning effect, so as to improve their teaching effect. In terms of team cooperation, the control group cultivates learning interest, problem-solving ability, thinking, and expression ability. It is suggested that the education system review recognized by the group can not only improve the educational effect but also cultivate the quality required by students' medical imaging study, improve students' comprehensive quality, and cultivate high-quality imaging students. The excellent teaching feedback rate reaches 95%, 80.5% higher than that in the control group, indicating that the patient teaching simulation scheme approved by the observation group can effectively

improve the excellent teaching feedback rate and provide better teaching services for students. Science and technology can effectively mobilize students' interest in learning, enhance students' sense of teamwork, and cultivate their ability of expression and thinking. And the ability to solve problems improves the teaching effect and the teaching quality, which has laid a certain foundation for students to enter clinical work in the future. The technology in teaching practice not only requires teachers to improve the virtual learning process but also must be very familiar with the teaching content, which is a challenge. In the medical field, the development of virtual case software usually cannot well reflect the key points and teachers' teaching level and cannot fully combine the benefits of virtual teaching with the existing courses, which hinders the development of VR technology in medical education. The combination of 3D VR technology and medical images will do better in the future research. This will be the gospel of people. Medical image 3D reconstruction is still a very new research direction in China and has developed rapidly. It is believed that, through the continuous efforts of Chinese researchers, China's medical 3D technology will provide a powerful tool for medical diagnosis and make science and technology benefit the people.

## Data Availability

No data were used to support this study.

## Retraction

# Retracted: Technical Evaluation of Commercial Sperm DFI Quality Control Products in SCSA Testing

### Journal of Healthcare Engineering

Received 11 July 2023; Accepted 11 July 2023; Published 12 July 2023

Copyright © 2023 Journal of Healthcare Engineering. This is an open access article distributed under the Creative Commons Attribution License, which permits unrestricted use, distribution, and reproduction in any medium, provided the original work is properly cited.

This article has been retracted by Hindawi following an investigation undertaken by the publisher [1]. This investigation has uncovered evidence of one or more of the following indicators of systematic manipulation of the publication process:

- (1) Discrepancies in scope
- (2) Discrepancies in the description of the research reported
- (3) Discrepancies between the availability of data and the research described
- (4) Inappropriate citations
- (5) Incoherent, meaningless and/or irrelevant content included in the article
- (6) Peer-review manipulation

The presence of these indicators undermines our confidence in the integrity of the article's content and we cannot, therefore, vouch for its reliability. Please note that this notice is intended solely to alert readers that the content of this article is unreliable. We have not investigated whether authors were aware of or involved in the systematic manipulation of the publication process.

Wiley and Hindawi regrets that the usual quality checks did not identify these issues before publication and have since put additional measures in place to safeguard research integrity.

We wish to credit our own Research Integrity and Research Publishing teams and anonymous and named external researchers and research integrity experts for contributing to this investigation.

The corresponding author, as the representative of all authors, has been given the opportunity to register their agreement or disagreement to this retraction. We have kept a record of any response received.

### References

- [1] T. Pang and X. Zhang, "Technical Evaluation of Commercial Sperm DFI Quality Control Products in SCSA Testing," *Journal of Healthcare Engineering*, vol. 2022, Article ID 9552123, 14 pages, 2022.

## Research Article

# Technical Evaluation of Commercial Sperm DFI Quality Control Products in SCSA Testing

Tao Pang and Xinzong Zhang 

NHC Key Laboratory of Male Reproduction and Genetics,  
Guangdong Provincial Reproductive Science Institute (Guangdong Provincial Fertility Hospital), Guangzhou 510600,  
Guangdong, China

Correspondence should be addressed to Xinzong Zhang; [zhangxinzong@nahaibio.com](mailto:zhangxinzong@nahaibio.com)

Received 11 December 2021; Revised 8 January 2022; Accepted 31 January 2022; Published 4 March 2022

Academic Editor: Yang Gao

Copyright © 2022 Tao Pang and Xinzong Zhang. This is an open access article distributed under the Creative Commons Attribution License, which permits unrestricted use, distribution, and reproduction in any medium, provided the original work is properly cited.

With the increase in population and the advancement of medicine, people even more hope that their offspring will be healthier. DNA fragmentation rate is currently one of the more common indicators for evaluating sperm fertility and predicting the outcome of pregnancy. In order to evaluate the technical performance and application value of commercial sperm DFI (DNA fragmentation index) quality control products in the flow cytometry sperm chromatin structure analysis (SCSA), this paper uses flow cytometry to test commercial sperm DFI quality control products (Celula) and laboratory routine self-made DFI quality control products. In this paper, the quality control of new commercial sperm DFI and laboratory-made quality control were compared and tested for 30 consecutive days. And this paper monitors the response of commercial quality control products to the interference of key reagent parameters. This paper compares the stability of the test results of two quality control products and their sensitivity to the interference of key performance parameters of the detection reagent. Experimental results show that commercial sperm DFI quality control products can simulate sperm DNA damage to achieve accurate detection of DNA integrity. The stability of commercial sperm DFI quality control ( $CV = 2.47\%$ ) is better than that of laboratory-made quality control ( $CV = 11.22\%$ ). The new commercial sperm DFI quality control product can sensitively detect changes in the concentration of acidified solution and staining solution at the same time. It can effectively control the quality of detection reagents and experimental procedures. The new commercial sperm DFI quality control product can effectively control sperm DNA integrity testing. It can be used as an external quality control product for quality control of test results to ensure that more accurate test results are provided to the clinic.

## 1. Introduction

**1.1. Background.** Sperm DNA fragmentation has been extensively studied for more than a decade. In the 1940s, people discovered the uniqueness of the sperm-protein complex that stabilizes DNA. In the 1950s and 1960s, people studied the relationship between unstable chromatin structure and infertility. In the 1970s, the effect of inducing DNA damage was studied. In the 1980s, the concept of sperm DNA fragmentation related to infertility was introduced, and the first DNA fragmentation test, sperm chromatin structure analysis (SCSA), was performed. The TUNEL test was introduced in the 1990s, followed by other

test methods. The link between DNA fragmentation in sperm and miscarriage has been extensively studied, which has stimulated the demand for treatment tools for these patients. This has caused increased interest in the etiology of DNA damage. However, the lack of necessary quality control products is one of the reasons why laboratory quality control cannot be carried out.

As a carrier of genetic material, sperm DNA not only is significantly related to sperm function but also can affect the division of fertilized eggs and the development of embryos. Among them, the rate of sperm fragmentation is a major influencing factor. Therefore, patients with severe sperm DNA damage will not only affect the quality of sperm but

also cause egg fertilization failure and reduce the chance of pregnancy (male infertility). Moreover, it affects the quality of the embryo. Even if the egg can be fertilized and divided normally, it often leads to poor embryonic development and miscarriage in the end.

With the improvement of modern industrialization, the proportion of infertility caused by environmental pollution, work pressure, and bad living habits is increasing year by year. Among them, the male infertility rate continues to increase, and the inspection methods for male infertility are mainly based on routine semen testing. Sperm chromatin structure analysis (SCSA), as the main detection method for evaluating the integrity of male sperm genetic material, plays a key role in evaluating sperm DNA quality, and it provides great help to the method of sperm detection. In clinical testing, sperm DNA integrity evaluation is mainly based on microscopy and flow cytometry. Flow cytometry is regarded as the “gold standard” for sperm DNA integrity testing because of its fast detection speed, simple operation, and high detection accuracy.

**1.2. Significance.** Numerous research results confirm the importance of sperm DNA fragmentation detection. It can reflect the integrity of sperm genetic material and in-depth assessment of male fertility, predict treatment outcomes, and guide treatment. However, the mechanism of DNA damage, the specific location of DNA damage, the treatment of sperm DNA fragmentation, and the establishment of a simple and easy-to-standardize clinical detection method all require further research.

Damage to the integrity of sperm DNA is also a common semen abnormality in modern men, and it is the main factor leading to the decline of male fertility. Sperm DNA fragmentation index is a commonly used index to judge sperm DNA damage. At present, the relationship between specific gene methylation and temporal rhythm changes and sperm DNA integrity is still unclear. Commercial sperm DFI quality control products are tested by SCSA, and the technical evaluation is quantitatively analyzed to determine the relationship between specific methylation and temporal rhythm changes and sperm DFI. Therefore, it is of practical significance to study the technical evaluation of commercial sperm DFI quality control products in SCSA testing, and such related research is also very much needed.

**1.3. Related Work.** In medicine, research on DFI has a history of more than ten years and has made great contributions to issues such as fertility. In order to explore the relationship between sperm DNA fragmentation index (DFI) and semen parameters, Jun et al. evaluated its application value in semen quality evaluation. His method is to collect a total of 9,694 semen samples and use flow cytometry-assisted sperm chromatin structure analysis (SCSA) to detect sperm DFI and high DNA staining (HDS). Pearson correlation and multiple linear regression analysis were used to analyze the correlation between sperm DFI and semen parameters. Experiments have shown that there is a moderate correlation between sperm DFI and semen

parameters, which can be used synergistically for the evaluation of semen quality [1]. Hongyi et al. pay more attention to the impact of DFI on fertility. They believe that the sperm DNA fragmentation index (DFI) is widely regarded as a key indicator of male fertility. However, DFI's predictive value for assisted reproductive technology (ART) outcomes remains controversial. In this study, they used a large sample to analyze the impact of sperm DFI on pregnancy outcomes after ART and its relationship with in vitro fertilization (IVF)/intracytoplasmic sperm injection (ICSI) oocyte fertilization and embryo development. They also explored the value of sperm DNA fragmentation (SDF) and related factors in assessing male fertility. They retrospectively analyzed the relationship between DFI measured by sperm chromatin structure measurement (SCSA) and pregnancy outcomes after ART during 2,622 ART treatment cycles. The results show that, as an increasingly common reproductive testing technique, sperm DFI has proven to be very valuable in male fertility assessment. However, its importance as a predictor of pregnancy outcome after ART needs further research [2]. Niederberger and Craig believe that the percentage of SCSA DFI and TUNEL positive sperm is a moderately correlated measure of sperm DNA integrity but produces different results in a large proportion of patients. DFI has a good correlation with semen analysis parameters, but TUNEL is not. These data indicate that the SCSA and TUNEL tests measure different aspects of sperm DNA integrity and should not be used interchangeably [3]. Bach PV and others have also done a lot of researches on infertility. They believe that semen analysis is traditionally used to distinguish fertile men from infertile men. But in the current era of assisted reproductive technology, its effectiveness is questioned. The need for more sophisticated diagnostic and prognostic tools has led to the increased use of sperm DNA damage in the management of male infertility. Although there are many methods to measure sperm DNA damage, our understanding of the etiology, measurement, and clinical significance of sperm DNA damage is still incomplete. Although the current evidence is full of heterogeneity, it complicates the attempts of comparison and meta-analysis. But in the era of in vitro fertilization (IVF) and intracytoplasmic sperm injection (ICSI), sperm DNA damage does seem to play a role in the development and maintenance of pregnancy. However, as pointed out by the American Society of Reproductive Medicine, the routine and widespread use of sperm DNA damage testing is not yet supported. This requires further research to standardize the measurement of sperm DNA damage and to clarify the exact role of sperm DNA damage in the countless other male and female factors that lead to IVF and ICSI reproductive outcomes [4]. Hallak is more inclined to DFI's evaluation criteria in this regard. For this reason, he believes that the Halosperm test kit is the latest sperm DNA fragmentation test. It becomes a suitable alternative to the sperm chromatin structure assay (SCSA) test. Although the test is clever and interesting, the data lack the statistical rigor of the SCSA test [5]. In terms of specific analysis, Asare N uses mice as experimental subjects. They found that silver nanoparticles (AgNPs) caused apoptosis, necrosis, and DNA strand breaks

in different cell models *in vitro*. These findings ensure the analysis of their relevance in the body. The results found that the transcription levels of some key genes were significantly induced in *Atm*, *Rad51*, *Sod1*, *Fos*, and *Mmp3* compared with the control group, especially in lung samples of KO mice exposed to Ag200. Ag200 causes genotoxicity and different gene expression patterns in selected genes related to DNA damage response and repair [6]. Rex AS et al. believe that some of the more novel methods that have recently been floated are the use of increased DNA fragmentation and hyaluronic acid (HA) combined technology to sort cells. The clinical value of these tests remains to be elucidated. Despite half a century of research in this field, this analysis is not routinely applied to fertility clinics. The root cause is multifaceted. Numerous reviews and meta-analyses have been published on the use of different analytical methods to analyze DNA fragments, different clinical artificial reproduction treatments (ART), different definitions of successful ART results, and small patient populations. Although the field of sperm DNA fragmentation is highly relevant to fertility clinics, further research is still needed, focusing on the standardization of methods and clinical implementation [7]. Kunkitti et al. physiologically evaluated the DNA fragmentation of frozen-thawed cat epididymal sperm from the body and tail regions through three different techniques and compared DNA fragmentation index (DFI) between the following techniques: sperm chromatin structure determination (SCSA®), acridine orange staining technique (AOT), and sperm chromatin dispersion (SCD). There are significant differences in DFI between different technologies ( $p < 0.05$ ), and there is no correlation. Only the DFI value obtained from the SCD showed that the DFI in the corpus was significantly higher than that of the sperm tail ( $p < 0.05$ ). The differences between technologies may be due to differences in the sensitivity of each technology and the severity of detectable DNA damage. The difference in DFI between the epididymal region of the SCD technique may indicate the different maturation stages of the sperm. Compared with the epididymal tail, the sperm has less chromatin condensation in the body [8].

**1.4. Innovation.** This paper discusses the technical evaluation of commercial sperm DFI quality control products in SCSA testing. Compared with related studies at home and abroad, this paper focuses on the performance of commercial sperm DFI quality control products. This makes the study more bold and maneuverable. Specifically, there are the following innovations. First, the selection of instruments: the reagents of the instruments are all internationally renowned samples, and domestic-related researches use more hospital sample banks. Second, the application of the method: this paper selects two indicators of day-to-day stability and batch-to-batch stability, which are also rare in previous studies. Third, this paper controls other influencing factors that cause DFI, such as the age of both parties, the history of infertility and current physical condition, and the type of assisted reproductive technology, especially the woman's factors, such as age, polycystic ovary syndrome,

endometrial disease, and hydrosalpinx. In addition, the woman's ovarian function is low, and her basic endocrine level is too high. These factors may have adverse consequences for the outcome of IVF and ET, and the DNA repair ability of its eggs is also very poor.

## 2. Material and Method

**2.1. Commercial Sperm DFI Quality Control and Chromatin Structure Analysis Method.** The integrity of mammalian sperm DNA is essential for producing normal offspring [9]. After a sperm with DNA damage conceives an egg, it may have adverse effects on fertilization, embryonic development, and adult health. In the past, commonly used indexes for evaluating semen quality in clinical practice were sperm density, vitality, morphology, body response, nuclear protein group conversion experiment, and so on [10].

Sperm chromatin structure analysis is a sensitive method for high-throughput and rapid detection of sperm DNA damage. Since Evenson Dp founded sperm chromatin structure assay (SCSA) technology to detect sperm DNA integrity, related basic and clinical research has been very active. And most of the research results believe that SCSA helps to assess the fertilization ability of animal sperm [11]. The assessment of male sperm fertilization ability can reflect male fertility. This will help doctors choose different methods of assisted pregnancy (IUI, IVF.ET, and ICSI) for the patient to obtain a successful pregnancy as soon as possible, thereby reducing the patient's psychological, physical, and economic burden. The founders of SCSA conducted a large number of studies on the use of SCSA parameters for male fertility assessment and prediction of subclinical infertility and reached a threshold for assessing human fertility potential: DFI of 0%–15% has high fertility potential; of 15%~30% has medium fertility potential; of >30% has low fertility potential; of >80% has no fertility. The basic principle is that after sperm enters the epididymis, a large number of thiol groups in the protamine are continuously oxidized into disulfide bonds. It binds more tightly with DNA, which makes DNA more resistant to acid, thereby maintaining the stability of the double-stranded structure [12]. In the sperm with DNA damage, most of the mercapto groups in protamine are not oxidized and are easily denatured to single-stranded DNA under the action of acid. According to this principle, the damaged DNA is denatured into single-stranded after acid treatment. Acridine orange combined with double-stranded DNA emits green fluorescence and combined with single-stranded DNA emits red or yellow fluorescence. It can be analyzed by flow cytometry [13].

**2.2. SPSS Introduction and Brief Description of Related Principles.** The SPSS software used in the experimental analysis of this paper is used for statistical analysis. Because of its visual operation interface and powerful statistical analysis capabilities, it is widely used in various scenarios [14]. In this paper, we use regression analysis in statistical analysis, so we will focus on it in the following introduction.

**2.2.1. The Basic Process of Using SPSS for Data Processing.** SPSS is powerful and easy to operate. This feature is reflected in his unified and simple operation process [15]. The basic process of SPSS statistical processing is shown in Figure 1.

**2.2.2. General Form of Multiple Regression Model.** Setting the random variable  $y$ , and the linear regression model of the general variable is  $x_1, x_2, \dots, x_p$ :

$$y = \beta_0 + \beta_1 x_1 + \beta_2 x_2 + \dots + \beta_p x_p + \varepsilon. \quad (1)$$

In formula (1),  $\beta_0$  is called the regression constant, and  $\beta_1, \beta_2, \dots, \beta_p$  are the regression coefficients.  $\varepsilon$  is called the random error term, and generally, we assume that

$$\begin{cases} E(\varepsilon) = 0, \\ V(\varepsilon) = \sigma^2. \end{cases} \quad (2)$$

$$E(y) = \beta_0 + \beta_1 x_1 + \beta_2 x_2 + \dots + \beta_p x_p. \quad (3)$$

Among them, (2) is the basic assumption, and (3) is called the theoretical regression equation [15]. However, in the actual problem processing, we obtain  $n$  sets of data, and the linear model is expressed as (4):

$$y = \beta X + \varepsilon. \quad (4)$$

**2.2.3. Basic Assumptions.**

- (i) Explanatory variables  $x_1, x_2, \dots, x_p$  are definite variables.
- (ii) The random error term has zero mean and equal variance; the formula is expressed as formula (5); namely,

$$\begin{cases} E(\varepsilon_i) = 0, & i = 1, 2, \dots, n, \\ \text{cov}(\varepsilon_i, \varepsilon_j) = \begin{cases} \sigma^2, & i = j \\ 0, & i \neq j \end{cases} \end{cases} \quad (5)$$

**2.2.4. The Assumption Condition Formula of Normal Distribution Is Expressed as Formula (6).**

$$\begin{cases} \varepsilon_i \sim N(0, \sigma^2), & i = 1, 2, \dots, n, \\ \varepsilon_1, \varepsilon_2, \dots, \varepsilon_n. \end{cases} \quad (6)$$

For the multiple linear regression matrix model  $y = \beta X + \varepsilon$ , this condition can be expressed as (7):

$$\varepsilon \sim N(0, \sigma^2 I_n). \quad (7)$$

It can be seen from the above-mentioned properties of the assumed multivariate normal distribution that the random vector  $y$  obeys the  $n$ -dimensional normal distribution, and the expected vector of the regression model  $y = \beta X + \varepsilon$  is (8) and (9):

$$E(y) = X\beta. \quad (8)$$

$$\text{Var}(y) = \sigma^2 I_n. \quad (9)$$

Therefore,

$$y \sim N(X\beta, \sigma^2 I_n). \quad (10)$$

Among them, (8) is the expected mean value, (9) is the expected variance, and the distribution of  $y$  in (10) is obtained.

**2.2.5. Regression Parameter Estimation.** The parameter ordinary least square estimation is expressed as follows: when  $A$  exists, the least square estimation can be obtained, as shown in formula (11):

$$\hat{\beta} = (X'X)^{-1}X'y. \quad (11)$$

$$\hat{y} = \hat{\beta}_0 + \hat{\beta}_1 x_1 + \hat{\beta}_2 x_2 + \dots + \hat{\beta}_p x_p. \quad (12)$$

Among them, formula (12) is called the empirical regression equation. Its regression value and residual are expressed as follows.

Call  $\hat{y}_i = \hat{\beta}_0 + \hat{\beta}_1 x_{i1} + \hat{\beta}_2 x_{i2} + \dots + \hat{\beta}_p x_{ip}$  the regression fitted value of the observed value  $y_i$  ( $i = 1, 2, \dots, n$ ), referred to as the regression value or fitted value. The residual satisfies the relationship, as in (13):

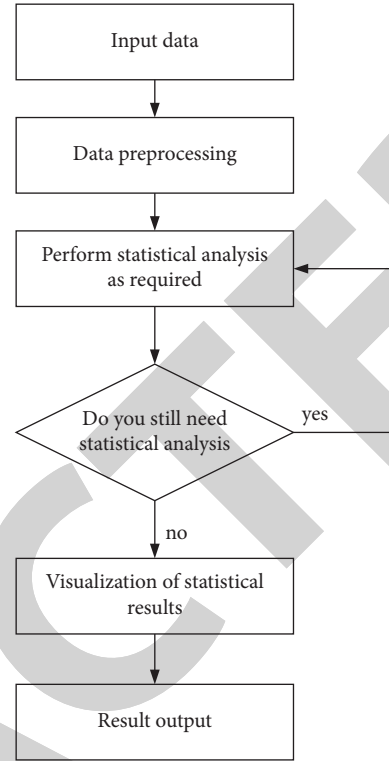


FIGURE 1: Basic diagram of the statistical process.

$$\begin{cases} \sum e_i = 0 \\ \sum e_i x_{i1} = 0 \\ \vdots \\ \sum e_i x_{ip} = 0 \end{cases} \quad (13)$$

In (13), the average value of the residuals is 0, and the weighted average of the residuals for each independent variable is 0.

**2.2.6. Maximum Likelihood Estimation of Regression Parameters.** The model is shown in formula (14):

$$\begin{aligned} y &= X\beta + \varepsilon \\ \varepsilon &\sim N(0, \sigma^2 I_n), \end{aligned} \quad (14)$$

where  $\varepsilon$  obeys a multivariate normal distribution, and then the probability distribution of  $y$  is shown in (15):

$$y \sim N(X\beta, \sigma^2 I_n). \quad (15)$$

At this time, the likelihood function is shown in (16):

$$L = (2\pi)^{-n/2} (\sigma^2)^{-n/2} \exp\left(-\frac{1}{2\sigma^2} (y - X\beta)' (y - X\beta)\right). \quad (16)$$

Among them, the unknown parameters  $L$  are  $\beta$  and  $\sigma^2$ , and the maximum likelihood estimation is to select  $\hat{\beta}$  and  $\hat{\sigma}^2$  that maximize the likelihood function  $L$ . To maximize  $L$ , take the logarithm of both sides of the equation, as shown in equation (17):

$$\begin{aligned} \ln L &= -\frac{n}{2} \ln(2\pi) - \frac{n}{2} \ln(\sigma^2) \\ &\quad - \frac{1}{2\sigma^2} (y - X\beta)' (y - X\beta). \end{aligned} \quad (17)$$

Obviously, it is necessary to maximize it, which is equivalent to the minimum of  $(y - X\beta)' (y - X\beta)$ ; that is, the maximum likelihood estimation of the error term variance  $\sigma^2$  is

$$\begin{aligned} \hat{\sigma}_L^2 &= \frac{1}{n} \text{SSE} \\ &= \frac{1}{n} (e'e). \end{aligned} \quad (18)$$

In (18), this is a biased estimate of  $\sigma^2$ , but it satisfies consistency. In the case of a large sample, this is an asymptotically unbiased estimate of  $\sigma^2$ .

**2.2.7. Significance Test of the Regression Equation.** This paper mainly describes the F test and the  $t$ -test. The F test is as follows: null hypothesis  $H_0: \beta_1 = \beta_2 = \beta_3 = \dots = \beta_p = 0$ . When  $F > F_\alpha(p, n - p - 1)$ , reject the null hypothesis  $H_0$ , thinking that, at the significance level  $\alpha$ ,  $y$  and  $x_1, x_2, \dots, x_p$  have a significant linear relationship; that is, the regression equation is significant. As shown in Table 1, the variance test table, the  $P$  value is the focus of our analysis.

The principle of the  $t$ -test is as follows: null hypothesis  $H_0: \beta_j = 0, j = 1, 2, \dots, p$ . Construct  $t$  statistics, as in the following:

$$t_j = \frac{\hat{\beta}_j}{\sqrt{c_{jj}} \hat{\sigma}}. \quad (19)$$

In formula (19),

$$\begin{aligned} \hat{\sigma} &= \sqrt{\frac{1}{n - p - 1} \sum_{i=1}^n e_i^2} \\ &= \sqrt{\frac{1}{n - p - 1} \sum_{i=1}^n (y_i - \hat{y}_i)^2}. \end{aligned} \quad (20)$$

Equation (20) is the regression standard deviation.

When the  $H_0: \beta_j = 0$  null hypothesis is true, the  $t$  statistic obeys the distribution with  $n - p - 1$  degrees of freedom. Given the significance level  $\alpha$ , the critical value  $t_{\alpha/2}$  of the two-sided test is found. When  $|t_j| \geq t_{\alpha/2}$ , reject the null hypothesis and think that  $\beta_j$  is significantly not zero, and the linear effect of the independent variable  $x_j$  on the dependent variable  $y$  is significant.

**2.2.8. Residual Error Analysis.** The residual A takes the independent variable B as the horizontal axis and the residual as the vertical axis to obtain a residual diagram. The residual diagram can be used to illustrate the different manifestations of sample data [16].

### 2.3. Instruments and Reagents

**2.3.1. Instrument.** The flow cytometer (Sparrow) is produced by Celula (China) Medical Technology Co., Ltd. The microscope (BX51) is produced by Olympus.

#### 2.3.2. Reagent.

- (1) Commercial sperm DFI quality control products are developed, produced, and provided by Celula (China) Medical Technology Co., Ltd. It includes two main components of nonsperm cells with specific proportions of DNA damage and internal reference products. Among them, the nonsperm cell is a mixture of nonsperm normal cells with intact DNA and nonsperm cells with DNA damage according to a preset ratio, which is used to simulate sperm with a certain degree of DNA damage; the internal reference product is composed of green and red microspheres with stable fluorescence intensity, which can be used as a reference for key operation steps and quality monitoring of sperm DNA reagents. The testing process of commercial sperm DFI quality control products is the same as the process of DNA integrity testing of sperm samples, and it can be stored at 2~8°C. The target value of the commercial

TABLE 1: Variance test table.

Variance analysis	Degree of freedom	Sum of square	Mean square	F value	P value
Return	p	SSR	SSR/p	(SSR/p)/(SSE/(n-p-1))	P(F>F value) = P value
Residual	n-p-1	SSE	SSE/(n-p-1)		
Sum	N-1	SST			

sperm DFI quality control product “DFI” in this test is  $38.20\% \pm 0.5\%$ .

- (2) Laboratory self-made sperm DFI quality control products are prepared and stored by Guangdong Family Planning Institute.
- (3) Sperm DNA integrity staining kit is produced by Celula (China) Medical Technology Co., Ltd. It is used for DNA integrity testing and technical performance evaluation of commercial sperm DFI quality control products and laboratory self-made sperm DFI quality control products [17].

**2.3.3. Sample.** The sample came from a sperm sample from the Andrology Clinic of our hospital in August 2021. The sample acquisition refers to the World Health Organization “Human Semen Examination and Processing Laboratory Manual” (5th edition). The project was approved by the hospital ethics committee, and the patient signed an informed consent form.

**2.4. Preparation Method of Laboratory Sperm DFI Quality Control Products.** Quality control preparation method is as follows: (1) Semen recovery: use conventional density gradient centrifugation to collect sperm in the bottom and subbottom layers. After washing, it is diluted to a recovered sperm fluid with a density of about 1 to  $2 \times 10^6/\text{ml}$ . (2) Hydroformylation fixation: add the sperm recovery solution to 0.5% glutaraldehyde in physiological saline solution, and fix it for 60 minutes at  $25^\circ\text{C}$  and room temperature. (3) Preparation of quality control products: collect the aldehyde spermatids, wash them with sperm diluent, separate them, and store them at  $-80^\circ\text{C}$ . (4) Determination of DFI target value of self-made quality control product.

**2.5. Test Method.** Following the Celula sperm DNA integrity staining kit operating instructions to perform flow cytometry detection of sperm DNA integrity, which mainly includes four steps, firstly dilute the semen; then acidify the sperm. The third step is to stain the DNA in different states. Finally, Sparrow flow cytometry was used to calculate the sperm DNA fragmentation index [18].

## 2.6. Detection Parameters

**2.6.1. DNA Fragmentation Index.** Flow cytometry was used to detect commercial sperm DFI quality control products and laboratory-made sperm DFI quality control products. The flow cytometer FL1 (FITC) and FL3 (PerCP), two

detection fluorescence channels, are used to distinguish cell populations and calculate DFI [19].

**2.6.2. Daytime Precision Study.** The laboratory-made sperm DFI quality control product was stored at  $-80^\circ\text{C}$ . Take out 1 sample a day for testing and make continuous testing for 30 days and parallel continuous testing of new commercial sperm DFI quality control products for 30 days. The commercial sperm DFI quality control product should be put back to  $2\sim 8^\circ\text{C}$  for storage immediately after use. By analyzing the DFI and coefficient of variation (CV) of laboratory-made quality control products and commercial sperm DFI quality control products at 30 days, the daytime precision was compared [20].

**2.6.3. Interassay Precision Study.** Test 3 batches of Celula commercial sperm DFI quality control products. The test was repeated 6 times for each batch, and the DFI and its coefficient of variation (CV) were analyzed [21].

## 2.6.4. Research on Reagent Interference.

- (1) In order to investigate the sensitivity of the Celula commercial sperm DFI quality control product, the acid denaturation reagent B in the sperm DNA staining kit was set with 4 gradients; the gradient setting is determined by the laboratory staining kit: 0.2X, 2X, 3X, and 1X (1X is the correct nominal dosage). Analyze whether the new commercial sperm DFI quality control product can be sensitive to the interference of the acid denaturation reagent B solution.
- (2) Set the staining solution in the sperm DNA staining kit to 4 gradients; the gradient setting is determined by the laboratory staining kit: 0.3X, 0.5X, 1.67X, and 1X (1X is the correct nominal amount). Analyze whether the commercial sperm DFI quality control product can be sensitive to the interference of the quality control to the staining solution C [22].

**2.7. Sperm DNA Fragments.** Sperm chromatin structure analysis (SCSA) method was used to detect sperm DNA fragments. Diluting the sperm cells with solution A to a final concentration of  $1\sim 210^6/\text{ml}$ , take  $100\mu\text{l}$  of the diluted semen, add  $200\mu\text{l}$  of B solution on ice, and add  $600\mu\text{l}$  of solution C, and mix well after 30S. Because of the loose structure of DNA-damaged sperm chromatin, it is easily cleaved under acid denaturation conditions to form single-stranded DNA, which binds to AO and emits yellow or red fluorescence, while normal sperm still maintains double-stranded DNA, and AO stains green fluorescence. Flow

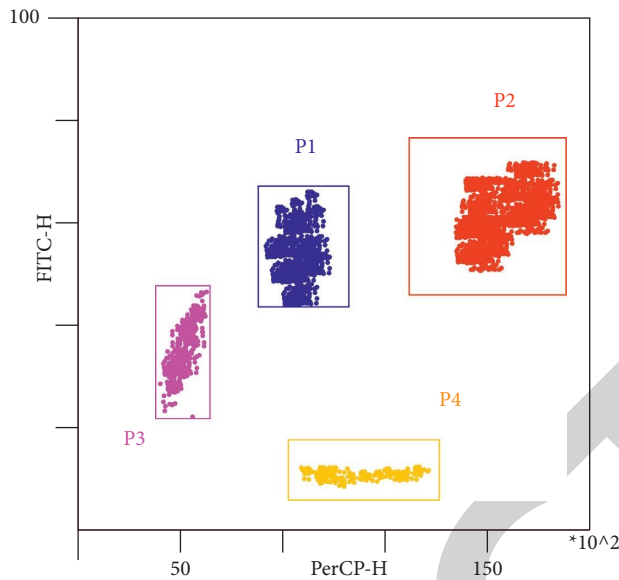


FIGURE 2: Commercial sperm DFI quality control product testing diagram.

cytometry analysis was used to detect the integrity damage of sperm DNA, and the results were expressed by DFI.

### 3. Experimental Results

**3.1. Effectiveness of New Commercial Sperm DFI Quality Control Products.** The flow diagram of the new commercial sperm DFI quality control after testing is shown in Figure 2. The P1 circle gate (blue part) indicates double-stranded DNA, that is, cell with intact DNA, and the P2 circle gate (red part) indicates DNA-damaged cells. From the results of stream clustering, it can be found that P1 and P2 can be effectively separated, and the calculation process of sperm DFI can be simulated in the same way. Therefore, the commercial sperm DFI quality control product can effectively simulate the DNA damage classification and the calculation of the fragment index for the DNA integrity test of the sperm sample. P3 (purple part) and P4 (orange part) are built-in reference products, which can be used for internal control calculation and the relative position of P1 and P2 circle gate, operation process interference, and reagent effectiveness evaluation; as you can see in Figure 2, all indicators are consistent with expectations. Therefore, commercial sperm DFI quality control products can effectively simulate sperm DNA damage to achieve sperm DNA integrity detection and can evaluate and control reagents and operations [23].

**3.2. Daytime Stability.** The test results of commercial sperm DFI quality control products and laboratory-made sperm quality control products for 30 days of continuous testing are shown in Figure 3. Calculating the sperm DNA fragmentation index and the 30-day CV value, respectively, the test results of commercial sperm DFI quality control products (DFI is  $38.20\% \pm 0.5\%$ ; CV is 2.47%) are better than those of laboratory self-made sperm quality control products (DFI is  $38.10\% \pm 0.5\%$ ; CV is 11.22%).

The preliminary reasons for the large fluctuations in laboratory-made sperm quality control products are as follows: (1) Sperm samples require high storage conditions, which are caused by improper control of storage conditions (freezing process and freezing conditions maintenance). (2) After the self-made quality control product is frozen and stored, the sperm DNA damage is caused by the thawing process (time and temperature), and the deviation is caused by the uneven operation. (3) The sample preparation process is cumbersome and lacks quality control links, uniformity is difficult to guarantee, and errors are prone to occur, resulting in large fluctuations in test results [24].

Furthermore, cosine analysis is used to check whether the time distribution of DFI conforms to the cosine curve. The amplitude of the fitted cosine curve is 8.4%, the phase is  $-330$ , and this shows that the activity level of commercial sperm DFI quality control products is stable during the day, as shown in Figure 4. Among them, the curve has a large dynamic range and does not fit well, indicating that the correlation is not particularly strong.

**3.3. Precision.** Calculate the average value of the sperm DNA fragmentation index of 3 batches of commercial sperm DFI quality control products and make a histogram. The results are shown as follows. The test results of the first batch of DFI conformed to  $38.20\% \pm 0.5\%$  and  $CV \leq 3.16\%$ . The test results of the second batch of DFI conformed to  $38.20\% \pm 0.5\%$  and  $CV \leq 0.66\%$ . The third batch of DFI test results meets  $38.20\% \pm 0.5\%$  and  $CV \leq 1.76\%$ . If the DFI target values of the three batches of quality control reagents are the same, the CV between the three batches of quality control products needs to be further calculated to prove the stability of the interbatch quality control products of the same detection system (DFI reagents, FCM, and operating procedures). All comply with the manufacturer's declaration, as shown in Figure 5.

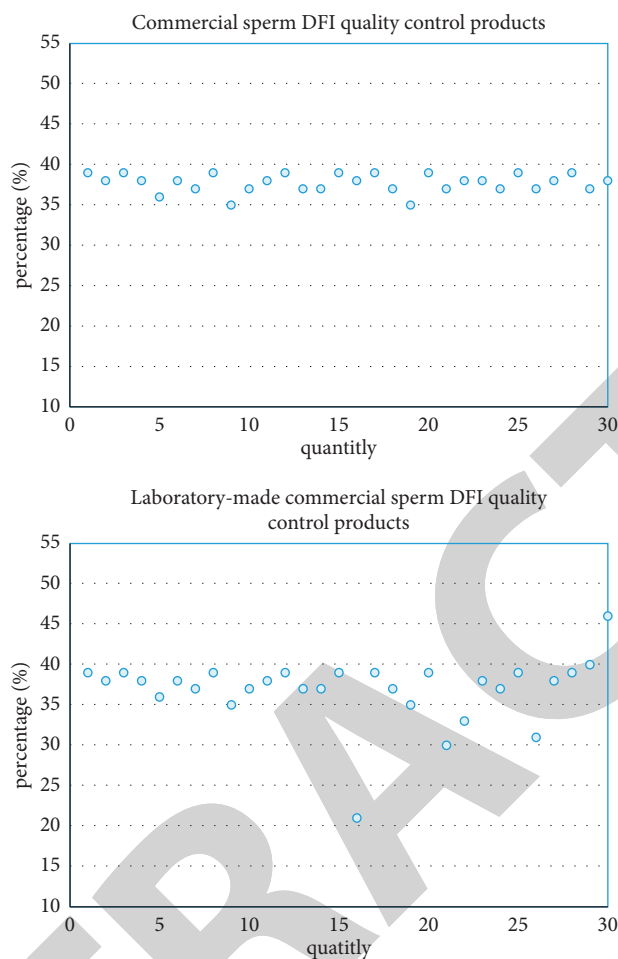


FIGURE 3: Daytime stability of commercial sperm DFI quality control products and self-made DFI quality control products.

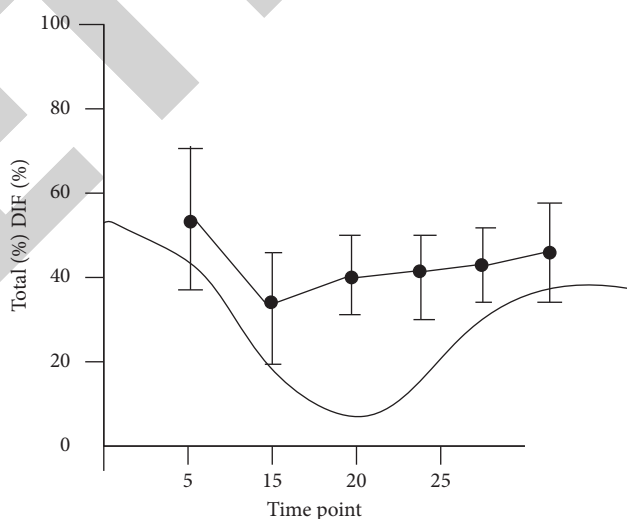


FIGURE 4: Sperm DIF activity level.

**3.4. Sperm Quality Difference between RMC Population and MARHCS Population.** Semen samples from the RMC population were collected from 7 am to 11 am, and semen samples from the MARHCS population were collected from 8 am to 20 pm. The characteristics of the population are

described in Table 2. The problem of sperm DFI can be explained by analyzing the difference in sperm quality of the population.

In the MARHCS population data, changes in sperm DFI over time were also found, as shown in Table 3.

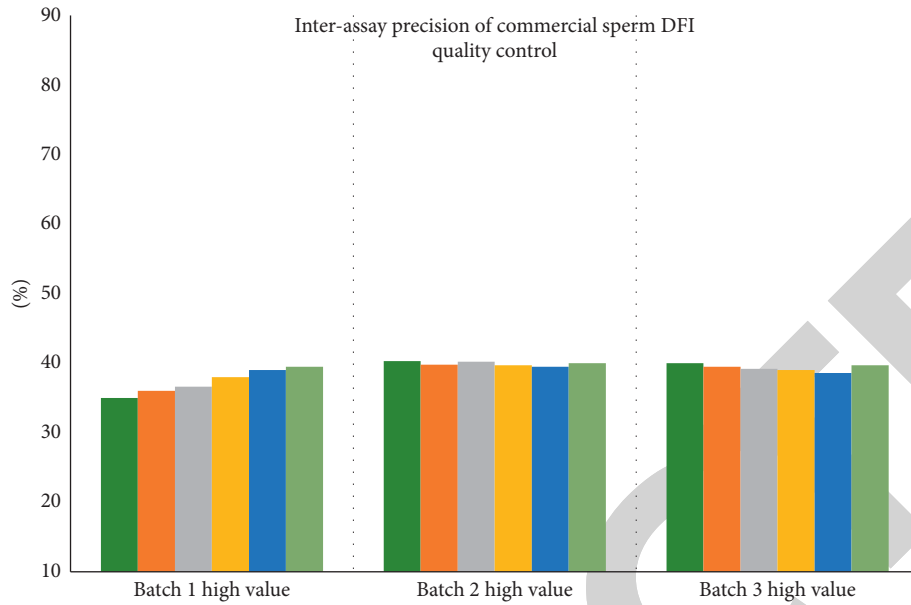


FIGURE 5: Interlot precision of commercial sperm DFI quality control products.

TABLE 2: Population characteristics table.

Variables	RMC		MARHCS	
	<i>n</i>	Total DFI%	<i>n</i>	Total DFI%
Age, years	10362	33 (30, 38)	630	21 (21, 22)
Abstinence period, days	10752	4 (3,5)	630	4 (3, 5)

TABLE 3: Single-factor analysis of sperm DFI.

Ejaculation time point	RMC		MARHCS	
	<i>n</i>	Value	<i>n</i>	Value
P-inequivalence	<0.001	0.131	<0.001	0.012
P-trend	<0.001	0.028	<0.001	0.335

In order to illustrate a relationship with time more intuitively, as shown in Figure 6, the sperm is in the day, from 8 am to 8 pm. At eleven o'clock, the absolute difference is the smallest, which means that the fragmentation rate becomes smaller at this time.

In order to illustrate the correlation, we used different cpg points for correlation analysis, and the principle is as follows: the total signal (M+U) of each cpg site of each sample is compared with the background signal, and the *P* value can be obtained. It is generally believed that a lower *P* value indicates that the site is more reliable. A cpg site with a *P* value greater than 0.01 is a site with relatively poor quality, and the results are shown in Figures 7 and 8.

It is obvious from the comparison between Figures 7 and 8 that each data point of the methylation level at the cpg20 point is near the potential line. However, the methylation level at the cpg4 point has a higher degree of dispersion between points, which can indicate that the methylation level at the cpg20 point has the highest correlation with the sperm DFI.

### 3.5. Key Operating Techniques

**3.5.1. Test Results of Different B Liquid Acid Denaturation Reagents.** In the use of standard B solution, the complete DNA and fragmented DNA on the scatter chart of commercial sperm DFI quality control products are in the preset fixed circle gate, and the position of the circle gate is constant with the built-in reference in the relative coordinate system (as shown in the upper left of Figure 9). Under the other different B liquid conditions, the intact DNA and fragmented DNA of the commercial sperm DFI quality control products deviate from the preset fixed circle gate, as shown in detail in Figure 9. Liquid B is 0.2X, 2X, and 3X from left to right. It can be seen that the commercial sperm DFI quality control product has the function of controlling whether the acid denaturation reagent of the staining solution is correct.

**3.5.2. Test Results of Dyeing Solutions of Different Concentrations.** In the use of standard C solution, the complete DNA and fragmented DNA on the scatter chart of commercial sperm DFI quality control products are in

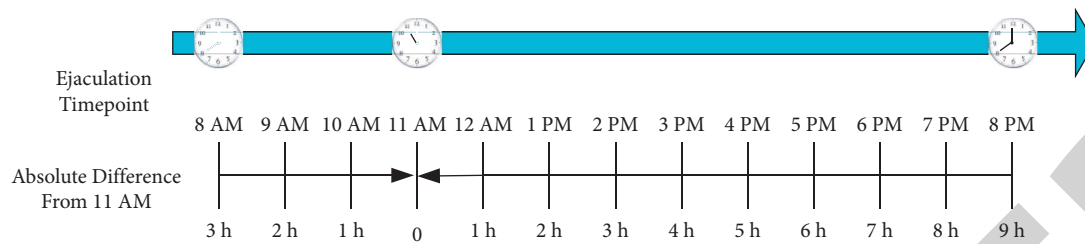


FIGURE 6: Absolute difference of sperm.

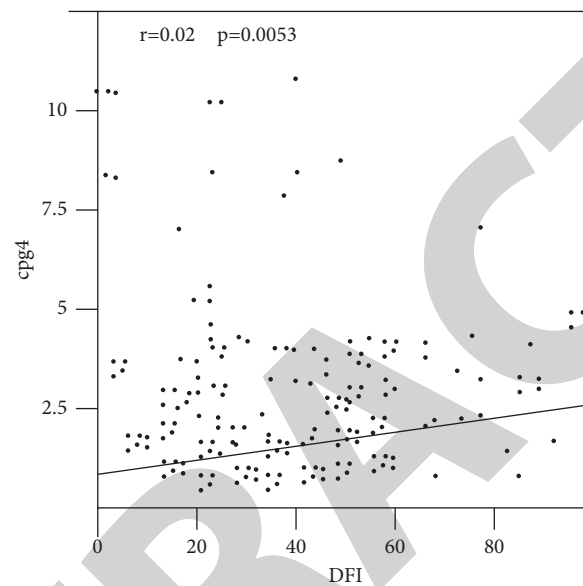


FIGURE 7: The correlation between the methylation level of cpg4 and the sperm DFI.

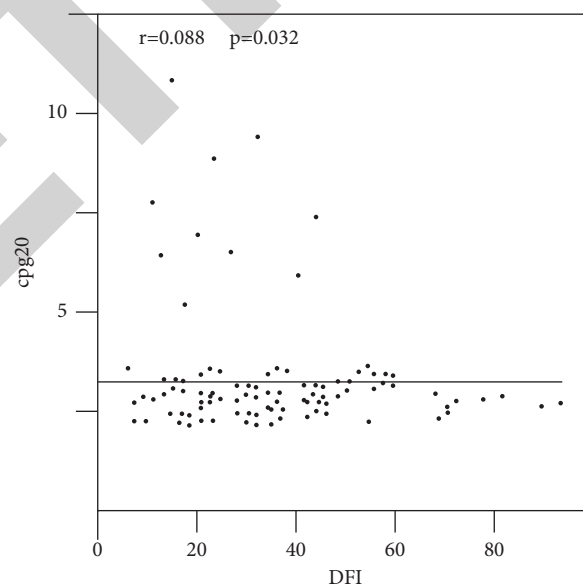


FIGURE 8: The correlation between the methylation level of cpg20 and the sperm DFI.

the preset fixed circle gate, and the position of the circle gate is constant relative to the built-in reference product (as shown in the upper left of Figure 10). Under the other

different C solution conditions, the intact DNA and fragmented DNA of commercial sperm DFI quality control products deviated from the preset fixed circle gate,

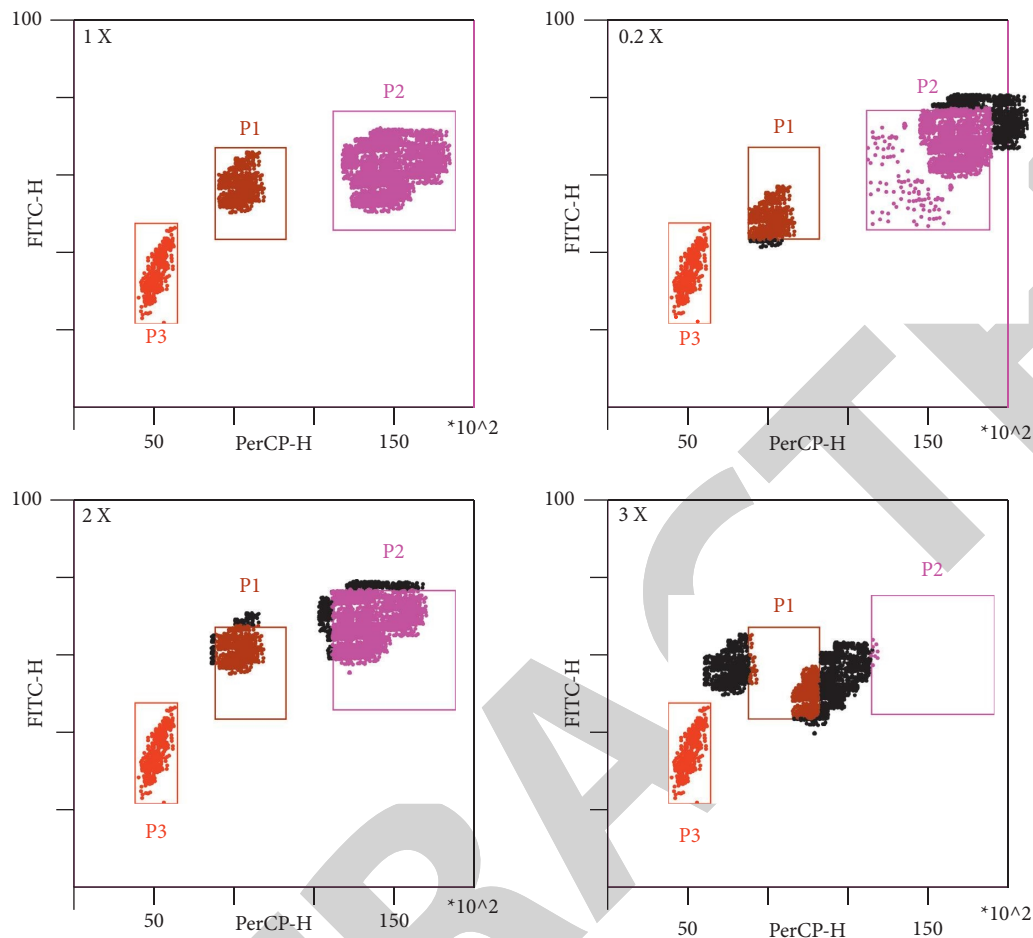


FIGURE 9: Commercial sperm DFI quality control product B liquid quality control.

as shown in Figure 10 for details. From left to right are C liquid 0.3X, 0.5X, and 1.67X. It can be found that the acidity of the p3 gate does not change much; only the p2 and p3 circle gates change with the change of acidity. It can be seen that the commercial sperm DFI quality control product has the function of the quality control reagent C solution staining solution.

## 4. Discussion

**4.1. Current Problems.** Flow cytometry is a novel and rapid tool for analyzing sperm integrity and DNA fragmentation. It is widely used in medical research and clinical diagnosis in the field of reproduction [25]. Many hospitals have successively launched sperm DFI testing projects. There are more than 10 DFI reagent providers on the market in China, and the test exceeds 40,000 cases per year. However, the biggest problem currently faced by andrology laboratories is the difference in test results, which brings some uncertainty to clinical diagnosis [26]. For example, 15 laboratories in the United Kingdom counted the same semen specimens in the early days, and the results showed that the percentage of normal sperm in each laboratory ranged from 12% to 80%. The main reason is the lack of quality assurance measures for semen analysis, such as the lack of standardized operating

procedures, the lack of corresponding quality control products, and the lack of quality control institutions to monitor the quality of semen analysis [27].

**4.2. Status of Traditional Quality Control Products.** How to solve the thorny problem of quality control, many scholars have focused on the exploration of establishing different quality control products. The sperm in the semen is recycled, and other processes are made to make sperm quality control products and conduct indoor quality control testing for no less than 7 months. The results showed that the CV of the DFI test results of sperm quality control products at about 5 months was less than 15%. iGnsb Ginsburg KA tried standard latex beads as quality control products for indoor quality control of sperm density counting [28]. But there is a certain gap from the ideal quality control products. The composition of the quality control product should be similar to or the same as the composition of the patient sample. The quality control product should be uniform and stable and can give a reminder of the result that exceeds the control limit when there is an error in the analysis process. At present, the self-made DFI quality control products in the laboratory cannot meet the above requirements, and at the same time, they cannot meet the needs of interchamber

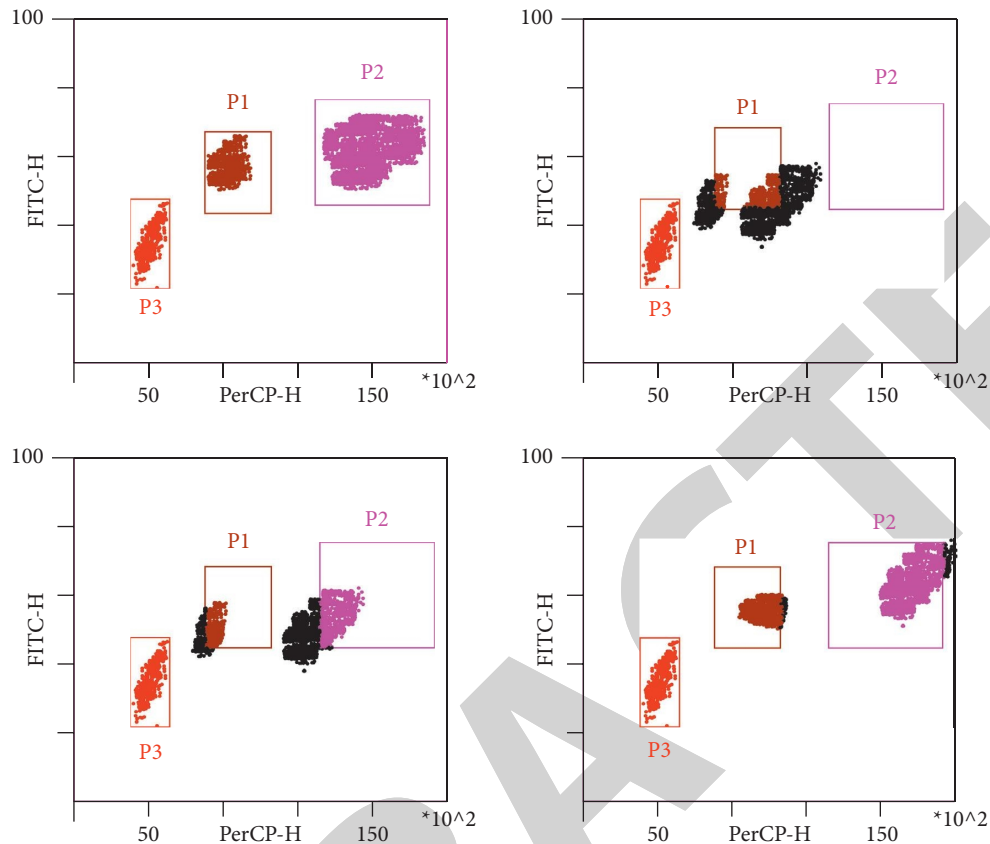


FIGURE 10: Quality control of liquid C of commercial sperm DFI quality control.

quality control, which severely limits the clinical application of sperm DNA integrity detection technology [29].

**4.3. Overview.** In this study, Celula provided commercial sperm DFI quality control products containing single-stranded and double-stranded simulated cells and the scattered dots of single-stranded DNA were scattered, which can effectively simulate the gradual development process of sperm DNA damage. At the same time, the concentration of acidification solution and staining solution and whether the sample addition operation is qualified can be indicated through the scattered circle gate, and the quality of the reagent and the test operation process can be controlled [30]. Compared with the sperm quality control products used in various laboratories (laboratory self-made quality control products), it has 4 obvious advantages: (1) Storing at 2–8°C, it is easier to manage and store. (2) The test results of continuous testing for 30 days show that the CV of commercial sperm DFI quality control products is much smaller than that of laboratory self-made DFI quality control products, which has a better stability. (3) The interbatch precision shows that the CV of commercial sperm DFI quality control products is  $\leq 6\%$ . However, laboratory-made quality control products use different sperm samples, and the uniformity of the cells in the samples is different, which is more likely to cause intra-assay and interassay variability. (4) In addition, laboratory-made quality control products

involve human genetic samples, which have many potential ethical and other risks and cannot be used for external quality control.

**4.4. Insufficient Essential Controls.** The raw materials of commercial sperm DFI quality control products are derived from animal cells. It is considered that the damaged DNA is processed and then mixed with intact DNA cells in proportion to simulate real sperm samples. Therefore, commercial sperm DFI quality control products are mainly used to simulate sperm DNA damage, and it is currently impossible to simulate and control the high DNA stainability index (HDS). But in any case, the quality control products provided by Celula break the gap of quality control products for sperm DNA integrity testing, allowing clinical testing laboratories and rooms to have stable and reliable quality control products to choose from. It needs more data to support its clinical application value.

## 5. Conclusions

This paper focuses on the technical evaluation of commercial sperm DFI quality control products in SCSA detection. The commercial sperm DFI quality control products can simulate sperm DNA damage to achieve accurate detection of DNA integrity; the new commercial sperm DFI quality control product can sensitively respond to changes in the

concentration of acidification solution and staining solution at the same time and can effectively control the detection reagents and experimental procedures. The new commercial sperm DFI quality control product can effectively control the sperm DNA integrity test and can be used as an external quality control product to control the test results to ensure that more accurate test results are provided to the clinic.

## Data Availability

The data that support the findings of this study are available from the corresponding author upon reasonable request.

## Conflicts of Interest

The authors declare that there are no conflicts of interest with respect to the research, authorship, and/or publication of this paper.

## Acknowledgments

This study was supported by the Guangzhou Municipal Science and Technology Bureau (Grant no. 202002030480) and the Guangdong Provincial Natural Science Foundation (Grant no. 2021A1515011544).

## References

- [1] S. Jun, L. Wu, Y. B. Gao, H. Shi, and Y. P. Sun, "[Correlation of sperm DNA fragmentation index with semen parameters]," *Zhonghua nan ke xue = National journal of andrology*, vol. 25, no. 2, pp. 129–134, 2019.
- [2] Hongyi and G. Yang, "The effect of sperm DNA fragmentation index on assisted reproductive technology outcomes and its relationship with semen parameters and lifestyle," *Translational Andrology and Urology*, vol. 8, no. 4, pp. 356–365, 2019.
- [3] C. Niederberger, "Re: concordance among sperm deoxy-ribonucleic acid integrity assays and semen parameters," *The Journal of Urology*, vol. 195, no. 2, 447 pages, 2016.
- [4] P. V. Bach and P. N. Schlegel, "Sperm DNA damage and its role in IVF and ICSI," *Basic and Clinical Andrology*, vol. 26, no. 1, p. 15, 2016.
- [5] J. Hallak, "Utility of sperm DNA fragmentation testing in different clinical scenarios of male reproductive abnormalities and its influence in natural and assisted reproduction," *Translational Andrology and Urology*, vol. 6, no. S4, pp. S509–S512, 2017.
- [6] N. Asare, N. Duale, H. H. Slagsvold et al., "Genotoxicity and gene expression modulation of silver and titanium dioxide nanoparticles in mice," *Nanotoxicology*, vol. 10, no. 3, pp. 312–321, 2016.
- [7] A. S. Rex, J. Aagaard, and J. Fedder, "DNA fragmentation in spermatozoa: a historical review," *Andrology*, vol. 5, no. 4, pp. 622–630, 2017.
- [8] P. Kunkitti, A. Sjö Dahl, A.-S. Bergqvist, A. Johannisson, and E. Axner, "Comparison of DNA fragmentation assay in frozen-thawed cat epididymal sperm," *Reproduction in Domestic Animals*, vol. 51, no. 4, pp. 618–622, 2016.
- [9] C. Bustamante, Z. Bryant, and S. B. Smith, "Ten years of tension: single-molecule DNA mechanics," *Nature*, vol. 421, no. 6921, pp. 423–427, 2016.
- [10] G. P. Mitchell, C. A. Mirkin, and R. L. Letsinger, "Programmed assembly of DNA functionalized quantum dots," *Journal of the American Chemical Society*, vol. 121, no. 35, pp. 8122–8123, 2016.
- [11] D. F. Bogenhagen, "Mitochondrial DNA," *Journal of Biological Chemistry*, vol. 278, no. 9–10, pp. 50961–50969, 2018.
- [12] J. Sandoval, H. Heyn, S. Moran et al., "Validation of a DNA methylation microarray for 450,000 CpG sites in the human genome," *Epigenetics*, vol. 6, no. 6, pp. 692–702, 2011.
- [13] B. Goldense and L. Dfi, "Design for IIoT & IoT," *Machine Design*, vol. 89, no. 4, 64 pages, 2017.
- [14] A. C. Komor, Y. B. Kim, M. S. Packer, J. A. Zuris, and D. R. Liu, "Programmable editing of a target base in genomic DNA without double-stranded DNA cleavage," *Nature*, vol. 533, no. 7603, pp. 420–424, 2016.
- [15] K. G. Lark, "Evidence for the direct involvement of RNA in the initiation of DNA replication in *Escherichia coli* 15T-," *Journal of Molecular Biology*, vol. 64, no. 1, pp. 47–60, 2016.
- [16] J. I. Fuxman Bass, C. Pons, and L. Kozlowski, "A gene-centered *C.elegans* protein–DNA interaction network provides a framework for functional predictions," *Molecular Systems Biology*, vol. 12, no. 10, pp. 1193–1205, 2016.
- [17] H. L. Klein, "Guidelines for DNA recombination and repair studies: cellular assays of DNA repair pathways," *Wiley Subscription Services, Inc. A Wiley Company*, vol. 17, no. 2, pp. 147–159, 2019.
- [18] C. D. Richardson, G. J. Ray, M. A. Dewitt, G. L. Curie, and J. E. Corn, "Enhancing homology-directed genome editing by catalytically active and inactive CRISPR-Cas9 using asymmetric donor DNA," *Nature Biotechnology*, vol. 34, no. 3, pp. 339–344, 2016.
- [19] M. Kenney and B. U. Von, "Technology, entrepreneurship and path dependence: industrial clustering in Silicon Valley and Route 128," *Industrial and Corporate Change*, vol. 8, no. 1, pp. 67–103, 1999.
- [20] A. Grosberg, Y. Rabin, S. Havlin, and A. Neer, "Crumpled globule model of the three-dimensional structure of DNA," *Europhysics Letters (EPL)*, vol. 23, no. 5, pp. 373–378, 1993.
- [21] J. M. Jakicic, K. K. Davis, R. J. Rogers et al., "Effect of Wearable Technology Combined With a Lifestyle Intervention on Long-term Weight Loss," *JAMA*, vol. 316, no. 11, pp. 1161–1171, 2016.
- [22] H. J. Lowe, E. C. Lomax, and S. E. Polonkey, "The World Wide Web: a review of an emerging internet-based technology for the distribution of biomedical information," *Journal of the American Medical Informatics Association*, vol. 3, no. 1, pp. 1–14, 1996.
- [23] K. Hart, N. Foloppe, C. M. Baker, E. J. Denning, L. Nilsson, and A. D. Mackerell, "Optimization of the CHARMM additive force field for DNA: improved treatment of the BI/BII conformational equilibrium," *Journal of Chemical Theory and Computation*, vol. 8, no. 1, pp. 348–362, 2012.
- [24] T. Luukkonen, O. Persson, and G. Sivertsen, "Understanding patterns of international scientific collaboration," *Science, Technology, & Human Values*, vol. 17, no. 1, pp. 101–126, 2016.
- [25] J. N. Acharya, A. J. Hani, J. Cheek, P. Thirumala, and T. N. Tsuchida, "American clinical neurophysiology society guideline 2: guidelines for standard electrode position nomenclature," *The Neurodiagnostic Journal*, vol. 56, no. 4, pp. 245–252, 2016.
- [26] B. R. Nelson, C. A. Makarewich, D. M. Anderson et al., "A peptide encoded by a transcript annotated as long noncoding RNA enhances SERCA activity in muscle," *Science*, vol. 351, no. 6270, pp. 271–275, 2016.

## Retraction

# Retracted: Design of Optimal Scheduling Model for Emergency Medical Supplies by Blockchain Technology

### Journal of Healthcare Engineering

Received 10 October 2023; Accepted 10 October 2023; Published 11 October 2023

Copyright © 2023 Journal of Healthcare Engineering. This is an open access article distributed under the Creative Commons Attribution License, which permits unrestricted use, distribution, and reproduction in any medium, provided the original work is properly cited.

This article has been retracted by Hindawi following an investigation undertaken by the publisher [1]. This investigation has uncovered evidence of one or more of the following indicators of systematic manipulation of the publication process:

- (1) Discrepancies in scope
- (2) Discrepancies in the description of the research reported
- (3) Discrepancies between the availability of data and the research described
- (4) Inappropriate citations
- (5) Incoherent, meaningless and/or irrelevant content included in the article
- (6) Peer-review manipulation

The presence of these indicators undermines our confidence in the integrity of the article's content and we cannot, therefore, vouch for its reliability. Please note that this notice is intended solely to alert readers that the content of this article is unreliable. We have not investigated whether authors were aware of or involved in the systematic manipulation of the publication process.

Wiley and Hindawi regrets that the usual quality checks did not identify these issues before publication and have since put additional measures in place to safeguard research integrity.

We wish to credit our own Research Integrity and Research Publishing teams and anonymous and named external researchers and research integrity experts for contributing to this investigation.

The corresponding author, as the representative of all authors, has been given the opportunity to register their agreement or disagreement to this retraction. We have kept a record of any response received.

### References

- [1] Y. Zhao, "Design of Optimal Scheduling Model for Emergency Medical Supplies by Blockchain Technology," *Journal of Healthcare Engineering*, vol. 2022, Article ID 4608761, 10 pages, 2022.

## Research Article

# Design of Optimal Scheduling Model for Emergency Medical Supplies by Blockchain Technology

Yan Zhao 

*College of Management, China University of Mining and Technology, Xuzhou, Jiangsu, China*

Correspondence should be addressed to Yan Zhao; [vivizhaoyan@xzit.edu.cn](mailto:vivizhaoyan@xzit.edu.cn)

Received 11 November 2021; Accepted 15 January 2022; Published 18 February 2022

Academic Editor: Yang Gao

Copyright © 2022 Yan Zhao. This is an open access article distributed under the Creative Commons Attribution License, which permits unrestricted use, distribution, and reproduction in any medium, provided the original work is properly cited.

The study aims to explore the scheduling plan for the emergency of blockchain technology in the medical industry. Network security architecture for medical supplies management based on the Hyperledger Fabric optimized consensus mechanism is established by studying the characteristics of blockchain technology and its data structure composition. The supply chain model for medical device scheduling based on intelligent contracts is selected for the particularity of the nature and shape of medical devices in medical supplies. Ant colony algorithm is used to solve it. Case analysis and verification results show that the improved Hyperledger Fabric consensus mechanism has better security performance. Under the condition of 10,000 transactions, the probability of an attacker with the optimized consensus mechanism successfully controlling the transaction is only 7.2%. The optimized solution is about 50% higher than the original solution in terms of transaction processing speed. Over 1000 transactions, the transaction latency optimization rate is more than doubled. The total order completion time of the medical device scheduling model adopted by the intelligent contract is 26.3% higher than the historical service time of 19 days. The performance of the medical emergency material scheduling program that is added to the supply chain technology is better.

## 1. Introduction

The handling of medical emergencies is related to everyone's life and health. For example, the rapid coronavirus disease 2019 (COVID-19) outbreak in the past two years has spread to the world [1]. The efficiency and accuracy of medical supplies dispatching in such incidents require close collaboration and cooperation between the medical staff of various medical institutions and personnel of multiple institutions, such as logistics systems in order to minimize the risk of human life safety [2]. The characteristics of decentralization, transparency, autonomy, and nontameability of blockchain technology can keep the quantity, location, and delivery status of medical supplies under real-time control during the medical supplies dispatching process. It can provide timely adjustment plans according to the development status of medical emergencies [3–5]. Therefore, the establishment of such a log scheduling system with the blockchain as the global control gives the platform the ability to trace any form of data modification, which can ensure that

any data modification operation is transparent to all personnel of the medical institution participating in the collaboration. It can ensure the integrity of data during the transportation of medical supplies, thereby establishing a trust relationship between multiple agencies involved in the prevention and control of public emergencies. Meanwhile, it can also greatly reduce the communication costs and conflicts caused by mutual distrust and improve the efficiency of material scheduling [6].

Regarding the application of blockchain technology in the scheduling of medical supplies, scholars have also achieved a lot of research results. The huge amount of data in the healthcare system makes it difficult to ensure safety and diagnostic procedures. In order to solve these problems, Sammeta and Parthiban [7] developed a new ultrazipper blockchain to support safe medical data management using deep learning diagnostic models. The presented model involves different stages of operation, such as encryption, optimal key generation, blockchain-based super-blockchain security data management, and diagnosis. The integration of

the Internet of Things (IoT) in the medical system can support medical events, such as real-time diagnosis, remote patient monitoring, and real-time drug prescriptions. However, the integrity and confidentiality of medical information on the Internet of Medical Things (IoMT) platform is still one of the controversies leading to medical service issues. Ogundokun et al. [8] proposed an Encryption-Stegno model to ensure medical information about the IoMT environment. In response to the Acquired Immune Deficiency Syndrome (AIDS) epidemic, stakeholders such as clinicians, community advocates, and researchers have used various forms of technology to alleviate the crisis. Garrett and Young [9] pointed out that blockchain was an emerging technology that originated from cryptocurrency. The function of the blockchain is very suitable for working in HIV. Its ability to safely transmit information and interact makes it a potentially useful tool. It can incorporate research and practice related to stigmatized diseases such as HIV, which require methods to maintain a high degree of security and confidentiality. There are many researches on the application of blockchain technology in the medical industry, but there are few studies in the field of medical material dispatching. The research on the dispatch of emergency supplies for medical emergencies can fill this research gap.

Using the methods of literature research and model verification, the study discusses the application of blockchain technology in medical material distribution. The innovation is that the optimized Hyperledger Fabric mechanism is adopted. The security, running speed, and transaction delay of the medical material dispatching network platform are improved. Ant colony algorithm is used to optimize the supply chain model for medical device scheduling logistics. Compared with similar studies in other related fields, this model can obtain shorter order completion time, and the transaction processing speed and transaction optimization rate have been greatly improved. The study is structured as follows. Section 1 describes the application background and current research status of blockchain technology in medical emergencies. Section 2 introduces the security analysis of medical material management based on the Hyperledger Fabric consensus mechanism. Section 3 compares and analyzes the corresponding research results given by the research method in Section 2, and Section 4 is the research conclusion.

## 2. Materials and Methods

**2.1. Blockchain Technology and Its Data Structure.** Blockchain technology is a decentralized distributed database integrated by multiple technologies. It uses Distributed Ledger Technology (DLT), which is a decentralized recording method [10]. There is no need to establish a trust relationship between each node of the blockchain. All node members in the blockchain can participate in data maintenance. Every node participating in the maintenance can obtain a complete copy of the blockchain data. Therefore, the blockchain is often described as a distributed ledger in which all nodes participate in the accounting records [11]. Each participant has their own complete copy of the ledger.

Compared with traditional databases that emphasize centralization, blockchain technology maintains the characteristics of decentralization, transparency, autonomy, and immutability [12].

The characteristic of decentralization means that all nodes in the blockchain have an equal relationship, and there is no trust center node. All nodes jointly maintain the data on the blockchain, which is the most fundamental feature of blockchain technology. Transparency is the basis for ensuring mutual trust among system nodes [13]. All update operations of nodes in the entire network are open and transparent to other nodes. All nodes can obtain any data and update records at any location in the blockchain at any time when needed [14]. No human intervention is required. All of its behaviors are autonomous, and only a predetermined algorithm determines how to operate. The cryptography technology in the blockchain can ensure that all data on the blockchain cannot be modified but can only be added. Because the cost of modifying the data on the blockchain is very high, this ensures that the blockchain data cannot be tampered with [15]. Blockchain architecture usually consists of a data layer, network layer, public awareness layer, incentive layer, contract layer, and application layer [16]. The data structure of the Bitcoin block is shown in Figure 1:

**2.2. Recent Research Work on Blockchain Technology.** In recent years, blockchain-based decentralized cryptocurrencies have attracted a lot of attention. Bitcoin is the first blockchain application, which has achieved great success and promoted more development in this field. However, the development of Bitcoin has encountered performance problems of low throughput and high transaction latency. Other cryptocurrencies based on proof-of-work also have these shortcomings, leading to more concerns about the scalability of the blockchain. Zhou et al. [17] tried to cover the existing extended blockchain solutions and classify them by level. In addition, they compared different methods and listed some potential directions for solving blockchain scalability issues. Various innovative applications are growing exponentially, such as smart agriculture, innovative healthcare, supply chain, logistics, commerce, tourism and hotels, energy management, etc. However, open channels for all applications, security, and privacy are the main issues. However, many security solutions and standards have been proposed to enhance the security level of intelligent applications. The existing solutions are either based on a centralized architecture or have high computing and communication costs. In addition, most existing security solutions only focus on a few aspects and fail to address the issues of scalability, robustness, data storage, network latency, immutability, and traceability. Blockchain technology has become one of the solutions to these problems. Based on these facts, Bodkhe et al. [18] conducted a systematic analysis of various blockchain-based solutions and their applicability in diverse industry 4.0-based applications. Many experts analyzed the potential applications of blockchain technology in different aspects of markets, institutions, or government

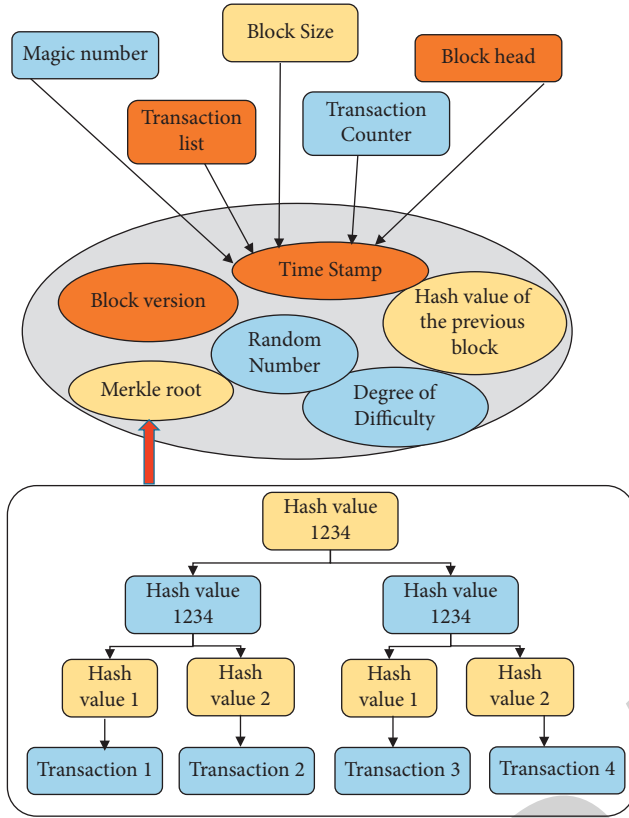


FIGURE 1: Block structure composition of Bitcoin.

organizations. In the brief history of blockchain, the use of blockchain has made incredible achievements. These aspects' sheer number and complexity may make it difficult to solve the blockchain problem. Nanayakkara et al. [19] found that the structure of blockchain and modern cloud edge computing are essential for new participants to realize the widespread adaptation and development of blockchain technology. The use of public and open-source codebases and tools will help ensure that the full potential is acknowledged of the blockchain.

**2.3. Security Analysis of Medical Supplies Management Using Hyperledger Fabric Consensus Mechanism.** Hyperledger Fabric network platform, as a kind of blockchain consensus mechanism, is an open and open-source project. Although the Hyperledger Fabric network platform is also decentralized like blockchain technology, the status of nodes in its network is different. Ordinary nodes must be authorized and authenticated by special nodes in the network before they can be added, which can reduce resource consumption while increasing transaction processing speed [20–22]. Applying it to the management part of material scheduling for medical emergencies can ensure data security and transmission speed in the material scheduling process. The original consensus mechanism of Hyperledger Fabric is shown in Figure 2:

First, the client will generate a proposal. Then, the proposal is sent to the endorsing node. The proposal has the on-chain code that needs to be executed, that is, the

smart contract and some other information that contains the signature carried by the client and the time stamp of the proposal generation. The endorsing node verifies whether the proposal is sent by the authenticated client by sending the signature in the proposal from the client. If not, the endorsing node will terminate the transaction. The result of the execution generates a set of read and write sets using the current ledger status. When there are multiple sorting nodes in all ledgers, the system will automatically call the Kafka cluster to sort transactions according to certain rules. There are some problems with this mechanism: after the transaction speed is increased, the existence of some key nodes will cause a certain “centralization” problem in the entire system due to the unequal relationship between nodes. In order to improve the security and performance of the Hyperledger Fabric consensus mechanism, a dynamic random method is used to determine the identity of the endorsing node. The optimized Hyperledger Fabric consensus mechanism is shown in Figure 3:

Since the endorsement node of the optimized scheme is randomly selected by using a verifiable random function, this virtually strengthens the security and privacy of the node and reduces the possibility of the node being attacked. The use of a verifiable random function can reduce the possibility of a fixed number of nodes always serving as endorsing nodes, which reduces the degree of centralization of endorsing nodes. Since the optimized node is no longer fixed because of the endorsement node, the probability of being attacked successfully will be reduced, which can improve the security of the system. Attacking hackers want to successfully attack and control a candidate endorsing node. Trying to use this as an opportunity to destroy the entire transaction is almost impossible. Because the system needs to select only one node during the attack, and this node happens to be controlled by the adversary. The probability of occurrence of this situation is shown in the following:

$$\text{pr} = \frac{1}{n} c_n^1 (1 - \lambda)^{n-1} = (1 - \lambda) \lambda^{n-1}. \quad (1)$$

$\lambda$  represents the present threshold for selecting endorsement nodes, and  $n$  represents the number of peer nodes included in the candidate endorsement node set. Assuming that the number of candidate endorsement nodes is 10, the threshold is 0.4. Then control an endorsement node, and the probability that the attacker can interfere with the transaction is as follows:

$$\text{pr}_i = \begin{cases} c_k^i (1 - \lambda)^i (\lambda)^{n-i}, & 0 < i \leq k, \\ c_{n-k}^{i-k} (1 - \lambda)^i (\lambda)^{n-i}, & k < i < 2k. \end{cases} \quad (2)$$

$\text{pr}_i$  represents the probability that the adversary can interfere with the transaction.  $k$  represents the number of endorsement nodes.  $\lambda$  represents the required threshold for selecting endorsement nodes set in advance.  $n$  represents the number of peer nodes contained in the candidate endorsement node set. The probability of an attacker who successfully interferes with the transaction by controlling  $k$  endorsing nodes is shown in the following:

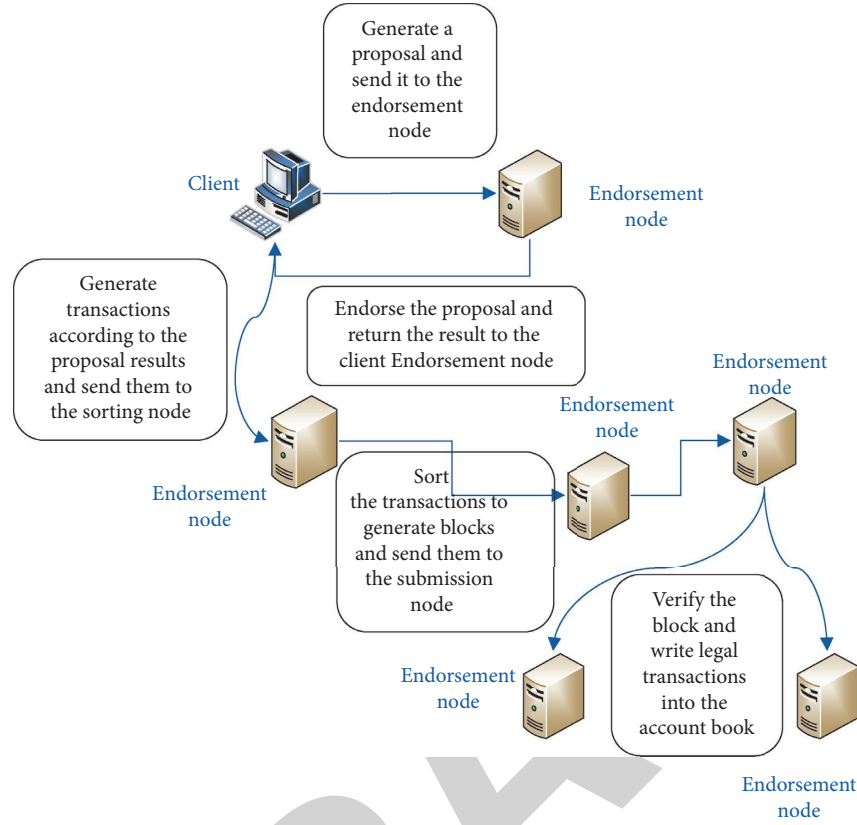


FIGURE 2: Schematic diagram of Hyperledger Fabric consensus mechanism.

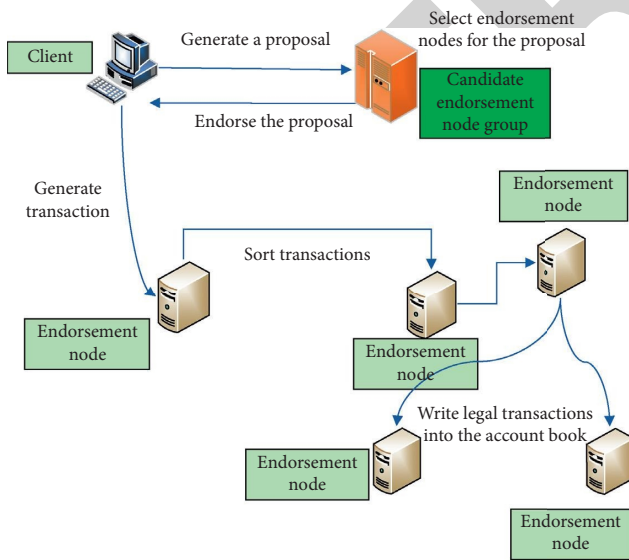


FIGURE 3: Schematic diagram of Hyperledger Fabric consensus mechanism.

$$pr = \sum_{i=1}^n pr_i. \quad (3)$$

When facing the same transaction, many clients have different random numbers, and their endorsement nodes are also different. Endorsement nodes that are not selected can

simultaneously endorse other clients. This parallel processing mode can speed up transaction processing. In addition, from the moment a client initiates a transaction until the transaction is recognized by the entire network, the process of endorsing the transaction by the candidate endorsing node may increase the transaction process time and cause transaction delay. There are usually some problems in applying this improved scheme to the existing medical material dispatching platform. The network deployment topology is shown in Figure 4. The disadvantages of centralized data storage are obvious. All electronic data are stored in a centralized central server. Once this server is attacked by hackers, it will face data leakage and malicious tampering of data. This will cause devastating consequences and immeasurable economic losses to all medical material platforms. If affected by natural disasters, the entire system will face collapse and system security will be low. As enterprise business expands and the number of orders increases, platform data will show explosive growth. This requires the establishment of a central server with stronger processing capabilities, and the centralized storage requires a huge amount of funds to be used for third-party centralized organizations to ensure the smooth operation of the system, and the cost is high. In addition, traditional electronic documents will go back and forth along the entire supply chain with the materials, requiring a lot of complicated operations. In order to ensure the safe operation of the system, a centralized third-party organization is often required to assist in the certification, which invisibly leads to

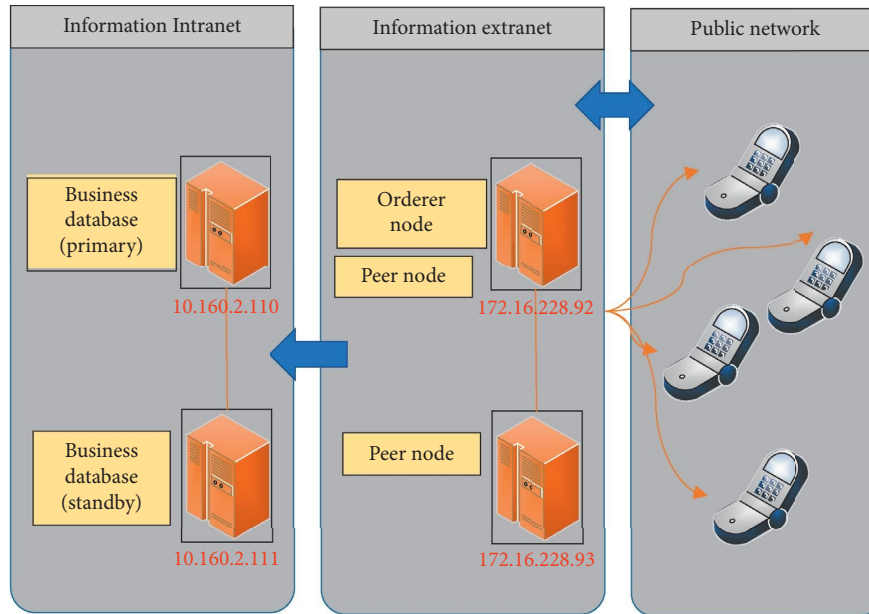


FIGURE 4: Network topology diagram of the current medical material platform.

relatively low efficiency of all processes. Applying the above-mentioned improvement scheme to this kind of medical material dispatching system can improve these problems to a great extent.

The application of blockchain technology in the material scheduling platform, and the private chain operation in the early stage, can not only ensure the security and authenticity of data but also improve the efficient collaboration of various units within the enterprise in the material fulfillment process. Suppliers and other external units use the “real-name identity authentication + service agreement” method to achieve business linkage through application identity access management and quick access to the platform. The core database is placed in the company’s information and communication computer room, and the database is used to store core business data.

In the mid-term, the system will build a larger range of alliance chains in conjunction with other organizations or authorities on the basis of the existing private chain. Meanwhile, the consortium chain can set an admission mechanism for the joining nodes, and the nodes can perform limited queries through the Application Programming Interface (API) [23] opened by the blockchain. The expanded network topology is shown in Figure 5:

In the later period, the robustness and stability of the entire platform is considered. If conditions permit, the platform will eventually adopt the Kafka cluster deployment mode. Among them, the order node will also be deployed in a cluster. In order to further ensure the immutability and authority of the consortium chain, by gradually increasing the members of the consortium chain, if conditions permit, at least one public trust institution shall be introduced as a consortium member to ensure the credibility of the consortium chain. Therefore, the final network topology is shown in Figure 6:

According to the final network structure, the minimum server configuration requirements are: a server with expansion requirements. It requires a 4-core Central Processing Unit (CPU), a memory of 4G, a hard disk capacity of 500G, and an operating system of Centos7.4. There are three servers each, ZooKeeper, Kafka, and Order in this configuration. To ensure consistent blockchain technology, superior stability and performance, the minimum hardware configuration requirements for the added node are: 1 server, Centos7.4 operating system, 4-core CPU, memory at least 4G, and hard disk capacity above 1T.

System performance is tested and safety is tested. Ten candidate endorsement nodes are selected, and 5 endorsement nodes successfully attacked by the adversary. Golang1.9 is used by the platform, and the crypto package in Golang is used to verify random functions. The curve-p256 elliptic curve is adopted. The hash function is sha-256, which can better show the advantages of the optimization scheme. The transaction speed is tested: the present number of candidate endorsement nodes is 10, and the threshold is 0.4. When 1, 10, 100, and 1000 transactions are initiated, the original plan and the optimized plan are compared with the average time it takes to successfully process each transaction in the medical material platform.

**2.4. Construction of Smart Contract Model of Medical Device Dispatching Supply Chain.** Medical emergencies often carry great safety risks. Therefore, timely measures such as emergency preparations, monitoring, prediction, early warning, reserve, and on-site disposal shall be taken to prevent possible factors that may cause public health emergencies, and to prevent the emergence of public health emergencies. The control of public health emergencies requires a certain degree of timeliness. As a kind of medical supplies, medical equipment has many problems in the

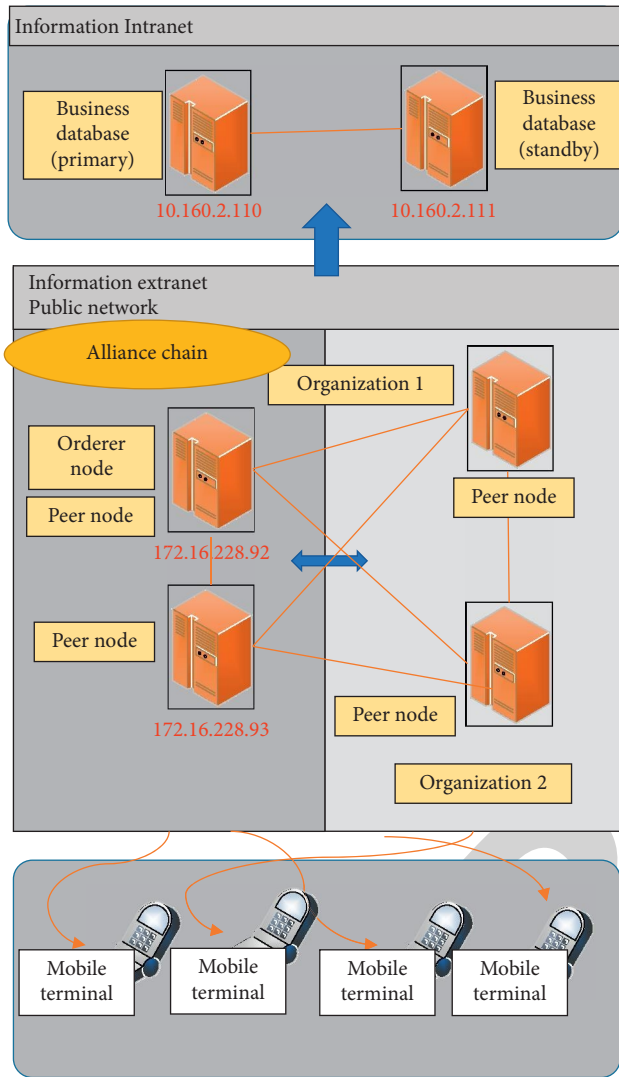


FIGURE 5: Network topology diagram of the expanded medical material platform.

dispatching process. Smart contracts are codes that are stored, verified, and executed on the blockchain and are a way of spreading through information channels. It completes the business logic assigned by the user according to the preset instructions to verify and execute the computer protocol of the task.

Because of the different types of medical devices and different models and sizes, biological and chemical reactions may occur between each other during the scheduling process. Therefore, there are higher requirements for storage and transportation conditions, logistics environment and timeliness, tracking and monitoring of the entire logistics, and management capabilities of logistics service providers. In addition, the lack of close cooperation among enterprises in the medical device logistics service supply chain, the lack of large-scale medical device logistics service integrators, and the lack of unified data management norms and standards for data collection among logistics enterprises have led to some links in the logistics service supply chain. "Information

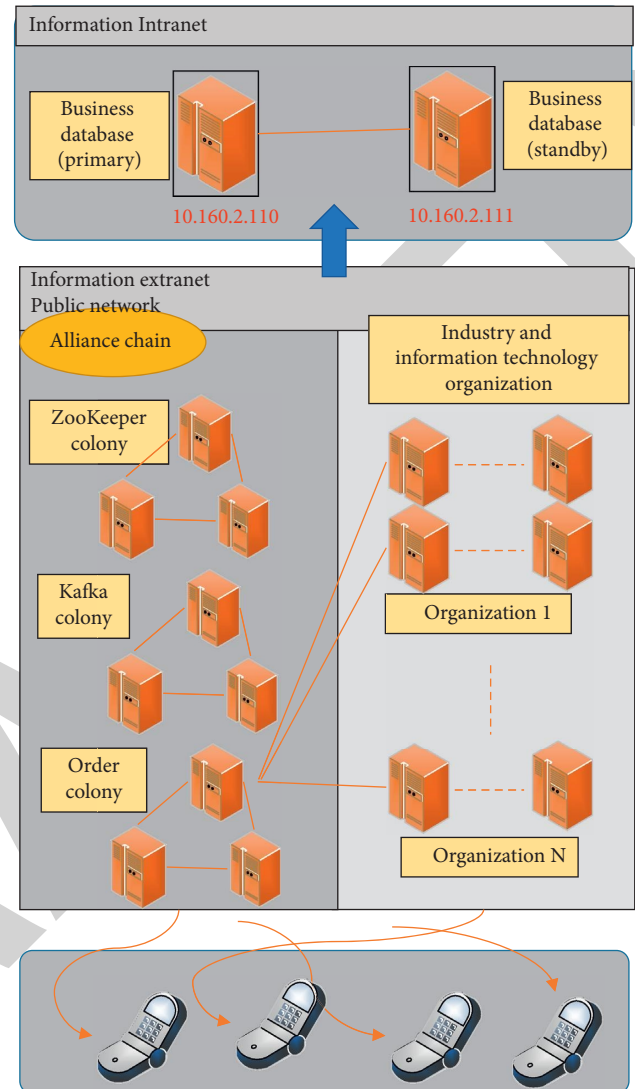


FIGURE 6: The final network topology diagram of the medical supplies platform.

distortion," resulting in poor timeliness of product traceability. Smart contracts can provide smart carriers for all kinds of information such as accounting, transactions, assets, funds, etc. Using the form of blockchain data code to spread across the network, after the security key and the auxiliary confirmation of the front and rear blocks, each node is stored in a time series information. This technology can improve information fraud, tampering, and even deletion. It has the advantages of efficient real-time update, accurate execution, reduced human influence, decentralization, and lower operating costs.

The smart contract technology is used in the supply chain of medical equipment logistics scheduling, and the process design of the smart contract model is shown in Figure 7. Many logistics service providers can perform operational services in the supply chain, and these operational services are arranged in order as a service process. In the design of smart contracts, the state change mechanism is one of the core mechanisms of logistics service supply chain

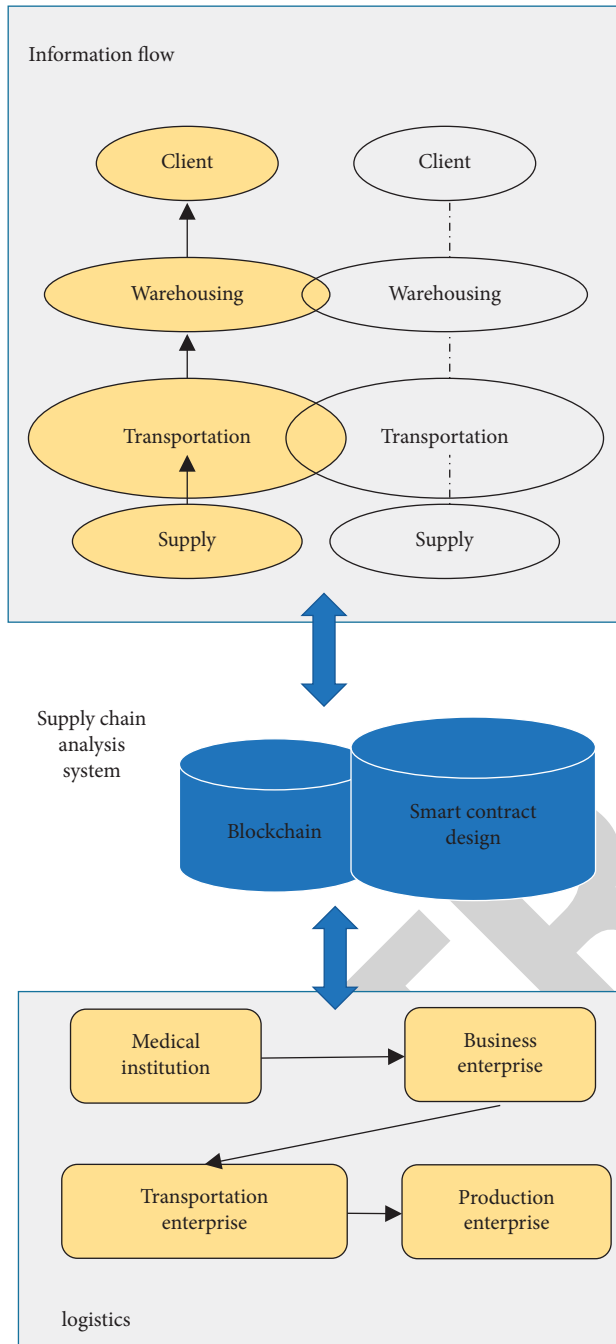


FIGURE 7: Smart contract model design in the context of blockchain.

and smart contract information. Participants are required to transmit data to update the content and state of the contract and synchronize with the actual business. In addition, the smart contract of the logistics supply chain has built-in state attributes to match each link of the logistics service. After the logistics service status is updated, the contract status information will also be updated synchronously.

After the medical device smart contract change mechanism is added, the contract status will be synchronized with the logistics service status. The business processes of logistics companies will be recorded on smart contracts and

blockchains in the form of state changes to achieve the effective integration of “logistics” and “information flow.” The construction of the smart contract model of the medical device service supply chain in the context of the blockchain is actually aiming at the shortest total order scheduling completion time, assigning the service operation to the logistics company and recording the start and end time of the operation in the blockchain. The proposed smart contract model is recorded on the blockchain in the form of code. When the conditions of the logistics service agreement become effective, the code will be automatically executed to complete the selection and scheduling of medical device logistics service providers.

The classic heuristic algorithm ant colony algorithm is used to solve the smart contract model, and the algorithm steps are shown in Figure 8. The ant colony algorithm uses the walking path of the ants to represent the feasible solution to the problem to be optimized. All paths of the entire ant colony constitute the solution space of the problem to be optimized. Ants with a shorter path release more pheromone. As time progresses, the accumulated pheromone concentration on the shorter path gradually increases, and the number of ants that choose this path increases. In the end, the entire ant will concentrate on the best path under the effect of positive feedback. At this time, it corresponds to the optimal solution of the problem to be optimized. The algorithm has good robustness.

The ant colony algorithm is used to select companies in the medical device scheduling service supply chain and coordinate the operations of each order to allocate the operations of scheduling each order to the companies that can provide services so that the order completion time is shortest. The basic idea is to let the ants schedule according to the corresponding service level information provided by the logistics enterprise and use the positive feedback characteristics of the ant colony algorithm to select the best feasible path for each order.

The effectiveness of the ant colony algorithm in the medical equipment logistics scheduling model is verified through experiments. The compilation environment uses PyCharm, the computer is configured as Inter (R) Core (TM) i5-7200, the main frequency is 2.50 GHz, and the installed and running memory is 8 GB.

### 3. Results

**3.1. Performance Analysis of Medical Supplies Management Using Hyperledger Fabric Consensus Mechanism.** When  $n = 10$ ,  $\lambda = 0.4$ , the rate of change of hacker attacking nodes is shown in Figure 9:

In Figure 9, the probability of the attacker’s success in control increases with the number of control nodes, but the trend is very flat. Only when the number of rules exceeds eight will the attack success rate be higher.

The security of the improved Hyperledger Fabric consensus mechanism is guaranteed and can be used.

The system security test result is shown in Figure 10:

In Figure 10, when more than half of the endorsing nodes are attacked for the original scheme, the attacker

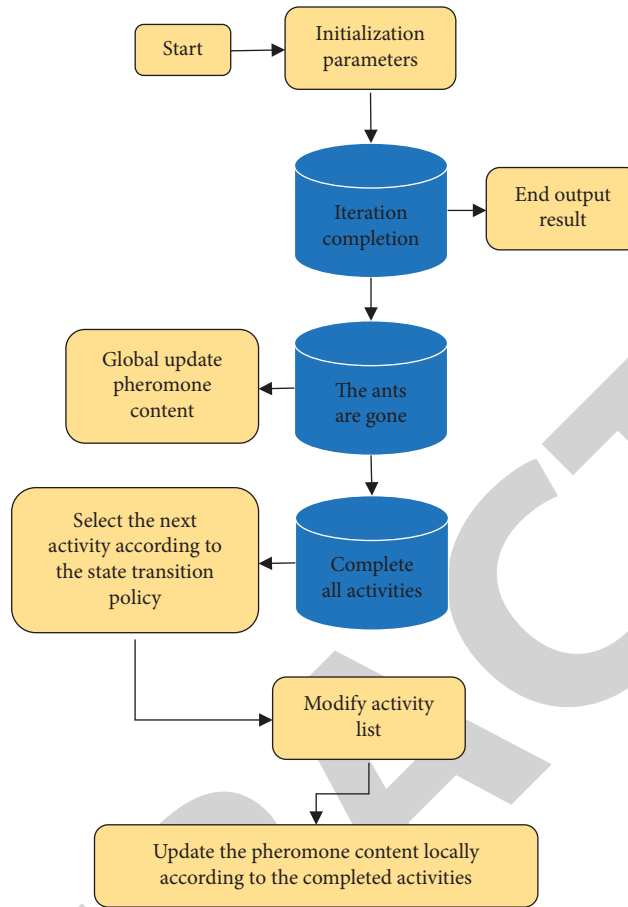


FIGURE 8: Flow chart of ant colony algorithm.

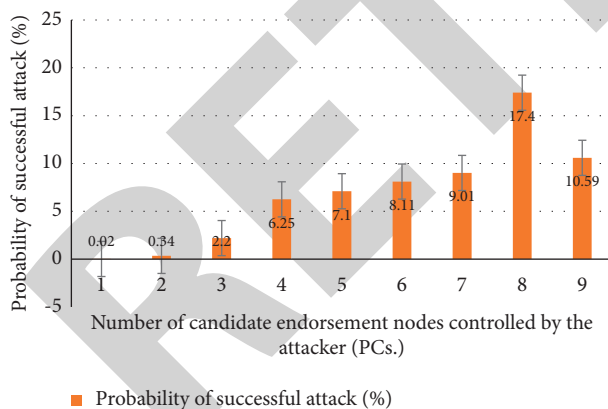


FIGURE 9: Probability of successful attack.

successfully manipulated all transactions. Under the condition of 10,000 transactions, the probability of an attacker with the optimized consensus mechanism successfully controlling the trade is only 7.2%.

Even if more than half of the endorsing nodes are attacked in the transaction after the optimized scheme is adopted, the optimized method can still run safely. The original consensus mechanism has completely fallen of fabric.

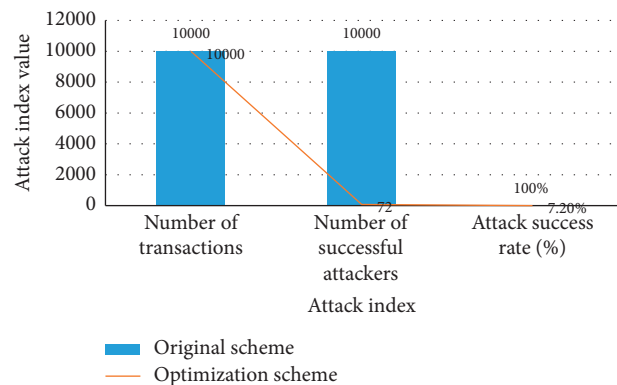


FIGURE 10: Number of occurrences of a node without endorsement.

The results of the time spent on processing each transaction are shown in Figure 11:

In Figure 11, as the number of transactions increases, the transaction time gradually gets longer. The optimized solution is about 50% faster than the original solution in transaction processing speed.

In terms of transaction processing speed, the proposed optimization scheme has advantages.

The comparison result of transaction delay is shown in Figure 12:

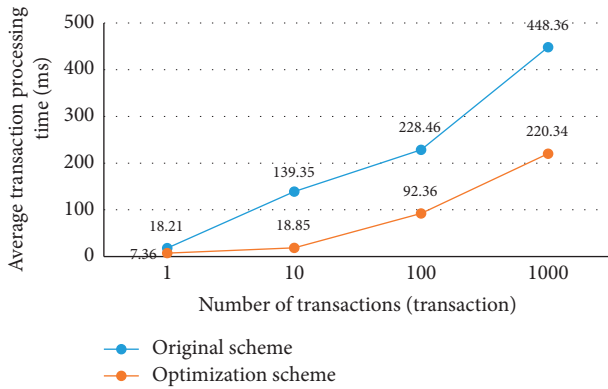


FIGURE 11: Comparison of transaction time between the two schemes.

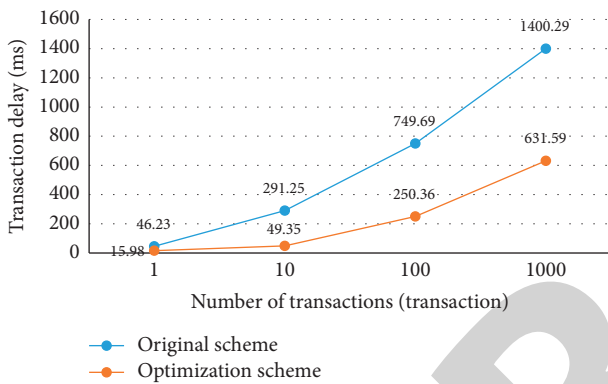


FIGURE 12: Comparison of transaction delay between the two schemes.

In Figure 12, as the number of transactions increases for the two schemes, transaction delays increase accordingly. However, the more the number of transactions increases, the more pronounced the optimized solution optimization of the transaction delay. The optimization rate reaches 128% at the time of 1000 transactions. This is more than twice as high as before being optimized.

The proposed optimization scheme has advantages in the optimization of transaction delay. As the difficulty of the task increases, its benefits become more pronounced.

**3.2. Performance Analysis of Smart Contract Model of Medical Equipment Dispatching Supply Chain.** The impact of the smart contract model on the order completion time is compared with the performance of similar medical device scheduling algorithms in literature [24] and literature [25], as shown in Figure 13:

As Figure 13 suggests, the total time to complete the order of the medical device scheduling model with a smart contract is saved by 5 days compared with the historical service time of 19 days, and the efficiency is improved by 26.3%, which is better than the performance of similar medical device scheduling algorithms.

The use of intelligent contracts saves a great deal of time and cost for the medical device logistics scheduling supply

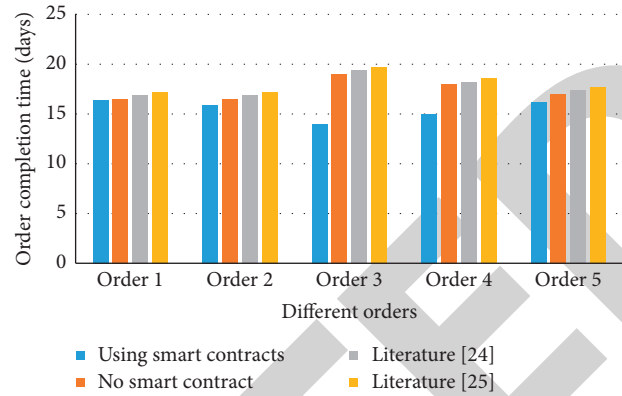


FIGURE 13: Influence of whether to adopt smart contract model on order completion time.

chain and can form economic benefits with obvious advantages.

## 4. Conclusions

With the popularization of the innovation, experimentation of new technologies such as blockchain, and the popularization of applications in multiple fields, including supply chain management, blockchain technology still has advantages for the dispatch of medical supplies for emergency emergencies in the medical industry. The use of blockchain technology in the medical material platform can better realize the real-time sharing of information. The upstream and downstream of the supply chain can achieve effective and trustworthy mutual cooperation and establish a low-cost and high-efficiency medical material supply system. Through the research of blockchain technology, using the drawbacks of Fabric's original consensus mechanism, a medical material management network security scheduling scheme using the Hyperledger Fabric consensus mechanism has been established. Aiming at the particularity of medical devices in medical supplies, a medical device scheduling supply chain model using smart contracts has been established and its performance has been verified. The proposed scheduling scheme that incorporates supply chain technology has been verified in terms of security, transaction time, and the probability of being successfully attacked. The proposed schemes all show superior performance. Some shortcomings still exist: in the medical device scheduling problem, the punishment mechanism for companies submitting information that does not meet actual requirements is not considered. A penalty function can be added in future research to make the proposed scheme more in line with actual requirements.

## Data Availability

The dataset used to support the findings of this study is available from the corresponding author upon request.

## Conflicts of Interest

The authors declare no conflicts of interest.

## Retraction

# Retracted: Analysis and Improvement of Nursing Quality Based on Standardized Information Integration

### Journal of Healthcare Engineering

Received 11 July 2023; Accepted 11 July 2023; Published 12 July 2023

Copyright © 2023 Journal of Healthcare Engineering. This is an open access article distributed under the Creative Commons Attribution License, which permits unrestricted use, distribution, and reproduction in any medium, provided the original work is properly cited.

This article has been retracted by Hindawi following an investigation undertaken by the publisher [1]. This investigation has uncovered evidence of one or more of the following indicators of systematic manipulation of the publication process:

- (1) Discrepancies in scope
- (2) Discrepancies in the description of the research reported
- (3) Discrepancies between the availability of data and the research described
- (4) Inappropriate citations
- (5) Incoherent, meaningless and/or irrelevant content included in the article
- (6) Peer-review manipulation

The presence of these indicators undermines our confidence in the integrity of the article's content and we cannot, therefore, vouch for its reliability. Please note that this notice is intended solely to alert readers that the content of this article is unreliable. We have not investigated whether authors were aware of or involved in the systematic manipulation of the publication process.

Wiley and Hindawi regrets that the usual quality checks did not identify these issues before publication and have since put additional measures in place to safeguard research integrity.

We wish to credit our own Research Integrity and Research Publishing teams and anonymous and named external researchers and research integrity experts for contributing to this investigation.

The corresponding author, as the representative of all authors, has been given the opportunity to register their agreement or disagreement to this retraction. We have kept a record of any response received.

### References

- [1] H. He, H. Li, K. Qiao, B. Hao, and D. Yu, "Analysis and Improvement of Nursing Quality Based on Standardized Information Integration," *Journal of Healthcare Engineering*, vol. 2022, Article ID 9172416, 10 pages, 2022.

## Research Article

# Analysis and Improvement of Nursing Quality Based on Standardized Information Integration

Huixia He,<sup>1</sup> Huiling Li,<sup>2</sup> Kong Qiao,<sup>1</sup> Bin Hao,<sup>2</sup> and Dong Yu<sup>3</sup> 

<sup>1</sup>Hand and Foot Microsurgery, Bayan Nur Hospital, Bayannur, Inner Mongolia 015000, China

<sup>2</sup>Department of Mathematics and Computer, Hetao College, Bayannur, Inner Mongolia 015000, China

<sup>3</sup>Department of Information Engineering, Bayan Nur Hospital, Bayannur, Inner Mongolia 015000, China

Correspondence should be addressed to Dong Yu; yd4306@126.com

Received 20 December 2021; Revised 4 January 2022; Accepted 5 January 2022; Published 11 February 2022

Academic Editor: Weiwei Cai

Copyright © 2022 Huixia He et al. This is an open access article distributed under the Creative Commons Attribution License, which permits unrestricted use, distribution, and reproduction in any medium, provided the original work is properly cited.

Information is becoming increasingly important in social development, and the medical industry's informatization has made significant progress. This paper evaluates the role of nursing informatization in improving nursing quality management by analyzing and comparing changes in nursing quality before and after the implementation of nursing informatization. Using modern computer network technology to evaluate nursing quality, monitor the implementation of nursing management plans, and control nursing quality links in real time has helped to promote and improve nursing quality. The integration mode of the existing hospital information system is sorted out and standardized according to the requirements of refined hospital management. We can optimize the overall architecture of the hospital information system, reduce the tight coupling between business systems, support rapid integration and flexible expansion of business systems, and lay a foundation for the cooperation and data sharing of medical resources in and out of the hospital by establishing a hospital information platform based on standardized specifications.

## 1. Introduction

With the rapid development of science and technology, the introduction of computers into the medical industry has become the basis of modern hospital management. For hospitals, medical quality is not only the lifeline, but also the main core of nursing management. Nursing quality is directly related to the medical level of hospitals [1]. The establishment of electronic information system in hospital is an indispensable tool and means in hospital management and an important measure to achieve the goal of modern hospital management [2]. Traditional nursing management is prone to the problems of slow information turnover, untimely business supervision, and poor standardization of organization and management. With the continuous improvement of information system, the rational use of informatization makes it a powerful helper for nursing managers [3]. The members of the quality control organization are composed of hospital leaders, the nursing staff are

not involved, and the quality control members do not understand the work status of grass-roots nursing staff [4]. Therefore, the quality control organization cannot fully consider some problems. From the perspective of nursing staff, the inspection team is a burden [5]. Therefore, in the face of examination, it is only regarded as a form. On the surface, the quality of nursing is high. However, in fact, there are all kinds of problems in nursing work. With the deepening of the reform of public hospitals, the original information infrastructure and business systems of many hospitals have been unable to meet the business needs of hospital fine management, especially in information integration and data analysis and utilization. Nursing quality is one of the important contents in hospital management, and the nursing quality management system includes quality construction, quality supervision, monitoring, evaluation, and quality continuous improvement [6].

Nursing is an important part of hospital work, and clinical nursing information systems have become one of the

components of hospital information systems, and their development has a direct impact on hospital and community health service management and effectiveness [7]. At this time, hospital development is heavily focused on information technology. Information collection, preservation, transmission, analysis, and processing are all aided by hospital informatization's progress toward electronization, mobility, and barcodes. It is convenient and efficient, increases accuracy and effectiveness, and reduces errors [8]. Because of its ease of data acquisition, the mobile nursing system is a new research direction in information integration and sharing application. In the regional context, a hospital information platform is a critical link in the realization of patient-centered interinstitutional medical information sharing and business collaboration services [9]. The core of nursing management is improving nursing quality and meeting patients' growing health needs. Creating and relying on an information platform is an effective way to promote continuous medical quality improvement.

The traditional business process-driven software development model and point-to-point business system integration model have been unable to meet the new requirements of hospital data planning, and a new model needs to be found for medical information construction [10, 11]. At present, Chinese hospitals are vigorously developing informatization construction so that informatization can better serve patients. Therefore, in the informatization construction, a series of models, application strategies, and methods have been formed [12]. "Hospital information platform based on electronic medical records" refers to the medical information sharing and business cooperation platform connecting clinical information system and management information system based on information collection, storage, and centralized management of patient electronic medical records [13]. It is the basis and carrier of unified integration, resource integration, and efficient operation among different business systems in the hospital. The hospital information platform based on electronic medical records has become an important support to overcome the obstacles of hospital information construction [14]. Hospital informatization construction is gradually shifting from business process software system as the core to a brand-new architecture model based on data planning and information platform as the core [15]. On the basis of perfecting the quality management system and establishing the quality control organization, this paper develops and applies nursing management assistant decision-making, head nurse electronic workbook, nursing electronic medical record, and nursing mobile ward round software step by step by using modern computer network technology. In this paper, a nursing quality basic data collection, management plan implementation, quality analysis and monitoring, and risk prospective prevention system was established, and the continuous improvement of nursing quality was realized.

## 2. Related Work

Literature [16] believes that the biggest problem facing the application of mobile nursing system technology is that there are greater difficulties in the seamless integration of

clinical information and real-time interconnection, which requires continuous optimization and improvement. Literature [17] shows that most tertiary hospitals in China have built a hospital information management system, and its development and application are developing in depth, from focusing on financial operation management, gradually extending to clinical applications and management decision-making applications. Literature [18] proposes that the construction of an information system in a hospital can improve efficiency, save resources, improve service quality, and increase benefits, which is an important way to become a modern hospital. Literature [19] pointed out that many hospitals have implemented inpatient nurse workstations, but they only deal with simple tasks such as doctor's order transfer, printing, and expense entry. Literature [20] developed a nurse human resource planning system based on a microcomputer. Literature [21] pointed out that the coverage of the front-end sensors of the hospital information system and the popularity of networking have become a prerequisite for its development. Therefore, at the level of information collection, it must be three-dimensional, full range, full coverage, and try to avoid omissions and leave no dead ends. Literature [22] believes that in order to realize medical informatization, it is necessary to realize that the human, financial, and material information of medical institutions, the electronic medical records of patients, the results of various testing and inspection equipment, and other complicated data information can be eliminated in this hospital information system. *Obstacle to Flow*. Literature [23] tries to design, develop, and demonstrate the planning, investment and control system of auxiliary hospital management. Literature [24] believes that the hospital information system is a kind of enterprise management system, but different from the general enterprise management system, it serves doctors and patients. Literature [25] pointed out that informatization construction is an important part of medical reform, and hospital informatization construction is imperative. In order to realize all-round medical informatization, medical data standardization must be at the forefront. Literature [26] mentioned that due to the change of medical model and the implementation of holistic nursing, the patient's demand for nursing is increasing, which makes the situation of insufficient nursing human resource allocation even more serious. Literature [27] believes that the developers of modern clinical information systems did not focus on the nursing profession in isolation, but instead focused on the establishment of a multidisciplinary system aimed at supporting a wide range of information systems. An information system with extensive patient clinical data can provide support for quality assessment and improvement of nursing and clinical treatment. Improving the quality of care and meeting the growing health needs of patients is the core of nursing management. Establishing and relying on an information platform is an effective way to promote continuous improvement of medical quality. Therefore, it is of great significance to establish a nursing information system. The information database of comprehensive nursing information platform constructed in this paper has strong expansibility and advanced technology.

Through the application of information technology, the nursing quality management can be guaranteed so as to maximize the safety of patients, improve the present quality of patients, and improve the management level of nursing managers. Save nurses' indirect nursing time and improve the standardization of nursing records. Electronic nursing record sheet is superior to handwritten record sheet in standardization, timeliness, and accuracy. The nursing information system improves the level of nursing quality management.

### 3. Methodology

**3.1. Nursing Information System.** The comprehensive information platform for nursing is a dynamic and visual comprehensive information platform for nursing management, which is supported by the hospital information system and focuses on daily management objectives such as doctor's advice management, electronic nursing medical records, and nursing quality management [28]. The nursing information system consists of four software. The overall design is based on the relatively independent and interrelated functions of four software, collecting basic data of nursing quality on the basis of nursing management decision-making software and nursing electronic medical record software, supervising the implementation of nursing management plan by means of head nurse electronic workbook software, automatically monitoring the nursing process of patients by using nursing mobile rounds software, and promoting the continuous improvement of nursing quality by computer. The nursing information system is shown in Figure 1.

Traditional nursing management has some flaws, such as poor organizational and management standardization, slow information turnover, and so on. Currently, the information system is improving all the time, and nursing managers can improve management quality by using information management in a scientific and rational manner. Nurses and computers make up a nursing information system, which collects, stores, and processes nursing management and business technical data [29]. In the development of hospitals, information technology is the most important factor to consider. Informatization in hospitals has progressed to the point where barcodes and electronization are used, making it easier to share and process information. Its benefits include increased efficiency and speed, which not only improves nursing quality but also reduces nursing errors.

The head nurse manages the work manual system and establishes the standard data query field database, and the head nurses and nursing department managers of each department can use it by multiple users with different permissions, and the head nurses can input and query the related nursing management contents of the department. The nursing department can inquire about the contents of all subjects in the whole hospital, but has no right to modify them. The head nurse's handbook is a memorandum of the head nurse's work. The main contents are as follows: (1) Formulating annual, monthly, and weekly nursing work plans and recording annual work summary. (2) Monthly record of self-examination and self-correction of nursing

quality. (3) Report nursing defects and corrective measures. (4) Continuous quality improvement plan and measures management. (5) Formulation of risk management projects, implementation of measures and effect evaluation. The function of the system in promoting the continuous improvement of nursing quality is to draft improvement plans according to the nursing quality feedback from the nursing department and the self-discovered undergraduate nursing quality problems and nursing defects, consciously implement improvement measures and self-evaluate the improvement effect.

The electronic nursing medical record system is applied to all nursing staff on the basis of strict authority and safety control. It is mainly used for computer management of nursing documents and real-time monitoring of the whole process of pre reminding, in-process supervision, and postevaluation of the writing time limit and writing quality of nursing electronic medical records. Main functions of the system: (1) Management of nursing admission evaluation form, nursing records, temperature list, and so on. (2) According to the time limit of all kinds of records in the nursing medical record writing specification, the computer automatically checks the timeliness and completeness of all kinds of records and reminds nurses in advance. (3) The nursing department queries the nursing medical records of the whole hospital in real time and grasps the nursing quality. And check the timeliness, accuracy, integrity, and other information of nursing medical records automatically counted by computer.

**Mobile Nursing Ward Round System.** On the basis of wireless network coverage in wards, barcode identification of patients' identities, medicines, and test specimens, automatic identification of nursing operation handheld computers is adopted to actively meet the standard requirements of three checks and seven pairs of nursing. It is applied to all nurses, mainly used for drug treatment, patient identity check during specimen collection, and basic nursing operation records. The main functions of the system are as follows: (1) Check the doctor's orders. (2) Check the collection information of test specimens. (3) Vital signs entry. (4) Nursing operation records.

The management assistant decision-making system is applied to the nursing quality control department, which mainly collects the registration, statistics and analysis of the data of previous department nursing quality inspection, nurses' personal business, and theoretical assessment. All data and contents are input after inspection and examination by the nursing department, and the computer automatically summarizes and calculates according to the required query items, and the analysis interface is illustrated with pictures and texts. The head nurse can check the current and historical quality through the network, but has no right to modify it. The main functions of the system are as follows: (1) The entry and statistics of the scores of previous nursing quality examinations in departments. (2) Entry and ranking of personal business and theoretical assessment results. (3) Longitudinal comparison of nursing quality in different periods. (4) Horizontal comparison of nursing quality in

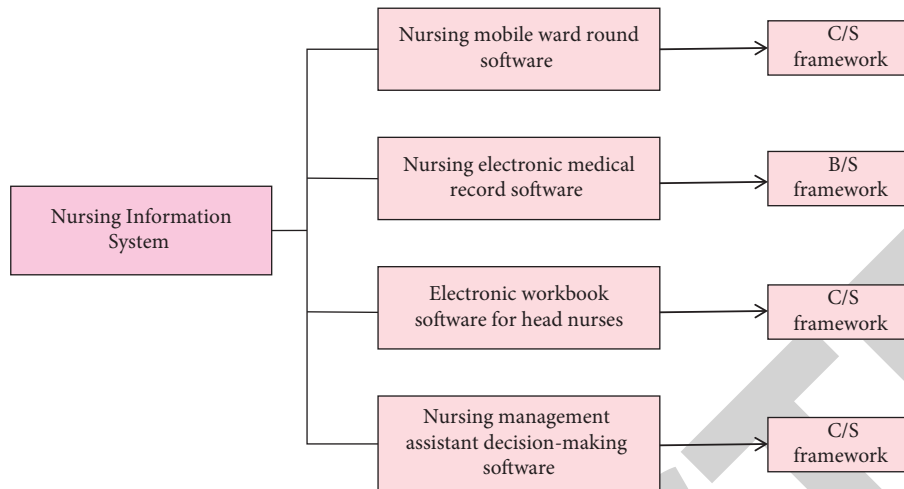


FIGURE 1: The composition of the nursing information system.

different departments. (5) Monthly dynamic analysis of nursing quality. (6) Quality analysis of nursing medical records. (7) Analysis of nursing defects. With the application of nursing management assistant decision-making software, the head nurses can understand the nursing quality problems existing in departments, check the dynamic nursing quality, and compare horizontally by departments or vertically by time, which not only introduces the competition mechanism among the head nurses, but also helps the head nurses to make targeted and timely improvement, which can effectively promote the improvement of nursing quality in the whole hospital year by year.

**3.2. The Role of Nursing Information System in Promoting Continuous Improvement of Nursing Quality.** The greatest advantage of information system is preventive quality improvement, and the focus of continuous quality improvement should be to prevent the occurrence of problems. Only prior quality control can achieve permanent and fundamental quality improvement [30]. At each stage of plan implementation, it is better to focus on preventing defects than to supervise problems.

Change nurses' perceptions of quality management by teaching them that the most important aspect of nursing care is to meet patients' needs as much as possible, rather than forcing patients to adapt to hospital management. Patients should be treated as nursing centers, and all nursing decisions should be made with their input. Reduce conflicts and disputes between doctors and patients by increasing nurses' acceptance of nursing quality control. Nurses can only improve their clinical work execution if they truly understand the assistance and guidance provided by nursing quality control. As a manager, communicate effectively with nurses to gain a better understanding of the practical difficulties and weaknesses that nurses face in their jobs and to address them appropriately in order to improve nurses' satisfaction with nursing quality control. Nurses should abandon the passive nursing mode of the past and actively implement nursing, not just strengthening the aseptic operation of nurses.

Informatization is an effective method for continuous quality improvement. With the help of hospital information system, the information of medical process can be directly collected and processed, the quality situation can be tracked, the quality problems can be found, the quality control can be implemented, and the quality can be evaluated. It is an effective method for continuous quality improvement to transform the traditional quality control after feedback of final quality evaluation into real-time tracking quality control of process quality control.

The scheme design is mainly divided into four parts, namely, input image preprocessing, classification feature selection, classifier training, and character recognition extraction. Its topology is shown in Figure 2.

Through the management of nursing information system, in different stages of nursing quality management, such as planning, implementation, inspection, and processing, the standard data collected by different information systems play their respective functions cooperatively and jointly promote the improvement of nursing quality. After each form, there are quality standards and scores. Inspectors only need to click against the standard, deduct points directly if they fail to meet the standard, and display the unqualified contents in the summary table below, and then the inspectors will write out the problem description and put forward rectification suggestions.

The focus of continuous nursing quality improvement should be on preventing problems rather than checking and correcting them after they occur. The only way to achieve permanent and fundamental quality improvement is to conduct quality control in advance, and the greatest benefit of a nursing information system is preventive quality improvement. Strengthen link control in the implementation process, and ensure timely information feedback to quickly correct errors and avoid negative consequences. Improve quality even more by using a combination of proactive reminders, on-the-job supervision, and postprocess evaluation. Use technological means to improve nursing quality by reforming workflow and preventing errors. A nursing information system can serve as a foundation for quality-

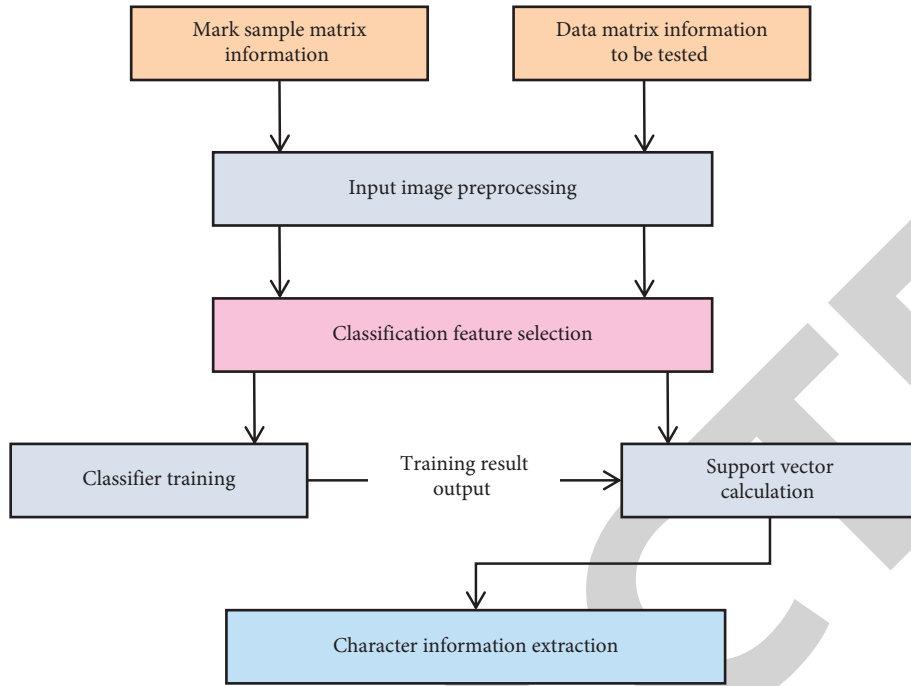


FIGURE 2: Topology diagram of medical monitoring data recognition algorithm scheme.

improvement decision-making in the long run. Facts and data must be used to make decisions, and improvement measures must be based on facts and data to ensure continuous quality improvement. The nursing quality inspection information is gathered by the management assistant decision-making system. We can quickly identify quality issues, assess the work effect, and determine whether there are opportunities to improve the work and solve problems using the directional analysis of the nursing information system.

Based on the hospital information system, all information data of various departments and nursing processes in the hospital were directly collected and processed. Through the information system, it provides the functions of optimal combination, intelligent judgment and assistant decision-making, tracking quality situation, finding quality problems, implementing quality control, and evaluating quality at any time. It is the development trend of medical quality management in the future and an effective method of continuous quality improvement to transform the traditional quality control after feedback of final quality evaluation into real-time tracking quality control of process quality control. Nursing information system can help nurses use modern tools and means to directly serve patients and improve work efficiency.

**3.3. Analysis and Improvement of Nursing Quality.** First, build a font library for all characters in each font to form a precorrelation template; then normalize the input image data to be recognized according to the resolution of the font library, perform two-dimensional cross-correlation matching between the input data and the prebuilt font library, and take the characters with the maximum

correlation in the font library as recognition results for output. Provide business logic methods to the presentation layer. The method itself judges whether the input data is legal and valid and calls the interface of data access layer after verification to realize data addition, deletion, and modification. After execution, return the processing result and processed data to the caller.

The set threshold  $a$  is the projection pixel accumulation threshold, and the set threshold  $b$  is the continuous fracture threshold. Scan the projection result from left to right. When a point less than a value appears in the statistical value of the projection result, it is judged that the point is broken. When the cumulative number of points less than the value of  $a$  in the projection result is greater than  $b$ , it is judged that the characters here can be divided.

The bilinear interpolation method only needs the pixel values of 4 adjacent points near the point to be interpolated to be calculated. The calculation process is as follows: Suppose the point to be interpolated is  $f(u, v)$ , where  $(u, v)$  is the decimal coordinate value; then the 4 adjacent points are  $f([u], [v])$ ,  $f([u] + 1, [v])$ ,  $f([u], [v] + 1)$ , and  $f([u] + 1, [v] + 1)$ ; let  $a = u - [u]$ ,  $b = v - [v]$ . The result of one-dimensional linear interpolation in the abscissa direction is

$$\begin{cases} t_1 = af([u] + 1, [v]) + (1 - a)f([u], [v]), \\ t_2 = af([u] + 1, [v] + 1) + (1 - a)f([u], [v] + 1). \end{cases} \quad (1)$$

In the same way, substituting the interpolation result into the ordinate direction for the second one-dimensional linear interpolation, then

$$\begin{aligned} g(x, y) &= f(u, v) \\ &= bt_2 + (1 - b)t_1. \end{aligned} \quad (2)$$

A one-dimensional difference template is used for gradient calculation for all pixels in each unit. Suppose the pixel value of each point in the image is  $f(x, y)$ ; then the one-dimensional gradient calculation formula corresponding to each point is as follows:

$$\begin{cases} \Delta_x(x, y) = f(x+1, y) - f(x-1, y), \\ \Delta_y(x, y) = f(x, y+1) - f(x, y-1), \end{cases} \quad (3)$$

where  $\Delta_x(x, y)$  is the horizontal gradient value, and  $\Delta_y(x, y)$  is the vertical gradient value. From the above formula, the one-dimensional difference template matrices used in gradient calculation are  $[-1 \ 0 \ 1]$  and  $[-1 \ 0 \ 1]^T$ , and the two templates are used to perform convolution calculations on the image data to obtain the one-dimensional gradient information  $D_{(x,y)}(\Delta_x, \Delta_y)$  of each point.

From the one-dimensional gradient information of each point, the gradient amplitude  $A(x, y)$  and the gradient direction  $\theta(x, y)$  corresponding to the pixel can be obtained as follows:

$$\begin{cases} A(x, y) = \sqrt{\Delta_x(x, y)^2 + \Delta_y(x, y)^2}, \\ \theta(x, y) = \arctan \frac{\Delta_x(x, y)}{\Delta_y(x, y)}. \end{cases} \quad (4)$$

Data integrity, in general, ensures the integrity of entities, references, and user-defined data, whereas entity integrity and reference integrity are the integrity requirements that databases must meet during the design process. The data usage specification that should be followed in database operations is known as user-defined integrity.

Solving the optimal classification hyperplane of support vector machine is mainly to solve the support vector samples in the sample space. When the sample set satisfies the condition of linear separability, the classification hyperplane equation satisfies the following conditions:

$$\begin{aligned} y_i &= \omega x_i + b \\ &= 0. \end{aligned} \quad (5)$$

Among them,  $x_i$  represents the  $i$ th data point,  $y_i$  represents the classification result corresponding to the  $i$ th data point,  $\omega$  represents the normal vector of the hyperplane, and  $b$  represents the intercept of the hyperplane to the feature space. According to the logistic regression model, let  $y_i = -1$  and  $y_i = 1$  represent two different classification results.

The hospital information integration platform enables real-time and data consistency between mobile application-specific data centers and clinical data centers. The nursing department or the department's head nurse set and distributed the quality control contents, and the nursing staff listed the quality control contents and presented the existing problems. The quality control personnel went to the department site for quality control and timely entry after receiving the quality control task, which was a problem. Each department's head nurses complete the problem cause analysis and corrective measures, while the nursing department examines quality control issues and improvement

effects, as well as tracks and supervises the major issues. After passing this quality control, there will still be an unqualified nursing department to assist in locating the source of the problem, as well as to monitor and supervise shift work until the quality control is passed.

Adopt a layered architecture. Call the services provided by the lower layer, and each layer is built on a more general layer. The advantage of the hierarchical structure of is that the attention is dispersed so that developers can only pay attention to one layer in the whole structure. Decentralized coupling makes it easy to replace the implementation of the original level with a new one, which can reduce the dependence between layers. Logic reuse can be beneficial to the reuse of each layer of logic.

Assuming that the projection point from the sample  $x$  to the classification hyperplane is  $x_0$ , the distance  $\gamma$  from the sample to the hyperplane satisfies the following formula:

$$x = x_0 + \frac{\gamma \omega}{\|\omega\|}. \quad (6)$$

From the above formula, it can be derived that the maximum separation of the classification hyperplane corresponding to the support vector sample is  $1/\|\omega\|$ ; that is, when  $\|\omega\|$  is the smallest, the classification distance is the largest to meet the requirements of the optimal classification result of the support vector machine. Taking the classification hyperplane equation as the constraint condition, when the convex quadratic programming problem  $f_x = 0.5\|\omega\|^2$  is satisfied, the required solution can be obtained.

For hospital nursing quality management, the networked nursing quality management system provides an effective platform. Management switched from terminal to link quality control, which improved nursing quality and decreased nursing risk significantly. Simultaneously, disparate and static data will become comprehensive and dynamic, allowing for tracking management to be carried out quickly, accurately, and consistently. To design and develop a comprehensive nursing management information platform, this chapter primarily uses wireless network technology and software development technology. Data connection and data conversion issues between the comprehensive nursing management information platform and other systems are addressed using database association technology. Database association technology can also perform statistical analyses on the system's various data. Also, set up a system for assessing nursing quality. It establishes a reporting system for nursing adverse events and provides a monitoring platform for nursing quality management. It optimizes the nursing management process and improves nursing management quality in the areas of clinical nursing quality index management, forward-looking risk assessment, and nursing management quality.

#### 4. Results Analysis and Discussion

Comprehensive nursing information platform highlights nursing modernization and humanized management means. It is beneficial to increase the nursing time of nurses and

improve the nursing quality. However, in the past, the simple nurse station could not effectively realize the closed loop of nursing process. Therefore, in the new system, new technologies and methods are added. It can greatly improve the potential safety hazard and improve the phase ratio. The efficiency and quality of nursing management have been improved. The application of hospital informatization has optimized the process and quality of nursing management. Especially, the process and reengineering of key links such as patient identification, doctor's advice handling, and doctor's advice checking can shorten the nursing quality control time, reduce the occurrence of nursing adverse events, and improve the efficiency of nursing management.

The collected effective data were processed by software, and descriptive statistics were made on general data, nursing practice status of patients after general anesthesia, and nurses' mastery of nursing knowledge of patients after general anesthesia by frequency, composition ratio mean, and standard deviation. Sample loss is shown in Figure 3.

The "dictionary database" of various nursing quality standards in the system is summarized and integrated according to a certain logical hierarchy to form a collection of information items with nursing management characteristics. A highly organized and integrated decision support system is formed by using the management information system, which can provide managers at all levels with the required information in an extremely complicated and rapidly changing external environment. Moreover, the system design is open, and the management model design is reasonable, and various statistical information can be quickly obtained, and then Excel tables can be exported for further statistical analysis.

Under the same scale of ensemble, the effect of selective ensemble is better than that of unselected ensemble, which shows that some base classifiers are redundant and the algorithm in this paper is effective. With the increase of integration scale, the improvement of integration effect is not obvious. The possible reason is that the difference caused by the added member classifiers to the whole integrated classifier is getting smaller and smaller. Therefore, when constructing the base classifier, we should comprehensively consider the storage and time overhead allowed in practical application to select the appropriate integration scale. The experimental results are shown in Figure 4.

Taking 4 adjacent segmentation units to form a feature block, the feature vector of  $4 \times 8 = 32$  dimensions can be obtained simultaneously. The normalized resolution of the input character image is  $16 \times 18$ , the characteristic block width is  $4 \times 2 = 8$ , and the length is  $6 \times 2 = 12$ . Taking the scanning step size as 2 pixels, the horizontal direction includes  $(16 - 8) / 2 = 4$  block scanning windows, and the vertical direction includes  $(18 - 12) / 2 = 3$  block scanning windows. Each scanning window contains 36 feature vectors, a total of  $4 \times 3 \times 32 = 384$  feature vectors. The model in this paper and the traditional model were used to carry out statistical experiments on the complications of patients after general anesthesia, and the statistical error rate and the time required for the statistics were compared. The comparison results are shown in Figures 5 and 6.

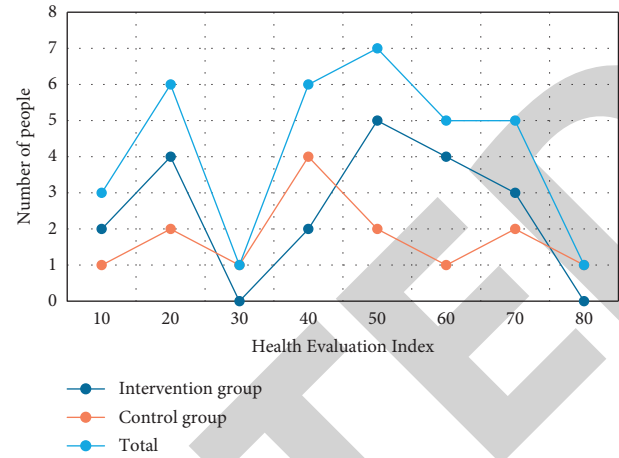


FIGURE 3: Sample loss.

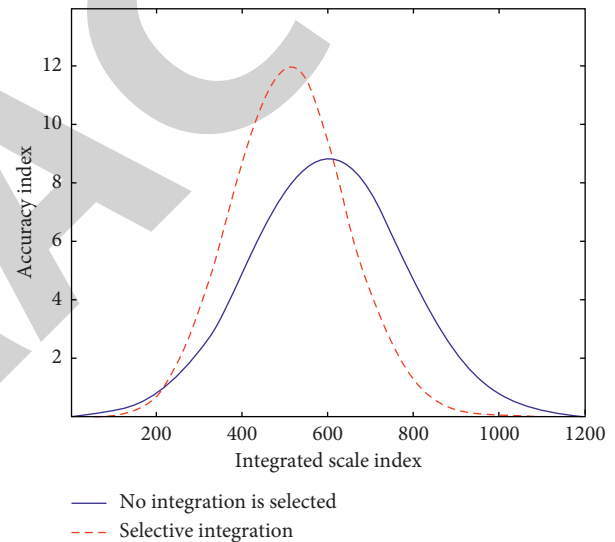


FIGURE 4: The impact of different integration scales on the accuracy of the classifier.

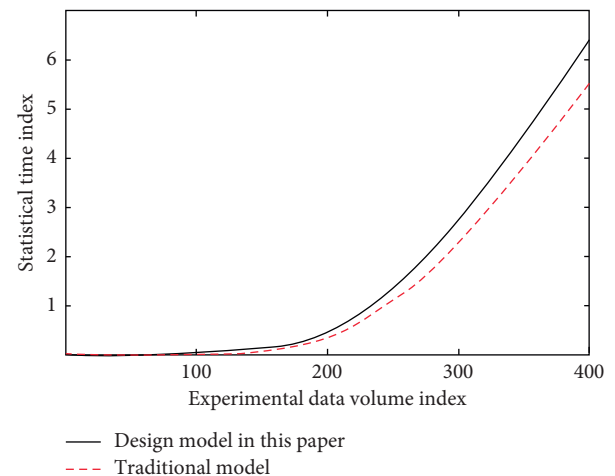


FIGURE 5: Comparison of statistical error rates of different models.

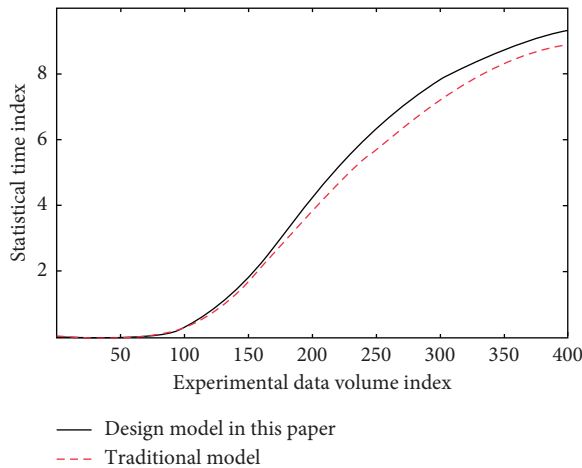


FIGURE 6: Comparison of statistical time of different models.

The superiority of nursing informatization implementation can be proven more accurately and concretely by comparing various special inspection data record indicators before and after the implementation of hospital nursing informatization, and the standardized nursing quality management model provides the foundation. The Clinical Data Repository (CDR) is the foundation of any hospital information system. To achieve rapid storage, retrieval, and reading of clinical data, the patient-centered reconstructed data repository standardizes and optimizes clinical data with different structures and terms. The goal and core of the mobile nursing system's development is to figure out the best way to process clinical data so that data and information can be shared across different clinical manifestations, nursing documents can be generated automatically in real time, and medical staff can record less information.

The concept of nonpunishment management encourages nurses to actively report and eliminate all kinds of worries in the development and application of electronic information for reporting adverse nursing events. At the same time, the system has established permissions for each department's operation. Departments can only see the data and information that their own departments have reported, and the nursing department can only see the data and information that each department in the hospital has reported. When analyzing, discussing, and commenting on adverse events, the nursing management committee follows the principle of confidentiality and does not reveal department information. Common problems will be discussed throughout the hospital, and solutions and measures will be proposed.

The fast and effective electronic statistics function standardizes the text format, which not only improves the efficiency, but also reduces the cost. There are 213 files in 20 folders in nursing management, which reduces the printing of about 1,300 manuals and the file transmission between nursing department and all nursing units for about 180 times throughout the year. The input and analysis of quality inspection data saved 7 working days per month on average. An initial node needs to be randomly selected, and the accuracy of generating the final model is different with different initial nodes. The model generated by traditional

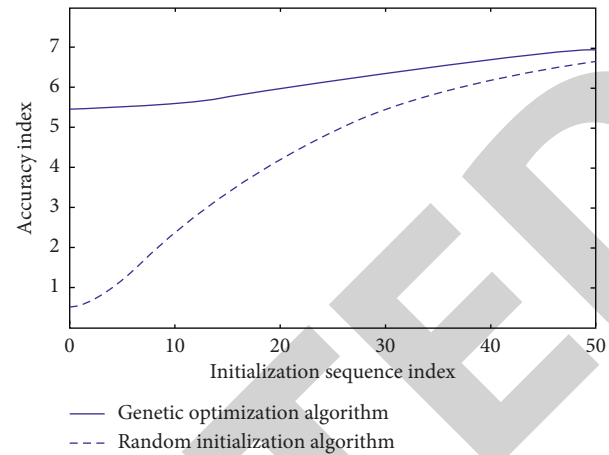


FIGURE 7: Different initialization sequence.

genetic algorithm is compared with the model generated by random initialization method. The experimental results are shown in Figure 7.

The construction of hospital information platform should take the opportunity of the maturity evaluation of standardization of hospital informatization interconnection and lay a solid foundation for information exchange, business collaboration, and management decision support inside and outside the hospital. Through standardized information integration, the analysis method of nursing quality can be improved, which is conducive to the improvement of analysis efficiency. The linear regression curve is calculated according to the stepwise multiple linear regression equation, as shown in Figure 8.

The development direction of nursing information system is nursing expert system, hospital nursing integrated management information system, and remote nursing. The tide of mobile medical care is overwhelming, and it has brought huge business opportunities and challenges to wireless, network, storage, security, software, integration, and other fields. This paper developed and utilized nursing information systems such as nursing management decision-making, head nurse's electronic manual, nursing electronic medical records, mobile nursing rounds software, and so on. According to the core system of nursing work, nursing quality indicators, nursing quality management standards, nursing quality standards, nursing quality control methods, and management measures, standardized management concept is transformed into an intelligent nursing quality control system and implemented. According to the research, the number of reported cases of nursing leak blocking incidents decreased. Improve nurses' satisfaction with nursing quality control and patients' satisfaction with nursing service. Nurses' satisfaction with nursing quality control has been significantly improved. Patients' satisfaction with nursing service after informatization is higher than before. The frequency of problems in electronic nursing records is less than that in handwritten records. The nursing information system established in this paper has strong expandability and advanced technology and improves the nursing quality management level.

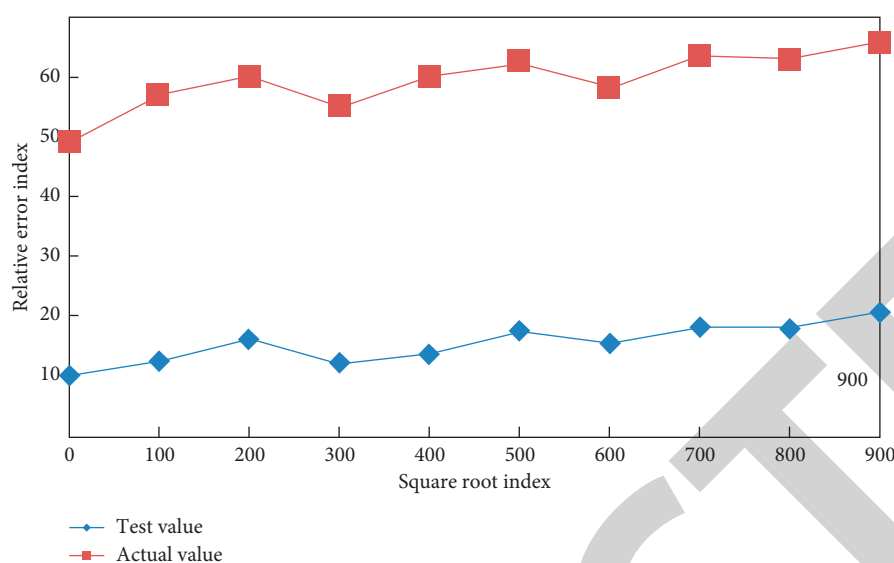


FIGURE 8: The relationship between the actual value and the calculated value of stepwise linear regression.

## 5. Conclusions

This paper can find quality problems in a timely manner, evaluate the work effect, and then analyze whether there is an opportunity to improve the work and solve the problems, and finally promote the continuous improvement of nursing quality through directional analysis of information systems. Nursing management, as an important part of hospital nursing ability, should be grasped at the pinnacle of modern nursing quality in order to discover the characteristics and laws of nursing management. Nursing management can only be implemented if the characteristics and laws are understood. The construction of a standardization system is a time-consuming and systematic process. Clinical nursing quality evaluation indexes are used to reflect the basis, process, and outcomes of nursing quality in a scientific and dynamic way. Scientific evaluation of nursing quality, continuous evaluation and monitoring of nursing quality, continuous improvement of nursing quality, and standardization, specialization, standardization, and refinement of nursing quality management are all carried out based on data. The information database of the comprehensive nursing information platform built in this paper is highly expandable and technologically advanced. At the same time, this paper has completed the design of various functions of the comprehensive nursing management information platform system, which endows the system with maintainability and manageability characteristics, based on the current state of hospital management and national medical and health management standards.

## Data Availability

The data used to support the findings of this study are included within the article.

## Conflicts of Interest

All the authors do not have any possible conflicts of interest regarding the publication of this paper.

## References

- [1] G. L. Alexander, R. W. Madsen, E. Miller, and K. Wise, "A national report of nursing home information technology adoption and quality measures," *Journal of Nursing Care Quality*, vol. 31, no. 3, pp. 201–206, 2016.
- [2] H. Haifeng, "Utilizing the national nursing quality data platform to improve the quality of nursing," *Chinese Health Quality Management*, vol. 148, no. 3, p. 8, 2019.
- [3] X. Zhu, Y. Liang, Y. Liang, and Y. Xie, "Application of quality control tools based on nursing information system in continuous quality improvement," *Nursing Research*, vol. 30, no. 23, pp. 2878–2881, 2016.
- [4] X. Sun, Y. Shi, M. Tian, M. Gong, X. Zhu, and Q. Wu, "Construction and continuous improvement of nursing management system based on information platform," *Nursing Research*, vol. 30, no. 28, pp. 3531–3534, 2016.
- [5] P. Li, J. M. Boyd, W. A. Ghali, and H. T. Stelfox, "Stakeholder views regarding patient discharge from intensive care: sub-optimal quality and opportunities for improvement," *Canadian Respiratory Journal*, vol. 22, no. 2, p. 109, 2016.
- [6] L. Qingfen, G. Jifang, and R. Jia, "Study on the effect of improving patient telephone information management subsystem on improving emergency diagnosis and treatment in outpatient and emergency department," *Chinese Journal of Practical Nursing*, vol. 35, no. 8, pp. 578–581, 2019.
- [7] L. Hongli and Y. Ya, "Construction and application of clinical nursing intelligent display platform based on information system," *Journal of Nursing*, vol. 25, no. 14, p. 5, 2018.
- [8] Technology Use and Nursing Home Quality, "Technology use and nursing home quality," *Journal of Gerontological Nursing*, vol. 46, no. 4, pp. 15–20, 2020.
- [9] G. L. Alexander and R. Madsen, "A national report of nursing home quality and information technology," *Journal of Nursing Care Quality*, vol. 33, no. 3, pp. 200–207, 2018.
- [10] X. Xue, L. Zhang, Y. Guo et al., "Using nursing information system to improve nursing quality management level," *China Digital Medicine*, vol. 13, no. 8, p. 3, 2018.
- [11] X. Jiao, G. Sun, and Z. Li, "Research on the integrated construction plan of hospital information system integration and

## Retraction

# Retracted: Construction of Sports and Health Data Resources and Transformation of Teachers' Orientation Based on Web Database

### Journal of Healthcare Engineering

Received 11 July 2023; Accepted 11 July 2023; Published 12 July 2023

Copyright © 2023 Journal of Healthcare Engineering. This is an open access article distributed under the Creative Commons Attribution License, which permits unrestricted use, distribution, and reproduction in any medium, provided the original work is properly cited.

This article has been retracted by Hindawi following an investigation undertaken by the publisher [1]. This investigation has uncovered evidence of one or more of the following indicators of systematic manipulation of the publication process:

- (1) Discrepancies in scope
- (2) Discrepancies in the description of the research reported
- (3) Discrepancies between the availability of data and the research described
- (4) Inappropriate citations
- (5) Incoherent, meaningless and/or irrelevant content included in the article
- (6) Peer-review manipulation

The presence of these indicators undermines our confidence in the integrity of the article's content and we cannot, therefore, vouch for its reliability. Please note that this notice is intended solely to alert readers that the content of this article is unreliable. We have not investigated whether authors were aware of or involved in the systematic manipulation of the publication process.

Wiley and Hindawi regrets that the usual quality checks did not identify these issues before publication and have since put additional measures in place to safeguard research integrity.

We wish to credit our own Research Integrity and Research Publishing teams and anonymous and named external researchers and research integrity experts for contributing to this investigation.

The corresponding author, as the representative of all authors, has been given the opportunity to register their agreement or disagreement to this retraction. We have kept a record of any response received.

### References

- [1] J. Yang and M. Chen, "Construction of Sports and Health Data Resources and Transformation of Teachers' Orientation Based on Web Database," *Journal of Healthcare Engineering*, vol. 2022, Article ID 4372406, 10 pages, 2022.

## Research Article

# Construction of Sports and Health Data Resources and Transformation of Teachers' Orientation Based on Web Database

Jiawen Yang<sup>1</sup> and Min Chen<sup>2</sup> 

<sup>1</sup>College of Physical Education and Health Science, Chongqing Normal University, Chongqing 401331, China

<sup>2</sup>School of Physical Education, Yulin Normal University, Yulin, Guangxi 537000, China

Correspondence should be addressed to Min Chen; [chenmin@ylnu.edu.cn](mailto:chenmin@ylnu.edu.cn)

Received 21 December 2021; Revised 5 January 2022; Accepted 6 January 2022; Published 7 February 2022

Academic Editor: Weiwei Cai

Copyright © 2022 Jiawen Yang and Min Chen. This is an open access article distributed under the Creative Commons Attribution License, which permits unrestricted use, distribution, and reproduction in any medium, provided the original work is properly cited.

In the intelligent era, emerging information technology helps to transform the information society into an intelligent society and the educational system into a new educational ecology. Teachers must change their roles to be competent for future education and teaching as a result of social transformation, technology application, and education development. Simultaneously, figuring out how to sort sports health data and analyze students' physical health information with a low error rate is an urgent problem that needs to be solved. Data management skills are an unavoidable requirement of the current state of school physical education. Sports health information management will become easier as computer technology advances and the country places a greater emphasis on computer networks. This paper proposes a Web database-based sports health data management system. This paper can help schools understand the relationship between important factors and indicators that affect students' health in order to guide them in making timely changes to their physical education programs. Provide a reasonable sports health plan based on scientific analysis and evaluation to achieve the goal of improving students' physical quality and reducing workload.

## 1. Introduction

With the gradual improvement of living standards, various factors such as unhealthy lifestyles directly threaten people's health, and the reason is that people's awareness and concept of personal health management are weak [1]. In daily life, there are many benefits of sports. It can enhance people's ability to resist diseases, and enhance various physical functions and potentials [2]. Moderate exercise can make you happy physically and mentally, relieve the pressure brought about by work and troubles, prevent various mental problems caused by psychological disorders, and add a lot of happiness to your life. Therefore, exercise is an important part of health management, which can bring personal health [3]. Based on this, it is imperative to strengthen modern people's personal health management, develop good habits of sports health, and implement scientific and reasonable sports health management. Sports health management is the management process of people's self-health risk factors, and

it has been paid more and more attention in the world [4]. With the continuous expansion of the scale of college students in China, the number of students increases rapidly, so the anthropometric data related to students also increases significantly, including student attendance information and physical health test data [5]. In the manual management of a large amount of information, mistakes often occur, which easily affect the enthusiasm of students to participate in sports and fail to achieve the purpose of urging students to exercise [6]. At the same time, it also brings many adverse effects to some schools to carry out sports activities. Therefore, how to conveniently and efficiently sort out sports health data and analyze students' physical health information with low error rate is an urgent problem to be solved. Doing a good job in data management is the inevitable requirement of the current development of school physical education.

With the constant awakening of people's health awareness, the sports health system has generated more and

more information, including students' sports information and students' physical health test data. Then, doing a good job in data management is the inevitable requirement of current development. Physical education and health course takes physical exercises as the main means and aims at improving students' health [7]. It adheres to the guiding ideology of "health first," takes students' development as the center, and always puts students' active development in a prominent position. Through rich and colorful sports activities, students' interest in sports is stimulated and their awareness of lifelong sports is cultivated [8]. The curriculum of physical education and health has changed from the direction of the organic combination of physical education and education, and the organic connection between physical education and health. Whether this idea and conception can be really implemented and they achieve the expected results depends on the concrete implementer-physical education teachers, the role played by physical education teachers in school education, and their understanding and understanding of their own roles [9]. For a long time, society has held the belief that physical education teachers should play a role. PE teachers have gradually formed their own role orientation, restricting their thoughts and behaviors with this role, influenced by societal expectations and their role consciousness—the role of their knowledge, attitude, and behavior tendency [10]. Teachers in the new era should consider the benefits and drawbacks of the new era and complete their own role positioning. As a result, research into the role orientation of physical education teachers in school physical education to promote sports and health is critical. Many schools are currently dealing with the issue of sloppy multi-campus sports health management [11]. To make sports health data management efficient and intelligent, it is necessary to research and develop a comprehensive sports health management system combined with modern network technology in order to better carry out school physical education. This paper summarizes the working principle of a World Wide Web (Web) database, proposes a sports and health data resource system based on a Web database, and describes the implementation process based on the development of management information systems.

A complete health plan should include three aspects: exercise, diet, and health guidelines. Sports health management is an important part of health management, and physical testing is an important link of sports health testing [12]. Exercise prescription is the process of reasonably guiding and formulating exercise plan according to various exercise test results. Give full play to the advantages of computer network technology, introduce it into modern sports health management, actively build an interactive platform for sports health management based on Web database technology, meet the sports health needs of the public, provide personalized physical fitness assessment, provide special sports health programs, and improve personal sports health level. It is an important content of personal health management [13]. This paper constructs student sports and health data resource database and video database based on Web database. The students' sports, health data, physique monitoring, and methods and means of improving students'

physique are systematized and shared with information, so as to improve the tedious work of students' physique monitoring. Strive to improve the diversification and scientificity of methods and means of students' physique, reduce the error probability of students' physique monitoring, improve students' physique work, and reduce the workload.

## 2. Related Work

According to the literature [14], users can log in to different database servers; select different authentication methods and log in users; and perform database, data table, and data view operations by designing and implementing a user database resource management system based on the Web. According to the literature [15], exercise prescription is the most common method of exercise health management. It is a healthy exercise program that is tailored to each person's specific needs. This method is quantitative, and the exercise mode is chosen with medical and health knowledge in mind. Literature [16] developed a Web database-based sports health management platform, created and adjusted intelligent sports prescriptions, and used information technology to assist people in improving their physical conditions. According to the literature [17], Internet users retrieve information using a unified web interface, which is less expensive than client software for document management systems and groupware. The combination of this integrated information network system database and web server has spawned a new area of Internet development for the next generation. According to literature [18], in order to be competent for future education and teaching, teachers must change their roles and reposition their work content from the dimensions of education and teaching, learning service, technology application, and subject attribute. According to literature [19], the core content of the construction of a sports health management platform is to create a networked and efficient personal sports health evaluation system as well as a personalized exclusive sports health scheme system. Literature [20] proposes that, thanks to the rapid development of Browser/Server structure (B/S), more and more software engineers began to focus on the design and development of Web applications. The load of client computers was greatly reduced, and the cost and workload of system maintenance and upgrading were reduced. Literature [21] in sports health management gives full play to the advantages of ASP technology and B/S structure technology, and establishes a scientific, practical, simple, and extensible sports health management platform based on Web database technology. Literature [22] proposed that when creating web pages and developing web database pages, first we should establish some static hypertext markup language (HTML) pages that support the whole web file system. We can also use InterDev to add files to them. Literature [23] considered that the application system based on Web development is a one-step development, which can enable different operators to access and operate the common database in different access ways from different places, and can effectively protect the server data platform. Literature [24] starts with the role

orientation of teachers in the intelligent era, puts in perspective the demands of teachers' literacy in the intelligent era, and then constructs the framework of teachers' intelligent education literacy, so as to provide reference for teachers' training and normal students' training. In literature [25], the Web-based user database resource management system is designed and implemented akin to the three-layer MVC architecture. The responsibilities and functions of each level are very clear, which greatly improves the scalability and maintainability. The developed system components have strong reusability and strong universality, which provides convenience for later transplantation to other management systems. Literature [24] discusses the transformation of teachers' role in the era of intelligence from four aspects. Based on the perspective of four dimensions, combined with the development and evolution of educational objectives, educational environment, and educational activities in the intelligent era, this paper combs the specific direction of teachers' role transformation in the future. Literature [26] mentioned that the Web is a global, interactive, dynamic, multi-platform and distributed graphic information system based on the Internet. It is an important means of retrieving information on the Internet. This paper designs and implements the student sports and health data resource management system. This system realizes the open and ecological linkage output of exercise and nutrition prescription, and makes the exercise video, which improves individual compliance. Combined with the analysis of sports data, the transfer progress degree of group exercise is obtained. Compared with the results of the traditional average evaluation method, it is found that the system can eliminate the differences in physical basis of individuals within the group and achieve a more fair and reasonable health evaluation of sports groups.

### 3. Methodology

**3.1. Design and Implementation of Web Database.** With the rapid growth of the Internet, the combination of database and network technology is becoming more and more common, and the development mode of network applications has shifted from C/S to B/S architecture. The question of how to create a reliable and efficient Web-based user database resource management system has risen to prominence in the field of information technology research [27]. At the same time, remote database resource management is realized, making database resource management more convenient for users.

At present, the integration schemes and technologies of Web and database are very complicated, which can be roughly divided into three categories. One is the technology developed by database manufacturers. Second, the technology developed by intermediate manufacturers. Third, the technology provided by Web server developers. The realization of various methods can be summarized as follows: the browser is used as the container for downloading the homepage from the Web server, the user fills in the query information in the form and gives it to the server, the server interfaces with the external database in different ways, runs

the operations such as query and update, returns the operation results to the server, and formats them into HTML pages and then sends them to the client browser.

Web database is mainly composed of four parts, that is, the design of HTML, Web editing language, common gateway interface (CGI), and database backend. The application of Web database consists of three parts: Web server, network database, and users [28]. Generally, the Web server and CGI external application exist on one host at the same time, while the database server and the Web server can be set up on one host at the same time or on two different hosts, respectively. From a technical point of view, there are four ways to realize the connection between Web and database. ① Use common gateway interface public gateway interface. ② Create a connection from the public gateway interface to the open database connection interface. ③ Use the Web server extension software to access the remote database. ④ Use a Web server with ODBC interface.

The working process of Web database is actually a CGI application process. The whole working principle can be roughly divided into five parts. ① From users to Web servers. ② From Web server to CGI external program. ③ CGI external program and database server. ④ From CGI external program to Web server. ⑤ From Web server to user. The Web server uses HTML language to return data to users in a specific form, and then completes an access operation to the Web server. The process is shown in Figure 1.

This sports health data management system uses a mature B/S architecture, which it effectively combines with the development of a Web database to create a three-tier B/S architecture. The sports network management system is developed using ASP technology, which combines the sports management and network platform. The data warehouse technology is introduced, and an innovative analysis module is added to analyze sports management results, provide timely feedback, and seek out the best management mode. In data management query, new methods of multi-keyword query and fuzzy query are introduced. In general, it meets the requirements for a sports network management system's development and is technically feasible. Web applications have obvious advantages over traditional desktop applications, including ease of development, installation, and post-maintenance, as well as a large user base [29]. Generally speaking, in a Web application, when a user submits a form, the server will accept the whole form and forward it to the script that processes the form, and then send a brand-new page back to the user after execution. The overall functional module structure diagram of the Web system in this paper is shown in Figure 2.

The problem to be solved in the realization of Web database is to configure the Web information server on IIS under the NTServer. At the back end of the database, create the network database with the SQLServer, and connect the Web with the network database with development tools, so as to realize the Web database. The core of the problem is how to realize the connection between Web and database. The server data (stored in the Web form) is returned to JavaScript code, which can quickly update the form data, and users can hardly feel any delay, and get new data without

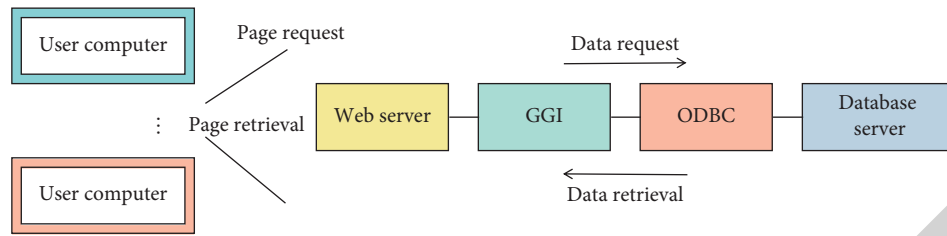


FIGURE 1: Access process of web server.

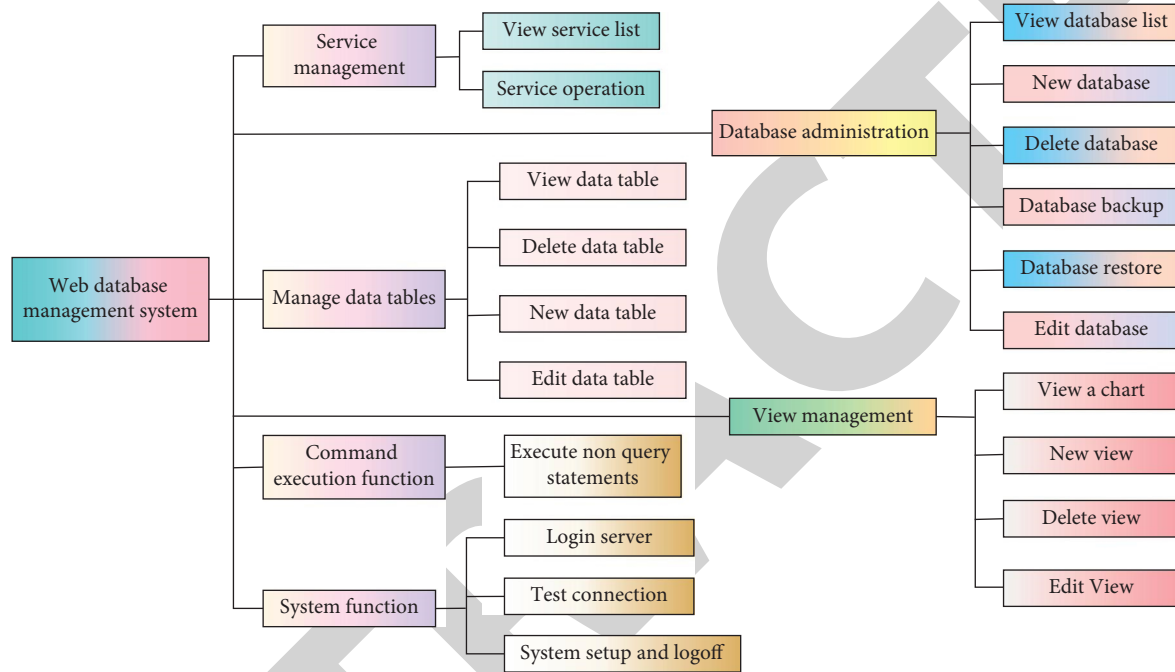


FIGURE 2: System function module structure diagram.

refreshing or submitting. The power of HttpRequest lies in this: it can interact with the server on its own according to needs, and users can even do everything without knowing the background at all. This is a dynamic, fast response, and highly interactive experience similar to desktop applications, and it also integrates the powerful power of the Internet.

**3.2. Teacher Orientation Change.** Emerging information technologies, such as artificial intelligence and virtual reality, are accelerating the transition to an intelligent society, resulting in shifts in talent demand. They are also remaking the learning environment and causing changes in the teaching process at the three levels of perception, knowledge, and cognition, paving the way for the development of human-computer collaborative teaching. Teachers will face new challenges as future education is reconstructed and reformatted. Teachers' roles must change and develop in the age of intelligence, taking into account aspects of education and teaching, learning and service, technology application, and subject attributes. Teachers must have technology cognition literacy, innovative teaching, human-computer cooperation, resource integration, data application, ethical security, and other skills. Under the influence of traditional

educational ideas, physical education teachers' role orientation has been in conflict with the role that physical education teachers should play under the guiding ideology of the Physical Education and Health Curriculum Standard, which appears out of place and leads to the phenomenon of dislocation of physical education teachers' roles in long-term practice of school physical education.

With the transformation of social productivity and form caused by the application of intelligent technology, the training of talents in the education system needs to meet the needs of social talents, and pay attention to the cultivation of higher-order thinking and accomplishment of learners to cope with future social life and professional challenges. At the same time, the in-depth application of intelligent technology in the education system will also lead to the changes of teaching environment, teaching activities, teaching modes, learning methods, management methods, etc., and promote the changes of educational subject view, educational communication view, and knowledge view, and help the systematic reform and reshaping of educational ecology. These changes will lead to the reconstruction of teachers' future professional division and orientation, and promote the transformation of teachers' roles. Under the new curriculum standard, PE teachers become promoters of

PE teaching and researchers of education and teaching activities accordingly.

Education in the era of intelligence requires teachers to have intelligent education literacy covering technology, education, and society; fully understand the nature, logic, enablement, and possibility of technology; innovatively design and implement human-computer collaborative education and teaching activities; and fully understand and respond to social risks and professional challenges brought about by technology application. As a promoter of sports health, physical education teachers' roles and behaviors are as follows: helping students decide appropriate learning goals, and confirming and coordinating the best way to achieve these goals; guiding students to form good study habits, master learning strategies, and cultivate the ability to exercise independently; creating rich teaching situations, stimulate students' learning motivation, cultivate their interest in learning and fully mobilize their learning enthusiasm; and providing various convenient services for students' study.

The change of teacher's role from the perspective of education mainly focuses on the change of teacher's teaching purpose, content, and method. At the level of teaching purpose, intelligent technology promotes the development of social productive forces, the transformation of industrial structure, and the reorganization of human-machine division of labor, which in turn creates new demands for the cultivation of educational talents and forces teachers to change their teaching. In school physical education, the teaching concept of competitive sports has been favored for a long time. At the technical level, the goal of school physical education is more defined, and the physical education teacher completely transforms into a coach engaged in sports technical training. Students have high expectations for establishing and maintaining a new teacher-student relationship with physical education teachers, according to the research. Teachers should be skilled at providing students with a sense of psychological safety and spiritual encouragement in a variety of ways, in order to stimulate their thinking and increase their exploration enthusiasm; actively create a learning environment for students; when exercises fail or movements are not standardized, teachers should understand and encourage them, in order to create a safe learning environment and promote their continuous exploration and thinking.

In the aspect of knowledge transmission, teachers will turn from instigator to guide, paying attention to inspiring and assisting learners' independent knowledge construction and cognitive development. In the aspect of educating people, education and teaching in the intelligent age pay more attention to the cultivation of learners' ability, wisdom enlightenment, and individual potential stimulation, and the cultivation of learners' higher-order rational thinking ability, interactive thinking, and lifelong learning ability. In terms of teaching content, teachers are no longer teaching based on specific textbooks and specific contents. They need to design and develop thematic and modular courses according to students' learning situation and needs, combined with various resources, and become teaching designers and

planners. At the level of teaching methods, teachers need to pay more attention to the support and precise guidance of learners' learning process, and give full play to students' learning initiative. With the implementation of the new curriculum in the context of quality education, the problems in the educational situation have greatly increased and become very complicated. Therefore, the requirement of "teachers are researchers" is particularly important in the context of the new curriculum. Teachers must gradually develop the consciousness and ability of self-reflection, scientific design of education and teaching behaviors, and engaging in educational action research, which is not only the need of the development of quality education, the need of promoting students' development, but also the need of teachers' self-development.

Physical education teachers should be fully aware that they are not only a coach engaged in sports technical training but also a real educator who can cultivate students' sound personality and healthy psychology, and promote their all-round development. Physical education teachers should not only pay attention to the teaching of basic knowledge and sports skills of sports and health, the exercise of sports skills and skills, and the development of students' physical quality and physical function but also impart scientific outlook on life and values to students, and guide students to form a good ideological style and attitude towards life.

### 3.3. Construction of Sports and Health Data Resource System.

Sports health management is a new health concept and health management method in recent years. It is mainly to scientifically and reasonably formulate some sports prescriptions according to users' sports data and natural conditions, and the ultimate goal is to improve users' health and physical fitness. Sports health management system has developed to a great extent in foreign countries, and it is increasingly accepted by the masses in China. At present, companies and institutions related to health management are constantly being established in China, but the construction of health management system in Chinese schools is still not to the desire level. According to the survey, at present, school students' awareness of physical health management is generally lacking.

The sports health management system described in this paper has several obvious advantages over traditional management methods, including the following: Modern Web technology can enable cross-platform message publishing and information browsing, as well as dynamic interactive management, thanks to advancements in computer network technology. Sports health management can be accomplished using network technology, computer technology, and database technology. The sports health data management platform is built and implemented using Web database technology, with ASP, HTML, and other web page programming languages and database technology serving as the primary technical support. Its network environment is primarily supported by the Internet, and unified management of individual sports health is realized using FTP tools, allowing users to access remote and personalized sports

health services. Users can not only make requests but also receive Web information via the Web browser.

In the scheduling of fitness benefit index heterogeneous data information resources,  $s_j^{(k)}$  and  $y_j^{(k)}$  are used to represent the linear input and reversible invariance output of the system, and the feature vector is expressed as:

$$x^{(k)} = [x_1^{(k)}, x_2^{(k)}, \dots, x_{N_{k-1}}^{(k)}]^T, \quad (1)$$

$$s^{(k)} = [s_1^{(k)}, s_2^{(k)}, \dots, s_{N_k}^{(k)}]^T, \quad (2)$$

$$y^{(k)} = [y_1^{(k)}, y_2^{(k)}, \dots, y_{N_k}^{(k)}]^T. \quad (3)$$

The time-frequency characteristics of cardiopulmonary function data under comprehensive fitness are to be studied, so as to use the characteristics as the medium to reflect the original characteristics of the cardiopulmonary function data. Suppose the value range of the range data is  $N$  discrete points  $A = \{a_1, \dots, a_N\}$ , then the time average value of the national fitness benefit index is calculated as follows:

$$t_m = \frac{1}{E_x} \int_{-\infty}^{+\infty} t |x(t)|^2 dt. \quad (4)$$

Frequency mean:

$$v_m = \frac{1}{E_x} \int_{-\infty}^{+\infty} v |X(v)|^2 dv. \quad (5)$$

The fitness benefit index system based on linear model or equivalent approximation is obtained.

The key technology of the sports health management platform is database technology. The platform's purpose is to extract, analyze, and process a large amount of data before providing feedback to customers. The database can perform data sorting and simple analysis on its own, and as a development tool, it can perform secondary development and data maintenance more quickly. To achieve data management, a database must design a large number of tables, for example, a user information table, a statistical information table, and so on. User name, gender, sports content, sports time, sports frequency, and sports intensity are all needed in the user information table. The five elements of exercise health management are represented as data items in the exercise prescription table, and each data table is linked by user name to enable basic keyword queries and facilitate feedback on reasonable exercise prescriptions. The relationship table between sports and diseases, in particular, must be designed in a one-to-many or one-to-one data storage mode, and these critical medical care data must be stored in a server that is easy to query and call.

Combine the weekly average energy consumption sequence of all exercise individuals for two consecutive weeks into one observation sequence, and first find the minimum value ( $e_{\min}$ ) and maximum value ( $e_{\max}$ ) of the sequence. Based on this,  $m$  state intervals are divided, and the span of each interval is  $\Delta e = (e_{\max} - e_{\min})/m$ , then the state interval of the energy consumption sequence is as follows:

$$[e_{\min}, e_{\min} + \Delta e], \dots, [e_{\min} + (m-1) \cdot \Delta e, e_{\max}]. \quad (6)$$

According to the transition probability matrix, the transition progress of the current Markov chain can be calculated:

$$K = \sum_{i=1}^m \sum_{j=1}^m (j-1)^3 \cdot p_{ij}, \quad i, j \in [1, m]. \quad (7)$$

After calculating the transfer progress degree of sports energy consumption of each group, respectively, it is used as the health evaluation model of sports groups to compare the exercise effects of sports groups.

The programming language for the sports health management platform is ASP, which stands for dynamic server page. ActiveX components work with ASP instructions to build Web server applications through an organic combination of HTML pages and ASP. Simultaneously, it can ensure that the application program is effective, interactive, and simple to use. The use of an ASP application in conjunction with HTML code and a scripting language can ensure that the ASP program runs safely and that the ASP source code is not transmitted to the client, which has strong applicability characteristics.

Build a nonlinear dynamic system that can fit many influencing factors, and realize the fitting of a benefit index parameter system. The fitting model is described as follows:

$$R_\beta X = U\{E \in U/R | c(E, X) \leq \beta\}, \quad (8)$$

$$R_\beta X = U\{E \in U/R | c(E, X) \leq 1 - \beta\}, \quad (9)$$

$$\text{bnr}_\beta(X) = R_\beta X - R_\beta X_1. \quad (10)$$

It is necessary to include the universal influence factor group, and select the number of principal components according to the contribution degree of cumulative variance. Only when the cumulative contribution rate reaches a certain amount, the corresponding  $m$  principal components can be selected as the principal components. The above fractal design provides accurate resource data basis for realizing a heterogeneous data mining model of sports health benefit index.

The development and design of a sports health management platform based on Web database technology adheres to the personal health management principle of "prevention first, sports intervention." We can work out the exercise mode suitable for individuals using the personal sports health plan module and the health information table, which we can combine with the specific characteristics of different groups of people. The sports data management platform's main functions include not only adjusting physical diseases and recovering quickly but also preventing diseases. Sports health management is a networked health management platform that selects sports methods and contents based on people's characteristics, according to relevant scientific data.

#### 4. Results Analysis and Discussion

Sports health management is a systematic project. Today, with the development of information network technology, we should give full play to its advantages and introduce it into the field of student health management. Actively establish the platform of sports health management system, strengthen personal sports health management, and improve students' sports health quality, so as to change health management from passive to active, and comprehensively improve students' health level. Abundant sports data can be generated in the process of exercise. By analyzing these sports data, we can find out the rules of people in the process of exercise. If the sports data are combined with the athletes' own physical fitness indexes for analysis, the physical health in the process of exercise can be evaluated.

According to the research, there is a certain gap in health status between students who participate in health management and those who do not. From the results of the experimental intervention group and the control group in Figure 3, it can be seen that the health status of the students who participated in health management has improved to some extent compared with those who did not participate in health management.

The ASP, B/S architecture, and Web database technology are used to create the sports health management platform described in this paper. Customers' sports health is managed and exercise prescriptions are given using a networked platform. Both unhealthy and healthy students are to be assisted in improving their physical condition. The platform's development language is ASP, which is a dynamic web page technology, and some common functions can be accomplished with HTML code. ActiveX controls can also be used by ASP to access users' sports health data. ASP has good interactive performance, can be used with a variety of software, and includes some built-in objects that can easily enhance the server's script function, allowing data uploaded by users to be further processed and stored in real time. The weight can be adjusted adaptively in this algorithm to achieve adaptive convergence, which improves the controllability and universality of the algorithm retrieval and data mining performance. The convergence curve of this algorithm is shown in Figure 4.

By analyzing the above experimental results, we can see that through heterogeneous data mining of the fitness benefit index, we get the promotion relationship model of sports health training for students' health benefit index, and master the improvement degree of fitness exercise for different groups' physical functions. Compared with traditional methods, the accuracy of this method is improved and the robustness is better.

After the user requests from the network enter the system, they are placed in a request task queue, waiting for the system to assign threads to execute. This request task queue is blocked, which can reduce the pressure on the server when the user requests too much. Access to shared resources with the system is protected by synchronization. In the multithreading concurrency model, the execution of each user request has gone through a complete set of

processes: accepting the request, assigning the thread to perform the task, and returning the processing result. The processing logic of this model is clear, and a complete request processing logic can be put together, which simplifies the development. Moreover, due to the introduction of threads, the processing of requests has good isolation. In addition, the synchronization mechanism is used to access shared resources, which ensures the consistency of the system. Figure 5 shows that the performance of multi-threaded concurrent server is affected by the change of the thread number.

System programming allows for logical control of the questionnaire and data, the avoidance of logical errors and abnormal values in the questionnaire data, and the assurance of data quality. However, in the design and application of this platform, it is worth noting that, in the case of a large amount of user data, databases such as Oracle or SQLServer are preferable to access databases in terms of practical performance. Because exercise intensity has a direct impact on human health, we can assess exercise health by examining exercise intensity changes. The expression of exercise intensity varies depending on the type of exercise. In this paper, we use a unified evaluation index to measure exercise intensity during exercise using a variety of sports data, laying the groundwork for future research into sports health evaluation models.

When all connections are established and sent, the timer starts. At this time, all connections start to send requests at the same time, and the timer stops after the last connection request receives a response, so as to calculate the number of connection requests that the server can handle per second under different concurrent connections. The test results are shown in Figure 6.

The student health management system has played a certain and positive role in improving students' health. However, due to the limited management time and the influence of many factors, the multi-directional and three-dimensional management system failed to show its full effectiveness, and the implementation of intervention measures failed to maximize, comprehensively and continuously. Therefore, there is no significant difference in individual items. This suggests that we need to continue to carry out sustainable health management for students. The comparison of the limit energy consumption rate and the energy consumption rate of athletes in each time period is shown in Figure 7.

From Figure 7, it can be found that since the 1100s, the athlete's energy consumption rate began to be lower than the limit energy consumption rate, and it continued to decrease with time. This indicates that his or her physical strength is beginning to decline. At this time, he or she should be advised to gradually reduce the intensity of exercise or stop exercising to have a rest, so as to ensure the benefit of exercise and minimize the occurrence of danger.

As for the health evaluation of sports groups, because of the differences in individual physical foundations within sports groups, only the average value of group sports result data is used to reflect the improvement degree of group exercise effect, without considering the individual

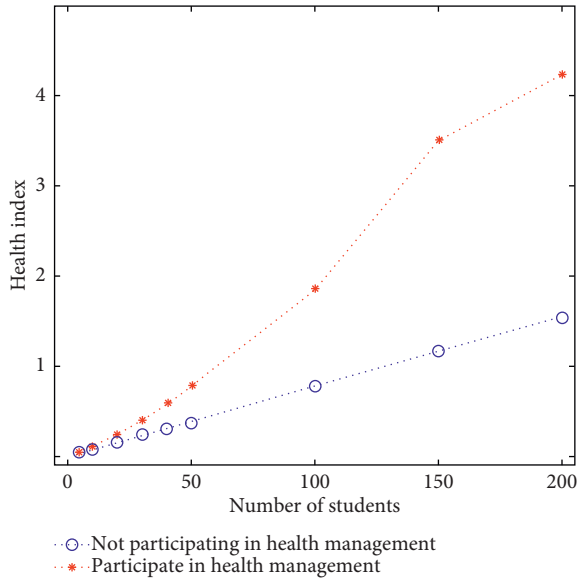


FIGURE 3: Comparison of health status between students who participated in health management and those who did not.

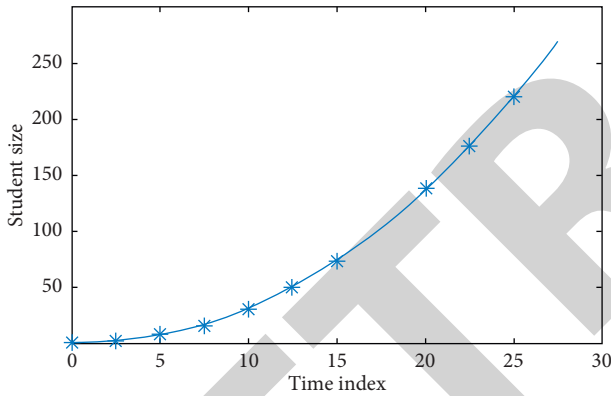


FIGURE 4: Convergence curve of the algorithm.

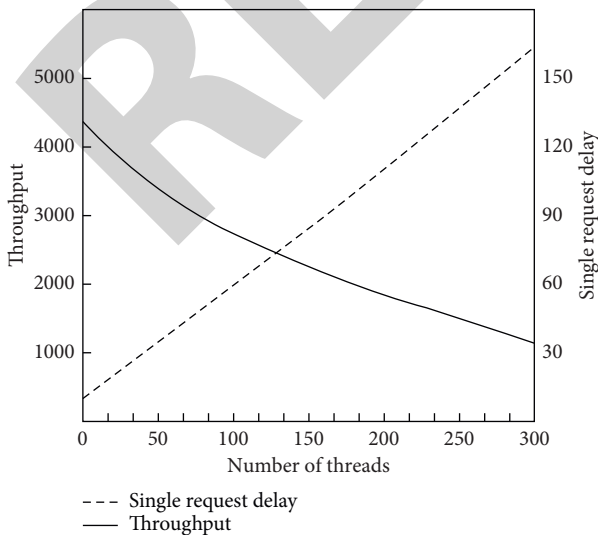


FIGURE 5: Multi-thread server performance test results.

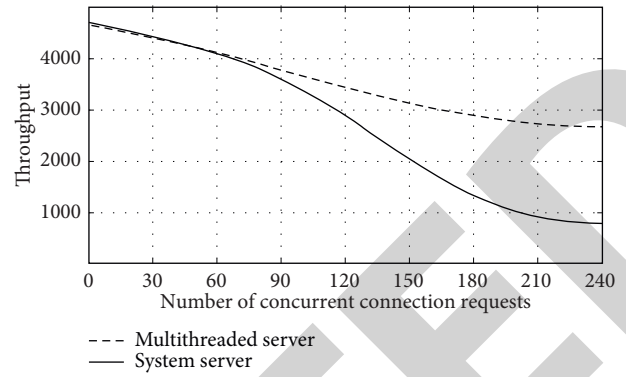


FIGURE 6: System server concurrent performance test results.

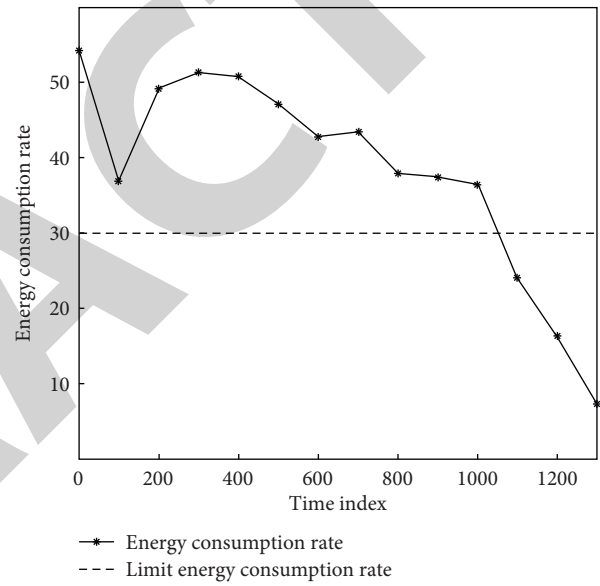


FIGURE 7: Comparison between energy consumption rate and limit energy consumption rate.

differences within groups, which cannot reflect the actual exercise effect of groups. Therefore, the sports group health evaluation model is based on Markov model, which calculates the data changes of two sports exercises of the group. This paper proposes to use the transfer progress degree to evaluate the improvement degree of sports exercise effect. Through the experiment, the errors produced by the sports individual health evaluation model in evaluating each sports individual are calculated, and the errors are plotted. The results are shown in Figure 8.

The health evaluation model for sports individuals proposed in this paper can accurately predict the exercise limits of sports individuals and provide reasonable exercise recommendations, as shown in the figure. Because the server database must store a large amount of medical care and rehabilitation knowledge, the system must be able to access data quickly. The user prescriptions generated by the platform will be automatically saved, and users will be able to rate these sports programs. Instead of constantly filling in follow-up data, the Web platform will display the excellent

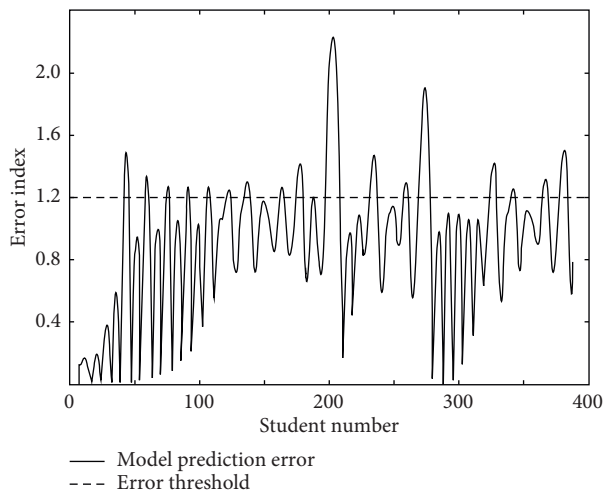


FIGURE 8: Error diagram of suggested time and actual time of the health evaluation model.

exercise prescription on the front page, allowing matching users to learn directly from it. Because the relational database is flawed, it is impossible to truly match well. Personalized sports scheme design also necessitates the active participation of users. In this case, the platform also designed the service of expert consultation, wherein athletes can send their own sports health data directly to experts, and more customers can refer to the sports prescriptions of successful cases.

The sports health management platform takes personal sports health data information recording as the fundamental starting point, realizes dynamic evaluation on the basis of personal sports health data analysis, and then provides personal sports health improvement schemes and plans, which is of great significance for improving people's sports health level.

## 5. Conclusions

The construction of sports resources is based on the individual's sports and living habits and the actual health status, with sports consultation and personal fitness assessment as the main means, fully understanding the individual's sports goals and needs, and providing personalized sports programs on this basis, so as to guide the individual's health behavior, and finally improve the individual's physical fitness and sports health. The sports and health data resource system based on the Web database is based on summarizing and accumulating existing systems, and it is an all-round and systematic comprehensive health management system that combines many factors related to students' health, such as health education, sports activities, family, and society. It classifies the main factors affecting students' health into three major aspects: society, school, and family. In this paper, through the construction of sports health data system, the function of sports intervention in physical education in the health management system is used to promote and improve students' health level. This system can delete or add dynamic changes; the prescription database is continuously

expanded and gradually improved; exercise mode, exercise belt, exercise amount, exercise intensity, exercise frequency, and other details are displayed, if requested; and the selected items are displayed visually by the built-in mathematical statistics formula in the system. It can provide convenient information collection, physical fitness evaluation, quick personalized nutrition prescription and exercise prescription output, and instant dietary nutrition evaluation, leading to an effective and convenient management platform for students' physical health promotion.

## Data Availability

The data used to support the findings of this study are included within the article.

## Conflicts of Interest

All the authors do not have any possible conflicts of interest.

## Acknowledgments

This work was supported by the project of science and technology research program of Chongqing Education Commission of China (Grant no. KJQN202000530).

## References

- [1] H. A. Jassas, H. A. Al-Bahadily, and Y. I. Al-Saady, "Integrating hydrogeological, geophysical, and remote-sensing data to identify fresh groundwater resources in arid regions: a case study from Western Iraq," *Environmental Earth Sciences*, vol. 78, no. 16, p. 521, 2019.
- [2] P. D. Glynn, A. A. Voinov, and C. D. Shapiro, "Earth's future from data to decisions: processing information, biases, and beliefs for improved management of natural resources and environments[J]," *Earth's Future*, vol. 5, no. 4, pp. 356–378, 2018.
- [3] R. C. Thomas, Q. Fang, D. Bibby, R. Mishra, and N. B. Schiller, "Left atrial strain responds to exercise and predicts exercise capacity in healthy subjects: the health eheart study," *Journal of the American College of Cardiology*, vol. 67, no. 13, p. 1805, 2016.
- [4] S. Ward, D. Scott Borden, A. Kabo-Bah, A. N. Fatawu, and X. F. Mwinkom, "Water resources data, models and decisions: international expert opinion on knowledge management for an uncertain but resilient future," *Journal of Hydroinformatics*, vol. 21, no. 1, pp. 32–44, 2019.
- [5] O. C. Witard, C. Mcglory, D. L. Hamilton, and S. M. Phillips, "Growing older with health and vitality: a nexus of physical activity, exercise and nutrition," *Biogerontology*, vol. 17, no. 3, pp. 529–546, 2016.
- [6] A. Rose, N. Belgrave, M. Lauren, A. Hennis, R. Delice, and L. R. Hambleton, "Predicting the burden of acute myocardial infarction in a country with limited resources: combining data from routine sources[J]," *International Health*, no. 1, pp. 53–58, 2016.
- [7] F. Pernollet, C. R. V. Coelho, and H. M. G. van der Werf, "Methods to simplify diet and food life cycle inventories: accuracy versus data-collection resources," *Journal of Cleaner Production*, vol. 140, no. 2, pp. 410–420, 2017.
- [8] F. Siyoum, M. Geilen, and H. Corporaal, "End-to-End latency analysis of dataflow scenarios mapped onto shared

## Retraction

# Retracted: Immunomodulatory Effect of *Lycium barbarum* Polysaccharides against Liver Fibrosis Based on the Intelligent Medical Internet of Things

### Journal of Healthcare Engineering

Received 9 December 2022; Accepted 9 December 2022; Published 3 January 2023

Copyright © 2023 Journal of Healthcare Engineering. This is an open access article distributed under the Creative Commons Attribution License, which permits unrestricted use, distribution, and reproduction in any medium, provided the original work is properly cited.

*Journal of Healthcare Engineering* has retracted the article titled “Immunomodulatory Effect of *Lycium barbarum* Polysaccharides against Liver Fibrosis Based on the Intelligent Medical Internet of Things” [1] due to concerns that the peer review process has been compromised.

Following an investigation conducted by the Hindawi Research Integrity team [2], significant concerns were identified with the peer reviewers assigned to this article; the investigation has concluded that the peer review process was compromised. We therefore can no longer trust the peer review process, and the article is being retracted with the agreement of the Chief Editor.

The authors agree to the retraction; author Wei Li could not be reached by the publisher using the e-mail address provided with the article submission.

### References

- [1] Y. Han, Y. Zhou, T. Shan, W. Li, and H. Liu, “Immunomodulatory Effect of *Lycium barbarum* Polysaccharides against Liver Fibrosis Based on the Intelligent Medical Internet of Things,” *Journal of Healthcare Engineering*, vol. 2022, Article ID 6280265, 13 pages, 2022.
- [2] L. Ferguson, “Advancing Research Integrity Collaboratively and with Vigour,” 2022, <https://www.hindawi.com/post/advancing-research-integrity-collaboratively-and-vigour/>.

## Research Article

# Immunomodulatory Effect of *Lycium barbarum* Polysaccharides against Liver Fibrosis Based on the Intelligent Medical Internet of Things

Yanzhen Han<sup>1</sup> , Yan Zhou,<sup>2</sup> Tieying Shan,<sup>2</sup> Wei Li,<sup>3</sup> and Haiping Liu<sup>4</sup>

<sup>1</sup>General Surgery, Affiliated Hospital of Hebei University of Engineering, Handan 056002, Hebei, China

<sup>2</sup>Medical College, Hebei University of Engineering, Handan 056002, Hebei, China

<sup>3</sup>International Exchange College, Hebei University of Engineering, Handan 056002, Hebei, China

<sup>4</sup>General Surgery, Handan Central Hospital, Handan 056002, Hebei, China

Correspondence should be addressed to Yanzhen Han; [yxyhulixi@hebeu.edu.cn](mailto:yxyhulixi@hebeu.edu.cn)

Received 3 November 2021; Revised 2 December 2021; Accepted 20 December 2021; Published 25 January 2022

Academic Editor: Yang Gao

Copyright © 2022 Yanzhen Han et al. This is an open access article distributed under the Creative Commons Attribution License, which permits unrestricted use, distribution, and reproduction in any medium, provided the original work is properly cited.

*Lycium barbarum* polysaccharide (LBP) is the main active component of *Lycium barbarum* and has many beneficial effects, including neuroprotection, antiaging, and antioxidation. This study mainly explores the immunomodulatory effect of *Lycium barbarum* polysaccharides against liver fibrosis based on the intelligent medical Internet of Things. This measure emphasizes that the current effective methods and methods for the treatment of liver cancer are mainly combined treatments of Western medicine and Chinese medicine. These treatments have a certain effect in preventing liver cancer, reducing recurrence, and reducing side effects. Among them, chemotherapy has unique advantages in improving the quality of life and prolonging survival. With the development of medical science and technology, the clinical efficacy and efficacy of traditional Chinese medicine in the treatment of liver cancer are constantly improving. The mechanism is also studied from many aspects. The treatment time of LBPs on fibrotic hepatocytes was set to 24 h. Take liver fiber cells in logarithmic growth phase and incubate them at 37°C for 24 h. The whole process uses a temperature sensor for intelligent temperature control. In the experiment, groups of LBPs with different concentrations and different molecular weight ranges were set up and each group had 6 multiple holes. The original medium was aspirated and replaced with a medium containing different concentrations of LBPs (12.5, 25, 50, 100, and 200 µg/mL) and cultured for 24 h. Based on the previous research, this study used in vitro cell experiments, microscopic observation, and MTT method to verify whether *Lycium barbarum* polysaccharides inhibit the proliferation of human liver cancer cells in vitro and whether they cooperate with the chemotherapy drug fluorouracil to play a tumor-killing effect. Animal experiments, using ELISA, HE staining, and other methods, explore the molecular and immunological mechanisms of LBP's antiliver cancer effect from the perspective of Th/Th2 differentiation balance and DC function, in order to provide experimental evidence for Chinese medicine polysaccharides in cancer immunotherapy and application. At different LBP concentrations (0 µmol/L, 5 µmol/L, 10 µmol/L, and 15 µmol/L), the inhibition rates were 0.80%, 20.06%, 35.44%, and 55.39%, respectively. This study provides a new method for large-scale expansion of hepatocytes in vitro, laying a stronger foundation for biological treatment of liver fibrosis.

## 1. Introduction

Tumor is a kind of common and frequently occurring disease that seriously harms human physical and mental health, among which malignant tumor is particularly serious. Worldwide, the incidence and mortality of cancer are increasing year by year. More than 7 million people die from malignant tumors every year. In some countries in Europe

and the United States, the death rate of cancer is second only to cardiovascular diseases. Due to the histological and anatomical characteristics of the liver itself, primary liver cancer is an extremely aggressive malignant tumor. Most patients are already in the middle and late stage when they are treated, and most patients are accompanied by cirrhosis, hepatitis, and the resulting liver function damage. As a result, the average survival time of patients who cannot be

treated is only 3-4 months, and the prognosis is extremely poor. Malignant tumors have become the most severe and urgent public health problem in the world due to their consistently high morbidity and mortality characteristics. Cancer deaths account for a quarter of all deaths. It has had a great destructive effect on human life and health. Factors that increase the risk of PHC (primary liver cancer) include long-term, heavy drinking and chronic infection with hepatitis B or C virus [1].

Although the level of diagnosis and treatment of liver cancer is constantly improving, the incidence and mortality of liver cancer are still high. The theoretical therapeutic potential of gene immunotherapy, which is considered as the most promising method in recent years, has not been fully realized. Liver transplantation is considered to be the most satisfied with the treatment, but difficult graft source and postoperative recurrence of problems, so liver transplantation is limited to the treatment of small tumors: early surgical resection does not change because of the large mass associated with recurrence of liver lesions, internal, anesthesia and surgery, liver blood flow blocking, and ischemia-reperfusion injury resulting in further suppressed immune function may cause cancer and further deterioration of the disease development. Liver transplantation is currently the most effective method, but the source of the liver, the cost of the operation, postoperative rejection, and recurrence make the transplantation operation not popular. Primary liver cancer (PHC) ranks sixth in the world among all cancers. Due to the increasing number of patients with liver fibrosis and alcoholic fatty liver (AFL) being its early reversible disease stage, therefore, the in-depth study of AFL is particularly important. Because primary liver cancer surgery resection rate is only 10% or so and postoperative recurrence rate is high, a variety of nonsurgical therapy remains: the main treatment of primary liver cancer, such as system and hepatic arterial infusion chemotherapy and embolization chemotherapy and radiotherapy (including radio frequency ablation or alcohol), have more severe immune and hematopoietic function of inhibiting and other side effects. Liver fibrosis is a compensatory response secondary to liver inflammation or tissue repair after injury. It is the common pathological basis of all chronic liver diseases and the main intermediate link in the development of liver cirrhosis. Its essence is the ECM when the tissue repair reaction occurs. The pathological process caused by the imbalance of synthesis, degradation and deposition, and liver fibrosis can eventually develop into liver cirrhosis and even liver cancer. Liver fibrosis and liver cirrhosis seriously affect human health. How to block the process of liver fibrosis is currently the focus of attention. This study uses smart medicine and *Lycium barbarum* polysaccharides to treat liver fibrosis, which has important clinical guiding significance.

At present, the treatment measures for liver cancer emphasize the implementation of comprehensive treatment, that is, through the combination of western medicine, traditional Chinese medicine, and other effective means and methods (such as cancer gene therapy and biological therapy). Traditional Chinese medicine has unique advantages in preventing the occurrence of liver

cancer, reducing recurrence, alleviating the toxic and side effects of radiotherapy and chemotherapy, improving the quality of life, and prolonging survival. With the development of medical science and technology, the clinical efficacy of traditional Chinese medicine in treating liver cancer has been continuously improved, and the research on the mechanism of drug action has been carried out from many aspects. Wolfberry has been used as a traditional medicinal herb and food supplement in China for more than 2,000 years. *Lycium barbarum* is rich in *Lycium barbarum* polysaccharides (LBP), betaine, phenols, cerebrosides, 2-O- $\beta$ -d-glucopyranosyl-l-ascorbic acid (AA-2 $\beta$ G), flavonoids, and vitamins. LBPs are the main active ingredients of wolfberry. Gao discussed the pharmacological activities of LBP and other main ingredients. They mediate significant antiaging effects through antioxidant, immunomodulatory, antiapoptotic activity, and reduction of DNA damage. Therefore, basic scientific evidence for the antiaging effects of LBPs is already available. However, more research is needed to understand the mechanism by which LBP mediates antiaging properties. The new findings of his research may pave the way for the clinical application of Chinese medicine wolfberry in modern evidence-based medicine [2]. Zhang's research aimed to determine whether *Lycium barbarum* polysaccharides (LBPs) can protect mice from cadmium- (Cd-) induced testicular toxicity. The four groups were given oral cadmium chloride (5.0 mg/kg body weight) for 35 days and combined treatment with LBPs (0, 10, 33.3, or 100 mg/kg), from the week before exposure to Cd until the end of the experiment. The other two groups were given oral administration only with vehicle or LBP (100 mg/kg). LBP pretreatment improved the decrease in body weight, sperm motility, and serum testosterone levels caused by Cd. In addition, cadmium-induced abnormal sperm increase decreased, and LBPs effectively attenuated Cd-induced degeneration of seminiferous tubules. Therefore, LBPs can reduce Cd-induced testicular damage by improving antioxidant enzyme activity and reducing oxidative stress, so it may be a potential adjuvant therapy for Cd-induced testicular toxicity [3]. Masci A. believes that in the past few decades, the sugar compound from the fruit of wolfberry (*Lycium barbarum*) has received great attention due to its potential health promotion effect. His review included investigations on the extraction and purification methods of these biologically active molecules (LBPs), as well as studies on the structural characteristics of carbohydrate components. In addition, an overview of in vitro, in vivo, and clinical studies on the hypoglycemic and hypolipidemic effects of the isolated LBP components is reported. In his research, these purified components of wolfberry fruit may be potentially useful as an adjuvant treatment of diabetes and related diseases [4]. Li et al. believe that due to the modern sedentary and food-rich lifestyle, nonalcoholic fatty liver disease (NAFLD) is one of the main causes of chronic liver disease around the world. Autophagy is the protective self-digestion of intracellular organelles, including lipid droplets (fat phagocytosis), to maintain homeostasis in response to stress. In addition to lipolysis, fat phagocytosis is another way of lipid

degradation. Impaired autophagy can also help treat NAFLD. Treatment with traditional Chinese herbal extracts may improve NAFLD. Their review will deeply explore the characteristics of autophagy in NAFLD and the traditions of resveratrol, wolfberry polysaccharides, dioscin, bergamot polyphenol components, capsaicin, and garlic derived S-allyl mercaptocysteine. The relevant actions/mechanisms of Chinese herbal extracts in inducing autophagy may inhibit the progression of NAFLD. In this research, the use of traditional Chinese herbal extracts to regulate autophagy/lipid autophagy may be a new method for the treatment of NAFLD, and its molecular mechanism should be further elucidated in the near future [5]. Yu et al. and Abdel-Basset et al. believes that the mechanism by which LBP prevents cerebral ischemia/reperfusion injury is still unclear. In addition, LBP was significantly reduced, and OGD/R induced apoptosis and autophagic cell death. LBP leads to the downregulation of cleaved caspase 3/caspase 3, LC3II/LC3I, and beclin 1, as well as the upregulation of Bcl-2/Bax and p62. In his research, only further analysis of the experiment was carried out, and the necessary research data was lacking [6, 7]. The body's antitumor immune relies mainly on T cell-mediated immune cells, T lymphocyte counts, the group of imbalance, and T lymphocyte activation barriers; increased apoptosis which is the main performance of the a tumor-burdened organism cellular immune function is low, and T lymphocytes in tumor local immune micro-environment and inhibition of function can directly reflect the body's antitumor cellular immune function.

T cell activation requires at least two signals. The first signal is the interaction between the specific antigen recognition receptor (TCR) on the surface of T cells and the antigen binding MHC complex on the antigen-presenting cells (tumor cells or macrophages, dendritic cells, etc.). The second signal is coordinated stimulus on the antigen-presenting cells and T cells in the corresponding receptors. There are a lot of synergy to stimulate molecules involved in T cell activation, such as cell adhesion molecules (ICAMs), vascular cell adhesion molecule (VCAMs), lymphocyte function associated antigen 3 (LFA-3), and heat shock protein, and no second signal of synergy. In this study, a mouse liver fibrosis model was constructed to further investigate the effects of different molecular weight LBP components on the growth of mouse fibrotic cells and the immune system from in vivo experiments. Liver fibrosis is continuously formed in the proliferation of cancer cells or the metastasis of signal transmission pathways in various ways under the action of multiple factors. The tumor micro-environment is complicated, and single treatment or drugs cannot effectively control the onset of liver cancer. Therefore, investigating methods and drug combination therapy is a new strategy for the treatment of liver cancer. This study focused on the early stage of steatosis of alcoholic liver disease, clarified the effect of ethanol on ALT, AST, and lipid peroxidation, further verified its etiology, and investigated the prevention and treatment of AFL and its molecular mechanism by LBP Effectiveness.

## 2. Research Methods

### 2.1. Cell Experiment Materials

**2.1.1. Cell Lines and Culture Methods.** The liver fiber cell line of human liver cancer was gifted by the medical school and preserved by the Biochemical Pathology Research Group of the University of Traditional Chinese Medicine. After the cells were resuscitated, they were subcultured in a medium incubator with (RPMI 1640 + 10% calf serum + 1% penicillin) for subsequent experiments.

**2.1.2. Drugs and Reagents.** Cell culture flasks, Pasteur pipettes, 96-well plates, 6-well plate culture plates, cryopreservation tubes, and so on are products of Nest company. Microporous membranes are purchased from Corning; syringes, medical cotton, and so on are purchased from Minkang Medical Equipment Co., Ltd. PBS buffer and pancreatin are prepared by our laboratory. PBS preparation method is as follows: weigh 8 g NaCl, 0.2 g KCl, 0.2 g  $\text{KH}_2\text{PO}_4$ , and 7.84 g  $\text{Na}_2\text{HPO}_4 \cdot (12\text{H}_2\text{O})$  into pure water and stir to dissolve the volume to 1 L and adjust the pH to 7.2–7.4 and high pressure of 0.22  $\mu\text{m}$  after sterilization.

Pore size microporous filter filtration is as follows. In pancreatin preparation method, add 0.25 g pancreatin and 0.02 g EDTA to 0 and 1L of PBS to fully dissolve and then slowly stir overnight at 4°C and pH value (7.2–7.4), and use 0.22  $\mu\text{m}$  microporous filter and cryopreserve.

**2.1.3. Instruments and Equipment.** Inverted phase contrast fluorescence microscope (Siemens, Germany), cell incubator (Invitrogen, US), cell cryopreservation tube (ABC, US), electric heating constant temperature water bath (Invitrogen, US), medical ultraclean workbench (Sigma, US), high-speed low-temperature desktop centrifuge (Invitrogen, USA) fluorescence quantitative PCR instrument, and horizontal electrophoresis equipment (BIO-RAD) were used.

**2.2. Preparation of Experimental Drugs.** Use an analytical balance to weigh 40 mg of *Lycium barbarum* polysaccharide powder, dissolve it in 8 mL of saline, mix well, and put it in a 10 mL EP tube and store it at 4°C. For cyclophosphamide injection, first use a syringe to inject 10 mL of normal saline into the bottle, shake it completely before the solution becomes transparent, and then prepare 0.29/mL of mother liquor. It can be used immediately, stored at 4°C for a short period of time, and then frozen at –20°C for a long time. The whole process uses a temperature sensor for intelligent temperature control. Dilute to the required concentration with sterile PBS buffer (pH 7.2, containing 5% trehalose).

The first-level total score of the survey patient is as follows [8]:

$$E = \sum_{j=1}^n \frac{PQ}{i}. \quad (1)$$

The total score of the second-level survey of patients is as follows [9]:

$$E = \sum_{j=1}^n \frac{PQ}{i}. \quad (2)$$

*Lycium barbarum* polysaccharide extracted from the traditional Chinese medicine *Lycium barbarum* has a variety of biological effects, such as enhancing the body's immune function, antitumor, and antioxidation, and can also reduce bone marrow suppression in radiotherapy and chemotherapy. The statistics on medical treatment are [10]

$$\begin{aligned} \text{CONT} &= \sum P(EP - 0.5), \\ \text{CONT} &= \sum P - \text{CONT}_{1,t}. \end{aligned} \quad (3)$$

The combination of traditional Chinese medicine polysaccharide with chemotherapy in the treatment of tumor patients showed that polysaccharide can not only produce obvious synergistic effect and enhance the immune function of tumor bearing body but also promote the development and differentiation of hematopoietic cells. For example, angelica polysaccharide can inhibit the proliferation of various malignant tumor cells in the blood system and promote the proliferation and differentiation of hematopoietic stem cells and progenitor cells. LBP can increase the number of nucleated cells and the number of granule/macrophage colonies in bone marrow and has the effect of endogenous CSF (colony stimulating factor).

The industrial characteristics of the Internet of Things are mainly reflected in the application field, and the intelligent application of the Internet of Things is realized through the combination of the application layer and industry requirements. In the medical field, the application of Internet of Things technology can realize smart medical care. In other words, the Internet of Things uses information recognition technologies such as sensors to build networks to realize smart medical services. The intelligent diagnosis of the Internet of Things is shown in Figure 1.

### 2.3. Experimental Method

**2.3.1. MTT Detection Method.** Chemotherapy is one of the main means of malignant tumor treatment, but chemotherapy has a severe immunosuppression and side effects of hematopoietic inhibition; combining therapy with Chinese medicine polysaccharide can improve the body's immune function as a whole; on the basis of killing tumor cells, at the same time, chemotherapy can reduce side effects, and the role in the field of polysaccharide in tumor immunotherapy has grabbed wide attention and been favored.

MTT colorimetric analysis is the relative quantification of the total number of liver fibrotic cells based on the optical density OD value determined by the enzyme plate. Normal pancreatic enzymes are used to digest cells that are growing well. In an appropriate amount of culture medium, the cells are blown to regenerate all cells. Next, according to the counting unit, the fibrotic cells inoculated on the 96-counting plate are combined with LBP-2 and LBP-3LB, respectively. The final concentrations of P-4 and LBP-5 were 400 and 800  $\mu\text{g/mL}$ , and 1200 and

1600  $\mu\text{g/mL}$  were set as well as the normal control group and the positive control group. The cells were incubated in the incubator for 24, 48, and 72 hours. The cells were collected in test tubes and washed twice with PBS, and finally PBS 2004 was added to each test tube. Use a flow cytometer to obtain 1 min under medium-speed conditions, and record the cell number, FSC, and SSC. The foundation of the Internet of Things center is now also the Internet. The network is expanded based on the Internet, and users exchange the expanded information. In other words, the Internet of Things is a new technology that connects sensors to the existing Internet. Today, smart medicine is an important development aspect in the medical field. The regional medical information platform is a regional medical service model established based on the information technology platform. It uses the Internet of Things technology to realize the interaction between patients and medical personnel, medical institutions, and medical equipment and provide health services. The medical IoT platform is shown in Figure 2.

**2.3.2. Effect of *Lycium Barbarum* Polysaccharides on Fibrosis.** Establishment and combination of experimental model are as follows: when the state of cell proliferation is 80% to 90% fusion, the liver fibroblasts used in the selection experiment are all in a good state of reproduction. The 6 holes were inoculated with cells at a density of  $2 \times 10^4/\text{ml}$ , and the glass cover for the immunofluorescence test was preinstalled with autoclaved glass. For different concentrations of LBP, different concentrations of LBP treat the cells for 24 hours. The effects of LBP culture with different concentrations on the proliferation of liver cancer cells were divided into 3 groups (5  $\mu\text{mol/L}$ , 10  $\mu\text{mol/L}$ , and 15  $\mu\text{mol/L}$ ), and the concentration as a control group was 0  $\mu\text{mol/L}$ . Next, observe the inhibitory effects of different concentrations of LBP on the proliferation of hepatocellular carcinoma cells.

**2.3.3. Effect of *Lycium Barbarum* Polysaccharide Combined with Positive Drug Fluorouracil on Killing Tumor Cells.** According to the results of preliminary experiments, the concentration gradient of LBP is 200  $\text{mg/L}$  and 400  $\text{mg/L}$ , respectively. On the other hand, a solution of a fixed concentration of 1  $\mu\text{mol/L}$  was combined as a fluorouracil (5FU) group, and a control group and a mixed group of LBP and fluorouracil were set. Each group has 3 composite holes. After 48 hours, the cell morphology and changes of each drug group were observed through a microscope and photographed, and the relative inhibition rate of each drug concentration group on the cells was detected by the MTT method.

**2.4. LBPs Affect the Viability of Liver Cells.** The processing time of LBPs was set to 24 h. Take L-02 cells in logarithmic growth phase and incubate at  $37^\circ\text{C}$  for 24 h. The experiment sets up different concentrations and different molecular weight ranges, and each group has 6 multiple holes. Change the original medium, change into the medium containing

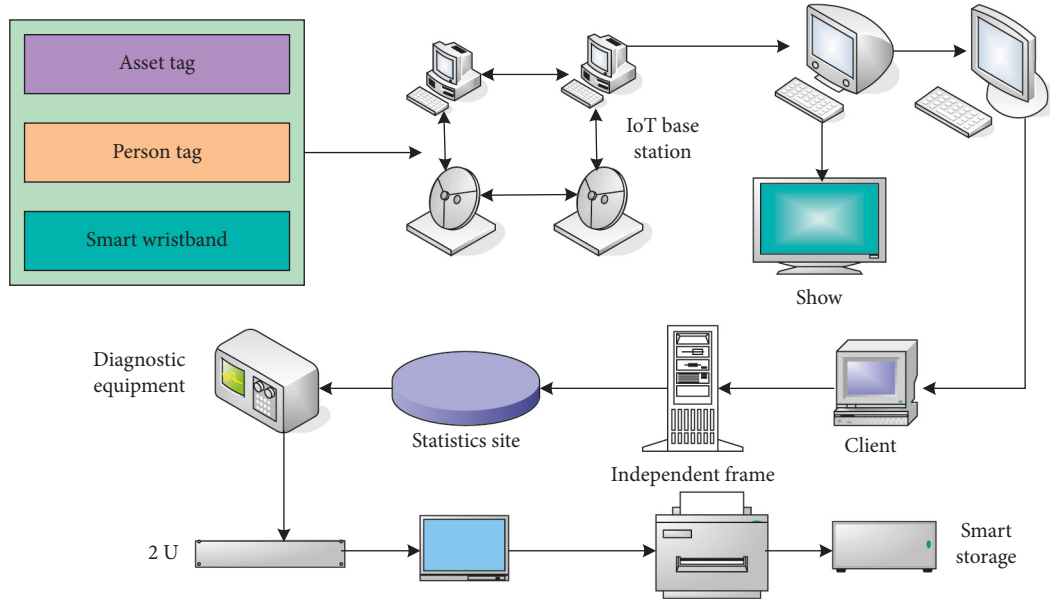


FIGURE 1: Intelligent diagnosis of the Internet of Things.

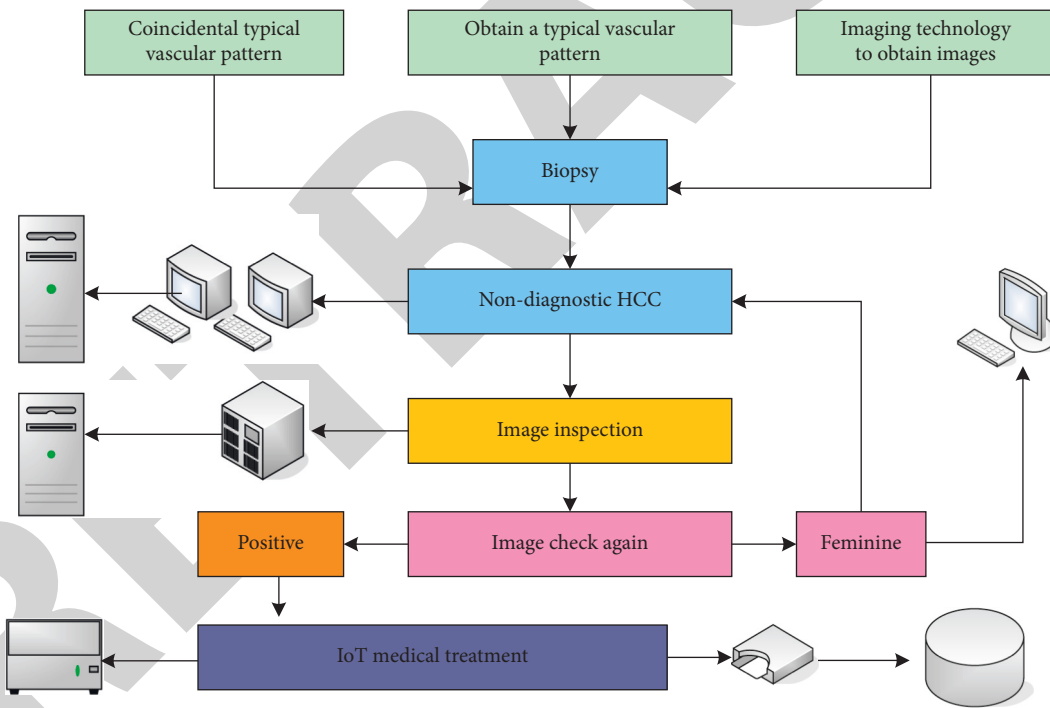


FIGURE 2: Medical Internet of Things platform.

different concentrations of LBPs (12.5, 25, 50, 100, and 200  $\mu\text{g/mL}$ ), and culture for 24 h. The original medium was replaced, the control group was replaced with fresh medium, and the ethanol injury group was replaced with a medium containing 5% ethanol and cultured for 4 hours. Take the cultured cell supernatant for testing. Calculate cell viability according to the following formula [6]:

$$H = \frac{A_G - A_K}{A_D - A_K} \times 100\%. \quad (4)$$

Calculate the consistency index [11] as follows:

$$CI = \frac{\lambda - N}{N - 1}. \quad (5)$$

There are  $n$  DMUs (decision-making units),  $X$  represents input indicators,  $Y$  represents output indicators, each DMU has  $m$  types of inputs and  $s$  types of output, and the weight coefficients  $p$  and  $q$  are used as variables to optimize the model for [12]

$$\begin{aligned} \max &= \frac{\sum_{k=1}^s qkykvo}{\sum_{l=1}^m pixivo} = pd, \\ \text{s.t. } &\frac{\sum_{k=1}^s qkykvo}{\sum_{l=1}^m jixiv} \leq 1. \end{aligned} \quad (6)$$

However, the antitumor mechanism of *Lycium barbarum* polysaccharides is not yet fully understood. Traditional Chinese medicine polysaccharide is a mixture of different molecular weight components extracted from traditional Chinese medicine. Current research shows that different molecular weight *Lycium barbarum* polysaccharide components may have different biological activities. Convert the above nonlinear fractional programming into the dual form of the equivalent linear programming [13]:

$$\begin{aligned} \text{s.t. } &\sum_{v=1}^n \beta_v x_v + s^- = \beta x_0, \\ &\beta_i y_i + s^+ = y_o. \end{aligned} \quad (7)$$

**2.5. In Vivo Experiment.** In recent years, the ethanol gavage method has been widely used in animal modeling. Depending on the ethanol concentration, dosage, time in the stomach, and additives, modeling is very unstable, or animal mortality is high. In vivo antitumor studies on the direct cytotoxic effects of LBP on liver cancer cells and tumor suppression experiments in animals have confirmed that polysaccharides can hinder the growth of liver fibrotic cancer in mice.

LBP's medium is as follows: weigh 10 mg of LBPs sample powder correctly, add 20 mL of complete medium, prepare 0.5 mg/mL LBPs stock solution, and completely dissolve it at 40°C for 5 minutes. Then, the culture solution is uniformly mixed and sterilized using a sterilized microsphere membrane. Stored at 4°C, it is effective within 2 weeks. The mother liquor is completely diluted to the required concentration of the culture medium.

**2.5.1. In Vivo Activated Metabolism of Ascites Cells in Mice and Subcutaneous Fibrotic Cell Tumor Modeling.** After microscopic observation of cells in a serum-free medium, 0.5 mL of cell suspension was prepared, all cell pellets were formed without exception, and male healthy mice of 229 g or more were used. In order to verify the activity, a cell suspension was prepared by injecting into the abdominal cavity of mice, and the size and mental state of the mice's abdomen were observed. For the third-generation mouse ascites, the third-generation mouse ascites has a good color and extracted 1 mL, respectively, extracted twice, mixed in the medium to dilute, and centrifuged to remove impurities; then add fresh serum-free medium to it, and count under a microscope. Constitutive cell concentration is  $1 \times 10^7$ /mL; select 50 mice, sterilize the mouse right axillary area with 75% ethanol cotton swab, and inoculate 0.2 mL tumor cells ( $1 \times 10^6$  cells); the tumor formation rate is 100%.

**2.5.2. Grouping of Experimental Animals and Methods of Administration.** The successfully prepared subcutaneous fibroma model mice were randomly divided into 5 groups, and the classification and label were written in the rearing cage. They were cyclophosphamide group, LBP low-dose group, fibroma model group, joint CXCL10LBP high-dose group, and *Lycium barbarum* polysaccharide. In the high-dose group, there are 10 animals in each group, but as a normal control group, there are 10 animals. Feed the animals on the third day after aseptic culture. In contrast, mice with liver fibrosis were given pelleted rat food and water before the 8th week. Add 2 mg/kg of *Lycium barbarum* (>95% purity; INDOFINE Chemical Company, Hillsborough, NJ) until the 8th week, and inject the *Lycium barbarum* solution with PBS and 5% Tween-80 (Solarbio, Beijing, China) compared. Observe for 14 days and continue medication. On the 15th day (at this time, some rats in the model group experienced cramps, fatigue, lack of food, etc.), the rats were anesthetized, blood was collected from the eyeballs, and the quality of the fibroids was determined by an analytical balance [14, 15]:

$$\begin{aligned} BE(1 - \gamma) &= CI_{1,\gamma} + CI_{2,\gamma}, \\ BE(1 - \gamma) &= CI_{3,\gamma} + CI_{4,\gamma} + CI_{5,\gamma}. \end{aligned} \quad (8)$$

Here,  $\gamma$  represents the self-pay ratio [16].

In essence, Euclidean distance represents the true distance between two points in a multidimensional space [17]:

$$d(x, y) = \sqrt{\left(\varphi \sum (x_i - y_i)^2\right)}. \quad (9)$$

The similarity expressed by Euclidean distance is [18]

$$\text{sim}(x, y) = \frac{1}{1 + d(x, y)} = \frac{1}{1 + \sqrt{\sum (x - y)^2}}. \quad (10)$$

Pearson correlation coefficient is as follows [19]:

$$\varepsilon(x, y) = \frac{\text{cov}(x, y)}{\sigma_y}. \quad (11)$$

The cosine similarity represents the cosine value of the angle formed by the vector value of two triples in the vector space [20]:

$$\cos(\beta) = \frac{\sum x \sum y}{1 + \sqrt{\sum x \sum y}}. \quad (12)$$

Calculate the product  $M$  of each row element of the judgment matrix [21, 22]:

$$M = \prod_{j=1}^n a_{i,j}. \quad (13)$$

Calculate the  $n$ th root of  $M$  [23]:

$$\begin{aligned} \bar{W} &= \sqrt{M}, \\ \bar{W} &= \frac{\sqrt{M}}{\sum_{j=1}^n W}. \end{aligned} \quad (14)$$

LBP is a well-known traditional Chinese medicine or a tonic. It has a great protective effect on the liver and eyes. Calculate the largest characteristic root of the judgment matrix [24]:

$$\lambda = \sum_{i=1} \frac{(AW)_i}{nW_i}, \quad (15)$$

$(AW)_i$  represents the  $i$ th element of the vector  $AW$  [25].

**2.5.3. Observation of Staining.** The wild balb/c mice (23–28 g) were divided into 2 groups ( $n=4$ ). Both the control group and the ZD group were fed normal food and water for 90 days. During this period, the wolfberry polysaccharide group was given 2 mg/kg of wolfberry red pigment every day for 90 days. Then, the serum ALT, AST, and TNF- $\alpha$  content were determined by the above-mentioned method, and the content of urea nitrogen (BUN) was determined using ADVIA2400 clinical instrument (Siemens Healthcare, Erlangen, Germany). The liver, heart, spleen, and kidney tissues of mice were stained with H&E to observe the damage.

### 3. Results

LBP is the most important part of *Lycium barbarum*. Modern medical research results show that LBP has a wide range of biological effects, including resistance to aging, nerve protection, glucose metabolism control, blood lipid reduction, oxidation prevention, enhance immune regulation, and other effects.

The rats in the normal control group were  $425 \pm 28$  grams by the end of the tenth week, and there was no death. Rats in the alcohol group were  $286 \pm 38$  g at the end of the tenth week, which was significantly different from the normal control group. The masses of the 5% LBP group, 10% LBP group, and 10% CSH treatment group were  $366 \pm 34$  g,  $363 \pm 37$  g, and  $371 \pm 33$  g at the end of the 10th week, respectively. There were 1 death, 3 deaths, and 1 death in each of the three treatment groups. At the end of the 10th week, the weight of the abstinence group was  $326 \pm 31$  g, 9 died, and the mortality rate was as high as 32.14%. The conditions of the rats that died and died abnormally in the experiment are shown in Figure 3.

NAFLD is one of the leading causes of chronic liver injury worldwide. It is also strongly associated with other pathological conditions, including obesity, diabetes, cardiovascular disease, and metabolic syndrome symptoms. Although the pathogenesis of NAFLD has not been fully characterized, it is generally believed to be caused by IR, lipid metabolism dysfunction, OS, inflammation, and necrotic cell apoptosis. Each potential therapeutic strategy should target these pathological conditions in the liver. In the past few decades, nonpharmacological treatments for NAFLD have received increasing attention. These substances are widely available and have fewer side effects than drugs, and their therapeutic mechanisms and benefits have been demonstrated in many studies.

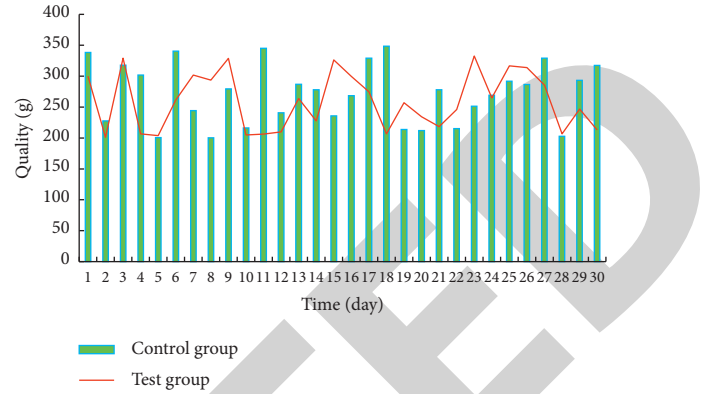


FIGURE 3: Conditions of rats executed and those that wrongfully died in the experiment.

For each concentration of LBP, three repeated inhibition tests were done. In one well (the number of cells in each well is  $125 \times 10^3$ ), when the concentration of *Lycium barbarum* polysaccharide is  $0 \mu\text{mol/L}$ , the average number of uninhibited cells is  $124.00 \times 10^3$ . The effect of fibrotic cell inhibitory concentration is shown in Table 1.

LBP is a famous Chinese medicine or tonic, which has shown great protective effect on liver and eyes. Mild to moderate abnormalities of ALT and/or AST are sometimes the only abnormal manifestations of NAFLD. Therefore, ALT and AST can be regarded as indicators of abnormal liver function. In this study, LBP was dry ALT and AST in pregroup were lower than those in NAFLD group, suggesting that LBP has protective effect on liver cells.

The immune system plays an important role in fighting tumors and fighting infections. Therefore, it is important to reduce the side effects and immunosuppression of chemotherapy drugs in the bone marrow and to protect the body's immune function. At present, biologics represented by stimulating factor (G-CSF) have various degrees of side effects in clinical use and even cause secondary tumors. People are strongly demanding to find new reagents for chemotherapy. The effect of suppressing the number of fibrotic cells is shown in Table 2.

Compared with the normal control group, the levels of lipofuscin and LPO in drosophila salivary gland cells in the group supplemented with LBP extract significantly decreased, suggesting that LBP can inhibit the production of ROS, reduce the effect of LPO, and protect cells to a certain extent. Clinical trials have also found that LBP can also increase serum antioxidant levels while reducing the formation of lipid peroxides.

*Lycium barbarum* polysaccharides can significantly inhibit the proliferation activity of HCCLM3 in in vitro experiments. At different LBP concentrations ( $0 \mu\text{mol/L}$ ,  $5 \mu\text{mol/L}$ ,  $10 \mu\text{mol/L}$ , and  $15 \mu\text{mol/L}$ ), the inhibition rates are 0.80%, 20.06%, 35.44%, and 55.39%, respectively. LBP concentration of  $5 \mu\text{g/mL}$ ,  $1 \mu\text{g/mL}$ , and  $2 \mu\text{g/mL}$  ( $1.008 \pm 0.090 \mu\text{g/mL}$  versus  $1.473 \pm 0.083 \mu\text{g/mL}$ ,  $1.063 \pm 0.050 \mu\text{g/mL}$  versus  $1.473 \pm 0.083 \mu\text{g/mL}$ , and  $1.040 \pm 0.078 \mu\text{g/mL}$  versus  $1.473 \pm 0.083 \mu\text{g/mL}$ ,  $P < 0.05$ ) had a greater impact on cell viability. The inhibition rate at different LBP concentrations is shown in Figure 4.

TABLE 1: Effect of the fibrotic cell inhibitory concentration.

LBP concentration ( $\mu\text{mol/L}$ )	First time	Second time	Third time	Average value
0	124.2	124.4	123.4	124.00
5	101.9	99.9	98.0	99.93
10	83.4	77.6	81.1	80.70
15	56.0	59.0	523	55.76

TABLE 2: Effect of fibrotic cell number inhibition.

LBP concentration ( $\mu\text{mol/L}$ )	Number of uninhibited cells	Number of suppressed cells	Total	Inhibition rate (%)
0	124.00	1.00	125.00	0.80
5	99.93	25.07	125.00	20.06
10	80.70	44.30	125.00	35.44
15	55.76	69.24	125.00	55.39

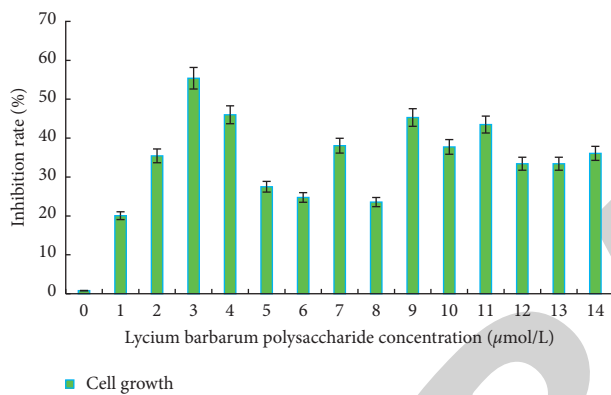


FIGURE 4: Inhibition rate at different LBP concentrations.

Radiotherapy is also the traditional method of liver cancer treatment. With the improvement of radiotherapy technology, radiotherapy plays an active role in palliative treatment of liver cancer. In recent years, molecular targeted therapy and immunotherapy have also been gradually applied in the treatment of liver cancer.

The western blot experiment is the average of three experimental results. The three experimental conditions are exactly the same. The VEGF protein concentration of the control group is set to  $1 \mu\text{mol/L}$ . In the results of this experiment, the ratio of the concentration of VEGF protein is 0.71, 0.57, and 0.27. In the second experiment, the ratio of VEGF protein concentration was 0.88, 0.59, and 0.47. Surgery is mainly the preferred treatment method for liver fibrosis including liver resection and transplantation. Surgical resection of the liver can effectively improve the survival rate of 50% of tumor patients, but surgical treatment is mainly suitable for early-stage patients. There are requirements for the size and nature of the tumor, as well as the status of patients with obvious heart and lungless patients, and no renal dysfunction is required. The results of the western blot experiment are shown in Figure 5.

However, the effect of any current treatment or drug therapy is not satisfactory, which is also the main reason for the high death rate of liver cancer. At present, comprehensive treatment is a new strategy for the treatment of liver cancer in different stages of development, such as

chemotherapy after surgical resection or liver transplantation to prevent recurrence. Or a combination of radiation and chemotherapy often works better than treatment alone.

When the LBP concentration is set to  $0 \mu\text{mol/L}$ , the protein concentration of VEGF is 1. When the LBP concentration is  $5 \mu\text{mol/L}$ ,  $10 \mu\text{mol/L}$ , and  $15 \mu\text{mol/L}$ , the protein concentration of VEGF is  $0.75 \pm 0.05$ ,  $0.56 \pm 0.03$ , and  $0.36 \pm 0.06 \mu\text{mol/L}$ , respectively. The protein concentration of VEGF is shown in Figure 6.

However, polysaccharide from traditional Chinese medicine is a mixture composed of a series of polysaccharide components with different molecular weight, which may have different biological activities. The main active components and mechanism of antitumor and immunomodulatory effects of LBP have not been clear, which also needs further study.

At present, the research on the modern molecular level of traditional Chinese medicine to prevent and treat ALD is still not deep enough, and the lack of exploration in signal transduction pathways, genome, and proteomics makes it difficult for traditional Chinese medicine to become the universal medical language in the world. The activity levels of ALT and AST in the cell culture medium of the ethanol injury group were 3.10 and 3.25 times that of the control group, respectively, and the difference was statistically significant ( $P < 0.01$ ). The results of this experiment show that the ethanol-induced hepatocyte injury model was successfully constructed. The cell culture condition of ethanol damage is shown in Figure 7.

*Lycium barbarum* polysaccharide (LBP) extracted from Chinese medicine *Lycium barbarum* has many biological effects, such as enhancing immune function, antitumor, and antioxidation and alleviating bone marrow inhibition by radiotherapy and chemotherapy. Existing studies suggest that LBP has the functions of antitumor and protective agent of chemotherapy and has the potential to reduce the immune toxicity of adriamycin and enhance its anti-liver cancer effect.

Compared with the control group, the cell viability of the ethanol injury group was significantly reduced ( $P < 0.01$ ), and the cell viability was  $66.48\% \pm 4.30\%$ . The cell viability of the ethanol injury group is shown in Figure 8.

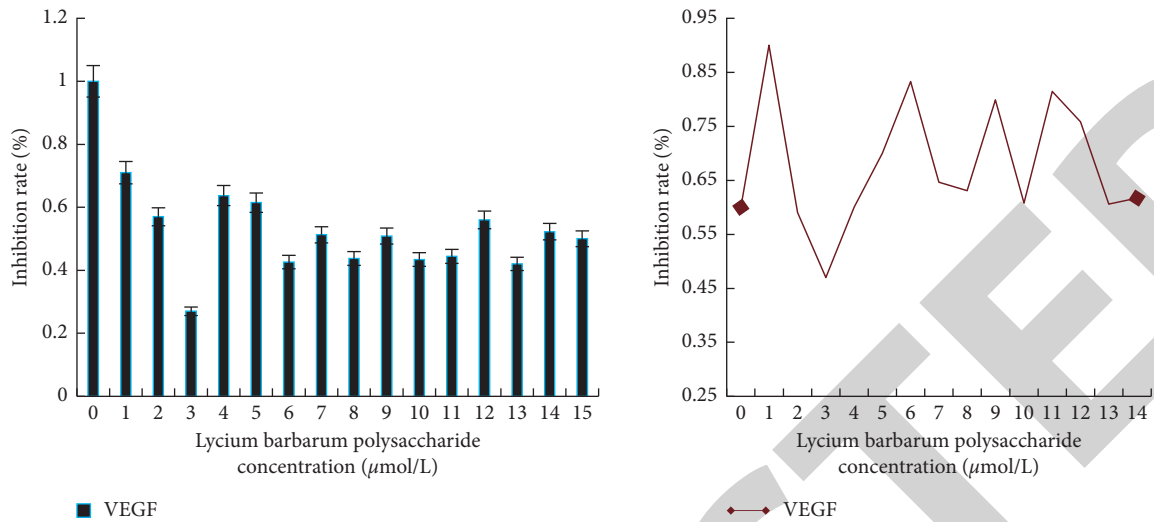


FIGURE 5: Results of the western blot experiment.

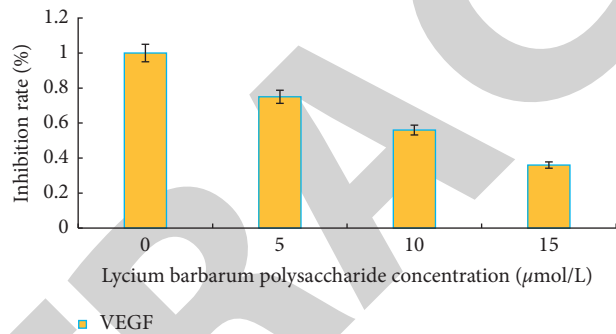


FIGURE 6: Protein concentration of VEGF.

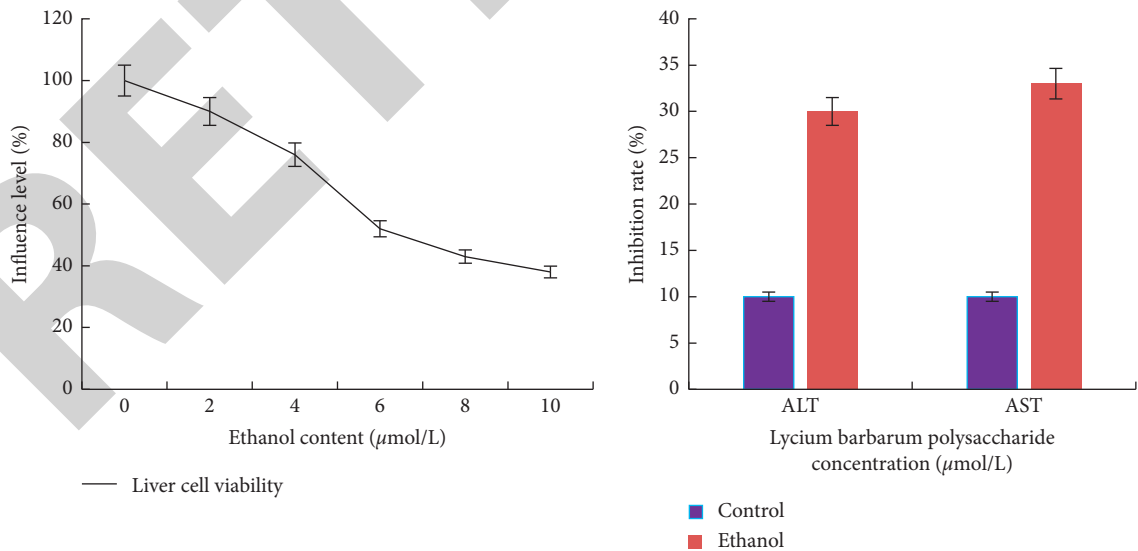


FIGURE 7: Situation of ethanol-damaged cell culture.

After 24 hours of plating, the cells of each group showed adherent growth, and the cell status was good. 48 hours after the addition of the drug, the low-dose wolfberry polysaccharide 200 mg/mL combination control group did not

change significantly compared with the cell morphology under the microscope, while some cells in the 400 mg/mL group rounding, the shrinking, and rounding of 800 mg/mL group showed that the number of apoptotic cells increased.

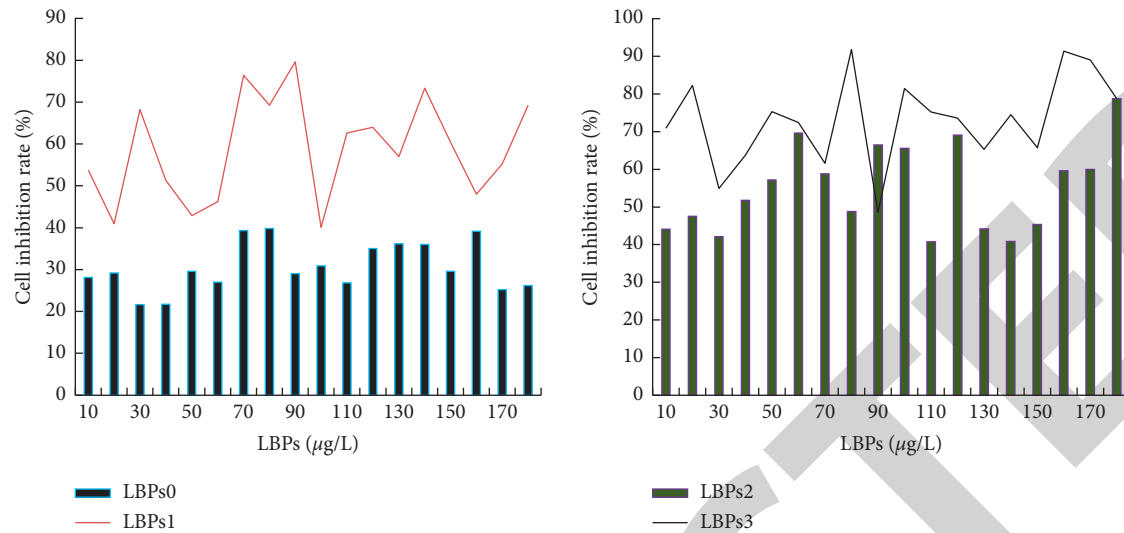


FIGURE 8: Cell viability in the ethanol damage group.

At high doses of *Lycium barbarum* polysaccharide, most of the adherent cells showed reduced volume and rounded growth, and the number of cells was very small. The cell growth is shown in Figure 9.

The results of MTT showed that each group of drugs had a certain inhibitory effect on cells and was dose-dependent. The inhibition rates of the *Lycium barbarum* polysaccharide group alone (200 mg/L, 400 mg/L, 800 mg/L, and 1000 mg/L) were 9.23%, 22.80%, 36.84%, and 76.25%, respectively. The MTT results are shown in Table 3.

Relative to the tumor quality of the model group, the low-dose LBP, high-dose LBP, LBP + CXCLIO, and CTX medication groups all showed a certain tumor inhibition trend, and the inhibition rates were 37.83%, 12.50%, 16.11%, and 59.20%, respectively. The changes of tumor mass in different groups are shown in Table 4.

The results of flow cytometry showed that the Th1/Th2 ratio of the LBP combined with CXC110 group increased significantly to  $6.12 \pm 3.89$ , while the model group was only  $0.87 \pm 0.42$ . The change of Th1/Th2 ratio is shown in Table 5. The effects of different molecular weight LBP components on the growth of mouse liver cancer xenografts in vitro experimental results show that different molecular weight LBP components have different effects on the proliferation of mouse H22 liver cancer cells and the function of lymphocytes and macrophages. However, the physiological environment in vivo is more complicated than the experimental environment in vitro. The inhibition of polysaccharides in vitro on fibrotic cells and the regulation of immune cell function cannot fully reflect its antitumor and immunoregulatory effects in vivo.

Among them, amino acid aminotransferase (ALT), aspartate aminotransferase (AST), lactate dehydrogenase (LDH), ALT, and AST can be regarded as indicators that reflect abnormal liver function. In this experiment, ALT and AST in the LBP intervention group were lower than those in the NAFLD group, suggesting that LBP has a protective effect on liver cells. Compared with the ethanol injury group,

the ALT, AST, and LDH activities of the 25 and 100 µg/mL LBPs groups were significantly reduced ( $P < 0.05$ ). The results showed that LBPs can inhibit the release of ALT, AST, and LDH in hepatocytes induced by ethanol. Make full use of postgenomics ideas and modern molecular biology technologies such as biochips, establish the concept of transformation mode related to genomics and proteomics and traditional Chinese medicine, link the modernization of traditional Chinese medicine research with life sciences, and make it a clear mechanism of action; the material basis is clear, and it is a modern and vigorous drug that is universally accepted internationally. The activities of ALT, AST, and LDH are shown in Figure 10.

#### 4. Discussion

Liver fibrosis (LF) is a general pathological feature of most chronic liver diseases and is an inevitable stage of the onset of liver cirrhosis. Because LF can be reversed, research on the treatment of liver fibrosis has become a hot topic. Because it is difficult to overcome the toxicity and side effects of western medicine treatment, it is difficult to be widely used in clinics. TCM has a long history in the treatment of liver fibrosis. In recent years, people have conducted extensive and detailed studies on the effective ingredients of many TCM extracts for liver fibrosis [26].

External pollutants (heavy metals such as cadmium, chromium, arsenic, organic poisons such as carbon tetrachloride, etc.) may cause chemical liver injury (CLI). CLI appears as fatty liver, hepatitis, fibrosis, and even liver cancer and has attracted the attention of researchers in the fields of toxicology, nutrition, and food science. Mitochondria have their own genome, but their synthesis and function require nuclear-encoded proteins. Under the action of various transcription factors and core collagen, these proteins regulate the transcription of nuclear and mitochondrial genetic factors, and regulate body temperature, energy intake, and exercise capacity. LBP of different molecular weights will

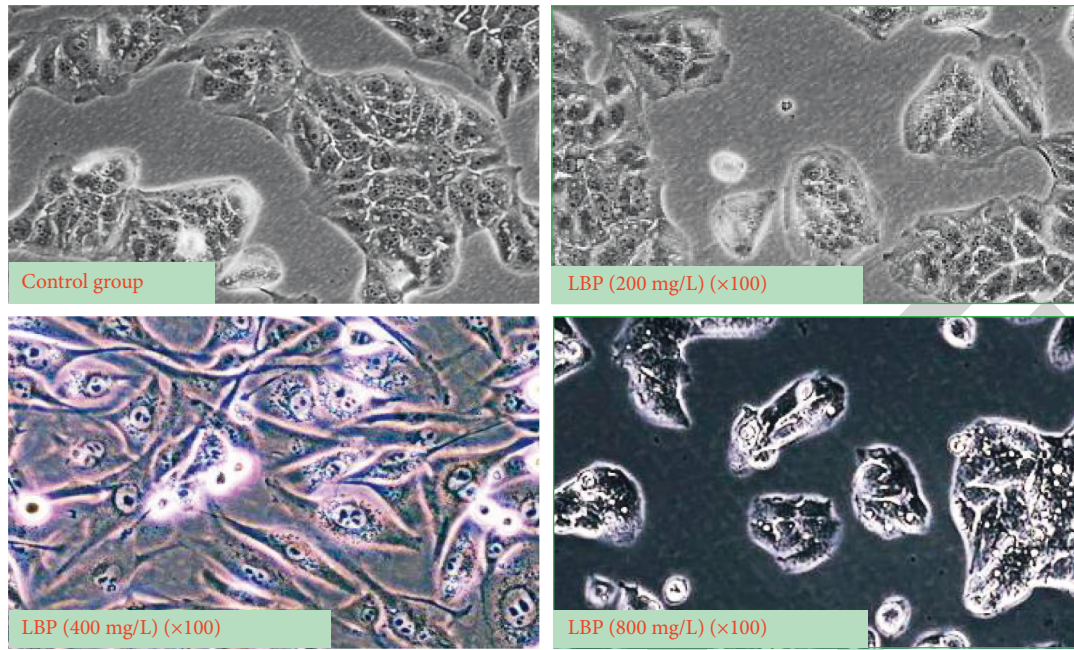


FIGURE 9: Cell growth.

TABLE 3: MTT bear fruit.

Group	LBP (mg/L)	5FU (umol/L)	Inhibition rate (%)
Blank control group	0	0	0
LBP1 group	200	0	9.23 ± 0.20
LBP2 group	400	0	22.80 ± 5.83
LBP3 group	800	0	36.84 ± 2.30
LBP4 group	1000	1	76.25 ± 8.23
5FU group	0	1	34.15 ± 0.73
Combine 1 group	200	1	45.15 ± 1.13
Combine 2 groups	400	1	81.10 ± 1.53

TABLE 4: Tumor mass in the different groups.

Group	N	Average tumor mass (g)	Tumor inhibition rate (%)
Normal	10	—	—
Model	7	3.04 ± 1.06	—
CTX	9	1.24 ± 0.84	59.20
Low-dose LBP	10	1.89 ± 1.21	37.83
High-dose LBP	8	2.66 ± 1.68	12.50

reduce cell viability and may hinder the proliferation of fibrotic cells. LBP-3 has the most important effect. Further studies have shown that LBP-3 has a dependent effect on the dosage of S phase arrested liver fibrotic cell cycle, reduces the mitochondrial membrane potential, and may cause liver fibrotic cell death [27].

Liver cancer is formed under the combined action of various factors. Cancer cells proliferate and metastasize through various methods or signal transmission pathways. Due to the complexity of the microenvironment of tumor

TABLE 5: Th1/Th2 ratio change.

Group	Th1 (%)	Th2 (%)	Th1/Th2
Normal	10.61 ± 4.72	7.75 ± 3.52	1.52 ± 0.59
Model	12.35 ± 7.74	21.48 ± 23.23	0.87 ± 0.42
CTX	4.05 ± 3.16	2.83 ± 2.05	2.01 ± 1.99
Low-dose LBP	28.38 ± 21.98	7.71 ± 5.24	6.05 ± 7.83
High-dose LBP	18.58 ± 7.61	18.88 ± 13.69	2.48 ± 2.93

tissues, a single treatment method cannot effectively control the onset of liver cancer. Therefore, exploring multiple methods and multiple drugs combined therapy has become a new strategy for the treatment of liver cancer. For mild alcoholic fatty liver and alcoholic hepatitis, control of alcohol and active treatment can restore the original state, but if not treated in time, all types of ALD will eventually lead to alcoholic liver cirrhosis, gastrointestinal bleeding, and development due to shock of all kinds of infections and other complications of liver cirrhosis. This is also the main cause of death in ALD patients [28].

Extrinsic chemicals are mainly produced by liver metabolism, and liver toxicity is mainly related to the formation of active metabolites. Normally, the liver is detoxified through phase I and phase II. When the cellular defense mechanism is disrupted, exogenous chemicals are usually metabolized by phase I phosphate P450 enzyme involved in oxidation, reduction, or hydrolysis, producing a large number of electron affinity groups and free radicals. In addition, the covalent protein binding produced by active metabolites may also cause immune damage.

LDH is widely present in the cytoplasm of hepatocytes and can indirectly evaluate the survival rate of cells and the degree of damage to cell membranes. Reducing the emission of transaminase and LDH is an important indicator for testing the preventive and therapeutic effects of natural

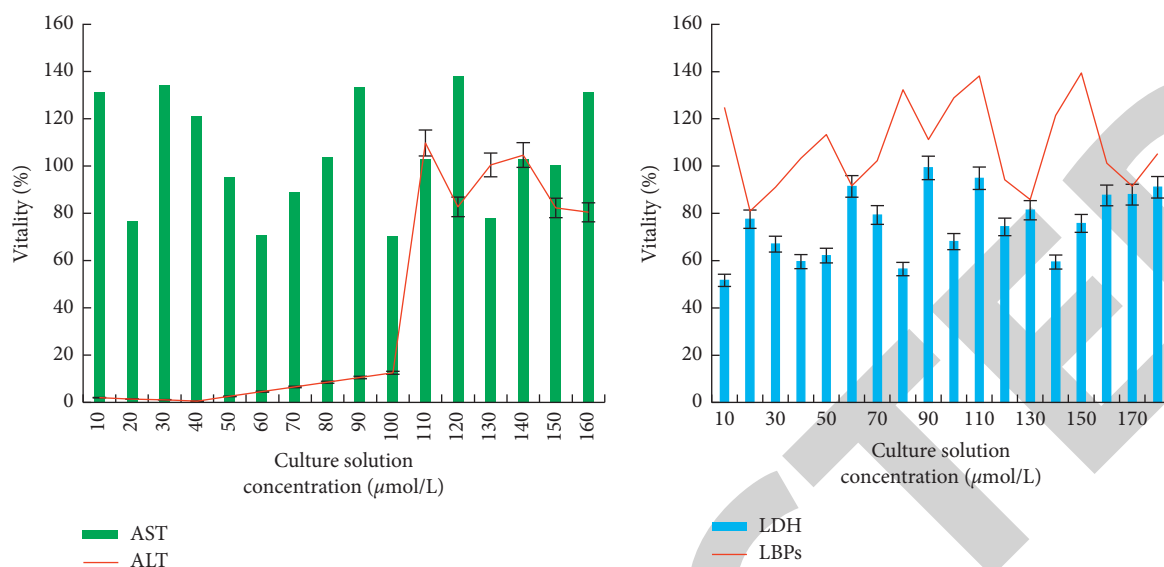


FIGURE 10: ALT, AST, and LDH vitality.

ingredients on liver dysfunction. The intervention of polysaccharides can reduce the release of ALT, AST, and LDH in liver cells. Therefore, by measuring the release of liver kinase and LDH in cell culture fluid, it can reflect the degree of damage to liver cells caused by ethanol and antifibrotic drugs [29].

In recent years, with the deepening of experimental research on the prevention and treatment of medical liver fibrosis and the research process mechanism, from the perspective of the effective ingredients of Chinese medicine, the preparation of single drugs and compounds has a good prospect, but from the perspective of pathology in the classic enzyme studies, most of the biochemistry, histochemistry, immunohistochemistry, radioimmunology, and so on show the mechanism of drugs by observing the pathological changes of the liver, the enzyme spectrum, and the cells of the liver [2].

## 5. Conclusion

This study found that LBPs can inhibit liver cell oxidative stress damage, and the Nrf2 pathway is a key transcription factor involved in liver cell metabolism and detoxification. Several downstream antioxidant enzymes are important components of the liver's antioxidant system. Excitogen plays a key role in maintaining cell oxidation homeostasis. Therefore, in order to explore the protective mechanism of LBPs on chemical hepatocyte damage caused by oxidative stress, this study used western blot to detect the effect of LBPs intervention on the expression of related proteins in the Nrf2 pathway of hepatocytes. The antitumor effect of *Lycium barbarum* polysaccharide has been confirmed. Research in recent years has shown that the biological activity of polysaccharide may be related to its chemical structure and molecular weight. In vitro experiments in this study have also confirmed that LBP has four different molecular weight soluble *Lycium barbarum* polysaccharide components. Strongly inhibit the proliferation of mouse liver cancer cells and enhance the function of immune cells. In this study, through in vivo tumor suppression

experiments, it was found that LBP can significantly inhibit the growth of liver cancer transplanted tumors in mice, and its antifibrotic tumor effect is significantly stronger than other molecular weight polysaccharide components. The effect of *Lycium barbarum* polysaccharide on transaminase does not show a linear dose-effect relationship with its dosage. The exact mechanism is not fully understood. With the development of medical immunology and molecular biology technology, the antitumor immune mechanism of polysaccharides will be more in depth. Liver fibrosis is a challenge in the new era, and it is the key to preventing and treating patients progressing to end-stage liver disease. Liver fibrosis and end-stage liver disease are problems affecting the world. Liver fibrosis determines the morbidity and death of patients with liver disease and causes liver failure and is related to the occurrence of primary liver cancer. In the process of liver fibrosis caused by various reasons, immune factors have played an important role. Various damage stimuli act on the liver, leading to the activation or inhibition of immune cells and the production of a variety of cytokines. The disorder of these cells and their cytokines promotes or inhibits the formation and development of liver fibrosis. However, these immune factors have not been fully elucidated, and further elucidation of these problems will provide us with various methods and basis for blocking the formation and development of liver fibrosis, which will help to treat this kind of diseases in a reasonable and effective clinical way. In the future, more drugs for treating liver fibrosis need to be studied.

## Data Availability

The data that support the findings of this study are available from the corresponding author upon reasonable request.

## Conflicts of Interest

The authors declare no conflicts of interest.

## *Retraction*

# **Retracted: An Early Warning of Atrial Fibrillation Based on Short-Time ECG Signals**

### **Journal of Healthcare Engineering**

Received 16 November 2022; Accepted 16 November 2022; Published 19 January 2023

Copyright © 2023 Journal of Healthcare Engineering. This is an open access article distributed under the Creative Commons Attribution License, which permits unrestricted use, distribution, and reproduction in any medium, provided the original work is properly cited.

*Journal of Healthcare Engineering* has retracted the article titled “An Early Warning of Atrial Fibrillation Based on Short-Time ECG Signals” [1] due to concerns that the peer review process has been compromised.

Following an investigation conducted by the Hindawi Research Integrity team [2], significant concerns were identified with the peer reviewers assigned to this article; the investigation has concluded that the peer review process was compromised. We therefore can no longer trust the peer review process, and the article is being retracted with the agreement of the Chief Editor.

The authors do not agree to the retraction.

### **References**

- [1] T. Zhao, X. Wang, and C. Qiu, “An Early Warning of Atrial Fibrillation Based on Short-Time ECG Signals,” *Journal of Healthcare Engineering*, vol. 2022, Article ID 2205460, 7 pages, 2022.
- [2] L. Ferguson, “Advancing Research Integrity Collaboratively and with Vigour,” 2022, <https://www.hindawi.com/post/advancing-research-integrity-collaboratively-and-vigour/>.

## Research Article

# An Early Warning of Atrial Fibrillation Based on Short-Time ECG Signals

Tianxia Zhao , Xin'an Wang , and Changpei Qiu 

*The Key Laboratory of Integrated Microsystems, Peking University Shenzhen Graduate School, Shenzhen 518055, Guangdong, China*

Correspondence should be addressed to Tianxia Zhao; 1501111264@sz.pku.edu.cn

Received 10 November 2021; Revised 14 December 2021; Accepted 30 December 2021; Published 18 January 2022

Academic Editor: Yang Gao

Copyright © 2022 Tianxia Zhao et al. This is an open access article distributed under the Creative Commons Attribution License, which permits unrestricted use, distribution, and reproduction in any medium, provided the original work is properly cited.

This study introduces a method to classify single-lead ECG signals by extracting features through traditional methods and deep neural network methods. At first step, the statistical type features of the ECG signals are extracted by traditional methods, including time domain features, frequency domain features, and medical domain features. And then, deep neural networks are used to extract the deeper features of the ECG signal. The database of ECG signals is from Cinc 17, which have 8528 samples of short-time ECG signal. The huge amount of data makes the classification and identification more accurate by atrial fibrillation, normal sinus rhythm, noise, and indiscernible. Compare the base model built by the classified data and the data collected by the ECG device of CareON to enable daily early screening and a remote alert function with WeChat app. This method can extend the prevention, detection, and diagnosis of heart disease to the family, company, and other out-of-hospital scenarios, thus enabling faster treatment of heart patients and saving medical resources.

## 1. Introduction

The heart completes the systolic and diastolic steps in sequence during the cardiac cycle, resulting in a potential change in the electrical charge of the heart on the human body surface, thus forming an electrocardiogram signal (ECG signal) [1]. The diagnosis and treatment of chronic diseases, such as cardiovascular disease, can be effectively diagnosed and treated through the highly accurate detection and analysis of ECG signals, which is why ECG testing is very important in the diagnosis and treatment of these chronic diseases [2].

Atrial fibrillation is one of the most common clinical arrhythmias [3], accounting for 1-2% of the general population [4]. As the population ages, the probability of atrial fibrillation occurring in the population will further increase [5]. Clinical medical studies have shown that the symptoms of atrial fibrillation are different in different patients. Some patients experience significant discomfort, while others have no obvious clinical symptoms. When the symptoms appear, the cardiovascular system is often already organically

diseased, leading to serious complications such as heart failure, coronary artery disease, stroke, and even death. Therefore, it is important to improve the vigilance of patients with paroxysmal atrial fibrillation to prevent adverse cardiovascular events [6]. Researchers have concluded from practical experience that there is a significant positive correlation between the degree of recovery from atrial fibrillation-induced disease and the timing of exposure to the disease. If the atrial fibrillation is found at earlier and the treatment is made earlier, the patient will recover easier and the effect of rehabilitation will be better. At the same time, the quality and quality of life for the atrial fibrillation patients will be reduced, the cost of living will increase, and the mood of patients will be affected. Therefore, it is important to manage patients with atrial fibrillation through early warning. Through some reasonable treatment and management methods, patients can live a normal life and improve their quality of life.

At present, domestic and foreign scholars have studies on atrial fibrillation recognition algorithms mainly based on atrial activity features [7] and RR interval characteristics [8].

Among them, the accuracy of atrial fibrillation automatic recognition algorithms based on atrial activity features is low, and the research on atrial fibrillation detection is usually limited in applicability, mainly because

- (1) The selected datasets show good performance, but may not be universal. Because, the strength of *P*-waves is weak compared to QRS complex and *T*-waves, and it is influenced by noise [9].
- (2) When atrial fibrillation occurs, the frequency domain segment of ECG waves may overlap with the frequency domain segment of atrial noise. If the frequency domain method is used, it is easy to cause misdiagnosis. The automatic recognition algorithm of atrial fibrillation based on RR interval is adopted to improve the accuracy and reduce the misdiagnosis rate [10], but this method cannot effectively distinguish atrial fibrillation from sinus rhythm.

To achieve high accuracy in detecting atrial fibrillation, in this study, the authors propose an architecture that combines common time-frequency domain features of ECG signals, medical features, and features extracted by deep neural networks, which can use the information contained in ECG signals in an all-round and multilevel way. The architecture diagram is shown in Figure 1. According to the comparison between the data collected by the portable ECG device CareON and the basic model, use a WeChat applet to enable remote alerting.

## 2. QRS Complex and RR Interregion Sequence

Figure 2 shows a schematic diagram of an ECG signal cycle. Usually, a normal ECG signal consists of multiple ECG signal cycles, and the ECG signal cycle consists of five parts: *P*-wave, PR interval, QRS complex, ST interval, and *T*-wave [11].

**2.1. Precise Positioning to QRS Complex.** As the most recognizable region of the ECG signal, the *R*-peak of the QRS complex becomes the basis of heart rate variability analysis due to its steep waveform and significant amplitude, and the accurate detection of the *R*-peak of the QRS complex of the ECG signal is a key precursor step to improve the quality of subsequent data analysis [12]. Locating the *R*-peaks of QRS complex, the detection of *P*-wave and *T*-wave of ECG signal can be further realized.

As a typical bioelectric signal, the ECG signal is susceptible to perturbation by interference noise, which mainly includes baseline drift, myoelectric interference, industrial frequency interference, and chemical voltage and electrode displacement interference. According to the frequency of QRS complex of ECG signal and the frequency of interference noise, the window function method is used for finite pulse response [13].

$$H(e^{j\omega}) = \sum_{n=0}^{N-1} h(n)e^{-j\omega n}. \quad (1)$$

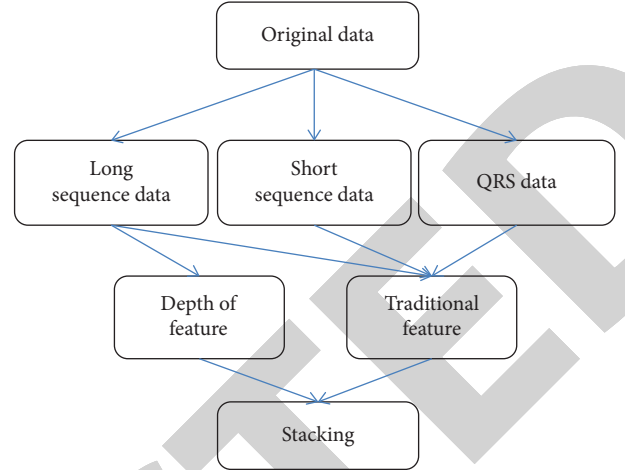


FIGURE 1: The architecture diagram of data classification.

After the bandpass filtering step, the first-order forward difference of the signal is calculated, as shown in formula (2). This calculation step can be used to suppress high *P*-wave and high *T*-wave while obtaining QRS complex slope information to improve the accuracy of the *R*-peak of the QRS complex detection algorithm for ECG signals.

$$d(i) = x(i+1) - x(i), \quad i = 1, 2, \dots, \text{length}(x) - 1. \quad (2)$$

After the first-order forward difference step, the signal is normalized in amplitude as shown in formula (3). This calculation step takes the signal itself as the numerator and the maximum absolute value of the signal as the denominator. After this calculation step, the range of the signal will be at  $[-1, 1]$  to prepare for the subsequent calculation of the Shannon energy envelope of the signal [14].

$$d(i) = \frac{d(i)}{\max(\text{abs}(d))}, \quad i = 1, 2, \dots, \text{length}(d). \quad (3)$$

In the digital filtering stage of the *R*-peak detection algorithm, the signal is bipolar signal after the first-order forward differential calculation step. In order to simplify the subsequent complexity of the *R*-peak detection, Shannon energy envelope is used to transform the signal from bipolar signal to unipolar signal, and the calculation method is shown in the following formula.

$$s(i) = -d(i)^2 \log(d(i)^2), \quad i = 1, 2, \dots, \text{length}(d). \quad (4)$$

In the *R*-peak detection algorithm, square envelope is used to achieve the purpose of converting the signal from bipolar signal to unipolar signal. The calculation method of square envelope is shown in the following formula.

$$s(i) = d(i)^2, \quad i = 1, 2, \dots, \text{length}(d). \quad (5)$$

After the zero-phase filtering in the Shannon energy envelope stage, the real *R*-peak and the pseudo *R*-peak exist in the processed ECG signal simultaneously. In order to improve the accuracy of the *R*-peak detection algorithm, the algorithm adopts the method of curve length transformation to remove pseudo *R*-peak [15].

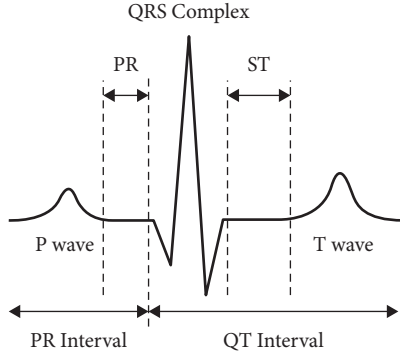


FIGURE 2: An ECG signal cycle.

In view of the difficulty of simultaneous amplification of QRS complex and suppression of noise, the Hilbert transform is used in this study to achieve high-quality  $R$ -peak detection of QRS complex [16]. Compared with the threshold-based  $R$ -peak detection algorithm, the advantage of Hilbert transform is that there is no threshold setting and no threshold adjustment strategy. The expression of the Hilbert transform is shown in the following formula.

$$H(x(t)) = \frac{1}{\pi t} \otimes x(t) = \frac{1}{\pi} \int_{-\infty}^{+\infty} \frac{x(\tau)}{t - \tau} d\tau. \quad (6)$$

The correspondence between the  $R$ -peak of the QRS complex and the positive zero crossing point is shown in Figure 3. The original ECG signal waveform is shown in Figure 3 which is used to simulate  $r(t)$ , and its expression is shown in equation (7). The signal after Hilbert transformation is simulated in  $H[r(t)]$ , and its expression is shown in equation (8). The position of  $R$ -peak and the positive zero crossing of the signal are identified by dots. Through Hilbert transform, the  $R$ -peak detection problem is transformed into a positive zero crossing detection problem [17].

$$r(t) = \frac{1}{1 + t^2}, \quad (7)$$

$$H[r(t)] = \frac{1}{1 + t^2}. \quad (8)$$

Since the index subscript corresponding to the forward zero crossing has some deviations from the index subscript corresponding to the real  $R$ -peak, the algorithm introduces the  $R$ -peak relocation process. When the sampling frequency is 360 Hz, 60 sampling points are detected forward to achieve high-quality  $R$ -peak detection.

Figure 4 shows the changes of the ECG signal after the calculation step of the Hilbert transform stage and the signal after  $R$ -peak relocation.

**2.2. RR Interregion Sequence.** The RR interval refers to the time interval between the  $R$ -peak of two adjacent QRS of the ECG signal. The heart rate can be calculated from RR interval [18], as shown in the following formula:

$$\text{Heart rate} = \frac{60}{RR}. \quad (9)$$

The heart rate can be calculated from the RR interval of the ECG signal, which is an important parameter of the heart's activity and can visually reflect the work done by the heart. A higher or lower heart rate often indicates a disease state or even a high risk state. Among them, the average of heart rate, as a circulatory parameter, contains less information as well as details. Compared to the average of heart rate, the instantaneous heart rate is more meaningful. Furthermore, RR interval sequences contain specific information about successive heart cycles. The study of heart rate variability (HRV) is a quantitative analysis method that found the variability of the continuous heartbeat cycle and thus its relationship with the human physiological state [19]. In fact, the transient heart rate of the human body is not constant even in the quiet state, and the corresponding RR interval series fluctuates slightly, and this fluctuation is more obvious when the physical state or health condition changes.

Heart rate variability analyses the variation and regularity of heart rate, namely, slight changes between successive cardiac cycles. Since cardiac excitation originates from the sinoatrial node, the  $P$ -wave appears first in a set of waves, so the PP interphase should use to calculate the sinus heart rate. However, due to  $P$ -wave amplitude is small and different dominant  $P$ -wave leads of each person,  $P$ -wave detection is not accurate, while  $R$ -wave amplitude is large and narrow which is easy to detect. Therefore, RR interval equal to PP interval is generally used for HRV correlation analysis.

### 3. Analysis of Atrial Fibrillation with Short-Term ECG Signal

In the study on the effectiveness of short-duration ECG signals, Tjin Hendriks et al. showed that intermittent short-duration ECG was more effective in detecting arrhythmias than 24-hour Holter electrocardiogram [20].

The common analysis methods of ECG signal in medicine include time domain analysis methods, frequency domain analysis methods, and nonlinear domain analysis methods. These methods have been proposed at an early stage, and their reliability has been clinically proven. In addition, they are commonly used in the medical field for detection and discrimination. The time domain analysis method of ECG signal is based on the time axis to represent the dynamic signal relationship, which can represent the signal visually from the morphology [21]. The frequency domain analysis method of ECG signal is to express the energy distribution of signal by frequency coordinate, which can analyze the problem more deeply and concisely. The nonlinear analysis method of ECG signal is studied in irregular time series which contains a deterministic mechanism in the same ECG signal. Thus, compared with the linear method, the nonlinear analysis method is likely to be more effective and can obtain more meaningful results.

The experimental data for this study were obtained from Cinc challenge 17 and included a total of 8528 single-lead

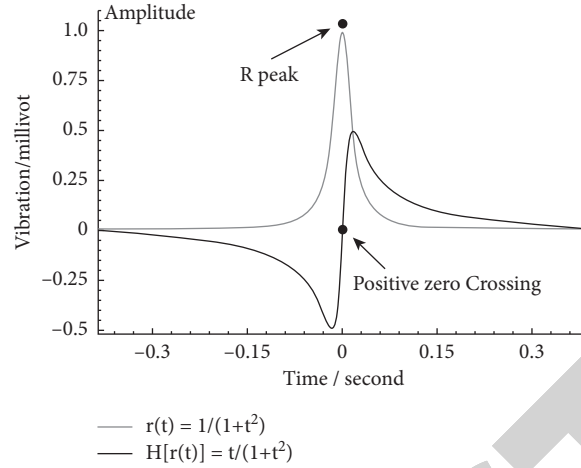


FIGURE 3: Relationship between the R peak and positive zero crossing.

300 Hz short-time ECG signals with ECG signal lengths ranging from 9 s to 61 s. These signals included 5154 normal sinus rhythm signals, 771 atrial fibrillation rhythm signals, 2557 ECG signals that could not be clearly diagnosed, and 46 noisy signals.

**3.1. Characteristic Value Extraction.** Before extracting the data, the raw data were preprocessed, and the following data were obtained.

**3.1.1. Time Domain Characteristics.** The time domain characteristics used in this study are statistical on the ECG signal sequence, and the statistical characteristics used value, mean, maximum, minimum, range, variance, skewness, kurtosis, and percentage.

**3.1.2. Frequency Domain Characteristics.** The frequency domain characteristics used in this study are the characteristics extracted from the conversion of ECG signals from time domain to frequency domain, and the characteristics used power, frequency band power, Shannon entropy, and signal-to-noise ratio. The Shannon entropy is calculated as [22]

$$H = - \sum_{i=1}^n p(x_i) \log_2 p(x_i). \quad (10)$$

**3.1.3. Medical Characteristics.** This part of characteristics is extracted based on the knowledge of medical field and divided into two parts. The first part is extracted from QRS data, including sample entropy, coefficient of variation, density histogram, median absolute deviation, and heart rate variability. The second part is extracted from short series data, including interval, length, amplitude, and slope.

**3.1.4. Nonlinear Characteristics.** This part of the characteristics contains turning points, excess zeros, autocorrelation coefficients, and trend fluctuation analysis coefficients.

**3.1.5. Depth Characteristics.** The deep neural network has been verified to be very effective in the processing of ECG signal [23]. In this study, we use a neural network constructed by a residual network to extract the depth features in ECG signals. Usually, the deep neural network model is an end-to-end model; so in this study, the output layer of the deep neural network model is removed, and the output of the hidden layer is treated as features.

### 3.2. Modeling Characteristics

**3.2.1. Long Sequence Data.** The raw data are converted into numeric sequences as long sequence data.

**3.2.2. Short Sequence Data.** Use the QRS detector to split the long sequence data into individual QRS waves as short sequence data. In this study, the QRS detector is realized on the Pan-Tompkins algorithm.

**3.2.3. QRS Data.** Calculate the length of each continuous QRS wave in long sequence data as QRS data.

**3.3. Model Performance.** The results of the model are offline verification. We use the five-fold cross-validation method to obtain the model results of training and verification conducted by five different training sets and verification sets and take the mean value as the offline verification score. The results were compared with those of Andrew Ng's team. Specific results are given in Table 1.

As shown in the above table,  $F_{1N}$  represents the  $F_1$ -score of normal sinus rhythm,  $F_{1A}$  represents the  $F_1$ -score of atrial fibrillation rhythm,  $F_{1O}$  represents the  $F_1$ -score of unclassified rhythm, and  $F_{1P}$  represents the  $F_1$ -score of noise. In this study, the number of noise samples in the original

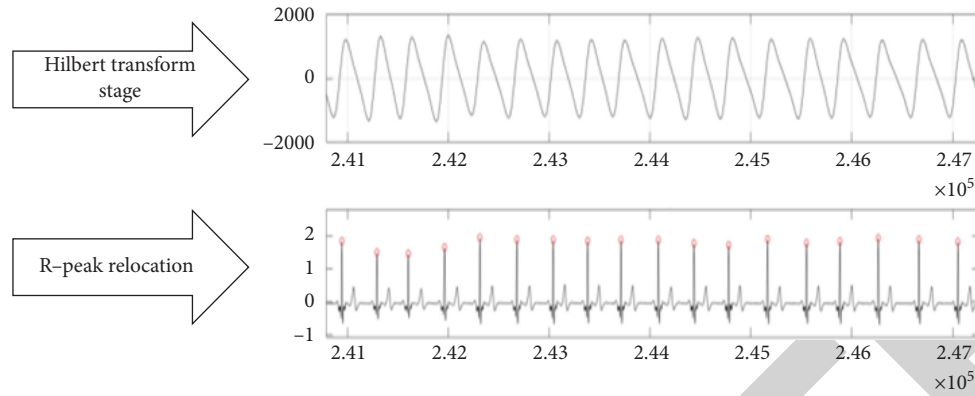


FIGURE 4: Hilbert transform.

TABLE 1: The results of verification in different teams.

Method	$F_{1N}$	$F_{1A}$	$F_{1O}$	$F_{1p}$	$F1$	$F_{1\_NAO}$
Cinc 2017 best score	0.9204	0.8692	0.8068	0.8156	0.8530	0.8655
Andrew Ng	0.9356	0.8680	0.8326	0.8041	0.8600	0.8787
This study	0.9430	0.8549	0.9103	0.7866	0.8682	0.8955



FIGURE 5: The moulding of CareON.

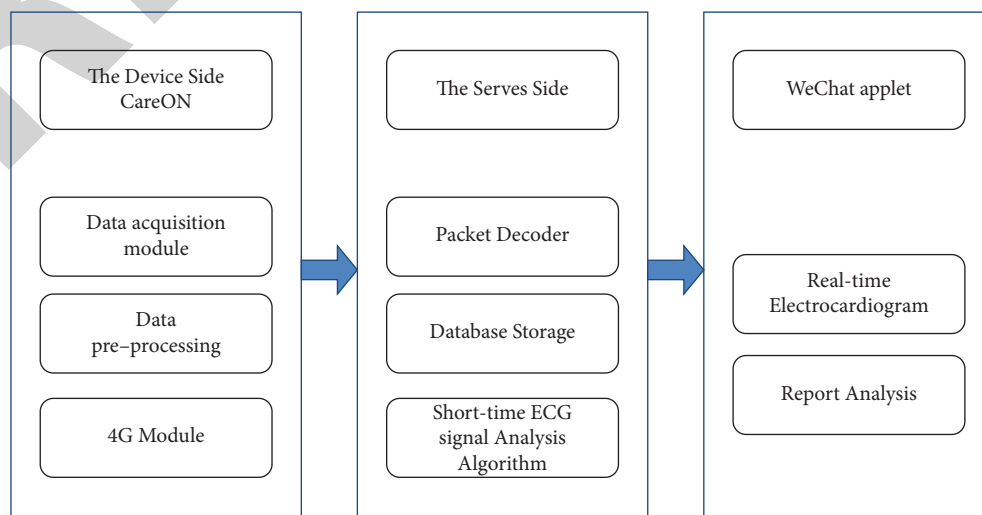


FIGURE 6: The short-time ECG signal detection system.

dataset is very small, and the data distribution of all kinds of samples is very uneven that leads to the instability of the trained model. Therefore, the final result will be more convincing if  $F_{1P}$  is removed, which is also the reason why there is a  $F_{1\_NAO}$ .

The algorithm is evaluated by using the Cinc 17 challenge database and achieves the average  $F1$ -score of 0.8682,  $F1\_NAO$  score of 0.8955, detection accuracy of atrial fibrillation 85.5%, and accuracy of ECG multiclassification 91%, which proves that this method has a certain degree of auxiliary diagnosis of ECG signals.

#### 4. Short-Term ECG Signal Detection System Based on CareON

The detection system based on short-term ECG signal includes three parts: the device side, the user side, and the server side. The device side adopts the single-lead ECG signal acquisition sensor CareON (Figure 5) which is developed by the team of Integrated Microsystems Laboratory of Peking University. The raw ECG signal is collected from the human body surface through electrode pads, processed by the internal integrated preprocessing module, and then, the data are sent to the server in real time through the 4G module, where the algorithm on the server analyzes the real-time data and returns the results to the user side and presents them to the user by means of an applet. The user side and the server side together constitute the software and algorithm part of the short-time ECG signal detection system.

The overall architecture of the short-time ECG signal detection system is shown in Figure 6. Patients can see their real-time ECG through the WeChat applet, and they can send requests on the applet side to get real-time analysis results. The server side includes MySQL database storage, packet parsing, and short-time ECG signal analysis algorithm, which can analyze the patient's ECG data in real-time in the background.

#### 5. Conclusion

In today's aging population, the incidence of atrial fibrillation is increasing day by day, though the ECG signal can effectively screen patients with atrial fibrillation. The hospital clinical electrocardiogram machine used by the static or dynamic electrocardiogram machine is expensive; it needs to be used in the hospital or go to the hospital. In order to enable patients with atrial fibrillation to assess their health status in daily life and to help patients know their condition recovery in real time, based on the MIT-BIH database, we propose a short-term ECG signal analysis architecture that combines traditional features, medical features, and depth features. This architecture can effectively improve the detection accuracy of atrial fibrillation rhythm. This model can effectively improve the detection accuracy of atrial fibrillation rhythm in short-term ECG signals, which can save the effort and time of clinical cardiologists to a certain extent, and can be used as an automatic aid for atrial fibrillation rhythm diagnosis.

#### Data Availability

The data used to support the findings of this study are available from the corresponding author upon request.

#### Conflicts of Interest

The authors declare that they have no conflicts of interest.

#### Acknowledgments

The project was funded by the Shenzhen (China) Future Industry Development Special Fund (JCYJ20170412151226061) and the Shenzhen (China) Technology Research and Development Fund (JCYJ20180503182125190).

#### References

- [1] M. Brennan, M. Palaniswami, and P. Kamen, "Do existing measures of Poincare plot geometry reflect nonlinear features of heart rate variability?" *IEEE Transactions on Biomedical Engineering*, vol. 48, no. 11, pp. 1342–1347, 2001.
- [2] M. García, J. Ródenas, R. Alcaraz, and J. J. Rieta, "Application of the relative wavelet energy to heart rate independent detection of atrial fibrillation," *Computer Methods and Programs in Biomedicine*, vol. 131, no. 7, pp. 157–168, 2016.
- [3] L. S. C. Li, C. C. Wang, Y. L. Xia et al., "Assessment of association of rs2200733 on chromosome 4q25 with atrial fibrillation and ischemic stroke in a Chinese Han population," *Human Genetics*, vol. 126, no. 6, pp. 843–849, 2009.
- [4] S. Kiranyaz, T. Ince, and M. Gabbouj, "Real-time patient-specific ECG classification by 1-D convolutional neural networks," *IEEE Transactions on Biomedical Engineering*, vol. 63, no. 3, pp. 664–675, 2016.
- [5] R. Sassi, S. Cerutti, F. Lombardi et al., "Advances in heart rate variability signal analysis: joint position statement by the e-cardiology ESC working group and the European heart rhythm association co-endorsed by the asia pacific heart rhythm society," *Europace*, vol. 17, no. 9, pp. 1341–1353, 2015.
- [6] T. Debnath, M. M. Hasan, and T. Biswas, "Analysis of ECG signal and classification of heart abnormalities using artificial neural network," in *Proceedings of the International Conference on Electrical and Computer Engineering*, pp. 353–356, IEEE, Dhaka, Bangladesh, December 2017.
- [7] C. Bian, Q. Ma, J. Si et al., "Sign series entropy analysis of short-term heart rate variability," *Science Bulletin*, vol. 54, no. 24, pp. 4610–4615, 2009.
- [8] R. B. Pachori, P. Avinash, K. Shashank, R. Sharma, and U. R. Acharya, "Application of empirical mode decomposition for analysis of normal and diabetic RR-interval signals," *Expert Systems with Applications*, vol. 42, no. 9, pp. 4567–4581, 2015.
- [9] M. A. Kabir and C. Shahnaz, "Denoising of ECG signals based on noise reduction algorithms in EMD and wavelet domains," *Biomedical Signal Processing and Control*, vol. 7, no. 5, pp. 481–489, 2012.
- [10] T. Nakamura, K. Kiyono, H. Wendt, P. Abry, and Y. Yamamoto, "Multiscale analysis of intensive longitudinal biomedical signals and its clinical applications," *Proceedings of the IEEE*, vol. 104, no. 2, pp. 242–261, 2016.
- [11] H. Gibbs, B. Freedman, M. Rosenqvist et al., "Clinical outcomes in asymptomatic and symptomatic atrial fibrillation

## Retraction

# Retracted: Effect of Protein Nutrition Level on Protein Metabolism during Volleyball Exercise Based on Edge Computing in the Medical System

### Journal of Healthcare Engineering

Received 16 November 2022; Accepted 16 November 2022; Published 20 January 2023

Copyright © 2023 Journal of Healthcare Engineering. This is an open access article distributed under the Creative Commons Attribution License, which permits unrestricted use, distribution, and reproduction in any medium, provided the original work is properly cited.

*Journal of Healthcare Engineering* has retracted the article titled “Effect of Protein Nutrition Level on Protein Metabolism during Volleyball Exercise Based on Edge Computing in the Medical System” [1] due to concerns that the peer review process has been compromised.

Following an investigation conducted by the Hindawi Research Integrity team [2], significant concerns were identified with the peer reviewers assigned to this article; the investigation has concluded that the peer review process was compromised. We therefore can no longer trust the peer review process, and the article is being retracted with the agreement of the Chief Editor.

The authors do not agree to the retraction.

### References

- [1] J. Yang, N. Du, W. Jiang, and C. Liu, “Effect of Protein Nutrition Level on Protein Metabolism during Volleyball Exercise Based on Edge Computing in the Medical System,” *Journal of Healthcare Engineering*, vol. 2022, Article ID 1614748, 9 pages, 2022.
- [2] L. Ferguson, “Advancing Research Integrity Collaboratively and with Vigour,” 2022, <https://www.hindawi.com/post/advancing-research-integrity-collaboratively-and-vigour/>.

## Research Article

# Effect of Protein Nutrition Level on Protein Metabolism during Volleyball Exercise Based on Edge Computing in the Medical System

Jicheng Yang,<sup>1</sup> Ning Du ,<sup>2</sup> Wei Jiang,<sup>2</sup> and Chenzhe Liu<sup>3</sup>

<sup>1</sup>Physical Education College, Jinan University, Guangzhou 510632, Guangdong, China

<sup>2</sup>School of Physical Education, South China Normal University, Guangzhou 510006, China

<sup>3</sup>Department of Sports Physiology, Beijing University of Physical Education, Beijing 100089, China

Correspondence should be addressed to Ning Du; [duning2021@scnu.edu.cn](mailto:duning2021@scnu.edu.cn)

Received 19 October 2021; Revised 1 December 2021; Accepted 24 December 2021; Published 12 January 2022

Academic Editor: Yang Gao

Copyright © 2022 Jicheng Yang et al. This is an open access article distributed under the Creative Commons Attribution License, which permits unrestricted use, distribution, and reproduction in any medium, provided the original work is properly cited.

With the rapid development of the Internet of Things, 5G, and communication technologies, the growth of various types of data has shown an exponential trend. Edge computing technology provides users with almost unlimited computing power through a large number of high-performance servers in the data center. It is one of the important solutions for big data analysis and processing. Volleyball has caused a great wave in China as early as the 1960s, but people pay little attention to the physical quality of volleyball players. At the same time, in the medical field, it is difficult to give a clear value to the athlete's protein requirement. Therefore, this article aims to observe the specific values of protein metabolism in volleyball at different levels of protein nutrition. By designing controlled experiments, then these rats under three nutrient levels of protein were observed and protein metabolism was analyzed after volleyball. The results of the study show that volleyball exercise can reduce the nitrogen balance and gastrocnemius nitrogen content. The nitrogen balance of the 17% group decreased from 388 mg/day before exercise to 336 mg/day, and the gastrocnemius nitrogen content decreased by up to 5.2%; serum urea nitrogen concentration and liver nitrogen content are increased, indicating the enhancement of protein catabolism. Different protein nutrition levels have different effects on protein metabolism during volleyball. The protein intake level of 17% is more conducive to resist the protein decomposition caused by volleyball. It can be seen that, based on edge computing technology, the influence factors of protein nutrition level on protein metabolism during volleyball sports can be well explored, and the research results are also very valuable.

## 1. Introduction

Human life involves many elements, and protein is one of the important elements. The human body needs a certain amount of protein every day to maintain balance. Protein supplements athletes' energy, strengthens human muscles, promotes the normal synthesis of human hemoglobin, accelerates metabolism, and eliminates fatigue. It has important practical significance. During exercise, the speed of protein synthesis will be greatly reduced [1]. Exercise, especially strength exercise, can stimulate muscle protein synthesis, leading to increased lean body mass and muscle mass; in addition, hemolysis intensifies in the early stage of heavy-load training, prompting red blood cells to strengthen

the synthesis of mitochondria and the synthesis of enzymes. Starting from volleyball, this article studies the effect of protein nutrition level on protein metabolism in a single sport, narrowing the research direction, making the entire research process more detailed and the research conclusions more authentic. Volleyball is one of the most popular sports in China. Men, women, young and old are happy to participate in it. Volleyball can improve people's physical quality and sports ability such as strength, speed, flexibility, endurance, bounce, and reaction and improve the functional status of various organs and systems of the body. Generally speaking, protein can provide 5.5% of the total calories consumed during exercise. However, further research is needed to determine the protein content required by the

body during sports and the relationship between the protein metabolism level of volleyball players during sports and the protein nutrition level of the body. Current research techniques cannot directly explore the reasons for this [2].

In recent years, society has gradually entered the “big data” era, and the emergence of cloud computing has enabled the ability to process and use big data to increase day by day. Cloud computing has been vigorously promoted with its advantages of low operating costs, dynamic scalability, and simplified operation and maintenance, and cloud computing-related industries have developed rapidly in China. On this basis, the state put forward medical informatization as an important development direction of medical physique reform [3]. Although cloud computing has announced the possibility of providing computer services at a lower cost, it also allows hackers to invest less money and obtain huge network computing power. Hacker attacks will pose a serious threat to user data security. Therefore, before these security problems and risk factors are properly managed, cloud computing is difficult to be effectively utilized. The nearby intelligent services provided by edge computing technology can meet the key requirements of agile connection, real-time business, data optimization, application intelligence, security, and privacy protection. An intelligent, flexible, and elastic medical network is built at the edge of the network. At the same time, its extremely strong computing power can do a good job on this subject [4, 5].

In order to use the edge cloud computing technology in the medical system to study the subject, Zhang et al. aim to use the security relationship of data information in edge technology computing and the technical characteristics of data privacy information protection to study the protection methods of commercially confidential information. He proposed a theoretical system and technical architecture centered on the application of data security technology. Experimental data shows that identification errors mainly occur when identifying nonabnormal data as abnormal data. The analysis and identification of abnormal information data are basically accurate, and various processing tasks can be completed quickly, and the abnormal information data can be eliminated to meet the requirements. However, the research motivation is unclear [6]. Mitchell’s research has shown that healthy individuals have a significantly constant skeletal muscle mass for most of their adult life, indicating the existence of homeostatic mechanisms. The amino acids consumed by dietary protein and the amino acids consumed by muscle protein synthesis are offset, making muscles exist in dynamic balance. The study uses atomic absorption spectroscopy, based on human studies, to describe the human bone protein metabolism in detail [7]. Ato proposed that the combination of exercise and nutritional intake can enhance protein anabolism more than exercise or nutritional intake alone. On this basis, the mechanism of protein anabolism based on the combination of exercise and nutritional intake was discussed, and recommendations were made to promote protein anabolism based on the latest research results. It is proposed that effective protein intake and functional food intake help to adapt to exercise to the maximum extent [8].

Compared with the previous studies on protein metabolism, the innovations of this paper are as follows: (1) the physiological function of the protein and the effect of endurance exercise on protein metabolism are analyzed in detail, which provides a comprehensive theoretical basis for the research. (2) The experiment was carried out in three batches to strictly control the experimental variables. The determination of serum urea nitrogen can also be used as a reliable chemical index to study the effects of different protein nutritional levels on protein metabolism in volleyball. (3) The third point is to use the nitrogen balance experiment method. The nitrogen balance experiment is an experiment to determine the protein demand of the human body, that is, to measure and compare the relationship between the intake of nitrogen and the discharge of nitrogen. It is difficult to directly measure the relationship between the protein content in the human body, and the change of nitrogen can reflect the protein metabolism. Combined with keas method, an experimental model of protein metabolism in Volleyball was established.

## 2. Introduction to Protein Nutrition Level Theory and Edge Computing

Protein is an important part of the human body. People need to consume a certain amount of protein every day to maintain the body’s balance. It can be seen that human life is inseparable from protein, and protein itself is also a part of the important structure of normal human cells. Proteins have different structures and many physiological functions, mainly four functions [9].

One is the catalytic function. Chemical reactions need to occur in the body to provide nutrients to maintain the normal functions of the body and maintain its balance. Enzymes are catalysts for many chemical reactions [10]. Only in this way can a person’s metabolism be more effectively and correctly controlled, and wastes from the body can be effectively discharged from the body as soon as possible. After a number of scientific experiments, protein coenzymes are the main components of more than 1,000 proteases in the human body [11]. Therefore, protein coenzymes have certain biocatalytic functions and are important substances for maintaining human body functions. Second is the transportation function. Human tissue is an organic whole, and various physiological digestive activities such as blood circulation and rapid oxygen delivery require organic carriers. Protein nutrition is an effective nutrient carrier that guarantees the maintenance of the normal physiological transportation of the human body, and an effective nutritional tool that promotes the maintenance of the normal physiological function of the human body. Therefore, the effective transportation of substances in the human body and the normal operation of human functions require proteins to complete the transportation activities and ensure its organic circulation. Third, motor function, as we all know, the human body mainly exercises through abdominal muscles. The main nutrient component of muscle is muscle protein, and the normal contraction and relaxation of human muscles are related to its protein

content. The muscle development of ordinary football players is more developed than the abdomen and other muscles of many ordinary people. This is because ordinary athletes have a certain measurement standard for their daily eating habits, and they need to consume a lot of protein, fat, water, and other substances every day. It can be seen that protein is an indispensable and important factor in human exercise and has certain exercise functions. Fourth is the hormonal function. Hormones play a role in drug therapy. From a biological point of view, many hormones are mainly composed of proteins, so proteins have certain hormone functions. Protein and peptide metabolism hormones are mainly important metabolic hormones in various animals, which can be used to regulate and help control the normal physiological metabolic activities of various animals. For example, insulin polypeptide can effectively reduce human blood sugar; however, heme polypeptide is an active polypeptide with 29 main amino acid residues and a molecular weight of 3585. Its pharmacological effect is completely opposite to that of active insulin, which can promote glycogenolysis and gluconeogenesis and increase blood glucose concentration [12]. The hormones in people's lives are often exposed to the outside, but it will cause certain damage to the human body to minimize the use of hormones.

Protein nutrition level plays an important role in maintaining human body functions. Among them, the level of protein nutrition directly affects the human immune system. Protein deficiency not only affects the body's cellular immunity but also hinders humoral immunity. Protein can accelerate the proliferation of neutral lymphocytes, differentiate, and delay allergic reactions. When the human body protein content is insufficient, the chemical reaction inhibition ability of the antibody or antigen binding to it will decrease, and the complement concentration will also decrease. The synthesis of antibodies requires the participation of a series of proteases. The level of antibody levels of immune proteins in the body will directly affect the antibody content of various immune enzymes in human cells, thereby directly changing the rate of cell synthesis and differentiation of antibodies in the body and directly affecting the effect of cellular humoral immunity effect. The low content of protein cannot fully meet the basic needs of ensuring the normal maintenance of the body's immune system. Only when the protein and fat content in the daily life diet gradually reaches a certain balance level, the body's autoimmune system potential damage can gradually reach the best defense state. However, if the protein nutrition level is too high, it will also cause adverse effects on the human immune function, such as causing excessive body burden.

The body's requirements for protein nutrition level when participating in sports activities are different from our daily activities. The diet of athletes has scientific standards. There is a certain relationship between the protein nutrition level of athletes and sports events and their own body weight. For the same sport, there are protein intake standards for different genders, weights, and training intensity. Nutritionists need to reasonably arrange specific diets according to the actual nutritional status of all athletes to effectively promote the reasonable diet and healthy growth of all athletes. The

results of the study show that the average daily protein requirement for long-term moderate and high-intensity weight-bearing exercise should be 2.5–3.0 g/kg, and the average daily protein requirement for speed and weight-bearing power athletes is 2.4–2.59 g/kg [13]. It is generally believed that when athletes are just beginning to perform strenuous exercise aerobic training because strenuous training is not fully adapted, the degree of damage to body cell function increases, and the metabolism of synthetic substances such as muscle collagen and red blood cell regeneration of the body is hyperactive. As well as the body's stress hormones and central nervous function regulation, other adverse reactions often lead to negative nitrogen balance and even cause severe exercise-induced anemia; strenuous exercise will also increase the amount of protein excreted in the urine. However, after a period of adaptation, the nitrogen balance will be improved. Therefore, in the early stage of strenuous exercise and when the exercise intensity is high, the protein nutrition level should be appropriately enhanced. According to the results of the nitrogen balance experiment, it is recommended that the daily protein intake of children participating in sports training should be between 2.0 g/kg and 3.0 g/kg. This is also a general standard, and different experts, scholars, and research data also have certain differences. Strictly speaking, every ball player will have his own special characteristics. Nutritionists should reasonably arrange the average intake of human protein according to the actual physical conditions of professional athletes and the actual working conditions in a timely manner to help ensure the normal sports training of professional athletes. This also promotes the continuous enhancement of professional trainers' performance.

Prolonged endurance exercise will increase protein metabolism, so protein nutrition levels will also increase. The increase in protein intake is also affected by glycogen storage. In endurance sports, when the concentration of muscle and glycogen is sufficient, the obvious increase in protein nutrition and energy consumption is limited to only 4% of the total human food nutrition and energy consumption. When the content of glycogen acid in a human body is completely exhausted, the loss can only increase downward by 10% at the same time. During long-term exercise (3.75 hours), the anaerobic energy consumption generated by the oxidation process of amino acids accounts for 4%–8% of the total oxidative energy consumption. Therefore, in addition to high-intensity endurance training, it is obviously reasonable to increase protein requirements by 10% [14]. Strength balance training also requires a slight increase in the total body protein and fat intake due to the increase in fat consumption of human muscles and soft tissues. The exercise intensity is high, the number of training sessions is large, and the protein metabolism is enhanced, which needs to be increased. In addition, for those professional ball players who need to strictly control their normal weight, they usually think that they should choose as many fish and meat as the main foods that are rich in protein, high in fat, and high in bone density to satisfy their demand. Protein foods can account for 18% of total calories. However, how the protein nutrition level affects the protein metabolism in volleyball and how much protein

content is the most appropriate, these specific situations still need to be known according to the specific situation of volleyball players. Therefore, the level of protein nutrition depends on the situation.

In order to better study how protein nutrition level affects protein metabolism in volleyball, we established a nitrogen balance measurement model and designed a data analysis system based on edge calculation.

Nitrogen balance is the balance between nitrogen intake and production. The nitrogen balance test is a classic method for studying protein requirements, measuring daily nitrogen intake and nitrogen excretion, and comparing the ratio of the two. Its main applications include the overall balance of nitrogen, the positive balance of nitrogen, and the negative positive balance of nitrogen. Its general form is as follows:

$$\frac{[d - (n + f + p)]}{\sqrt{n^2 + (f - p)^2}} = dt. \quad (1)$$

Among them,  $d$  is the intake of nitrogen, and  $n$ ,  $f$ , and  $p$  represent the emissions of carrying nitrogen. We need to use the keas method to determine the value of  $N$ ,  $F$ , and  $P$ . The calculation formula of crude protein in the keas method is as follows:

$$X = (V1 - V2) \times C \times 0.0140 \times 6.25. \quad (2)$$

Edge computing is a new ecological model. By converging five types of resources, including network, computing, storage, application, and intelligence, at the edge of the network, it can improve network service performance and open network control capabilities, thereby inspiring new models similar to the mobile Internet.

Edge computing was originally a key technology to solve the 5G network delay problem. In recent years, it has been tried to be used in emerging fields such as the Internet of Vehicles and the Internet of Things [15]. The above-mentioned problems in the processing of cloud computing can be solved by edge computing technology. As a hot technology, edge computing has been widely used in the business field. Among them, Internet companies hope to extend their existing cloud service capabilities to edge networks with the help of their own relevant advantages in the service industry. Communication companies hope to use edge computing technology to further tap the value of network connection equipment and improve their technological status in the consumer Internet of Things and Industrial Internet by strengthening the relevant performance of the access side network. The approach of industrial enterprises is to combine IT and OT. That is, traditional enterprises use IT solutions in local cloud architecture and add industrial operation technology to GE or non-GE facilities. They hope to use the Industrial Internet as their main position, use their own industrial network connections and industrial Internet platform services to give full play to their advantages, and establish new business models [16].

On the basis of edge computing, it provides medical workers with a medical management system that supports hierarchical division, two-way referral, and provides data

analysis services. The mobile medical information system integration platform is a medical data sharing platform designed for mobile terminals, primary medical care, and community family medical care based on the IHE (Integrating the Healthcare Enterprise) technical framework of medical information system integration. IHE is a technical framework designed to improve the sharing of information and data between medical systems. It specifically describes the information transmission between various systems based on the IHE system document standard. On this platform, the advantages of edge computing can be better utilized, and protein metabolism can be explored in depth from a clinical perspective.

### 3. Theory of Endurance Exercise and Protein Metabolism

In endurance exercise, most of the protein synthesis of muscle tissue is inhibited, but there is no instance in the exercise of muscle protein being broken down. Otherwise, it is not in it. On the one hand, the liver, muscle vasoconstrictor enzyme, and protein binding decomposition reaction speed varies. The speed of the synthetase slows down, the release of amino acids increases, and the amino acids in the metabolic pool increase; on the other hand, exercise will increase the alanine released by glucose, especially in this process (when the rate of alanine release 30 mol/L, moderate-intensity exercise to 70 mol/L, and vigorous exercise soaring to 170 mol/L) cycle in order to maintain blood sugar levels; during the recovery period after exercise, the exercise muscles produce methyl histamine cad, urine excretion increased, methyl histidine excretion increased, to provide evidence for conversion into muscle protein; exercise has a stable isotope tracing method, which can show exercise in the process of protein metabolism, so exercise has an effect on protein synthesis and decomposition has obvious effects [17].

Long-term endurance exercise consumes the sugar in the body. Due to the limited sugar reserves in the body, the glycosylation pathway of amino acids is activated. After removing amino acids, the carbon skeleton of most amino acids in the body can enter the triaxial cycle or anaerobic glycolysis metabolic pathway and can also be converted into glucose after oxidation to help maintain blood sugar [18]. Alanine and glutamine account for 30% of the amino acid. In the process of exercise metabolism in human muscles, acetylacetonate produced by the oxidation reaction of glucose reacts with other amino acids (such as lysine) to hydrolyze. Alanine can enter the human blood and directly return to the human liver. In the human liver, it directly generates a large amount of glucose through the pathway of gluconeogenic enzymes and metabolic enzymes, which greatly increases the main source of blood glucose metabolism in the blood of human exercise hypoxia. The biological oxidation process of glutamine glucose should also have a similar cyclic glutamine-glucosamine oxidation cycle, which is also related to the maintenance of blood sugar during exercise.

Generally, protein provides a small proportion of energy during exercise, accounting for about 5% to 7% of the total

heat energy demand. In endurance exercise, the percentage of amino acid supply increases after muscle glycogen is depleted. In the process of alanine-hydroxy glucose and glutamine-hydroxy glucuronide cycle conversion, part of the hydroxy glucuronide produced by the enzymatic conversion process of alanine and glutamine in the liver can be reoxidized and enter the human muscles. Fat cells oxidize fat to produce more energy. During the oxidation of phenylalanine and glutamine produced by keto acids in human musculoskeletal tissues, an amino acid that provides this amino acid is converted into keto acid by invertase, which can enter into the synthesis of aerobic keto acid metabolism enzyme pathways to provide keto acid oxidase function. In addition, muscles use amino acids circulating in the blood. Some studies have shown that the muscle uptake rate of branched-chain amino acids increases during exercise, while long-term vigorous exercise can increase the amount of oxidation several times [19]. As mentioned above, the increase in alanine concentration during exercise is mainly due to the enhancement of protein metabolism during exercise, which makes the amino acids produced, especially branched-chain amino acids, easily converted into pyruvate under the catalysis of pyruvate and produce alanine. In the constant perfusion experiment of isotope  $^{13}\text{C}$ -labeled leucine, it was observed that the oxidation rate of leucine increased by 2 times after 50% intensity exercise for 2 hours, and the absolute value of leucine increase was equal to the requirement of 90 for the amino acid. Therefore, the powerful effect of supplementing branched-chain amino acids has attracted widespread attention. Although the use of branched-chain amino acids, in theory, can improve the energy supply of working muscles, so far, it has not been proven to improve performance in well-designed randomized controlled clinical trials.

As mentioned above, in the process of endurance exercise, the oxidative exercise effect of leucine is also greatly enhanced. However, whether it can increase the mutual oxidative combination of all two amino acids remains to be proved by experiments. The intermediate metabolism of certain important amino acids can produce tricarboxylic acids or cyclic metabolic catalyst products, which have a good regulatory effect on the human body's exercise metabolism process and the human muscle metabolism process. Because it greatly increases the active oxidation reaction capacity of the ethyl cycle to the formyl ethyl peptide cocoa produced by the reaction of glucosamine and other free amino fatty acids. In addition, the main metabolites of these major amino acids can also be converted into pyruvate by dodecyl phosphate pyruvate oxidative kinase and pyruvate oxidative kinase. The increase in pyruvate production can lead to an increase in amino acid oxidation during exercise. The oxidation of amino acids is an important process in the human body.

#### **4. Establishment of an Experimental Model of the Protein Metabolism in Volleyball**

*4.1. Experimental Animals and Establishment of Model.* The Zoology Center of the Medical Sciences provided 96 male Wistar rats weighing  $(69 \pm 7)$  g. During the experiment,

each rat was fed separately in a cage. Specially prepared feed was required during feeding, free drinking water, room temperature  $(25 \pm 2)^\circ\text{C}$ , and natural light.

*4.1.1. First Batch of Experiments.* 24 male Wistar rats are the only choice for introducing experimental animals, and in order to study the effect of different content of protein feed on energy supply in Wistar rats, they are randomly divided into 3 groups, namely, three different levels of protein intake groups (hereinafter referred to as each group is 7%, 17%, 27%), each grouped in eight cage methods, according to the main nutrient composition of the feed ain-76 animal species, as shown in Table 1.

The various nutrients in various types of feed animals mainly refer to the weight of various feed animals. The percentage of carbohydrates is also different. The energy provided by the three levels of protein accounted for 7.8%, 18.6%, and 29.9% of the total energy of the feed, respectively. Based on the average food of the rats with the least food intake as the standard, each group was given an equal weight of feed so that the energy intake of each rat was equal. After eating for 45 days, the rats were forced to play volleyball until they collapsed, and the fatigue time of each rat was recorded.

*4.1.2. The second Batch of Experiments.* There are 24 male Wistar rats, and the animal source is the same as above. In order to study different levels of protein metabolism, they were randomly divided into 3 groups with 8 animals in each group. They were fed the above three protein levels separately and fed in a metabolic cage. The feeding method is the same as above. After the 3rd day, they were fed, urinated for 1 hour a day, exercised continuously for 5 days, and collected the daily urine and feces. During the urination period, feces were collected on the 3rd, 2, 4, and 6 days after urination. The keas method analyzes the nitrogen intake in urine, and the feces excrete nitrogen. Nitrogen balance is equal to nitrogen intake minus emissions.

*4.1.3. The Third Batch of Experiments.* In order to study the effect of protein nutrition level on the nitrogen content of gastrocnemius muscle and liver, they were randomly divided into 6 groups, each with 8 animals, namely the control group and the experimental group with several protein intake levels. The control group did not play volleyball, and the feed formula and measurement method were the same as those mentioned above. After 45 days, the experimental group performed volleyball exercises for two hours at a temperature of  $(25 \pm 2)^\circ\text{C}$ . Immediately after exercise, they were killed by decapitation. Blood samples, insulin, and gastrocnemius muscle were taken at 3000 rpm/heart was separated for 15 minutes. They were stored in a low temperature environment. The serum urea concentration was determined by the diacetyl method, and the instrument was Shimadzu UN-120-20 spectrophotometer. The content of gastrocnemius muscle nitrogen and serum nitrogen is determined by the advanced keas method.

TABLE 1: Feed formula with three protein nutrition levels (g/100 g).

Ingredient	Protein nutrition level		
	7%	17%	27%
Casein	8.3	20.1	31.9
Methionine	0.3	0.3	0.3
Corn starch	15.0	15.0	15.0
Sucrose	61.8	50.0	38.2

**4.2. Observation Items and Methods.** Every 5 days, the weight of the rats was measured by an accurate electronic balance, and the average body weight of rats with a protein level of 7%, a protein level of 17%, and a protein level of 27% was calculated, respectively. In the preexercise, mid-exercise, and postexercise periods, nitrogen intake, urine, and excrement are measured for nitrogen balance, and nitrogen balance is calculated. The urine and stool samples collected were analyzed for the last three consecutive days in the fourth week before exercise. Urine and stool samples collected on the third, fourth, and fifth days of the exercise were analyzed for urine and fecal nitrogen, respectively. Urine and stool samples were collected 2, 4, and 6 days after exercise, and the nitrogen in the urine and stool was analyzed daily. The nitrogen balance is determined by the kea's method. The serum urea nitrogen was determined by the diacetyl method. The automatic keas method was used to determine the content of amino acid carbon and nitrogen compounds in the gastrocnemius muscle and liver blood. Use automatic amino acid concentration analyzer to determine serum amino acids, use 5% of serum to combine with sulfosalicylic acid to precipitate protein, and the volume ratio of serum to the salicylic acid to precipitate protein is 1:1.5. After fully mixing with serum, put the instrument at  $-18^{\circ}\text{C}$  and freeze for more than 30 minutes, and analyze the amino acid concentration of the supernatant. The amino acid condition of the instrument should be a physiological liquid column (4.0 mm\*150 mm), lithium salt buffer system, filler 2619f resin, 34~ 68°C temperature gradient $\times 4$ .

**4.3. Western Blot Detection of Protein Metabolism.** The extensor muscles of each test rat's limbs were taken out and stored frozen at  $-80^{\circ}\text{C}$  and 50 mg, respectively. It was quickly extracted and put into a small tube containing polymerization inhibitor and lysate and washed for 20 s three times. Centrifuge the supernatant for 30 minutes. Using BCA to measure proteins and compounds, it can be directly used to accurately measure the average concentration of various proteins and compounds in all test samples when determining the measurement kit and adding the corresponding ratio of lysis substances and buffers. Adjust the concentration to the same level, and denature at  $70^{\circ}\text{C}$  for 10 minutes. SDS-PAGE gel electrophoresis at 200 V for 45 minutes. Prepare 5% skimmed milk to seal the PVDF membrane for 1 hour. Prepare with 5% BSA solution and incubate overnight on a shaker at  $4^{\circ}\text{C}$ . After washing the next day, incubate for 1 hour on a shaker at room temperature. After cleaning, put the

adhesive strip into the chemiluminescence reagent imaging and development system, and add a chemiluminescence reagent meter on the adhesive strip to expose and develop the adhesive strip. Use Image Lab5.1 software to analyze the gray value of the fluorescent protein in the gel strip to accurately calculate the gray relative expression of the gel strip and the target protein [20]. Use SPSS to process the experimental data and describe the results in the form of mean  $\pm$  standard deviation. A one-way variance test was used for comparison between groups.

## 5. Analysis of the Effect of Protein Nutrition Level on Protein Metabolism in Volleyball

**5.1. Analysis of Three Protein Nutrition Levels on Rats' Body Weight Gain during Volleyball Sport.** First, statistical analysis of the weight of experimental rats. Considering the influence of food on the weight of rats, the weight of rats was measured twice in the morning and evening. Therefore, the data in the figure is based on time and presents certain distribution characteristics. It was found that under the nutritional levels of the three proteins, there was no significant difference in the weight gain of rats. Although there was no significant difference in the nutritional levels of the three proteins in rats, the volleyball exercise time of the 7% group and the 17% group was 22% and 25% longer than that of the 27% group and 22%, respectively. The 17% group has the longest time for volleyball.

As shown in Table 2, when the protein nutrition level reaches 17%, the volleyball exercise time is extended. In other words, the replacement protein intake has an inhibitory effect on volleyball, but more than 17% of protein absorption does not promote the effect of volleyball. On the contrary, it will increase the burden on the body, which is counterproductive.

As shown in Figure 1, as the number of days of feeding increased, the weight distribution of rats with three protein nutritional levels increased. However, as can be seen, there is still a certain difference in weight between the 7%, 17%, and 27% groups. From the tenth day of feeding, the body weights of the three groups of rats began to differ. On the tenth day, the average weights of the three groups of rats were 92 g, 95 g, and 95 g, respectively. However, after 15 days of feeding, the average body weights of the three groups of rats were 110 g, 122 g, and 130 g, respectively, and the gap gradually widened. Overall, 7% of rats weighed slightly less than 17% and 27%, mainly because they played volleyball. Protein, sugar, and other substances are consumed during exercise, and the protein nutrition level of the 7% group obviously cannot meet the consumption demand of endurance sports such as volleyball. There was almost no difference between the 17% group and the 27% group.

**5.2. Analysis of the Results of Nitrogen Balance Determination of Protein Metabolism in Volleyball.** As shown in Figure 2, the nitrogen balance values before, during, and after

TABLE 2: Three protein nutritional levels volleyball time (minutes).

Protein nutrition level (%)	Volleyball time	Percentage (%)
7	374.2 ± 141.0	122
17	405.4 ± 154.6	125
19	400.2 ± 148.8	123
21	385.1 ± 140.8	118
27	308.2 ± 108.4	108

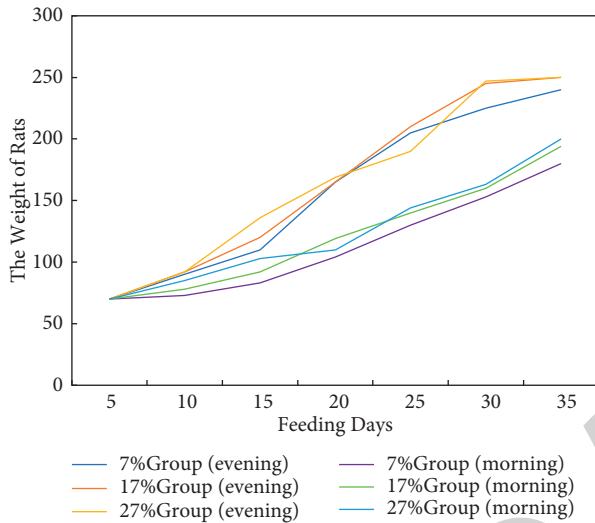


FIGURE 1: Feeding days and weight gain in 7% group, 17% group, and 27% group.

volleyball in the 7% group, 17% group, and 27% group were analyzed. Due to the different levels of protein nutrition before exercise, the nitrogen balance of the three groups showed different degrees of positive nitrogen balance. The nitrogen balance data of the 17% group is in the middle. Compared with the other two groups, the nitrogen balance value of this group has a smaller degree of change. The 27% group had the highest nitrogen balance value and the degree of change was also greater. The nitrogen balance value of the 7% group was lower and showed a downward trend after volleyball, from 293 mg/day before exercise to 246 mg/day after exercise. During and after exercise, the nitrogen balance of each group changed significantly. On the third day of exercise, there was a significant difference in the positive nitrogen balance between the 7% group and the 17% group. On the fourth day of exercise, the positive nitrogen balance values of each group showed a downward trend, while the 7% group was still significantly lower than the 17% group, the 7% group was 250 mg/day, and the 17% group was 343 mg/day. On the fifth day of exercise, the nitrogen balance of the 7% group continued to decline, and a negative nitrogen balance appeared. On the second day after the rest, the nitrogen balance of group 7%, group 17%, and group 27% began to rise and returned to the preexercise state. There was no significant difference between the groups. On the 4th day after exercise, the nitrogen balance value of the 7% group fluctuated downward, which was

significantly different from the 17% group and the 27% group. On the sixth day after exercise, the nitrogen balance of each group returned to the level before the experiment, and there was no significant difference between the groups. Before exercise, during, and after exercise, the nitrogen balance values of each group were different, but overall, there was no significant difference between the nitrogen balance values of the 17% group and the 27% group, which was significantly higher than that of the 7% group.

**5.3. Analysis of the Effect of Protein Nutrition Level on Gastrocnemius Muscle Nitrogen Content and Liver Nitrogen Content during Protein Metabolism.** Blood urea nitrogen (BUN) is the end product of protein metabolism, which is mainly discharged with urine through glomerular filtration. The determination of serum urea nitrogen can also be widely used as a reliable chemical indicator to measure the decomposition and metabolism of protein in the body. The increase in the content of urea nitrogen in the human blood indicates an increase in the normal catabolism of protein. Input the data of serum urea nitrogen concentration into MATLAB to establish the analysis model of serum urea nitrogen concentration of three protein nutrition levels.

As shown in Figure 3, after volleyball, the serum urea nitrogen concentrations of group 7%, group 17%, and group 27% were significantly higher than those of the control group, indicating that exercise can lead to increased protein catabolism. In volleyball, the experimental group increased the serum urea nitrogen concentration by 7%, 17%, and 27%, respectively. The difference was obvious. In volleyball, the 7% group had the largest increase in the concentration of urea nitrogen, and the 27% increase had the smallest increase, which was only 13.4%. The 27% group had a very high prevolleyball serum urea nitrogen level due to high protein intake. This level has increased before and after the experiment, but it still does not mean that the protein decomposition level of this group is low. The serum nitrogen concentration of the 17% group was elevated at a moderate level, slightly lower than that of the 7% group. This indicates that the protein nutrition level during volleyball exercise has no significant effect on the serum urea concentration in the body.

As shown in Figure 4, the first and second groups show the data of the gastrocnemius nitrogen content of the control group and the experimental group, and the fourth and fifth groups show the data of the liver nitrogen content of the control group and the experimental group. There was no significant difference in the content of gastrocnemius muscle nitrogen in the control group 7% group, 17% group, and 27% group. After volleyball, the gastrocnemius nitrous content of the three nutritional levels of the experimental group was significantly lower than that of the control group. The content of gastrocnemius in the third group was decreased in 7% group, 17% group, and 27% group. It can be seen that with the improvement of protein nutrition level, the content of gastrocnemius muscle nitrogen

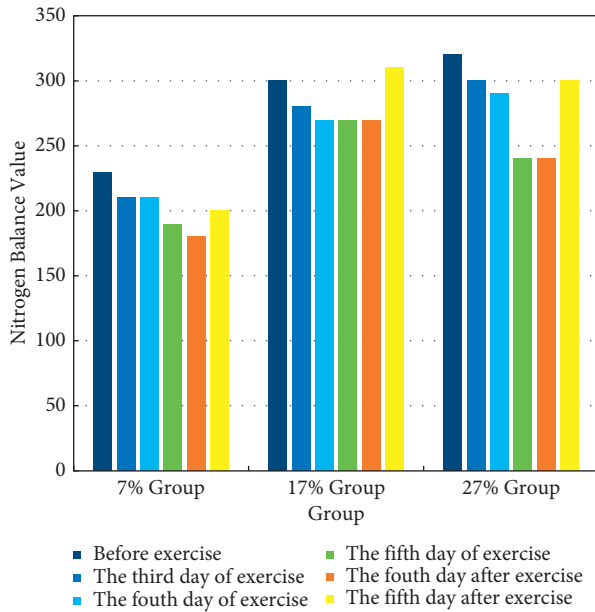


FIGURE 2: Nitrogen balance of rats during volleyball sport with three protein nutrition levels.

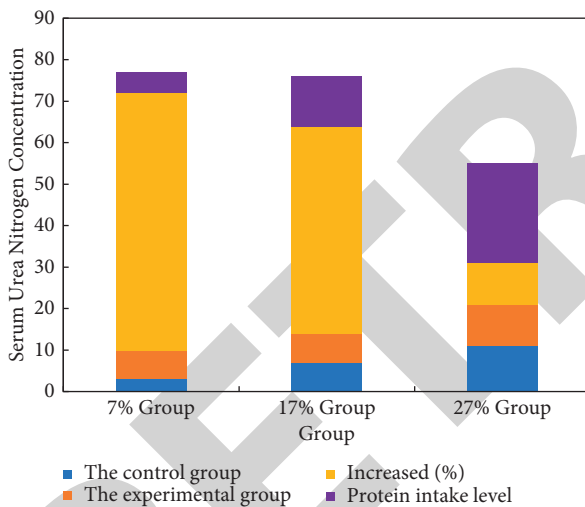


FIGURE 3: Comparative analysis of the effect of protein nutrition level on serum urea nitrogen concentration.

gradually decreases after exercise. The ability of skeletal muscles to degrade amino acids is not strong. After exercise, a large amount of muscle amino acids must be transported to the liver for metabolism. Decreased skeletal muscle nitrogen content indicates increased protein breakdown. In this experiment, it was observed that the gastrointestinal nitrogen content of all experimental groups decreased after exercise, and the gastrointestinal nitrogen content of the 7% group significantly decreased, reaching 5.2%, indicating strong protein decomposition. The reduction in gastrocnemius nitrous acid was similar in the 17% and 27% groups (4.3% and 3.6%, respectively) but less than in the 7% group.

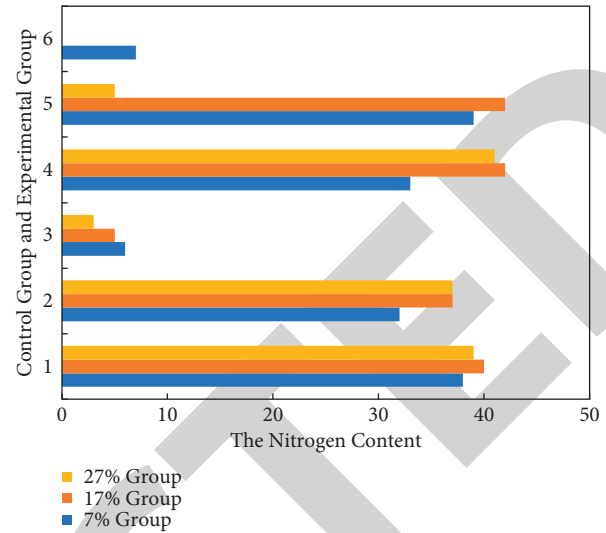


FIGURE 4: Gastrocnemius muscle nitrogen content and liver nitrogen content of the control group and the experimental group.

## 6. Conclusions

Aiming at some shortcomings and shortcomings of cloud computing itself, this paper implements a data analysis system based on edge computing. Corresponding designs and implementations are made for the specific application of the algorithm under different experiments. Successfully exploring the experimental results in line with the theme of the article, the following are specific experimental data results.

- (1) 7% of the rats ingested the protein level required by physiology, 17% of the rats ingested the protein level of a balanced diet, and 27% of the rats ingested high protein. In the experiment, the time from volleyball to exhaustion was used to observe the effects of different protein levels on the exercise endurance of rats. The 17% group had the longest exercise time, which could be extended by 25%, and showed stronger exercise endurance, while the 27% group did not show stronger exercise endurance.
- (2) Nitrogen balance test is a classic method for studying protein requirements. After volleyball, the nitrogen balance of rats in each group was significantly lower than before volleyball, indicating that the decomposition and utilization of protein were enhanced. The nitrogen balance values of the 7% group and the 27% group have been changing greatly and have been showing a downward trend, and this exercise has a great influence on the nitrogen storage in the body, indicating that the intake of low protein and high protein is not conducive to the body's nitrogen storage. This experiment also observed the nitrogen content in the rat's gastrocnemius muscle and liver after volleyball. The results also show that an appropriate level of protein nutrition can help reduce the breakdown of muscle protein during exercise.

## Research Article

# Performance Prediction of Listed Companies in Smart Healthcare Industry: Based on Machine Learning Algorithms

**Baobao Dong , Xiangming Wang, and Qi Cao**

*School of Management, Jilin University, Changchun 130025, Jilin, China*

Correspondence should be addressed to Baobao Dong; [markruby@126.com](mailto:markruby@126.com)

Received 14 November 2021; Revised 25 November 2021; Accepted 11 December 2021; Published 7 January 2022

Academic Editor: Weiwei Cai

Copyright © 2022 Baobao Dong et al. This is an open access article distributed under the Creative Commons Attribution License, which permits unrestricted use, distribution, and reproduction in any medium, provided the original work is properly cited.

With the development of wireless network, communication technology, cloud platform, and Internet of Things (IOT), new technologies are gradually applied to the smart healthcare industry. The COVID-19 outbreak has brought more attention to the development of the emerging industry of smart healthcare. However, the development of this industry is restricted by factors such as long construction cycle, large investment in the early stage, and lagging return, and the listed companies also face the problem of financing difficulties. In this study, machine learning algorithm is used to predict performance, which can not only deal with a large amount of data and characteristic variables but also analyse different types of variables and predict their classification, increasing the stability and accuracy of the model and helping to solve the problem of poor performance prediction in the past. After analysing the sample data from 53 listed companies in smart healthcare industry, we argued that the conclusion of this study can not only provide reference for listed companies in smart healthcare industry to formulate their own strategies but also provide shareholders with strategies to avoid risks and help the development of this emerging industry.

## 1. Introduction

The World Health Organization defines smart health (eHealth) as the use of information and communication technologies (ICT) to provide comprehensive services in healthcare. The healthcare information system can be more easily managed by improving the design of information flow. This new healthcare mode provides a new path for the development of global healthcare industry. Moreover, with the advent of the aging era, how to live healthy is one of the important issues that modern people pay attention to. Through the application of wireless network communication technology, cloud platform, and Internet of Things (IOT) in healthcare treatment, smart healthcare care has become an indispensable smart health technology for people [1, 2]. In the era of big data, smart healthcare technology can also help improve healthcare efficiency and service quality. More importantly, since the end of 2019, the outbreak of COVID-19 has aroused the importance of Internet healthcare, and the smart healthcare industry has ushered in significant development opportunities, but at the same time, it is also

facing great challenges and risks [3]. In order to develop the emerging industry of smart healthcare, sufficient funding is needed. The construction cycle of smart healthcare treatment is long, the initial investment is huge, and the return lags behind [1]. In order not to let the capital chain restrict the development of companies, many smart healthcare companies choose to go public, but the performance of these companies in the stock market is not satisfactory. Many smart healthcare companies are facing serious financial risks and heavy costs, which affect their performance [4–6].

After analysing the performance of listed companies in the smart healthcare industry, we find that there are also many problems in the development process of the companies, and the financial risks in its development are relatively large. As an emerging industry, healthcare industry must solve many problems we will face in the future. So, we should give support to this industry. But the current situation is not so amiable to the development of this industry. The development of many companies presents strong fluctuation and instability. Therefore, a detailed analysis of the performance of listed smart

healthcare companies can provide valuable reference for the long-term development of companies and shareholders' investment.

However, the current predictive analysis of performance is lack of reasonable explanation, and the research methods are mainly focused on the traditional regression analysis technology to analyse the main influencing factors of performance [7]. For example, Booth, regressed and based on the sample data of 10 countries in developing countries, found that debt service ratio had the same influence on the development of listed companies in both developing and developed countries. The most important factor was profitability, and capital structure had a negative correlation with corporate business performance [8]. Li et al. empirically examined the effect of firm performance on CSR disclosure in terms of disclosure frequency and quality among Chinese listed firms and the possible mediating effect of corporate ownership on the relationship between firm performance and CSR disclosure. They argued that performance influenced CSR and then the future investment [9]. Traditional measurement indicators are based on the assumption of normal distribution, but in fact, the performance of listed smart healthcare companies is not normal distribution, which results in bad prediction of the performance. In this study, machine learning is used to predict performance, which can not only deal with a large amount of data and characteristic variables but also analyse different types of variables and predict their classification, increasing the stability and accuracy of the model and helping to solve the problem of poor performance prediction in the past. This study may be the pioneer to study performance prediction of listed companies in healthcare industry by using machine learning, which can give some hints or directions for future research in prediction for companies.

Therefore, this paper will study the performance of listed companies in the smart healthcare industry, provide reference for companies to formulate their own strategies, and provide shareholders with risk-avoiding strategies to facilitate the development of this emerging industry.

## 2. Literature Review

**2.1. Operating Performance of Listed Companies.** Performance is the result of the enterprise's work to achieve the established goal. Performance of an enterprise refers to the operating results of an enterprise and the performance of an operator during a certain operating period. The level of business efficiency is mainly reflected in the profitability, asset operation level, debt paying ability, and follow-up development ability of the enterprise. The performance of managers is mainly reflected by the achievements and contributions made by managers to the operation, growth, and development of companies in the process of operating and managing companies [1]. Enterprise management performance evaluation includes two aspects of enterprise management benefit and operator performance evaluation.

Listed companies in different industries have different market structure, growth capacity, correlation with macroeconomic cycle, and life cycle stage of the industry, so their

business performance is also significantly different. This paper intends to make a comprehensive evaluation of the business performance of listed smart healthcare companies by analysing the index system reflecting the business performance of listed companies in the smart healthcare industry and using the machine learning method. On this basis, it attempts to study the business performance of listed smart healthcare companies in China from the perspective of the industry, so as to provide predictive reference for their future development.

**2.2. Smart Healthcare Industry.** In addition to the definition of eHealth by WHO, some scholars believe that eHealth is also related to public health and commercial healthcare information [7]. Broadly speaking, apart from the technical level, smart healthcare also includes an attitude of thinking to enhance healthcare care [10]. eHealth covers a wide range, including mHealth and smart health [11]. According to the U.S. Food and Drug Administration (FDA), smart healthcare in the broad sense includes mobile healthcare (mHealth), health information technology, wearable devices, remote healthcare, and personalized healthcare technology [12]. Smart healthcare promises to improve overall healthcare efficiency and make it easier for patients and users to track and manage personal health information.

The development of smart healthcare mainly relies on three aspects to build the health data ecosystem. The first is the data source, that is, sensors, wearable devices, and real-time monitoring devices are used to obtain users' physiological health data, and the second is that the above data are combined with more diversified living environment and user behaviour information. The third is to adapt to the technological or industrial environment changes of the first two, and the participation of stakeholders will also change the overall health information environment system [3].

Smart healthcare treatment integrates artificial intelligence, big data, Internet of Things, and other technologies and uses the Internet and other emerging things to integrate resources [12]. Doctors in large hospitals can make inquiries through the computer screen, and the examination data of each hospital can be connected to reduce multiple examinations of patients, and timely investigation of the past healthcare history of patients or emergency patients can greatly facilitate the basic needs of the people, so that doctors can stay at home, and data sharing does not waste healthcare resources. Smart healthcare consists of smart hospital system, regional health system, and family health system.

**2.3. Machine Learning.** Machine learning is a popular algorithm in recent years. In the past, the variables analysed by traditional methods must be independent, and the amount of data should not be too large, especially when extreme values are encountered, which also leads to relatively limited performance prediction [13]. However, machine learning overcomes the limitations of traditional data and adapts to the requirements of the era of big data. It can deal with high-dimensional and nonlinear problems and can not only analyse numerical variables but also explore category-based

variables to increase the diversity of variables. The accuracy of prediction is greatly improved by constantly updating the model through learning.

Some scholars have predicted the performance model based on the relevant data of listed companies, which provides valuable reference for the development of listed companies. For example, fund performance can be predicted by multiple fund rating indicators, and fund level can be predicted by random forest, which can not only process high-dimensional data but also perform very well in noise reduction, increasing model stability and improving accuracy. Some scholars studied the time series of financial commodities [14]. Support vector machine (SVM) and random forest can realize the principle of minimum risk, reduce the error ratio, and improve the accuracy of the overall model, which is superior to the general traditional model and neural network analysis methods. Zhang et al. proposed extreme gradient boosting (shortly XGB), which is highly efficient in machine learning algorithm [15]. The above analysis shows that the machine learning algorithm has high precision and reliability for the prediction model of some indicators of listed companies.

### 3. Methodology

**3.1. Data Collection.** The samples in this paper are from listed companies in the smart healthcare industry of the A share of Shanghai and Shenzhen Stock Markets. The sample data are collected from 2015 to 2020. The source of the original data is mainly collected through the Chinese stock market research database developed and produced by Shenzhen Guotai'an Information Technology Co., Ltd. In order to avoid unnecessary errors and the authenticity of the results, the data should be processed as follows:

- (1) Companies that are not listed within three years are excluded, that is, companies listed after 2017 (including 2017) are not included in the statistical data. Because of their short listing time and insufficient financial data, it is easy to cause sample error.
- (2) Eliminate ST and \*ST companies. These companies are generally due to the lack of financial motivation caused by poor management. These companies have extreme performance phenomenon.
- (3) Eliminate companies with incomplete data in the dataset. Incomplete data may occur during data collection, which may affect the objectivity and impartiality of the results.

Referring to the existing evaluation system at home and abroad, this paper selected sales profit margin, return on assets, asset turnover, cost of sales rate, total asset growth rate, inventory turnover rate, and receivables turnover rate from 53 listed smart healthcare companies as the sample data. The calculation process of each original indicator is shown in Table 1.

**3.2. Modelling.** This research mainly uses machine learning and deep learning for modelling. Machine learning includes

logistic regression, random forest and gradient boosting. The above methods are all classification of machine learning, while deep learning is multilayer perceptron [16]. However, we only choose random forest, XGB, and deep learning methods because random forest follows standard procedures to solve problems. It divides problems into several parts, solves them separately, and then combines the results to obtain the required answers. XGB is committed to pushing the lifting tree beyond its computational limits to achieve the engineering goal of fast computation and excellent performance. Deep learning, on the other hand, solves problems in a centralized manner rather than having to break them down [17]. Through the comparison of the two analysis results, we can clearly understand the “interior” of the deep network.

Random forest is a classifier that uses multiple trees to train and predict samples. In machine learning, a random forest is a classifier containing multiple decision trees, and its output categories are determined by the mode of the categories output by individual trees. Leo Breiman and Adele Cutler developed algorithms for random forests. It comes from random decision forests, which were proposed in 1995 by Tin Kam Ho of Bell Laboratories. This approach combines Breimans’ “bootstrap aggregating” idea with Ho’s “random subspace method” to build a collection of decision trees [18]. It uses the set of trained classifiers to classify new samples and then counts the classification results of all classifiers by majority voting or averaging the output, and the category with the highest result is the final standard [19]. This kind of algorithm can effectively reduce the bias and the number of variation. The random forest flow is shown in Figure 1.

XGB is a general regression analysis algorithm to enhance the performance of basic algorithms. It does not need to construct a high-precision regression analysis, just a rough basic algorithm, and then repeatedly adjust the basic algorithm which can get a better combination of regression model. It can improve the weak learning algorithm to strong learning algorithm and can be applied to other basic regression algorithms, such as linear regression and neural network, to improve the accuracy. Bagging and artificial neural network algorithms are similar but slightly different. The main idea of bagging is to give known weak learning algorithms and training sets. It needs to go through several rounds of calculation to get the prediction function column. The following is the loss function of XGB.

$$L(\phi) = \sum_i l(\hat{y}_i, y_i) + \sum_k \Omega(f_k), \quad (1)$$

where  $i$  represents the  $i$ th sample,  $l(\hat{y}_i, y_i)$  represents the prediction error of the  $i$ th sample, and the smaller the error, the better.  $\sum_k \Omega(f_k)$  is the function of the tree’s complexity, the smaller the complexity, the stronger the generalization ability and  $\Omega(f) = \gamma T + 1/2\lambda ||w||^2$ .

Then, the objective function in iteration  $t$  can be written as

$$L(t) = \sum_{i=1}^n l(y_i, \hat{y}_i^{t-1} + f_t(X_i) + \Omega(f_t)). \quad (2)$$

TABLE 1: Performance indexes.

Number	Index	Formula	Note
1	Profit margin on sales	Total profit/operation revenue $\times 100\%$	It represents the profitability of the enterprise. The higher the index, the stronger the ability of the enterprise to create profits.
2	Return on assets	Net profit after tax/total assets $\times 100\%$	It measures how much net profit is generated per unit of assets
3	Asset turnover	Total revenue/total asset $\times 100\%$	It measures the efficiency of corporate asset management
4	Cost of sales rate	Sales cost/sales revenue $\times 100\%$	It reflects the cost expenditure required by each unit of sales revenue of the enterprise
5	Total asset growth rate	Growth in total assets/total assets at the beginning of the year $\times 100\%$	It expresses the capital accumulation ability and development ability of the enterprise
6	Inventory turnover rate	Cost of sales/average inventory $\times 100\%$	It reflects the turnover speed of inventory, that is, the liquidity of inventory and whether the amount of inventory capital occupied is reasonable
7	Accounts receivable turnover ratio	Revenue/accounts receivable $\times 100\%$	It measures the turnover speed and management efficiency of enterprise accounts receivable

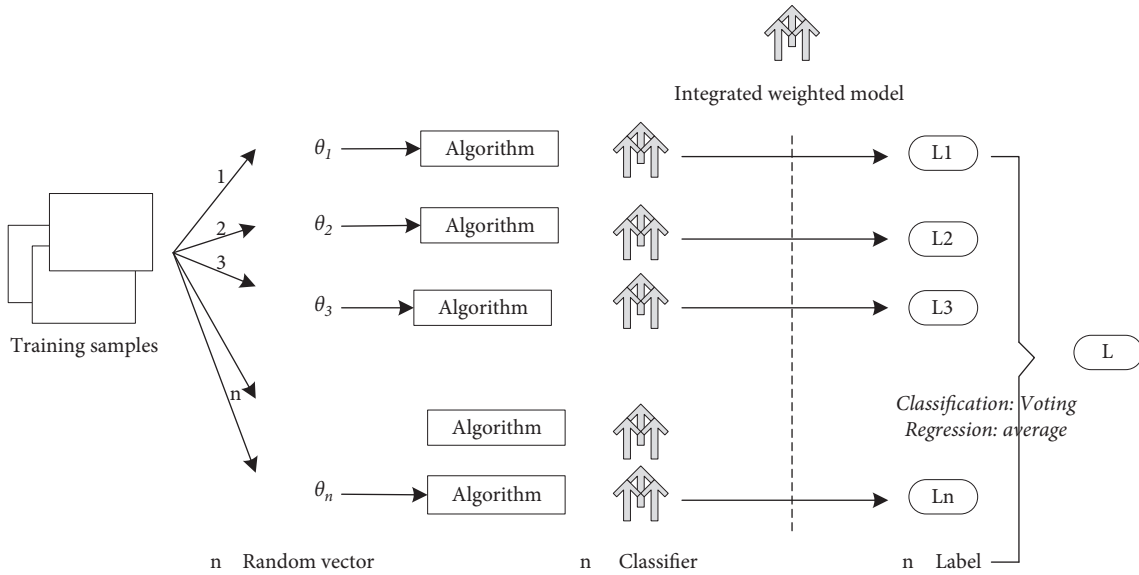


FIGURE 1: The random forest flow chart.

Deep learning (DL) is a new research direction in the field of machine learning. It is introduced into machine learning to make it closer to its original goal—artificial intelligence (AI). Deep learning is to learn the internal rules and representation levels of sample data, and the information obtained in the learning process is of great help to the interpretation of data such as text, image, and sound [18, 19].

The concept of deep learning originates from the research of artificial neural network. Multilayer perceptron with multiple hidden layers is a kind of deep learning structure. Deep learning discovers distributed feature representation of data by combining low-level features to form more abstract high-level representation attribute categories or features. The motivation for deep learning research is to build neural networks that mimic the human brain for analytical learning, which can interpret data, such as images, sounds, and texts, by imitating the mechanisms of the human brain [20].

The computation involved in producing an output from an input can be represented by a flow graph: a graph that represents a computation in which each node represents a basic computation and a calculated value, the result of which is applied to the values of the node's children. Consider a set of computations that can be allowed to define a family of functions in each node and possible graph structure. Figure 2 shows the deep learning model with multiple hidden layers (source: Wei J., Liu A., Tang J., “Alarm model of digital TV monitoring platform: Based on deep learning neural network technology”. *CATV Technology*, vol.11, no.7, pp. 78–82, 2017).

#### 4. Performance Evaluation

Random forest, XGB, and deep learning are used to predict the future performance of listed companies in the healthcare industry, that is, whether the performance at next phase will rise or fall, and the confusion matrix is drawn to accurately

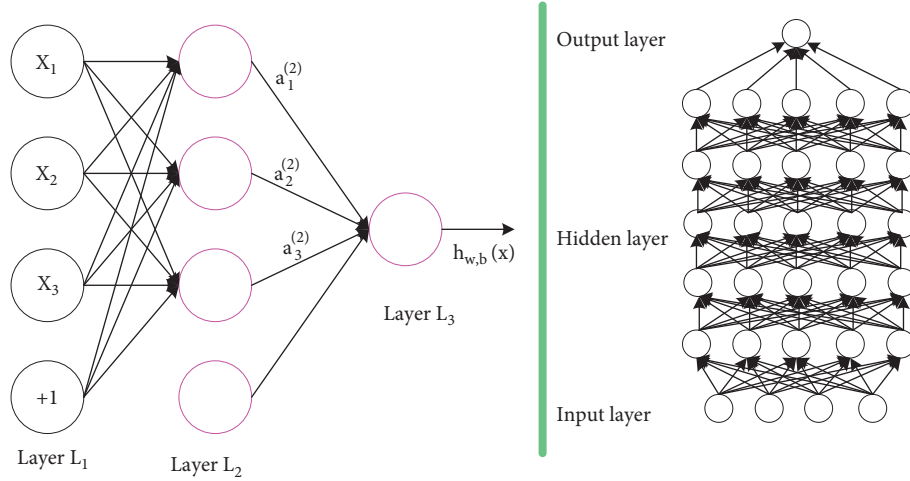


FIGURE 2: Deep learning model with multiple hidden layers.

judge the accuracy, precision, recall, type I error, and type II error [21]. Taking the above five items as the performance evaluation indicators, we will compare the quality of the classification model. Before explaining accuracy, precision, and recall, we need to define the classification of TP, FN, FP, and TN, which are shown in Table 2.

**Accuracy.** The ratio of correctly classified samples to total samples, and it equals to  $(TP + TN)/(ALL)$ .

**Precision.** Ratio of the number of correctly retrieved samples to total retrieved samples, and it equals to  $TP/(TP + FP)$ .

**Recall.** Ratio of the number of correctly retrieved samples to the number of samples that should have been retrieved, and it equals to  $TP/(TP + FN)$ .

The higher the value is, the better the prediction ability is, and the lower it is, the vice versa.

The first type of error, i.e., type I error, refers to the error that rejects  $H_0$ , which is actually true, and is “truth-rejecting.” Its probability is usually represented by  $\alpha$ , which is called significance level.  $\alpha$  can be unilateral or bilateral, generally stipulated  $\alpha = 0.05$  or  $\alpha = 0.01$ .

The second type of error, namely, type II error, refers to the error that does not reject  $H_0$ , which is actually untenable. It is a “false” error, and its probability is usually expressed by  $\beta$ .  $\beta$  is a single tailed. Generally, the value of  $\beta$  is not known during hypothesis testing, but can be calculated under certain conditions (such as the difference between two populations  $\delta$ , sample content  $n$ , and test level  $\alpha$ ). Table 3 shows type I error and type II error.

## 5. Results

In this study, random forest, XGB, and deep learning were used to predict all performance indicators, respectively, in an attempt to compare the accuracy of each machine model

TABLE 2: Confusion matrix.

	Positive	Negative
Retrieved	True positives (TP)	False positives (FP)
Not retrieved	False negatives (FN)	True negatives (TN)

*Note.* TP: positive sample retrieved, actually positive sample (correct identification). FP: positive sample retrieved, actually negative sample (a type of misidentification). FN: positive sample is not retrieved, but is actually positive sample. Type II error identification. TN: the positive sample was not retrieved, which was actually negative sample. (correct identification).

TABLE 3: Type I error and type II error.

	Decision making	
	Accept $H_0$	Reject $H_0$
$H_0$ is true	Correct	Type I error ( $\alpha$ )
$H_0$ is false	Type II error ( $\beta$ )	Correct

in performance prediction. The results are shown in Table 4.

According to the selected important performance variables, machine learning predictions are checked in this study. Table 4 shows that the overall prediction rate of deep learning is the best than that of random forest and XGB. Accuracy, precision, and recall are all higher than those of competitive model. Type I error is also low. However, random forest has a lower type II error. In terms of specific indicators, especially cost of sales rate, the model prediction rate of random forest is the highest than that of deep learning and XGB, but its type I error is higher. In general, deep learning is the best prediction model, while random forest is the best in reducing type II error. In the other six indicators, the predictive power of deep learning has obvious advantages. It can be seen that the deep learning model is more stable for the performance prediction of listed smart healthcare companies.

TABLE 4: Comparative analysis of performance.

Performance indexes	Evaluation indexes	Random forest	XGB	Deep learning
Profit margin on sales	Accuracy	0.73774	0.70449	0.81584*
	Precision	0.74	0.69	0.83*
	Recall	0.75	0.75	0.80*
	Type I error	0.39176	0.34129	0.28132*
	Type II error	0.09317*	0.17804	0.18359
Return on assets	Accuracy	0.70927	0.73504	0.79304*
	Precision	0.71	0.75	0.80*
	Recall	0.74	0.80	0.83*
	Type I error	0.43914	0.40827	0.30471*
	Type II error	0.08932*	0.12737	0.17588
Asset turnover	Accuracy	0.80931	0.83649	0.84297*
	Precision	0.70	0.77	0.84*
	Recall	0.71	0.74	0.82*
	Type I error	0.38394	0.35127	0.20315*
	Type II error	0.09355*	0.24294	0.16721
Cost of sales rate	Accuracy	0.80319*	0.79339	0.80171
	Precision	0.85*	0.81	0.80
	Recall	0.79*	0.76	0.74
	Type I error	0.43086	0.35149	0.28413*
	Type II error	0.08047*	0.17306	0.14931
Total asset growth rate	Accuracy	0.80106*	0.79254	0.79538
	Precision	0.75	0.77	0.84*
	Recall	0.74	0.73	0.81*
	Type I error	0.50179	0.38147	0.30147*
	Type II error	0.05142*	0.11597	0.10789
Inventory turnover rate	Accuracy	0.78505	0.76582	0.81137*
	Precision	0.80	0.81	0.87*
	Recall	0.79	0.82	0.84*
	Type I error	0.36921	0.30297	0.20762*
	Type II error	0.09399*	0.27446	0.17582
Accounts receivable turnover ratio	Accuracy	0.74209	0.76934	0.81776*
	Precision	0.81	0.80	0.84*
	Recall	0.77	0.79	0.84*
	Type I error	0.46237	0.35887	0.28149*
	Type II error	0.08337*	0.13572	0.14642

\*indicates that the value is superior to the competitive model.

## 6. Conclusions

In recent years, the number and scale of listed smart healthcare companies are growing steadily. How to acquire stable remuneration among many listed companies has become an important issue. In this study, three kinds of machine learning algorithms are used to predict the future performance of listed companies in the smart healthcare industry. According to the results of accuracy, prediction, recall, type I error, and type II error, deep learning can improve the prediction ability better and stably. There are three findings in this study: first, compared with random forest and XGB, deep learning has relatively stable performance evaluation and accurate prediction, with the lowest type I error. Second, compared with deep learning and XGB, random forest has the lowest type II error. Third, in terms of cost of sales rate, one of the performance indicators, besides type I error, each evaluation index of random forest is better than that of deep learning and XGB. It can be seen that deep learning has the higher accuracy and the prediction model is

more stable in predicting the performance of listed companies in smart healthcare industry.

In addition to random forest, XGB, and deep learning, machine learning also includes logistic regression, which also have certain effectiveness for performance prediction. In the future, this model can be applied to the performance prediction model of listed companies to increase the predictive power of the model. In addition, 7 indicators of performance are selected for prediction in this study. In the future, more performance indicators, such as asset-liability ratio, can be added to analyse the development trend of future performance through big data, so as to increase the breadth and accuracy of prediction.

Besides, improving enterprise performance and increasing investor confidence are the main reasons for management to adopt machine learning. These algorithms help enterprise management make correct decisions and mobilize their actions. Machine learning algorithms can provide valuable references for corporate investors to help them avoid risks. Smart healthcare industry is a

comprehensive industry integrating health, computer, and artificial intelligence, which has infinite development space in the future. We studied the smart healthcare industry as a whole. So, it is a great pity that it cannot be specific to a specific branch of the smart healthcare industry. In the future, machine learning can be applied to some subindustries of smart healthcare to analyse its future development trend. But no algorithm is optimal, and machine learning is more like an experiment than a Bible.

## Data Availability

The data used to support this study are available upon request.

## Conflicts of Interest

The authors declare that they have no conflicts of interest.

## Acknowledgments

This paper was financially supported by the Soft Science Project of Science and Technology Department of Jilin Province entitled “Research on the Factors and PATH of Ambidexterous Innovation of Technological Entrepreneurial Enterprises in Jilin Province” under grant no. 20190601060FG.

## References

- [1] D. Sarno, “Capital structure and growth of the firms in the backward regions of the South Italy,” *Applied Financial Economics*, vol. 18, no. 10, pp. 821–833, 2010.
- [2] V. Lex, H. Hermie, and W. O. -N. d’Hollosy, “A maturity model for interoperability in eHealth,” in *Proceedings of the 2016 IEEE 18th International Conference on E-Health Networking, Applications and Services (Healthcom)*, Munich, Germany, September 2016.
- [3] W. L. Currie and J. J. Seddon, “A cross-national analysis of eHealth in the European Union: some policy and research directions,” *Information & Management*, vol. 51, no. 10, pp. 783–797, 2014.
- [4] M. Scott and M. Richard, “Principles and framework for eHealth strategy development,” *Journal of Medical Internet Research*, vol. 15, no. 7, pp. 1–18, 2013.
- [5] K. A. Stroetmann, J. Artmann, and V. Stroetmann, “Developing national eHealth infrastructures – results and lessons from Europe,” in *Proceedings of the AMIA Annual Symposium*, pp. 1347–1354, Washington, DC, USA, October 2011.
- [6] W. Fatehi and R. Farhad, “Telemedicine, telehealth or e-health? a bibliometric analysis of the trends in the use of these terms,” *Journal of Telemedicine and Telecare*, vol. 8, no. 18, pp. 460–464, 2011.
- [7] Y. Tifani, B. Lee, and E. Jeong, “A patient’s indoor positioning algorithm using artificial neural network and SVM,” *Journal of Theoretical and Applied Information Technology*, vol. 95, no. 16, pp. 3758–3766, 2017.
- [8] L. Booth, V. Aivazian, A. Demircug-Kunt, and V. Maksimovic, “Capital structures in developing countries,” *The Journal of Finance*, vol. 56, no. 1, pp. 87–130, 2001.
- [9] Q. Li, W. Luo, Y. Wang, and L. Wu, “Firm performance, corporate ownership, and corporate social responsibility disclosure in China,” *Business Ethics: A European Review*, vol. 22, no. 2, pp. 159–173, 2013.
- [10] D. Mascharka and E. Manley, “Machine learning for indoor localization using mobile phone-based sensors,” 2015, <https://arxiv.org/abs/1505.06125>.
- [11] T. Kohonen, “Self-organized formation of topologically correct feature maps,” *Biological Cybernetics*, vol. 43, no. 1, pp. 59–69, 1982.
- [12] S. H. Shah and I. Yaqoob, “A survey: internet of things (IoT) technologies, applications and challenges,” in *Proceedings of the In 2016 IEEE Smart Energy Grid Engineering (SEGE)*, pp. 381–385, Oshawa, Canada, August 2016.
- [13] F. Zargoun, I. M. Henawy, and N. I. Ziedan, “Effects of walls and floors in indoor localization using tracking algorithm,” *International Journal of Advanced Computer Science and Applications*, vol. 7, no. 3, pp. 34–39, 2016.
- [14] M. A. Bitew, R.-S. Hsiao, H.-P. Lin, and D.-B. Lin, “Hybrid indoor human localization system for addressing the issue of RSS variation in fingerprinting,” *International Journal of Distributed Sensor Networks*, vol. 11, no. 3, Article ID 831423, 2015.
- [15] C. Zhang, P. Patras, and H. Haddadi, “Deep learning in mobile and wireless networking: a survey,” *IEEE Communications Surveys & Tutorials*, vol. 21, no. 3, pp. 2224–2287, 2019.
- [16] Y. Bengio, I. Goodfellow, and A. Courville, *Deep Learning*, Vol. 1, MIT press, Cambridge, MA, USA, 2017.
- [17] P. Georgiev, S. Bhattacharya, N. D. Lane, and C. Mascolo, “Low-resource multi-task audio sensing for mobile and embedded devices via shared deep neural network representations,” *Proceedings of the ACM on Interactive, Mobile, Wearable and Ubiquitous Technologies*, vol. 1, no. 3, p. 50, 2017.
- [18] M. Wang, Y. Cui, X. Wang, S. Xiao, and J. Jiang, “Machine learning for networking: workflow, advances and opportunities,” *IEEE Network*, vol. 32, no. 3, pp. 92–99, 2017.
- [19] S. Marsland, *Machine Learning: An Algorithmic Perspective*, Chapman and Hall/CRC, Boca Raton, FL, USA, 2014.
- [20] Z. Ghahramani, “Probabilistic machine learning and artificial intelligence,” *Nature*, vol. 521, no. 7553, pp. 452–459, 2015.
- [21] Y. Zhu, H. Luo, Q. Wang et al., “A fast indoor/outdoor transition detection algorithm based on machine learning,” *Sensors*, vol. 19, no. 4, p. 786, 2019.

## *Retraction*

# **Retracted: Discussion on Health Service System of Mobile Medical Institutions Based on Internet of Things and Cloud Computing**

### **Journal of Healthcare Engineering**

Received 16 November 2022; Accepted 16 November 2022; Published 24 January 2023

Copyright © 2023 Journal of Healthcare Engineering. This is an open access article distributed under the Creative Commons Attribution License, which permits unrestricted use, distribution, and reproduction in any medium, provided the original work is properly cited.

*Journal of Healthcare Engineering* has retracted the article titled “Discussion on Health Service System of Mobile Medical Institutions Based on Internet of Things and Cloud Computing” [1] due to concerns that the peer review process has been compromised.

Following an investigation conducted by the Hindawi Research Integrity team [2], significant concerns were identified with the peer reviewers assigned to this article; the investigation has concluded that the peer review process was compromised. We therefore can no longer trust the peer review process, and the article is being retracted with the agreement of the Chief Editor.

### **References**

- [1] J. Tang, “Discussion on Health Service System of Mobile Medical Institutions Based on Internet of Things and Cloud Computing,” *Journal of Healthcare Engineering*, vol. 2022, Article ID 5235349, 12 pages, 2022.
- [2] L. Ferguson, “Advancing Research Integrity Collaboratively and with Vigour,” 2022, <https://www.hindawi.com/post/advancing-research-integrity-collaboratively-and-vigour/>.

## Research Article

# Discussion on Health Service System of Mobile Medical Institutions Based on Internet of Things and Cloud Computing

Jinzhou Tang 

*School of Health Management, Xi'an Medical University, Xi'an 710021, Shaanxi, China*

Correspondence should be addressed to Jinzhou Tang; [tangjinzhou@ximu.edu.cn](mailto:tangjinzhou@ximu.edu.cn)

Received 29 October 2021; Revised 25 November 2021; Accepted 7 December 2021; Published 7 January 2022

Academic Editor: Yang Gao

Copyright © 2022 Jinzhou Tang. This is an open access article distributed under the Creative Commons Attribution License, which permits unrestricted use, distribution, and reproduction in any medium, provided the original work is properly cited.

Because modern human beings pay more and more attention to physical health, and there are many problems in the traditional medical service system, human beings have a higher and higher voice for the new medical model. At present, there are many researches on the application of modern science and technology to put forward solutions to medical development, but they generally pay attention to some details and ignore the construction of the whole medical service system. In order to solve the problems of low efficiency of the traditional medical model, difficult communication between doctors and patients, unreasonable allocation of medical resources, and so on, this article proposes establishing a perfect medical and health service system. First, the correlation functions are used, such as cosine correlation, to calculate the correlation of various medical products, and then the correlation measurement methods of cloud computing and the Internet of Things are used to realize the network connection of smart medical equipment, efficiently store, calculate and analyze health data, and realize online outpatient services, health file management, data analysis, and other functions. Then, the energy consumption formula of the wireless transceiver was used to reduce the resource loss in the operation of the system. Then, we use the questionnaire to understand the current situation of mobile medical and put forward improvement suggestions. This article also scores the performance of the system. The experimental results show that the performance rating of traditional medical institutions is B, while the model rating of mobile medical institutions is A, and the efficiency is optimized by 4.42%.

## 1. Introduction

**1.1. Background.** In recent years, with the popularization and expansion of mobile smart devices and global mobile communication networks, the Internet of Things technology has been spawned, which is based on the Internet and extends the user side to between things. With the gradual increase in the business volume of the Internet of Things, a large amount of information exchange and communication has increased the demand for data storage, analysis, and computing capabilities, and cloud computing technology has emerged. Various mobile applications and services based on the Internet of Things and cloud computing have emerged. Many “ready-to-use” services have a lasting impact on people’s lives. Application in the medical field can greatly improve the quality of services, expand the scope of services, and solve some of them [1, 2]. The problem of uneven distribution of medical resources has created a new medical

method of “mobile medical.” Today’s mobile medical institutions have implemented mobile application solutions such as wireless ward rounds, network calls, remote outpatient clinics, and mobile nursing services [3, 4]. Mobile technology can optimize patient consultation procedures such as inpatient registration, dispensing, sampling, surgery, and discharge. At the same time, it can benefit patients and healthcare professionals. Therefore, with the continuous development of mobile technology, users are increasingly demanding new medical service systems.

**1.2. Significance.** At present, the application of mobile medical services mainly focuses on providing services for medical staff and improving the efficiency of medical operations while ignoring personal tracking, electronic medical record management, etc. The health service system is not yet perfect. In this regard, this article proposes research on the

medical and health service system of mobile medical institutions based on the Internet of Things and cloud computing [5]. Through the research of this article, a set of mobile medical and service systems based on mobile smart terminal equipment has been designed, which integrates various mobile medical data to achieve a more friendly service. There is a certain guiding significance.

The health service system is divided into three levels of management. The first layer is the community basic medical system, the second layer is the community general clinic, and the third layer is the urban comprehensive hospital. Community clinics provide the most basic healthcare services 24 hours a day. If necessary, doctors will transfer patients to the upper-level hospital. Such a system has played an important role for a long time and was once advertised by the British as “the most complete medical service system in the West.” The health service system of mobile medical institutions based on the Internet of Things and cloud computing can make today’s health service system more scientific. Combining the transmission efficiency of the Internet of Things and the processing power of cloud computing can make the health service system have high efficiency and high data processing capabilities.

**1.3. Related Work.** With the progress of society, more and more people have conducted research on mobile medical institutions. Xa et al. defined cloud computing as a model that can realize ubiquitous, convenient, and on-demand network access and sharing of configurable computing resource pools. Their purpose was to develop and verify a tool to determine the determinants that affect the use of cloud computing. The factors include the attitude toward using cloud computing services (CCS), perceived privacy/security, perceived behavior control, the intention to use cloud computing services (CCS), and subjective norms. This research focuses not only on subjective factors but also on objective factors such as hardware facilities and other insufficient attention [6]. Huo et al. believed that while the computing efficiency of the industrial Internet of Things system is greatly improved, privacy issues may seriously damage the interests of users. They summarized the privacy issues in the industrial Internet of Things system and provided privacy when using software to define networks and blockchains. However, this solution can only solve network problems and has little effect on the physical level [7]. Yu et al. wanted to explore unique urban development models through new technologies such as the Internet of Things, cloud computing, and 4G and introduced successful experiences into all walks. However, building a smart city is a complex issue that requires multiple considerations of human factors and not just through technical means [8]. Avula believed that it was necessary to redesign the medical system to meet the needs of the people and quickly solved many complex problems in a shorter time and at a lower cost. He focused on the possibility of cloud computing technology in the medical field but only stayed at the theoretical research with no actual investigation [9]. Jeong et al. described the medical image information system for medical image sharing and used cloud services for the external

interface of the system. They adjusted the connection of the device with PACS and smart devices and synchronized the data of the image application service based on cloud computing services. The research is a specific application case of the Internet of Things and cloud computing in mobile medical institutions, but it requires a lot of infrastructure investment, and small and medium medical institutions cannot achieve this effect [10]. Li et al. proposed two secure and efficient dynamic searchable symmetric encryption (SDSSE) schemes for medical cloud data: using secure k-nearest neighbor (kNN) and attribute-based encryption (ABE) technology to construct a dynamic searchable symmetric encryption scheme; these two security attributes are crucial and extremely challenging in the field of dynamic searchable symmetric encryption. However, the problem of key sharing has not been solved yet, so that most people do not have the right to view information [11, 12]. Cao et al. believed that in the process of extensive deployment of the intelligent medical system, with the rapid development of medical equipment and the continuous increase of the number of medical equipment, it will become extremely difficult to plan or manage large-scale medical Internet of Things systems on the traditional single cloud platform. Various technologies should merge to reduce workload and provide medical data storage and backup mechanisms. However, medical service systems are rarely regular, and the work of merging similar items is not easy, but over-institutionalized drawbacks will appear [13].

**1.4. Innovation.** The main innovations of the research content of this article are as follows. (1) Based on the development and deployment of the application platform, this article selects a mature and technologically advanced cloud service platform and makes full use of distributed database technology and distributed computing technology to realize data distributed storage. (2) Based on the analysis of the development status of Internet and cloud computing applications in the medical industry, we will boldly combine mobile information technology, apply our advantages to the field of medical services, and propose a mobile medical institution service system based on Internet of Things and cloud computing. (3) Pay attention to the current imbalance in the development of mobile medical institutions, focus on providing mobile medical solutions for vulnerable service institutions, shape a new industry service model, and realize the rational allocation of medical resources.

## 2. Methods of Mobile Medical Service System

**2.1. Relevance Measurement of Cloud Computing.** Many recommended algorithms use item correlation, and there are three most commonly used measurement methods: cosine similarity, adjusted cosine similarity, and correlation similarity [14].

**Cosine correlation:** cosine similarity measures the similarity between two vectors by calculating the cosine of the angle between them. It is widely used in calculating document similarity. The  $i_{th}$  column of the user evaluation

matrix, that is, the score vector of item  $i$ , is denoted as  $r_i$ ; the  $j$ th column, the score vector of item  $j$ , is denoted as  $r_j$ ; the set of users who have purchased item  $i$  and item  $j$  at the same time is  $U_{ij}$ . The correlation  $W_{ij}$  between item  $i$  and item  $j$  can be measured by the angle between the vectors as follows:

$$\begin{aligned} W_{ij} &= \cos(\mathbf{r}_i, \mathbf{r}_j) \\ &= \frac{\mathbf{r}_i \cdot \mathbf{r}_j}{\|\mathbf{r}_i\| \cdot \|\mathbf{r}_j\|} \\ &= \frac{\sum_{u \in U_{ij}} \mathbf{r}_{ui} \mathbf{r}_{uj}}{\sqrt{\sum_{u \in U_i} \mathbf{r}_{ui}^2 \sum_{u \in U_j} \mathbf{r}_{uj}^2}}. \end{aligned} \quad (1)$$

Modified cosine correlation: the purpose of correcting the cosine similarity is to solve the cosine similarity that only considers the similarity in the direction of the vector dimension and does not consider the difference in the dimensions of each dimension. Therefore, when calculating the similarity, a correction operation of subtracting the mean value of each dimension will be performed. This method improves the cosine correlation without considering the insufficiency of different users' different scoring habits (high or low). It is calculated as follows:

$$W_{ij} = \frac{\sum_{u \in U_{ij}} (\mathbf{r}_{ui} - \mathbf{r}_u)(\mathbf{r}_{uj} - \mathbf{r}_u)}{\sqrt{\sum_{u \in U_{ij}} (\mathbf{r}_{ui} - \mathbf{r}_u)^2 \sum_{u \in U_{ij}} (\mathbf{r}_{uj} - \mathbf{r}_u)^2}}. \quad (2)$$

Correlation is also known as Pearson correlation. Correlation mainly considers a linear correlation, which is defined as the quotient of the covariance and standard deviation between two variables and is widely used to measure the degree of correlation between two variables. Correlation is the average score formula (3) of a single item and the average score formula (4) for calculating Pearson's correlation when calculating the item relevance.

$$W_{ij} = \frac{\sum_{u \in U_{ij}} (\mathbf{r}_{ui} - \mathbf{r}_i)(\mathbf{r}_{uj} - \mathbf{r}_j)}{\sqrt{\sum_{u \in U_{ij}} (\mathbf{r}_{ui} - \mathbf{r}_i)^2 \sum_{u \in U_{ij}} (\mathbf{r}_{uj} - \mathbf{r}_j)^2}}. \quad (3)$$

$$W_{uv} = \frac{\sum_{i \in I_{uv}} (\mathbf{r}_{ui} - \mathbf{r}_u)(\mathbf{r}_{vi} - \mathbf{r}_v)}{\sqrt{\sum_{i \in I_{uv}} (\mathbf{r}_{ui} - \mathbf{r}_u)^2 \sum_{i \in I_{uv}} (\mathbf{r}_{vi} - \mathbf{r}_v)^2}}. \quad (4)$$

It is generally believed that diversity is the opposite of correlation [15]. In the actual situation, recommending a group of similar items to users takes a lot of time to traverse the complete collection of items. If the similarity between items  $j$  and  $i$  is represented by  $W_{ij}$ , where  $W_{ij} \in [0,1]$ ,  $L(u)$  is the list of items recommended by the system for user  $U$ , so the diversity of  $L(u)$  can be expressed by the following formula:

$$\text{diversity} = \frac{\sum_{i,j \in L(u), i \neq j} W_{ij}}{1/2|L(u)|(|L(u)| - 1)}. \quad (5)$$

When considering the list of recommended items of all users, the overall diversity should be averaged [16], and the following formula can be used:

$$\text{diversity} = \frac{1}{|U|} \sum_{u \in U} \text{Diversity}(L(u)). \quad (6)$$

In the actual situation, the prediction accuracy of the recommendation algorithm will increase as the number of items increases and the additional calculations account for a small proportion of the total and can be ignored, but the introduction of the user list can increase the coverage, optimize resource allocation, and improve user satisfaction. [17]. It is generally believed that the coverage rate (Coverage) describes the share of items that can be recommended by the recommendation system. Simply put, it is the percentage of all items that can be recommended by the recommendation system. This formula can meet the docking of user and business information, achieve the accurate matching, and reduce resource waste. In formula (7),  $U$  is the user set,  $L(u)$  is the recommended item, and  $G$  is the set of all items. From a commercial point of view, the higher the coverage rate is, the more products we recommend to users. We can recommend the most in-demand medical products to users, which may result in higher user satisfaction and adequate and reasonable allocation of medical resources [18].

$$\text{coverage} = \frac{|U_{u \in U} L(u)|}{|G|}. \quad (7)$$

The above is a recommendation algorithm based on item relevance and diversity, and the main idea of a content-based recommendation algorithm is to identify the common characteristics and attributes of items that have been given higher ratings by users and then identify those that have the same attributes as the item recommend new items to users [19]. The information containing the properties of item  $j$  is generally recorded in the form of the feature vector  $x_j$ . User  $u$ 's preference feature vector  $x_u$  generally needs to be obtained from the user's rated item subset  $L(u)$ . After the user's preference vector  $x_u$  is obtained, it can be found that those new items whose feature vector  $x_j$  is similar to  $x_u$  are recommended to users [20].

$$X_u = \sum_{j \in L_u} \mathbf{r}_{uj} \mathbf{x}_j. \quad (8)$$

The  $U_{ser}CF$  algorithm predicts the user's rating  $r_{uj}$  of item  $j$  using some users' ratings of item  $j$  similar to user  $u$  and uses  $W_{uv}$  to represent the similarity between two users. We denote such a group of neighbors as  $N(u)$  [21]. Then,  $r_{ui}$  can be estimated by averaging the scores of these neighbors on  $j$ .

$$r_{uj} = \frac{1}{|N_j(u)|} \sum_{v \in N_j(u)} r_{vj}. \quad (9)$$

However, this formula still has a problem. It does not take into account the fact that each user has different evaluation standards and levels for items. The following formula gives a new method of score prediction [22]:

$$r_{uj} = h^{-1} \left( \frac{\sum_{v \in N_j(u)} w_{uv} h(r_{vj})}{\sum_{v \in N_j(u)} |w_{uv}|} \right). \quad (10)$$

$h(r_{vj})$  in the formula represents the relative rating considering the average rating level of user  $v$  and  $h^{-1}$  is the

inverse function of  $h$ . For further explanation, see the following formula:

$$h(r_{uj}) = r_{uj} - r_u. \quad (11)$$

If  $W_{ij}$  is the similarity between items  $i$  and  $j$  and  $L(u)$  is the number of items that the user has rated, then the user's rating prediction for item  $i$  can be calculated by the weighted average of the ratings of all items in user  $u$ 's item list  $N_{ui}$ . Formula (12) is obtained. In the same way, formula (13) can be used for predictive scoring considering differences in personal scoring standards.

$$r_{ui} = \frac{\sum_{j \in L(u)} w_{ij} r_{uj}}{\sum_{j \in L(u)} |w_{ij}|}, \quad (12)$$

$$r_{ui} = h^{-1} \left( \frac{\sum_{j \in L(u)} w_{ij} h(r_{uj})}{\sum_{j \in L(u)} |w_{ij}|} \right). \quad (13)$$

There is a distance threshold  $d_0$  for communication between nodes that consume energy for wireless transmission between items and its value is determined by the external environment [23]. When the distance between the sending node and the receiving node is less than  $d_0$ , the energy consumed to send data is proportional to the square of the distance [24]; it can be seen that the energy  $E$  consumption required to transmit bit information when the distance between nodes is  $d$  is as follows:

$$E = \begin{cases} kE_{elec} + k_{ef}d^2, & d < d_0, \\ kE_{elec} + k_{emp}d^4, & d > d_0. \end{cases} \quad (14)$$

$E_{elec}$  represents the energy consumed by the wireless transceiver circuit;  $k_{ef}d^2$  and  $k_{emp}d^4$  represent the energy consumed by the signal amplifier to transmit each bit of data;  $k$  represents the length of the data packet;  $d$  represents the distance between the nodes. The energy consumption  $E_r$  of the received signal and the formula considering the energy consumption of data fusion are as follows [25]:

$$\begin{aligned} E_r &= kE_{elec}, \\ E_r &= k(E_{elec} + E_{df}). \end{aligned} \quad (15)$$

Although cloud computing and the Internet of Things are advanced science and technology, their basic application principles in the medical field are as follows. The main roles are only users (patients) and doctors, and the main medium is smart devices that can be combined through the network, supplemented by the service platform, solve practical problems, and improve efficiency for both parties [26, 27]. The basic schematic diagram is shown in Figure 1.

**2.2. The Performance Evaluation Model of the Mobile Medical Institution Model.** Compared with the traditional service model, the biggest difference of the mobile medical institution model is that the service process is realized by using the Internet of Things technology and a virtual cloud computing platform. Using the Internet of Things and cloud computing, it is possible to integrate the management

and planning of the mobile medical institution model, resource supply and allocation, performance evaluation, etc., to build a systematic and holistic comprehensive system, and to easily integrate the medical information, which is passed to the hands of every citizen, realizing the full coverage of medical services in different regions and urban and rural areas [28, 29]. Therefore, to evaluate the performance of the mobile medical institution model, it is necessary to discuss the three aspects of service model innovation, service process reengineering, and public interest realization [19]. This article draws up initial performance evaluation indicators. The weighted average score refers to the average score calculated by multiplying each score by its weight ratio. Medical assessment scores can be set, and then, weights are set according to the contribution of each person's work, and the weighted average is used to reasonably evaluate the distribution performance. According to the structure of the construction and operation process of the cloud computing platform of the mobile medical institution, the first-level indicators of performance evaluation are constructed: (1) whether the mobile medical institution model is constructed in accordance with a reasonable plan; (2) whether the mobile medical institution model is operating in accordance with reasonable design requirements.

The construction process and operation process of the mobile medical institution model are subdivided, and six secondary indicators have been constructed: (1.1) whether the project management is normal; (1.2) whether the plan for model construction is implemented; (1.3) whether the process of managing nongovernmental organizations and enterprises participating in the construction of the model is carried out; (2.1) whether the platform is fully prepared for operation; (2.2) whether the management process of the model is effectively controlled; (2.3) whether the medical public service management planning process is effectively controlled and a quantifiable evaluation for each secondary index is established. Each of the five tertiary indicators is used to quantify and evaluate the construction process and operation process of the mobile medical institution model.

The relevance of each three-level indicator is assessed and scored. The classification of each level is based on the content of the hospital assessment and is divided into excellent, qualified, basic qualified, and unqualified according to the degree of completion of the work content. The scoring rules are as follows: 10 points, requirements are fully implemented; 8 points, more than 3/4 requirements are implemented; 6 points, some requirements are implemented; 4 points, most requirements are not implemented, 0 points, there is no progress at all. According to the scoring of the third-level indicators, the implementation of the second-level indicators is calculated, and the calculation formula is as follows:

$$ex = \sum \frac{\text{three-level indicator score}}{\text{the highest possible score for the three-level indicator}} [\%]. \quad (16)$$

Among them,  $x$  refers to each secondary index. According to the scores of the second-level indicators, the

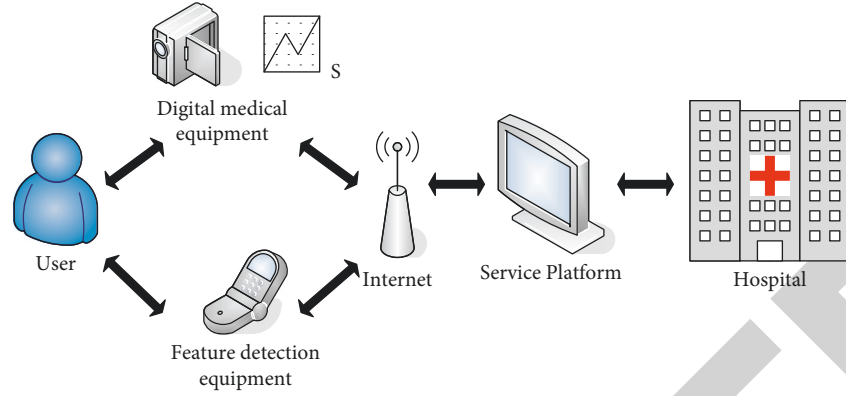


FIGURE 1: Basic principles of mobile healthcare.

implementation of the first-level indicators can be calculated as follows:

$$\begin{aligned}
 e_1\% &= \frac{e_{1.1} + e_{1.2} + e_{1.3}}{3} [\%], \\
 e_2\% &= \frac{e_{2.1} + e_{2.2} + e_{2.3}}{3} [\%], \\
 e_{\text{overall}}\% &= \frac{e_{1.1} + e_{1.2} + e_{1.3} + e_{2.1} + e_{2.2} + e_{2.3}}{3 + 3} [\%].
 \end{aligned}
 \tag{17}$$

Among them,  $e_1$  reflects the implementation of the mobile medical institution model during the construction process;  $e_2$  reflects the implementation during the operation process;  $e_{\text{overall}}$  reflects the implementation of the entire system from construction to operation. According to the scores of  $e_1$ ,  $e_2$ , and  $e_{\text{overall}}$ , the construction and operation process of the mobile medical institution model can be graded [30]. See Table 1 for grading standards.

When the level is A, it means that there is basically no problem in the construction and operation of the mobile medical institution model, and the relevant departments can correct the related problems by themselves. When the grade is B, it indicates that there are certain problems in the construction and operation of the mobile medical institution model. The government department can rectify the related problems and then report to the performance evaluation department for review. When the level is C, it indicates that there are serious problems in the construction and operation of the mobile medical institution model. It should be reported to the superior authority immediately, and the rectification should be carried out under the supervision of the superior agency. After the rectification is completed, an application for a new performance evaluation should be applied.

### 2.3. Health Service System Architecture Diagram Design.

This article selects Android and iOS devices, such as mobile devices, and sends real-time requests to the back-end server via HTTP. According to the user type and request type, the back-end service program makes the first evaluation, physical sign recording, patient browsing, and other

operations according to the response type and stores them in the corresponding database. Do the corresponding data storage and data echo operations [15]? Business logic analysis and functional modeling for the system are conducted. The complete use case diagram includes the relationship between use cases, actors, and the system, which can effectively express a complete function provided or defined in the system and be perceived by users. The medical service system based on mobile smart terminals aims at medical service. The system is used to process, collect, and store patient information and diagnose diseases [31, 32]. The service system modeling is shown in Figure 2.

With the development of science and technology, mobile medicine plays an important role in clinical diagnosis, scientific research, and education [33]. How to effectively display a large amount of medical information on a limited number of mobile smart devices is a question worth considering. However, due to the resource limitations of mobile smart devices, mobile smart devices cannot handle complex tasks for a long time, like desktop systems. Therefore, this article proposes a threshold-based level set segmentation method for data segmentation under multi-threaded conditions.

## 3. Mobile Medical Service System Development and Achievement Analysis

### 3.1. The Public's Willingness to Adopt Mobile Healthcare.

The mobile medical market in my country started late because of the slow process of informatization promotion, the low penetration rate of smartphones, the large and widespread population, and the imperfect medical system [34]. However, with the development of mobile technology becoming more and more mature and the popularization of smart terminals, China's mobile medical market has begun to sprout and emerge on a large scale. The experiment first analyzes the influencing factors of the people's willingness to use mobile medical applications so that the government can improve mobile medical according to the needs of the public, better realize the interaction between the government, enterprises, and the public, and play the role of mobile medical [35]. The questionnaire surveyed the medical needs of doctors and patients so as to realize the matching of needs

TABLE 1: Grading standards.

Grade	Score	Illustration
A	$e \geq 90\%$	There is basically no problem in the construction and operation of the system
B	$80\% \leq e < 90\%$	There are certain problems in the construction and operation of the system
C	$e \leq 80\%$	There are serious problems in the construction and operation of the system

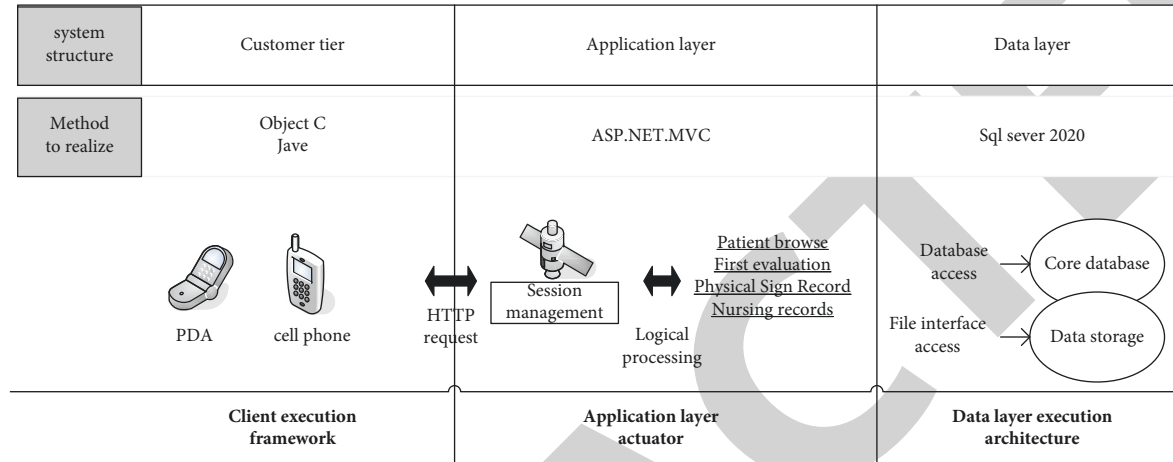


FIGURE 2: Business analysis of the health service system of mobile medical institutions.

and better optimize medical resources. The theme of the article is to build a medical exchange platform. First, study the development status of domestic mobile medical care. Taking Nanchang Maternity and Child Health Hospital as an example, the amount of medical payment and the number of payments in different ways are shown in Figure 3.

This shows that while the volume and number of online transactions increase, the market share of autonomous transaction machines is declining, and other forms of transactions, including traditional over-the-counter cash payments, are also being affected. To some extent, the number of transactions has dropped significantly.

Subsequently, the influencing factors of mobile healthcare were formally investigated. This article is designed after consulting related literature. Many experts and scholars at home and abroad have conducted research on this. The data is true and effective, which can guide article design very well, integrate various mobile medical data, and achieve more friendly services. At the same time, the survey questionnaire was distributed online and offline, and the questionnaire star was used online for questionnaire editing; offline questionnaires were distributed in universities, office buildings, hospital waiting rooms, and other places. A total of 300 questionnaires were distributed online and offline. The questionnaire of the article is a one-to-one collection of data, the data are true and effective, and the degree of feasibility is extremely high. The data we collect is true and valid, and there is no invalid data. Among the valid samples in this questionnaire survey, the gender ratio is similar, with males accounting for 53% and females accounting for 47%. Young people aged 21–30 years old accounted for 58.3%, followed by people aged 31–40 years old accounting for 16%. In terms of education level, 77.3% of the population has a bachelor's

degree or above, of which 20.3% have a master's degree or above and 57% have a bachelor's degree, indicating that the respondents generally have a higher degree of education. The respondents with a college degree accounted for 12% and a high school degree or below accounted for 11%. The young adults in the sample we selected came from other age groups. Their statements can guide the needs of other age groups. The popularity of the results is beyond doubt. See Table 2 for the details of the respondents.

Through the analysis of the collected 300 valid questionnaires, descriptive statistics and correlation analysis methods are used to test the hypotheses proposed in the previous article. Based on the data of 300 surveys, we carried out the descriptive analysis and correlation tests and found that the survey results showed the needs of users very well, with advantages such as perceived usefulness, perceived ease of use, compatibility, social influence, and personal innovation can better know the upgrade and optimization of mobile medical. The results show that among a large number of influencing factors, perceived usefulness, perceived ease of use, compatibility, social influence, personal innovation, and willingness to adopt mobile medicine are significantly positively correlated. The correlation analysis coefficients are shown in Table 3.

### 3.2. Analysis of the Use of Mobile Medical Institutions.

According to the survey results, with the advancement of national medical progress, mobile medical has developed rapidly. Thanks to the era of knowledge payment and the liberalization of medical e-commerce policies, the market scale of the mobile medical industry has grown rapidly, reaching 23.14 billion yuan in 2017, and the scale of the

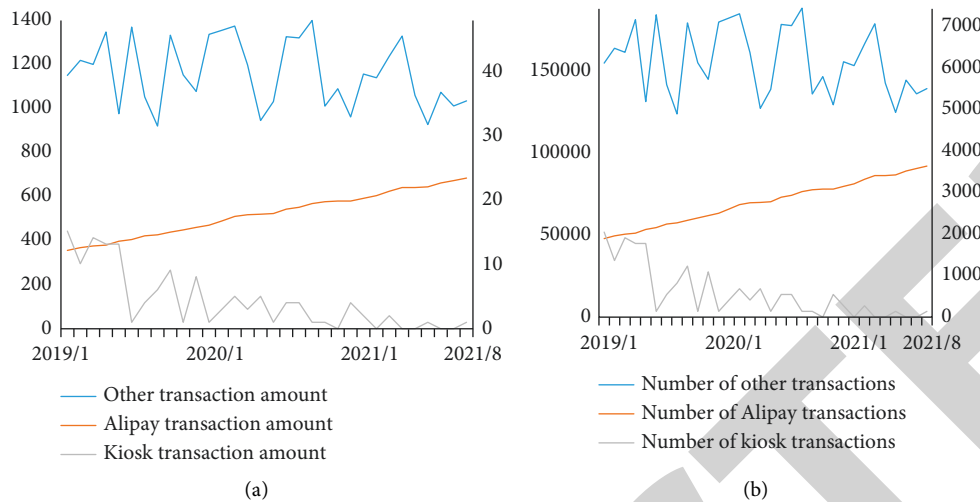


FIGURE 3: Statistics chart of the payment amount (ten thousand yuan) and the number of transactions by different payment methods.

TABLE 2: Basic information of survey samples.

Variable	Type	Frequency	Percentage
Gender	Male	159	53.0
	Female	141	47.0
	Total	300	100.0
Age	Under 20	17	5.7
	21–30 years	175	58.3
	31–40 years	48	16.0
	41–50 years	38	12.7
	Above 50	22	7.3
	Total	300	100.0
Education	High school	32	10.7
	Junior college	36	12.0
	Undergraduate	171	57.0
	Master	58	19.3
	PhD and above	3	1.0
	Total	300	100.0
Income	3000 yuan and below	176	58.7
	3000–5000 yuan	83	27.7
	5000–8000 yuan	35	11.7
	8000 yuan and above	6	2.0
	Total	300	100.0
Profession	Student	169	56.3
	Civil servants	19	6.3
	Institutional personnel	15	5.0
	Enterprise personnel	45	15.0
	Individual/private owners	34	11.3
	Freelancer	5	1.7
	Unemployed	8	2.7
	Others	5	1.7
	Total	300	100.0

mobile medical market has reached 53.96 billion yuan in 2020. The scale of the medical market reached 53.96 billion yuan, and the growth is shown in Figure 4.

The questionnaire survey data indicated that patients hope to monitor their own health, medical history, and drug records through mobile medical services in the future, communicate with doctors better and more conveniently,

and even realize remote monitoring of doctors. Doctors hope that mobile medical can help them increase real-time communication with patients, improve the quality of consultations, and optimize internal processes. The feedback from the questionnaire also showed that among the needs of doctor users, the expected data that have significantly changed from the current status also include communication with suppliers. The current needs of patients are covered by the needs they want to meet, and the two data can be directly synchronized. The demand situation of the patient and the doctor is shown in Figure 5.

As of September 2021, according to the data obtained from the survey, as a comprehensive health app, “Good Doctor Online” has been downloaded more than 180 million times. However, a more professional content system that can provide core medical services is relatively lacking. Mobile in the future medical developers has great prospects in providing more professional medical services based on how to deeply understand the needs of patients. On the other hand, statistics on doctor users show that as of September 2021, Dingxian-gyuan’s “Medical Time” active user market coverage reached 41.5%, and the second and third software belonged to Xingshulin among these applications that doctors often use. It is obvious that patients do not use them often. This is because these two have different expertise and needs and doctors and patients are still in different systems. When communicating, the transparency and openness of all information are limited. In general, the number of downloads by patients and doctors can be a good measure of coverage, and data collection is easy, and market coverage can be clearly perceived. The detailed market coverage of each application is shown in Figure 6.

**3.3. Function Demonstration Based on Cloud Computing and Internet of Things.** General mobile medical apps adopt the following model. Third parties such as smart medical equipment and pharmaceutical factories provide medical data. The app uses these data to build a two-way communication bridge between users and doctors. Doctors make

TABLE 3: Correlation coefficients between willingness to adopt and predictors.

		Optimism	Usefulness	Ease of use	Compatible	Resistance	Risk	Social	Innovation
Optimism	Correlation	1	0.619**	0.561**	0.460**	-0.136*	-0.06	0.441**	0.556**
	Significance	0.0	0.0	0.0	0.0	0.349	0.034	0.0	0.0
Usefulness	Correlation	0.475**	1	0.620**	0.624**	-0.07	-0.018	0.383**	0.401**
	Significance	0.0		0.0	0.0	0.258	0.78	0.0	0.0
Ease of use	Correlation	0.621**	0.561**	1	0.529**	-0.079	-0.032	0.479**	0.370**
	Significance	0.0	0.0		0.0	0.625	0.221	0.0	0.0
Compatible	Correlation	0.460**	0.475**	0.529**	1	-0.158*	-0.033	0.355**	0.480**
	Significance	0.0	0.0	0.0		0.014	0.61	0.0	0.0
Resistance	Correlation	-0.136*	-0.073	-0.079	-0.158*	1	0.245**	-0.04	-0.247**
	Significance	0.034	0.258	0.221	0.014		0	0.535	0.0
Risk	Correlation	-0.06	-0.017	-0.032	-0.033	0.245**	1	0.042	-0.029
	Significance	0.349	0.78	0.625	0.61	0.0		0.613	0.557
Social	Correlation	0.456**	0.401**	0.481**	0.356**	-0.04	-0.029	1	0.237**
	Significance	0.0	0.0	0.0	0.0	0.042	0.657		0.0
Innovation	Correlation	0.541**	0.383**	0.370**	0.480**	-0.251**	0.535	0.236**	1
	Significance	0.0	0.0	0.0	0.0	0.0	0.514	0.0	

\*\*Significantly correlated at the .01 level (two-sided). \*Significantly correlated at the 0.05 level (two-sided).

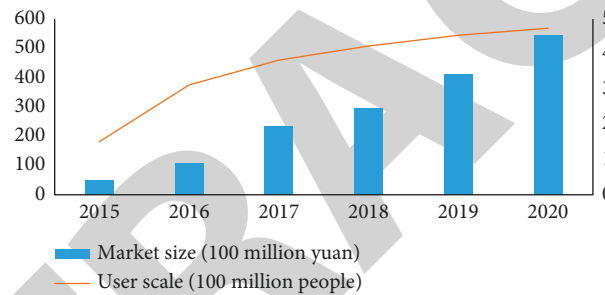


FIGURE 4: 2015–2020 China's mobile medical (service) market status.

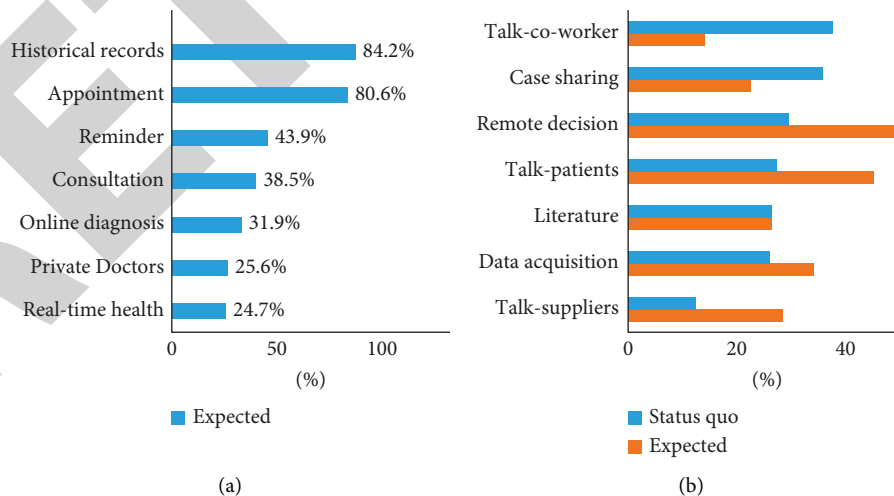


FIGURE 5: Patient-doctor's functional requirements for mobile medical institutions.

diagnosis decisions based on the feedback data, and users follow the service. Scores are made to form a closed loop, and data generated during communication, such as electronic medical records, will provide samples for the database. Big data is provided by everyone who uses the system, and it is

the ultimate storage terminal that can connect to all data. The detailed operation process is shown in Figure 7.

According to the existing mobile medical ecosystem in the abovementioned market, the mobile medical organization designed in this article relies on hardware and software.

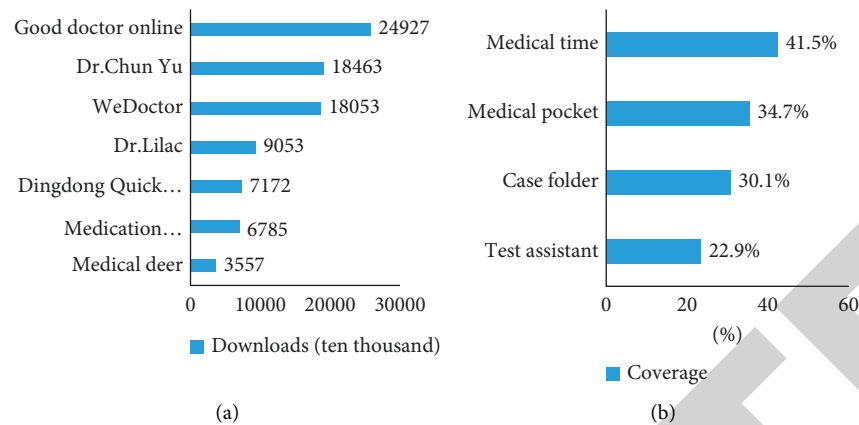


FIGURE 6: The number of patient app downloads, doctor app coverage.

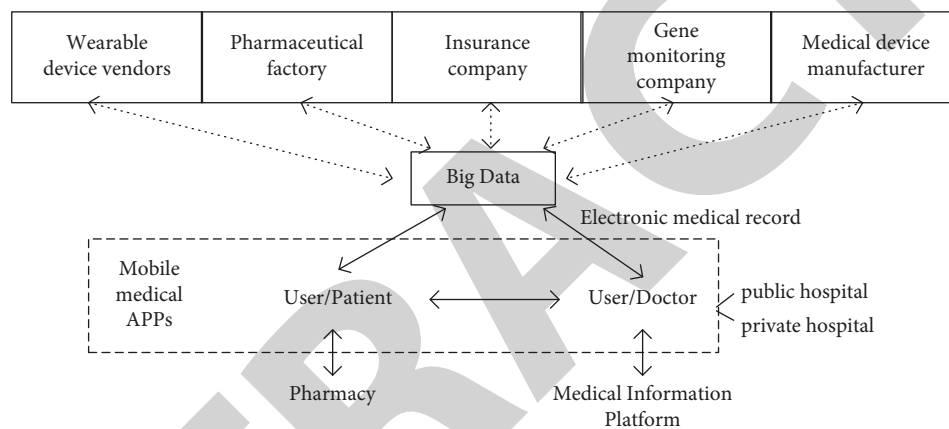


FIGURE 7: Mobile medical ecosystem.

The hardware adopts sensor terminal products. There are many types of sensor terminals. Mainstream and high-quality sensor terminals on the market are chosen and their communication interfaces are transformed to make them compatible with mobile health protection projects. The relevant specifications of the project are connected to the gateway terminal of this project to complete the overall function of the system. At present, terminal hardware is divided into household multiparameter terminals and portable measurement terminals (including exercise blood glucose meters, monitoring rings, antidrop Bluetooth headsets, wrist blood pressure monitors, wrist electrocardiographs, and ECG phones) [36]. The software adopts the cloud platform service system, and the mobile medical health service system based on the cloud platform is composed of business processing, user service, business management, system management, expert system, user, and other subsystems [37]. The software architecture diagram of the mobile health service system platform is shown in Figure 8.

The business processing subsystem provides remote diagnosis, treatment, and health consultation services. Hospital experts use the physiological indicators collected by the health terminal to make preliminary and follow-up diagnoses of user indicators, give doctors guidance, start a

rescue, make diet and medical plans, recommend services, etc. There are many types of service products, such as SMS, voice, video, and access [38]. At the same time, we can also provide call center agent services. The business processing subsystem also provides emergency rescue services. In other words, the user can initiate a "one-key rescue" request through a dedicated button on the emergency rescue terminal. The system recognizes the user's identity according to the user's rescue terminal number, confirms it, and then sends a rescue request work order to the rescue system (ambulance or medical institution in a nearby hospital). The user service subsystem is located in the user service subsystem. Users can measure indicators and upload data to the business platform through health sensing terminals and health information gateways. Users can change and update their personal profile information and view location information and billing status. Users can also create medical advice, weekly and monthly reports, health information, health indicators, and other information [39].

With this system, the author simulated online consultation, commuting time, case acquisition, registration, payment, laboratory test receipt, insurance reimbursement, and multiple processes, which is shown in a scatter chart. Figure 9 shows the processing time of the seven processes in order from left to right, including online consultation,

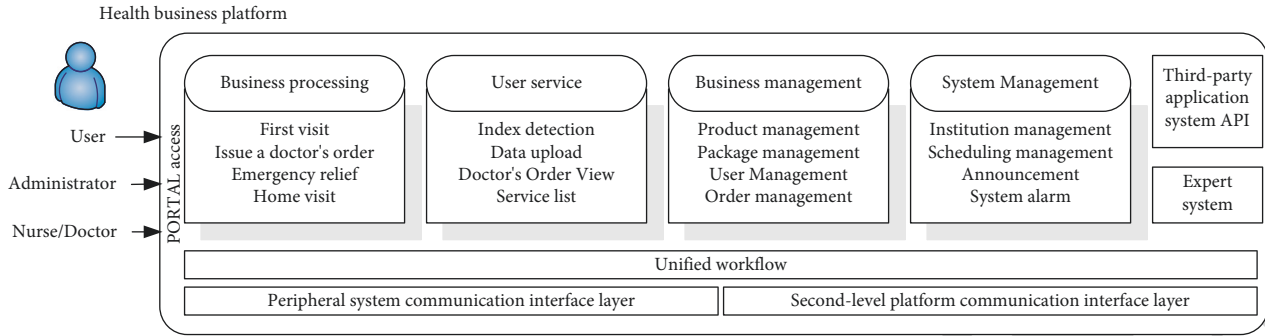


FIGURE 8: Software operation architecture diagram.

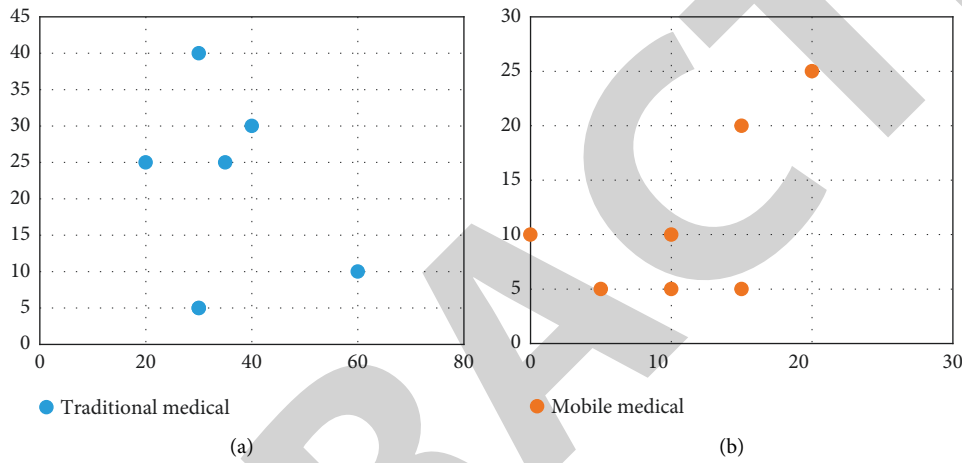


FIGURE 9: Scatter plot of processing time for different medical modes (minutes).

commuting time, case acquisition, registration and call, payment, test paper collection, and insurance reimbursement. It can be seen from Figure 9 that the processing time of mobile medical treatment far exceeds that of traditional medical treatment in many aspects, and the efficiency is improved significantly.

The traditional medical model determines the performance based on the performance of the medical workers, and the mobile medical institution evaluates the performance based on the weighted average of the level of the hospital's assessment, which is fairer. According to the performance of the evaluation model of the traditional medical institution model proposed above, this system is evaluated, and the calculated scores are shown in Table 4.

According to the formula, the traditional medical institution score of  $e_1$  is 88.20%, the mobile medical institution score is 93.81%, the traditional medical institution score of  $e_2$  is 90.67%, and the mobile medical institution scores 93.89%. In the aggregate score  $e_{\text{overall}}$ , the traditional medical institution scores 89.43%. Mobile medical institutions scored 93.85%. Figure 10 is obtained according to the scoring details.

Traditional medical institutions have  $e_{\text{overall}}$  score of 89.43%, less than 90%, and a performance rating of B, while the mobile medical institution model proposed in this article has a score of 93.85% and a rating of A. In addition, the small

scores are also higher than the traditional medical institution as a whole. It can be seen that the health service system is efficient and executable.

#### 4. Discussion

This article first introduces technologies such as the Internet of Things and cloud computing, understands the research status of mobile medical institutions through previous literature reviews, and designs mobile medical institutions through experimental methods such as cloud computing correlation measurement and mobile medical institution performance evaluation models. The health service system, through the experimental method of the questionnaire survey, understands the current status and problems of the current mobile medical service system and proposes the author's suggestions accordingly, intending to perfect this system. This article conducted a questionnaire survey on the public's willingness to adopt mobile medical services and obtained more real first-hand data. However, limited by the author's personal ability, time, and funding, this research has some shortcomings. Opinions are for reference for follow-up research. (1) The study sample has limitations. The sample in this article mainly covers Nanchang, but the population and medical conditions of various regions in China are different, and there is no nationwide sampling. (2)

TABLE 4: Performance scoring table of the traditional medical model and mobile medical institution model.

Project	Existing medical model		Mobile medical service system	
	Average	Ideal highest	Average	Ideal highest
1.1. Is the project management normal	5.8	7	8.7	9
1.2. Has the construction plan been implemented	4.4	5	5.6	6
1.3. Whether to manage NGOs and businesses	7.5	8	6.4	7
2.1. Is the preparation before operation sufficient	5.8	6	8.7	9
2.2. Whether the management is effectively controlled	4.6	5	7.5	8
2.3. Whether the plan is effectively controlled	5	6	7.3	8

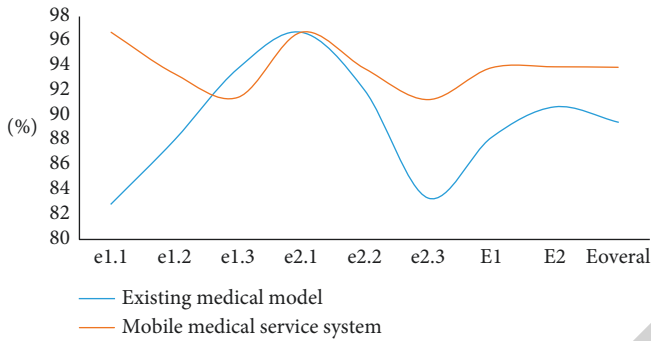


FIGURE 10: Performance score chart of the traditional medical model and mobile medical institution model.

This article is mainly based on cloud computing for the application of medical software for the Internet of Things; future scholars can consider research on users' willingness to adopt more new technologies such as artificial intelligence. (3) The deep integration of sensors and smartphones is promoted to eliminate the demand for a variety of complex and bulky medical devices.

## 5. Conclusions

Based on the use of hardware and software facilities, this article relies on cloud computing and Internet of Things technology to realize online outpatient services, health file management, data analysis, and other functions. Mobile medical software can meet the needs of patients seeking medical advice. Users can browse Internet information and communicate directly with doctors and experts. Through research, this article puts forward the following suggestions for the health service system of mobile medical institutions. Intelligent medical equipment to carry health monitoring and personal monitoring services for people living alone can be connected with the hospital system to collect health-related data to the greatest extent. The mobile medical service system uses various ready-made resources such as health sensor terminals, communication networks, medical and health institutions, and communication operators, which reduces the cost of building a cloud platform. To improve the mobile medical system, we must give full play to the government's advantages, improve the establishment of related systems, and strengthen publicity and promotion to let more people understand the mobile medical system. The design of

mobile medical applications is optimized to ensure the security and user privacy of a large amount of health data.

## Data Availability

The data that support the findings of this study are available from the corresponding author upon reasonable request.

## Conflicts of Interest

The author declares no potential conflicts of interest with respect to the research, authorship, and/or publication of this article.

## Acknowledgments

The author acknowledges Xi'an Medical College National Fund Cultivation Project "Comprehensive Evaluation Research on Health Service Capacity of Primary Medical Institutions under Hierarchical Diagnosis and Treatment System" (Project No. 2018GJFY18). This work was supported by the fourth batch of university-level key disciplines of Xi'an Medical College.

## References

- [1] X. Li, H. Jianmin, B. Hou, and P. Zhang, "Exploring the innovation modes and evolution of the cloud-based service using the activity theory on the basis of big data," *Cluster Computing*, vol. 21, no. 1, pp. 907–922, 2018.
- [2] S. Namasudra and P. Roy, "PpBAC popularity based access control model for cloud computing," *Journal of Organizational and End User Computing*, vol. 30, no. 4, pp. 14–31, 2018.
- [3] Y. Zhang, L. Sun, H. Song, and X. Cao, "Ubiquitous WSN for healthcare: recent advances and future prospects," *IEEE Internet of Things Journal*, vol. 1, no. 4, pp. 311–318, 2014.
- [4] F. Xiao and W. Ding, "Divergence measure of pythagorean fuzzy sets and its application in medical diagnosis," *Applied Soft Computing*, vol. 79, pp. 254–267, 2019.
- [5] Z. Lv, D. Chen, H. Feng, Z. Hu, and H. Lv, "Digital twins in unmanned aerial vehicles for rapid medical resource delivery in epidemics," *IEEE Transactions on Intelligent Transportation Systems*, 2021.
- [6] Z. Xa, M. Abdekhoda, and H. Nadrian, "Cloud computing services adoption among higher education faculties: development of a standardized questionnaire," *Education and Information Technologies*, vol. 25, no. 1, pp. 175–191, 2020.
- [7] Y. Huo, C. Meng, and R. Li, T. Jing, An overview of privacy preserving schemes for industrial internet of things," *China communication*, vol. 17, no. 10, pp. 6–23, 2020.

## Retraction

# Retracted: Investigation on Quality of Life and Economic Burden of Children with Cerebral Palsy in Changzhou

### Journal of Healthcare Engineering

Received 11 July 2023; Accepted 11 July 2023; Published 12 July 2023

Copyright © 2023 Journal of Healthcare Engineering. This is an open access article distributed under the Creative Commons Attribution License, which permits unrestricted use, distribution, and reproduction in any medium, provided the original work is properly cited.

This article has been retracted by Hindawi following an investigation undertaken by the publisher [1]. This investigation has uncovered evidence of one or more of the following indicators of systematic manipulation of the publication process:

- (1) Discrepancies in scope
- (2) Discrepancies in the description of the research reported
- (3) Discrepancies between the availability of data and the research described
- (4) Inappropriate citations
- (5) Incoherent, meaningless and/or irrelevant content included in the article
- (6) Peer-review manipulation

The presence of these indicators undermines our confidence in the integrity of the article's content and we cannot, therefore, vouch for its reliability. Please note that this notice is intended solely to alert readers that the content of this article is unreliable. We have not investigated whether authors were aware of or involved in the systematic manipulation of the publication process.

Wiley and Hindawi regrets that the usual quality checks did not identify these issues before publication and have since put additional measures in place to safeguard research integrity.

We wish to credit our own Research Integrity and Research Publishing teams and anonymous and named external researchers and research integrity experts for contributing to this investigation.

The corresponding author, as the representative of all authors, has been given the opportunity to register their agreement or disagreement to this retraction. We have kept a record of any response received.

### References

- [1] C. Bian, F. Peng, H. Guo, and K. Chen, "Investigation on Quality of Life and Economic Burden of Children with Cerebral Palsy in Changzhou," *Journal of Healthcare Engineering*, vol. 2022, Article ID 1519689, 9 pages, 2022.

## Research Article

# Investigation on Quality of Life and Economic Burden of Children with Cerebral Palsy in Changzhou

**Chaorong Bian** <sup>1</sup>, **Feng Peng** <sup>1</sup>, **Haibin Guo** <sup>1</sup> and **Kejin Chen** <sup>2</sup>

<sup>1</sup>Changzhou Children's Hospital Affiliated to Nantong University, Changzhou 226019, Jiangsu, China

<sup>2</sup>Changzhou Maternal and Child Health Care Hospital, Changzhou 213000, Jiangsu, China

Correspondence should be addressed to Kejin Chen; [chenkejin@njmu.edu.cn](mailto:chenkejin@njmu.edu.cn)

Received 9 October 2021; Revised 2 December 2021; Accepted 20 December 2021; Published 4 January 2022

Academic Editor: Yang Gao

Copyright © 2022 Chaorong Bian et al. This is an open access article distributed under the Creative Commons Attribution License, which permits unrestricted use, distribution, and reproduction in any medium, provided the original work is properly cited.

Based on the data of children with cerebral palsy (CP) in Changzhou obtained by the Disabled Persons' Federation, this study sampled some children with CP and investigated their survival status, treatment cost, and family burden so as to provide scientific decision-making basis and policy suggestions for coping with disease hazards and improving children's quality of life. In this study, a simple random sampling method was used to conduct household surveys of the selected children with CP. The economic burden of CP is measured by direct and indirect methods, and the quality of life of patients of children with CP and their families is analyzed qualitatively and quantitatively by the EuroQol Five Dimensions (EQ-5D) Questionnaire. The average family economic burden of each case of CP in Changzhou was about 4,188,500 yuan, of which the direct medical burden was 205,800 yuan and the indirect economic burden was 3,982,700 yuan. The socioeconomic burden of CP in Changzhou is as high as about 2.244 billion yuan. From the EQ-5D measurement results of 55 children with CP, the average index score was 0.423, which was lower than the national general population level. The proportions of patients with CP who have problems in the five aspects of action, self-care, daily activities, pain/discomfort, and anxiety/depression are 72.73%, 81.82%, 81.82%, 83.64%, and 92.73%, respectively, which are significantly higher than those of the national general population. The average score of the Visual Analogue Scale (VAS) is 58.09, which is significantly lower than the national general population level. The only major factor affecting the quality of life of patients with CP and their families is the health status represented by the EQ-5D score. To liberate and develop the labor ability of patients and their direct caregivers through clinical treatment, rehabilitation, and special education is the most effective way to reduce the socioeconomic burden of CP. Relevant government departments should perform their duties, integrate social assistance resources, implement early intervention, and launch targeted support and assistance policy.

## 1. Background

Cerebral palsy (CP) in children has become the most serious disease problem affecting children's health worldwide. The incidence of CP in China is about 2.48% [1]. Based on a population of 12 million born in 2020 [2], there were approximately 29,760 children with CP born in China. Cerebral palsy patients are mainly manifested as dyskinesia and abnormal posture, accompanied by mental retardation, epilepsy, sensory disturbance, language disorder, and abnormal mental behavior. CP not only has an irreversible impact on the health of patients but also seriously affects their quality of life. In the meantime, it also brings a heavy

economic burden to society and families, causing a series of social problems.

In terms of physical function, patients with CP have poor normal mobility and self-care ability, and most of them cannot take care of themselves. From the point of view of emotional function, they are emotionally unstable and vulnerable, and they are prone to fear, depression, anxiety, and other negative emotions. As far as social interaction, they rarely communicate with other children normally and lack corresponding entertainment activities. The total scores of children with CP in the Pediatric Quality of Life Inventory Measurement Models (PedsQL™) are lower than those in the normal control group or the general disease group [3].

Therefore, the training they usually have to receive includes big motor training, fine motor training, language cognitive training, life self-care ability training, and sensory integration training.

The economic burden of CP includes direct medical expenses, rehabilitation costs, long-term care costs, special education, and other expenses, as well as indirect loss of their productivity and the parents' income. The cost of the disease is an "opportunity cost" that reflects the burden of disease on society. If the disease can be reduced or even eliminated, society can reduce the cost of the disease and thus obtain benefits [4]. At present, research on the economic burden of CP is mainly concentrated in developed countries with abundant data resources and relatively prominent birth defects. The Nordic countries are known for their strong welfare systems, yet it is unknown to what extent the added burden related to disability is actually compensated for [5]. In Canada, direct health care costs in constant 2010 Canadian dollars were about \$11,700 for children with cerebral palsy aged 1–4 years versus about \$600 for those without the condition [6]. China has less research literature on this. Searching for "cerebral palsy" and "disease burden," "economic burden," "costs," and "economic evaluation," respectively, as keywords, there are fewer documents. Part of the literature only briefly describes the family economic burden of children with CP, which is not conducive to the government and society to provide targeted support and assistance, especially in Jiangsu Province, which accounts for 6% of the Chinese population [7]. Therefore, this study is based on the data obtained by Disabled Persons' Federation for children with CP in Changzhou, Jiangsu Province. We did a random sample and then investigated the quality of life and economic burden of those children to evaluate and analyze the related issues caused by CP from multiple perspectives such as society, family, and intervention.

Theoretically, the total economic burden of disease should be composed of direct economic burden, indirect economic burden, and intangible economic burden. We plan to use quantitative and qualitative analysis methods for evaluation. Among them, the direct and indirect economic burdens, such as the expenses invested by the family of children with CP, the time consumed, and the items purchased, can be directly obtained through questionnaire surveys, then calculated through quantitative analysis methods and mathematical formulas, and expressed in the form of monetary amounts. Limited by actual conditions, the actual number of patients receiving treatment is generally less than the number of illnesses or patients, so the direct economic burden of the disease will be overestimated by the direct method. In order to avoid overestimation, it is necessary to comprehensively consider the utilization rate of receiving medical services. We have taken this into consideration when calculating the economic burden of children with CP in Changzhou. The intangible burden is mainly qualitatively evaluated through interviews, which can understand the main problems, practical difficulties, ideological concerns, mental pressure, and needs of patients and their families.

The economic burden of CP is very sensitive to many objective factors such as China's regional socioeconomic development, family economic conditions, parents' educational level, disease severity, and treatment and rehabilitation methods, so in fact, the family economic burden of patients varies greatly. It is more difficult to calculate the economic burden. The direct economic burden of most surviving patients with birth defects is relatively small, and the indirect and intangible burdens are relatively large. This calculation requires more data sources, which greatly limits the estimation of the economic burden. Although the current research on the economic burden of CP has obtained some meaningful results, our research can provide the possibility of further improvement.

## 2. Materials and Methods

**2.1. Survey Object.** The inclusion criteria of the study objects are children under 14 years of age who have lived in Changzhou for more than one year with a clear diagnosis of cerebral palsy. Using the random number table method, a random sampling was carried out from 220 children with confirmed CP under 14 years old in Changzhou. The 55 selected children with CP were investigated one by one. Randomly selected children and their caregivers (parents, grandparents, etc.) were the respondents of this survey.

**2.2. Survey Content and Methods.** The questionnaire used in this survey has been used in the investigation of children with CP in Hebei Province in China [8]. The questionnaire contains five parts: sociodemographic characteristics, direct economic burden, indirect economic burden, daily activity ability, and quality of life of children with CP and their families (see Appendix 1). The questionnaire has been verified to have high reliability and validity. The measurement and evaluation methods of quality of life and economic burden are scientific and rigorous (see Appendix 2).

The investigator used a household survey to interview each child with CP and his family's direct caregiver and filled out questionnaires. The survey was jointly completed by children follow-up personnel and researchers in the area where the samples were located.

**2.3. Statistical Analysis Methods.** All questionnaires and content items are uniformly coded and entered by EpiData (Version 3.1). After checking the errors of the input data manually and computer logic, the conversion is performed, and SAS (Version 9.3) is used for statistics and analysis. If the measurement data obey a normal distribution, the discrete trend is expressed by the mean plus and minus the standard deviation; otherwise, the median (lower quartile; upper quartile) is used to express. The classification data is described by rate or composition ratio. The correlation of the quality of life of children with CP and their families was analyzed by the Spearman rank correlation analysis. The factors affecting the quality of family life were analyzed by logistic regression, with the inclusion criteria  $\alpha = 0.05$  and the exclusion criteria  $\alpha = 0.10$ .

**2.4. Investigation Quality Control.** We conducted unified training for investigators participating in household surveys to clarify the purpose of the investigation, the investigation discipline, the tasks, and the requirements of the investigators and to be familiar with the investigation items. At the same time, the relevant knowledge of birth defect diseases, quality of life, and disease economic burden was briefly introduced.

Make sure that the investigator visits the families with cerebral palsy within the sample range one by one, without any omissions. Make sure that all the questionnaire items are filled in truthfully, and there are no missing items. In this study, a total of 55 questionnaires were distributed, and 55 valid questionnaires were returned. The effective response rate was 100%. After the on-site investigation, we reviewed the questionnaires, found problems, and resolved them in a timely manner. Researchers also conduct random surveys based on the telephone numbers or addresses of the respondents to ensure the quality of the questionnaire survey. In the entry part, the specially assigned persons entered and reviewed data to ensure that logging data was accurate.

### 3. Results

**3.1. Demographic Characteristics of Children with Cerebral Palsy and Their Parents.** Among the children with CP investigated, the youngest is 1 year old, the oldest is 13, and the average age is 5 years. Those under 10 years old accounted for 90.91% (50/55). Male children accounted for 70.91% (39/55), and females accounted for 29.09% (16/55).

The survey shows that 82% (45/55) of families live in cities. The average age of the mother is 33 years, and the father is 34. About 75% of parents have college, university, and above education level (father 41/55; mother 42/55). Most of their mothers were unemployed or private enterprise employees, accounting for 66.64% (35/55) of the total number, and most of their fathers were private enterprise employees or self-employed individuals, accounting for 74.55% (41/55) (Table 1).

**3.2. Daily Activity Ability of Children with Cerebral Palsy.** The vast majority of children with CP are poor in daily activities. Only 27.27% (15/55) of them can walk around, 20% (11/55) can take care of themselves, 18.18% (10/55) can perform daily activities, and 16.36% (9/55) do not have any pain or discomfort. Only 7.27% (4/55) of the children did not feel anxious or depressed (Table 2).

**3.3. Direct Economic Burden of Children with Cerebral Palsy.** Among the children with CP under investigation, 27.78% of them had comorbidities, and 9.62% had undergone surgery. 32.73% had been hospitalized in addition to surgery, and 65.45% of children had purchased rehabilitation equipment. 30.91% have purchased over-the-counter (OTC) drugs or nutritional products. 92.72% of them received rehabilitation treatment (Table 3).

According to the questionnaire conditions, 53 children should answer the source of medical expenses. The medical

expenses of 68% of the children are sourced from social medical insurance and partially self-financed, and 22% are partially self-financed. Only 6% are completely self-financed, but only 4% completely come from social medical insurance (Figure 1).

The 33 children with cerebral palsy who had comorbidities without surgery or hospitalization were mainly due to mild symptoms (96.97%), followed by financial difficulties (3.03%).

Among the 55 valid questionnaires, we know that 100% of children with CP underwent general diagnosis and treatment, and their medical expenses averaged 15,900 yuan. Their accumulative total of transportation, accommodation, and escort expenses were 22,100 yuan. Twelve children (accounting for 21.82%) received surgical treatment, and their average medical expenses were 37,800 yuan, and the traffic, accommodation, and nursing fees added up to 71,600 yuan. There are 22 nonsurgical hospitalizations (accounting for 40%); the average was 35,800 yuan, and the addition of cost of transportation, accommodation, and accompany resulted a grand total of 44,800 yuan. Almost everyone chose rehabilitation treatment, the average medical cost was 105,900 yuan, and the cumulative total of others was 130,600 yuan. Among these expenses, the main one is medical expenses, followed by transportation costs, and the accommodation and escort costs are relatively low. Among the types of expenditures, the proportion of purchasing rehabilitation equipment for children is relatively high, and the proportion of purchasing nutritional products is relatively low (Table 4).

**3.4. Indirect Economic Burden of Children with Cerebral Palsy.** Among children with CP who cannot take care of themselves, the daily expenses of taking care of them cost an average of 5,500 yuan per month, and the total average family burden is about 293,500 yuan. In the survey, 11 children with CP received school education (including special kindergartens and auxiliary schools), accounting for 20%. The monthly special education fee is about 3,000 yuan, totaling 106,300 yuan (Table 5).

**3.5. Economic Burden Calculation.** Children with CP have different medical and family conditions. Not only are their treatment methods and types different, but also the utilization rate of various medical services is different. As a result, families actually bear different direct economic burdens. Children with serious comorbidities that require surgery, rehabilitation, and systemic treatment cost more. Those who are generally in better condition and have only undergone general diagnosis and treatment have relatively little medical expenses. In general, the direct economic burden of families with children ranges from 22,100 yuan to 285,600 yuan, with an average of 205,800 yuan.

According to the data released by Changzhou Municipal Government, in 2020, the urban per capita disposable income is 60,529 yuan, and the rural is 32,364 yuan [9]. It can be estimated that the actual indirect economic burden of each family is about 2.3006 million yuan for rural patients and about 4.3565 million yuan for urban patients, and the average is 3.9827 (2.306, 4.3565) million yuan. Affected by

TABLE 1: Demographic characteristics of parents of children with cerebral palsy.

		Mother (n, %)	Father (n, %)
Age		33.24 ± 4.20	34.18 ± 4.45
Profession	Unemployed	18 (35.73)	1 (1.82)
	Self-employed	3 (5.45)	8 (14.55)
	Employees of government agencies	12 (21.82)	5 (9.09)
	Migrant workers	1 (1.82)	1 (1.82)
	Others	3 (5.45)	1 (1.82)
	Employees of private enterprises	17 (30.91)	33 (60.00)
	Professional technicians	1 (1.82)	6 (10.91)
	Illiterate or semi-illiterate	0 (0.00)	0 (0.00)
Degree of education	Primary school and below	0 (0.00)	0 (0.00)
	Junior middle school	6 (10.91)	5 (9.09)
	High school, vocational school, and technical secondary school	7 (12.73)	9 (16.36)
	College, university, or above	42 (76.36)	41 (74.55)

TABLE 2: Daily activity ability of children with cerebral palsy.

		Number of people	Proportion (%)
D1 action	I can walk around without any difficulty	15	27.27
	It is a little inconvenient for me to move	26	47.27
	I cannot get out of bed and move around	14	25.45
	I can take care of myself without any difficulties	11	20.00
D2 self-care	I have some difficulties in washing my face, brushing my teeth, bathing, or getting dressed	26	47.27
	I cannot wash my face, brush my teeth, bathe, or dress myself	19	34.55
	I can carry out daily activities without any difficulties	10	18.18
D3 daily activities (such as work, study, housework, family, or leisure activities)	I have some difficulties in carrying out daily activities	29	52.73
	I cannot carry out daily activities	16	29.09
	I do not have any pain or discomfort	9	16.36
D4 pain or discomfort	I feel moderately pain or discomfort	33	60.00
	I feel extremely painful or uncomfortable	13	23.64
	I do not feel anxious or depressed	4	7.27
D5 anxiety (such as nervousness, worry, anxiety, etc.)/ depression (such as lack of interest in doing things, no fun, lack of energy, etc.)	I feel moderately anxious or depressed	36	65.45
	I feel extremely anxious or depressed	15	27.27

TABLE 3: Treatment of children with cerebral palsy.

	Number of people who should be answered	Answer "yes" (n, %)
Whether there are comorbidities	54	15 (27.78)
Whether to undergo surgery	52	5 (9.62)
In addition to surgery, whether to be hospitalized	55	18 (32.73)
Whether to buy rehabilitation equipment	55	36 (65.45)
Whether to take over-the-counter drugs or nutritional products	55	17 (30.91)
Whether to receive rehabilitation	55	51 (92.73)

the income difference between rural residents and urban residents, the indirect burden of urban CP families is much higher than that of rural families. If patients with CP and their caregivers are transformed into normal labor, they will create value for society. Due to CP disease, this part of the production value is lacking, which constitutes the indirect

economic burden of the society of this disease. According to the seventh census data [10], as of 0:00 on November 1, 2020, the permanent population of Changzhou is 5278121. In 2020, Changzhou achieved a regional gross product (GDP) of 780.53 billion yuan [9], so the per capita GDP is 147,800 yuan (Table 6).

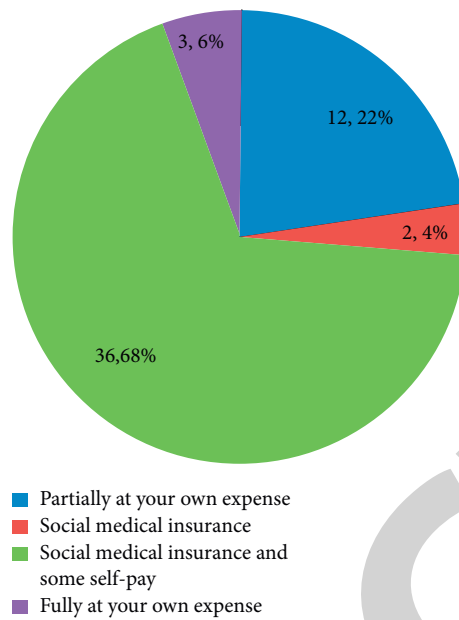


FIGURE 1: Sources of medical expenses for children with cerebral palsy.

TABLE 4: Relevant treatment costs for children with cerebral palsy (unit: ten thousand yuan).

	Number of people	Medical expense	Transportation expense	Accommodation expense	Escort expense	Total
General diagnosis and treatment expenses	55	0.50 (0.20, 2.00)	0.23 (0.03, 0.2)	0.03 (0, 0.2)	0.27 (0.13, 0.65)	1.56 (0.46, 4.58)
Surgical treatment expenses	12	3.00 (3.00, 5.25)	0.06 (0.05, 0.50)	0.3 (0, 0.46)	0.25 (0.20, 0.54)	3.74 (1.65, 6.99)
Nonsurgical hospitalization expenses	22	2.5 (1.00, 5.00)	0.10 (0.05, 0.175)	0.3 (0.00, 0.3)	0.49 (0.33, 0.61)	3.56 (0.61, 6.53)
Rehabilitation treatment expense	55	7.20 (5.00, 7.20)	0.50 (0.24, 1.00)	2.00 (0.50, 7.00)	0.35 (0.00, 0.40)	11.03 (5.12, 9.55)
The cost of purchasing supplements	18	0.4 (3, 0.97)	—	—	—	0.4 (0.13, 0.97)
The cost of purchasing rehabilitation equipment	36	0.29 (18, 0.56)	—	—	—	0.29 (0.18, 0.56)

TABLE 5: Indirect economic burden of children with cerebral palsy.

	Number of people	Time (month)	Average monthly cost (ten thousand yuan)	Total cost (ten thousand yuan)
Daily care expenses	12	47.70 (5.28, 67.65)	0.55 (38, 0.6)	29.35 (5.64, 38.47)
Special education expenses	11	42.00 (6.00, 62.00)	0.30 (14, 0.35)	10.63 (56, 19.68)

To sum up, the economic burden of each family is 4.1885 (2.3227, 4.6421) million yuan. The actual social economic burden of 220 families with children with CP in Changzhou is about 2.244 billion yuan.

**3.6. Quality of Life and Influencing Factors of Patients with Cerebral Palsy.** The EQ-5D five-dimensional health status of patients with CP is not optimistic. The proportions of

patients with CP who have moderate and severe problems in the five dimensions of action, self-care, daily activity ability, pain/discomfort, and anxiety/depression are 72.73%, 81.82%, 81.82%, 83.64%, and 92.73%, respectively (Table 7).

The average score of the 55 children with CP on the EQ-5D index was 0.423 (see Appendix 3).

The family life quality of patients with CP (VAS measurement data) is also low. In a total of 55 valid questionnaires, the average family score was 58.09, with the highest

TABLE 6: Calculation table of actual indirect family burden and social indirect burden of children with cerebral palsy.

	Time (year)	Per capita annual income (ten thousand yuan)		GDP per capita (ten thousand yuan)	Number of children or caregivers		Total social indirect burden (ten thousand yuan)
		Urban	Rural		Urban	Rural	
Patient labor	42	6.0529	3.2364	14.788	45	10	34160.28
Direct caregiver labor	27	6.0529	3.2364	14.788	45	10	21960.18
Special education	9	—	—	—	11	0	—
The actual indirect burden of each family	—	435.65	230.06	—	—	—	56120.46

TABLE 7: EQ-5D five-dimensional health status of children with cerebral palsy.

Total number of valid questionnaires	No problem		Moderate problems		Severe problems	
	Number of people	Composition ratio (%)	Number of people	Composition ratio (%)	Number of people	Composition ratio (%)
55	15	27.27	26	47.27	14	25.45
55	11	20.00	26	47.27	19	34.55
55	10	18.18	29	52.73	16	29.09
55	9	16.36	33	60.00	13	23.64
55	4	7.27	36	65.45	15	27.27

self-rating score of 90 and the lowest of 25. Only 19 patients scored 60 points or more, accounting for 34.55% of the total (Table 8).

We performed a grade correlation analysis on the EQ-5D index scores of children with CP and the family VAS scores and found that there was a significant correlation between the two ( $R = 0.811$ ,  $P < 0.05$ ). Those with a score less than 30 were regarded as the low quality of life group; otherwise, it was regarded as the high quality of life group. We first conduct a single-factor analysis of 13 factors and then include the meaningful variables (X7:  $r = -0.25422$ ,  $P = 0.0611$ ; X9:  $r = 0.27527$ ,  $P = 0.0419$ ; X13:  $r = 0.35902$ ,  $P = 0.0071$ ) into logistic regression analysis (see Appendix 4). The stepwise logistic regression analysis showed that the only factor affecting the quality of family life of the children was the health status represented by the EQ-5D score (OR = 12.499 (1.338, 116.787)).

#### 4. Discussion

According to calculations, the average family economic burden of each patient with cerebral palsy in Changzhou is about 4,188,500 yuan, of which the indirect economic burden accounts for the vast majority, and the direct medical burden accounts for only 4.91%. If calculated according to the average direct economic burden of each patient with CP, 193,500 yuan, it is 5.98 times as the per capita disposable income of rural residents in Changzhou in 2020 and 3.20 times as the per capita disposable income of urban residents. Meanwhile, owing to the fact that patients with CP and their caregivers are unable to engage in normal production all year round, their family income is low, which is generally lower than the average family income. Moreover, they

TABLE 8: Visual Analogue Scale of children with cerebral palsy.

Score	Number of people	Percentage	Cumulative percentage
0~10	0	0	0
~20	0	0	0
~30	5	9.09	9.09
~40	11	20	29.09
~50	12	21.82	50.91
~60	8	14.55	65.46
~70	5	9.09	74.55
~80	10	18.18	92.73
~90	4	7.27	100
~100	0	0	100
Total	55	100	100

seldom participate in social production and create labor value, which leads to a significantly larger indirect economic burden on society. In the light of the human capital method, the socioeconomic burden of 220 children with CP in Changzhou is as high as 2.244 billion yuan, accounting for 0.29% of Changzhou's GDP in 2020.

The data on direct family medical costs of patients with CP is distributed skewedly and varies greatly. This is mainly related to service utilization, family economic status, urban-rural differences, and social security. Our investigation found that the utilization rate of general diagnosis and rehabilitation treatment is very high, but the rate of purchasing nutritional products and rehabilitation equipment is low. Moreover, rural patients' access to related services is significantly harder than that of urban patients. Most of these patients with CP have a poor prognosis and usually fall into a vicious circle where the less the money they have for treatment, the worse their health and self-care ability and the heavier the indirect burden. Social security will reduce the

financial burden of patients' families to a certain extent, but it is difficult to achieve full coverage.

Our further analysis found that the main factors affecting the social and economic burden are the incidence of disease and the rate of recovery. Obviously, reducing the incidence of diseases can directly reduce the number of patients with CP, thereby reducing the socioeconomic burden. Increasing the recovery rate means liberating and developing the labor force, and it can also fundamentally reduce the indirect economic burden. Due to motor dysfunction, children with cerebral palsy often have changes in their psychology and mental state, and it is difficult to adapt to society. Therefore, special education must be carried out to correctly understand themselves, build confidence, and eliminate man-made bad psychological factors. As long as they are given the help they deserve, children with cerebral palsy can become talents and contribute to society. Without special education, other rehabilitation works will be difficult to carry out. Therefore, on the whole, interventions and funding of social and government should mainly focus on three aspects: early clinical treatment, standardized rehabilitation, and science education for patients with CP.

Through family interviews, we also learned about the invisible burden of CP patients and their families. Because of communication problems in patients with CP, most of our interviews were with their parents or direct caregivers. In the interview, almost all the interviewees believed that CP disease not only brought heavy economic pressure to the family but also overwhelmed the invisible burdens such as social discrimination, psychological load, and family problems. Many family members expressed pain, helplessness, grief, and despair.

From EQ-5D measurement results, the proportions of patients with CP who have problems in five aspects, namely, action, self-care, daily activity ability, pain/discomfort, and anxiety/depression, are 72.73%, 81.82%, 81.82%, 83.64%, and 92.73%, respectively. The average EQ-5D score of 55 children with CP in Changzhou is 0.423. According to the EQ-5D scale survey for 2994 urban residents in Beijing, the proportions of problems in the five aspects are 3.4%, 1.4%, 2.2%, 13.0%, and 5.3%, respectively. The average score of their EQ-5D index is 0.77 [11]. The proportions from 2830 rural residents in Kaiyang County, Guizhou Province, are 5.95%, 3.39%, 8.19%, 25.03%, and 33.23%, and the average EQ-5D score is 0.67 [12]. The proportions of the five aspects of children with CP in Hebei Province are 87.81%, 94.34%, 94.34%, 58.43%, and 72.05%, and the average score of the EQ-5D index is 0.44 [8]. By comparison, we find that the proportion of children with CP in Changzhou who have problems in the five dimensions is significantly higher than that of the general population, and the average score of the EQ-5D index is significantly lower than that of the general population. Our results are similar to those of the children with CP in Hebei Province.

We asked the direct caregivers to score themselves based on the current quality of life. The average score is 58.09, and there are 19 people with a score of 60 or more, accounting for 34.55% of the total. This result is significantly higher than

that in Hebei Province [8]. The average VAS score of children in Hebei Province is 27, 50% of which scored below 30, and those with a score of 60 or above accounted for only 5.9% of the total.

With reference to VAS scores of the health-related quality of life of the general population, the fourth health service survey in China in 2008 [13] showed that the VAS scores of the general population in rural areas was 80.4. Comparing the VAS score, we found that the VAS score of patients with CP and their families in Changzhou is lower than that of the general population but higher than that in Hebei Province [8]. Parents of most families who take care of children with cerebral palsy often have mental and physical disorders such as perseverance and sensitivity and may be accompanied by emotional problems such as autism, depression, and anxiety. These health problems and negative emotions make them show strong dissatisfaction with the status quo of the family. Well-being is thus reflected in the low scores of VAS. Similarly, the quality of life of parents of patients with CP has also significantly decreased [14–16]. Through stepwise logistic regression analysis, we found that the only factor affecting the quality of life of the children's family was the EQ-5D score. Domestic research in Hebei Province shows that EQ-5D score, hospitalization, surgical treatment, mother's education level, presence of brothers and sisters, and school education are the influencing factors. Schneider's research has shown [17] that parental care time, family cohesion, and the ability to receive school education significantly affect the quality of life of children with CP. Our conclusions are similar to and different from those of domestic and foreign research. The different conclusions may be that our sample size needs to be further expanded.

In recent years, the news media has repeatedly reported on cases of CP patients and family plights. The misfortune of CP patients' families has attracted more and more social attention. However, due to the lack of basic data on cerebral palsy, most people believe that the incidence of this disease is low and the disease burden is limited, especially since it has not received high attention and policy support from relevant government departments. From an empirical point of view, this study demonstrates that not only does cerebral palsy restrict family development but also the economic burden of the disease is quite alarming. At the same time, from a social perspective, cerebral palsy can also lead to social problems such as abandonment of infants and family breakdown. Therefore, relevant government departments should attach great importance to the major harm of cerebral palsy and take active and effective countermeasures.

Although the demographic characteristics, sociological characteristics, and health conditions of our respondents and the participants of other groups are not very homogeneous, such intuitive comparison may not be able to directly draw an authoritative conclusion, but the serious impact of CP on the quality of life of patients and their families is obvious. Some treatments and interventions have been shown to be cost-effective, although stronger evidence of clinical effectiveness is needed [18].

## 5. Conclusion

This paper adopts a quantitative analysis method to calculate the present situation of the family and socioeconomic burden of cerebral palsy in Changzhou. The calculated data intuitively reflects that the economic burden caused by cerebral palsy is very heavy. At the same time, a comprehensive evaluation of the quality of life of children with cerebral palsy and their families was carried out by using the EQ-5D scale, which objectively reflects that cerebral palsy has seriously affected the quality of life, family happiness, and social harmony. We found that to liberate and develop the labor capacity of patients and their direct caregivers through clinical treatment, rehabilitation, and special education is the most effective way to reduce the socioeconomic burden of cerebral palsy and improve the quality of life. This study is conducive to government departments and social community to fully understand the great harm of cerebral palsy and the necessity and urgency of intervention measures.

## Data Availability

The data in this study are all derived from questionnaire surveys. As it involves the privacy of cerebral palsy patients and their direct caregivers, the data cannot be fully disclosed. If the research colleagues are interested in this, you can contact the corresponding author via email to obtain the data.

## Ethical Approval

The authors are accountable for all aspects of the work in ensuring that questions related to the accuracy or integrity of any part of the work are appropriately investigated and resolved. This research, including the consent procedure, was approved by the Ethics Committee of Changzhou Maternal and Child Health Care Hospital (no. 2019006). All procedures performed in this study involving human participants were in accordance with the Declaration of Helsinki (as revised in 2013).

## Consent

All participants provided their written informed consent to participate in this study anonymously. The data were also collected and analyzed anonymously.

## Conflicts of Interest

The authors declare no conflicts of interest.

## Authors' Contributions

K Chen contributed to conception and design; K Chen and C Bian contributed to administrative support and data analysis and interpretation; F Peng and H Guo contributed to provision of study materials or patients; C Bian contributed to collection and assembly of data. All authors contributed to manuscript writing and final approval of the manuscript.

## Acknowledgments

The authors are most grateful to the children with cerebral palsy and their direct caregivers in Changzhou who made it possible for them to perform this study. They extend their thanks to the follow-up personnel for children in various neighborhoods and towns for working with them. This work was supported by Jiangsu Province Maternal and Child Health Research Project (F201834) and Changzhou Health Young Cultivation Project (CZQM2020101).

## Supplementary Materials

Appendix 1: the informed consent form and the questionnaire used in this survey. Appendix 2: the detailed introduction of the calculation method of economic burden and the EQ-5D scale. Appendix 3: the EQ-5D index of 55 children with cerebral palsy. Appendix 4: the specific assignment of a dependent variable and 13 independent variables. (*Supplementary Materials*)

## References

- [1] X. J. Li, H. B. Qiu, and Z. M. Jiang, "Epidemiological characteristics of cerebral palsy in twelve Province in China," *Chinese Journal of Applied Clinical Pediatrics*, vol. 33, no. 05, pp. 378–383, 2018.
- [2] China Planning Development and Informationization Department, *Statistical Bulletin of China's Health Development in*, <http://www.nhc.gov.cn/guihuaxxs/s10743/202107/af8a9c98453c4d9593e07895ae0493c8.shtml,%202021-07-13/2021-8-24, 2020>.
- [3] Z. H. Liu, q. M. Lin, and R. P. Wan, "Study on quality of life in children with cerebral palsy," *Chinese Journal for Clinicians*, vol. 3, no. 8, pp. 1327–1334, 2009.
- [4] S. L. Hu, "Research on the burden of disease (Part 1)," *Health Economics Research*, 2005.
- [5] A. I. Alriksson-Schmidt, M. Ahonen, and G. L. Andersen, "CP-North: living life in the Nordic countries? A retrospective register research protocol on individuals with cerebral palsy and their parents living in Sweden, Norway, Denmark, Finland and Iceland," *BMJ Open*, vol. 9, no. 10, Article ID e024438, 2019.
- [6] N. Amankwah, M. Oskoui, R. Garner et al., "Cerebral palsy in Canada, 2011-2031: results of a microsimulation modelling study of epidemiological and cost impacts," *Health Promotion and Chronic Disease Prevention in Canada*, vol. 40, no. 2, pp. 25–37, 2020.
- [7] National Bureau of Statistics of China, *Bulletin of the Seventh National Census*, [http://www.stats.gov.cn/tjsj/zxfb/202105/t20210510\\_1817179.html,%202021-05-11/2021-8-24 No. 3, 2021](http://www.stats.gov.cn/tjsj/zxfb/202105/t20210510_1817179.html,%202021-05-11/2021-8-24 No. 3, 2021).
- [8] W. Cui, *Evaluation of Hebei Province to Investigate the Quality of Life and Economic Burden in Children with Cerebral Palsy*, pp. 46–51, Jilin University, China, 2014.
- [9] Changzhou Bureau of Statistics, *Statistical Bulletin of National Economic and Social Development in Changzhou in*, [http://www.changzhou.gov.cn/ns\\_news/668161482201017,%202021-03-04%20/%202021-8-24, 2020](http://www.changzhou.gov.cn/ns_news/668161482201017,%202021-03-04%20/%202021-8-24, 2020).
- [10] Jiangsu Provincial Bureau of Statistics, *Bulletin of the Seventh National Census of Jiangsu Province*, [http://tj.jiangsu.gov.cn/art/2021/5/18/art\\_80066\\_9819836.html,%202021-05-18/2021-8-24\(No. 2\) \[EB/OL\], 2021](http://tj.jiangsu.gov.cn/art/2021/5/18/art_80066_9819836.html,%202021-05-18/2021-8-24(No. 2) [EB/OL], 2021).

## Retraction

# Retracted: The Potential Mechanism of Exercise Combined with Natural Extracts to Prevent and Treat Postmenopausal Osteoporosis

### Journal of Healthcare Engineering

Received 16 November 2022; Accepted 16 November 2022; Published 23 January 2023

Copyright © 2023 Journal of Healthcare Engineering. This is an open access article distributed under the Creative Commons Attribution License, which permits unrestricted use, distribution, and reproduction in any medium, provided the original work is properly cited.

*Journal of Healthcare Engineering* has retracted the article titled “The Potential Mechanism of Exercise Combined with Natural Extracts to Prevent and Treat Postmenopausal Osteoporosis” [1] due to concerns that the peer review process has been compromised.

Following an investigation conducted by the Hindawi Research Integrity team [2], significant concerns were identified with the peer reviewers assigned to this article; the investigation has concluded that the peer review process was compromised. We therefore can no longer trust the peer review process, and the article is being retracted with the agreement of the Chief Editor.

The authors do not agree to the retraction.

### References

- [1] T. Zhou, Z. Gai, X. Gao, and L. Li, “The Potential Mechanism of Exercise Combined with Natural Extracts to Prevent and Treat Postmenopausal Osteoporosis,” *Journal of Healthcare Engineering*, vol. 2021, Article ID 2852661, 9 pages, 2021.
- [2] L. Ferguson, “Advancing Research Integrity Collaboratively and with Vigour,” 2022, <https://www.hindawi.com/post/advancing-research-integrity-collaboratively-and-vigour/>.

## Review Article

# The Potential Mechanism of Exercise Combined with Natural Extracts to Prevent and Treat Postmenopausal Osteoporosis

Tongxi Zhou, Zhuo Gai, Xing Gao, and Li Li 

College of Sports and Human Sciences, Harbin Sport University, Harbin 150008, Heilongjiang, China

Correspondence should be addressed to Li Li; [lili@hrbipe.edu.cn](mailto:lili@hrbipe.edu.cn)

Received 27 October 2021; Revised 19 November 2021; Accepted 9 December 2021; Published 17 December 2021

Academic Editor: Yang Gao

Copyright © 2021 Tongxi Zhou et al. This is an open access article distributed under the Creative Commons Attribution License, which permits unrestricted use, distribution, and reproduction in any medium, provided the original work is properly cited.

Postmenopausal osteoporosis (PMOP) is a systemic chronic bone metabolic disease caused by the imbalance between bone formation and bone resorption mediated by estrogen deficiency. Both exercise and natural extracts are safe and effective means to prevent and control PMOP. The additive effect of exercise synergy extract against PMOP may be no less than that of traditional medicine. However, the mechanism of action of this method has not been clarified in detail. A large number of studies have shown that the pathogenesis of PMOP mainly involves the OPG-RANKL-RANK system, inflammation, and oxidative stress. Based on the abovementioned approaches, the present study reviews the anti-PMOP effects and mechanisms of exercise and natural extracts. Finally, it aims to explore the possibility of the target of the two combined anti-PMOP through this approach, thereby providing a new perspective for joint intervention research and providing a new direction for the treatment strategy of PMOP.

## 1. Introduction

Postmenopausal osteoporosis (PMOP) refers to women after menopause due to ovarian atrophy, functional degeneration, and estrogen secretion lack, which then induces a reduction in bone mass, bone trabecular structure changes, bone fragility, and easy fracture systemic bone metabolic disease. The traditional prevention method for PMOP mainly uses estradiol and bisphosphonates, but long-term use of such drugs may improve the incidence of cancer and osteonecrosis risk [1]. At present, 200 million women worldwide suffer from osteoporosis. It is expected that by 2050, the number of patients with osteoporotic fractures will double compared with now, which represents a huge medical care and economic burden [2]. Based on this, a proposed study explores the effect of exercise combined with natural extracts on postmenopausal osteoporosis.

## 2. Mechanism of Osteoporosis Formation after Menopause

*2.1. Bone Resorption Is Uncoupled from Bone Formation.* Bone is a multifunctional and changing organ that can support the activities of the motor system and maintain the

metabolic balance of minerals such as calcium and phosphate. In order to ensure the homeostasis of the bone microenvironment and meet the needs of body activities, bone tissue should be ablated and regenerated continuously, which is called bone remodeling. Bone remodeling is mainly completed by osteoclasts (OC), osteoblasts (OB), and osteocytes in the bone remodeling cavity. Bone cells in the deep layer of bone can sense the microcracks caused by external force or growth and development, or respond to hormone changes such as estrogen deficiency, transmit signals to the bone surface, and then cause osteoclasts and osteoblasts to function. Osteoclasts are developed from blood-derived mononuclear precursor cells. They are the only bone resorption cells. They can produce enzymes related to the acid dissolution of mineral salts in bone tissue and the degradation of organic matter. They will adhere to the surface of the bone matrix for bone resorption, such as eliminating bone tissue microcracks. In this process, the bone matrix will release a variety of growth factors. Osteoblasts differentiate from bone marrow mesenchymal stem cells and are the main functional cells of bone formation [3]. Stimulated by the direct contact of osteoclasts or cytokines, osteoblasts continue to mature, mineralize, and deposit to form new bone.

In this process, osteoblasts can negatively regulate the intensity of osteoclast bone resorption by secreting osteoprotegerin (OPG). Bone remodeling is a dynamic coupling process of bone resorption and bone formation. Therefore, estrogen is very important for the balance of the bone remodeling coupling process.

Both OC and OB are target cells of estrogen, which activates hormone response elements if combined to the estrogen receptor (ER) within OC, can reduce the transcription factor c-jun activity in OC precursors and OC, inhibit osteogenesis induced by RANKL and M-CSF, and attenuate bone resorption [4]. Binding of estrogen to ER also causes upregulation of the apoptosis-associated factor ligand (FASL) of OC that binds to Fas on OC in an autocrine manner and induces OC apoptosis through the Fas/FasL pathway [5]. In OB, estrogen can induce GSK3 $\beta$  phosphorylation which blocks  $\beta$ -catenin degradation, activates the Wnt/ $\beta$ -catenin pathway, binds to the TCF/LEF transcription factor family, and initiates cell cycle genes such as downstream cyc D and c-myc to mediate OB proliferation; and it also upregulates BMP-2 expression, which phosphorylates Smad1/5/8, activates the intranuclear gene expression, and promotes osteogenic differentiation [6]. Estrogen is also able to regulate many transcription factors' activity that in turn inhibits OB apoptosis through activation of Src/Shc/ERK signaling. Less estrogen caused by menopause leads to enhanced OC differentiation and reduced surface FasL expression, and OC escapes apoptosis. It also leads to decreased OB proliferation and differentiation capacity and increased apoptosis. Ultimately, bone resorption capacity is greater than bone formation, causing osteoporosis.

**2.2. The OPG-RANKL-RANK Signaling System Influences the Bone Remodeling Mechanisms.** The OPG-RANKL-RANK signaling system is very important for the process of bone remodeling. Before the discovery of this system, people could not explain the regulatory mechanism of bone resorption and metabolism. Until 1997, Tsuda found a glycoprotein that can specifically inhibit the differentiation of osteoclasts. In the same year, Simonet found a secretory protein that can inhibit the differentiation of osteoclasts and increase bone mineral density. Later, different students found substances with similar functions. After identification, these molecules are the same substance, named osteoprotegerin. The relationship between osteoprotegerin (OPG), nuclear factor- $\kappa$ B receptor activation factor ligand (RANKL), and nuclear factor- $\kappa$ B receptor activation factor (RANK) was found in the subsequent study. In the stable state, the contents of OPG and RANKL are in a balanced state, and their relative contents maintain the number of osteoclasts and support the normal level of bone resorption. When the change of one or more upstream factors excessively tilts this balance to the function of RANKL, the number of active osteoclasts increases and bone resorption is too strong; when the balance tilts too much to the function of OPG, the number of osteoclasts decreases and bone formation is too strong [7].

The mechanisms by which osteoblasts regulate the differentiation and maturation of osteoclasts are influenced by three cytokines, OPG, RANKL, and RANK. RANK belongs to the type I transmembrane receptor protein and is the only receptor for OC surface-mediated RANKL activity, a critical gate for differentiation and activation signaling pathways. RANKL is a member of the tumor necrosis factor (TNF) superfamily that can be secreted by OB, T cells, and endothelial cells and has a role in regulating OC proliferation and differentiation [8].

It has been shown that anti-RANKL treatment can enhance skeletal mechanical properties [9]. Osteoprotegerin, a member of the tumor necrosis factor receptor superfamily, is an osteoclast repressor secreted during OB differentiation and is able to negatively regulate the bone resorption process. OPG acts as an inhibitor of RANK activation by binding to RANKL with a higher affinity, blocking the OC precursor differentiation, inhibiting the function of OC, and preventing excessive bone resorption. Osteoprotegerin presented significant regulation of bone metabolism, with evidence of greater advantage for maintenance of skeletal and muscle function compared to gene deletion or selective inhibition of RANKL, a single treatment with OPG supplementation [10]. Thus, the proportion of OPG/RANKL is the lever that regulates the balance between bone resorption and bone formation. Estrogen downregulates RANKL, induces OC formation, and also promotes OB OPG. The sudden decrease in estrogen secretion after menopause triggered increased RANKL secretion, reduced OPG synthesis, active OC, enhanced bone resorption, and a dynamic imbalance of bone remodeling.

**2.3. Effects of the Inflammatory Response on Bone Mass.** Cells in the bone marrow are functionally divided into cells involved in bone metabolism and hematopoietic cells involved in the immune response, and both share the same microenvironment in the bone marrow and interact to perform functional activities of the skeletal system. It has been clear that osteoclasts and immune cells have common progenitor cells and are also regulated by many common regulators. T cells, B cells, cytokines, chemokines, and costimulatory molecules interact with immune cells under physiological and pathologic conditions, with the OPG-RANKL-RANK signaling system as a bridge to regulate bone formation and bone resorption, and then affect the bone remodeling process [11]. Several studies have shown that almost all chronic diseases are linked to inflammation and that inflammation and immunity are complementary processes, with many immunoactive substances and immune cells involved in the inflammatory response.

B cells and T cells in immune cells are involved in bone formation and bone resorption processes. B lymphocytes were shown to secrete OPG to maintain OPG/RANKL balance and promote bone formation [12]. Interferon  $\gamma$  (I FN- $\gamma$ ) secreted by helper T lymphocytes 1 (Th1) are important anti-inflammatory factors that have been clinically used in the treatment of severe osteoporosis. IFN- $\gamma$  is able to bind to the OC surface receptor IFNGR, activate TRAF6,

inhibit downstream NF- $\kappa$ B, JNK, and exert antiresorption; in OB, IFN- $\gamma$  upregulates Runx2, Osterix expression, and osteocalcin and ALP synthesis, which confirmed that the number of OB was significantly decreased in IFN- $\gamma$  receptor gene knockout mice [13]. In contrast to this effect, interleukin 4 (IL-4), mainly secreted by Th2 cells, suppresses OB differentiation by upregulating and downregulating RANKL expression [14]. The specific IL-17 secreted by Th17 in subsets of CD4<sup>+</sup> cells can stimulate OB and fibroblasts and also mediate the secretion of the inflammatory factors IL-1, TNF- $\alpha$ , and IL-6, further promoting bone resorption and inhibiting bone formation [15]. Furthermore, other inflammatory factors are also involved in the regulation of bone remodeling, and binding of the tumor necrosis factor  $\alpha$  (TNF- $\alpha$ ) as a ligand to OC surface receptors can either cooperate with RANKL to induce OC formation or directly activate TRAF6 to upregulate OC expression without RANKL dependence [16]; Smad6/7 activated by TNF- $\alpha$  within OB can inhibit Smad1/5/8, to further inhibit BMP-mediated OB differentiation processes. IL-1 is able to bind to OC surface IL1R, which indirectly activates TRAF6, which upregulates OC gene expression through multiple pathways and promotes the bone resorption process [17]. It has also been shown that IL-6 promotes OB-mediated osteogenic differentiation through the activation of JAK 2 and RANKL, and also cooperates with IL-1 and TGF- $\beta$  to induce T cell differentiation into Th17 [18]. There are estrogen targets on T cells that can be directly regulated by the latter, and estrogen can also inhibit the expression of bone resorption factors like TNF- $\alpha$ , IL-1, and IL-6 at the gene level, increase the expression of osteogenic factors such as TGF- $\beta$ , and then initiate OC apoptosis and prevent bone loss. Submenopausal estrogen reduction leads to T cell expansion, significantly increased content of proinflammatory factors IL-1, IL-6, IL-17, TNF- $\alpha$ , and IFN- $\gamma$ , enhanced OC function, reduced OB bone deposition capacity, and bone resorption greater than bone formation, resulting in reduced bone mass and osteoporosis formation [19].

**2.4. Oxidative Stress Affects Bone Metabolism.** Oxidative stress (OS) is also an important pathogenetic factor of postmenopausal osteoporosis. Active oxygen species, such as hydrogen peroxide and hydroxyl groups are produced during cell metabolism, and antioxidant enzyme lines in the body, including catalase (CAT), glutathione peroxidase (GPX), and superoxide dismutase (SOD), are responsible for removing free radicals from protected cells. Under the dual effects of aging and estrogen reduction, the body's oxidative stress response is enhanced, leading to an imbalance of bone remodeling [20]. In physiological states, intracellular ROS can indirectly activate JNK and serine/threonine kinase (MST1), which then phosphorylates the forkhead transcription factor (FOXO) to nucleate, induce DNA expression, and activate activities like DNA repair, cell cycle, apoptosis, and autophagy [21]. ROS inhibits OB occurrence and reduces its lifespan, so during OB transcription maturation, the transcription factor FOXO protects against

increased ROS caused by inducing autophagy and reducing enhanced mitochondrial respiration in osteoblasts [22]. Moreover, FOXO also prevents oxidative stress within OB by increasing SOD, CAT expression, and accumulation of GPX [23]. On the contrary, ROS is required for OC production, function, and survival. ROS can activate JNK and p38 to phosphorylate AP-1 and, in turn, enhance OC differentiation [24], suggesting that FOXO may inhibit bone resorption in an antireactive oxygen species manner. Studies have shown that estrogen can remove reactive oxygen species and protect bone health by fighting body oxidation. Estradiol can significantly enhance autophagy to reduce OB apoptosis through the ERs/ERK/mTOR pathway [25]; RANKL can increase ROS [26], estrogen in osteoclast progenitors can induce the effect of OPG secretion to inhibit RANKL and attenuate the function of OC. Higher serum levels of inflammatory factors and prooxidative biomarkers in menopausal women mean a state of high oxidative stress. Estrogen deficiency increases NADPH oxidase (NOX) on the membrane, decreasing antioxidant system capacity, and ROS accumulation triggers oxidative stress. At the same time, this process exacerbates OB apoptosis and OC differentiation, with bone resorption greater than bone formation and eventually PMOP.

**2.5. Exercise Affects the Postmenopausal Osteoporosis Mechanism.** In recent years, exercise has attracted much attention as a nondrug treatment of osteoporosis. Studies show that exercise effectively controls and prevents osteoporosis and is also a potential intervention strategy to overcome postmenopausal complications due to changes in metabolic hormones, especially estrogen levels [27]. Exercise regulation of the postmenopausal female estrogen secretion mechanism is not clear; the existing studies show the following associations: sports cause the hypothalamus-pituitary-gonadal axis, a study in strict accordance with the ASCM standard for postmenopausal women showed that 12 weeks of exercise can effectively improve female estradiol levels, and compared with aerobic exercise, anaerobic exercise has a more significant effect on bone density [28]. However, the impact of exercise on estrogen secretion is somewhat contradictory. Past studies have shown that adipose tissue can synthesize estrogen, while exercise is conducive to reduce fat quality, so it helps to reduce estrogen levels [29]. Previous studies believe that aerobic exercise has negative effects on estrogen levels, and the effect of resistance exercise is unknown [30]. Another study of postmenopausal obese women showed that estrogen levels increased in aerobic, resistance, and control groups, but there were no significant differences [31]. In short, exercise has a regulatory effect on estrogen, but the specific mechanism and effect results have not been uniformly determined and may be affected by the individual physiological state, exercise strength, and other factors.

A large number of current studies point to the significant positive effect of mechanical loads generated by exercise on maintaining bone mass and that amputation leads to accelerated bone loss in the affected limb [32]. Mechanical

stimulation mainly fights the PMOP from several aspects. On the one hand, mechanical load can directly stimulate the ER response and slow down the ER reduction due to estrogen deficiency. Experiments showed that ERK is not activated by pulling tension in OB and osteocytes that knocked down the ER $\alpha$  and ER $\beta$  genes, suggesting that ERs are ligand-independent and are directly involved in the conversion of mechanical forces into mechanical signals in osteocytes [33]. On the other hand, mechanical stress may modulate bone remodeling by regulating osteogenic differentiation of myeloid marrow mesenchymal cells. Fluid hydrodynamic regulation of osteogenic differentiation of bone marrow mesenchymal cells is reported to upregulate Runx2 expression in mouse bone marrow mesenchymal cell lines by both classical and nonclassical Wnt pathways, whereas mechanical unloading reduces  $\beta$ -catenin expression and suppresses OB proliferation [34]. In addition, exercise also showed upregulation of collagen expression in OB, and mechanical stress affects collagen arrangement upon the formation of new bone, thereby enhancing bone strength. Without physical activity, bed rest or weightlessness negatively affects the bone by inhibiting OB activity and/or enhancing OC activity [35]. In conclusion, the mechanical load induced by exercise has a positive effect on the proliferation and activity of osteoblasts, thereby promoting bone formation under physiological and pathological conditions.

Exercise may cause amelioration of inflammatory cytokines by upregulating anti-inflammatory cytokines, which in turn affect bone metabolism [36]. Low-impact, high-intensity interphase exercise has been reported to stimulate responses to bone transformation markers and cytokines such as IL-1, IL-6, and TNF- $\alpha$  which are significantly above baseline, suggesting a correlation between this form of exercise and immune and skeletal responses [37]. The body is in motion. It can also affect the OPG/RANKL/RANK system. Endurance treadmill exercise increases OPG expression and decreases RANKL levels in rats [38]. Resistance exercise increases OPG in adult rats and then upregulates the OPG/RANKL ratio to inhibit bone resorption. Several animal experiments reported similar effects on other forms of exercise: reduced RANKL levels and increased OPG levels were observed in osteoblast experiments in acutely trained mice [39]. Diabetic model rats showed significant OPG in bone and serum and decreased mRNA and protein expression of RANKL after forced swimming training [40]. However, another study found that exercise may not change the level of RANKL and OPG and their expression: a 12-week joint exercise experiment for healthy female college students showed that the bone metabolic response of OPG/RANKL/RANK signaling is not obvious. This speculation is due to the way of exercise. Long-term low-intensity exercise is not enough to improve body function, so the role of the RANKL signaling system is also limited [41]. Long and moderate-intensity regular physical exercise can reduce bone absorption and increase bone mass in healthy people and pathological patients [42]. From the above discussion, it can be concluded that OPG/RANKL changes may be affected by motor mode, motor intensity, and cycle, but still need to be further confirmed by more evidence.

*2.6. Effects of Natural Plant Extracts on Postmenopausal Osteoporosis.* It has been proved that the effective components of various natural plants and Chinese herbal medicines have significant prevention and control effects on PMOP, and the toxic side effects of traditional drug treatment have not been found, which is considered as a potential alternative therapy for traditional drugs for PMOP. It was found that multiple natural components control PMOP as dependent on their estrogen-like effects. It was shown that echinacoside (ECH), a novel phytoestrogen, effectively reverses uterine atrophy in ovariectomy (OVX) rats by enhancing in utero ER expression [43] and upregulating OB proliferation and differentiation via ER-mediated OPG/RANKL [44]. At the same time, ECH can promote osteogenesis and differentiation of bone marrow mesenchymal cells [45, 46] through activation of the classical Wnt pathway and autophagy; EHC can also regulate the NF- $\kappa$ B pathway and MAPK pathway to inhibit RANKL-induced osteogenesis and reduce bone loss [47]. Similarly, XSPS can promote the nuclear accumulation of  $\beta$ -catenin in bone marrow stromal cells without affecting BMP signaling, inducing osteogenic differentiation while inhibiting RANKL induced osteoclast differentiation [48]. Naringin modulates the classical Wnt pathway, upregulates OB differentiation, and downregulates ERK activity, which in turn suppresses bone resorption [49]. Glycyrrhizate directly attenuates OC specific genes and inhibits OC maturation induced by the NF- $\kappa$ B, ERK and MAPK pathways [50]. In addition, genoflavone, soy isoflavone, and resveratrol are also phytoestrogens that can replace estrogen to promote mesenchymal cell osteogenic differentiation and regulate bone remodeling balance [51].

Other native components can also improve bone remodeling imbalance by regulating the OPG/RANKL axis: salidroside suppresses bone turnover and upregulates bone OPG/RANKL expression, thus increasing bone density in OVX rats [52]. Ginsenoside, the main active ingredient of TCM panax ginseng, significantly suppresses RANKL-induced IKK activity and NFATc1 activity, as well as inhibition of OC synthesis, cathepsin K, MMP, and TRACP, suggesting that ginsenoside can inhibit osteoclast by inhibiting the RANKL-induced NF- $\kappa$ B pathway and Ca<sup>2+</sup> pathway [53]. Violoxin not only inhibits RANKL mediated expression of OC specific marker genes such as NFATc1 and TRACP, but also promotes expression of factors in OB, thus alleviating bone loss in OVX rats [54]. There is additional evidence that calycosin inhibits the RANKL mediated MAPK pathway and downregulates ALP and TRACP expression [55]. Mountain seed polysaccharide from cypress roots can upregulate OPG to downregulate RANKL expression and regulate the latter-mediated PI3K/Akt pathway [56]. Both components significantly fight osteoporosis in OVX rats, suggesting use as a potential surrogate for PMOP.

Plant components have antioxidative and anti-inflammatory effects, and they realize the prevention of PMOP by preventing inflammation and inhibiting oxidative stress. Epimedium prevents IL-1-induced apoptosis through the PI3K/AKT pathway [57] and also inhibits STAT3 activation and reduces Th-17 cells [58]. Melon polyphenols and lutein are all-natural antioxidants, which have positive effects on

protecting bone loss in OVX rats, and lutein can also inhibit OC-specific protein expression and bone resorption [59, 60]. Plant active components can influence oxidative stress levels by upregulating the expression of antioxidant enzyme lines, such as cocoa and lycopene, which can all upregulate GPX and SOD activity within OB and inhibit bone turnover in OVX rats to restore bone strength and microstructure [61, 62]. The advantage of natural ingredients is that there are no toxic side effects. Studies show that pomegranate seed oil extract is rich in phytoestrogens and antioxidants, which have therapeutic effects on osteoporosis and have no adverse effects on blood lipids, uric acid, liver, and kidney function [63]. In conclusion, the estrogen-like effects and antioxidant and anti-inflammatory effects of natural components make them of great research value in the prevention and control of PMOP.

**2.7. Antimenopausal Osteoporosis Effects of Exercise Combined with Natural Extracts.** The PMOP effects of exercise control were limited, and studies showed that exercise intervention in OVX rats could not prevent bone loss after OVX but alleviated the dramatic reduction in estrogen-dependent physiological processes due to estrogen deficiency, and the motor effects were much lower in estradiol than in the OVX rat group [64]. Early studies found that estrogen and mechanical stimulation synergistically inhibit OC generation [65], suggesting that they may work better against PMOP. Alendronate was reported to prevent bone loss in low-intensity whole-body vibration groups in OVX rats, but the combined intervention group was better, suggesting that low-intensity vibration enhances the effect of alendronate on OVX rats by further improving bone trabecular structure [66]. However, high-frequency loading combined with bisphosphonate intervention in OVX rats indicate that a single factor improved bone microstructure, but the combination had no additive effect [67]. The above findings suggest that the effect of the combined intervention may be affected by the exercise mode or exercise intensity as well as the drug type. But traditional drug treatment has limitations and disadvantages, such as estrogen, calcitonin increases the risk of cancer, bisphosphonate has a very low probability of jaw necrosis, and new drugs such as cathepsin K inhibitors, and sclerosing inhibitors clinical application have side effects and lack of long-term efficacy research data [68], which lead to patients' low acceptance and poor compliance with such drug treatments. Natural plant ingredients replace traditional drugs, and in combination with exercise, they may be highly potential and valuable therapies against PMOP.

The effect of PMOP investigated by motion combined with natural extracts is in the exploratory stage, and existing studies illustrate that the efficacy of natural composition and biomechanical stimulation have an additive effect on bone. It is found that the combined intervention can significantly increase the expression of osteoblast transcription factor osterix and inhibit GSK-3 $\beta$ , thereby promoting the proliferation and differentiation of osteoblasts and enhancing bone formation. The combination of naringin combined

with exercise has been reported to significantly enhance bone strength, bone mass, type I collagen C terminal peptide (CTX), and osteocalcin expression in OVX rats and is superior to a single intervention [69]. The combination of goldfinch isoflavone with resistance exercise prevented femur loss caused by OVX compared to experiments alone [70]. However, the mechanism of joint intervention on PMOP has not been defined, and based on the previous analysis, several pathways of action may involve the following. On the one hand, the estrogen-like effects of natural components can substitute for the mechanical stimulation produced by estrogen synergistic movement and improve bone loss due to hormone deficiency. It has been reported for both phytoestrogen 8-prenylnaringenin (8-PN) and vibration to stimulate ER $\alpha$  expression in OVX rats, and it is speculated that vibrations combined with 8-PN stimulation have synergistic effects on OVX rat ER $\alpha$ , making the combined group have a more pronounced effect on bone than the 8-PN group [71]. Experiments using rats intervening with the dye lutein (GEN) found a more pronounced reduction in bone mineral density than animals with voluntary exercise. Data show that GEN has no skeletal protection in the absence of physical activity. Meanwhile, the bone-protective effect of GEN may be mediated by ER $\alpha$ -dependent mechanisms, and physical exercise has a strong effect on the bone-protective capacity of this phytoestrogen [72]. On the other side, regulation of OPG/RANKL, anti-inflammatory, and antioxidant may also be a combination therapy for anti-PMOP pathway. It was reported that both platform exercise and puerarin alone or combined could downregulate RANKL content in high-fat-raised OVX rats, with no significant effect on mRNA expression of OPG, suggesting that this intervention may be a direct inhibition of RANKL induction of OC formation in OVX rats. Moreover, the combined intervention had a sexual effect on the trabecular quality, and ALP, CTX, and ALP were even better than those of estrogen treatment [73]. A 6-month randomized experiment showed that green tea polyphenols combined with Taijiquan were effective in reducing oxidative stress levels in postmenopausal women, suggesting that the combination therapy may improve PMOP [74]. Through the antioxidant pathway another study showed that soybean isoflavone significantly improved GSH levels in OVX rats but had no SOD activity, while 12-week platform exercise enhanced SOD activity and H<sub>2</sub>O<sub>2</sub> induced significantly increased DNA tail length, suggesting that moderate exercise binding soy isoflavone protected rats from oxidative stress through different pathways [75]. In addition, isoflavone synergy with weekly aerobic and resistance training for six months reduced TNF- $\alpha$  and IL-6 levels in postmenopausal obese women and superior to exercise alone [76].

Furthermore, the combined means may also affect osteogenic differentiation or bone formation marker expression, which in turn affects bone metabolism. It was reported that  $\beta$ -catenin, Akt, ER $\alpha$ , and Runx2 expression were significantly increased in OB in the treadmill-bound Epimedii intervention group, compared with exercise alone. Combination treatment significantly prevented OVX-induced bone loss and increased OB differentiation and

mineralization ability, some of which may be regulated by the ER $\alpha$ /Akt/ $\beta$ -catenin pathway, but whether combination intervention affected OC differentiation remains unclear [77]. In vitro experiments by domestic scholars have shown icariin combined with exercise coupling stimulation may inhibit bone resorption by regulating NF- $\kappa$ B signaling and influence the upregulation of OB proliferation by the classical Wnt/ $\beta$ -catenin pathway. Soybean isoflavone cooperative treadmill exercise intervention can restore bone mass to sham surgical levels in OVX rats with the same effect of estradiol treatment [78]. However, the effect of soy protein combined with moderate endurance exercise in postmenopausal women showed that there was no intervention effect on bone density [79]. In addition, it is speculated that exercise intensity and dosage may affect the combined effect, and the molecular mechanisms of maintaining bone mass may be different, not simply synergy [80].

### 3. Conclusions

In a summary, it is possible that motor binding to natural extracts may involve multiple pathways including mechanical signaling, estrogen deficiency-mediated OPG/RANKL alterations, and anti-inflammatory and antioxidant control of PMOP. Most of the existing studies have shown the additive effect of combination interventions, but several data show no additional efficacy, which may be affected by the choice of exercise regimen and extract dosage. Therefore, the effect and mechanism of combination treatment still need to be further explored by extensive experimental data. Exercise and natural ingredients have great potential and advantages with their low cost, nontoxic, and other advantages, which have been widely valued by the medical community. We are eager to select the best treatment scheme based on various therapies in the future to greatly reduce the pain of patients with osteoporosis and help potential patients stay away from the threat of osteoporosis.

### Data Availability

The data that support the findings of this study are available from the corresponding author upon reasonable request.

### Conflicts of Interest

The authors declare that they have no conflicts of interest.

### Acknowledgments

This work was founded by the Natural Science Foundation of Heilongjiang Province (LH2020H011), Discipline Echelon's Construction Foundation of Harbin Sport University (XKB10 and XKL10), and Basic Science Foundation of Heilongjiang Provincial Undergraduate Universities in 2021 (2021KYYWF-PY04).

### References

- [1] J. A. Kanis, C. Cooper, R. Rizzoli, and J. Y. Reginster, "Correction to: European guidance for the diagnosis and management of osteoporosis in postmenopausal women," *Osteoporosis International: A Journal Established As Result of Cooperation Between the European Foundation for Osteoporosis and the National Osteoporosis Foundation of the USA*, vol. 31, no. 1, p. 801, 2020.
- [2] P. Paola, M. Daniela Renna, F. Conversano et al., "Major osteoporotic fragility fractures: risk factor updates and societal impact," *World Journal of Orthopedics*, vol. 7, no. 3, pp. 171–181, 2016.
- [3] S. Khosla, M. J. Oursler, and D. G. Monroe, "Estrogen and the skeleton," *Trends in Endocrinology and Metabolism*, vol. 23, no. 11, pp. 576–581, 2012.
- [4] J.-E. Huh, W. I. Lee, J. W. Kang et al., "Formononetin attenuates osteoclastogenesis via suppressing the RANKL-induced activation of NF- $\kappa$ B, c-Fos, and nuclear factor of activated T-cells cytoplasmic 1 signaling pathway," *Journal of Natural Products*, vol. 77, no. 11, pp. 2423–2431, 2014.
- [5] A. Krum Susan, A. Miranda-Carboni Gustavo, V. Hauschka Peter et al., "Estrogen protects bone by inducing Fas ligand in osteoblasts to regulate osteoclast survival," *The EMBO Journal*, vol. 27, no. 3, 2008.
- [6] R. Y. Kim, H. J. Joo, S. Y. Mi, K. I. Sook, and J. S. Jung, "Estrogen modulates bone morphogenetic protein-induced sclerostin expression through the Wnt signaling pathway," *Tissue Engineering. Part A*, vol. 21, no. 13-14, 2015.
- [7] L. C. Hofbauer, S. Khosla, C. R. Dunstan, L. Lacey, J. Boyle, and B. L. Riggs, "The roles of osteoprotegerin and osteoprotegerin ligand in the paracrine regulation of bone resorption," *Journal of Bone and Mineral Research*, vol. 15, no. 1, 2010.
- [8] M. Nakamura and U. Nobuyuki, "Osteoporosis and RANKL signal," *Clinical Calcium*, vol. 21, no. 8, 2011.
- [9] H. Dounia, M. Laetitia, P. B. Antoine et al., "An anti-RANKL treatment reduces muscle inflammation and dysfunction and strengthens bone in dystrophic mice," *Human Molecular Genetics*, vol. 28, no. 18, pp. 3101–3112, 2019.
- [10] S. S. Dufresne, A. Boulanger-Piette, S. Bossé et al., "Genetic deletion of muscle RANK or selective inhibition of RANKL is not as effective as full-length OPG-fc in mitigating muscular dystrophy," *Acta Neuropathol Commun*, vol. 6, no. 1, p. 31, 2018.
- [11] K. Okamoto, T. Nakashima, M. Shinohara et al., "Osteoimmunology: the conceptual framework unifying the immune and skeletal systems," *Physiological Reviews*, vol. 97, no. 4, p. 1295, 2017.
- [12] L. Yan, T. Gianluca, A. Li et al., "B cells and T cells are critical for the preservation of bone homeostasis and attainment of peak bone mass in vivo," *Blood*, vol. 109, no. 9, 2007.
- [13] T. Maruhashi, T. Kaifu, R. Yabe et al., "DCIR maintains bone homeostasis by regulating IFN- $\gamma$  production in T cells," *The Journal of Immunology*, vol. 194, no. 12, pp. 5681–5691, 2015.
- [14] S. G. Kamel Mohamed, E. Sugiyama, K. Shinoda et al., "Interleukin-4 inhibits RANKL-induced expression of NFATc1 and c-Fos: a possible mechanism for downregulation of osteoclastogenesis," *Biochemical and Biophysical Research Communications*, vol. 329, no. 3, 2005.
- [15] G. H. Tso, H. K. Law, W. Tu, G. C. F. Chan, and Y. L. Lau, "Phagocytosis of apoptotic cells modulates mesenchymal stem cells osteogenic differentiation to enhance IL-17 and RANKL expression on CD4+ T cells," *Stem Cells*, vol. 28, no. 5, 2010.
- [16] L. Zha, L. He, Y. Liang et al., "TNF- $\alpha$  contributes to postmenopausal osteoporosis by synergistically promoting RANKL-induced osteoclast formation," *Biomedicine & pharmacotherapy=Biomedecine & pharmacotherapie*, vol. 102, p. 369, 2018.

- [17] N. C. Huynh, V. Everts, P. Pavasant, and R. S. Ampornaramveth, "Interleukin-1 $\beta$  induces human cementoblasts to support osteoclastogenesis," *International Journal of Oral Science*, vol. 9, no. 4, pp. 216–223, 2017.
- [18] Q. Wu, X. Zhou, D. Huang, Y. Ji, and F. Kang, "IL-6 enhances osteocyte-mediated osteoclastogenesis by promoting JAK2 and RANKL activity in vitro," *Cellular Physiology and Biochemistry: International Journal of Experimental Cellular Physiology, Biochemistry, and Pharmacology*, vol. 41, no. 4, 2017.
- [19] R. Zhao, "Immune regulation of bone loss by T h17 cells in oestrogen-deficient osteoporosis," *European Journal of Clinical Investigation*, vol. 43, no. 11, 2013.
- [20] D. A. Callaway and J. X. Jiang, "Reactive oxygen species and oxidative stress in osteoclastogenesis, skeletal aging and bone diseases," *Journal of Bone and Mineral Metabolism*, vol. 33, no. 4, pp. 359–70, 2015.
- [21] L.-O. Klotz, C. Sánchez-Ramos, I. Prieto-Arroyo, P. Urbánek, H. Steinbrenner, and M. Monsalve, "Redox regulation of FoxO transcription factors," *Redox Biology*, vol. 6, 2015.
- [22] S. Gavali, M. K. Gupta, B. Daswani, M. R. Wani, R. Sirdeshmukh, and M. Ikram Khatkhatay, "Estrogen enhances human osteoblast survival and function via promotion of autophagy," *BBA -Molecular Cell Research*, vol. 1866, no. 9, pp. 1498–1507, 2019.
- [23] A. Fatemeh, M. Ali, and S. Pepper Michael, "The role of reactive oxygen species in mesenchymal stem cell adipogenic and osteogenic differentiation: a review," *Stem Cells and Development*, vol. 24, no. 10, 2015.
- [24] T. S. Agidigbi and C. Kim, "Reactive oxygen species in osteoclast differentiation and possible pharmaceutical targets of ROS-mediated osteoclast diseases," *International Journal of Molecular Sciences*, vol. 20, no. 14, 2019.
- [25] Y. H. Yang, K. Chen, B. Li et al., "Estradiol inhibits osteoblast apoptosis via promotion of autophagy through the ER-ERK-mTOR pathway," *Apoptosis*, vol. 18, no. 11, pp. 1363–1375, 2013.
- [26] X. C. Bai, D. Lu, A. L. Liu et al., "Reactive oxygen species stimulates receptor activator of NF-kappaB ligand expression in osteoblast," *Journal of Biological Chemistry*, vol. 280, no. 17, Article ID 17497, 2005.
- [27] J. Iwamoto, T. Takeda, and S. Ichimura, "Effect of exercise training and detraining on bone mineral density in postmenopausal women with osteoporosis," *Orthop Sci*, vol. 6, pp. 128–132, 2001.
- [28] Z. A. Razzak, A. A. Khan, and S. I. Farooqui, "Effect of aerobic and anaerobic exercise on estrogen level, fat mass, and muscle mass among postmenopausal osteoporotic females," *International Journal of Health Sciences*, vol. 13, no. 4, pp. 10–16, 2019.
- [29] F. E. Rossi, C. Buonani, J. Viesel et al., "Effect of combined aerobic and resistance training in body composition of obese postmenopausal women," *Motriz Revista De Educao Física*, vol. 21, no. 1, pp. 61–67, 2015.
- [30] A. C. Hackney, "Exercise as a stressor to the human neuroendocrine system," *Medicina*, vol. 42, no. 10, pp. 788–797, 2006.
- [31] J. R. Yoon, G. C. Ha, K. J. Ko, and S. J. Kang, "Effects of Exercise Type on Estrogen, Tumor Markers, Immune Function, Antioxidant Function, and Physical Fitness in Postmenopausal Obese Women," *Exerc Rehabil*, vol. 14, no. 6, pp. 1032–1040, 2018.
- [32] H. C. Cunningham, D. W. D. West, L. M. Baehr, F. D. Tarke, K. Baar, and B. A. Christiansen, "Age-dependent bone loss and recovery during hindlimb unloading and subsequent reloading in rats," *BMC Musculoskeletal Disorders*, vol. 19, no. 1, p. 223, 2018.
- [33] N. Swift Sibyl, M. Swift Joshua, and A. Bloomfield Susan, "Mechanical loading increases detection of estrogen receptor-alpha in osteocytes and osteoblasts despite chronic energy restriction," *Journal of Applied Physiology*, vol. 117, no. 11, pp. 1349–55, 2014.
- [34] C. Yin, Y. Zhang, L. Hu et al., "Xian. Mechanical unloading reduces microtubule actin crosslinking factor 1 expression to inhibit  $\beta$ -catenin signaling and osteoblast proliferation," *Journal of Cellular Physiology*, vol. 233, no. 7, 2018.
- [35] G. Armbrecht, D. L. Belavý, D. L. Belavý et al., "Trabecular and cortical bone density and architecture in women after 60 days of bed rest using high-resolution pQCT: wise 2005," *Bone and Mineral Research*, vol. 26, no. 10, pp. 2399–2410, 2011.
- [36] Y. A. Mezil, D. Allison, K. Kish et al., "Response of bone turnover markers and cytokines to high-intensity low-impact exercise," *Medicine & Science in Sports & Exercise*, vol. 47, no. 7, pp. 1495–1502, 2015.
- [37] A. Mezil Yasmeen, D. Allison, K. Kimberly et al., "Response of bone turnover markers and cytokines to high-intensity low-impact exercise," *Medicine & Science in Sports & Exercise*, vol. 47, no. 7, 2015.
- [38] A. Troib, M. Guterman, R. Rabkin, D. Landau, and Y. Segev, "Endurance exercise and growth hormone improve bone formation in young and growth-retarded chronic kidney disease rats," *Nephrology Dialysis Transplantation*, vol. 31, pp. 1270–1279, 2016.
- [39] L. Tang, Z. Lin, and Y. M. Li, "Effects of different magnitudes of mechanical strain on Osteoblasts in vitro," *Biochemical and Biophysical Research Communications*, vol. 344, no. 1, pp. 122–128, 2006.
- [40] L. Pezhman, F. Sheikhzadeh Hesari, and R. Ghiasi, "The impact of forced swimming on expression of RANKL and OPG in a type 2 diabetes mellitus rat model," *Archives of Physiology and Biochemistry*, vol. 125, no. 3, pp. 195–200, 2019.
- [41] J. Y. Kim, H. J. Kim, and C. S. Kim, "Effects of 12-week combined exercise on RANKL/RANK/OPG signaling and bone-resorption cytokines in healthy college females," *Exerc Nutrition Biochem*, vol. 23, no. 1, pp. 13–20, 2019.
- [42] Z. Qi, W. Liu, and J. Lu, "The mechanisms underlying the beneficial effects of exercise on bone remodeling: roles of bone-derived cytokines and microRNAs," *Progress in Biophysics and Molecular Biology*, vol. 122, pp. 131–139, 2016.
- [43] F. Li, X. Yang, Y. Yang et al., "Antiosteoporotic activity of echinacoside in ovariectomized rats," *Phytomedicine*, vol. 20, no. 6, 2013.
- [44] L.-J. Sun, L. Chong, X.-H. Wen et al., "Icariin Stimulates hFOB 1.19 Osteoblast Proliferation and Differentiation via OPG/RANKL Mediated by the Estrogen Receptor," *Current pharmaceutical biotechnology*, vol. 22, no. 1, 2020.
- [45] J.-M. Huang, B. Yuan, W. Xiang et al., "Icariin Regulates the Bidirectional Differentiation of Bone Marrow Mesenchymal Stem Cells through Canonical Wnt Signaling Pathway," *Evid Based Complement Alternat Med*, vol. 2017, pp. 1–12, 2017.
- [46] X. Liang, Z. Hou, Y. Xie et al., "Icariin promotes osteogenic differentiation of bone marrow stromal cells and prevents bone loss in OVX mice via activating autophagy," *Cell Biochem*, vol. 120, no. 8, pp. 13121–13132, 2019.
- [47] G. Qiang, G. Chen, X. Liu, M. Dai, and B. Zhang, "Icariin inhibits RANKL-induced osteoclastogenesis via modulation of the NF- $\kappa$ B and MAPK signaling pathways," *Biochemical*

- and *Biophysical Research Communications*, vol. 508, no. 3, pp. 902–906, 2018.
- [48] L. Du, M. N. Nong, J. M. Zhao, X. M. Peng, S. H. Zong, and G. F. Zeng, “Polygonatum sibiricum polysaccharide inhibits osteoporosis by promoting osteoblast formation and blocking osteoclastogenesis through Wnt/ $\beta$ -catenin signalling pathway,” *Scientific Reports*, vol. 6, Article ID 32261, 2016.
  - [49] H. Wang, C. Li, J. Li et al., “Naringin enhances osteogenic differentiation through the activation of ERK signaling in human bone marrow mesenchymal stem cells,” *Iranian Journal of Basic Medical Sciences*, vol. 20, no. 4, pp. 408–414, 2017.
  - [50] Z. Yin, W. Zhu, Q. Wu et al., “Glycyrrhizic acid suppresses osteoclast differentiation and postmenopausal osteoporosis by modulating the NF- $\kappa$ B, ERK, and JNK signaling pathways,” *European Journal of Pharmacology*, vol. 859, Article ID 172550, 2019.
  - [51] B. Saud, R. Malla, and K. Shrestha, “A review on the effect of plant extract on mesenchymal stem cell proliferation and differentiation,” *Stem Cells International*, vol. 2019, no. 5, 13 pages, 2019.
  - [52] H. Zheng, S. Qi, and C. Chen, “Salidroside improves bone histomorphology and prevents bone loss in ovariectomized diabetic rats by upregulating the OPG/RANKL ratio,” *Molecules*, vol. 23, no. 9, 2018.
  - [53] H. B. Hsiao, H. Lin, J. B. Wu, and W. C. Lin, “Kinsenoside prevents ovariectomy-induced bone loss and suppresses osteoclastogenesis by regulating classical NF- $\kappa$ B pathways,” *Osteoporosis International*, vol. 24, no. 5, pp. 1663–1676, 2013.
  - [54] Y. Chen, Z. Xie, Y. Zhang, C. Xia, M. Yang, and X. Hu, “Shikonin relieves osteoporosis of ovariectomized mice by inhibiting RANKL-induced NF- $\kappa$ B and NFAT pathways,” *Experimental Cell Research*, vol. 394, no. 1, Article ID 112115, 2020.
  - [55] N. Li, T. Yan, S. Yin, Y. Qin, L. Chao, and X. Liu, “Calycosin attenuates osteoporosis and regulates the expression of OPG/RANKL in ovariectomized rats via MAPK signaling,” *Die Pharmazie*, vol. 71, no. 10, 2016.
  - [56] X. Sun, B. Wei, Z. Peng et al., “Protective effects of Dipsacus asper polysaccharide on osteoporosis in vivo by regulating RANKL/RANK/OPG/VEGF and PI3K/Akt/eNOS pathway,” *International Journal of Biological Macromolecules*, vol. 129, pp. 579–587, 2019.
  - [57] X. Deng, W. Wu, H. Liang et al., “Icariin prevents IL-1 $\beta$ -induced apoptosis in human nucleus pulposus via the PI3K/AKT pathway,” *Evidence-based Complementary and Alternative Medicine: eCAM*, vol. 2017, no. 1, 12 pages, Article ID 2198323, 2017.
  - [58] L. Chi, W. Gao, X. Shu, X. Lu, and J. Galvez, “A Natural Flavonoid Glucoside, Icariin, Regulates Th17 and Alleviates Rheumatoid Arthritis in a Murine Model,” *Mediators of Inflammation*, 10 pages, 2014.
  - [59] B. Kim, L. Sung-Ho, S. Su-Jin et al., “Protective effects of melon extracts on bone strength, mineralization, and metabolism in rats with ovariectomy-induced osteoporosis,” *Antioxidants*, vol. 8, no. 8, p. 306, 2019.
  - [60] H. Li, C. Huang, J. Zhu, K. Gao, J. Fang, and H. Li, “Lutein suppresses oxidative stress and inflammation by Nrf2 activation in an osteoporosis rat model,” *Medical Science Monitor: International Medical Journal of Experimental and Clinical Research*, vol. 24, pp. 5071–5075, 2018.
  - [61] B. Sarmadi, A. Ismail, L. Yusof, M. Faridz, and M. Yunoh, “Mechanism of action of cocoa on bone metabolism in calcium and estrogen-deficient rat model of osteoporosis: evidence for site and dose-related responses and involvement of IGF-I,” *Journal of Functional Foods*, vol. 66, Article ID 103793, 2020.
  - [62] M.-S. M. Ardawi, M. H. Badawoud, S. M. Hassan et al., “Lycopene treatment against loss of bone mass, micro-architecture and strength in relation to regulatory mechanisms in a postmenopausal osteoporosis model,” *Bone*, vol. 83, pp. 127–140, 2016.
  - [63] N. Z. Shaban, I. M. Talaat, F. H. Elrashidy, A. Y. Hegazy, and A. S. Sultan, “Therapeutic role of punica granatum (pomegranate) seed oil extract on bone turnover and resorption induced in ovariectomized rats,” *The Journal of Nutrition, Health & Aging*, vol. 21, no. 10, pp. 1299–1306, 2017.
  - [64] S. T. Müller, A. M. Keiler, K. KraKer, O. Zierau, and R. Bernhardt, “Influence of Estrogen on Individual Exercise Motivation and Bone protection in Ovariectomized Rats,” *Laboratory Animals*, vol. 52, no. 5, pp. 479–489, Article ID 002367721875645, 2018.
  - [65] H. Allison and L. M. McNamara, “Inhibition of osteoclastogenesis by mechanically stimulated osteoblasts is attenuated during estrogen deficiency,” *American Journal of Physiology. Cell Physiology*, vol. 317, no. 5, pp. C969–C982, 2019.
  - [66] C. Guo-Xian, S. Zheng, S. Qin et al., “Effect of low-magnitude whole-body vibration combined with alendronate in ovariectomized rats: a random controlled osteoporosis prevention study,” *PLoS One*, vol. 9, no. 5, 2014.
  - [67] K. Hatori, G. V. Camargos, M. Chatterjee et al., “Single and combined effect of high-frequency loading and bisphosphonate treatment on the bone micro-architecture of ovariectomized rats,” *Osteoporosis International: A Journal Established As Result of Cooperation Between the European Foundation for Osteoporosis and the National Osteoporosis Foundation of the USA*, vol. 26, no. 1, 2015.
  - [68] S. Khosla and L. C. Hofbauer, “Osteoporosis treatment: recent developments and ongoing challenges,” *The Lancet Diabetes & Endocrinology*, vol. 5, no. 11, 2017.
  - [69] X. Sun, F. Li, X. Ma et al., “The effects of combined treatment with naringin and treadmill exercise on osteoporosis in ovariectomized rats,” *Scientific Reports*, vol. 5, Article ID 13009, 2015.
  - [70] D. Nakajima, C.-S. Kim, T.-W. Oh et al., “Suppressive effects of genistein dosage and resistance exercise on bone loss in ovariectomized rats,” *Physiol Anthropol Appl Human Sci*, vol. 20, no. 5, 2001.
  - [71] M. Komrakova, C. Rechholtz, N. Pohlmann et al., “Effect of alendronate or 8-prenylnaringenin applied as a single therapy or in combination with vibration on muscle structure and bone healing in ovariectomized rats,” *BoneKey Reports*, vol. 11, Article ID 101085, 2019.
  - [72] T. Hertrampf, M. J. Gruca, J. Seibel, U. Laudénbach, K. H. Fritzemeier, and P. Diel, “The bone-protective effect of the phytoestrogen genistein is mediated via ER  $\alpha$ -dependent mechanisms and strongly enhanced by physical activity,” *Bone*, vol. 40, no. 6, pp. 1529–1535, 2007.
  - [73] H. M. Ok, M. R. Gebreamanuel, S. A. Oh, H. Jeon, W. J. Lee, and O. Kwon, “A root-based combination supplement containing pueraria lobata and rehmannia glutinosa and exercise preserve bone mass in ovariectomized rats fed a high-fat diet,” *Calcified Tissue International*, vol. 97, no. 6, 2015.
  - [74] G. Qian, K. Xue, L. Tang et al., “Mitigation of oxidative damage by green tea polyphenols and tai chi exercise in postmenopausal women with osteopenia,” *PLoS One*, vol. 7, 2012.

## Retraction

# Retracted: Deep Learning-Based Cervical Spine Posterior Percutaneous Endoscopic Disc Nucleus Resection for the Treatment of Cervical Spondylotic Radiculopathy

### Journal of Healthcare Engineering

Received 11 July 2023; Accepted 11 July 2023; Published 12 July 2023

Copyright © 2023 Journal of Healthcare Engineering. This is an open access article distributed under the Creative Commons Attribution License, which permits unrestricted use, distribution, and reproduction in any medium, provided the original work is properly cited.

This article has been retracted by Hindawi following an investigation undertaken by the publisher [1]. This investigation has uncovered evidence of one or more of the following indicators of systematic manipulation of the publication process:

- (1) Discrepancies in scope
- (2) Discrepancies in the description of the research reported
- (3) Discrepancies between the availability of data and the research described
- (4) Inappropriate citations
- (5) Incoherent, meaningless and/or irrelevant content included in the article
- (6) Peer-review manipulation

The presence of these indicators undermines our confidence in the integrity of the article's content and we cannot, therefore, vouch for its reliability. Please note that this notice is intended solely to alert readers that the content of this article is unreliable. We have not investigated whether authors were aware of or involved in the systematic manipulation of the publication process.

In addition, our investigation has also shown that one or more of the following human-subject reporting requirements has not been met in this article: ethical approval by an Institutional Review Board (IRB) committee or equivalent, patient/participant consent to participate, and/or agreement to publish patient/participant details (where relevant).

Wiley and Hindawi regrets that the usual quality checks did not identify these issues before publication and have since put additional measures in place to safeguard research integrity.

We wish to credit our own Research Integrity and Research Publishing teams and anonymous and named external researchers and research integrity experts for contributing to this investigation.

The corresponding author, as the representative of all authors, has been given the opportunity to register their agreement or disagreement to this retraction. We have kept a record of any response received.

### References

- [1] Y. Zhang, H. Zhu, Z. Zhou et al., "Deep Learning-Based Cervical Spine Posterior Percutaneous Endoscopic Disc Nucleus Resection for the Treatment of Cervical Spondylotic Radiculopathy," *Journal of Healthcare Engineering*, vol. 2021, Article ID 7245566, 12 pages, 2021.

## Research Article

# Deep Learning-Based Cervical Spine Posterior Percutaneous Endoscopic Disc Nucleus Resection for the Treatment of Cervical Spondylotic Radiculopathy

**Yang Zhang, Hengjie Zhu, Zheng Zhou, Yinming Sun, Xiang Shen, Jixiang Wu, and Chengcun Li** 

*Neurosurgery, Yangzhou Hongquan Hospital, Yangzhou 225200, Jiangsu, China*

Correspondence should be addressed to Chengcun Li; [lichengcun2021@126.com](mailto:lichengcun2021@126.com)

Received 8 October 2021; Revised 24 November 2021; Accepted 2 December 2021; Published 17 December 2021

Academic Editor: Yang Gao

Copyright © 2021 Yang Zhang et al. This is an open access article distributed under the Creative Commons Attribution License, which permits unrestricted use, distribution, and reproduction in any medium, provided the original work is properly cited.

In the past 10 years, the technology of percutaneous spine endoscopy has been continuously developed. The indications have expanded from simple lumbar disc herniation to various degenerative diseases of the cervical, thoracic, and lumbar spine. Traditional surgery for the treatment of cervical radiculopathy includes anterior cervical decompression surgery, anterior cervical decompression plus fusion surgery, and posterior limited fenestration surgery. This article mainly studies the treatment of cervical spondylosis caused by radiculopathy caused by the nucleus resection of the posterior cervical spine percutaneous spinal endoscopy based on deep learning. In the PPECD group, the height of the intervertebral cavity was measured before the operation and during the final follow-up, and the height change of the intervertebral cavity was evaluated. The relative angle and relative displacement of the sagittal plane of the operation segment in the PPECD group were measured, and the stability was evaluated. Using the cervical spine X-ray Kelvin degeneration evaluation criteria, before and during the final follow-up operation, the degeneration of the adjacent segments of the two groups was evaluated. A retrospective analysis of 26 cases of cervical radiculopathy that met the criteria for diagnosis, inclusion, and exclusion was reviewed. Among them, 11 cases were treated with PPECD surgery; 15 cases were treated with ACDF surgery. According to the evaluation method of Odom, the excellent rate and the good rate of the two groups were compared. According to the location of the lesion, the nerve detection or dull tip device is exposed under the armpit or shoulder of the nerve root, and the protruding nucleus pulposus tissue is explored and removed, and annulus fibrosus is performed as needed. After hemostasis was detected, the surgical instruments were removed and the surgical incision was completely sutured. Before the operation and 3 months after the operation, the final follow-up made no significant difference in the overall average height of the intervertebral cavity ( $F = 2.586$ ,  $P > 0.05$ ). The results show that posterior foramen expansion is an effective surgical method for the treatment of cervical spondylotic radiculopathy, but surgical adaptation requires strict management. In order to achieve satisfactory results, appropriate cases must be selected.

## 1. Introduction

Traditional surgery for the treatment of radiculopathy of cervical spondylosis includes anterior cervical decompression surgery, anterior cervical decompression plus fusion surgery, and posterior limited fenestration surgery. Anterior cervical discectomy can completely remove the intervertebral disc from the front, but there are complications such as segmental instability and local kyphosis after the operation, and the reoperation rate is about 10%. This article explores it

based on deep learning. The current development status of deep learning has great development prospects in computer vision, speech recognition, natural language processing, and other fields.

Percutaneous total endoscopy is the fastest-growing minimally invasive spinal surgery in recent years. Due to its more advanced technical design concept, the intraoperative visual field is clearer than that of microendoscopy. It has been widely used in lumbar degenerative diseases and obtained satisfactory clinical efficacy. With the pursuit of

clinicians to improve the efficacy of surgery, to control or reduce trauma, and the development of supporting devices for percutaneous total endoscopic surgery, the application of this technology to cervical degenerative diseases has become a reality. Posterior cervical disc herniation resection, alias posterior cervical disc herniation, nucleus pulposus, percutaneous posterior cervical disc herniation, and cervical disc herniation through posterior approach are mainly used for patients with lateral cervical disc herniation with shoulder and arm pain.

In recent years, with the advancement of minimally invasive spine surgery technology, the development of percutaneous endoscopic techniques has been remarkable, among which the cervical percutaneous endoscopic technique of disc nucleus pulposus removal for the treatment of cervical spondylosis has developed rapidly and has become one of the surgical modalities for the treatment of neurogenic cervical spondylosis. Deep learning is becoming the mainstream intelligent auxiliary diagnosis and intelligent diagnosis algorithm in the field of medical image processing. Matthew believes that deep learning uses a hierarchical structure of hidden variables to construct nonlinear high-dimensional predictors. His goal is to develop and train deep learning architectures for spatiotemporal modeling. Through stochastic gradient descent and parameter regularization to exit training deep structure, the goal is to minimize the mean square error of out-of-sample prediction. He first predicted sharp discontinuities in the traffic flow data, and secondly, he developed a classification rule that used the order book to deeply predict short-term futures market prices [1]. Wang believes that with the advent of advanced metering infrastructure, smart meters widely deployed in modern power grids continue to generate a large amount of electricity consumption data. He proposed a new concealed black box attack construction model, which targets the deep learning model for non-intrusive load monitoring based on smart meter data. Through comprehensive theory, practice, and comparative analysis, he demonstrated the profound impact of the proposed stealth attack structure on the energy analysis and decision-making process. His work reveals the loopholes of the ML model in the smart grid environment and provides valuable insights for safely adapting to the increasing popularity of artificial intelligence in modern power grids [2]. Thanh believes that student performance prediction is one of the most concerned issues in the field of education and training, especially in the field of educational data mining. He proposed a method of using various deep learning techniques to predict student performance. In addition, he also analyzed and introduced several data preprocessing techniques (such as quantile transformation and min-max scaler) and then extracted them into well-known deep learning models, such as long- and short-term memory (LSTM) and volume product neural network (CNN) to perform prediction tasks. The results show that this method has a good predictive effect, especially when using data conversion [3]. Alrahhal proposed a new convolutional neural network framework for COVID-19 detection using computed tomography (CT) images. The network uses the EfficientNet architecture as the

backbone structure to extract feature maps of different scales from the input CT scan images. In addition, different rates of ATRUS convolution are applied to these multiscale feature maps to generate denser features, which helps to obtain COVID-19 findings in CT scan images [4]. Chen C. believes that deep learning (DL) has continuously made significant progress in the field of intelligent sensing due to its huge advantages over traditional machine learning. The prospect of wide application puts forward requirements for the universal deployment of DL in various environments. Therefore, executing DL on mobile or embedded platforms has become a common requirement. He summarized the typical applications of deep learning with limited resources and pointed out that deep learning is an indispensable driving force for pervasive computing. Later, he reviewed the basic concepts of neural network capacity, generalization, and backpropagation and discussed the root cause of high DL computing overhead [5]. Carrillo proposed a deep learning tracking control scheme based on game theory, which allows the complete flight system to perform autonomous trajectory tracking tasks in consideration of saturated actuators, adversarial inputs, and nonquadratic cost functions [6]. However, these studies are not comprehensive enough for the medical processing system design of deep learning, and further improvements are needed.

The innovations of this paper are mainly reflected in the following. (1) Posterior cervical percutaneous endoscopic discectomy (PECD) is gradually being used to treat disc stenosis and cervical disc herniation. (2) With this procedure, blood loss during surgery can be reduced and damage to the anterior muscles can be minimized. (3) Micro-endoscopic discectomy can reduce the incision of the neck muscles, but narrow surgical access, poor microscopic field of view after intraoperative bleeding, and only two-dimensional images can be observed, lacking three-dimensional operation space, resulting in long operation time and increasing the risk of spinal nerve injury.

## 2. Methods and Experiments

**2.1. Deep Learning.** The main research task of biomedical information extraction relies on accurate disease named entity recognition. How to accurately identify disease named entities is a key research problem in medicine. Disease NER involves many complex problems, and it is often difficult to identify. Since medical texts usually contain medical vocabulary and phrases, it is not easy to identify word prefix and suffix information. Using character-level deep representation learning can effectively promote the recognition performance of the NER method. The advantage of learning character-level embedding is that it can capture content-specific features, which play an important role in learning rich text information [7]. Deep learning is to learn the internal laws and representation levels of sample data. The information obtained in the learning process is of great help to the interpretation of data such as text, images, and sounds. Its ultimate goal is to enable machines to have the ability to analyze and learn like humans and to recognize data such as text, images, and sounds.

Given a text composed of a character table, each word can be decomposed into character-level word elements. Then, according to the character lookup table, this character-level representation is connected together to become a word-level representation. Input  $X = [x_1, \dots, x_n]$ , the input weight is  $W = [w_1, \dots, w_n]$ ,  $b$  is the bias term, and  $f$  is the activation function; then the output of the neural unit  $t$  is  $h_t$ , and the expression is as follows [8]:

$$h_t = f\left(\sum_{i=1}^n w_i x_i + b\right). \quad (1)$$

The commonly used activation functions sigmoid, tanh, and relu are as follows [9]:

$$\begin{aligned} \sigma(x) &= \frac{1}{(1 + e^{-x})}, \\ \tanh(x) &= \frac{(e^x - e^{-x})}{(e^x + e^{-x})}, \\ \text{relu}(x) &= \max(ax, x). \end{aligned} \quad (2)$$

For the input sentence,  $P$  represents the output matrix from the two-way LSTM network. The number of labels is  $k$ . The probability of the  $i$ th word being assigned the label  $j$  is calculated as  $P_{i,j}$ . Define the expectation as [10]

$$s(x, y) = \sum_{i=0}^n A_{y_i, y_{i+1}} + \sum_{i=1}^n P_{i, y_i}. \quad (3)$$

The label probability matrix is as follows:

$$p(y|x) = \frac{e^{s(x,y)}}{\sum e^{s(x,y)}}. \quad (4)$$

The maximum probability of the tag sequence is as follows:

$$\begin{aligned} \log(p(y|x)) &= s(x, y) - \log\left(\sum e^{s(x,y)}\right) = s(x, y) - \text{logadd}(s(x, y)), \\ \ln p &= \ln(p_1 + p_2) = \ln(e^{\ln p_1} \times (1 + e^{\ln p_2 - \ln p_1})) = \ln p_1 + \ln(1 + e^{\ln p_2 - \ln p_1}). \end{aligned} \quad (5)$$

Maximize the probability to  $y^*$  to predict the potential tag sequence, as follows [11]:

$$y^* = \arg \max(\log P(y|x)). \quad (6)$$

The loss function of negative samples is as follows:

$$L_\theta(w_t, c_t) = \log \sigma(s(w_t, c_t; \theta)) + \sum_{i=1}^k \log \sigma(-s(\tilde{w}_t, c_t; \theta)). \quad (7)$$

Considering that the goal of NER is to mark the sequence, the linear chain CRF can calculate the global optimal sequence, so it is widely used to solve the NER problem, as follows [12]:

$$P(y|x) = \frac{1}{z(x)} \exp\left(\sum_{k=1}^k \lambda_k f_k(y_t, y_{t-1}, x_t)\right). \quad (8)$$

In the formula,  $f_k(y_t, y_{t-1}, x_t)$  is the feature function,  $\lambda_k$  represents the learning weight of the functional feature, and  $z(x)$  is the normalization factor as follows [13]:

$$z(x) = \sum_y \exp\left(\sum_{k=1}^k \lambda_k f_k(y_t, y_{t-1}, x_t)\right). \quad (9)$$

The objective function  $s(x, y)$  is used to calculate the probability of each label. The higher the value, the higher the probability of choosing the predicted label [14]. Its expression is as follows:

$$s(x, y) = \sum_{i=1}^n P_{i, y_i}^{sem} + \sum_{i=0}^n A_{y_i, y_{i+1}}. \quad (10)$$

The final calculation task is to find all possible output point estimates of  $y$  to maximize the conditional log-likelihood probability, as shown in the formula [15]:

$$y^* = \arg \max(\log P(y|x)). \quad (11)$$

In the document-level attention layer, let  $A$  denote the weight vector and  $A_{i,j}$  denote the similarity weight value between the current  $i$ th word  $h_i$  and the  $j$ th word  $h_j$  in the document. The softmax function is as follows [16]:

$$A_{i,j} = \text{soft max}(\text{score}(h_i, h_j)) = \frac{\exp(\text{score}(h_i, h_j))}{\sum_k (\text{score}(h_i, h_k))}. \quad (12)$$

The input of a single neuron is as follows:

$$y = \sum_{i=0}^{n-1} w_i x_i. \quad (13)$$

The different  $x_i$  parameters in the formula represent the input and output of the neuron, while  $w_i$  represents the interconnection weight between neurons, so the output of the neuron is as follows [17]:

$$y = f\left(\sum_{i=0}^{n-1} w_i x_i - \theta\right). \quad (14)$$

The  $\theta$  parameter in the formula is the bias term of the formula, its value is a real number, and  $f$  is an activation

function, which determines whether the output of this neuron is 1 or 0.

The perceptron formula is as follows:

$$o(x_1, \dots, x_n) = \begin{cases} 1, & w_0 + w_1x_1 + \dots + w_nx_n > 0, \\ -1, & \text{otherwise.} \end{cases} \quad (15)$$

The error formula is as follows:

$$E(\bar{w}) = \frac{1}{2} \sum_{d \in D} \sum_{k \in \text{output}} (t_{k,d} - o_{k,d})^2. \quad (16)$$

In the formula, outputs are the set of top-level output results and  $t_{k,d}$  and  $o_{k,d}$  are the output results of different training levels [18].

The structure of the conviction network model is hierarchical, and each layer is composed of several neurons. The probability relationship between the visual data  $v$  of the network and the hidden vector  $h$  is as follows [19]:

$$P(v, h^1, \dots, h^l) = \left( \prod_{k=1}^{l-2} P(h^k | h^{k+2}) \right) P(h^{l-2}, h^l). \quad (17)$$

The flow of the deep learning algorithm is shown in Figure 1. Deep learning has yielded many results in search technology, data mining, machine learning, machine translation, natural language processing, multimedia learning, speech, recommendation and personalization techniques, and other related areas. In general, the proportions of the three data sets are different for different data volumes. The training set is the data set used for deep learning network training. This data set determines how well the deep learning model can be trained and is the main component of the data set. The validation set is mainly used to verify tests and select parameters during deep learning model training. Under normal circumstances, the deep learning process is long and time-consuming. It is difficult to select the optimal parameters of the network by simply using loss in the training set during the training process. The set is new data that the network has never seen before. The evaluation of the deep learning model on the validation set can select network parameters with better generalization ability. The test set is generally used to evaluate the quality of the network, and the comparison of network capabilities is performed on this data set [20, 21].

**2.2. Research Objects.** A retrospective analysis of 26 cases of cervical spondylotic radiculopathy that met the criteria for diagnosis, inclusion, and exclusion was performed. Among them, 11 cases were treated with PPECD operation and 15 cases were treated with ACDF operation.

### 2.3. Experimental Method.

- (1) Contrast group: First, sterilize the curtain and cut it laterally to expose the anterior muscle membrane layer by layer. Use the vertebral body pump to open at the correct position and remove the intervertebral disc. Wipe off the end cartilage and cut the longitudinal ligament to expose the dura mater. After

decompression, the protruding tissue was bitten off and an artificial bone intervertebral fusion cage was inserted [22].

- (2) Observation group: Configure the head with the fluoroscopy head frame, take the abdomen and supine position, perform single-lumen endotracheal intubation under general anesthesia, and determine the surgical site (outside the vertebral arch cavity of the surgical site). First, the sterilization curtain is cut along the puncture point, the soft tissue is expanded, and the working sleeve is inserted to confirm the position of the opening of the sleeve (the outer edge of the interlayer space and the inner side of the outer joint). Use normal saline, use high-frequency electrodes to clean and remove soft tissues, exposing the "V" point. The dynamic system cuts off the upper and lower sides of the inside of the joint, and removes the nucleus pulposus. Stretch or shrink the dura mater. After high frequency hemostasis, please completely remove the compressive material. Pull off the working sleeve and lens, and sew. The two groups of patients came out of bed 12 hours after the operation and were discharged 3 days after the operation. Chest protectors must be worn within one month after discharge. The pain and movement caused by gravity must be avoided within 3 months [23]. Then carry out necessary experimental operations on the observation group, observe the resulting phenomenon, and compare it with the control group, compare the similarities and differences between the two, and analyze the reasons.

**2.4. Anesthesia and Position.** Local anesthesia (2% lidocaine 10 ml + 0.1% ropivacaine 10 ml + 0.9% saline 20 ml), take the prone position, hang the chest and abdomen, use a non-invasive Mayfield head frame or tape to fix the patient's head in a neutral position and keep it bend the head and neck forward about 20 degrees, fix the patient on the operating table from below the back, and pull the upper limbs distally along the axis of the body [24].

**2.5. Operation under the Mirror.** Use cervical vertebral rongeurs (Kerrison forceps), basket forceps or nucleus pulposus forceps to peel off the ligamentum flavum from its attachment points on the upper and lower lamina and articular processes from the inside to the outside to initially reveal the dural sac, the nerve root and the deep intervertebral space. After exploring hemostasis, the surgical instruments were removed, and the surgical incision was sutured across the entire thickness [25].

**2.6. ACDF.** General anesthesia endotracheal intubation, take the supine position, suspend the chest and abdomen, fix the patient's head in the neutral position with adhesive tape, and maintain the moderate over extension position of the head and neck, fix the patient on the operating table from below the back, and pull the bilateral upper limbs to the

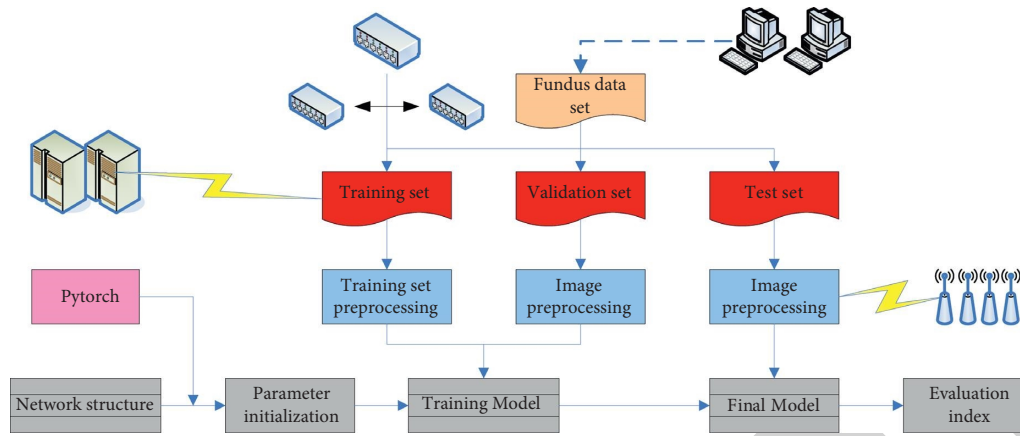


FIGURE 1: Deep learning algorithm flow.

distal end along the body axis. For routine disinfection and towel laying, a transverse incision of about 5 cm is taken at the right front of the neck according to the plane of the surgical segment, and the platysma muscle is cut layer by layer.

After blunt separation along the potential gap between the tracheoesophageal sheath and the vascular sheath, it reaches the prevertebral fascia. Conventionally, vertebral nails are placed at the upper edge of the lower endplate of the upper vertebral body and the lower edge of the upper endplate of the lower vertebral body. The responsible intervertebral disc tissue was removed to the posterior longitudinal ligament for spinal canal expansion and decompression.

After carefully separating and protecting the dural sac, the posterior longitudinal ligament at the intervertebral space plane was smoothly cut off and removed. The decompression window was used to decompress the bilateral posterior wall to the uncinate vertebral joint. After exploration again, it was found that the spinal canal was unobstructed, the dural sac was swollen, and the pulsation was satisfactory. After the bone block was trimmed to an appropriate size, it was implanted into the responsible intervertebral space. The anterior cervical titanium plate with an appropriate length was tiled in front of the vertebra. The internal fixation position of C-arm fluoroscopy was satisfactory. After repeated flushing with normal saline and complete hemostasis, a drainage tube was routinely reserved for the neck incision, the neck incision was sutured layer by layer, and covered and fixed with gauze dressing. This is because the incision retains the drainage tube, and the neck incision is sutured layer by layer, covered and fixed with gauze dressing, which can effectively accelerate the healing of the wound.

**2.7. Measurement of Imaging Parameters.** The image processing of the cervical spine is shown in Figure 2. On the PscView imaging system workstation, obtain the patient's cervical spine CT three-dimensional reconstruction image data and cervical spine MRI image data, and perform imaging data measurement [26, 27]. On the corresponding

images obtained, first, establish a sagittal plane parallel to the central axis of the human body with the midline of the spinous process, and then establish a transverse section parallel to the horizontal plane with the C3/4, C4/5, C5/6, and C6/7 intervertebral spaces.

## 2.8. Observation Indicators and Evaluation Standards. (1)

McNabb's therapeutic effect: 3 months after the operation, according to the modified McNabb's assessment of the surgical effect of the two groups of patients, the symptoms disappeared and you can live before the disease; the symptoms are mild, the activities are slightly reduced, and there is no affect work and life. Because the symptoms are improved, activities are restricted, which affects work and life. The difference is that there is no difference before and after treatment, and even the state deterioration.

(2) Cervical spectacle angle (CA): The angle between the C2 lower end plate and the C7 lower end plate is measured by the 4-line method. NDI Index: using NDI scaling, the neck dysfunction of the two groups was evaluated before and after 3 months. The surgical index and ratio contained 10 items worth 5 points respectively. Cervical spine flexion and extension activity (ROM): the two groups received X-ray examinations before and 3 months after the operation, and were performed by the surgical method of measuring cervical spine flexion and extension activities.

(3) Complications: The occurrence of postoperative complications (traumatic edema, epidural hematoma, epidural hematoma, nerve root rupture, etc.) was recorded in two groups.

## 2.9. Data Collection.

(1) Collection of case data: Sort out the case data that meet the inclusion and exclusion criteria, record the age, gender, course of disease, and diseased segment of the two groups respectively, and measure the physiological curvature of the two groups before

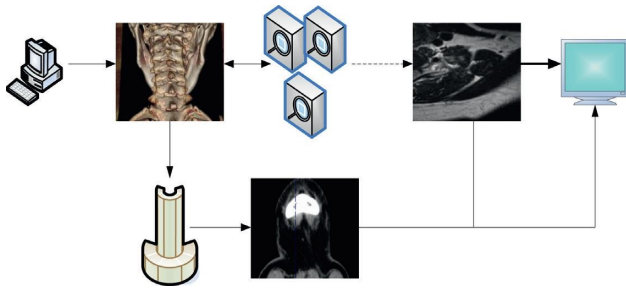


FIGURE 2: Cervical spine image processing.

surgery, and read the pictures before surgery according to Kellgren Degradation classification standards are used for classification. Summarize the patient's operation time, fluoroscopy time, intra-operative blood loss, hospitalization costs, and the number of complications; check the previous follow-up records to summarize the preoperative, postoperative 2 hours, 1 week, 1 month, 3 months, and 6 months. The neck VAS score and upper limb VAS score at 12 months and the last follow-up, as well as the NDI score at 1 week, 1 month, 3 months, 6 months, 12 months, and the last follow-up, and the number of complications in the two groups. And through the image reading of the last follow-up, the two groups of patients were again classified according to the Kellgren degeneration grading standard, and the physiological curvature was measured; and the stability and intervertebral space height of the PPECD group were measured, and evaluated according to Odom's grading evaluation method the number of cases with excellent, good, acceptable and poor.

- (2) Follow-up measures: Follow-up of patients through various channels such as WeChat, telephone and follow-up software, including completing the VAS score sheet, NDI score sheet questionnaire, the last Odom's grading evaluation sheet, and imaging examination for the different time periods mentioned above after surgery. Follow up every 3 months after discharge.

**2.10. Statistical Processing.** The variance of intraoperative blood loss, incision length, and time in bed was uneven, using approximate  $t$  test. The two groups were compared by sex, using chi-square test. The two groups of diseased segments, Kellgren cervical degeneration classification, the last follow-up Odom's clinical efficacy evaluation, and the comparison of complications were all performed by Fisher's exact test. The comparison of the cervical spine physiological curvature, the height of the intervertebral space, the relative sagittal angle, and the sagittal displacement before the operation and the last follow-up within the group was performed by paired  $t$  test. The neck VAS score, upper limb VAS score, and NDI score were analyzed by variance analysis at each time point before and after operation in the two groups.

### 3. Results

Table 1 shows the comparison of the efficacy of Macnab between the two groups. Compared with the control group, the effect of Macnab in the observation group was not statistically different ( $P > 0.05$ ). As can be seen from the table, the efficacy of the observation group was better compared to the control group, indicating that the results of the study were favorable for the treatment of the patients.

During the training of the CRF model, there are two parameters that affect the performance of the model,  $c$  represents the hyperparameter related to the fitting rate, and  $f$  represents the cut-off threshold in feature selection. In order to find the best combination of  $c$  and  $f$ , we test different values of  $c$  and  $f$  to test NER performance changes. The final best combination of  $c$  and  $f$  is  $c = 1.5$  and  $f = 3$ , and the F1 score at this time is 74.5%. The result is shown in Figure 3. Figure 3 shows the test results of the model, in which the CRF model is effectively combined with deep learning algorithms to add accuracy to the experiment.

The dimensional performance comparison between word embedding and BiLSTM is shown in Figure 4. In terms of word embedding dimension, set from 50 to 200 respectively. When the size is equal to 100, the overall performance of the model is the best, with an F1 score of 78.95%. In the dimensions of BiLSTM, they are set to 50 to 200 respectively. The results show that when the dimension of the BiLSTM network is 100, the F1 value is best 80.22%.

In order to study the influence of the vertebral perforation diameter on the stress distribution of the cancellous bone inside the vertebral body, we selected the bone tunnel sidewall with the stress concentration inside the vertebral body as the research object, and measured the vertebral bone tunnel sidewall with different perforation diameters. The trend of Von Mises stress distribution from the ventral to dorsal path is shown in Figure 5. When the cervical vertebrae were flexed, the lateral walls of the two model tunnels showed stress concentrations in the ventral and dorsal portions of the vertebral bodies. The Von Mises stress value increases with the increase of the tunnel diameter. The maximum stress of the A10 and B10 models are 3.58 MPa and 3.74 MPa, respectively, and the maximum stress of the complete model in this path is 0.9 MPa.

The surface location of nerve block is shown in Figure 6. The PPECD group had less blood loss, smaller incision length, hospitalization time, and bed time than the ACDF group, and the hospitalization cost was also lower than that of the ACDF group. However, the operation time of the PPECD group was longer than that of the ACDF group, and the fluoroscopy time was longer than that of the ACDF group. Through the statistical analysis of the measurement data of the intervertebral space height, the relative sagittal plane angle, relative displacement, and other indicators in the PPECD group, the PPECD group postoperative intervertebral space height, the sagittal plane relative angle and relative displacement were compared with those before the operation, and there was no difference. It is statistically significant, and the relative angulation and relative displacement of the sagittal plane are compared with the

TABLE 1: Comparison of the efficacy of Macnab between the two groups.

Group	Excellent (%)	Good (%)	Middle (%)	Poor (%)	Excellent and good (%)
Control group	45.45	36.36	9.09	9.09	81.81
Observation group	40.00	26.67	20.00	13.33	66.67

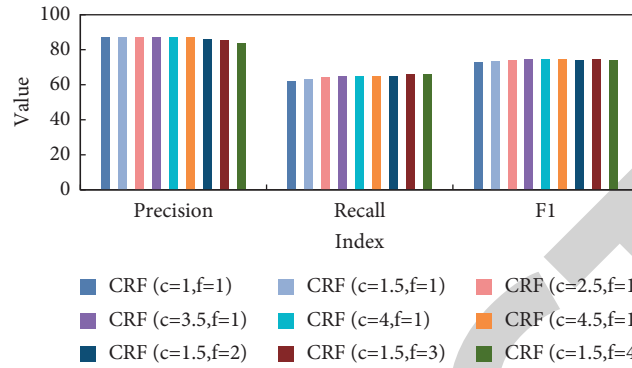


FIGURE 3: Model test results.

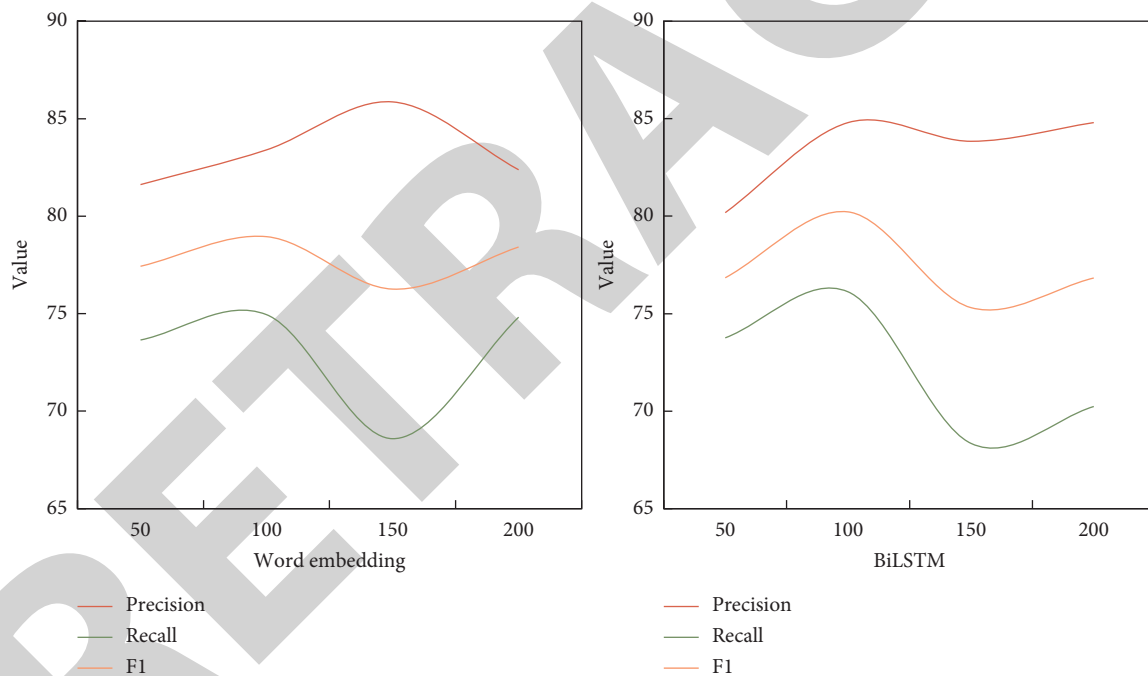


FIGURE 4: Dimensional performance comparison between word embedding and BiLSTM.

reference value of instability, which are all smaller than the reference value of instability, and the differences are statistically significant, indicating that there is no instability in the surgical segment after PPECD.

The measurement distance of the measured parameters after the parameters on the left and right sides are combined is shown in Table 2. After combining the left and right parameters, calculate the average distances from the V point to the lateral edge of the adjacent lower pedicle isthmus as  $1.54 \pm 0.20$  mm,  $2.18 \pm 0.27$  mm,  $2.99 \pm 0.18$  mm,  $5.55 \pm 0.16$  mm, from C3/4~C6/7 showed a gradually increasing trend, and the distance of C6/7 was the largest.

ACDF is also known as anterior decompression and fusion for cervical spondylosis, which is a kind of orthopedic surgery.

Table 3 shows the VAS score and improvement rate of neck, shoulder and upper limb pain. All patients alleviated the pain of the upper limbs to varying degrees. The average VAS scores of the two groups on the day after the operation were greatly improved compared with those before the operation ( $P < 0.05$ ), and with the extension of the follow-up time, there was also a further improvement. There was no significant difference in the improvement rate of VAS scores ( $P > 0.05$ ).

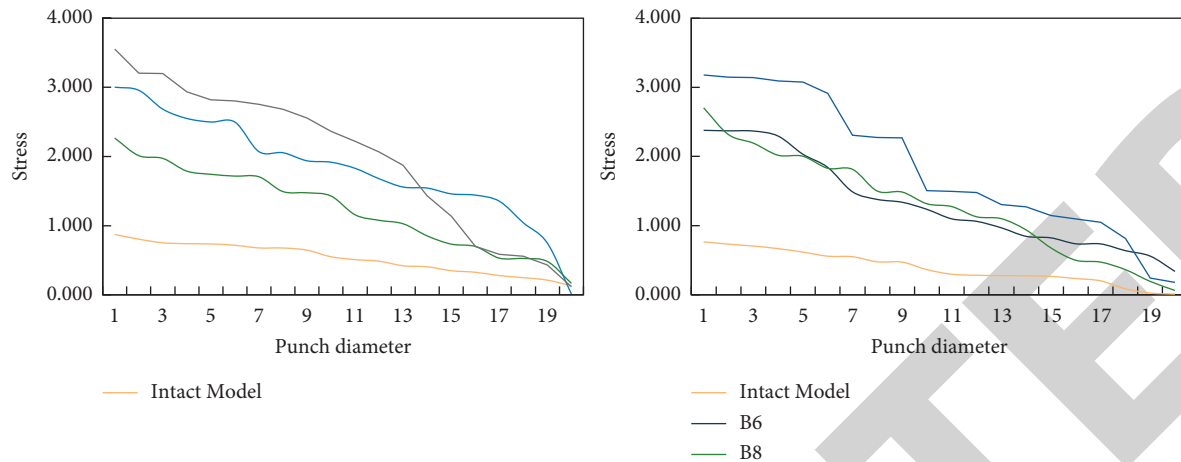


FIGURE 5: Trend of stress distribution.

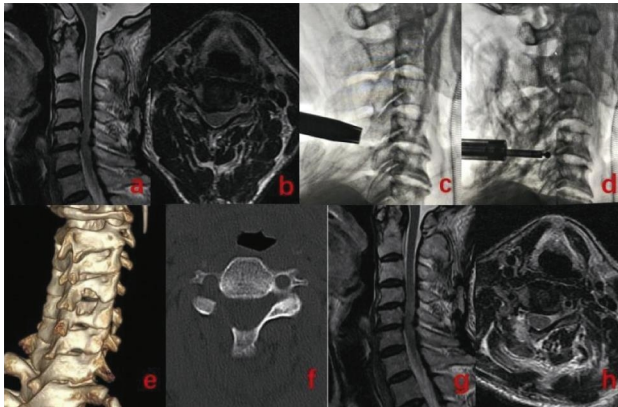


FIGURE 6: Surface location of nerve block.

The VAS score of wound pain is shown in Figure 7. The VAS score of trauma pain in the PPECD group on the first day after surgery was significantly lower than that in the ACDF group ( $P < 0.05$ ), but there was no significant difference between the two groups at 1 week, 1 month, and 3 months ( $P > 0.05$ ).

The operation time of the patients in this group is 100–150 minutes, the intraoperative blood loss is 10–35 mL, and the postoperative hospital stay is 3–5 days. There are no complications such as spinal cord and nerve root injury, and the incision site heals well. Table 4 shows the patients' VAS, JOA pain scores, and NDI improvement scores before and after surgery. A summary comparison with the previous VAS scores was made to better highlight the authenticity of the experimental results.

The VAS score of patients after surgery was significantly lower than that before surgery, and the JOA score was significantly higher than before surgery. The incidence of symptoms before and after NDI surgery was significantly reduced, and the difference was statistically significant ( $P < 0.05$ ). The image data of a typical situation is shown in Figure 8.

The height of the intervertebral space and the curvature of the cervical spine at the surgical segment are shown in

Figure 9. Disc height and cervical curvature were unchanged preoperatively, at three months postoperatively, and at the last follow-up observation. The degree of activity segment is shown in Figure 10. Before the operation and 3 months after the operation, the final follow-up made no significant difference in the overall average height of the intervertebral cavity ( $F = 2.586$ ,  $P > 0.05$ ). Before the operation and 3 months after the operation, there was no significant difference in the overall mean value of the neck curvature due to the final follow-up ( $F = 2.680$ ,  $P > 0.05$ ). Before the operation and 3 months after the operation, the overall average of the last follow-up upper segment movement was not statistically significant ( $F = 1.162$ ,  $P > 0.05$ ). Before surgery and 3 months after surgery, the overall average of the lower migration rate at the last follow-up was not statistically significant ( $F = 0.167$ ,  $P > 0.05$ ). Combined with preoperative MRJ and other imaging studies, clarifying the anatomical location of the intervertebral disc herniation and nerve roots can help improve the safety of surgery and effectively reduce the occurrence of nerve root damage.

Table 5 shows the distance of re-examination of cervical spine CT three-dimensional reconstruction to remove bone after operation. In the 4 patients treated with PPECD, the protruding nucleus pulposus tissue was completely removed during the operation, the nerve root was completely decompressed, the bleeding was completely stopped during the operation, and there was no leakage of cerebrospinal fluid due to dural sac injury or dura mater.

#### 4. Discussion

When the operation is performed on the epidural plexus, it is easy to cause bleeding of the venous plexus and affect the field of vision of the operation. Therefore, the control of the bleeding of the jugular plexus should be the focus of the operation. In this step, the use of radiofrequency or hemostatic agents is effective, and the pressure can also be increased by temporarily sealing the pipeline to achieve the purpose of hemostasis. During disc exploration and discectomy, the oblique section of the working pipe can be used as a protector to protect the outlet nerve root. In order to

TABLE 2: The measured distance of the measured parameters after the parameters on the left and right sides are combined.

Segments	<i>a</i>	<i>b</i>	<i>c</i>	<i>d</i>
C3/4	$2.31 \pm 0.15$	$1.54 \pm 0.20$	$4.57 \pm 0.21$	$3.82 \pm 0.30$
C4/5	$1.98 \pm 0.20$	$2.18 \pm 0.27$	$4.76 \pm 0.26$	$3.72 \pm 0.32$
C5/6	$1.95 \pm 0.16$	$2.99 \pm 0.18$	$5.65 \pm 0.22$	$3.14 \pm 0.27$
C6/7	$1.13 \pm 0.15$	$5.55 \pm 0.16$	$4.96 \pm 0.29$	$3.07 \pm 0.28$

TABLE 3: VAS score and improvement rate of neck, shoulder and upper limb pain.

	PPECDF group		ACDF group	
	VAS score	ROC (%)	VAS score	ROC (%)
1d	$1.54 \pm 0.51$	52.8	$2.32 \pm 0.66$	56.1
1 week	$1.91 \pm 0.39$	63.2	$1.86 \pm 0.46$	66.7
1 month	$1.74 \pm 0.41$	64.3	$1.81 \pm 0.61$	70.4
3 months	$1.13 \pm 0.28$	81.2	$1.44 \pm 0.52$	83.5

ensure the effect, adequate decompression is the key point of surgery.

In the establishment of the surgical channel, the foramen should be enlarged and formed under the microscope first, and the protruding nucleus pulposus can be removed only after the ligamentum flavum is removed. According to the anatomical characteristics and clinical experience, the protruding operation on the shoulder is safer, while the axillary and free types require more ligamentum flavum removal, which increases the risk of nerve root injury. Therefore, combining preoperative MRJ and other imaging studies to clearly determine the anatomical position of the intervertebral disc herniation and the nerve root will help improve the safety of the operation and effectively reduce the occurrence of nerve root injury.

The advantages of PECDF are mainly: (1) The introduction of water medium, while the water pressure can avoid massive bleeding during the operation. (2) The field of view can be enlarged under the endoscopy, and the doctor can clearly distinguish the tissue, combined with radiofrequency to stop bleeding, and reduce the damage to the tissue. (3) The operation does not require stripping of soft tissues, which can effectively protect the physiological structure of the spine. (4) Preserve motion segments and avoid segment fusion, thereby avoiding degeneration of adjacent segments. (5) Promote rehabilitation and ensure satisfactory results. At the same time, speed up the patient's work and life to return to normal.

In addition, this study was followed up for less than one year, and the impact of adjacent segments could not be evaluated. In-depth long-term research is needed. However, when applying PECDF, it should be noted that: (1) The operation needs to have a sense of three-dimensional space and can be proficient in open surgery. (2) Because of the stenosis of the surgical indication, it is necessary to choose to be located in the intervertebral foramen or external soft protrusion. However, from the current follow-up results, the patient's recovery after the operation is also very successful.

Effectively avoid interference with the spinal canal, and only need to slightly stretch the nerve roots without affecting the dural sac; at the same time, the soft protrusion facilitates

decompression and reduces the use of drills to ensure the successful completion of the operation; if the technique is skilled. For those with bony stenosis of the intervertebral foramen, the surgical operation still needs to be gentle. The contraindication of PECDF is a herniated intervertebral disc attached to the front of the spinal cord in the central part. ACDF is required to remove the nucleus pulposus tissue.

The degeneration of cervical intervertebral disc causes the herniated disc and the secondary stenosis of the nerve root canal is the main cause of nerve radiation-like pain in the upper limbs. Metabolism of the degenerated intervertebral disc tissue is disordered, which in turn produces inflammatory mediators that stimulate the nerve roots and cause nerve root pain. The upper limb muscle strength, skin tactile decrease and muscle strength decrease are mainly thought to be caused by nerve root compression.

ACDF completely removes the intervertebral disc from the front to relieve the compression of the nerve root, but due to the limitation of intraoperative exposure and traction, the compression of the nerve root cannot be completely removed under direct vision, and bleeding occurs during the operation, which will cause postoperative inflammatory substances. Aggregation affects the curative effect of postoperative surgery. The existing finite element model is smaller than the in vitro experimental results in flexion, extension, rotation, and lateral bending. This is because the number of in vitro experimental samples is limited and the difference is large.

There is also a certain gap between them, but the overall distribution trend of the results is more consistent. Secondly, the current digital modeling technology cannot fully simulate the geometric properties and material properties of the normal cervical spine structure, and ignores the influence of muscles on the cervical spine, which inevitably has certain limitations, but for simple mechanical loading simulation, its accuracy and the reliability has reached sufficient experimental requirements.

MED surgery has a small operating space, and the surgical field is enlarged by 8 to 16 times. A small amount of bleeding can fill the entire surgical field, which will cause inconvenience to the operator. When the MED operation is first carried out. Some doctors spend more time on hemostasis than the operation. So it is very important to completely stop bleeding during the operation. After decompression of the intervertebral foramina during the operation, it is necessary to carefully explore whether there is a herniated disc, the part and type of herniation. For those who have prolapsed intervertebral disc and dissociated in the intervertebral space, it is necessary to completely clean up the intervertebral disc fragments and completely decompress the nerve roots. Anterior surgery does not cut the

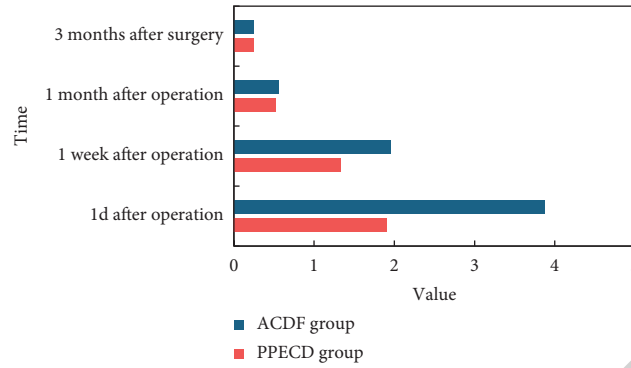


FIGURE 7: VAS score of wound pain.

TABLE 4: Patients' VAS, JOA pain scores, and NDI improvement scores before and after surgery.

Number of cases	VAS score	JOA score	NDI score
Before therapy	$5.58 \pm 0.44$	$10.74 \pm 0.79$	$47.67 \pm 3.68$
After treatment	$2.4 \pm 0.46$	$14.13 \pm 0.61$	$8.76 \pm 3.57$



FIGURE 8: Image data of a typical situation.

posterior longitudinal ligament and the annulus fibrosus, the disc fragments protruding from the spinal canal cannot be removed, and the nerve roots are not completely released.

This may be one of the reasons for the poor effect of anterior surgery in the treatment of lateral disc herniation. However, with the improvement of people's living standards and higher requirements for surgical experience, the minimally invasive and precise surgery has become the goal of surgical doctors under the premise of ensuring clinical efficacy. In this study, the last VAS score and NDI score of the PPECDF group and the ACDF group were not statistically

different, and the excellent and good rates of the two groups were 86.36% and 85%, respectively, indicating that the two surgical methods have the same effect. Compared with ACDF, the advantage of the PPECDF group is first reflected in the anesthesia method. PPECDF can be operated under local anesthesia, avoiding the risk of general anesthesia. The last follow-up imaging measurement in the PPECDF group showed that the height of the intervertebral space did not change significantly compared with that before the operation, indicating that the PPECDF operation had little interference with the responsible disc.

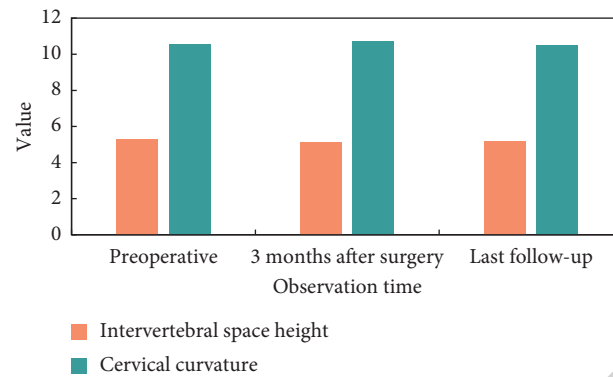


FIGURE 9: The height of the intervertebral space and the curvature of the cervical spine.

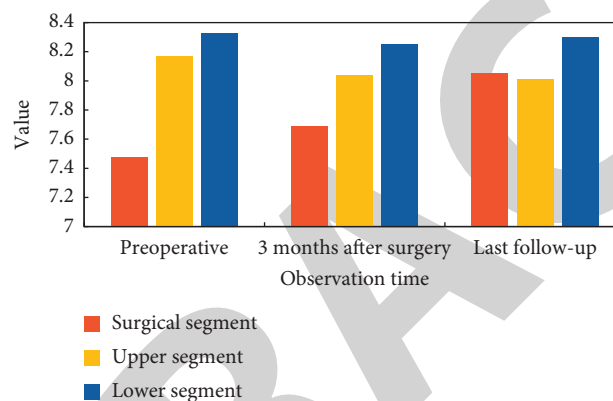


FIGURE 10: Motion segment degree.

TABLE 5: Postoperative re-examination of cervical spine CT three-dimensional reconstruction of the bone removal distance.

Segments	Outside		Superior		Down	
	Pre operative	Post operative	Pre operative	Post operative	Pre operative	Post operative
Neck4/5	2.5	3.9	5.1	3.4	4.2	6.7
Neck5/6	3.2	4.7	5.4	3.7	2.6	5.7
Neck6/7	4.9	6.8	3.7	1.7	2.9	5.8

## 5. Conclusions

Posterior foraminal expansion angioplasty is an effective method for the treatment of intractable cervical spondylomyelopathy. It can directly remove the proliferative osteophytes and scar tissues of the facet joints, can relax the nerve roots directly, ensure the decompression effect, the operation difficulty is relatively low, which can effectively protect the integrity of other bones and soft tissues of the cervical spine, and reduce the instability and instability of the cervical spine. Risk of complications such as worsening degeneration. In short, posterior foraminoplasty is an effective surgical method for the treatment of cervical spondylotic radiculopathy, but the surgical indications must be strictly controlled, and the appropriate cases must be selected to achieve satisfactory results. MED surgical procedures have a small surgical space and expand the surgical area by 8 to 16

times. A small amount of bleeding can fill the entire surgical area and can cause inconvenience to the operator. When performing a MED operation for the first time. Some surgeons spend more time on stopping bleeding than on the procedure. It is very important to stop bleeding completely during the procedure. During the operation, try to protect the rear soft tissue structure and combine with the internal fixation system to maintain the stability of the cervical spine and reduce the occurrence of complications.

## Data Availability

No data were used to support this study.

## Conflicts of Interest

The author states that this article has no conflicts of interest.

## Retraction

# Retracted: Qualitative Diagnosis of Liver Tumors Based on Ultrasound-Guided Automatic Biopsy

### Journal of Healthcare Engineering

Received 29 August 2023; Accepted 29 August 2023; Published 30 August 2023

Copyright © 2023 Journal of Healthcare Engineering. This is an open access article distributed under the Creative Commons Attribution License, which permits unrestricted use, distribution, and reproduction in any medium, provided the original work is properly cited.

This article has been retracted by Hindawi following an investigation undertaken by the publisher [1]. This investigation has uncovered evidence of one or more of the following indicators of systematic manipulation of the publication process:

- (1) Discrepancies in scope
- (2) Discrepancies in the description of the research reported
- (3) Discrepancies between the availability of data and the research described
- (4) Inappropriate citations
- (5) Incoherent, meaningless and/or irrelevant content included in the article
- (6) Peer-review manipulation

The presence of these indicators undermines our confidence in the integrity of the article's content and we cannot, therefore, vouch for its reliability. Please note that this notice is intended solely to alert readers that the content of this article is unreliable. We have not investigated whether authors were aware of or involved in the systematic manipulation of the publication process.

Wiley and Hindawi regrets that the usual quality checks did not identify these issues before publication and have since put additional measures in place to safeguard research integrity.

We wish to credit our own Research Integrity and Research Publishing teams and anonymous and named external researchers and research integrity experts for contributing to this investigation.

The corresponding author, as the representative of all authors, has been given the opportunity to register their agreement or disagreement to this retraction. We have kept a record of any response received.

### References

- [1] B. Peng, "Qualitative Diagnosis of Liver Tumors Based on Ultrasound-Guided Automatic Biopsy," *Journal of Healthcare Engineering*, vol. 2021, Article ID 8585887, 12 pages, 2021.

## Research Article

# Qualitative Diagnosis of Liver Tumors Based on Ultrasound-Guided Automatic Biopsy

Bin Peng 

The Central Hospital of Xiaogan, Xiaogan, Hubei 432000, China

Correspondence should be addressed to Bin Peng; nome2021@163.com

Received 11 October 2021; Revised 29 October 2021; Accepted 30 October 2021; Published 18 November 2021

Academic Editor: Weiwei Cai

Copyright © 2021 Bin Peng. This is an open access article distributed under the Creative Commons Attribution License, which permits unrestricted use, distribution, and reproduction in any medium, provided the original work is properly cited.

The goal of this study was to see if automatic biopsy guided by ultrasound could be used to provide a qualitative diagnosis of a liver tumor. *Methods.* A total of 40 patients (101 focuses) were treated with automatic liver parenchyma biopsy under ultrasound guidance, and the correlation between pathological outcomes and ultrasound images was investigated. The lesion size in the observation group was compared to that in the control group using conventional ultrasound ( $P > 0.05$ ), and there was no significant difference. Under contrast-enhanced ultrasound (CEUS), there was no statistically significant difference in lesion size between the observation and control groups ( $P > 0.05$ ). The difference in lesion size between the conventional ultrasonography and CEUS observation groups was statistically significant ( $P 0.05$ ). *Conclusion.* Ultrasound-guided automated biopsy of the liver parenchyma is a simple and effective procedure with fewer problems and a high diagnostic rate, and it deserves to be promoted clinically.

## 1. Introduction

In recent years, ultrasound-guided automated biopsy has become widely used in qualitative diagnosis of abdominal and pelvic space-occupying focus. The mortality rate of liver cancer has been rising in European and American countries in recent years. In China, the frequency of liver cancer remains high, and the overall incidence of liver cancer is expected to continue to climb. Hepatic hemangioma is a frequent benign liver tumor caused by a congenital blood vessel abnormality. Cavernous hemangioma, sclerosing hemangioma, hemangioendothelioma, and capillary hemangioma are the pathological classifications for hepatic hemangioma. The bulk of them are cavernous hemangiomas of the liver, and the last three are uncommon in clinic. Cavernous hemangioma is the most common type of hepatic hemangioma seen in clinic. Hemangioma is more frequent in the liver than in other organs. Because the tumors are so small, the majority of patients do not experience any symptoms. Liver cancer and liver hemangioma are two distinct diseases with distinct occurrences, progressions, treatments, and prognoses. As a result, in clinical work,

determining the nature of focused focus detected in liver tests is quite useful in guiding treatment.

To date, surgical resection remains the most effective treatment for primary liver cancer. However, due to the influence of tumor scope, location, and liver function, the patients who can be given surgical treatment only account for about 20% of HCC patients, and the true success rate of surgical resection is only 30%, with a high recurrence rate after surgery [1]. It has been reported in the literature [2] that the sensitivity, specificity, and negative predictive value of benign and malignant tumors identified by morphology, site, boundary, and echo of the mass were 98%, 68%, and 99%, respectively. In addition, morphological changes of the mass after pressure from the probe can also help distinguish benign from malignant. Several diagnostic criteria have been proposed in the literature [3], including visualization, relative brightness, boundary uniformity, and lesion size of focus compared with elastic and two-dimensional images. These researchers found that the size of malignant tumors was larger than that of conventional ultrasound on elastic images. Literature [4] also proposed an elastic classification method based on the degree and distribution of strain, with

the sensitivity, specificity, and accuracy of 87%, 90%, and 88%, respectively, for malignant diagnosis of breast tumor based on the elastic score of 3-4.

Clinically, imaging examination methods such as ultrasonography and CT are used to diagnose liver space-occupying focus, although these approaches are not suitable for differentiating between benign and malignant foci [5]. Ultrasound-guided percutaneous needle biopsy has become a crucial diagnostic tool in clinical practice for qualitative diagnosis of liver space-occupying focus, thanks to the widespread use of interventional ultrasound in clinical practice. The manifestations of contrast-enhanced ultrasound (CEUS) of primary liver cancer are characteristic, mainly characterized by rapid overall enhancement of the arterial phase, which has a short duration and hypoechoic changes in the portal phase, showing the overall change of "fast in and fast out" [6]. However, the contrast manifestations of some primary liver cancers are atypical and difficult to distinguish from benign focus. On the basis of CEUS, we used the analysis software to analyze and compare the contrast-related data. To further explore the clinical application value of quantitative analysis of CEUS in qualitative diagnosis of liver tumors.

The current study is unique in that it is the first to use ultrasound-guided automatic biopsy for the qualitative diagnosis of abdominal and pelvic space-occupying foci. Its use in the qualitative diagnosis of liver tumors, on the other hand, is restricted. The goal of this research is to provide a reference for clinical qualitative diagnosis of liver tumors using ultrasound-guided automatic biopsy.

## 2. Literature Review

*2.1. Application Progress of Contrast-Enhanced Ultrasound in Interventional Ultrasound.* In recent years, CEUS technology has become increasingly mature in the clinical diagnosis of many diseases. At the same time, interventional ultrasound has been widely used in clinical diagnosis. The close combination of CEUS and interventional ultrasound can find new advantages in clinical diagnosis.

*2.1.1. Application of Contrast-Enhanced Ultrasound in Percutaneous Transhepatic Biliary Puncture and Drainage.* The most common causes for surgical jaundice in patients are biliary tract obstruction caused by inflammation, tumor, and calculus, which can cause increased pressure in small bile ducts and capillary bile ducts, dilation and rupture of lumens, and then bile overflow to small veins and reflux to increased blood circulation and biliary tract pressure. Patients gradually suffer from decreased hepatocyte function and increased heme, with clinical manifestations including obvious yellow staining of skin and sclera and skin pruritus.

Reasonable use of CEUS for accurate catheterization and drainage, judging the drainage range and predicting the drainage effect will have an important impact on the prognosis of patients. Some scholars used rabbit as the animal model for research and explored whether bile duct perfusion studied by CEUS via biliary tract is feasible. The

rabbits were divided into four groups according to the concentration of diluted contrast agent. After administration, the perfusion of contrast agent in intrahepatic bile duct was observed, including whether the contrast agent completely filled the bile duct, whether it overflowed and the satisfactory duration of imaging. Finally, it was concluded that it was feasible to apply CEUS to the biliary system to study bile duct perfusion, and it was considered that the concentration of contrast agent should not be too low, and the imaging effect was best with a concentration of 1/200 dilution [7].

*2.1.2. Application of Contrast-Enhanced Ultrasound in Percutaneous Nephrostomy.* Congenital abnormalities of the urinary system, stones, tumors, trauma, and other common causes of urinary system obstruction, resulting in different degrees of kidney water, further development will cause renal damage, and even the late occurrence of uremia. In order to relieve the clinical symptoms of patients with hydronephrosis, control infection, improve renal function, or prepare for the removal of the cause of obstruction, percutaneous nephrostomy under the guidance of B ultrasound is often required to directly drain the urine to relieve the compression on the renal parenchyma [8].

Percutaneous nephrostomy can not only protect the renal function but also greatly improve the quality of life of patients. Although percutaneous nephrostomy can be completed in most cases under the guidance of conventional ultrasound, the ability of conventional ultrasound is often limited when the puncture point and puncture direction are selected in some cases of mild hydronephrosis, upper calyx sputum production, and high kidney [9, 10]. Therefore, conventional ultrasound-guided percutaneous nephrostomy cannot fully meet the clinical needs, and it is necessary to explore a safer and more reliable puncture-catheter drainage method, so as to provide further help for finding the cause of obstruction.

*2.1.3. Application of Contrast-Enhanced Ultrasound in Radiofrequency Ablation of Liver Cancer.* Tumor tissue ablation is another significant component of interventional ultrasound, and hepatocellular carcinoma ablation has been widely used in clinical practice. At present, the ablation treatment methods for liver cancer with more clinical applications include radio frequency activation (RFA), microwave coagulation activation (MWA), cryoablation and high intensity focused ultrasound activation (HIFU). The basic principle of most treatment methods is to destroy the tumor tissue using its unique physical characteristics to cause coagulation and necrosis of the tumor tissue for local treatment. Among them, RFA was carried out early and to a certain extent it was representative.

The efficacy of RFA in the treatment of liver cancer is also closely related to the tumor size. Therefore, we should decide whether RFA is feasible or not to improve the cure rate of RFA for liver cancer on the premise of fully understanding the lesion size. In the previous study [11], a total of 222 focuses were grouped and compared in 167 patients who met

the treatment indications of RFA. Among the 81 cases with 110 focuses that underwent CEUS before RFA, and 86 cases with 112 focuses that did not undergo CEUS before RFA, the results showed that seven new focuses were found during CEUS examination, which were not found in conventional ultrasound examination or enhanced CT examination. Moreover, 56.4% of the focuses were found to be larger than conventional ultrasound, and 49.1% of the focuses were more irregular in boundary than conventional examination.

Literature [12] A retrospective study was conducted to analyze 64 ablation cases. The subgroups in this study found that the residual tumor rate in the CEUS group at the end of treatment was 0%, while the residual tumor rate in the non-CEUS group was 16.7%. The results showed that performing CEUS immediately at the end of RFA treatment to evaluate the ablation effect could effectively reduce the incidence of residual tumors after thermal ablation, and provide accurate information for RFA operators to guide ablation treatment. Besides, a study evaluating the intraoperative application of CEUS found that CEUS can immediately evaluate the ablation effect, not only without increasing the patient's cost, but on the contrary, it can reduce the treatment cost for patients with liver cancer and alleviate the economic burden on patients [13].

In summary, CEUS has broken the traditional concept that imaging of the target area can be achieved by injection of contrast agent through the external elbow vein, and imaging can also be provided with valuable information for clinical diagnosis and treatment by injection through non-vascular lacunar ducts. Ultrasound-guided therapy has been increasingly accepted and recognized clinically because of its advantages such as small trauma, no radiation, accuracy and real-time dynamics. Reasonable and standardized application of CEUS in interventional ultrasound diagnosis and treatment and playing the important role of interventional CEUS not only can improve the disease diagnosis efficiency, but also can efficiently guide clinical treatment, provide the most valuable information for clinical doctors and bring the least pain and maximum benefit to patients.

**2.2. Pathogenesis of Liver Cancer.** Primary liver cancer is one of the most common malignant tumors in China, coming in second only to lung cancer in terms of incidence. According to statistics, China has the highest incidence of liver cancer in the world, with more males than females. With recent advances in molecular biology, virology, and genetics, it is now widely assumed that primary liver cancer is caused by a combination of multifactor, multipathway, and multistep long-term effects, including external environmental carcinogenic factors as well as its own genetic factors.

**2.2.1. Virus Infection.** There is a close relationship between hepatitis B virus (HBV) infection and the occurrence of hepatocellular carcinoma (HCC). The results of several epidemiological studies have shown that worldwide, with few exceptions, chronic HBV infection has great similarities with HCC occurrence regions [14, 15], and the incidence of HCC is also relatively low in regions with low HBV

infection. The mechanism of direct carcinogenesis of HBV is that the integration of HBV genome into host cells causes the simultaneous destruction of HBV DNA sequence and host cell gene sequence, or the occurrence of reintegration, which leads to the activation of oncogenes and inactivation of tumor suppressor genes, leading to cell carcinogenesis. Chronic hepatitis B can cause liver fibrosis and uncontrolled hepatocyte growth, and monocytes present in inflammatory liver tissue can locally produce reactive oxygen species, which can promote the occurrence of liver cancer.

Hepatitis C virus (HCV) has been proved by the research in China and abroad. Hepatitis C and B are the important causes of liver cancer. HBV is the main cause of liver cancer in developing countries, while HCV is the main cause in developed countries [16]. At present, it is generally believed that continuous infection is obtained due to HCV sequence variation and evasion of immune recognition and hepatocyte degeneration, necrosis, and regeneration occur repeatedly, leading to the accumulation of gene mutations. The C protein and NS3 structural region of HCV destroy the dynamic balance of cell proliferation by regulating the expression of related genes and participating in signal transduction regulation, leading to cell canceration [17].

**2.2.2. Aflatoxin.** A large number of epidemiological investigations and laboratory studies have confirmed that the incidence of liver cancer has a graded correlation with the amount of aflatoxin intake, and HBV and aflatoxin have a synergistic carcinogenic effect [18]. At present, aflatoxin is considered to be closely related to the mutation of tumor suppressor gene p53. Researchers in China and abroad can detect p53 gene mutation in liver cancer patients with high aflatoxin exposure, and it mainly occurs at codons 249 and 254.

**2.2.3. Relationship between Alcohol, Tobacco, and Occurrence of Liver Cancer.** Drinking alcohol mainly plays an auxiliary role in the occurrence of liver cancer. There is little evidence that alcohol itself is a carcinogen, but studies have shown a relationship between alcohol intake and the risk of liver cancer (OR): OR < 1 at low doses; The medium dose was OR > 1; Severe alcohol consumption increased the OR value by 2.75 times, and the OR value increased with the increase of drinking dose in a significant dose-response relationship [19].

The risk of liver cancer and liver cancer mortality caused by smoking increase with the increase of cigarette smoking, and there is a significant positive correlation between cigarette smoking and liver cancer [20]. There was a synergistic effect between alcohol consumption, smoking, and hepatitis B virus infection [21].

**2.2.4. Relationship between Genetic Factors and Occurrence of Liver Cancer.** Epidemiological studies have shown that after exposure to the same environment, the genetic susceptibility of the exposed plays an important role in the

pathogenesis of environmental factors. The genetic susceptibility indicators studied at present include

- (1) GST gene polymorphism, including GSTM1, GSTT1, GSTP1. Polymorphism in the coding sequence of GST gene may affect the carcinogenic function of the metabolic environment of the body [22].
- (2) Cytochrome P4501A gene polymorphism. It can cause a large amount of final carcinogen accumulation in the body, making the chance of final carcinogen binding to p53 gene greatly increased, resulting in p53 gene mutation [23].
- (3) Acetaldehyde dehydrogenase 2 gene polymorphism. It can affect alcohol metabolism, and the increased acetaldehyde concentration in the body can lead to an increased risk of hepatocellular carcinoma [24].

**2.2.5. Relationship between *Helicobacter pylori* Infection and Hepatocellular Carcinoma.** Studies outside China have found that *Helicobacter pylori* can cause chronic active hepatitis in some strains of mice and induce liver cancer in sensitive mice [25]. Making it the first time that bacterial infections have been linked to cancer. Of the 28 HCC specimens detected by PCR, 17 were positive for 16SrRNA gene of *Helicobacter pylori* (60.7%). Using the specific probe southern hybridization as a method for identifying *Helicobacter pylori*, the results showed that 60.7% of patients with primary liver cancer did experience infection with *Helicobacter pylori*, and sequencing results confirmed that the *Helicobacter pylori* 16SrRNA sequence in their liver cancer tissues shared 97.8% homology with *Helicobacter pylori*.

*Helicobacter pylori* reaches the liver through the portal vein, lymphatic circulation and other pathways, and is mostly distributed in the capillary bile duct between the hepatocytes, and the possible mechanism of cancer is:

- (1) *Helicobacter pylori* itself and its metabolites have hepatotoxic effect [26]
- (2) Inflammatory infections release cytokines that drive the cell cycle and increase the expression of endogenous associated antigens to cause abnormalities in cell proliferative kinetics

### 3. Experimental Part

**3.1. Research Objects.** The research subjects were primary and metastatic liver cancer patients who visited our hospital. All of them were clinically diagnosed (surgical pathology or biopsy pathology) and applied for ultrasound-guided radiofrequency ablation of liver tumors, a total of 40 cases with 101 focuses.

According to the consensus, inclusion and exclusion criteria for all cases were established and grouped according to the location of liver tumors and tumor volume, that is, research subjects were divided into two groups: treatment difficulties observation group (hereinafter referred to as the observation group) and control group, depending on whether liver tumors were difficult and complex to treat.

There were 45 focuses in the observation group and 56 focuses in the control group.

Inclusion criteria:

- (1) Liver malignant tumors that cannot be resected by surgery or for which the patient voluntarily selects ultrasound-guided RFA treatment
- (2) Patients with liver tumors had no vascular tumor thrombi or invasion of adjacent organs
- (3) Liver function classification Child-Pugh Grade A or B

Exclusion criteria

- (1) Diffuse hepatocellular carcinoma
- (2) Accompanied with vascular cancer thrombi or invasion of adjacent organs
- (3) Child-pughc of liver function, which could not be improved after liver protection treatment
- (4) Esophageal (gastric) variceal hemorrhage occurs within one month before treatment
- (5) Irreversible coagulation disorder and severe hemogram abnormality with severe bleeding tendency
- (6) Recalcitrant massive ascites, cachexia
- (7) Active infection, especially inflammation of the biliary system
- (8) Severe liver, kidney, heart, lung, brain, and other major organ failure
- (9) Patients with disturbance of consciousness or inability to cooperate with therapy

### 3.2. Experimental Installation

**3.2.1. Ultrasonic Instrument.** The ultrasonic instrument used in this study was PHILIPS IU22. The device is a multifunctional color Doppler ultrasound diagnostic apparatus. Has the advantages of high image quality, powerful functions, simple operation, and the like. The PHILIPS iU22 has a fully digital xSTREAM host architecture that can handle multiple data streams simultaneously—real-time processing—and supports an ultrawideband beam transmitter. Fast operation, running more than 250 billion times per second, makes real-time processing possible in all modes, including real-time three-dimensional volumetric imaging.

**3.2.2. Contrast-Enhanced Ultrasound Agent.** Sonovue, sulfur hexafluoride microbubbles for injection, manufactured by BRACCO, Italy, with a specification of 59 mg sulfur hexafluoride, was used. Before use, 5 mL normal saline for injection (0.9% NaCl) was injected with matching instruments, fully shaken and homogenized to obtain microbubble suspension for later use.

**3.2.3. Ultrasound-Guided Percutaneous Liver Puncture Biopsy Device.** Italian PRE TruCut needle was used for biopsy,

with a diameter of 20G, a length of 10 cm and a cutting groove length of 2 cm.

**3.2.4. Contrast-Enhanced Ultrasound Quantitative Analysis Software.** QLAB CEUS Image Analysis Software is a new contrast analysis software released by PHILIPS, which can be run on personal computers and also used in various computer operating systems such as windows XP. Compared with the previous contrast analysis software, when using this software for CEUS, the acquisition of contrast images has the following requirements:

- (1) The settings of contrast conditions of ultrasonic instruments shall be adjusted according to the recommended use and adjustment requirements of different instruments, and the concentration of contrast agent in the circulating blood and the stability of microbubbles shall be maintained to the maximum extent, for example, the settings of two-dimensional gray scale gain, TGC, mechanical index (MI) and other parameters
- (2) For CEUS, the section image should be located on the largest section of the lesion and the image should be kept on the same section to the maximum extent
- (3) In order to minimize the images caused by breathing or probe jitter, the patient should be asked to maintain stable breathing as much as possible and keep the stability of the probe
- (4) The injection method of contrast agent should be bolus injection
- (5) Contrast images should be recorded continuously for at least 180 seconds

**3.3. Method.** The technical route is shown in Figure 1:

**3.3.1. Conventional Ultrasonic Examination Method.** A comprehensive scan of the liver was performed to confirm the focus's location and number, to fully comprehend the focus's size, morphology, internal echo structure, color blood flow signals, spectral characteristics, and the relationship between the focus and the surrounding important tissues and structures, as well as to measure and record the relevant data and store the static and dynamic imprints.

The description of routine ultrasound results of focal liver focus includes the following aspects:

- (1) *The Size of the Lesion.* The maximum diameter was measured on that largest section shown in the lesion.
- (2) *The Morphology of Focus.* The spherical or ellipsoidal shape of focal liver focus is defined as regular morphology, and it is called irregular morphology when the focus have no certain morphology and grow irregularly.
- (3) *Echo Types of Focus.* The normal liver parenchyma echo was taken as the reference, and the normal spleen echo could be taken as the reference when the liver was accompanied

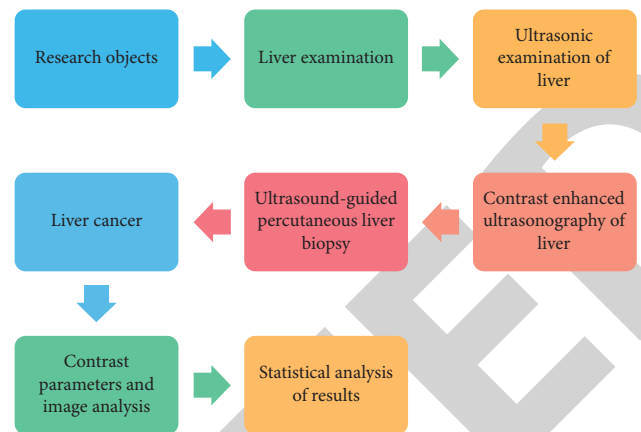


FIGURE 1: Method road map.

with diffuse focus. A lesion with an echo similar to that of the lesion was defined as isoecho, and the lesion with an echo higher than that was defined as hyperecho, and that with an echo lower than that was defined as hypoecho.

(4) *The Boundary of the Lesion.* The focus with complete and continuous capsule and clear boundary with liver parenchyma were called with clear boundary, while the focus without obvious capsule or with discontinuous capsule and unclear boundary with liver parenchyma were called with unclear boundary.

(5) *Focal Blood Flow Signal.* There were two types according to the abundance of blood flow signals in and around the focus: linear and branched blood flow signals in and around the tumor focus were defined as the rich blood supply type, and no blood flow signal in the focus was defined as the less blood supply type.

(6) *Spectral Doppler Characteristic of Focus.* According to the RI, it was divided into two types, low resistance type ( $RI < 0.7$ ) and high resistance type ( $RI > 0.7$ ).

**3.3.2. Contrast-Enhanced Ultrasound Targeted Spot Selection.** The patient was in the supine or left lateral position, and the morphological characteristics of the lesion, including lesion size, echo, and boundary, were recorded using conventional two-dimensional ultrasound with an abdominal probe. Then color Doppler ultrasonography was performed to observe the blood supply. The contrast agent was prepared in advance. Using SonoVue produced by Bracco, Italy, 5 ml normal saline was injected into the SonoVue lyophilized powder bottle, and the bottle was vigorously shaken for several seconds until the lyophilized powder was completely and uniformly mixed to form an opalescent suspension.

Set the scan tool to contrast mode. A rapid bolus of 2.4 ml of SonoVue Suspension was injected through the superficial vein at the elbow and the tube was rinsed with 5 ml of normal saline. Timing was immediately started from the injection, and lesion enhancement characteristics in arterial phase, portal phase and delayed phase of the lesion

were continuously observed in real time and dynamically according to the guidelines of the European Committee on Ultrasound Medicine and Biology for CEUS of the liver, and images were stored. According to the contrast results, the puncture biopsy was performed using the contrast-enhanced active region as the target.

**3.3.3. Ultrasound-Guided Percutaneous Liver Biopsy.** Routine blood test and coagulation function examination before operation. The puncture biopsy can be performed only for patients who have no coagulation dysfunction or bleeding tendency and can tolerate the operation. Patients and their families were informed of the surgical risks and possible complications before surgery and informed consent was signed.

After routine disinfection and towel laying, the ultrasonic probe was covered with a sterile probe sleeve, a special puncture holder was mounted, and 2% lidocaine was used for local anesthesia. An 18G BARD needle biopsy was performed through the normal liver parenchyma to avoid large vessels. One to two needles were punctured conventionally. The average number of punctures was equal to the total number of punctures divided by the total number of punctures. The specimens obtained from the biopsy were fixed in 10% formaldehyde solution and then sent to the Pathology Department for histological examination. The ultrasound-guided puncture process is shown in Figure 2:

**3.3.4. Contrast-Enhanced Ultrasound Analysis of Liver.** The QLAB software will first be started and the contrast files stored on the CD will be imported into the analysis software. Secondly, various parameters of the software are set, and the settings of the parameters should be consistent with those of the ultrasound instrument during contrast. Selection of region of interest, which should include all the regions of the lesion as much as possible.

**3.3.5. Postoperative Observation and Treatment.** After the patient's vital signs were stabilized, the stretcher was returned to the ward and he was told to stay in bed for 24 hours. Monitoring of blood pressure, oxygen saturation and other vital signs and abdominal conditions, focusing on observing whether there is a complication. Patients were routinely treated with related therapies such as hemostasis, analgesia, liver protection and anti-inflammation, and the changes of the disease conditions were monitored.

**3.3.6. Statistical Treatment.** SPSS14.0 statistical software was used. Taking the pathological results as the gold standard, calculating the sensitivity, specificity, positive predictive value and negative predictive value of elastography in the diagnosis of liver malignant tumor; The Chi-square test was used to compare the accuracy of elastography in diagnosing malignant tumors  $\leq 2$  cm and  $> 2$  cm.

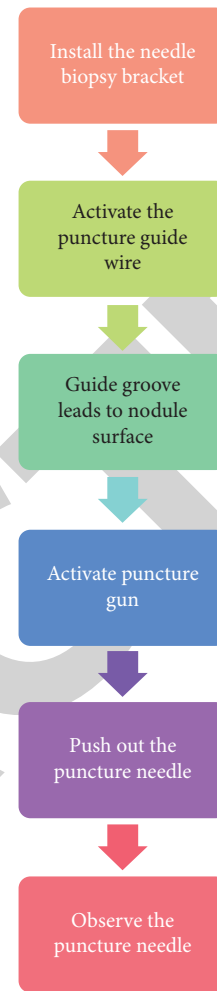


FIGURE 2: Ultrasound-guided puncture process.

## 4. Result

**4.1. Routine Ultrasound Observations.** In the observation group, there were 45 focuses, with the largest lesion being 10.3 cm, and the smallest lesion being 0.7 cm, with the average size of  $(3.22 \pm 2.51)$  cm. Among them, 33 focuses were located in special locations, including six adjacent to the diaphragm, 11 located under the liver capsule, four close to the gastrointestinal tract, three adjacent to the gallbladder, and 10 adjacent to the great vessels. In addition, there were 12 cases with the maximum diameter  $\geq 5$  cm. The composition of the difficult factors for focus in the observation group is shown in Figure 3.

In the control group, 56 focuses were identified, of which 4 focuses were newly detected by CEUS before RFA treatment and were not measured under conventional ultrasound before operation. Among the remaining 52 focuses, the largest lesion was 4.6 cm and the smallest was 0.3 cm, with an average of  $(23.35 \pm 0.88)$  cm.

The average values of the lesion sizes in the observation group and the control group are compared, and the results are shown in Table 1. By rank sum test,  $Z = -0.714$ , and  $P = 0.476 > 0.05$  indicated that there was no significant

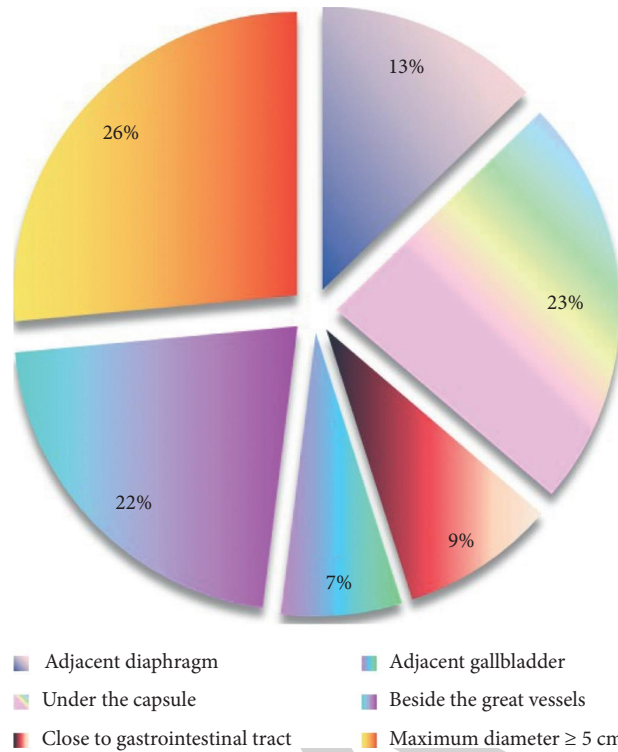


FIGURE 3: Schematic diagram of constitution of lesion difficult factors in observation group.

TABLE 1: Under conventional ultrasound, the average value of the maximum diameter of the observation group was compared with that of the control group.

	Observation group ( $n = 45$ )	Control group ( $n = 56$ ).	Z	P
Measurement under conventional ultrasound.	$3.24 \pm 2.17$	$2.36 \pm 0.87$	-0.714	0.476

difference in the lesion sizes between the two groups when measured by conventional ultrasound.

**4.2. Test Results of Contrast-Enhanced Ultrasound.** Preoperative CEUS evaluation was performed on 80 focuses. Satisfactory contrast images were obtained for 45 focuses in the observation group and 55 focuses in the control group, while repeated observation of one lesion in the control group could not obtain a satisfactory effect. Under contrast conditions, the average maximum diameter of 45 focuses in the observation group was  $(3.36 \pm 2.27)$  cm, and that of 55 focuses in the control group was  $(2.43 \pm 0.78)$  cm. The lesion sizes of the two groups were compared, and  $Z = -0.963$ ,  $P = 0.357 > 0.05$  by rank sum test. There was no significant difference in lesion size between the two groups measured in the CEUS shape.

In the observation group, 53% (24/45) of the focuses were  $\leq 3$  cm, 18% (8/45) were between 3 cm and 5 cm, and the other 29% (9/45) were  $> 5$  cm.

In the control group, 84% (46/55) of the focuses were  $\leq 3$  cm, and 16% (9/55) of the focuses were within the range of 3 cm to 5 cm (Figure 4).

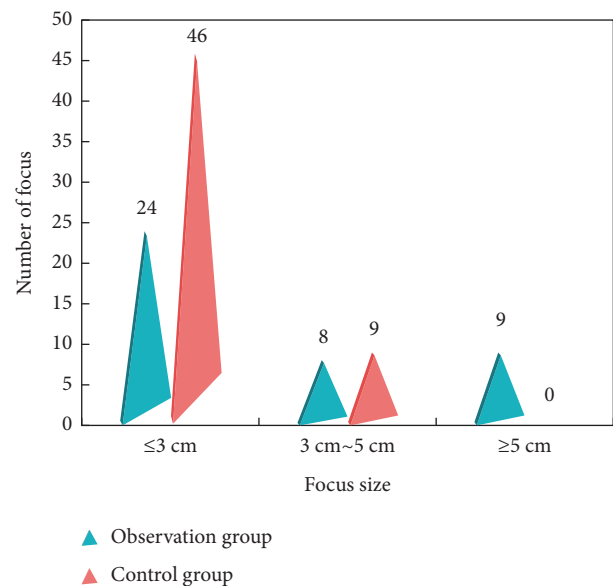


FIGURE 4: Schematic diagram of lesion size distribution in two groups of CEUS.

A total of 101 focuses were treated with RFA, and CEUS was performed immediately to observe the size of ablation focus. The average maximum diameter of 45 ablation focuses in the observation group was  $(3.98 \pm 2.51)$  cm, and that of 56 ablation focuses in the control group was  $(3.22 \pm 0.84)$  cm.

**4.3. Comparison of Lesion Size Measurement Results Using Conventional Ultrasound and Contrast-Enhanced Ultrasound.** The average size of 45 focuses in the observation group was  $(3.23 \pm 2.45)$  cm under conventional ultrasound and  $(3.41 \pm 2.23)$  cm under CEUS.  $Z = -2.801$  and  $P = 0.003 < 0.05$  in rank sum test, and there was statistical difference in the lesion sizes measured by the two methods. The lesion CEUS measurement in the observation group was larger than that under conventional ultrasound.

A total of 56 focuses were found in the control group. The paired analysis of conventional ultrasound and CEUS was performed on the 56 focuses in the control group. The average lesion size was  $(2.36 \pm 0.88)$  cm under conventional ultrasound and  $(2.63 \pm 0.87)$  cm under CEUS.  $Z = -4.177$ ,  $P < 0.05$  by rank sum test. There was statistical difference in the lesion sizes measured by the two methods. The lesion size measured by CEUS in the control group was larger than that measured by conventional ultrasound.

In the observation group, the CEUS measurement result of 64% (29/45) of all focuses was larger than the conventional ultrasound measurement result, 16% (7/45) of the focuses were consistent with the conventional ultrasound measurement result, and 20% (9/45) of the focuses were smaller than the conventional ultrasound measurement result (Figure 5).

Among them, 68% (38/56) of the focuses in the control group had an increase in CEUS measurement of lesion diameter compared with the conventional ultrasound measurement, and 25% (14/56) of the focuses had the same measurement results under the two methods. Only 7% (4/56) of the focuses had CEUS measurement results smaller than the conventional ultrasound measurement (Figure 5).

**4.4. Effect Evaluation.** One month after RFA treatment of 101 focuses, CEUS follow-up was performed to evaluate the efficacy of biopsy. CEUS indicated that a total of 85 focuses were completely ablated, and the overall complete ablation rate was 85%.

Among the 45 focuses in the observation group, 33 focuses were completely ablated, and 12 focuses were not completely ablated, with the complete ablation rate of 73.3%. In the control group, 48 of the 56 focuses were completely ablated, and eight focuses were not completely ablated. The complete ablation rate was 85.7% (Figure 6).

The complete ablation rate of focus between the two groups was compared. Although the complete ablation rate in the observation group was slightly lower than that in the control group, according to the chi-square test,  $\chi^2 = 0.407$ , and  $P = 0.516 > 0.05$  indicated that there was no significant difference in the complete ablation rate between the two groups.

**4.5. Patient Serum AFP Content Results.** The patients with primary liver cancer were followed up for serum AFP content one month after operation and compared with those before operation. The results are shown in Figure 7.

Among the 13 cases of primary liver cancer in the observation group, AFP was always in the normal range in two patients, declined to varying degrees in eight patients, increased in four patients, and the level of AFP in one patient was the same as that before surgery.

In the control group, including 22 patients with primary liver cancer, the serum AFP values of six patients were consistent within the normal range, 10 patients experienced different degrees of AFP decline, five patients had higher AFP than before, and one patient was the same as the preoperative AFP.

**4.6. Follow-Up of Survival Rate and Local Recurrence Rate after Surgical Treatment.** The follow-up results of survival rate and local recurrence rate after treatment are shown in Figure 8.

This study was started in October 2019, and the complete case follow-up was conducted until January 2020. The survival rate and local recurrence rate of 101 patients with liver cancer treated by ultrasound-guided automatic biopsy were followed up for half a year and one year.

In the observation group, the half-year and one-year survival rates of 45 patients were 78% (35/45) and 69% (31/45), respectively, and the local recurrence rates were 11% (5/45) and 18% (8/45), respectively.

In the control group, the half-year and one-year survival rates of 56 patients were 80% (46/56) and 75% (42/56), respectively, and the local recurrence rates were 7% (4/56) and 11% (6/56), respectively.

## 5. Discussion

During CEUS of the normal liver, the microbubble contrast agent was injected through the peripheral vein and entered the abdominal aorta through the pulmonary circulation, and a part of the microbubbles traveled from the abdominal aorta to the hepatic artery, where their introduction led to enhanced blood flow in the hepatic arterial system (early enhancement). Some microvesicles: transabdominal artery-splenic artery-splenic vein-portal vein; Through superior mesenteric artery-superior mesenteric vein-portal vein, liver entry results in increased flow (delayed enhancement) in the portal system. Primary liver cancer is a multi-vascular malignant tumor, and 90% of its blood supply is derived from the hepatic artery. Moreover, tumor cells can secrete angiogenic factors, stimulate neoangiogenesis, and have abnormal anastomosis with arterioles and venules. Deformation, shift, abnormal proliferation, vascular encircling, arteriovenous fistula, etc. of the tissue and vessels can be seen from the tissue morphology. The peripheral liver parenchyma was mainly supplied by portal vein.

A large number of studies have shown that angiogenesis is the prerequisite and basis for tumor growth and metastasis. Malignant tumors without neovascularization are

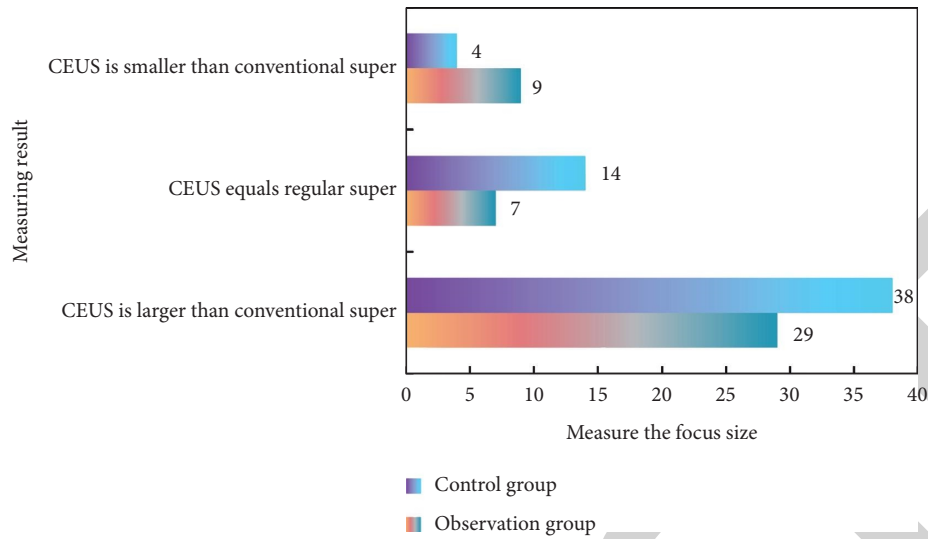


FIGURE 5: Comparison between CEUS measurement and conventional ultrasound measurement in two groups.

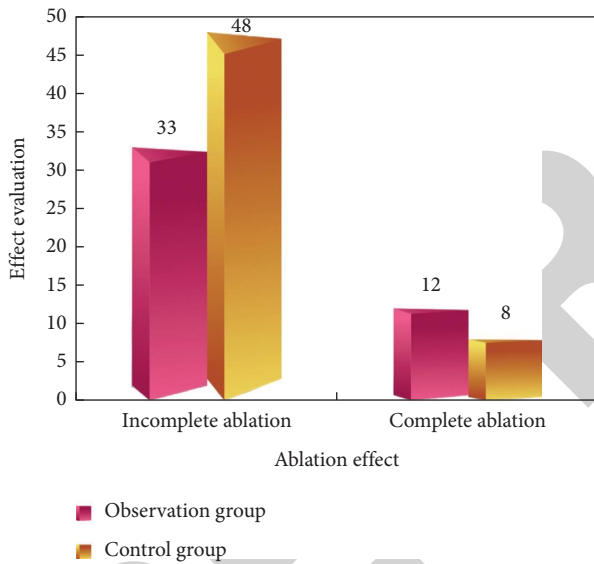


FIGURE 6: Schematic diagram of ablation efficacy evaluated by CEUS in two groups one month after treatment.

usually in a semi-dormant state, limited to the primary site, and grow slowly. In the pre-vascular stage where solid tumors are formed, the primary tumors are usually 1–3 mm in diameter and the number of cells is limited to 106. The focus is in a static state for a long time, such as carcinoma in situ. Once the angiogenesis enters the late vascular stage, the tumor will grow uncontrollably, and the tumor volume can reach 10,000–20,000 times of the original size within two weeks, while a large number of tumor cells metastasize to the distant via blood vessels [27].

Transhepatic biopsy can not only identify the benign and malignant focus, but also carry out pathological classification, understand the cell morphology, tissue structure characteristics and differentiation degree, identify the malignant tumor as primary or metastatic, and guide clinical

analysis of the etiology and treatment of various benign focus. Another study [28] has revealed that the size, location of liver cancer focus and the background of liver cirrhosis are the main causes of missed diagnosis by conventional ultrasound. Based on the above existing problems, it is not enough to rely on conventional ultrasound to evaluate the basic situation of the focus in liver malignant tumors before RFA treatment. It is necessary to further understand the true size, boundary range, location and adjacent relationship as well as the blood supply characteristics of the focus through other methods.

The tissues obtained from ultrasound-guided needle biopsy are only a small part of the diseased tissues, which cannot completely represent the whole lesion. The puncture pathological results of different regions within the same lesion may be completely different. Therefore, detecting positive and representative diseased tissues by needle biopsy is the key to improving the success rate of needle biopsy, the positive rate of needle biopsy, the diagnostic coincidence rate of needle biopsy and the diagnostic accuracy of malignant focus. CEUS increases the blood supply information of liver space-occupying focus and helps to judge whether the focus are active or not. The blood supply of some hepatic space-occupying focus is not rich, and conventional ultrasound cannot meet the needs of the diagnosis of the focus and the evaluation of curative effects after treatment. The active tissue can be determined as soon as the contrast-enhanced area on CEUS is present, while the less active part shows mild enhancement in the arterial phase, and the non-active part shows no enhancement. CEUS can sensitively and delicately provide the internal microvascular distribution of liver space-occupying focus and judge the carcinomatous residue and recurrence of liver cancer after treatment, which is clinically of great significance.

Tumor angiogenesis plays an important role in the pathogenesis of tumors. Malignant tumors can secrete tumor angiogenic factors, and under their stimulation, tumors and surrounding tissues begin to produce new blood vessels,

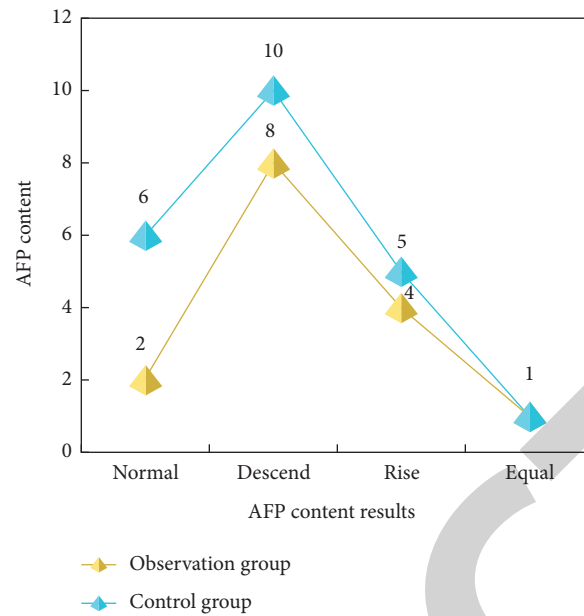


FIGURE 7: Results of serum AFP content in patients with primary liver cancer after one month follow-up.

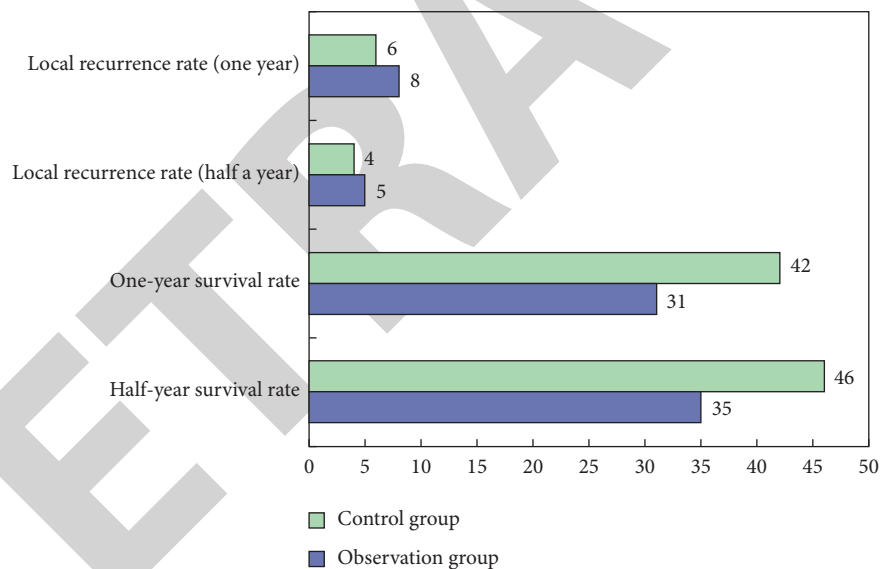


FIGURE 8: Follow-up of survival rate and local recurrence rate after treatment.

which are different from those of benign tumors in morphology, quantity and function. Some studies have applied the information technology [29] to observe the morphology of new blood vessels of hepatocellular carcinoma tumors, and the results show that the distribution of new blood vessels is disordered. The above pathological characteristics of tumor blood vessels led to abnormal tumor blood perfusion, and CEUS as a blood pool tracer imaging provided the theoretical basis for reflecting the true size of the lesion.

In this clinical study, the rank sum test was used to compare the lesion sizes of the two groups under conventional ultrasound and CEUS, and  $P > 0.05$  meant that there was no significant difference in the lesion sizes between the

two groups. However, in the treatment observation group, the largest diameter of tumors in seven of the 45 focuses was  $> 5$  cm, while all focuses in the control group were  $< 5$  cm. For analysis, there was no statistical difference in lesion size between the two groups probably due to the small sample size. If the sample size of focus with the largest diameter  $> 5$  cm was increased, the focus in the observation group would likely be larger than those in the control group.

In this study, three cases of liver cancer CEUS showed atypical manifestations, and no significant contrast agent regression was observed in the portal venous phase and the delayed phase. The puncture pathological results of these cases confirmed highly differentiated liver cancer, while 25

cases of CEUS showed typical “fast-forward and fast-out” liver cancer. The puncture pathological results confirmed medium-to low-differentiated liver cancer. These differences reflect the sequential changes in hemodynamics during the formation of HCC, namely, with the increase of the malignancy of the nodules, the portal blood supply will gradually decrease and the arterial blood supply will gradually increase. In addition, CEUS parameter values of benign and malignant focus overlapped in some parts of the study, and it is difficult to identify the nature of the lesion in this case by only relying on the parameter values. These cases deserve further study in the future.

## 6. Conclusion

For qualitative diagnosis of liver tumors, ultrasound-guided automatic biopsy is an effective method with fewer complications and a high diagnosis rate. This technique is deserving of further clinical promotion due to its ease of use, high sampling quality, and lack of pain for patients. Furthermore, for nodular foci in the liver that are difficult to characterize with routine imaging and laboratory examination, clinicians should consider ultrasound-guided automatic biopsy as the first alternative qualitative diagnosis method.

## Data Availability

The data used to support the findings of this study are included within the article.

## Conflicts of Interest

The author declares that there are no conflicts of interest in association with the publication of this article.

## References

- [1] M. Zamzam, A. A. El-Aziz, I. El-Mahallway, G. AbdeLaal, and M. A. El-Mageed, “Role of ultrasound-guided transthoracic biopsy versus computed tomography-guided biopsy in the diagnosis of peripheral intrathoracic focus,” *Egyptian Journal of Chest Diseases and Tuberculosis*, vol. 69, no. 1, p. 183, 2020.
- [2] S. Kajikawa, I. Naoyuki, S. Okachi et al., “Diagnostic contribution of cytological examination to endobronchial ultrasound-guided transbronchial biopsy for lung malignancies,” *Nagoya Journal of Medical Science*, vol. 81, no. 4, pp. 613–620, 2019.
- [3] G. Zanetta, A. Brenna, M. Pittelli, A. Lissoni, D. Trio, and S. Riotta, “Transvaginal ultrasound-guided fine needle sampling of deep cancer recurrences in the pelvis: usefulness and limitations,” *Gynecologic Oncology*, vol. 54, no. 1, pp. 59–63, 1994.
- [4] S. Lahiri, H. Justino, J. Heinle, J. Hernandez, and C. Miyake, “Ultrasound-guided intraoperative trans-epicardial needle biopsy of an intracardiac tumor,” *Annals of Pediatric Cardiology*, vol. 13, no. 4, p. 346, 2020.
- [5] Z. H. Gou, F. Yan, H. Y. Wang et al., “Application value of diffusion-weighted imaging signal pattern in the qualitative diagnosis of renal focus with T(2)WI hypointensity,” *National Medical Journal of China*, vol. 99, no. 35, pp. 2756–2760, 2019.
- [6] X. Tan, B. Liu, R. Wang, and Y. Zhang, “Diagnostic value of transbronchial ultrasound-guided needle aspiration biopsy in the diagnosis of small cell lung cancer and non-small cell lung cancer,” *Zhongguo fei ai za zhi = Chinese journal of lung cancer*, vol. 23, no. 6, pp. 466–471, 2020.
- [7] M. Tttrup, J. D. Eriksen, M. B. Hellfritsch, F. B. Sørensen, and T. B. Hansen, “Diagnostic accuracy of ultrasound-guided core biopsy of peripheral nerve sheath tumors,” *Journal of Clinical Ultrasound*, vol. 48, no. 3, pp. 134–138, 2020.
- [8] Y. Luo, Q. Gao, J. Guo, Y. Zhang, J. Sun, and W. Li, “Ultrasound-guided co-axial introducer needle biopsy in the diagnosis of eosinophilic cystitis in children,” *Chinese Medical Journal*, vol. 134, no. 15, pp. 1872–1873, 2021.
- [9] A. Hormati, M. R. Ghadir, S. Rezvan, A. Mohammadbeigi, and F. Alemi, “Comparison of the success rate and complications of blind liver biopsy and ultrasound-guided liver biopsy,” *Govaresh*, vol. 24, no. 1, pp. 59–64, 2019.
- [10] J. Kuijvenhoven, F. Leoncini, L. Crombag, and R. Spijker, “Endobronchial ultrasound for the diagnosis of centrally located lung tumors: a systematic review and meta-analysis,” *Respiration*, vol. 99, no. 5, pp. 1–10, 2019.
- [11] L. Xin, J. Wang, and H. Chen, “Etc. Diagnostic value of ultrasound-guided fine needle aspiration biopsy for TI-RADS 4-5 nodules,” *Journal of Dali University*, vol. 4, pp. 65–68, 2020.
- [12] P. VlasakJ. Bouda et al., “Diagnostic reliability, accuracy and safety of ultrasound-guided biopsy and ascites puncture in primarily inoperable ovarian tumours,” *Anticancer Research*, vol. 40, no. 6, pp. 3527–3534, 2020.
- [13] F. H. Kawshty, A. A. Abd Elradi, and A. M. Ahmed, “Diagnostic yield of ultrasound-guided transthoracic biopsy in peripheral lung lesions,” *Egyptian Journal of Bronchology*, vol. 13, no. 4, pp. 469–476, 2019.
- [14] J. Phan, D. W. Dawson, A. Sedarat et al., “Clinical utility of obtaining endoscopic ultrasound-guided fine-needle biopsies for histologic analyses of pancreatic cystic lesions,” *Gastroenterology*, vol. 158, no. 3, pp. 475–477, 2020.
- [15] S. Choudhery, J. A. Stellmaker, A. L. Hanson et al., “Utilizing time-driven activity-based costing to increase efficiency in ultrasound-guided breast biopsy practice,” *Journal of the American College of Radiology*, vol. 17, no. 1, pp. 131–136, 2020.
- [16] P. Kabalak, D. Kizilgoz, U. Yilmaz, and F. Demirag, “Application of endobronchial ultrasound-guided transbronchial needle aspiration for re-biopsy in lung cancer,” *Annals of Medical Research*, vol. 28, no. 3, p. 454, 2021.
- [17] Z. Wang, Q. Qu, K. Cai, and T. Xu, “CT image examination based on virtual reality analysis in clinical diagnosis of gastrointestinal stromal tumors,” *Journal of Healthcare Engineering*, vol. 2021, Article ID 9996565, 10 pages, 2021.
- [18] C. A. A. Febres, S. Alghamdi, K. Krishnamurthy, and R. J. Poppiti, “Liver fibrosis helps to distinguish autoimmune hepatitis from dili with autoimmune features: a review of twenty cases,” *Journal of Clinical and Translational Liver Diseases(English Version)*, vol. 007, no. 1, pp. 21–26, 2019.
- [19] L. Cheng and H. Hu, “Clinicoradiological features and value of BI-RADS classification standard for qualitative diagnosis in breast phyllodes tumors,” *Guangxi medicine*, vol. 041, no. 4, pp. 439–442, 2019.
- [20] A. Howell, A. Lambert, M. M. Pinkston et al., “Sustained sobriety: a qualitative study of persons with HIV and chronic hepatitis C coinfection and a history of problematic drinking,” *AIDS and Behavior*, vol. 6, pp. 1–11, 2020.